ORNL/SPR-2016/276

FY 2016 Status Report: CIRFT Testing Data Analyses and Updated Curvature Measurements

Fuel Cycle Research & Development

Prepared for
US Department of Energy
Used Fuel Disposition Campaign

J.-A. Wang, H. Wang
B. B. Bevard, J. M. Scaglione
Oak Ridge National Laboratory

July 24, 2016
M4FT-16OR080202032

ORNL/SPR-2016/276

Materials Science and Technology Division

FY 2016 Status Report: CIRFT Testing Data Analyses and Updated Curvature Measurements

Jy-An John Wang and Hong Wang

Program Manager
Bruce Bevard

Date Published: July 24, 2016

Prepared by
OAK RIDGE NATIONAL LABORATORY
Oak Ridge, TN 37831-6283
managed by
UT-BATTELLE, LLC
for the
US DEPARTMENT OF ENERGY
under contract DE-AC05-00OR22725

This page intentionally left blank.

SUMMARY

This report provides a detailed description of FY15 test result corrections/analysis based on the FY16 Cyclic Integrated Reversible-Bending Fatigue Tester (CIRFT) test program methodology update used to evaluate the vibration integrity of spent nuclear fuel (SNF) under normal transportation conditions. The CIRFT consists of a U-frame testing setup and a real-time curvature measurement method. The three-component U-frame setup of the CIRFT has two rigid arms and linkages to a universal testing machine. The curvature of rod bending is obtained through a three-point deflection measurement method. Three linear variable differential transformers (LVDTs) are used and clamped to the side connecting plates of the U-frame to capture the deformation of the rod.

The contact-based measurement, or three-LVDT-based curvature measurement system, on SNF rods has been proven to be quite reliable in CIRFT testing. However, how the LVDT head contacts the SNF rod may have a significant effect on the curvature measurement, depending on the magnitude and direction of rod curvature. It has been demonstrated that the contact/curvature issues can be corrected by using a correction on the sensor spacing. The sensor spacing defines the separation of the three LVDT probes and is a critical quantity in calculating the rod curvature once the deflections are obtained.

The sensor spacing correction can be determined by using chisel-type probes. The method has been critically examined this year and has been shown to be difficult to implement in a hot cell environment and thus cannot be implemented effectively. A correction based on the proposed equivalent gauge-length has the required flexibility and accuracy and can be appropriately used as a correction factor.

The correction method based on the equivalent gauge length has been successfully demonstrated in CIRFT data analysis for the dynamic tests conducted on Limerick (LMK) (17 tests), North Anna (NA) (6 tests), and Catawba mixed oxide (MOX) (10 tests) SNF samples. These CIRFT tests were completed in FY14 and FY15. Specifically, the data sets obtained from measurement and monitoring were processed and analyzed. The fatigue life of rods has been characterized in terms of moment, curvature, and equivalent stress and strain..

This page intentionally left blank.

ACKNOWLEDGMENTS

This research was sponsored by the US Department of Energy (DOE) Used Fuel Disposition Campaign (UFDC) under DOE contract DE-AC05-00OR22725 with UT-Battelle, LLC. The authors thank ORNL program managers Bruce Bevard and John Scaglione for their support and guidance during the project, Chuck Baldwin for post-irradiation examination (PIE), Josh Schmidlin for fuel rod cutting and dimension measurement, Bryan Woody and Scott Thurman for hot-cell operation support, Brian Sparks and Randy Parten for drawing and machining support, and Rose Raney for editorial review of this report.

This page intentionally left blank.

CONTENTS

LIST OF FIGURES

LIST OF TABLES

This page intentionally left blank.

ACRONYMS

AP	alumina pellets
BWR	boiling water reactor
CIRFT	Cyclic Integrated Reversible-Bending Fatigue Tester
DOE	US Department of Energy
FCRD	Fuel Cycle Research & Development
FEA	finite-element analysis
FY	fiscal year
GWd/MTU	gigawatt-days per metric ton of uranium
HBR	H. B. Robinson Nuclear Power Station
HBU	high burn-up
ID	identification numbers
LMK	Limerick Nuclear Power Station
LVDT	linear variable differential transformer
MOX	mixed uranium-plutonium oxide
NA	North Anna Power Station
NCT	normal conditions of transport
NRC	US Nuclear Regulatory Commission
NUREG	Nuclear Regulatory Commission technical report
NUREG/CR	NUREG contractor report
OD	outer diameter
ORNL	Oak Ridge National Laboratory
PCI	peripheral component interconnect
PIE	post-irradiation examination
PNNL	Pacific Northwest National Laboratory
PPI	pellet-to-pellet interface
PWR	pressurized water reactor
RT	room temperature
SNF	spent nuclear fuel
SS	stainless steel
SSAP	stainless steel alumina pellets
UFDC	Used Fuel Disposition Campaign
SNF	spent nuclear fuel

This page intentionally left blank.

USED FUEL DISPOSITION CAMPAIGN

FY 2016 Status Report: CIRFT Testing Data Analyses and Updated Curvature Measurements

1. CYCLIC INTEGRATED REVERSIBLE-BENDING FATIGUE TESTER

The Cyclic integrated reversible-bending fatigue tester (CIRFT), developed by ORNL,[1,2,3,4,5,6,7,8] consists of a U-frame as shown in Fig 1. The U-frame includes two rigid arms, connecting plates, and universal testing machine links. The rod specimen is coupled to the rigid arms through two specially designed grips. The U-frame setup is oriented in a horizontal plane and is driven by electromagnetic-force–based Bose dual linear motors. With help from the coupling, linear motions applied at the loading points of the rigid arms are converted into bending moments. The dual linear motor (model LM2) test bench has a maximum load capacity of ±3,000 N and a maximum stroke of ±25.6 mm. Bending is imposed through a U-frame with dual driving points and a 101.60 mm loading arm. Under a pair of forces or displacements that face outward, the rigid arms are opened, and bending moments force the rod to deflect outward (away from operator). Under a pair of forces facing each other, the rigid arms are closed, forcing the rod to deflect inward. The CIRFT can deliver dynamic loading to a rod specimen in the load-control mode at 5 to 10 Hz. The current configuration enables the system to test a rod 9.70 mm to 11.74 mm in diameter, 152.40 mm (6 in.) in length, and 50.80 mm (2 in.) in gage section. Three LVDTs measure rod deflections at three adjacent points within the gage section to determine rod curvature, which is then correlated to the applied moment to characterize the mechanical property of the bending rod. Online monitoring can capture mechanical property changes to reveal fatigue behavior during testing.

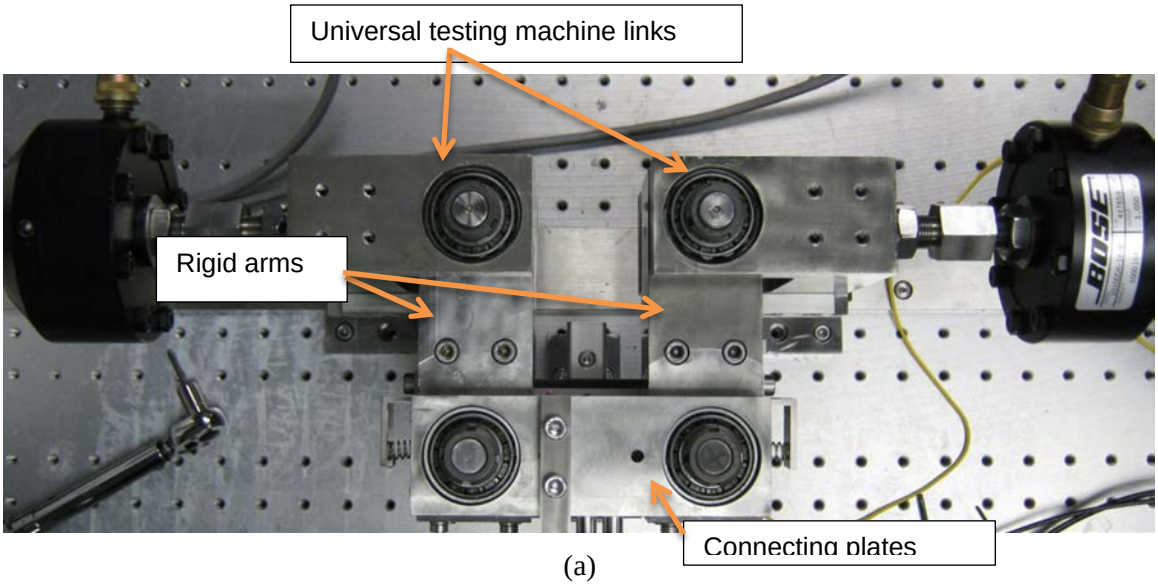
Universal testing machine links
Rigid arms
Connecting plates

(a)

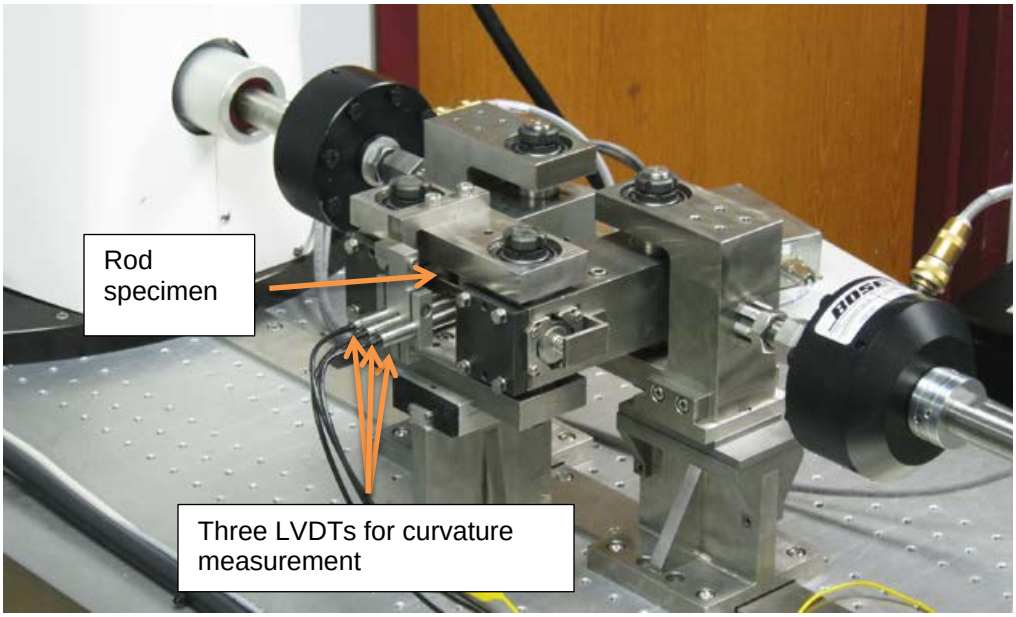
Rod specimen
Three LVDTs for curvature measurement

(b)

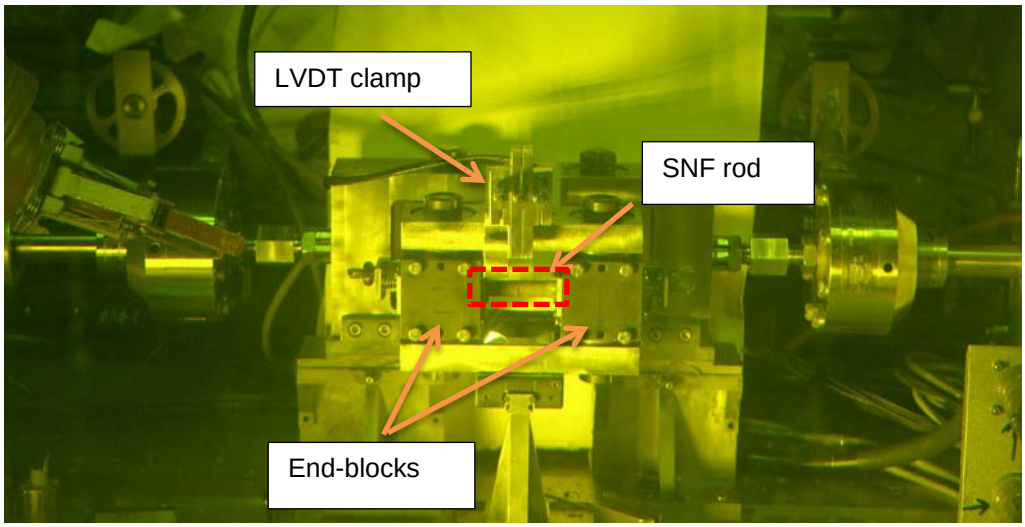

(c)

Fig. 1. (a) Horizontal layout of ORNL U-frame setup, (b) rod specimen under test and three LVDTs for curvature measurement (operator is facing the three LVDTs), and (c) front view of CIRFT installed in ORNL hot cell.

1.1 Moment and Curvature Calculations

Measurement data are converted into the applied moment and curvature based on the load channel (load1 and load2) information, the loading arm length (101.60 mm), and LVDT data (LVDT1, 2, and 3).

The moment was estimated by

$$M = F \times L \tag{1}$$

where F is the averaged value of applied loads (load1 and load2) from the Bose dual motors, and L is the loading arm length, 101.60 mm.

Theoretically, the bending radius and maximum strain of a rod can be estimated on the basis of the traveling displacement at the loading points of the rigid arm. However, the displacement measured contains the contribution of the compliant layers depending on the materials used in the compliant layers and the level of loading.

To address this issue, direct measurement of the specimen displacement at three adjacent points along the rod method was adopted[9] and has been implemented to evaluate the curvature of a bending rod in this study.[2,3]

Given the deflections from three LVDTs, d_1, d_2, and d_3, as shown in Fig. 2**.**, the curvature κ of the bending rod can be evaluated as follows:

$$\kappa = [(x_0 - d_2)^2 + y_0^2]^{-1/2}, \qquad x_0 = \frac{-2m_a m_b h - m_a(d_2 + d_3) + m_b(d_1 + d_2)}{2(m_b - m_a)}, \tag{2}$$

$$y_0 = -\frac{1}{m_a}\left(x_0 - \frac{d_1 + d_2}{2}\right) - \frac{h}{2},$$

where

$$m_a = \frac{h}{d_2 - d_1},$$

$$m_b = \frac{h}{d_3 - d_2},$$

and h is the sensor distance, 12 mm.

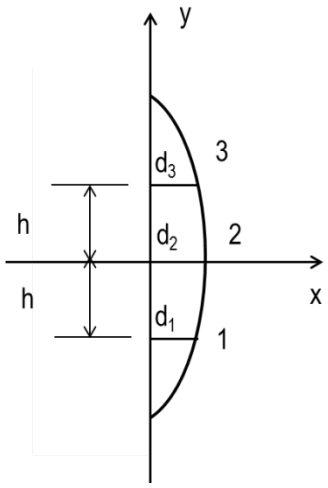

Fig. 2. Determination of the bending curvature of the rod by use of deflections measured at three points.

The arrangement of the three LVDTs and their installation in the setup can be seen in Fig. 3**.** An equivalent strain-stress curve (illustrated in Eq. 3) can be obtained under the assumption that the SNF rod can be idealized as a linear elastic homogeneous material without t consideration of the effects induced by pellet-clad interaction. The equivalent stress was calculated using:

$$\sigma = M \times y_{max}/I \quad (3)$$

where I is the moment of inertia, $I = I_c + I_p$, I_c and I_p are moments of inertia of cladding and pellet, respectively, and y_{max} is the maximum distance to the neutral axis of the test rod of the section and is measured by the radius of the cladding. The calculation of stress disregards the difference of elastic moduli between clad and pellets.

The equivalent strain is then:

$$\varepsilon = \kappa \times y_{max}. \quad (4)$$

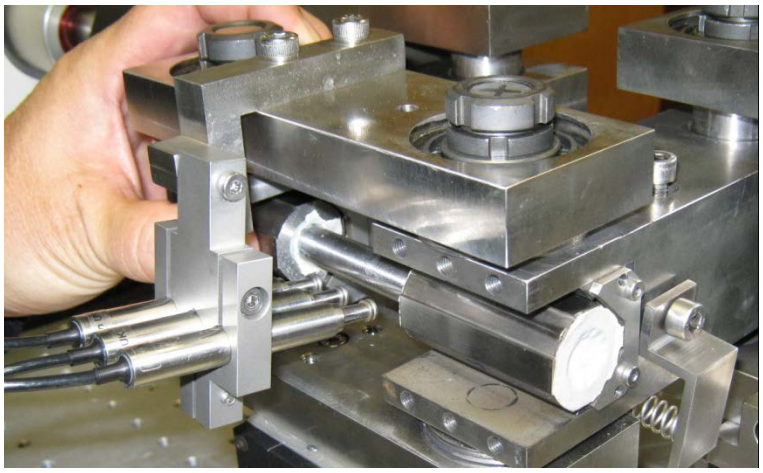

Fig. 3. Grip design of CIRFT with one end-block removed.

1.2 Sensor Spacing Correction for Curvature Measurement

The contact of LVDT probe with the rod under testing depends on the bending direction and induced curvature, especially when the contact is a disk with a flat head. This resulted in the deviation of sensor spacing from the ideal condition (Fig. 4).

For positive curvature when tensile load was applied to U-frame, actual sensor spacing h_2 is,

$$h_2 = h + \Delta h \tag{5}$$

and for negative curvature when compressive load was applied to U-frame, actual sensor spacing h_1 is

$$h_1 = h - \Delta h\,. \tag{6}$$

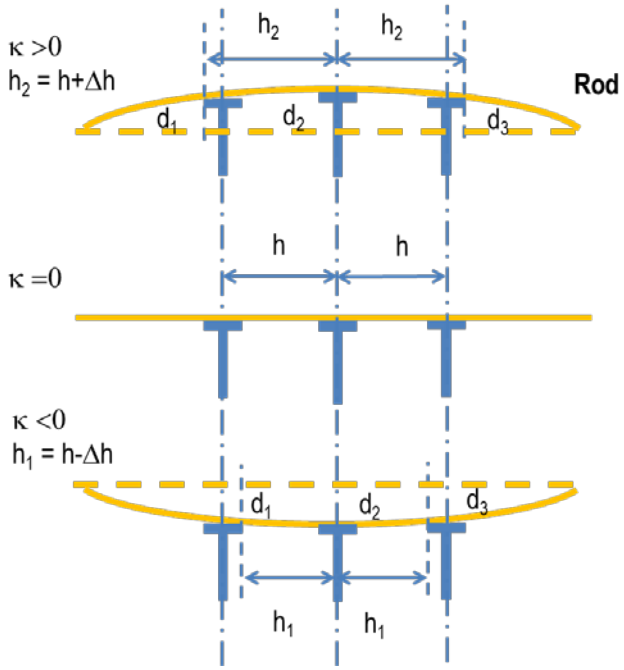

Fig. 4. Deflections measured by LVDTs may be at different points from initial positions, and sensor spacing h needs to be corrected.

A polycarbonate rod (0.4375 in diameter and 6 in length) specimen PC01 was tested under -6 mm and +6 mm with disk-head LVDTs. The curvatures in positive and negative direction appeared to be quite different as seen below (Fig. 5).

The same specimen PC01 was tested under the same level of applied displacement, but curvatures were based on chisel head LVDTs. The curvatures in both directions were very close near 2 m^{-1}. The repeatable results indicated that the PC01 behaved elastically as designed, and at the same time, the effect of chisel head on the curvature measurement is negligible.

Analysis revealed that:

- For a positive curvature induced by tension on the U-frame, a sensor adjustment of 2.90 mm is needed to have the disk-based measurement matched with the chisel-based measurement.

- For a negative curvature induced by compression on the U-frame, a sensor adjustment of 2.40 mm is needed to have the disk-based measurement matched with the chisel-based measurement.

The obtained sensor spacing adjustments for two conditions will be used in the data analysis in Sect. 2.

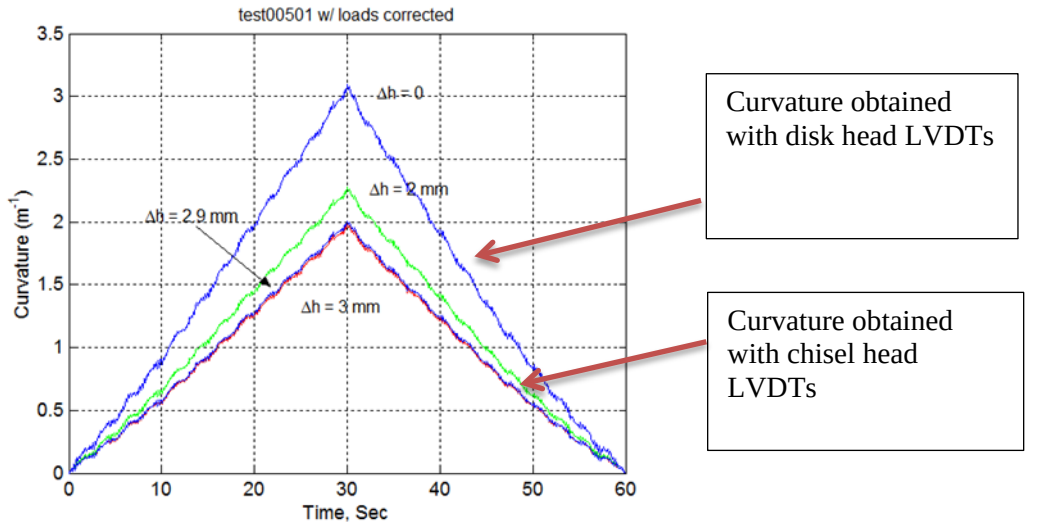

(a)

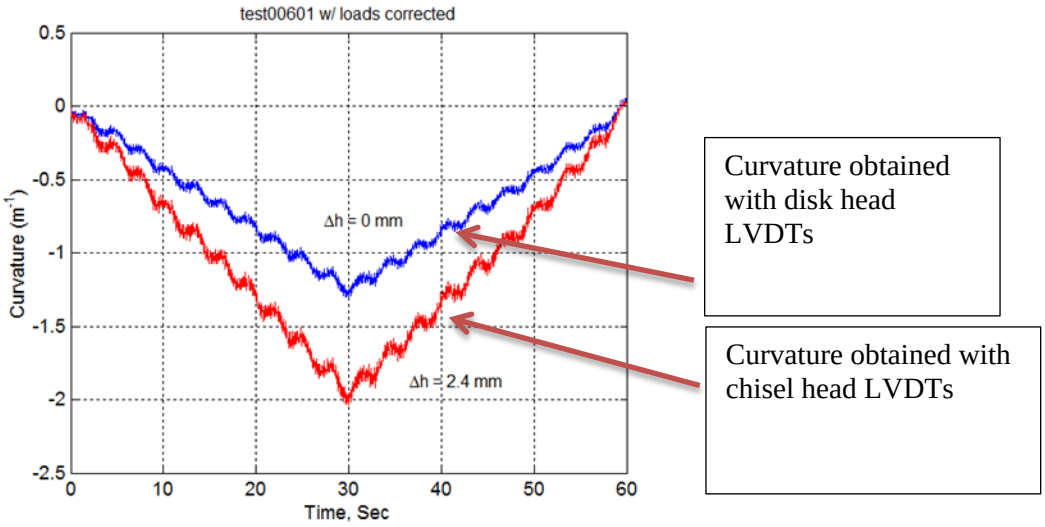

(b)

Fig. 5. (a) For a positive curvature induced by tension on U-frame, a sensor adjustment of 2.9 mm is needed to have the disk-based measurement matched with the chisel-based measurement. (b) For the negative curvature induced by compression on U-frame, a sensor adjustment of 2.4 mm is needed to have the disk-based measurement matched with the chisel-based measurement.

2. VERIFICATION OF CURVATURE MEASUREMENT

2.1 Technical Issues

Technical issues exist regarding the curvature measurement in CIRFT testing:

1) Can the curvature measured by the three LVDTs be evaluated? If so, how?

2) How close is the corrected curvature to the actual curvature?

3) Is the correction method applicable to all the levels of curvature?

4) Is the correction method applicable to both static and dynamic cases?

2.2 Technical Approach

ORNL proposed to use strain gage measurements to further benchmark the three LVDT curvature measurements. The rationale behind this is as follows:

1) When using a homogenous bending rod, the maximum strain at the extreme fiber can be evaluated because the estimate of that strain has been established theoretically. The deformation of the rod shall be limited within the elastic region of the material to enable the calculation to be effective.

2) The three LVDT-based curvatures in step 1 can be converted into the strain at the extreme fiber.

3) The strain at the extreme fiber can be measured by a strain gage.

4) The strain gage-based strain in step 3 can thus be compared with the three-LVDT-based strains to verify the curvature measurement in step 1.

2.3 Experimental Results

ORNL accomplished the following:

1) Purchased a four-channel strain gage signal conditioning amplifier Micro Measurement 2310B.

2) Integrated the conditioning amplifier 2310B into the PCI-82 control box in Bose testing machine (L218, 4515).

3) Studied the strain gages for the surrogate rod in-out cell testing in both small and large deformation cases.

4) Performed the CIRFT test on the surrogate rod made of 304 cladding only (no pellets involved) in small deformation.

5) Performed the CIRFT test on the surrogate rod made of polycarbonate in large deformation.

6) Analyzed the hot cell CIRFT testing data on MOX SNF and other SNF tested under DOE sponsorship (see Sect. 3)

The 4-channel 2310B amplifier (Raleigh, NC, Fig. 6) has following features:

- Fully adjustable calibrated gain from 1 to 11,000
- Accepts all strain gage inputs (foil or piezoresistive), potentiometers, direct current differential transformers (DCDTs), etc.
- Bridge excitation from 0.7 to 15Vdc (11 steps) plus 0.2 to 7 volts continuously variable
- Input impedance above 100 megohms
- Two simultaneous buffered outputs: ±10V, ±1.4V (for tape recorders)
- Wide band operation exceeding 60 kHz, -0.5 dB at all gains and output levels
- Four-frequency active 6-pole filter (10 to 10 000 Hz)
- Dual-range (±5000 and ±25000με) automatic bridge balance, with keep-alive power to preserve balance for months without external power
- Dual-polarity two-step double-shunt calibration

Fig. 6. Strain gage signal conditioning amplifier 2310B, Micro-Measurements.

Two types of strain gages (Micro-Measurements, Raleigh, NC) were identified for this study, and the gage factors are given in Table 1. The setups of surrogate rods with the strain gage mounted are shown in Figs. 7 and 8.

Table 1. Strain gages used in out-cell verification tests

Surrogate rod	Strain gage designation	Gage factor
SS304 surrogate rod	EA-06-250BF-350	2.055 +/- 0.5%
Polycarbonate rod	CEA-06-125UW-350	2.095+/-0.5%

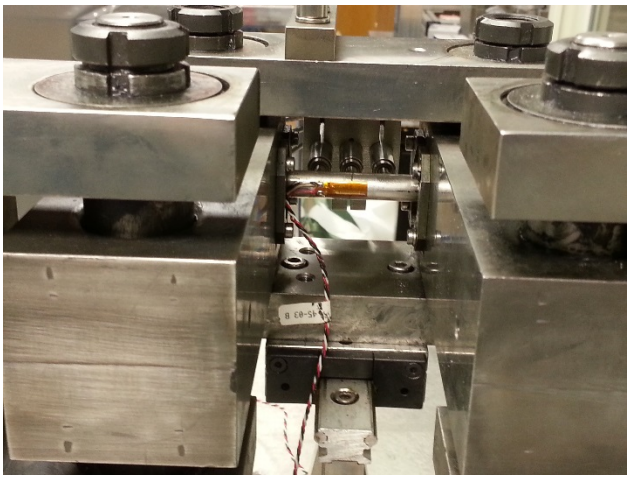

Fig. 7. Setup of SS304 surrogate rod with strain gage mounted in CIRFT testing.

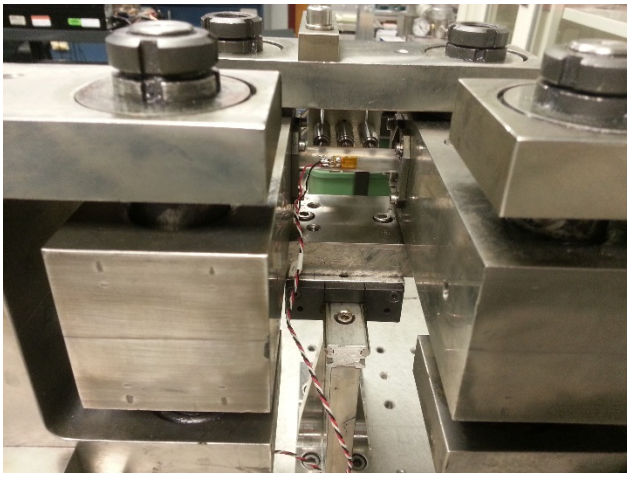

Fig. 8. Setup of polycarbonate surrogate rod with strain gage mounted in CIRFT testing.

2.3.1 CIRFT Testing and Data Analysis on SS304 Surrogate Rod

The proposed curvature correction was tested against several established methods including curvature measurement using a chisel type probe and a strain gage.

2.3.1.1 Base Considerations in Data Analysis

The following information was used in the data analysis:

1) The LVDT-based strain calculation was based on the discussion in Sect. 1.1.

2) The correction was based on the assumption of the equal gage length in both peak and valley of one data block (two cycles of sine wave). The half gage length Lg/2 was calculated according to the equation as follows

$$Lg/2 = \sqrt{2d_2/\kappa} \tag{7}$$

where d_2 is the middle LVDT reading in m and κ is the calculated curvature in m^{-1}.

3) The gage-based strain was obtained according the following equation,

$$\varepsilon = 10^6/(0.25*V_{BR}*A*S_g) \quad (8)$$

where ε is micro strain or με, V_{BR} is the bridge voltage, A is the amplification, and S_g is the gage factor.

4) The strain can be estimated according to the condition of the rod by

$$\varepsilon = (M / EI) y_{max} \quad (9)$$

where M is the applied moment amplitude, EI is estimated 42.8 Nm^2, y_{max} = 4.78mm.

2.3.1.2 Chisel Type Probe as Calibration Method

Testing on surrogate rod SS30402 was conducted in 0.05 Hz and 5 Hz to simulate the static and dynamic loading (Table 2).

Table 2. Testing condition of surrogate rod SS30402 with disk and chisel types

No.	pk1 (mm, N)	pk2 (mm, N)	Frequency	Cycles	Sum	LVDT type
44	-0.4	0.4	0.05	3		Flat disk, D6
45	-0.6	0.6	0.05	3		Flat disk, D6
46	-0.8	0.8	0.05	3		Flat disk, D6
47	-75	75	5	500	500	Flat disk, D6
48	-0.4	0.4	0.05	3		Flat disk, D6
49	-0.6	0.6	0.05	3		Flat disk, D6
50	-0.8	0.8	0.05	3		Flat disk, D6
51	-100	100	5	500	1,000	Flat disk, D6
52	-0.4	0.4	0.05	3		Flat disk, D6
53	-0.6	0.6	0.05	3		Flat disk, D6
54	-0.8	0.8	0.05	3		Flat disk, D6
55	-125	125	5	500	1,500	Flat disk, D6
56	-0.4	0.4	0.05	3		Chisel, D6
57	-0.6	0.6	0.05	3		Chisel, D6
58	-0.8	0.8	0.05	3	0	Chisel, D6
59	-75	75	5	500	500	Chisel, D6
60	-0.4	0.4	0.05	3		Chisel, D6
61	-0.6	0.6	0.05	3		Chisel, D6
62	-0.8	0.8	0.05	3		Chisel, D6
63	-100	100	5	500	1,000	Chisel, D6
64	-0.4	0.4	0.05	3		Chisel, D6
65	-0.6	0.6	0.05	3		Chisel, D6
66	-0.8	0.8	0.05	3		Chisel, D6
67	-125	125	5	500	1,500	Chisel, D6

The curvature values based disk-type probe and the corrected are presented in the Figs. 9–12, along with those based on flexural rigidity (EI) and the chisel-type probe. The major observations can be summarized as follows,

1) Measurement with the chisel type probe showed uncertainty in curvature; no defined trend can be seen in the measured curvatures as compared to those using the disk-type probe.

2) The tests with the chisel type and disk type probes were not conducted concurrently. The probe contact condition was changed in the session when the probe was changed and the three LVDTs were remounted; the sensor spacing was sensitive to the change of contact condition.

3) The corrected curvature was shown to be close to the EI-based curvature.

4) Spacing correction (Δh) seemingly exhibited a trend to increase with the level of displacement input (disp1 on the side of motor 1). However, a large variance of correction was seen near small displacement.

5) The level of correction was also far less than those based on the calibration of chisel type probe (2.40 or 2.90 mm).

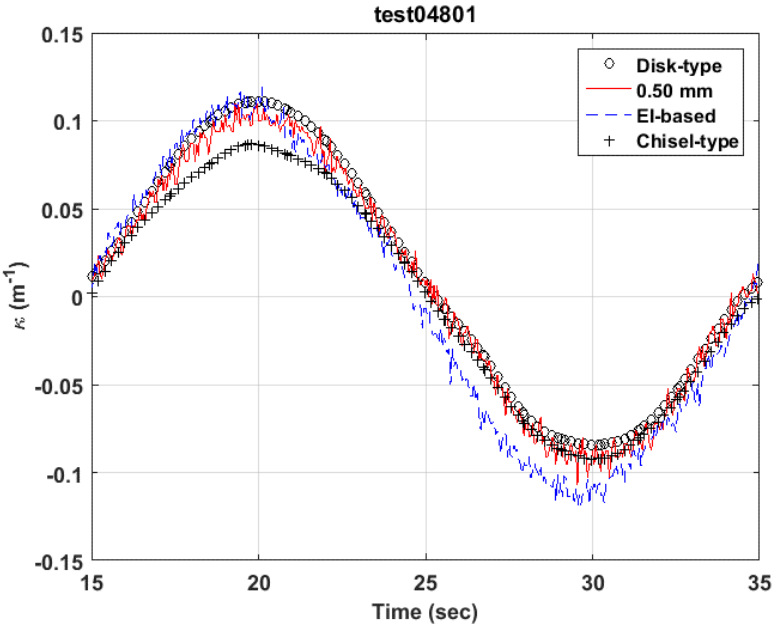

(a) 0.4 mm

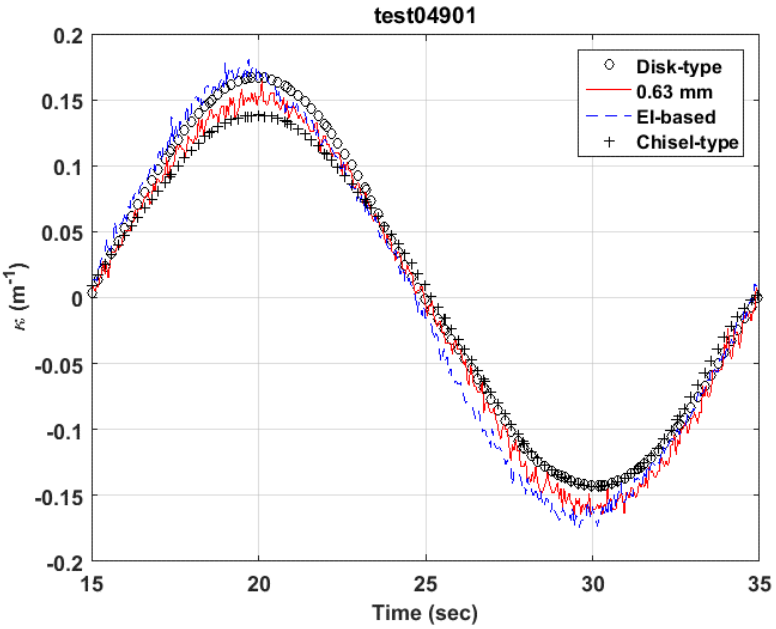

(b) 0.6 mm

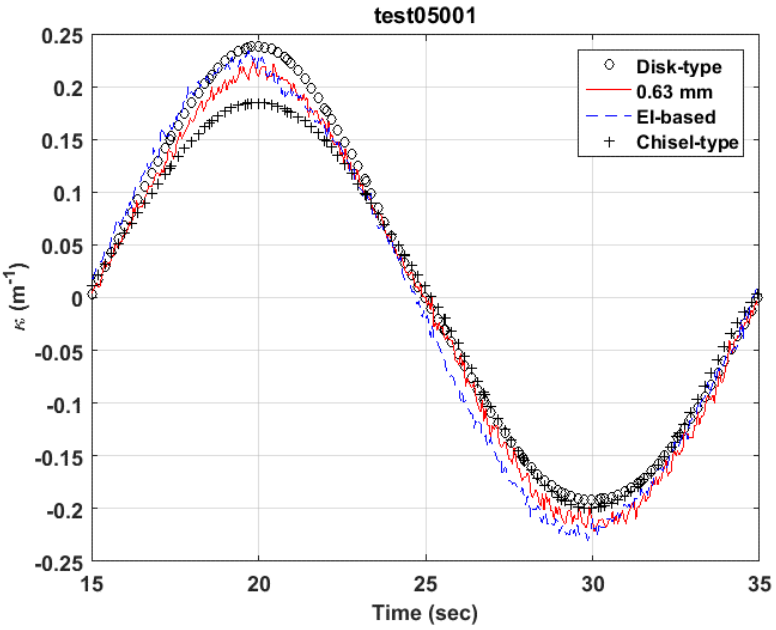

(c) 0.8 mm

Fig. 9. Curvatures based on disk-type probe, corrected, EI-based, and chisel-type probe, for 0.05 Hz displacement at loading point of U-frame arm: (a) 0.4 mm, (b) 0.6 mm, and (c) 0.8 mm. EI=42.8 Nm^2.

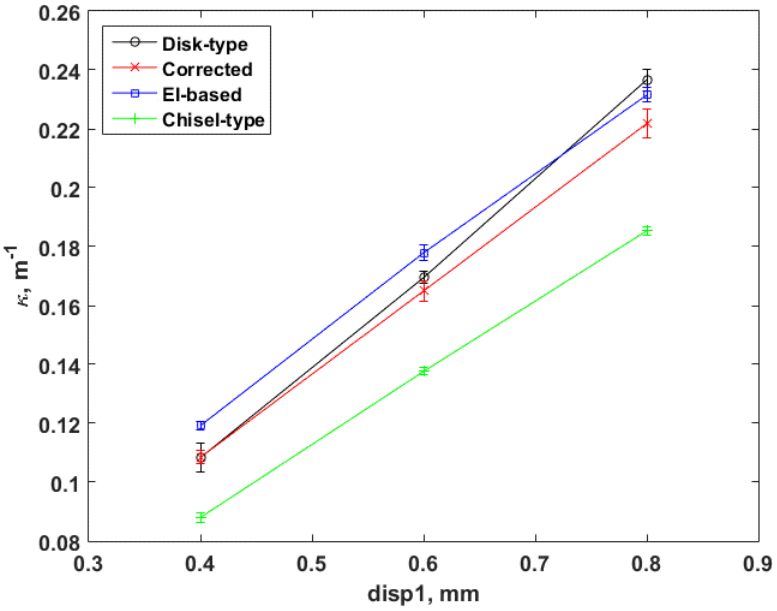

(a) Peak

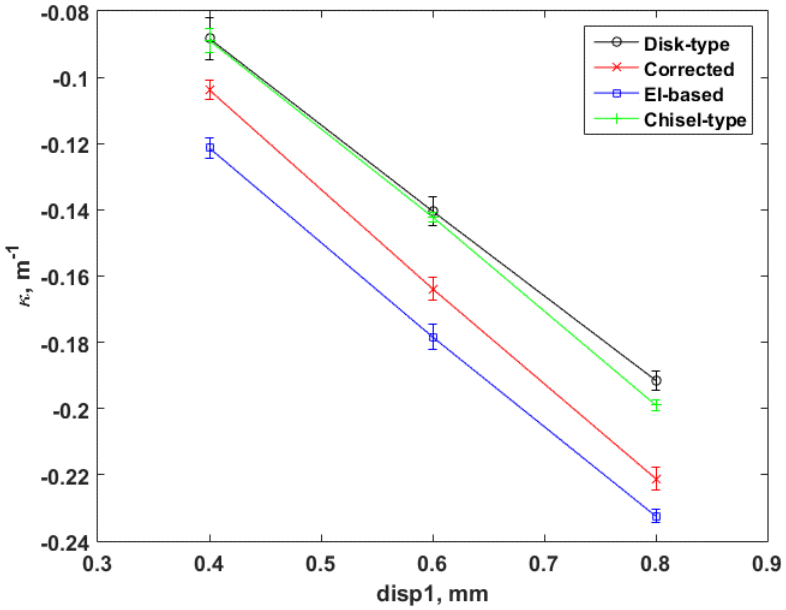

(b) Valley

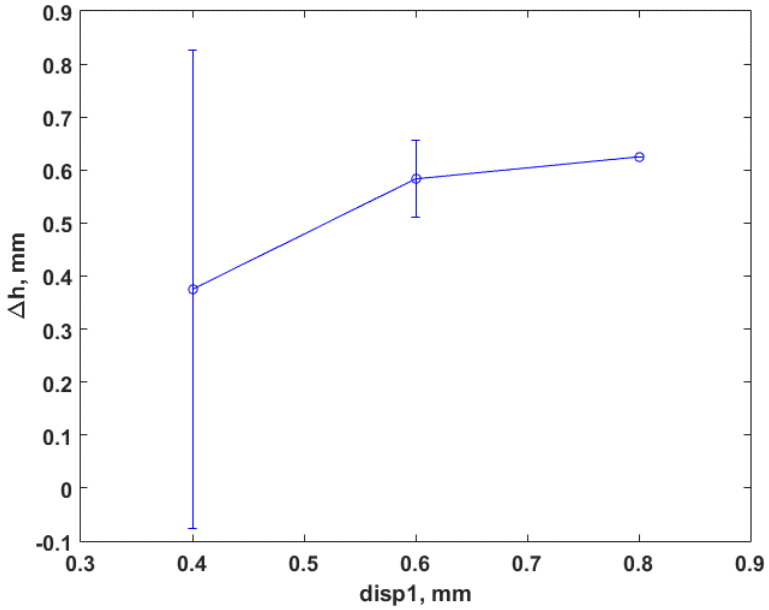

(c) Spacing correction

Fig. 10. (a) Peak and (b) valley responses of curvature waveform and (c) spacing corrections under various disp1 amplitudes at 0.05Hz.

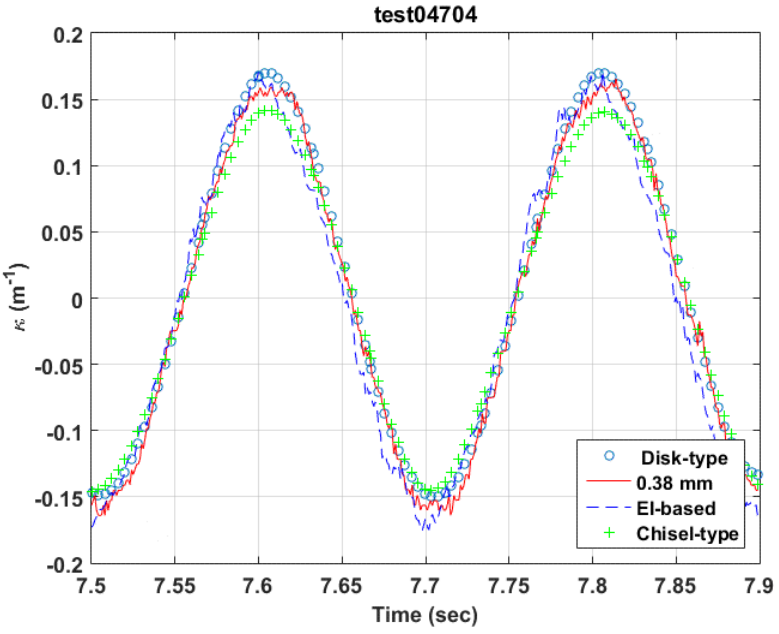

(a) 75N

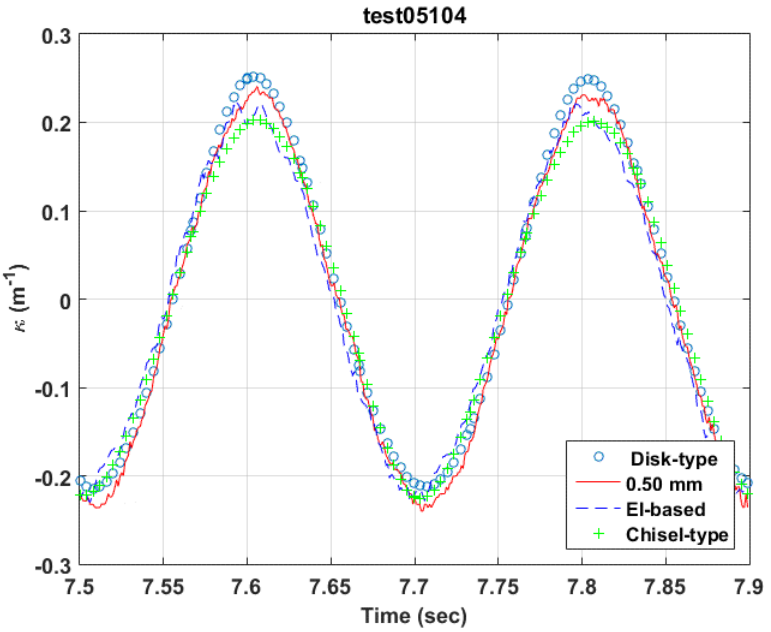

(b) 100N

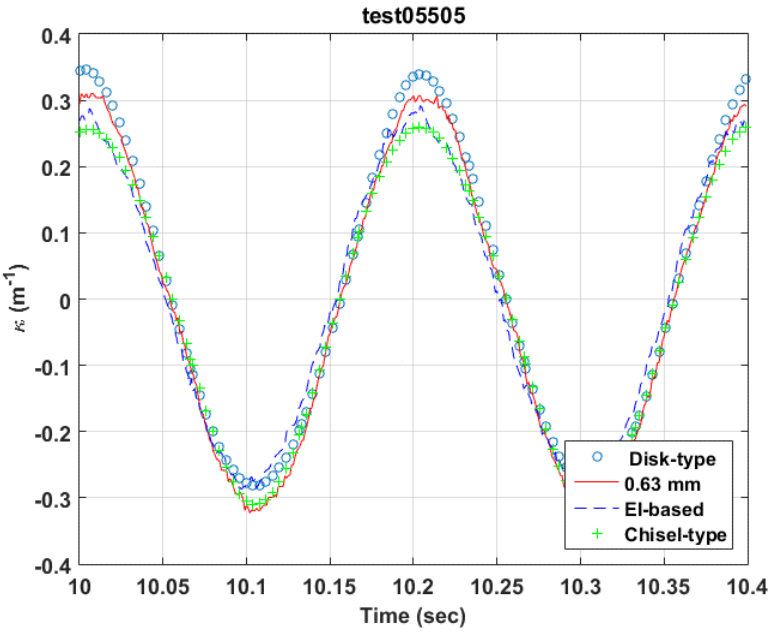

(c) 125N

Fig. 11. Curvatures based on disk-type probe, corrected, EI-based, and chisel-type probe for 5 Hz load at loading point of U-frame arm: (a) 75 N, (b) 100 N, and (c) 125 N. EI=42.8 Nm^2.

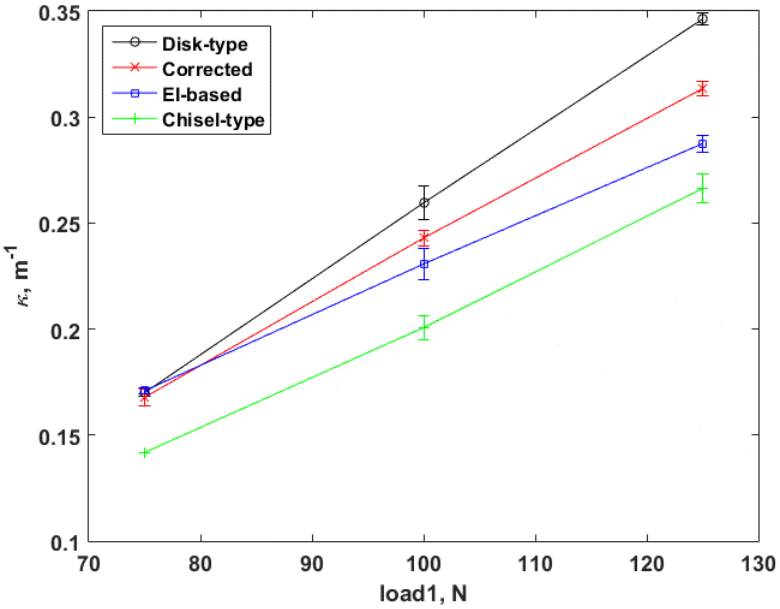

(a) Peak

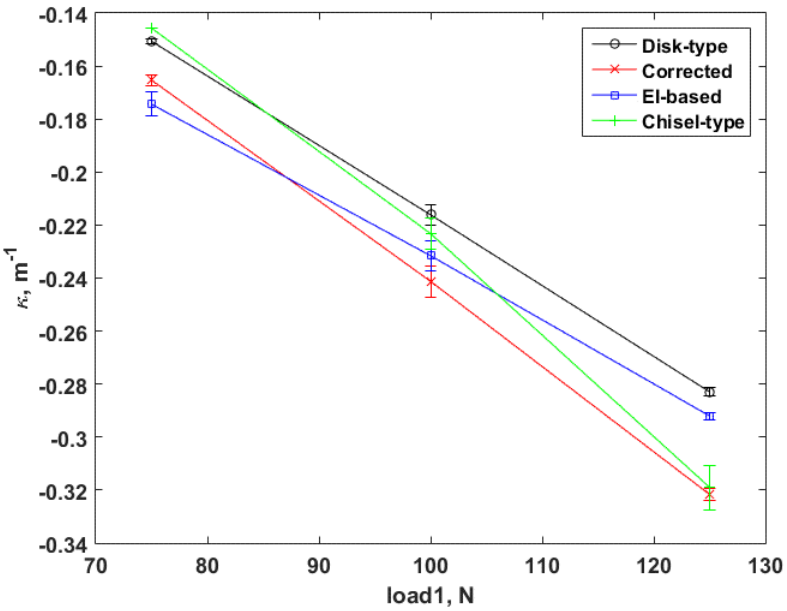

(b) Valley

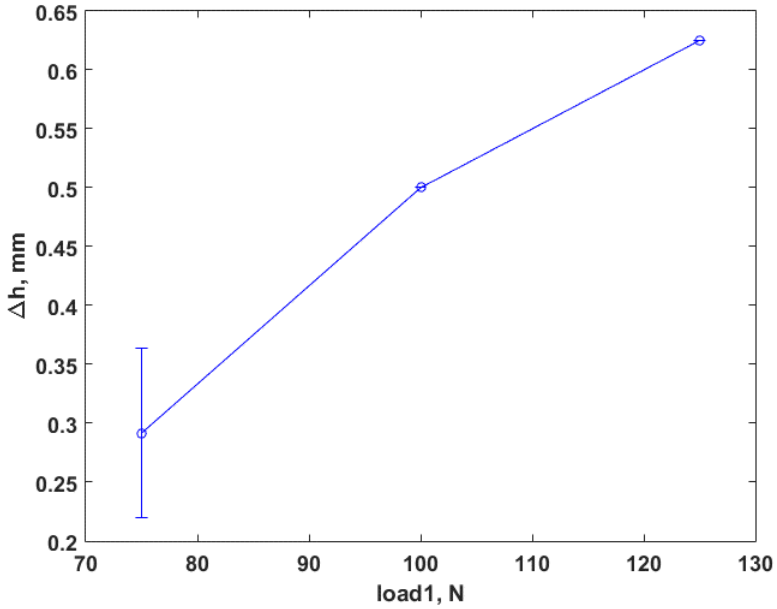

(c) Spacing correction

Fig. 12. (a) Peak and (b) valley responses of curvature waveform, and (c) spacing corrections under various load1 amplitudes at 5Hz.

2.3.1.3 Strain Gage as Calibration Method

The strain gage was installed on the surface of the bending rod opposite the three LVDTs as shown in Fig. 7. The test conditions using 0.05 Hz sine wave with varying amplitudes are given in Table 3. The strains were acquired in #71–73 using a P3 strain indicator and recorder (Vishay Micro-Measurement, Raleigh, NC) and in #81–84 using strain signal conditioning amplifier 2310B (Vishay Micro-Measurement, Raleigh, NC).

Table 3. Test condition with strain gage installed

No.	pk1 (mm, N)	pk2 (mm, N)	Frequency	Cycles	LVDT type
71	-0.4	0.4	0.05	3	Flat disk, D5
72	-0.6	0.6	0.05	3	Flat disk, D5
73	-0.8	0.8	0.05	3	Flat disk, D5
81	-0.4	0.4	0.05	3	Flat disk, D5
82	-0.6	0.6	0.05	3	Flat disk, D5
83	-0.8	0.8	0.05	3	Flat disk, D5
84	-100	100	5	500	Flat disk, D5

The curvatures measured using three LVDTs were converted into the maximum strain at outer fiber of bending rod. The results of tests #71–73 are illustrated in Figs. 13 and 14.

1) Overall, the strain gage has a synchronized response with curvature-based strain, although the curvature-based strain at 0.6 mm lagged a little in the first half of period.

2) The peak/valley response of the curvature-based strain with the correction applied matched the strain gage measurement well.

3) Spacing correction (Δh) demonstrated again an increasing trend with the displacements. However, the correction, especially at small displacement input, showed a lower level than in the previous test session (Fig. 10).

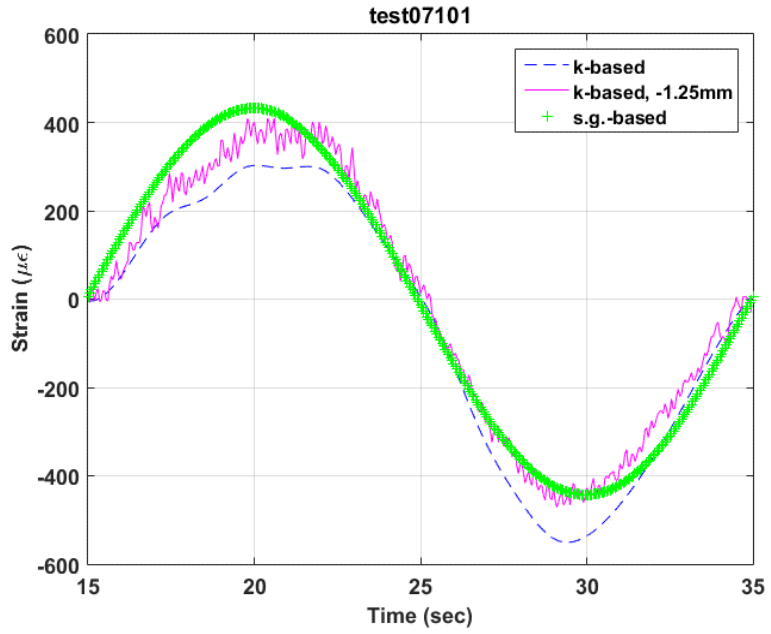

0.4 mm

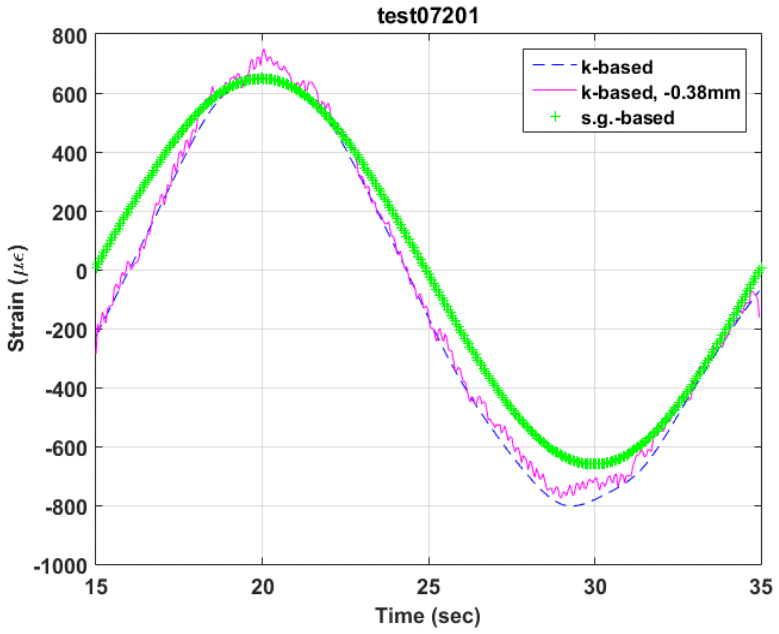

0.6 mm

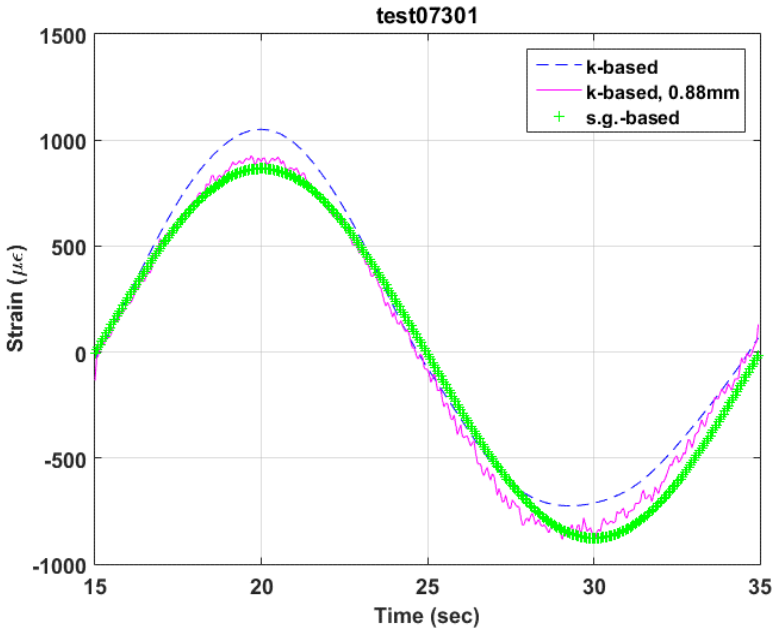

0.8 mm

Fig. 13. Strain curves based on original disk-type curvature, corrected curvature, and strain gage for 0.05 Hz displacement at loading point of U-frame arm: (a) 0.4 mm, (b) 0.6 mm, and (c) 0.8 mm.

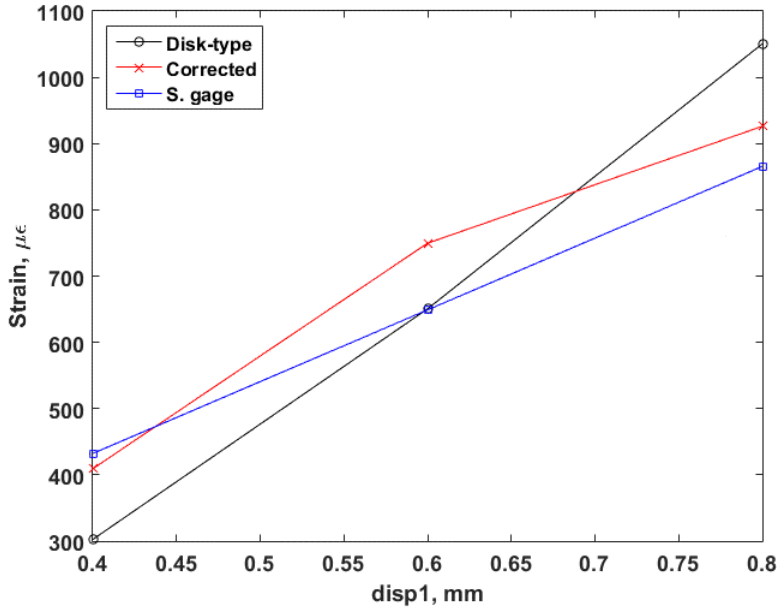

(a) Peak

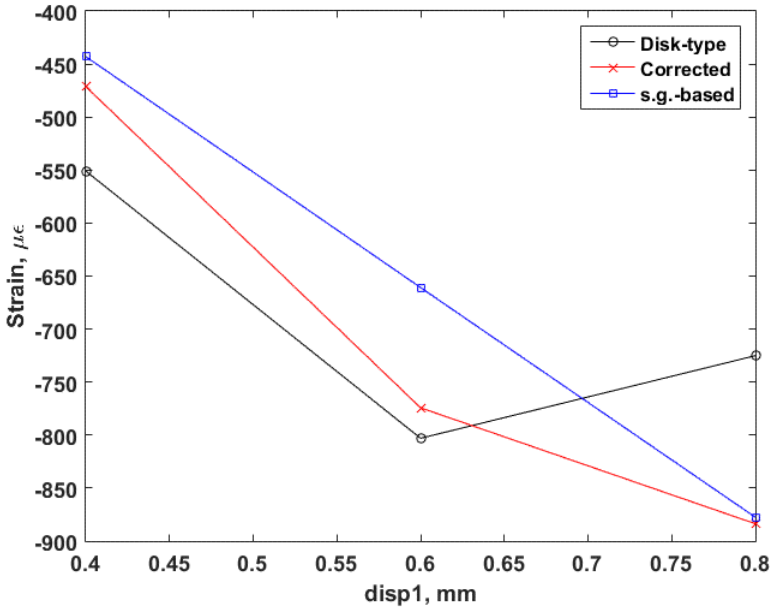

(b) Valley

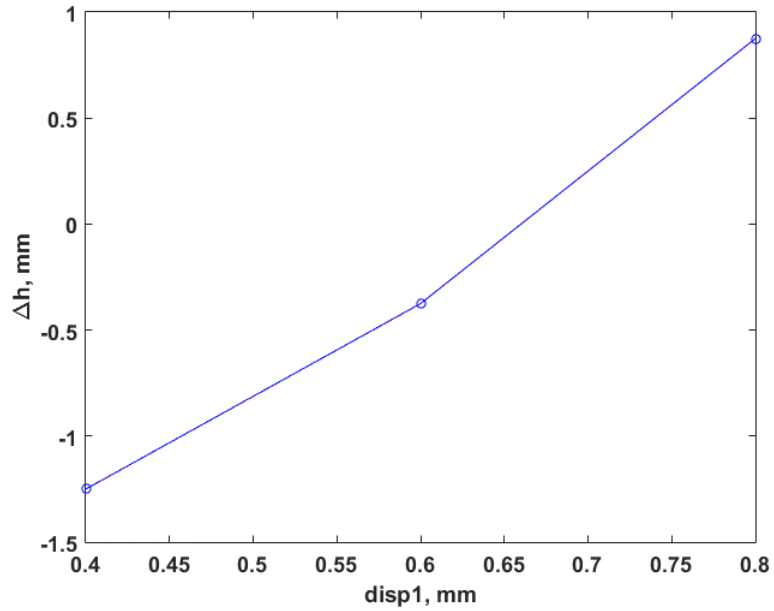

(c) Spacing correction

Fig. 14. (a) Peak, (b) valley responses of strain waveform, and (c) spacing corrections under various disp1 amplitudes at 0.05 Hz.

The results of tests #81–84 are given in Fig. 15 for 0.05 Hz and Fig. 16 for 5 Hz. The following observations can be made:

1) The strain gage showed a lower level of strain than those of curvature-based strain.

2) The spacing correction Δh and its variation with displacements were smaller compared with previous tests (Figs. 10 and 14). The degree of correction on κ-based strain was smaller, as well.

3) The corrected curvature-based strains were seen close to EI-based strains.

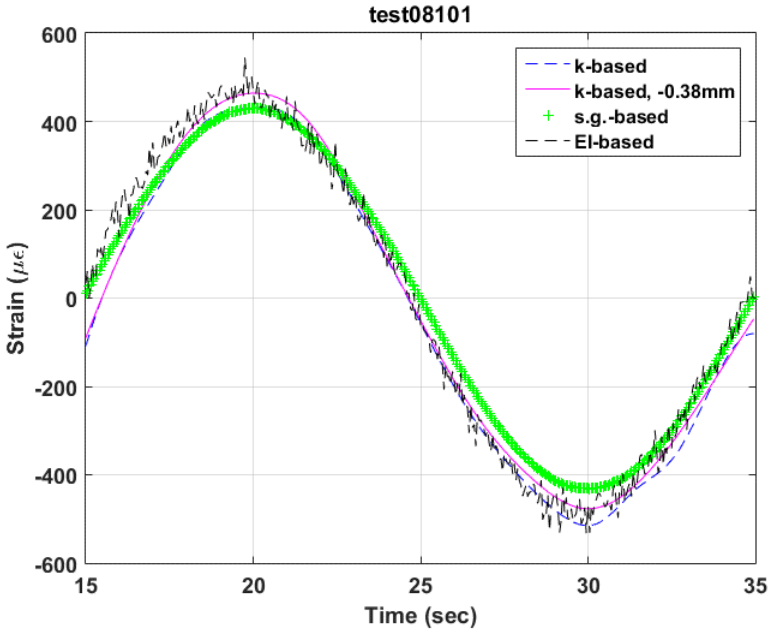

(a) Displacement amplitude 0.4 mm

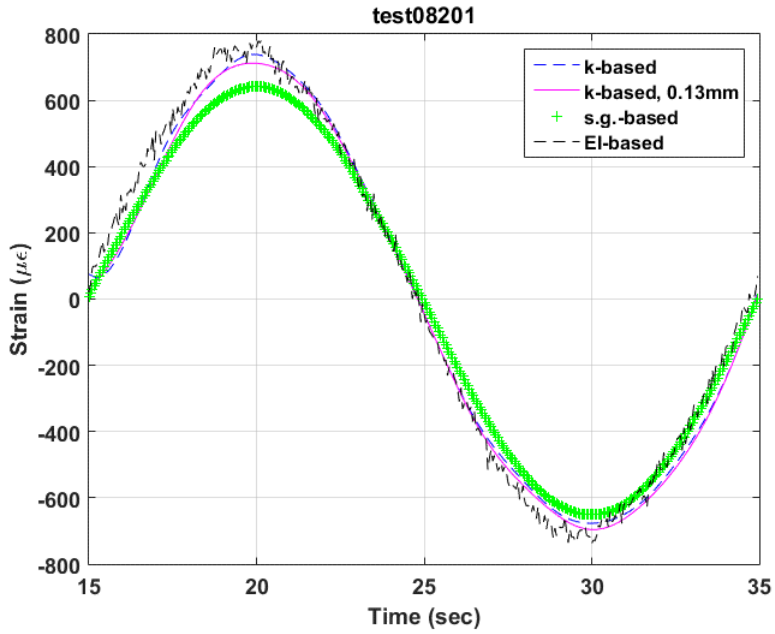

(b) Displacement amplitude 0.6 mm

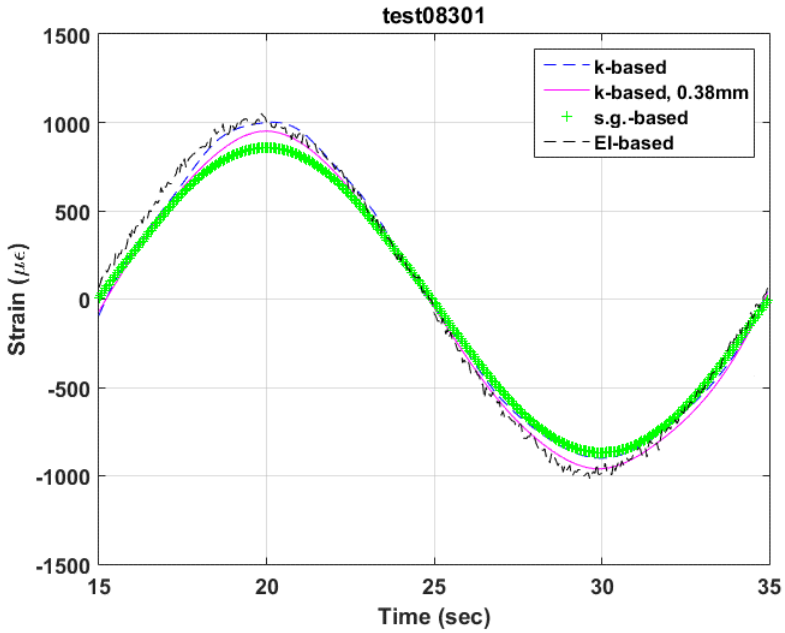

(c) Displacement amplitude 0.8 mm

Fig. 15. Strain results based on original curvature, corrected curvature, strain gage, and flexural rigidity EI for 0.05 Hz tests under three displacement amplitudes.

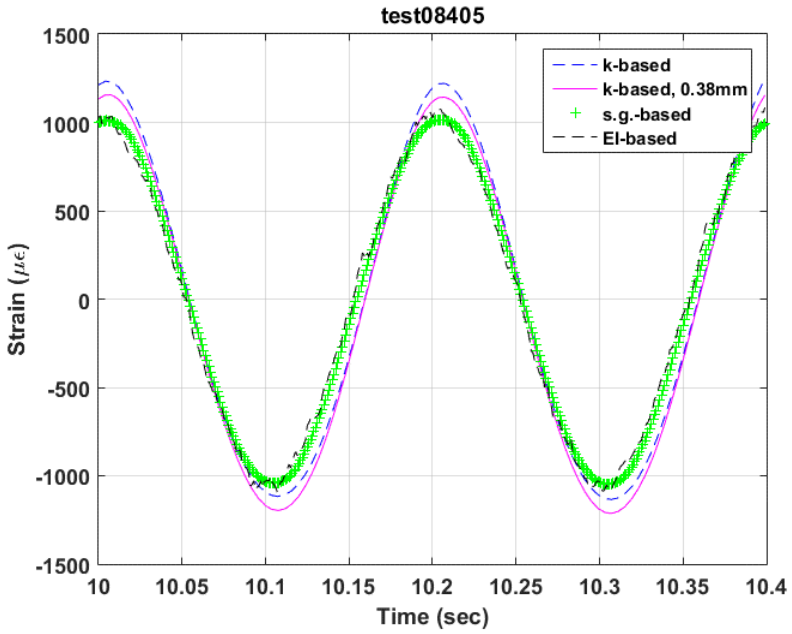

(a) Data block 5

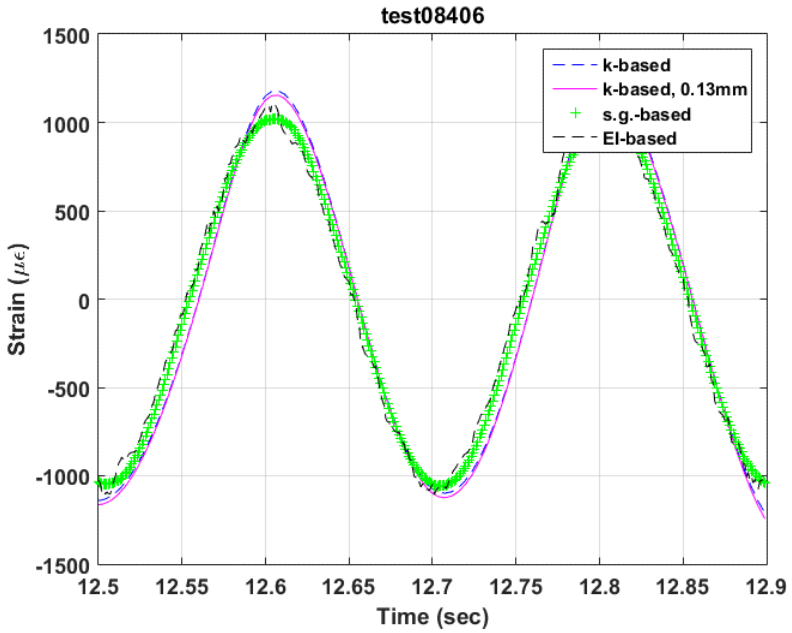

(b) Data block 6

Fig. 16. Strain results based on original curvature, corrected curvature, strain gage, and flexural rigidity EI for 5 Hz tests under amplitude 100N.

2.3.1.4 Summary

The use of a SS304 surrogate rod in the out-cell study provided the opportunity to examine the small curvature measurement currently used in CIRFT tests. The following summarizes the major observations:

1) The corrected curvature was shown to be close to an EI-based curvature; the corrected curvature-based strain was also demonstrated to be agreed with strain gage measurement.

2) The spacing correction (Δh) was smaller than those based on large curvature measurement. The degree of correction on curvature-based strain was also smaller.

3) The spacing correction exhibited a defined trend to increase with the level of displacement input, but it also showed a large variance at the small displacements.

4) The level of spacing correction in specified displacement input varied among test sessions. The change of contact condition between probe and surface of rod is believed to contribute the variation. A systematic correction scheme was also developed accordingly.

2.3.2 CIRFT Testing on Polycarbonate Surrogate Rod Material

The test condition on a polycarbonate rod (PC01) consists of two load waveforms: ramp and sine.

2.3.2.1 Ramp Waveform Test

The displacement at each loading point of the U-frame ramped up to a designated level and then down to zero; one loading cycle was used. The bending in ramp was unidirectional with a single wave pule pointed in either positive or negative direction.

Two types of LVDT probes were tested, namely flat disk type and chisel type. Test condition can be seen in Table 4.

Table 4. Test condition using ramp process

No.	pk1 (mm)	pk2 (mm)	rate(mm/s)	Cycles	LVDT
1	0	6	0.2	1	flat disk, D5
2	0	-6	0.2	1	flat disk, D5
7	0	6	0.2	1	chisel, D5
8	0	-6	0.2	1	chisel, D5

The data sets for a specified probe were assembled to obtain a whole waveform of reversed bending. The three LVDT-based curvatures obtained with both disk type and chisel type probes are presented, along with the corrected curvature in Fig. 17, in which EI = 1.8 Nm^2 was used for EI-based estimate.

1) The correction procedure suggests that a sensor spacing correction of 2.50 mm is needed. With the suggested procedure, only one correction is needed instead of two corrections in positive (2.90mm) and negative direction (2.40 mm), as used before.

2) The corrected curvature showed a good correspondence with both chisel type measurement and EI-based estimate.

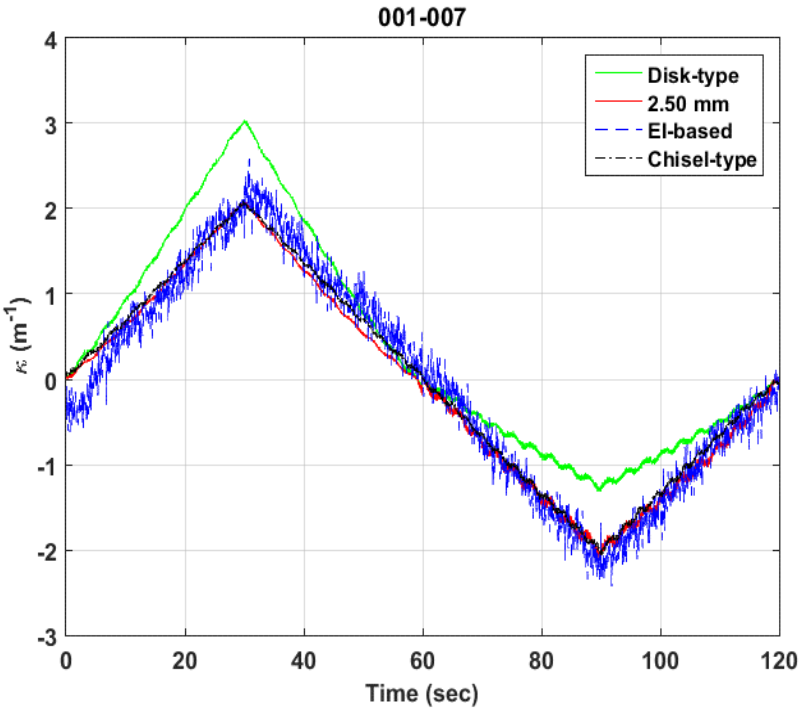

Fig. 17. Curvature measurements of polycarbonate surrogate rod based on disk and chisel type probe, 2.50 mm sensor spacing correction, and EI-based estimate.

2.3.2.2 Sine Waveform Test

Reverse bending was conducted directly by using a 0.05 Hz sine wave. A total of 12 amplitudes were tested with one LVDT probe, flat disk type. Strain gage measurement was enabled, and strains were acquired using a P3 strain indicator and recorder. The tests condition can be seen from Table 5.

Table 5. Test condition using sine wave

No.	pk1 (mm)	pk2 (mm)	F(Hz)	Cycles	LVDT
35	0.5	-0.5	0.05	3	flat disk, D5
36	1	-1	0.05	3	flat disk, D5
37	1.5	-1.5	0.05	3	flat disk, D5
38	2	-2	0.05	3	flat disk, D5
39	2.5	-2.5	0.05	3	flat disk, D5
40	0.3	-0.3	0.05	3	flat disk, D5
41	0.3	-0.3	0.05	3	flat disk, D5
42	0.3	-0.3	0.05	3	flat disk, D5
43	0.5	-0.5	0.05	3	flat disk, D5
44	0.5	-0.5	0.05	3	flat disk, D5
45	0.5	-0.5	0.05	3	flat disk, D5
46	1	-1	0.05	3	flat disk, D5
47	1	-1	0.05	3	flat disk, D5
48	1.5	-1.5	0.05	3	flat disk, D5

Table 5. (continued)

No.	pk1 (mm)	pk2 (mm)	F(Hz)	Cycles	LVDT
49	1.5	-1.5	0.05	3	flat disk, D5
50	2	-2	0.05	3	flat disk, D5
51	2	-2	0.05	3	flat disk, D5
52	2.5	-2.5	0.05	3	flat disk, D5
53	2.5	-2.5	0.05	3	flat disk, D5
54	3	-3	0.05	3	flat disk, D5
55	3	-3	0.05	3	flat disk, D5
56	3	-3	0.05	3	flat disk, D5
57	3.5	-3.5	0.05	3	flat disk, D5
58	3.5	-3.5	0.05	3	flat disk, D5
59	3.5	-3.5	0.05	3	flat disk, D5
60	4	-4	0.05	3	flat disk, D5
61	4	-4	0.05	3	flat disk, D5
62	4	-4	0.05	3	flat disk, D5
63	4.5	-4.5	0.05	3	flat disk, D5
64	4.5	-4.5	0.05	3	flat disk, D5
65	4.5	-4.5	0.05	3	flat disk, D5
66	5	-5	0.05	3	flat disk, D5
67	5	-5	0.05	3	flat disk, D5
68	5	-5	0.05	3	flat disk, D5
69	5.5	-5.5	0.05	3	flat disk, D5
70	5.5	-5.5	0.05	3	flat disk, D5
71	5.5	-5.5	0.05	3	flat disk, D5
72	6	-6	0.05	3	flat disk, D5
73	6	-6	0.05	3	flat disk, D5
74	6	-6	0.05	3	flat disk, D5
75	6	-6	0.05	3	flat disk, D5

The typical results from tests using a 0.05 Hz sine wave are given in Fig. 18. The peak and valley values of the strain waveforms obtained for various cases are shown in Fig. 19, including strains based on original curvature (disk-type probe), corrected curvature, and strain gage. The variation of spacing correction as a function of displacement input is also presented.

1) The strains from the strain gage usually agreed well with those based on the corrected curvatures, but they deviated from the corrected curvature-based strain at high levels.

2) The spacing correction (Δh) again exhibited a defined trend to increase with the displacement input and also a larger variance at the small displacements.

3) The spacing corrections were again lower than those obtained in ramping.

4) The corrected ultimate curvatures obtained in ramp and sine waveforms were the same (around 2 m^{-1} at 6.00 mm disp1). There was perhaps a significant change of the contact condition between probe and surface of rod as the tests were carried out in different periods of the project.

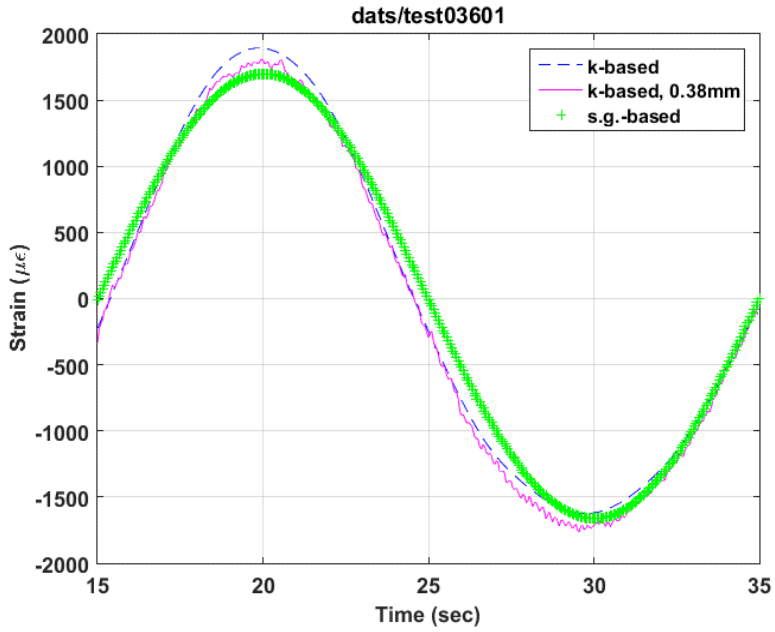

(a)

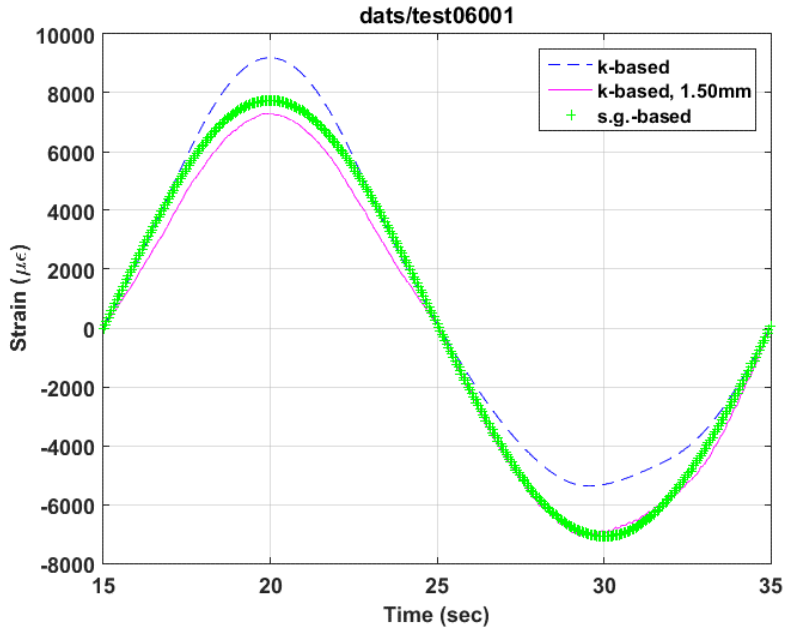

(b)

Fig. 18. Strain wave forms obtained from original curvature, corrected curvature, and strain gage: (a) displacement amplitude 1.00 mm, and (b) 4.00 mm.

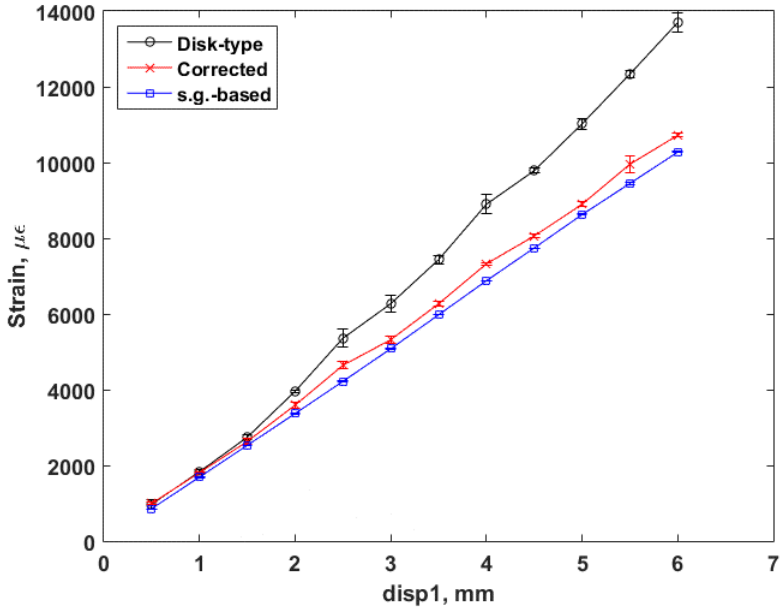

(a) Peak

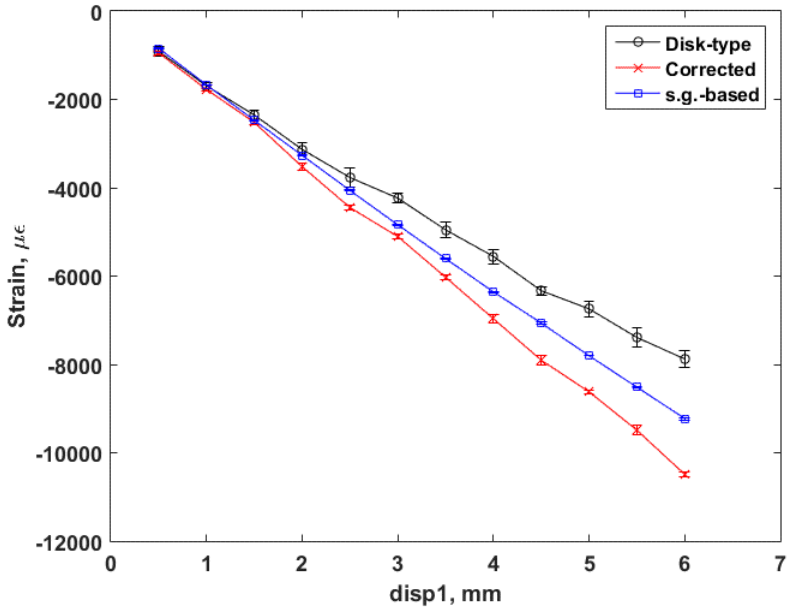

(b) Valley

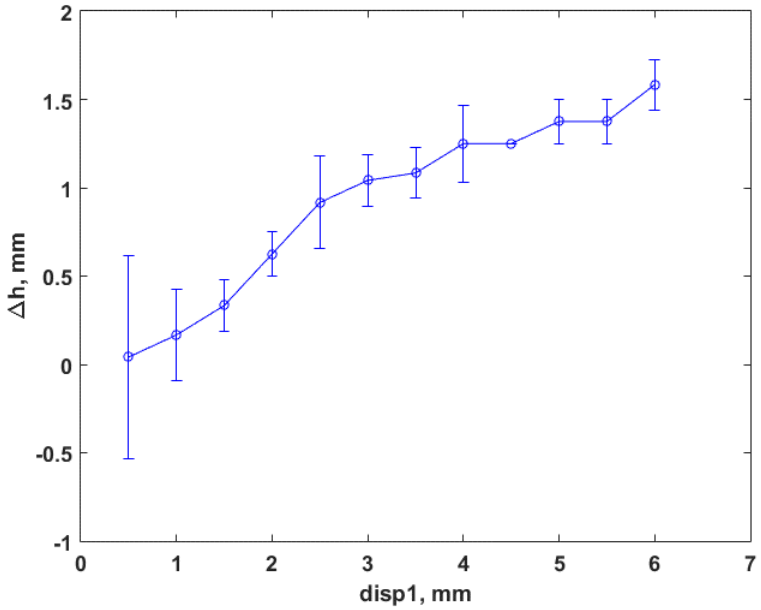

(c) Spacing correction

Fig. 19. (a) Peak and (b) valley responses of strain waveform, and (c) spacing corrections under various disp1 amplitudes at 0.05 Hz.

2.3.2.3 Summary

Based on the tests of the polycarbonate rod, observations with respect to disk-type curvature measurement and correction can be summarized as follows:

1) The corrected curvature showed a good correspondence with chisel type measurements and the EI-based estimate. The corrected curvature-based strain has good agreement with that of strain gage measurement, particularly near small-to-intermediate levels of displacement input.

2) The spacing correction (Δh) again exhibited a defined trend to increase with the displacement input with a larger variance at the small displacements.

3) The correction procedure suggested a spacing correction of 2.50 mm (at 6.00 mm disp1) other than dual corrections reported in ramping (2.40 mm in negative curvature and 2.90 mm in positive curvature). However, the corrected ultimate curvatures obtained in ramp and sine waveforms were the same (approximately 2 m^{-1} at 6.00 mm disp1).

4) The change of the contact condition between the probe and surface of the rod in different test sessions may be responsible for the variation of spacing correction observed.

2.4 Recommendation

It has been shown that the sensor spacing correction depends on the level of imposed displacement. The corrected curvature based on disk-type probes agrees to a varying extent with the EI-based estimate in both small and large curvature measurements and with chisel-type probe measurements in the large curvature case. The corrected curvature-based strain was also shown to correspond to the strain gage measurement, particularly at the small-to-intermediate level of displacement input.

There is some uncertainty involved with the contact of the probe against the rod during reversible bending testing. However, the proposed dynamic correction method of LVDT probes is independent of contact spacing correction mentioned earlier. The identification of sensor spacing correction dynamically accounts for the changes and evolution of contacts, this effect is still working in progress and will be reported in next performance period.

The proposed correction procedure will be applied to data analysis of the all CIRFT test results. The analysis results of LMK, NA, and MOX fuels is presented below.

3. DATA ANALYSIS OF CIRFT TESTING ON Limerick BWR SNF

3.1 Overview of CIRFT Tests on LMK Fuel Rods

A total of 16 specimens—LM1–LM4 and LM5–LM17—were tested in the hot cell. LM1 was used in the tuning and static test. The remaining 15 specimens were used in dynamic tests. The dynamic tests were conducted with a range of moment amplitudes from 7.11 to 30.48 N·m. A total of 13 specimens failed with fatigue lives from 10^4 to 4.7×10^6 cycles. LM12 and LM17 were cycled to more than 3.4×10^6 cycles without failure. LM12 was stopped at 7.6×10^6 cycles, and LM17 was tested continuously but to an increased amplitude 30.48 Nm and failed at 1.3×10^4 cycles.

3.2 Results on Data Analysis for Dynamic Tests

The data sets for each of the dynamic tests, including measurement data and online monitoring data, were processed by using the procedure suggested in Sect. 2.

Results for each test are given in Appendix A. For each test:

1) The variations of curvature range, moment range, flexural rigidity, curvature peak/valley, and moment peak/valley are presented whenever they are available.

2) The curvature and moment plots are given for the beginning data block of a test session when the load reaches the designated level. The results for two test sessions are presented, namely, the first (tested to 1000 cycles) and last sessions.

3) Finally, the data based on online monitoring are presented, including the variations of curvature range, moment range, flexural rigidity, curvature peak/valley, and moment peak/valley as a function of number of cycles or the cycles to failure.

For each cyclic test, several measurement data sets were obtained between test sessions. These measurements were made with small displacement amplitudes at 0.05 Hz. With such input, both moment and curvature varied or decreased along with the accumulated number of cycles. The obtained rigidities were generally higher than those from monitoring data, and the degree of changes was similar to those of monitoring data.

The corrected curvature depends on the spacing correction applied. Generally, the correction observed for the curvature is not quite significant because of the small input. However, the signal-to-noise ratio becomes much smaller at the lower input. The amplitude of de-noised curvature was thus lowered relatively compared to original noisy data, which can be seen from the pots of specimen LM12 in Fig. A.40.

Major results for the dynamic tests are summarized in Table 6. The table is self-explained, including the following columns:

1) TN – test number

2) Spec – Specimen ID

3) ID – inside diameter of cladding

4) OD – outside diameter of cladding

5) Dia – diameter of pellet

6) Load – load amplitude at the loading point of U-frame

7) N – number of cycles accumulated or the cycles to failure

8) Fail – 1 as failure, and 0 as no failure

9) ma – mean of moment amplitude ($\Delta M/2$) based on de-noised monitoring data

10) ma_std – standard deviation of moment amplitude (4 inch or 101.60 mm loading arm) based on de-noised monitoring data

11) ka – mean of curvature amplitude ($\Delta\kappa/2$) based on corrected and de-noised monitoring data

12) ka_std – standard deviation of curvature amplitude based on corrected and de-noised monitoring data

13) km – mean of curvature extreme values based on corrected and de-noised monitoring data, km = $\max\{|\kappa_p|,|\kappa_v|\}$, where κ_p and κ_v are peak/valley values

14) km_std – standard deviation of curvature extremes based on corrected and de-noised monitoring data

15) R – mean of flexural rigidity

16) R_std – standard deviation of flexural rigidity

17) sa – mean of equivalent stress amplitude ($\Delta\sigma/2$) based on de-noised monitoring data

18) sa_std – standard deviation of equivalent stress amplitude based on de-noised monitoring data

19) ea – mean of equivalent strain amplitude ($\Delta\varepsilon/2$) based on corrected and de-noised monitoring data

20) ea_std – standard deviation of equivalent strain amplitude based on corrected and de-noised monitoring data

21) em – mean of strain extreme values based on corrected and de-noised monitoring data, em = $\max\{|\varepsilon_p|,|\varepsilon_v|\}$

22) em_std – standard deviation of strain extremes based on corrected and de-noised monitoring data

23) Lg2 – mean of half gauge length, Lg/2

24) Lg2_std – standard deviation of half gauge length

25) dh – mean of sensor spacing correction, Δh

26) dh_std – standard deviation of sensor spacing correction

The plots based on the mean values of major quantities can be found in Fig. 20 (a)–(d), where the circles represent the tests with failure and the circles with arrows designate the tests without failure. The results obtained from the follow-up tests for LM1 and LM17 are also included.

The fatigue life increased with decreasing amplitude as expected, but the variation was not continuous. A discontinuity or knee was observed near 7 Nm and 0.2 m^{-1} in the moment – N and curvature – N curves, respectively. For this SNF, these parameters correspond to 50 MPa of equivalent stress and 0.1% of equivalent strain. At the same time, curvature extreme values were generally higher than curvature amplitudes as expected, but the difference was small.

The flexural rigidity was mostly shown to be either quite flat or featuring a decreasing trend with the number of cycles. Several tests also suggested a tendency to increase with number of cycles, including LMK2, 8, and 14. Overall, the degree of variation of rigidity is limited. Meanwhile, no relation of rigidity to the number of cycles to failure can be seen.

The effective half-gage length was found out to be limited with a range between 38 and 50 mm and to increase with increased amplitude of moment. On the other hand, the sensor spacing correction did not suggest any relation to the moment amplitude.

Table 6a. Dynamic test results for LMK SNF rods

TN	Spec	ID	OD	Dia	Load	N	Fail	ma	ma_std	ka	ka_std	km	km_std
		inch	inch	inch	N	cycles		Nm	Nm	m^1	m^-1	m^-1	m^-1
1	LM1	0.394	0.450	0.374	250.000	9.40E+03	1	23.426	0.087	0.901	0.027	1.007	0.027
2	LM2	0.391	0.447	0.374	125.000	1.71E+05	1	11.468	0.090	0.266	0.006	0.275	0.008
3	LM3	0.392	0.448	0.374	100.000	4.92E+05	1	9.016	0.081	0.243	0.008	0.258	0.011
5	LM5	0.392	0.448	0.374	85.000	2.49E+05	1	7.570	0.074	0.165	0.008	0.205	0.013
6	LM6	0.392	0.448	0.374	75.000	1.79E+06	1	6.488	0.071	0.154	0.008	0.201	0.008
7	LM7	0.392	0.448	0.374	150.000	1.22E+05	1	13.930	0.085	0.347	0.005	0.362	0.009
8	LM8	0.392	0.448	0.374	75.000	4.70E+06	1	6.601	0.077	0.128	0.007	0.192	0.007
9	LM9	0.392	0.448	0.374	100.000	7.31E+05	1	9.058	0.077	0.216	0.004	0.226	0.007
10	LM10	0.392	0.448	0.374	200.000	5.20E+04	1	18.903	0.089	0.490	0.004	0.496	0.005
11	LM11	0.392	0.448	0.374	85.000	3.55E+05	1	7.657	0.111	0.162	0.007	0.194	0.010
12	LM12	0.392	0.448	0.374	70.000	7.58E+06	0	6.141	0.087	0.206	0.014	0.226	0.021
13	LM13	0.392	0.448	0.374	250.000	2.10E+04	1	21.396	2.415	0.533	0.071	0.553	0.073
14	LM14	0.392	0.448	0.374	100.000	3.90E+05	1	9.048	0.082	0.198	0.008	0.228	0.010
15	LM15	0.392	0.448	0.374	100.000	4.41E+05	1	8.997	0.073	0.225	0.007	0.230	0.007
16	LM16	0.392	0.448	0.374	300.000	1.36E+04	1	28.560	0.168	0.654	0.008	0.679	0.014
17	LM17	0.392	0.448	0.374	85.000	3.37E+06	0	7.459	0.374	0.204	0.011	0.212	0.013
18	LM17	0.392	0.448	0.374	300.000	1.31E+04	1	28.063	0.131	0.853	0.006	0.863	0.011

Table 6b. cont'd

TN	Spec	R	R_std	sa	sa_std	ea	ea_std	em	em_std	Lg2	Lg2_std	dh	dh_std
		Nm^2	Nm^2	MPa	MPa	%	%	%	%	mm	mm	mm	mm
1	LM1	26.017	0.809	179.649	0.667	0.515	0.015	0.575	0.015	43.766	0.767	0.279	0.182
2	LM2	43.120	0.891	88.227	0.691	0.151	0.004	0.156	0.005	44.250	0.634	-0.084	0.347
3	LM3	37.187	1.025	69.286	0.623	0.138	0.004	0.147	0.007	44.455	0.738	0.325	0.298
5	LM5	45.948	2.117	58.177	0.566	0.094	0.005	0.117	0.007	41.932	0.756	-1.436	0.577
6	LM6	42.226	2.287	49.862	0.548	0.088	0.005	0.114	0.005	40.157	0.749	-1.723	0.312
7	LM7	40.176	0.586	107.050	0.656	0.197	0.003	0.206	0.005	45.455	0.565	-0.426	0.190
8	LM8	51.567	2.504	50.733	0.590	0.073	0.004	0.109	0.004	42.342	0.890	2.568	0.338
9	LM9	41.880	0.736	69.615	0.590	0.123	0.003	0.129	0.004	43.120	0.698	0.206	0.215
10	LM10	38.563	0.336	145.272	0.684	0.279	0.002	0.282	0.003	46.986	0.528	0.355	0.173
11	LM11	47.437	2.009	58.848	0.856	0.092	0.004	0.110	0.006	41.396	0.757	-1.864	0.362
12	LM12	29.879	1.859	47.196	0.665	0.117	0.008	0.129	0.012	38.475	0.965	0.732	0.683
13	LM13	40.225	0.903	164.428	18.563	0.303	0.040	0.315	0.042	47.411	0.705	-0.138	0.143
14	LM14	45.659	1.768	69.535	0.632	0.113	0.005	0.130	0.006	44.092	0.781	-1.307	0.387
15	LM15	40.008	1.219	69.141	0.561	0.128	0.004	0.131	0.004	44.196	0.698	-0.148	0.585
16	LM16	43.672	0.480	219.490	1.295	0.372	0.005	0.386	0.008	50.296	0.440	-0.435	0.153
17	LM17	36.630	1.138	57.325	2.872	0.116	0.006	0.121	0.007	44.656	0.919	-0.849	0.338
18	LM17	32.913	0.252	215.671	1.004	0.485	0.003	0.491	0.006	47.420	0.331	1.211	0.092

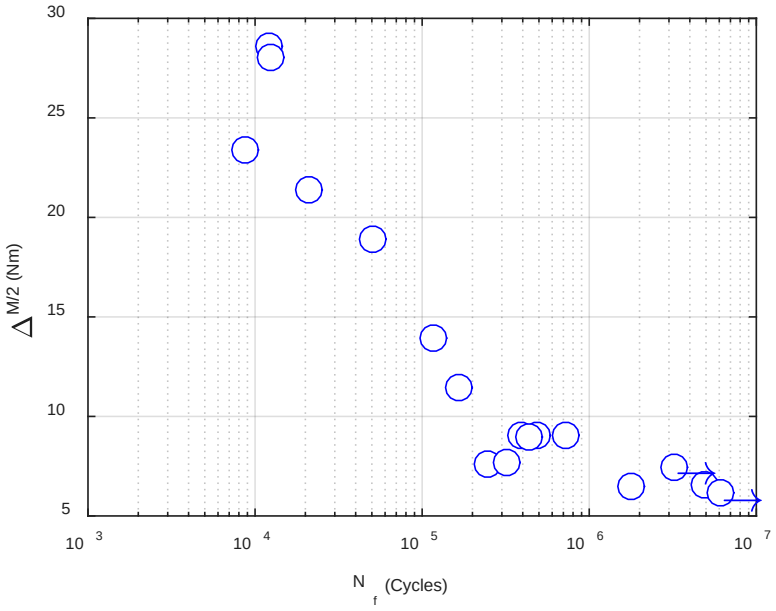

(a)

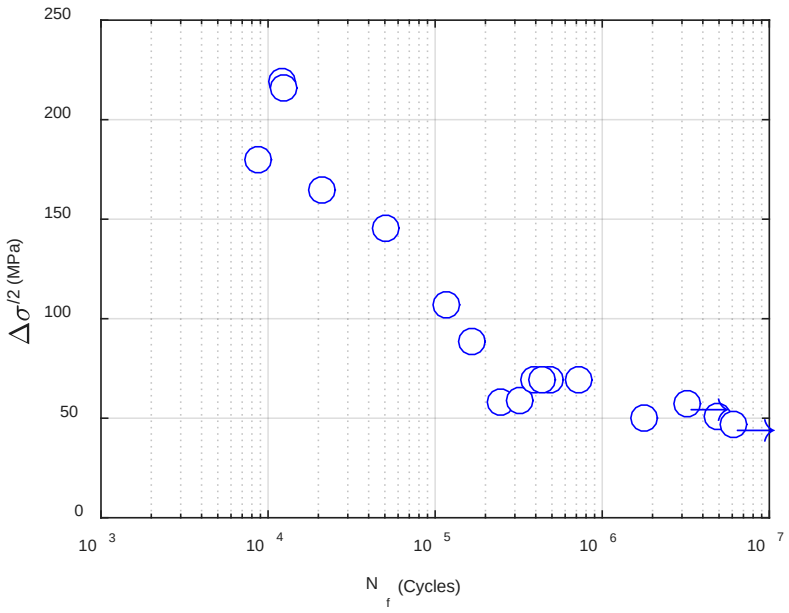
250
200
150
100
50
0
$\Delta\sigma^{/2}$ (MPa)
10 3
10 4
10 5
10 6
10 7
N f (Cycles)

(b)

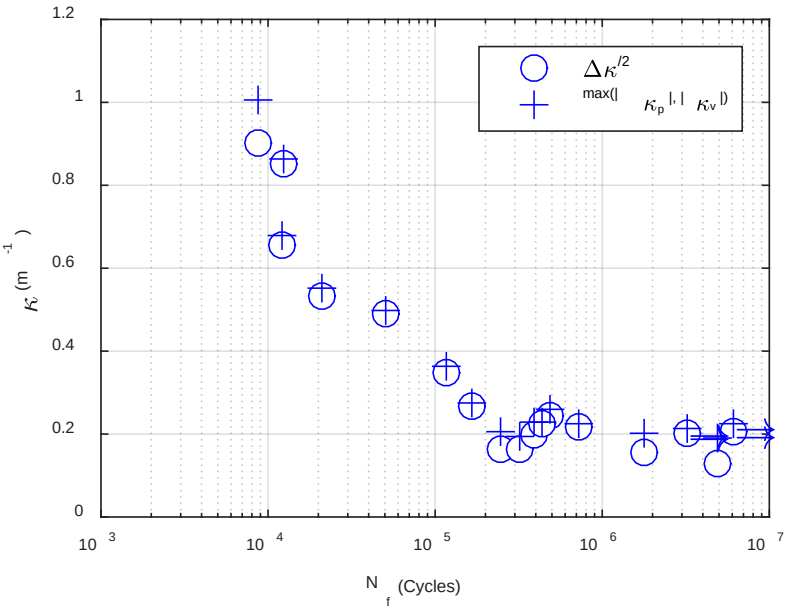
1.2
1
0.8
0.6
0.4
0.2
0
κ (m -1)
$\Delta\kappa^{/2}$
max(|
κ_p |, |
κ_v |)
10 3
10 4
10 5
10 6
10 7
N f (Cycles)

(c)

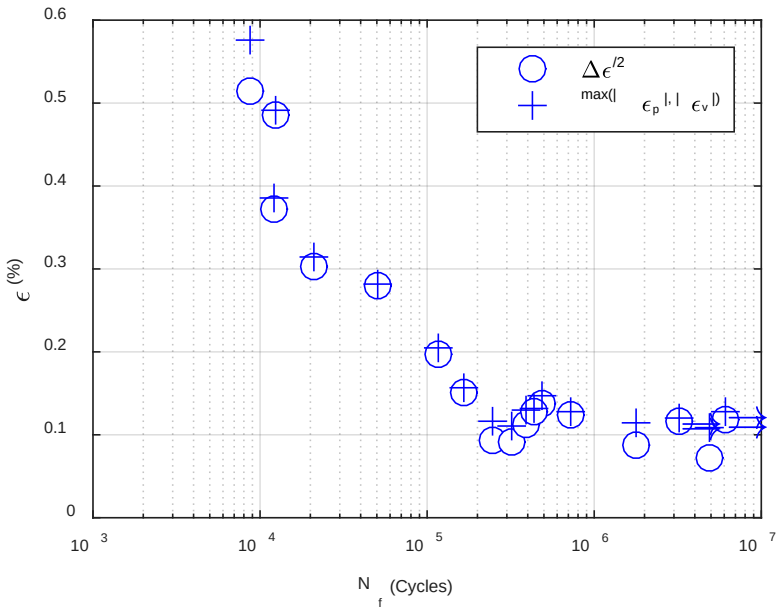

(d)

Fig. 20. (a) Moment amplitude, (b) stress amplitude, (c) curvature amplitude/ maximum, and (d) strain amplitude/ maximum as a function of cycles or cycles to failure.

4. DATA ANALYSIS OF CIRFT TESTING ON North Anna FUEL

4.1 Overview

A total of 6 dynamic tests was conducted with applied amplitudes from 5.08 to 15.24 N·m; 5 specimens failed, and fatigue life ranged from 1.26×10^4 to 4.27×10^5 cycles. One specimen (NA5) was cycled to 5.11×10^6 cycles without failure and stopped.

4.2 Results on Data Analysis for Dynamic Tests

The results for each test are given in Appendix B. For each test, the plots similar to those of LMK fuels are presented for NA fuel as well, including the variations of curvature range, moment range, flexural rigidity, curvature peak/valley, and moment peak/valley values.

The results for the dynamic tests are summarized in Table 7. The items of the columns are the same as those of LMK fuels in Sect. 3.2.

The plots based on the mean values of quantities can be found in Fig. 21 (a)–(d). In the moment – N and curvature – N curve, it seemed that there are knee points near 4 Nm and 0.05 m^{-1}. However, the knee was not defined well because of the limited data points.

The variation of rigidity was generally limited for a specified cyclic test, but abrupt change was observed in several tests. On the other hand, the effective half-gage length was found out to be limited with a range between 40 and 49 mm, increasing with increased amplitude of moment.

Table 7. Dynamic test results for NA SNF rods

TN	Spec	ID	OD	Dia	Load	N	Fail	ma	ma_std	ka	ka_std	km	km_std
		inch	inch	inch	N	cycles		Nm	Nm	m^1	m^-1	m^-1	m^-1
1	NA1	0.334	0.379	0.323	125.000	1.57E+04	1	11.001	0.053	0.512	0.007	0.536	0.013
2	NA2	0.332	0.377	0.323	100.000	2.20E+04	1	8.802	0.082	0.391	0.013	0.412	0.017
4	NA4	0.334	0.379	0.323	75.000	6.10E+04	1	6.331	0.083	0.221	0.009	0.255	0.010
5	NA5	0.334	0.379	0.323	50.000	5.11E+06	0	3.982	0.068	0.143	0.014	0.161	0.014
6	NA6	0.334	0.379	0.323	50.000	4.27E+05	1	3.986	0.090	0.121	0.010	0.163	0.009
7	NA7	0.335	0.380	0.323	150.000	1.26E+04	1	13.540	0.542	0.610	0.039	0.629	0.026

TN	Spec	R	R_std	sa	sa_std	ea	ea_std	em	em_std	Lg2	Lg2_std	dh	dh_std
		Nm^2	Nm^2	Mpa	MPa	%	%	%	%	mm	mm	mm	mm
1	NA1	21.494	0.268	135.887	0.650	0.246	0.003	0.258	0.006	46.055	0.469	-0.359	0.247
2	NA2	22.561	0.695	108.926	1.017	0.187	0.006	0.197	0.008	45.473	0.670	1.271	0.371
4	NA4	28.676	0.888	78.196	1.023	0.106	0.004	0.123	0.005	45.209	0.775	1.248	0.353
5	NA5	28.084	2.764	49.186	0.842	0.069	0.007	0.078	0.007	40.101	1.533	-0.148	0.770
6	NA6	33.140	2.801	49.237	1.113	0.058	0.005	0.078	0.004	43.153	0.968	1.745	0.404
7	NA7	22.261	1.174	167.085	6.690	0.295	0.019	0.303	0.013	49.444	1.317	0.163	0.345

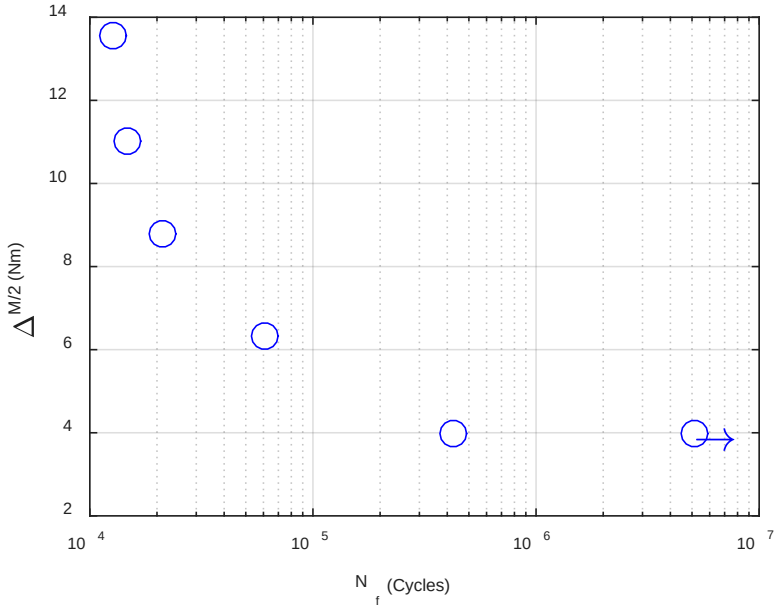
14
12
10
8
6
4
2
ΔM/2 (Nm)
10 4
10 5
10 6
10 7
N f (Cycles)

(a)

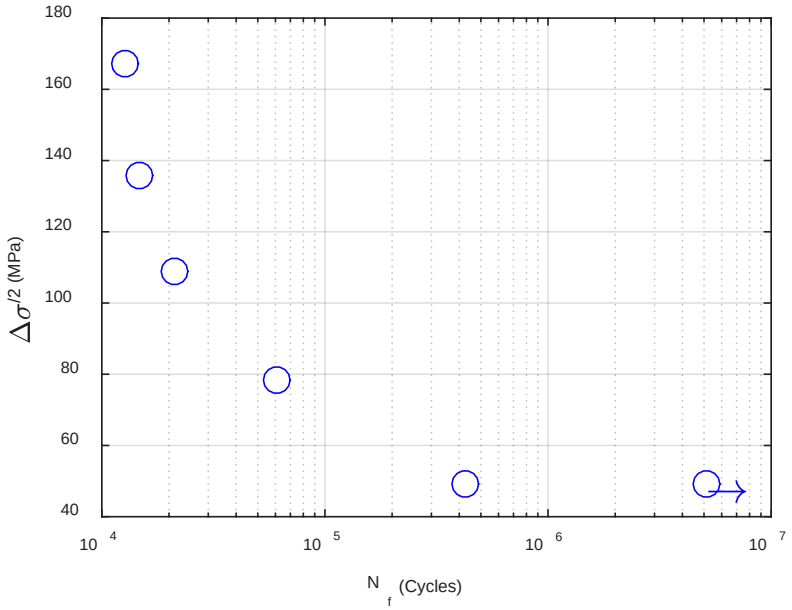
180
160
140
120
100
80
60
40
Δσ/2 (MPa)
10 4
10 5
10 6
10 7
N f (Cycles)

(b)

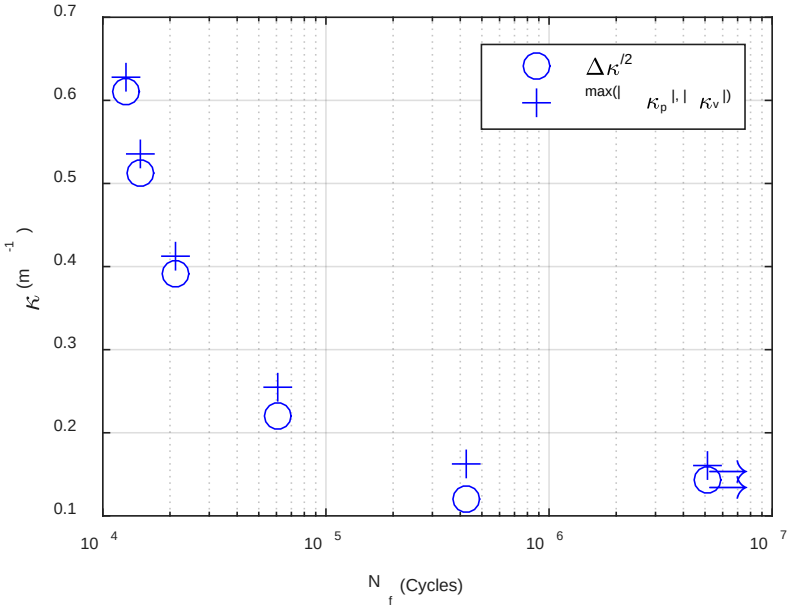

(c)

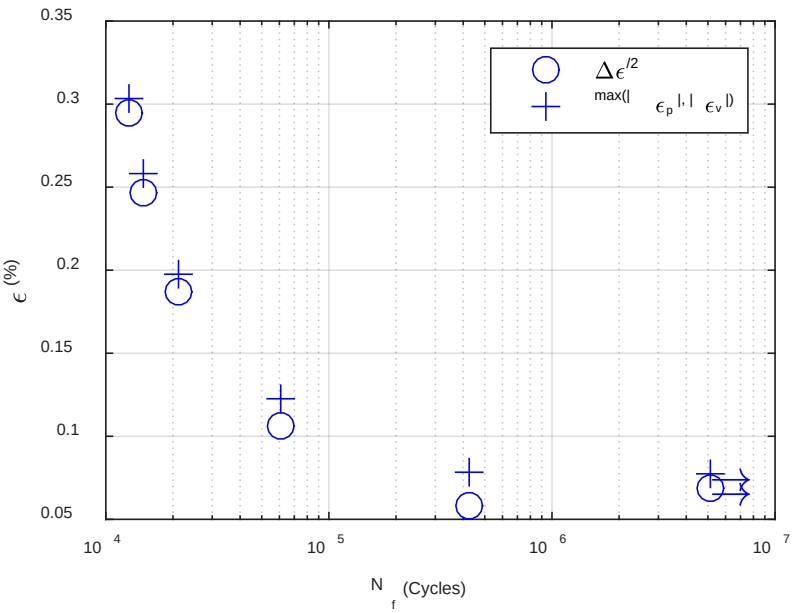

(d)

Fig. 21. (a) Moment amplitude, (b) stress amplitude, (c) curvature amplitude/ maximum, and (d) strain amplitude/ maximum as a function of cycles or cycles to failure.

5. DATA ANALYSIS OF CIRFT TESTING ON MOX FUEL

5.1 Overview

10 dynamic tests were completed with the applied amplitudes from 5.08 to 15.24 Nm, and all specimens failed. The fatigue life ranged from 1.29×10^4 and 2.15×10^6 cycles.

5.2 Results on Data Analysis for Dynamic Tests

The results for each test are given in Appendix C. The plots similar to those of LMK fuels are presented for MOX fuel, as well including the variations of curvature range, moment range, flexural rigidity, curvature peak/valley, and moment peak/valley values.

The results for the dynamic tests of MOX fuel are summarized in Table 8. The items of the columns are the same as those of LMK fuels in Sect. 3.2.

The plots based on the mean values of quantities can be found in Figs 22 (a)–(d). In the moment – N curve, it seemed that there is knee point near 4 Nm. However, the variation of fatigue life in curvature –N curve appeared to be continuous within the tested amplitude range.

The fatigue response of rigidity depends on the moment amplitudes applied. Under a high level such as >10.2 Nm, the rigidity was either relatively stable, or it showed a trend of decreasing with the accumulated number of cycles. Under the low level, it tended to increase during the cyclic test, but it was indeed observed that the fatigue life of MOX fuel increased with the increasing initial rigidity.

On the other hand, the effective half-gage length was determined to be limited with a range between 40 and 52 mm, increasing with increased amplitude of moment.

Table 8a. Dynamic test results for MOX SNF rods

TN	Spec	ID	OD	Dia	Load	N	Fail	ma	ma_std	ka	ka_std	km	km_std
		inch	inch	inch	N	cycles		Nm	Nm	m^1	m^-1	m^-1	m^-1
2	MOX2	0.333	0.378	0.323	100.000	3.70E+04	1	8.480	0.103	0.425	0.010	0.437	0.012
4	MOX4	0.333	0.378	0.323	50.000	2.15E+06	1	3.900	0.075	0.132	0.016	0.148	0.017
5	MOX5	0.333	0.378	0.323	60.000	4.49E+05	1	4.794	0.061	0.179	0.009	0.186	0.010
6	MOX6	0.333	0.378	0.323	50.000	5.42E+05	1	3.830	0.054	0.169	0.008	0.174	0.010
7	MOX7	0.333	0.378	0.323	150.000	1.55E+04	1	13.857	0.127	0.629	0.008	0.640	0.009
8	MOX8	0.333	0.378	0.323	125.000	1.29E+04	1	11.036	0.104	0.542	0.009	0.587	0.013
9	MOX9	0.333	0.378	0.323	75.000	8.98E+04	1	6.294	0.084	0.319	0.009	0.353	0.015
10	MOX10	0.333	0.378	0.323	100.000	3.85E+04	1	8.729	0.068	0.378	0.016	0.397	0.017
11	MOX11	0.333	0.378	0.323	100.000	4.23E+04	1	8.662	0.047	0.375	0.008	0.415	0.011
12	MOX12	0.333	0.378	0.323	100.000	4.23E+04	1	8.711	0.067	0.415	0.005	0.439	0.010

Table 8b. (continued)

TN	Spec	R	R_std	sa	sa_std	ea	ea_std	em	em_std	Lg2	Lg2_std	dh	dh_std
		Nm^2	Nm^2	Mpa	MPa	%	%	%	%	mm	mm	mm	mm
2	MOX2	19.955	0.533	104.839	1.274	0.204	0.005	0.210	0.006	43.811	0.621	1.243	0.291
4	MOX4	29.939	3.703	48.216	0.932	0.063	0.008	0.071	0.008	40.575	2.133	-1.512	0.927
5	MOX5	26.797	1.235	59.265	0.758	0.086	0.004	0.089	0.005	43.766	1.027	-1.178	0.684
6	MOX6	22.744	1.021	47.347	0.662	0.081	0.004	0.084	0.005	43.751	0.867	0.059	0.395
7	MOX7	22.042	0.316	171.317	1.569	0.302	0.004	0.307	0.004	48.523	0.454	0.409	0.129
8	MOX8	20.377	0.282	136.440	1.282	0.260	0.004	0.282	0.006	49.223	0.484	0.441	0.144
9	MOX9	19.716	0.470	77.823	1.041	0.153	0.004	0.169	0.007	45.835	0.536	-0.505	0.190
10	MOX10	23.127	0.855	107.918	0.840	0.181	0.008	0.190	0.008	49.626	1.075	-0.428	0.276
11	MOX11	23.098	0.534	107.096	0.585	0.180	0.004	0.199	0.005	52.390	0.622	-1.036	0.260
12	MOX12	20.979	0.242	107.694	0.825	0.199	0.002	0.211	0.005	48.820	0.550	-0.678	0.182

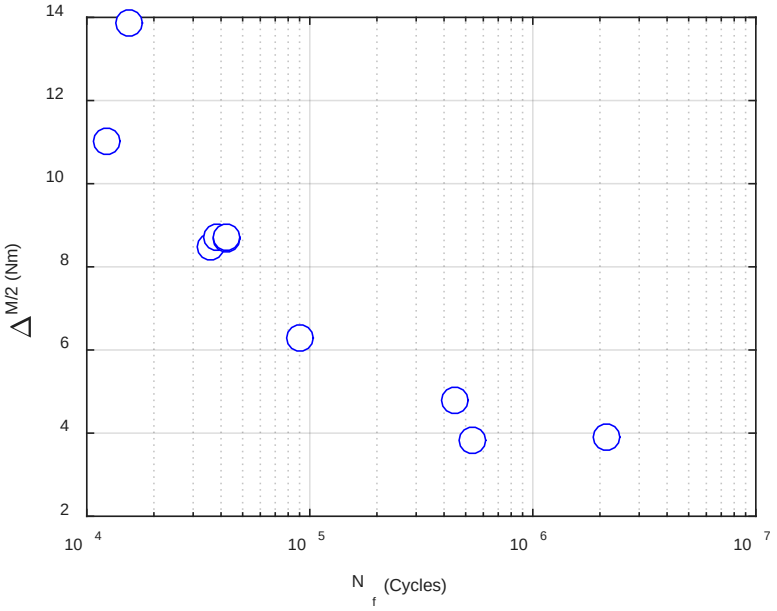

(a)

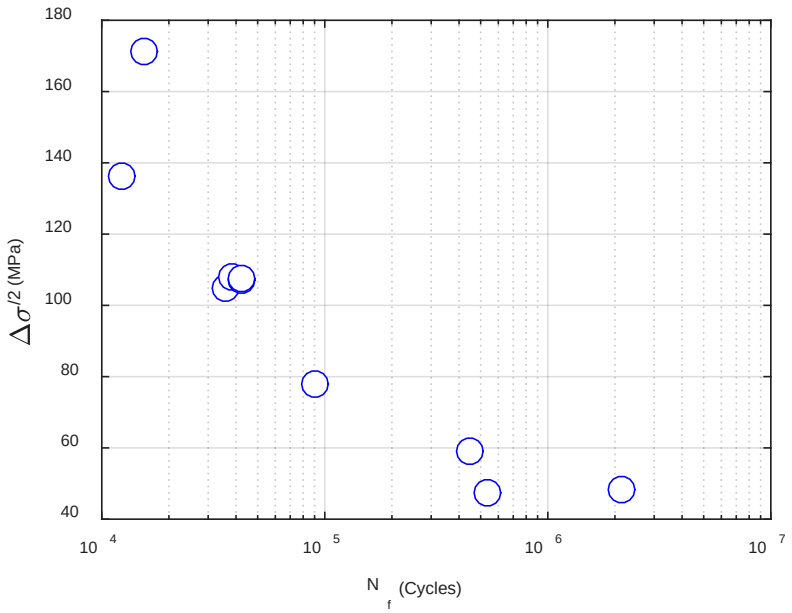
180
160
140
120
100
80
60
40
$\Delta\sigma^{/2}$ (MPa)
10^4
10^5
10^6
10^7
N_f (Cycles)

(b)

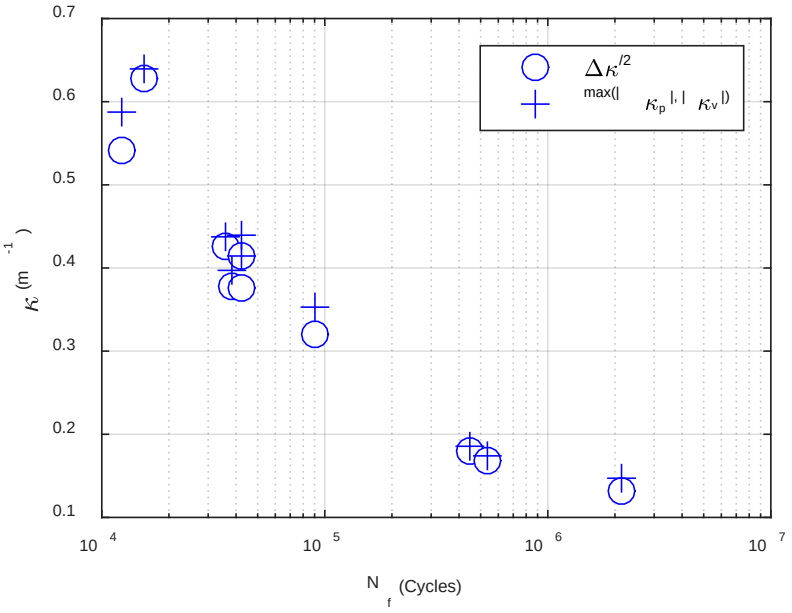
0.7
0.6
0.5
0.4
0.3
0.2
0.1
κ (m^{-1})
$\Delta\kappa^{/2}$
max(| κ_p |, | κ_v |)
10^4
10^5
10^6
10^7
N_f (Cycles)

(c)

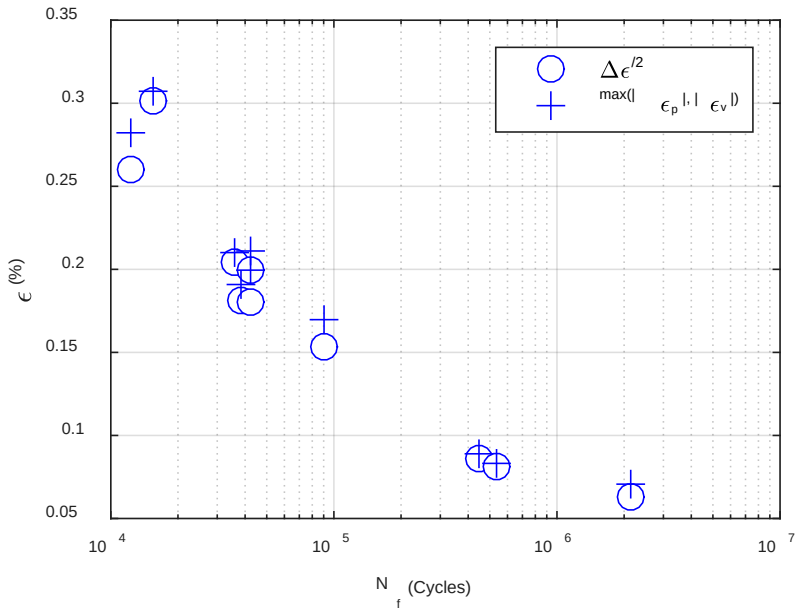

(d)

Fig. 22. (a) Moment amplitude, (b) stress amplitude, (c) curvature amplitude/ maximum, and (d) strain amplitude/ maximum as a function of cycles or cycles to failure.

6. DISCUSSION AND REMAINING ISSUES

6.1 Fatigue Life of SNF

The variations of fatigue life are given in Fig. 23 in terms of moment, equivalent stress, curvature and equivalent strain for the tested SNFs.

The equivalent stress indeed collapsed the data points from all of the SNFs into a single zone. A detailed examination revealed that, at same stress level, the LMK fuel showed a longer fatigue life than the other two SNFs between 10^4 and 10^6 cycles. The strain – N curve shows that the LMK fuel has a longer fatigue life in a wider range from 10^4 to 10^7 cycles.

The knee point in the curve of moment and curvature or equivalent quantities is more clearly defined for LMK fuel than for the other two fuels.

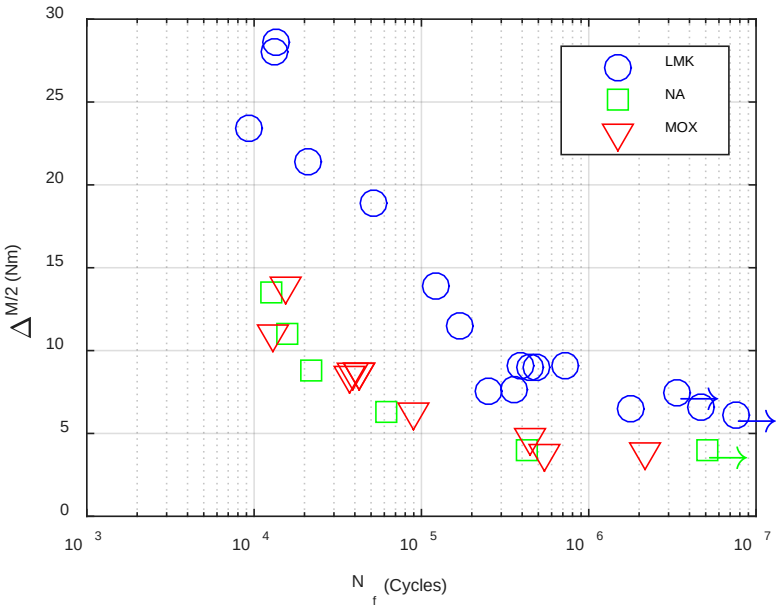

(a)

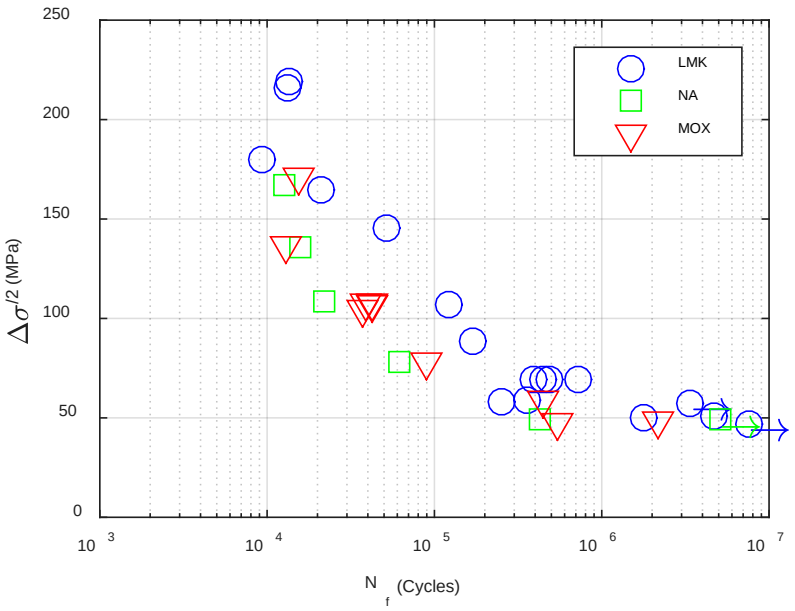
LMK
NA
MOX
250
200
150
100
50
0
$\Delta\sigma^{1/2}$ (MPa)
10^3
10^4
10^5
10^6
10^7
N_f (Cycles)

(b)

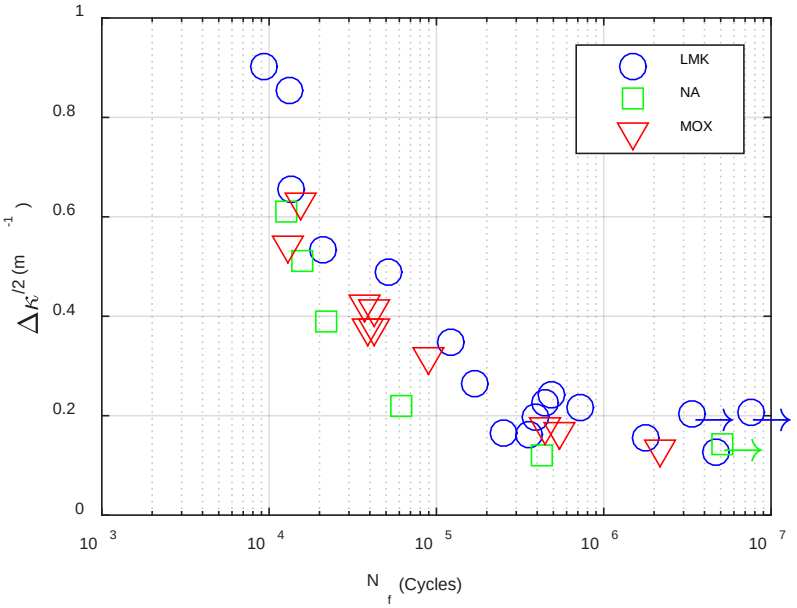
LMK
NA
MOX
1
0.8
0.6
0.4
0.2
0
$\Delta\kappa^{1/2}$ (m^{-1})
10^3
10^4
10^5
10^6
10^7
N_f (Cycles)

(c)

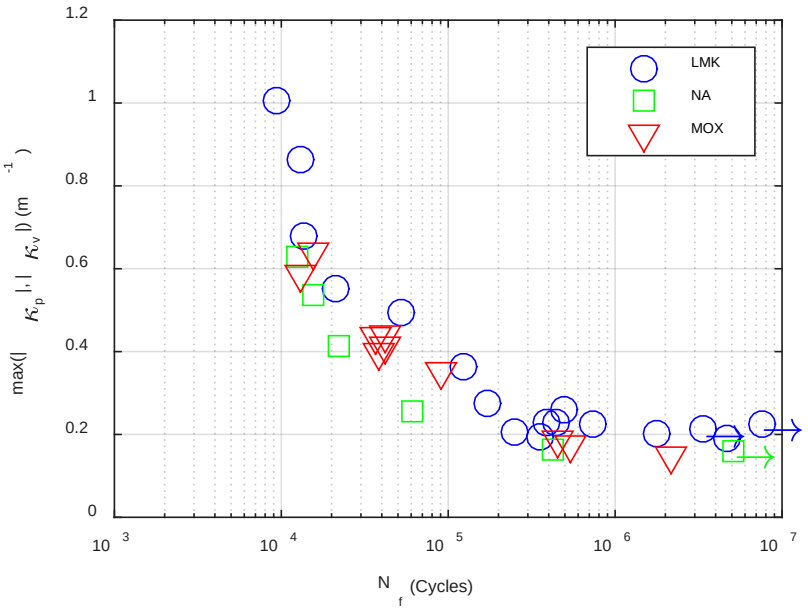
LMK
NA
MOX
max(| κ_p |, | κ_v |) (m^{-1})
N$_f$ (Cycles)

(d)

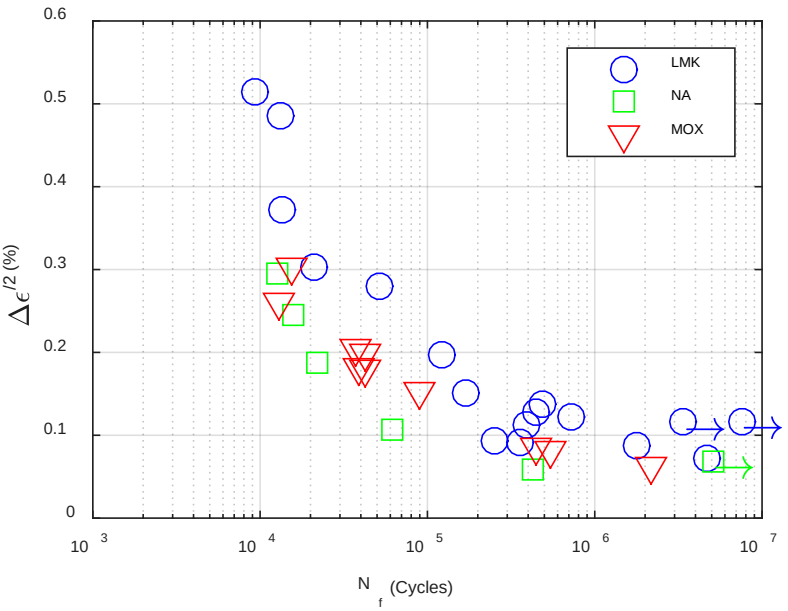
LMK
NA
MOX
$\Delta\epsilon^{/2}$ (%)
N$_f$ (Cycles)

(e)

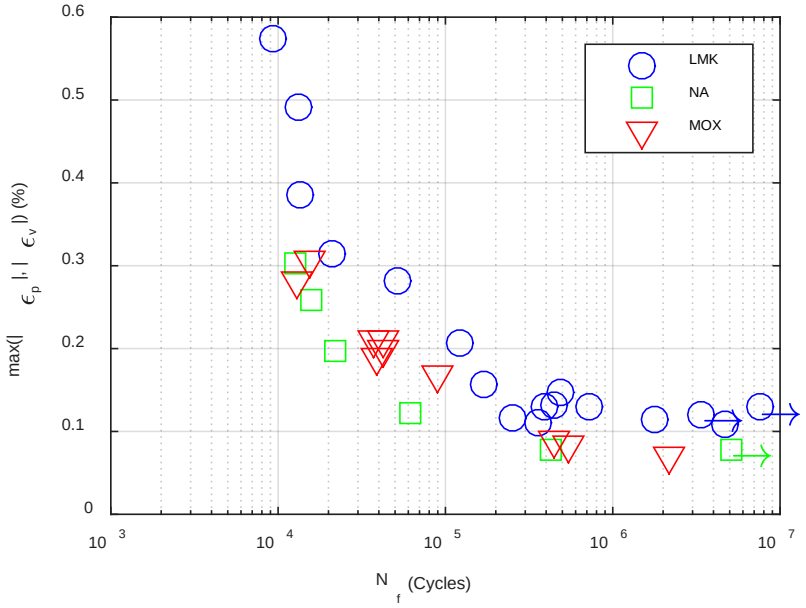

(f)

Fig. 23. (a) Moment amplitude, (b) stress amplitude, (c) curvature amplitude, (d) curvature maximum, (e) strain amplitude, and (f) strain maximum as a function of cycles or cycles to failure.

6.2 Remaining Issues with Curvature Measurement

6.2.1 Small Amplitude Curvature

In CIRFT tests, the small curvatures usually occur in the dynamic tests. Remaining issues exists with respect to the small curvature measurement.

1) How close is the contact condition of SS cladding-only surrogate rods to that of SNF rods?
   This question is critical because the contact dominates the sensor spacing used in the calculation of curvature. This is mainly because the cladding material, and especially the surface condition of the SNF rod, vary from those in the surrogate rod. The initial engagement and the subsequent contact of LVDT probes with the rod will be affected by these factors.

2) How much impact of the transverse motion of LVDT probes is imposed on curvature measurement?
   There is a clearance between the measurement probe and LVDT cylinder designed to ensure a smooth longitudinal motion of the LVDT probe within the measurement cylinder. This clearance introduces an inevitable transverse motion of probe, which affects the initial engagement of probe with the rod and also the subsequent translational movement of the probe in measurement.

3) What is the effect of driving frequency on the curvature measurement?
   It has been shown that there is an effect of frequency on the response of bending rod. The issue remaining to be addressed here is to determine how the frequency will impact the curvature measurement itself. This effect occurs because the contact of probe against the rod is influenced by the dynamics of system.

6.2.2 Large Amplitude Curvature

There are some outstanding issues with regard to the large curvature measurement.

1) The impact of pellet-cladding mechanical interaction (PCMI) may be important when the deformation becomes large.
   This is obvious because the local plastic deformation can be substantial due to local buckling in compressive side, for instance. This alters the surface condition, and in turn, it alters the contact of the probe against the rod.

2) How will the transverse motion of the probe be changed with large deformation?
   The transverse motion is associated with clearance of LVDT measurement. Large deformation of the rod may close the gap between the measurement rod and the cylinder on one side and open it on other side.

3) How is the correction applicable to the real SNF rods?
   The spacing correction relation has been developed using a flexible rod made of materials like polycarbonate. This provides a useful approach to investigate the response of the rod system in large deformation, but it needs to be justified before being migrated into the CIRFT data analysis.

7. CONCLUSION

1) There is an effect from the contact of the probe on the curvature measurement in current CIRFT tests. The effect of the contact can be corrected by using the correction of sensor spacing that is defined between LVDT probes used for curvature measurement.

2) The sensor spacing correction can be determined by using a chisel-type probe. However, this method is limited in its application and cannot be implemented effectively.

3) The sensor spacing correction based on equivalent gage length has the required flexibility and can meet the challenge from application.

4) The correction method based on the equivalent gage length has been demonstrated in this report in CIRFT data analysis for the dynamic tests on LMK (17), NA (6), and MOX (10) fuel rods.

5) Some important issues such as the effects of large amplitude curvature, transverse movement of probes, etc., remain to be investigated in future.

REFERENCES

1. J.-A. J. Wang, H. Wang, Y. Yan, R. Howard, and B. Bevard, *High Burn-up Spent Fuel Vibration Integrity Study Progress Letter Report (Out-of-Cell Fatigue Testing Development–Task 2.1)*, ORNL/TM-2010/288, Oak Ridge National Laboratory, Oak Ridge, TN, January 2011.

2. J.-A. J. Wang, H. Wang, T. Tan, H. Jiang, T. Cox, and Y. Yan, *Progress Letter Report on U Frame Test Setup and Bending Fatigue Test for Vibration Integrity Study (Out-of-Cell Fatigue Testing Development–Task 2.2)*, ORNL/TM-2011/531, Oak Ridge National Laboratory, Oak Ridge, TN, January 2012.

3. J.-A. J. Wang, H. Wang, T. Cox, and Y. Yan, *Progress Letter Report on U-Frame Test Setup and Bending Fatigue Test for Vibration Integrity Study (Out-of-Cell Fatigue Testing Development–Task 2.3)*, ORNL/TM-2012/417, Oak Ridge National Laboratory, Oak Ridge, TN, August 2012.

4. J.-A. J. Wang, H. Wang, and Ting Tan, *An Innovative Dynamic Reversal Bending Fatigue Testing System for Evaluating Spent Nuclear Fuel Rod Vibration Integrity or Other Materials Fatigue Aging Performance*, ORNL Invention Disclosure 201102593, DOE S 124,149, April 8, 2011, Patent in review, 13/396,413, February 14, 2012.

5. H. Wang, J.-A. J. Wang, T. Tan, H. Jiang, T. S. Cox, R. L. Howard, B. B. Bevard, and M. E. Flanagan, "Development of U-frame Bending System for Studying the Vibration Integrity of Spent Nuclear Fuel," *Journal of Nuclear Materials* 440, 201–213 (2013).

6. J.-A. J. Wang, H. Wang, B. B. Bevard, R. L. Howard, and M. E. Flanagan, "SNF Test System for Bending Stiffness and Vibration Integrity," *International High-Level Radioactive Waste Management Conference*, Albuquerque, NM, April 28–May 2, 2013.

7. J.-A. J. Wang, H. Wang, T. Cox, and C. Baldwin, *Progress Letter Report on Bending Fatigue Test System Development for Spent Nuclear Fuel Vibration Integrity Study (Out-of-Cell Fatigue Testing Development–Task 2.4)*, ORNL/TM-2013/225, Oak Ridge National Laboratory, Oak Ridge, TN (2013).

8. J.-A. J. Wang, H. Wang, B. B. Bevard, R. L. Howard, and M. E. Flanagan, "Reversible Bending Fatigue Test System for Investigating Vibration Integrity of Spent Nuclear Fuel During Transportation," *Proceedings of the 17th International Symposium on the Packaging and Transportation of Radioactive Materials* PATRAM 2013, San Francisco, CA, August 18–23, 2013.

9. G. Bjorkman, "High Burnup Spent Fuel Testing Program Objectives," NRC Program Review Meeting, Oak Ridge National Laboratory, August 8, 2011.

This page intentionally left blank.

APPENDIX A CIRFT TESTING RESULTS OF LIMERICK BWR SPENT NUCLEAR FUEL

TABLE OF CONTENTS

Measurement and monitoring rigidity curves for Limerick (LMK) BWR Spent Nuclear Fuel

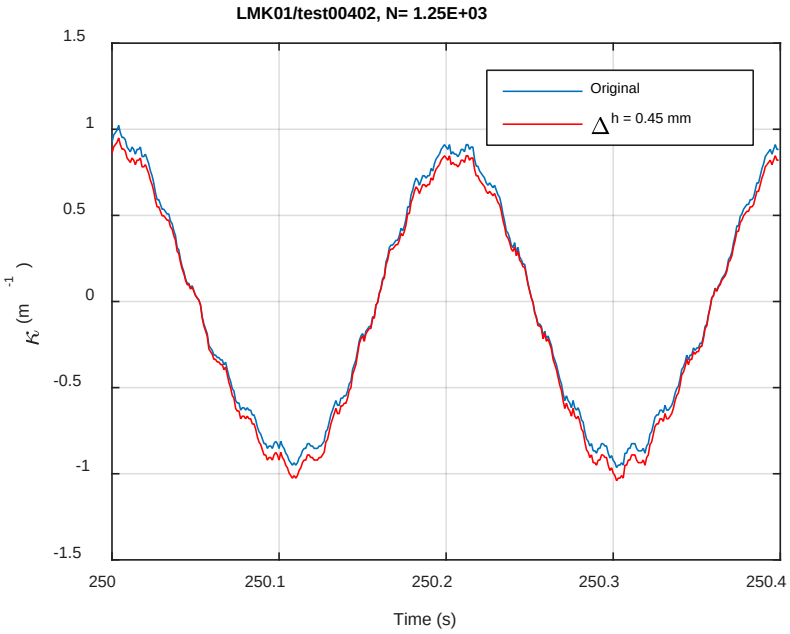
LMK01/test00402, N= 1.25E+03
Original
Δh = 0.45 mm
κ (m-1)
Time (s)
1.5
1
0.5
0
-0.5
-1
-1.5
250
250.1
250.2
250.3
250.4

(a)

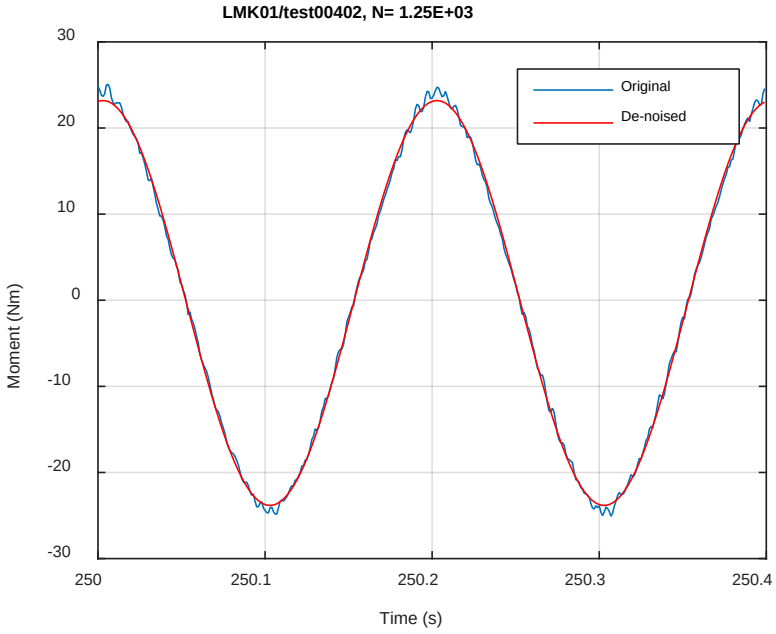
LMK01/test00402, N= 1.25E+03
Original
De-noised
Moment (Nm)
Time (s)
30
20
10
0
-10
-20
-30
250
250.1
250.2
250.3
250.4

(b)

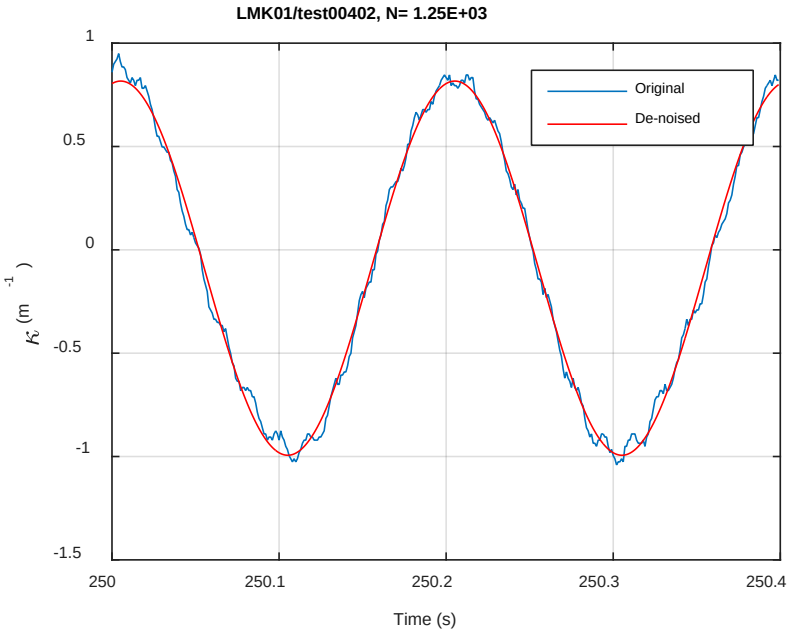

(c)

Fig. A.1. Monitoring-based responses: (a) curvature, (b) moment, (c) curvature, LMK01, 25.40 Nm, Ns = 1.25E+03 cycles.

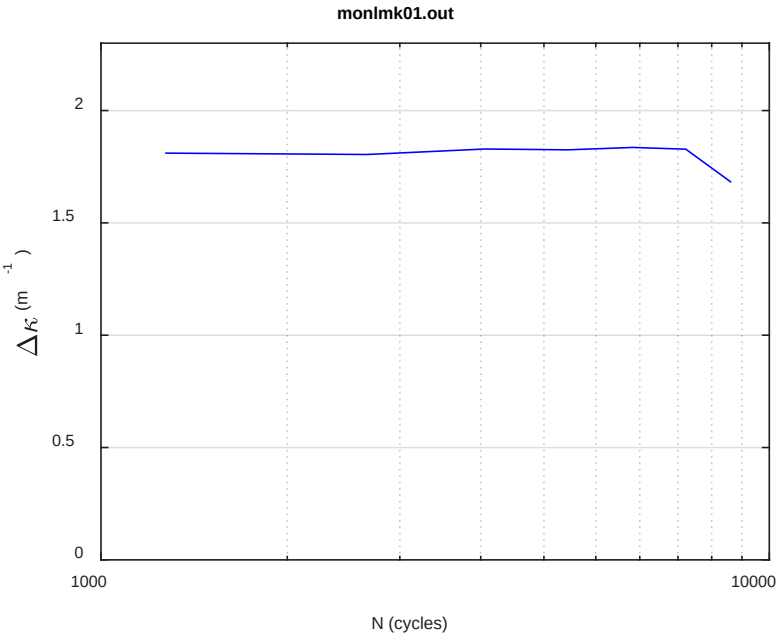
monlmk01.out
2
1.5
1
0.5
0
Δκ (m-1)
1000
10000
N (cycles)

(a)

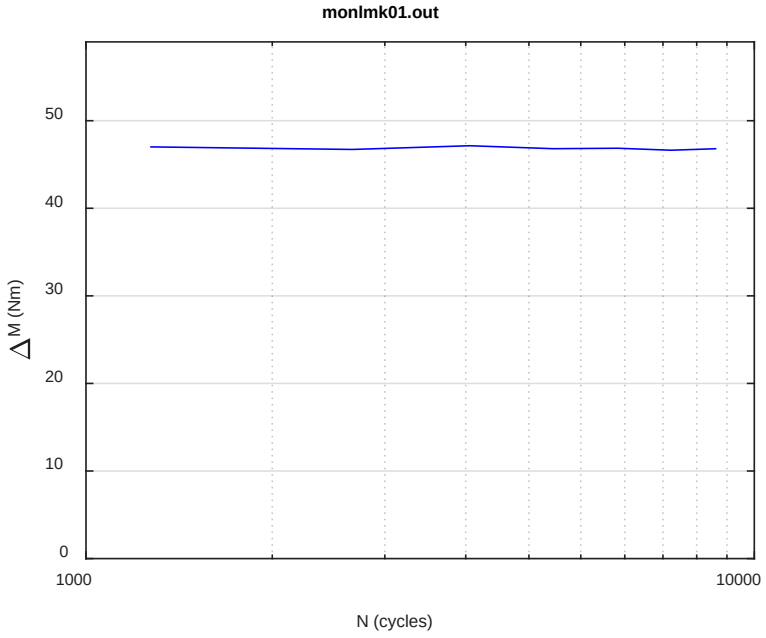
monlmk01.out
50
40
30
20
10
0
Δ M (Nm)
1000
10000
N (cycles)

(b)

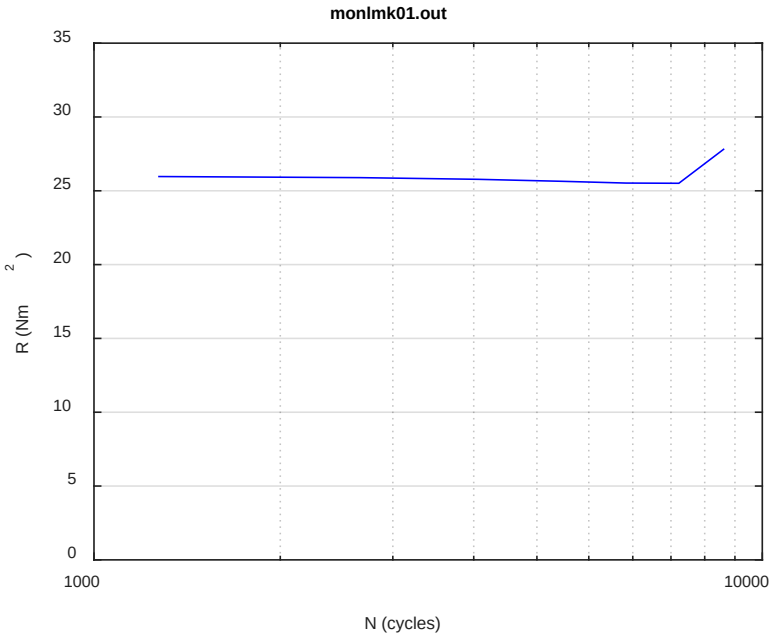
monlmk01.out
35
30
25
20
15
10
5
0
R (Nm 2)
1000
10000
N (cycles)

(c)

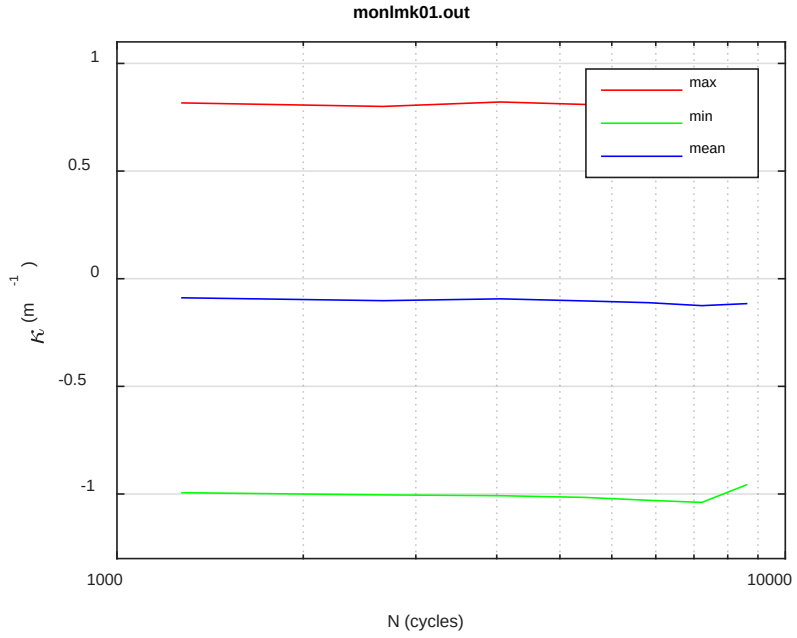
monlmk01.out
1
0.5
0
-0.5
-1
κ (m -1)
max
min
mean
1000
10000
N (cycles)

(d)

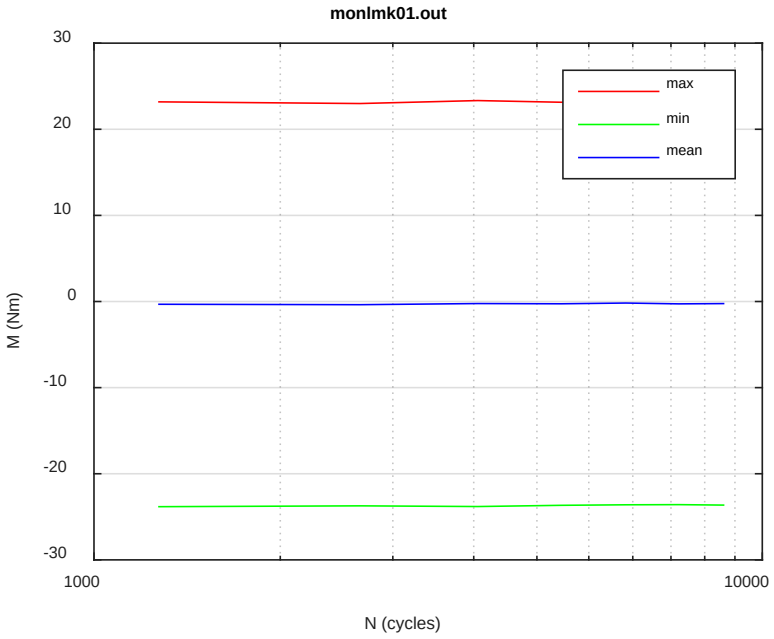

(e)

Fig. A.2. Monitoring-based responses: (a) curvature range, (b) moment range, (c) rigidity, (d) curvature peak/valley, (e) moment peak/valley, LMK01, 25.40 Nm, Nf = 9.40E+03 cycles.

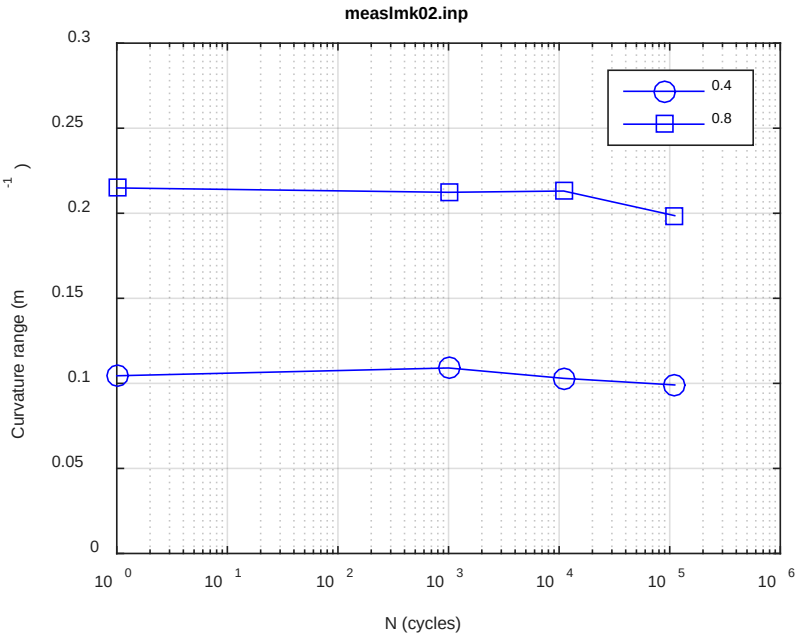
measlmk02.inp
0.3
0.25
0.2
0.15
0.1
0.05
0
Curvature range (m-1)
0.4
0.8
10 0
10 1
10 2
10 3
10 4
10 5
10 6
N (cycles)

(a)

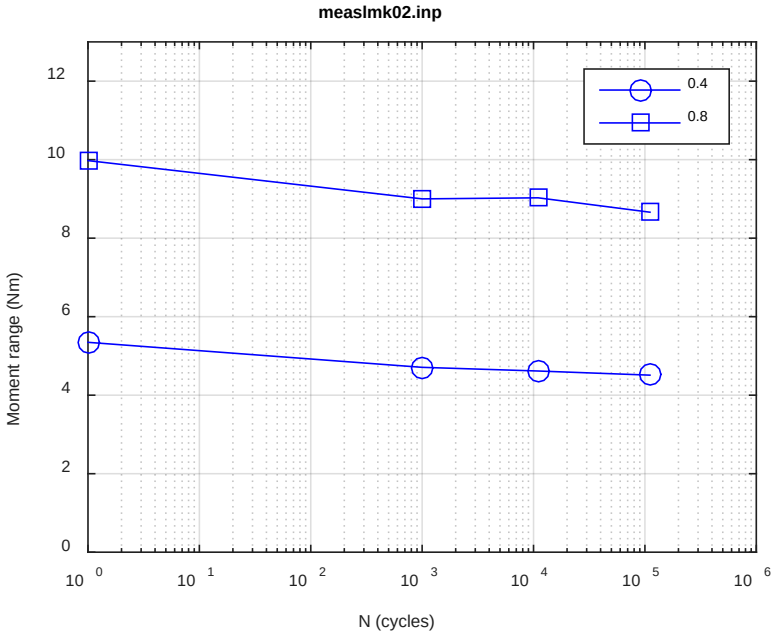
measlmk02.inp
12
10
8
6
4
2
0
Moment range (Nm)
0.4
0.8
10 0
10 1
10 2
10 3
10 4
10 5
10 6
N (cycles)

(b)

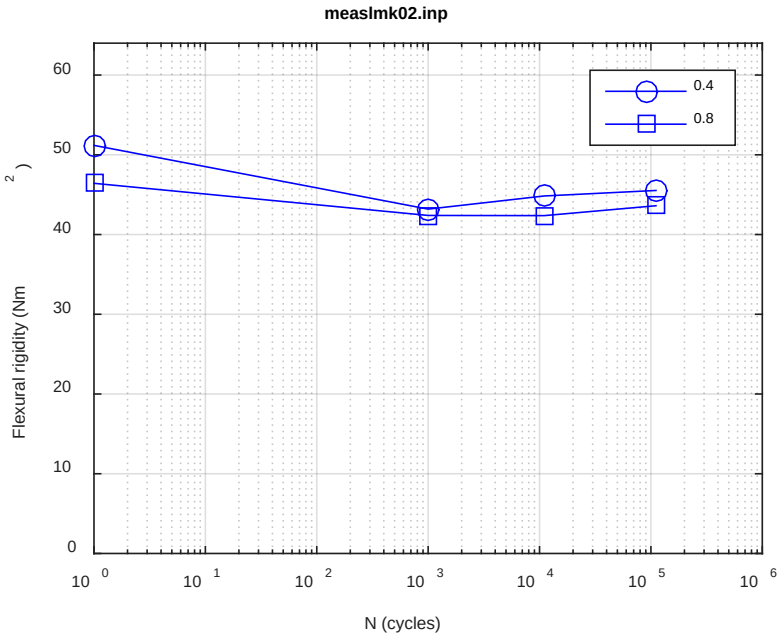
measlmk02.inp
Flexural rigidity (Nm 2)
N (cycles)
0.4
0.8

(c)

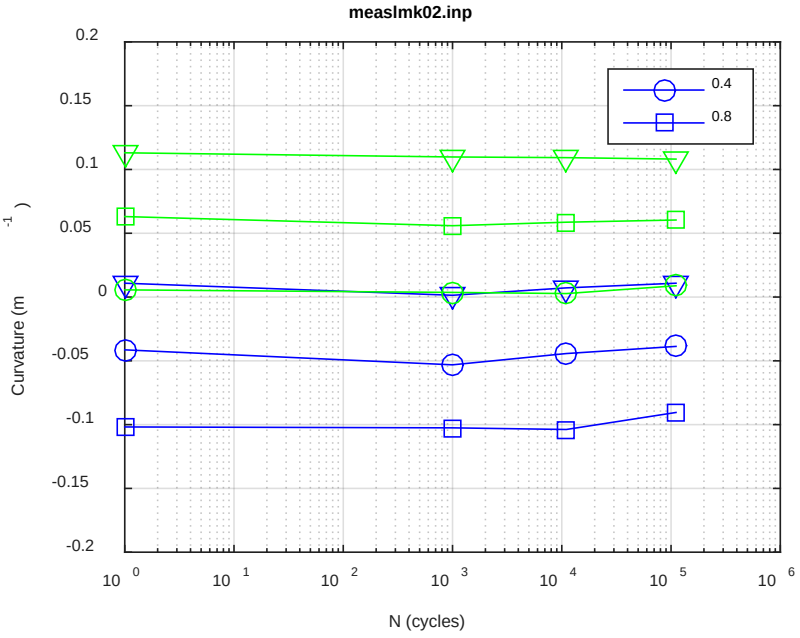
measlmk02.inp
Curvature (m -1)
N (cycles)
0.4
0.8

(d)

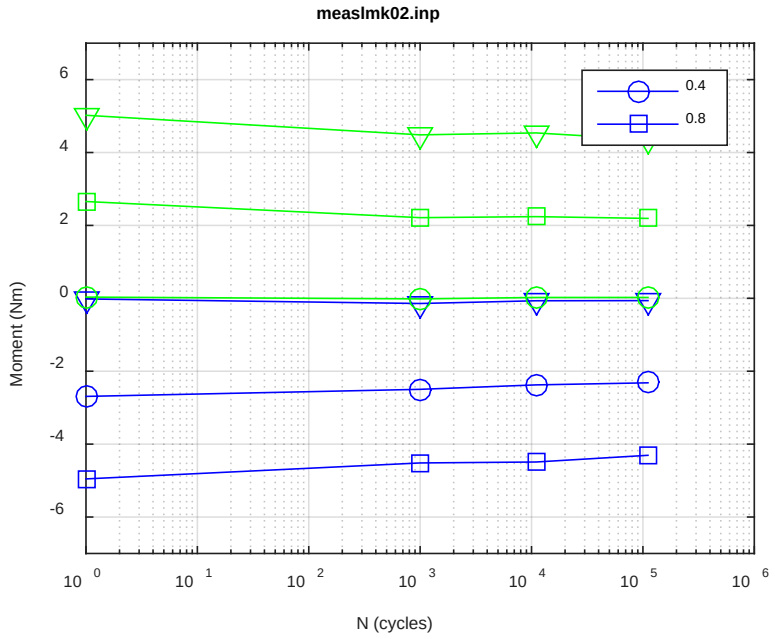

(e)

Fig. A.3. Measurement-based responses: (a) curvature range, (b) moment range, (c) rigidity, (d) curvature peak/valley, (e) moment peak/valley, LMK02, 12.70 Nm.

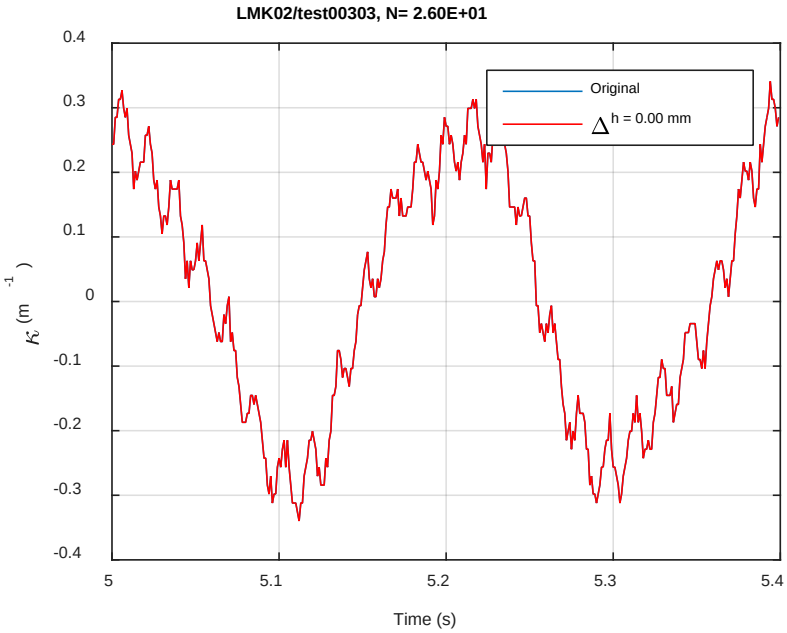
LMK02/test00303, N= 2.60E+01
Original
Δh = 0.00 mm
κ (m-1)
Time (s)

(a)

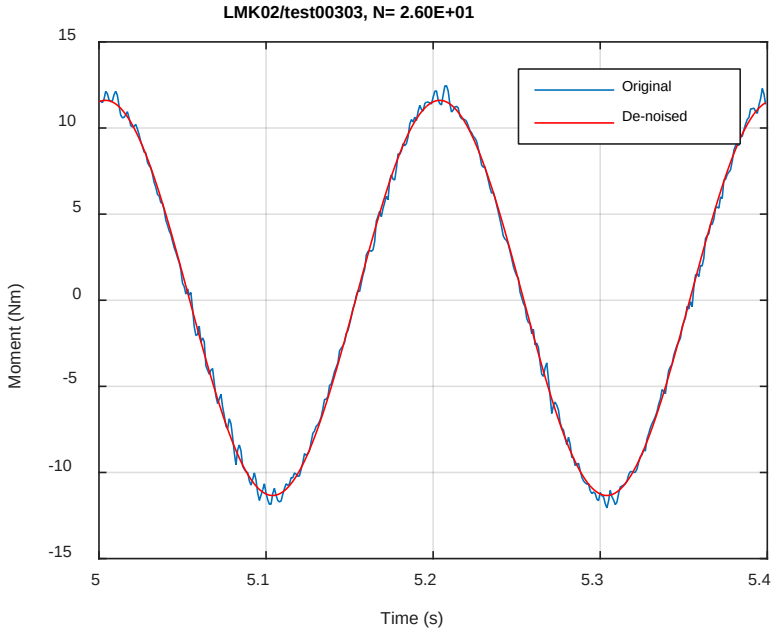
LMK02/test00303, N= 2.60E+01
Original
De-noised
Moment (Nm)
Time (s)

(b)

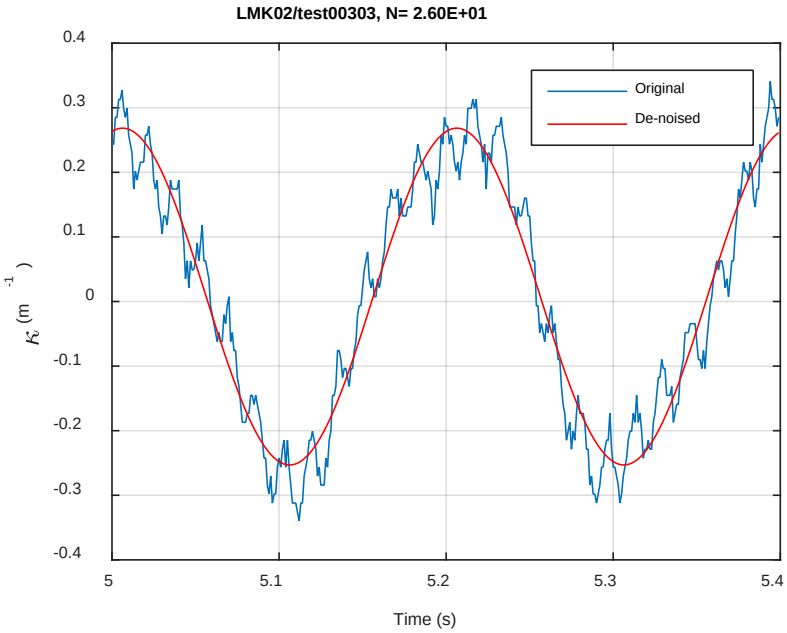

(c)

Fig. A.4. Monitoring-based responses: (a) curvature, (b) moment, (c) curvature, LMK02, 12.70 Nm, Ns = 2.60E+01 cycles.

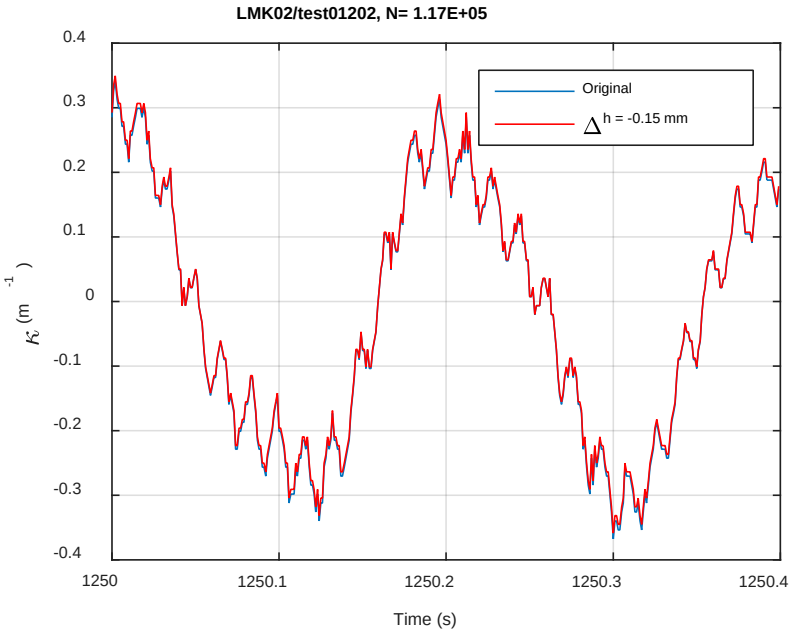
LMK02/test01202, N= 1.17E+05
Original
Δh = -0.15 mm
κ (m-1)
Time (s)
0.4
0.3
0.2
0.1
0
-0.1
-0.2
-0.3
-0.4
1250
1250.1
1250.2
1250.3
1250.4

(a)

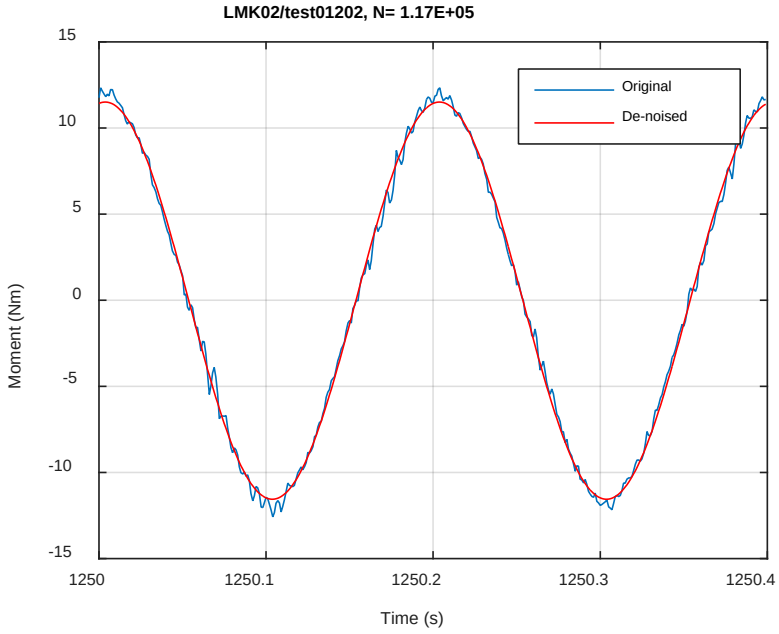
LMK02/test01202, N= 1.17E+05
Original
De-noised
Moment (Nm)
Time (s)
15
10
5
0
-5
-10
-15
1250
1250.1
1250.2
1250.3
1250.4

(b)

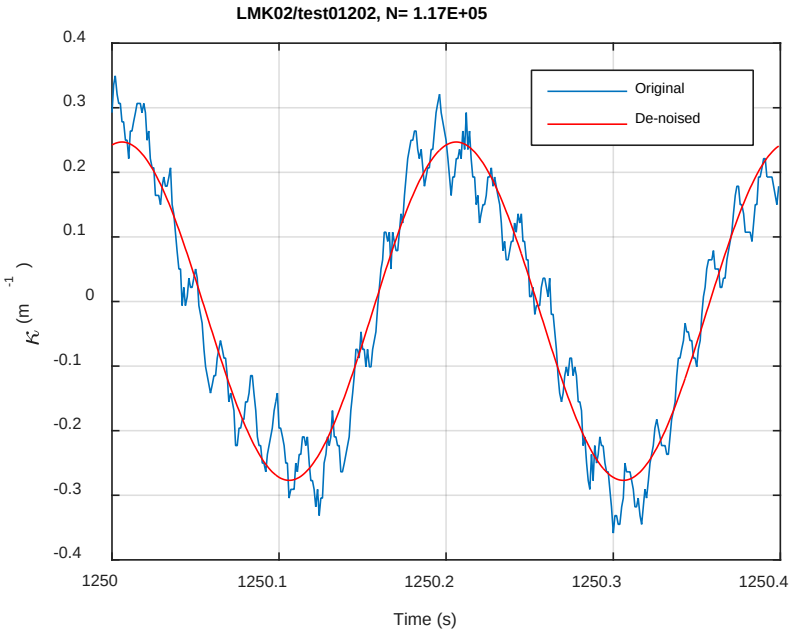

(c)

Fig. A.5. Monitoring-based responses: (a) curvature, (b) moment, (c) curvature, LMK02, 12.70 Nm, Ns = 1.17E+05 cycles.

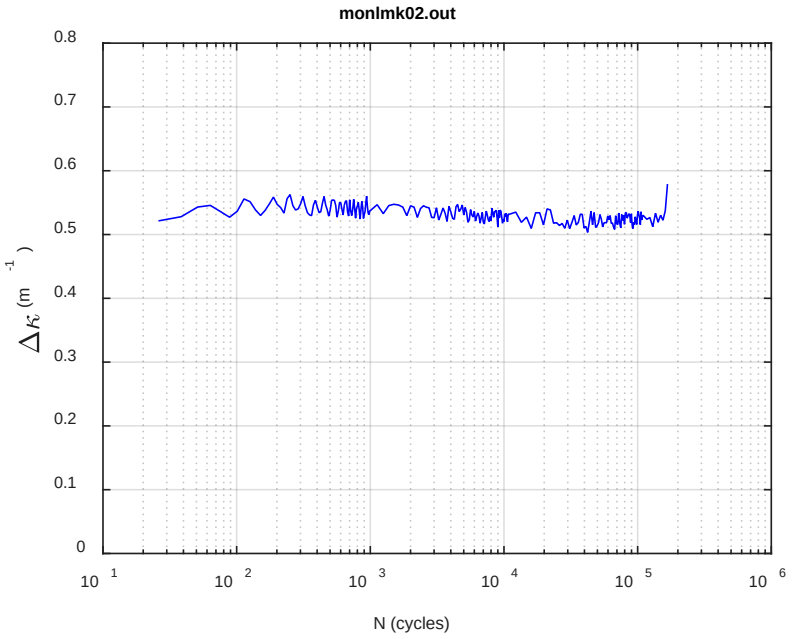
monlmk02.out
0.8
0.7
0.6
0.5
0.4
0.3
0.2
0.1
0
Δκ (m -1)
10 1
10 2
10 3
10 4
10 5
10 6
N (cycles)

(a)

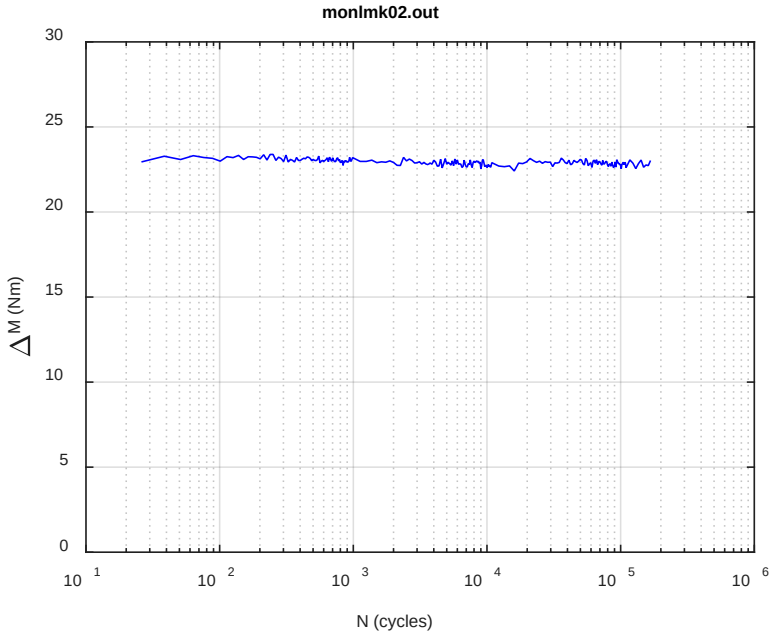
monlmk02.out
30
25
20
15
10
5
0
Δ M (Nm)
10 1
10 2
10 3
10 4
10 5
10 6
N (cycles)

(b)

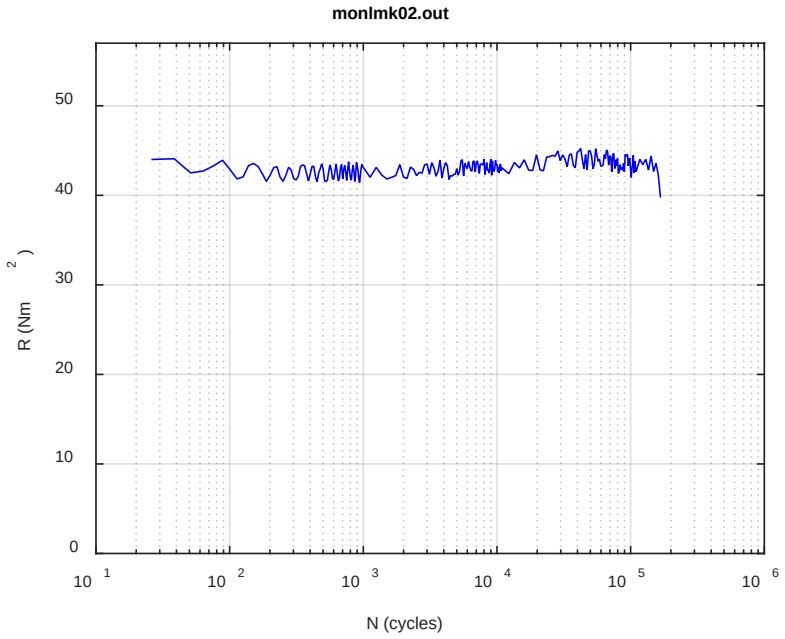
monlmk02.out
R (Nm 2)
N (cycles)

(c)

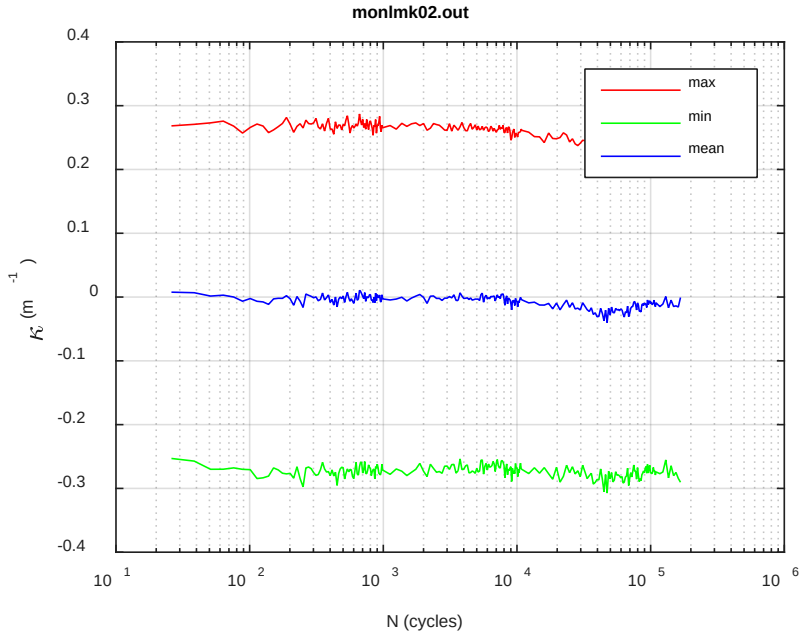
monlmk02.out
max
min
mean
κ (m -1)
N (cycles)

(d)

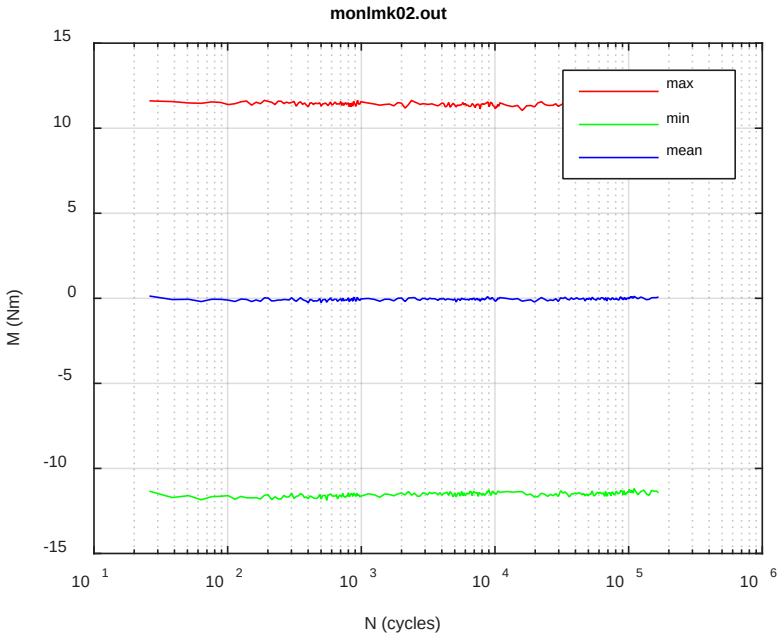

(e)

Fig. A.6. Monitoring-based responses: (a) curvature range, (b) moment range, (c) rigidity, (d) curvature peak/valley, (e) moment peak/valley, LMK02, 12.70 Nm, Nf = 1.71E+05 cycles.

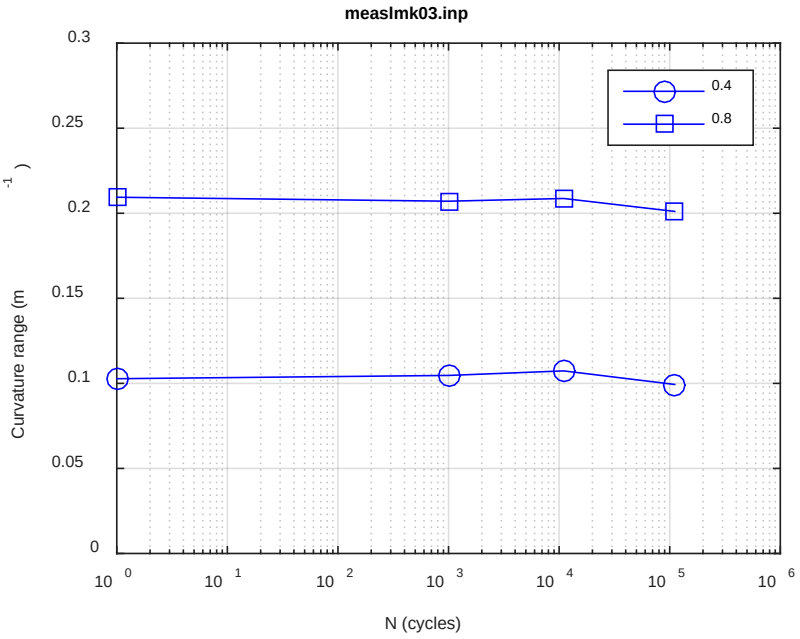
measlmk03.inp
0.3
0.25
0.2
0.15
0.1
0.05
0
Curvature range (m-1)
0.4
0.8
10 0
10 1
10 2
10 3
10 4
10 5
10 6
N (cycles)

(a)

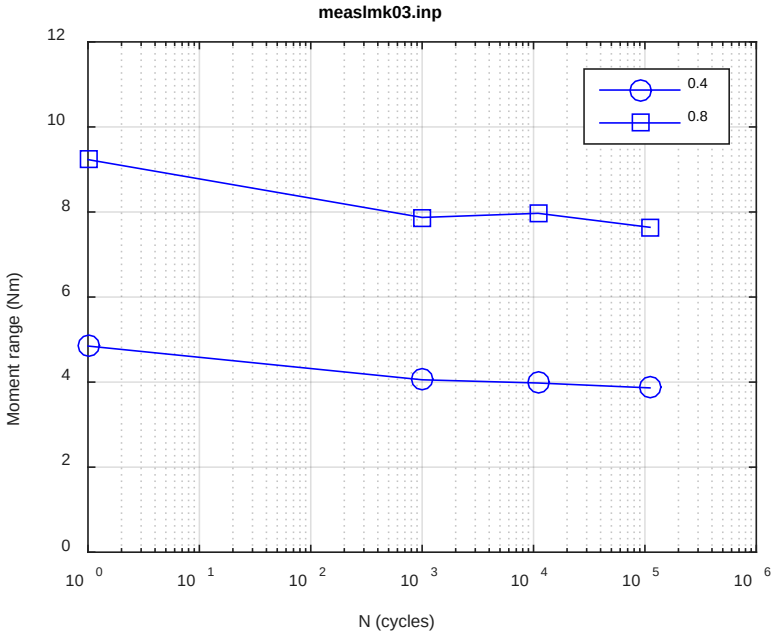
measlmk03.inp
12
10
8
6
4
2
0
Moment range (Nm)
0.4
0.8
10 0
10 1
10 2
10 3
10 4
10 5
10 6
N (cycles)

(b)

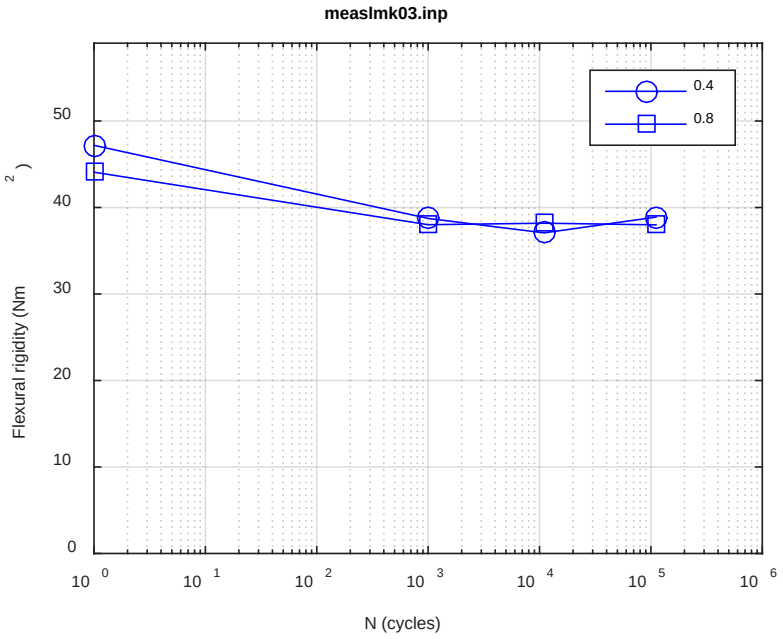
measlmk03.inp
0.4
0.8
Flexural rigidity (Nm 2)
N (cycles)

(c)

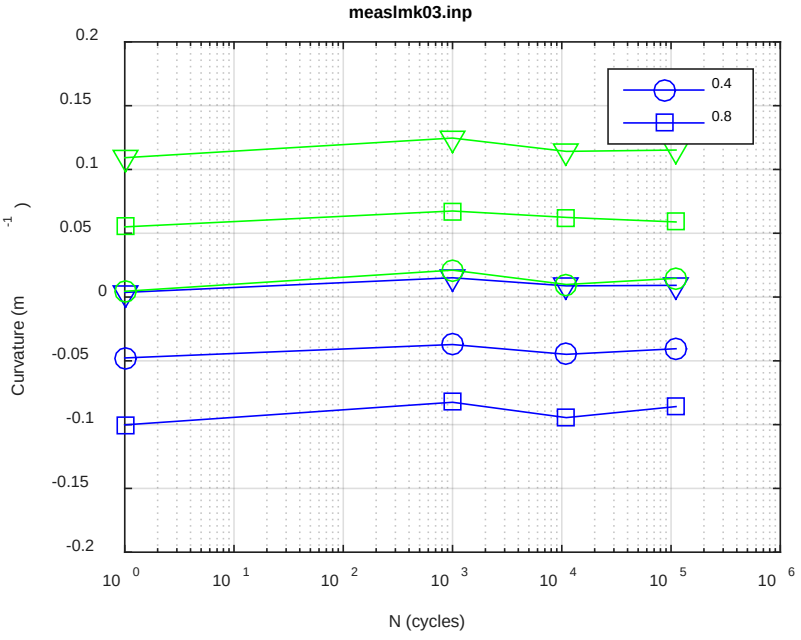
measlmk03.inp
0.4
0.8
Curvature (m -1)
N (cycles)

(d)

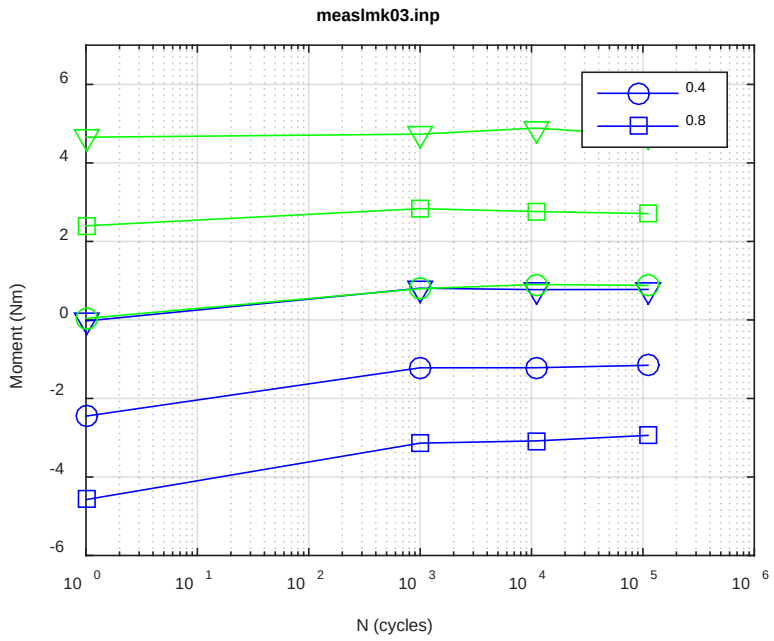

(e)

Fig. A.7. Measurement-based responses: (a) curvature range, (b) moment range, (c) rigidity, (d) curvature peak/valley, (e) moment peak/valley, LMK03, 10.16 Nm.

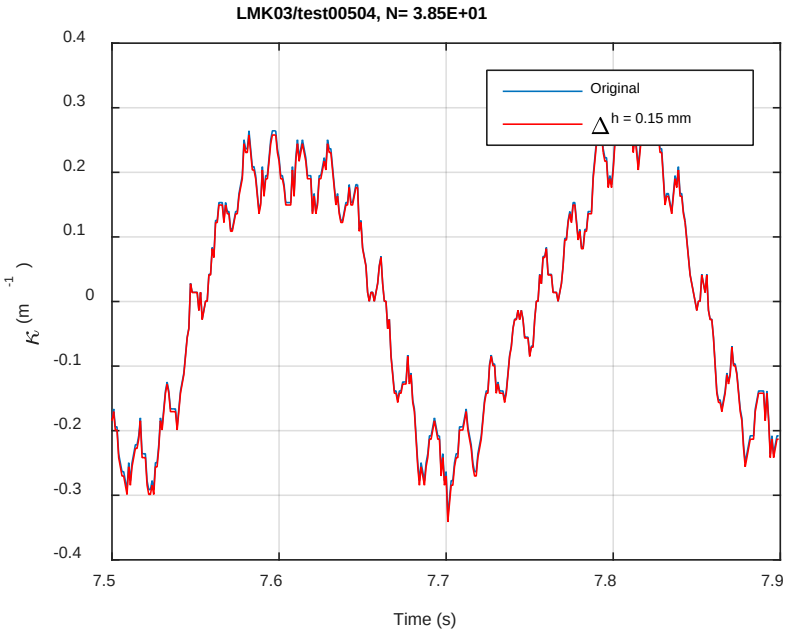
LMK03/test00504, N= 3.85E+01
Original
Δh = 0.15 mm
κ (m-1)
Time (s)

(a)

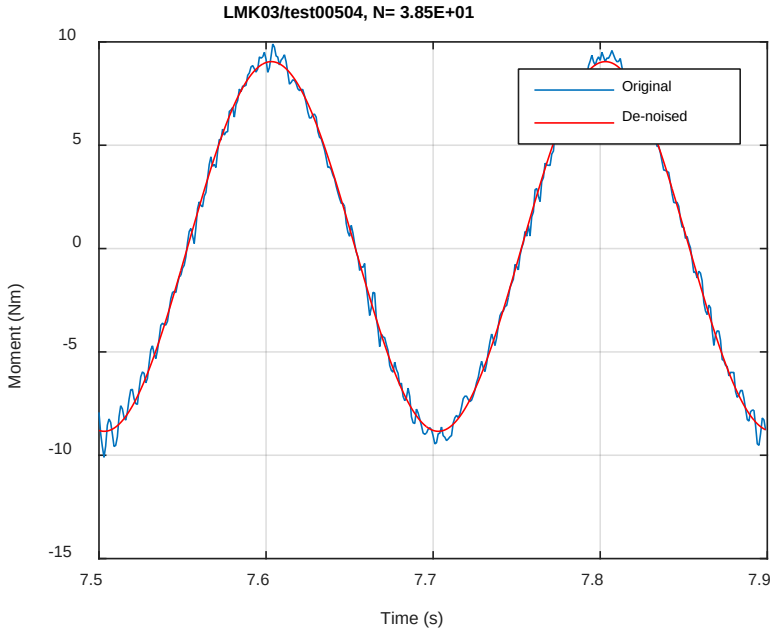
LMK03/test00504, N= 3.85E+01
Original
De-noised
Moment (Nm)
Time (s)

(b)

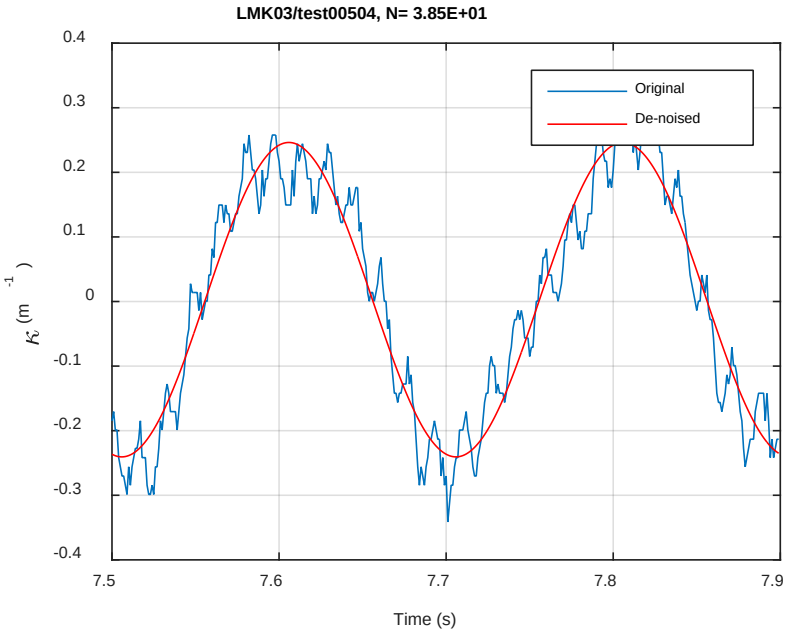

(c)

Fig. A.8. Monitoring-based responses: (a) curvature, (b) moment, (c) curvature, LMK03, 10.16 Nm, Ns = 3.85E+01 cycles.

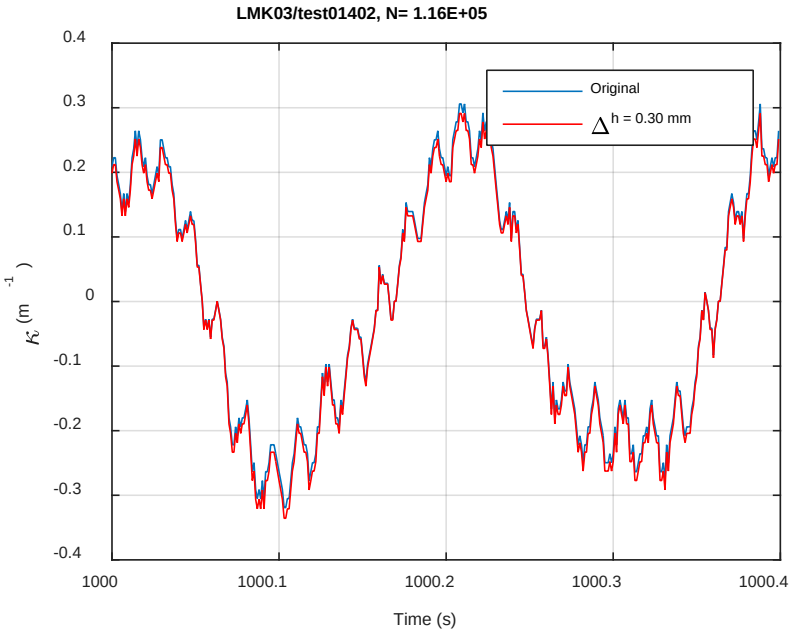
LMK03/test01402, N= 1.16E+05
Original
Δh = 0.30 mm
κ (m-1)
Time (s)
0.4
0.3
0.2
0.1
0
-0.1
-0.2
-0.3
-0.4
1000
1000.1
1000.2
1000.3
1000.4

(a)

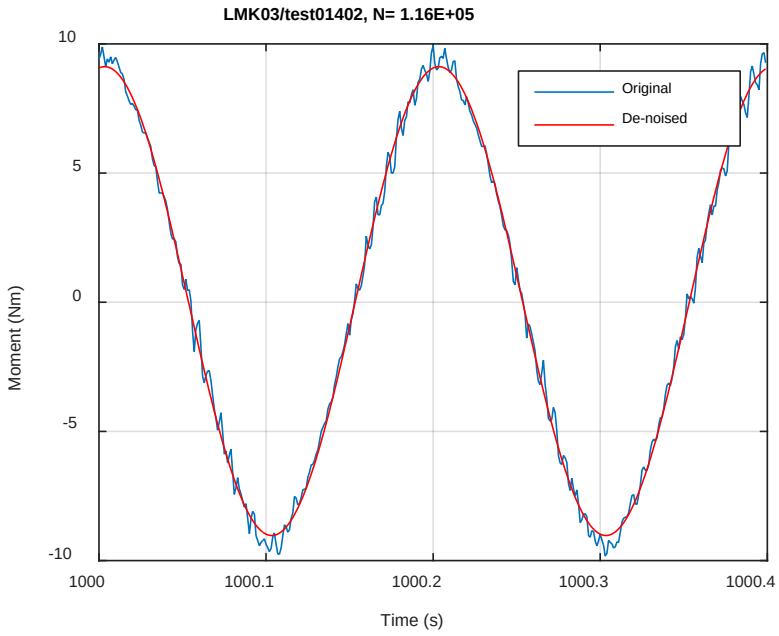
LMK03/test01402, N= 1.16E+05
Original
De-noised
Moment (Nm)
Time (s)
10
5
0
-5
-10
1000
1000.1
1000.2
1000.3
1000.4

(b)

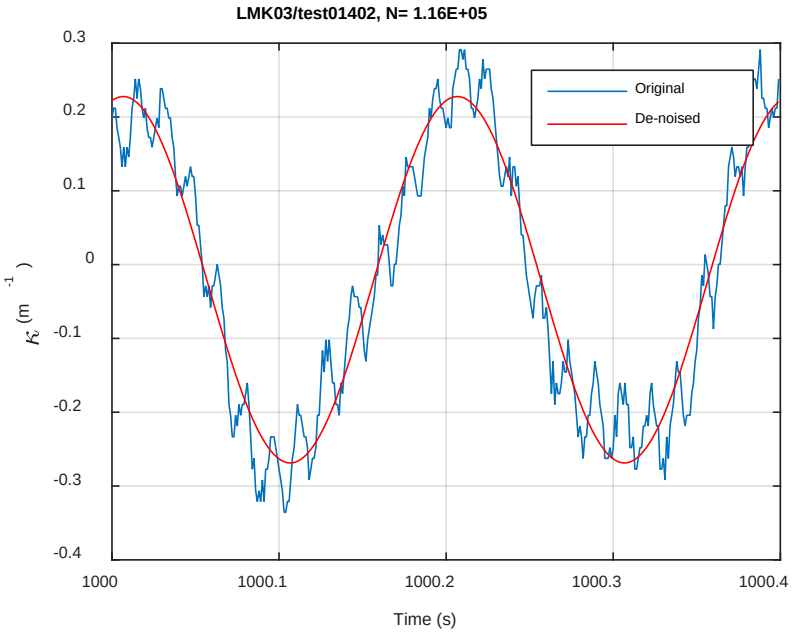

(c)

Fig. A.9. Monitoring-based responses: (a) curvature, (b) moment, (c) curvature, LMK03, 10.16 Nm, Ns = 1.16E+05 cycles.

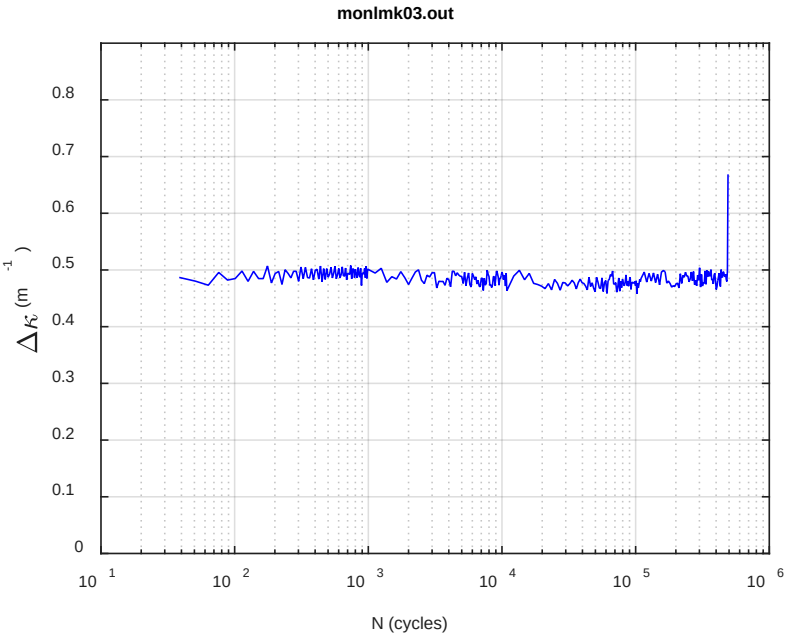
monlmk03.out
0.8
0.7
0.6
0.5
0.4
0.3
0.2
0.1
0
Δκ (m-1)
10 1
10 2
10 3
10 4
10 5
10 6
N (cycles)

(a)

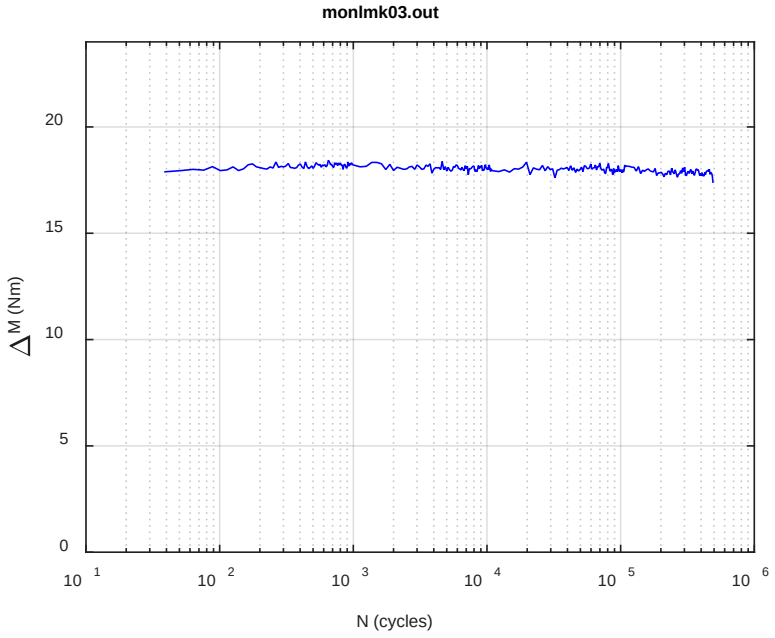
monlmk03.out
20
15
10
5
0
Δ M (Nm)
10 1
10 2
10 3
10 4
10 5
10 6
N (cycles)

(b)

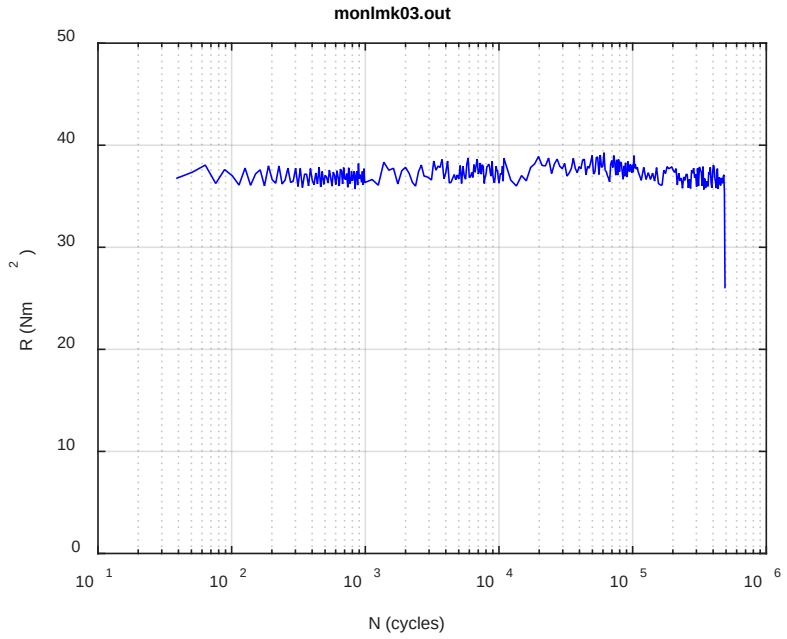
monlmk03.out
R (Nm 2)
N (cycles)

(c)

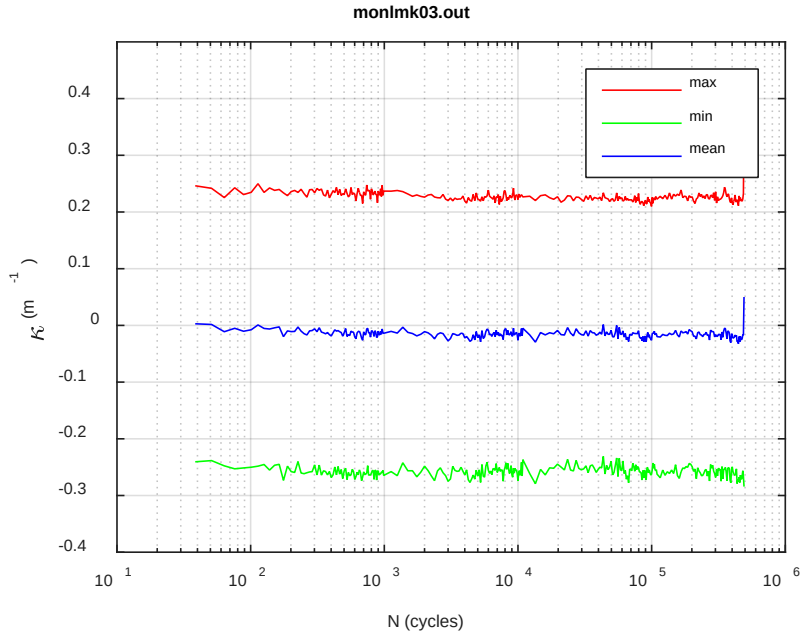
monlmk03.out
max
min
mean
κ (m -1)
N (cycles)

(d)

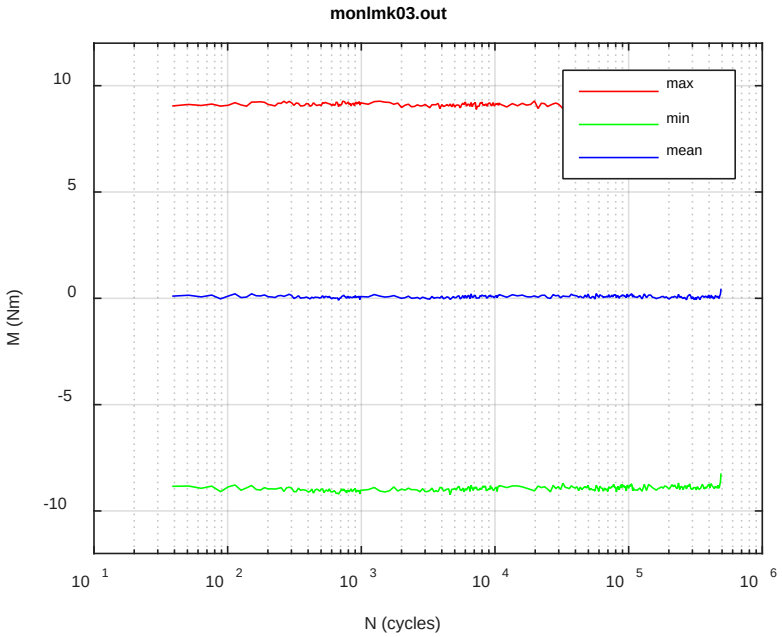

(e)

Fig. A.10. Monitoring-based responses: (a) curvature range, (b) moment range, (c) rigidity, (d) curvature peak/valley, (e) moment peak/valley, LMK03, 10.16 Nm, Nf = 4.92E+05 cycles.

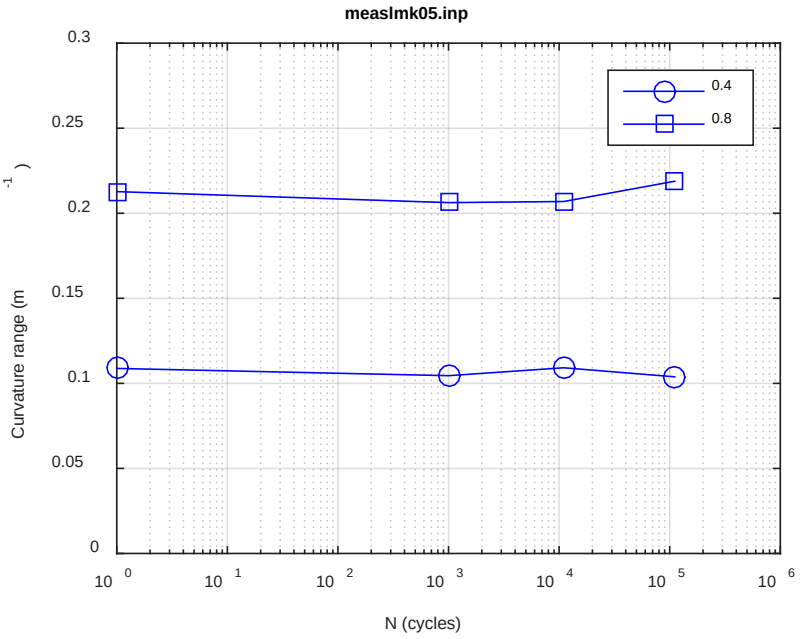
measlmk05.inp
0.3
0.25
0.2
0.15
0.1
0.05
0
Curvature range (m -1)
0.4
0.8
10 0
10 1
10 2
10 3
10 4
10 5
10 6
N (cycles)

(a)

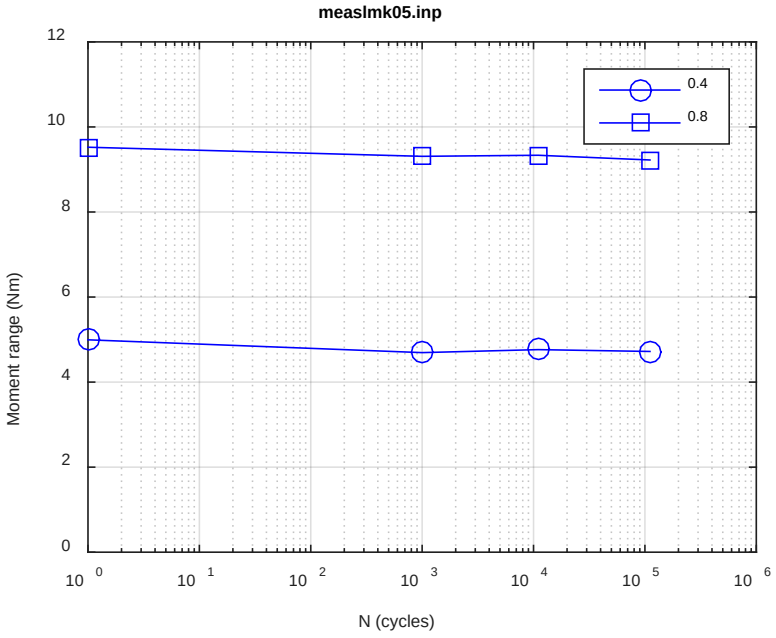
measlmk05.inp
12
10
8
6
4
2
0
Moment range (Nm)
0.4
0.8
10 0
10 1
10 2
10 3
10 4
10 5
10 6
N (cycles)

(b)

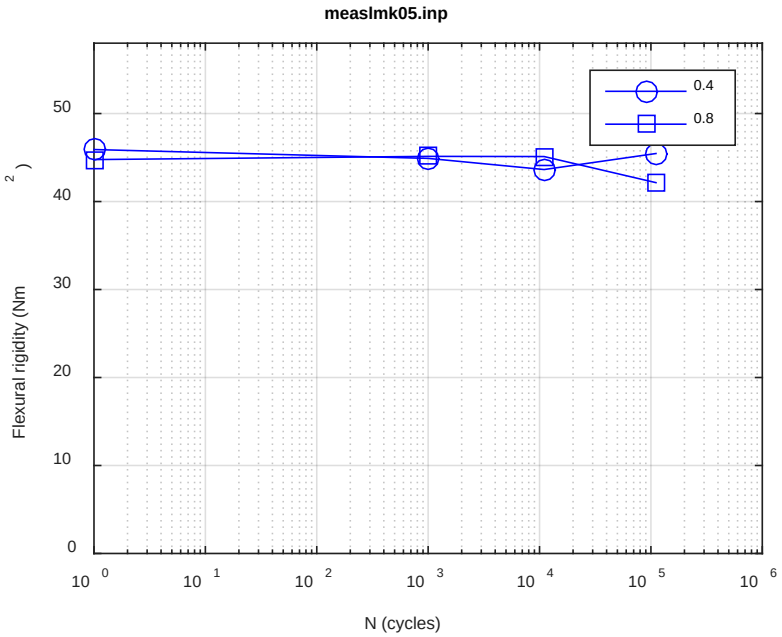
measlmk05.inp
0.4
0.8
Flexural rigidity (Nm 2)
N (cycles)

(c)

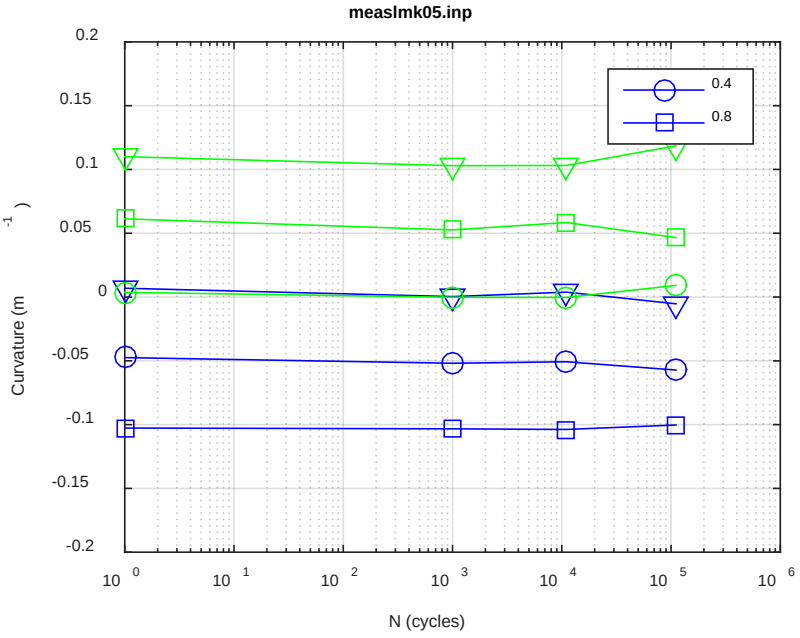
measlmk05.inp
0.4
0.8
Curvature (m -1)
N (cycles)

(d)

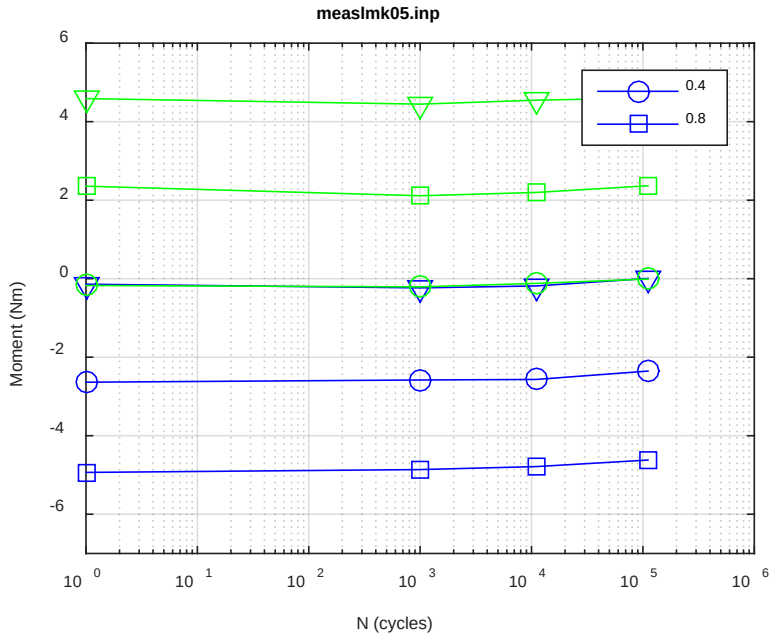

(e)

Fig. A.11. Measurement-based responses: (a) curvature range, (b) moment range, (c) rigidity, (d) curvature peak/valley, (e) moment peak/valley, LMK05, 8.64 Nm.

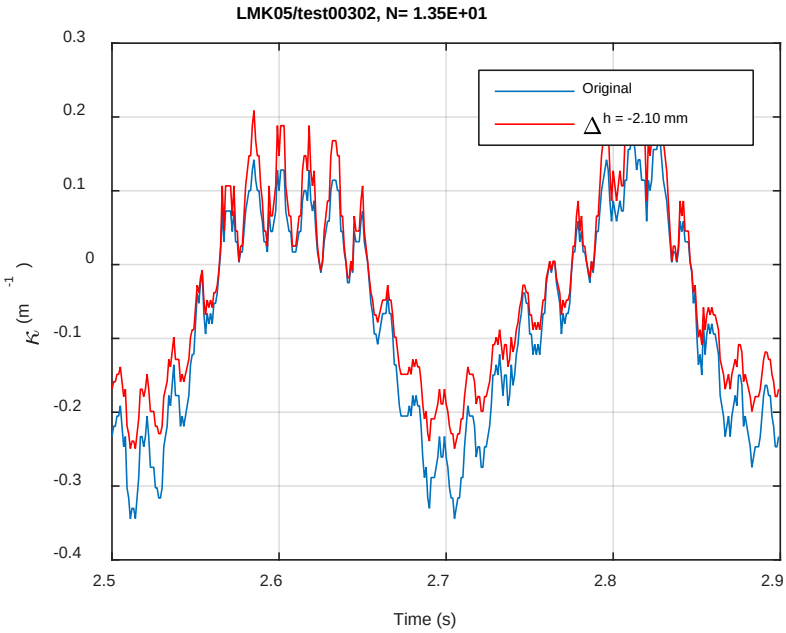
LMK05/test00302, N= 1.35E+01
Original
Δh = -2.10 mm
κ (m-1)
Time (s)

(a)

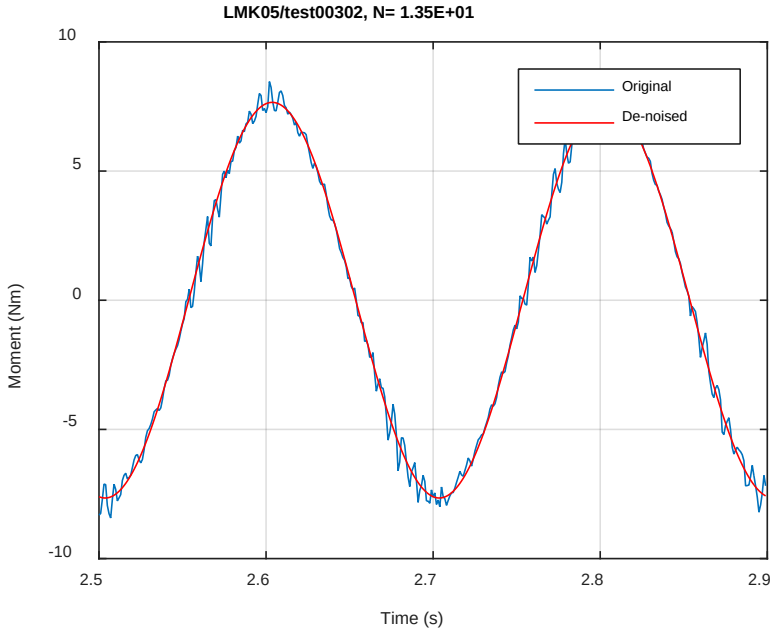
LMK05/test00302, N= 1.35E+01
Original
De-noised
Moment (Nm)
Time (s)

(b)

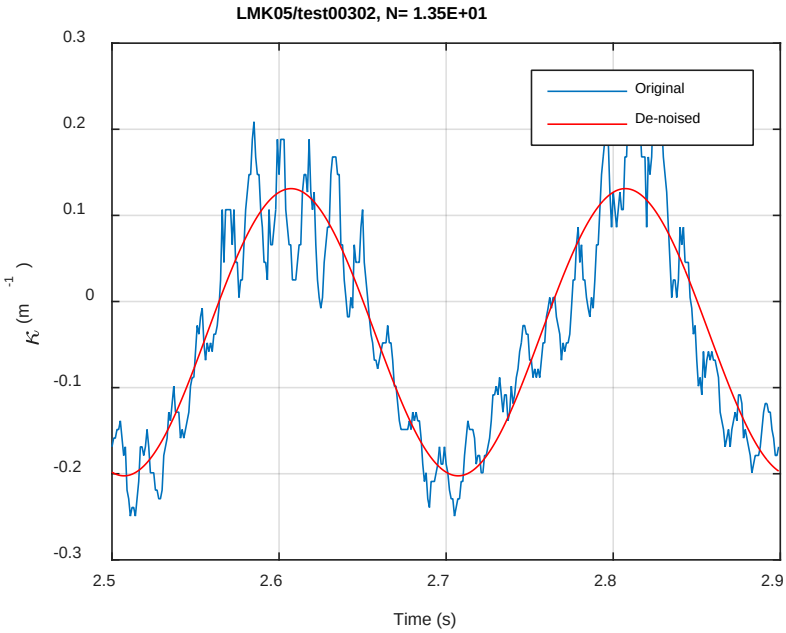

(c)

Fig. A.12. Monitoring-based responses: (a) curvature, (b) moment, (c) curvature, LMK05, 8.64 Nm, Ns = 1.35E+01 cycles.

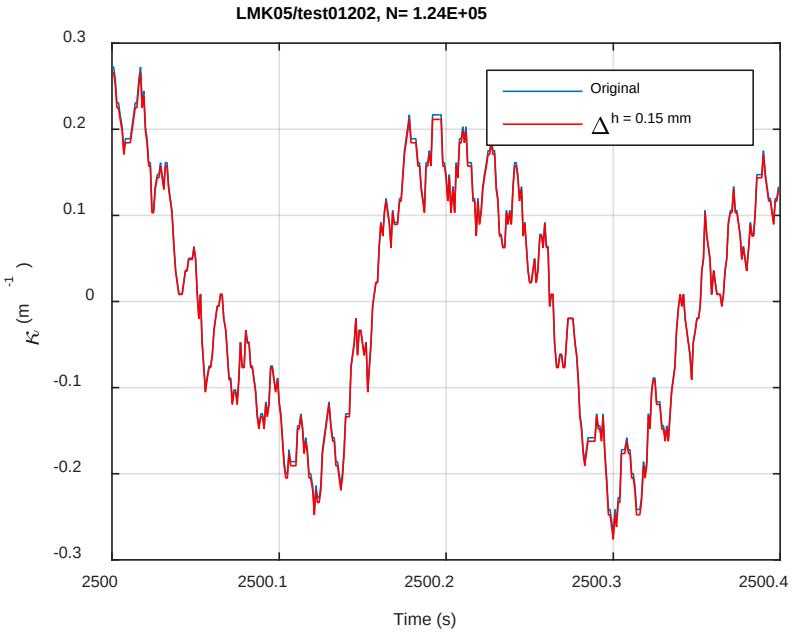
LMK05/test01202, N= 1.24E+05
Original
Δh = 0.15 mm
κ (m-1)
Time (s)
0.3
0.2
0.1
0
-0.1
-0.2
-0.3
2500
2500.1
2500.2
2500.3
2500.4

(a)

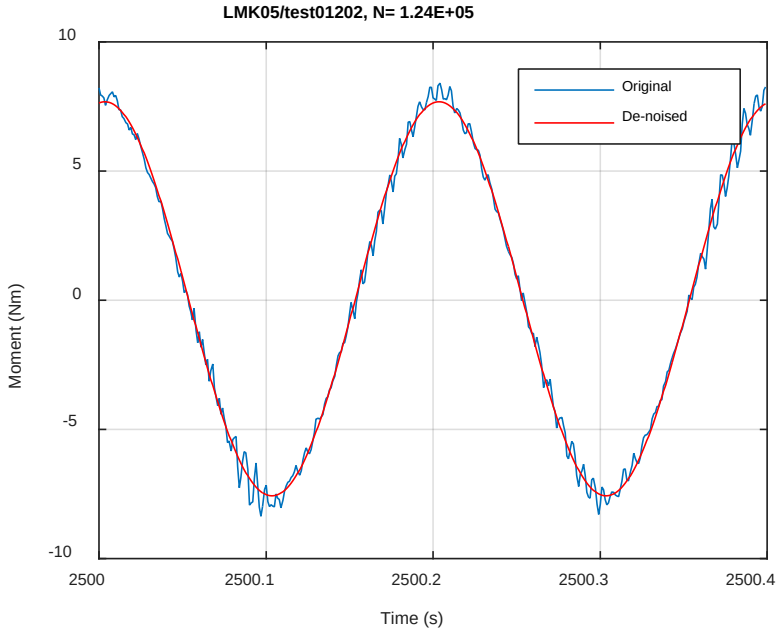
LMK05/test01202, N= 1.24E+05
Original
De-noised
Moment (Nm)
Time (s)
10
5
0
-5
-10
2500
2500.1
2500.2
2500.3
2500.4

(b)

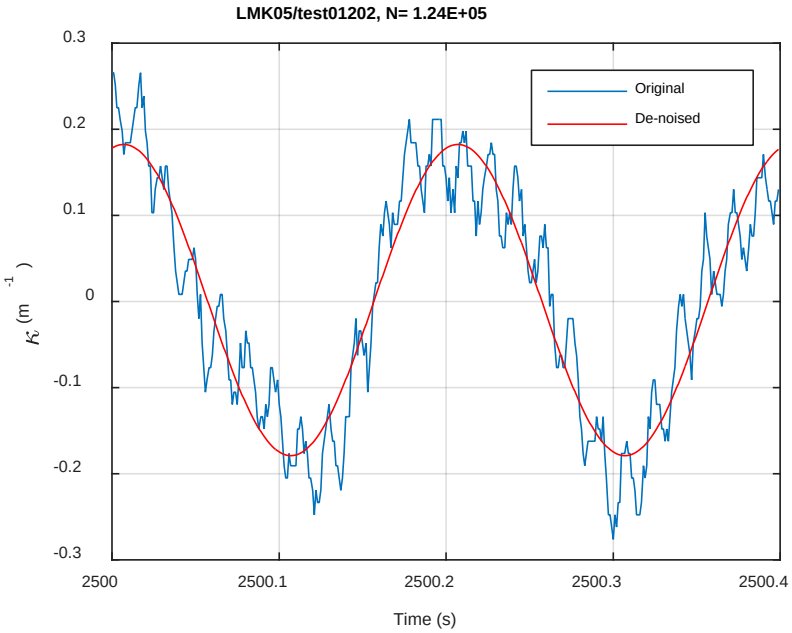

(c)

Fig. A.13. Monitoring-based responses: (a) curvature, (b) moment, (c) curvature, LMK05, 8.64 Nm, Ns = 1.24E+05 cycles.

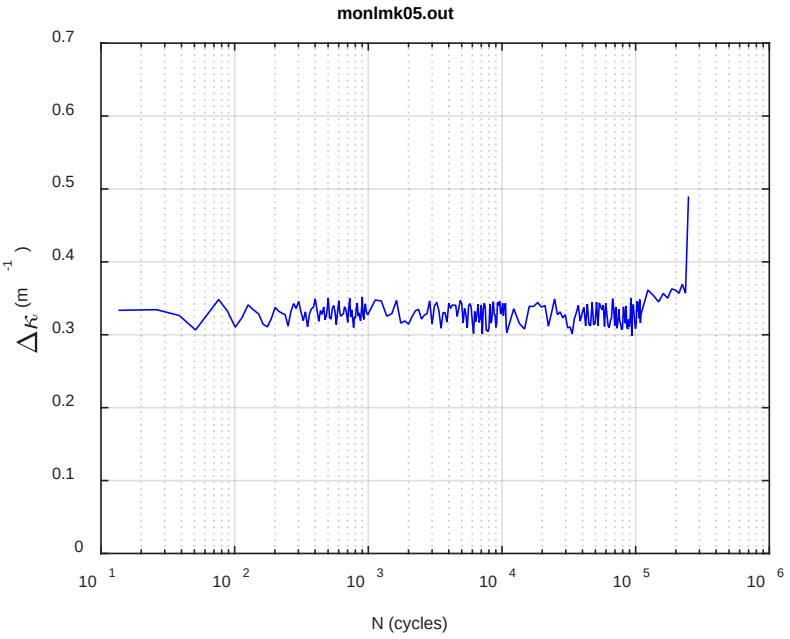
monlmk05.out
0.7
0.6
0.5
0.4
0.3
0.2
0.1
0
Δκ (m -1)
10 1
10 2
10 3
10 4
10 5
10 6
N (cycles)

(a)

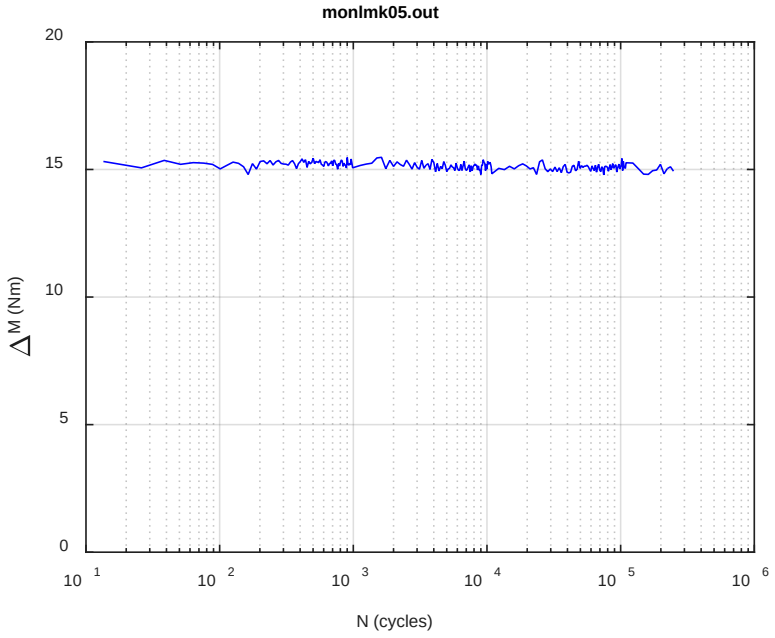
monlmk05.out
20
15
10
5
0
Δ M (Nm)
10 1
10 2
10 3
10 4
10 5
10 6
N (cycles)

(b)

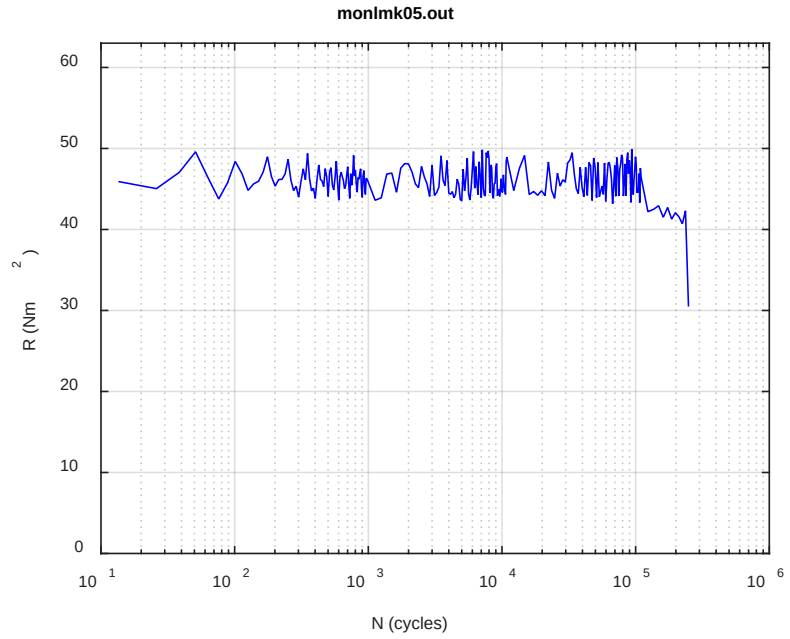
monlmk05.out
R (Nm 2)
N (cycles)

(c)

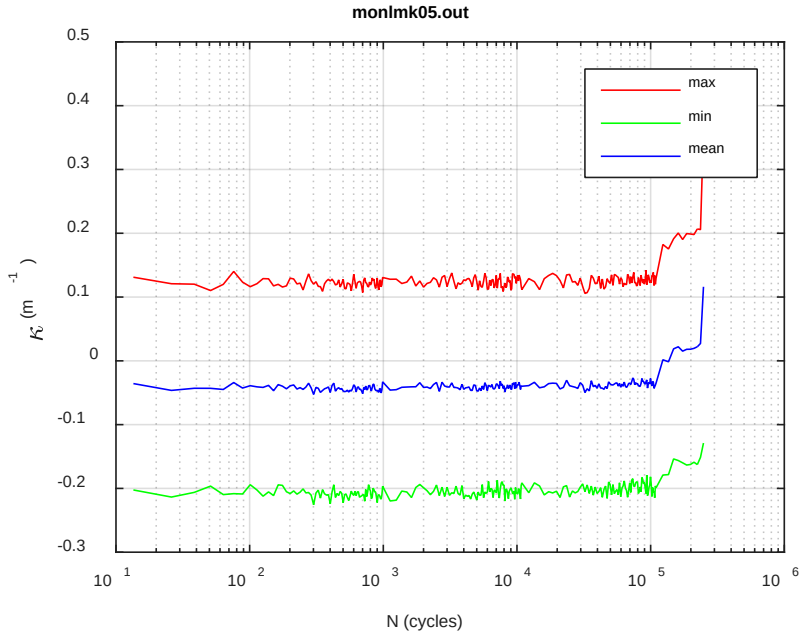
monlmk05.out
max
min
mean
κ (m -1)
N (cycles)

(d)

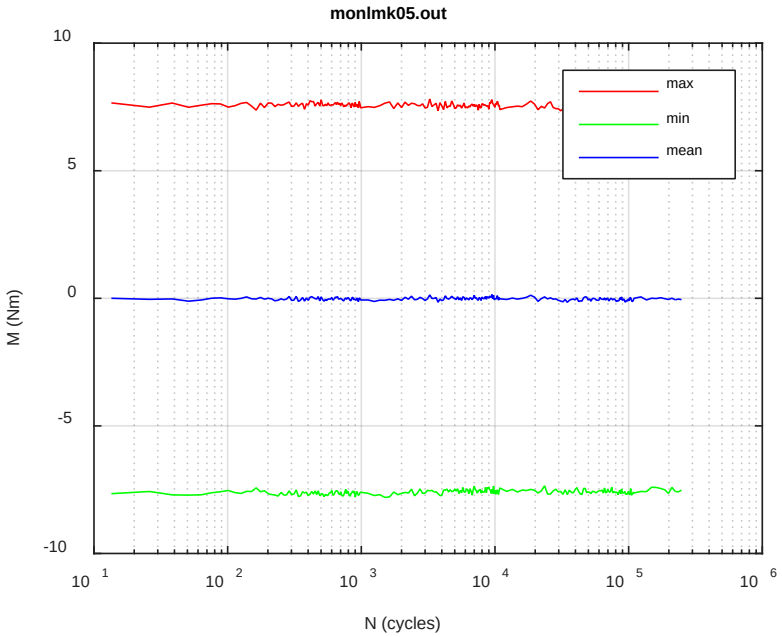

(e)

Fig. A.14. Monitoring-based responses: (a) curvature range, (b) moment range, (c) rigidity, (d) curvature peak/valley, (e) moment peak/valley, LMK05, 8.64 Nm, Nf = 2.49E+05 cycles.

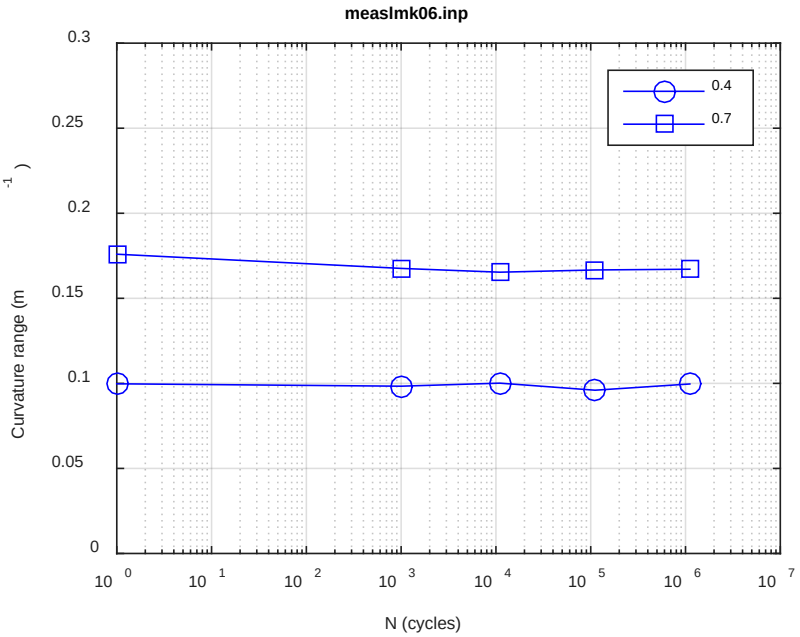
measlmk06.inp
0.3
0.25
0.2
0.15
0.1
0.05
0
Curvature range (m-1)
0.4
0.7
10 0
10 1
10 2
10 3
10 4
10 5
10 6
10 7
N (cycles)

(a)

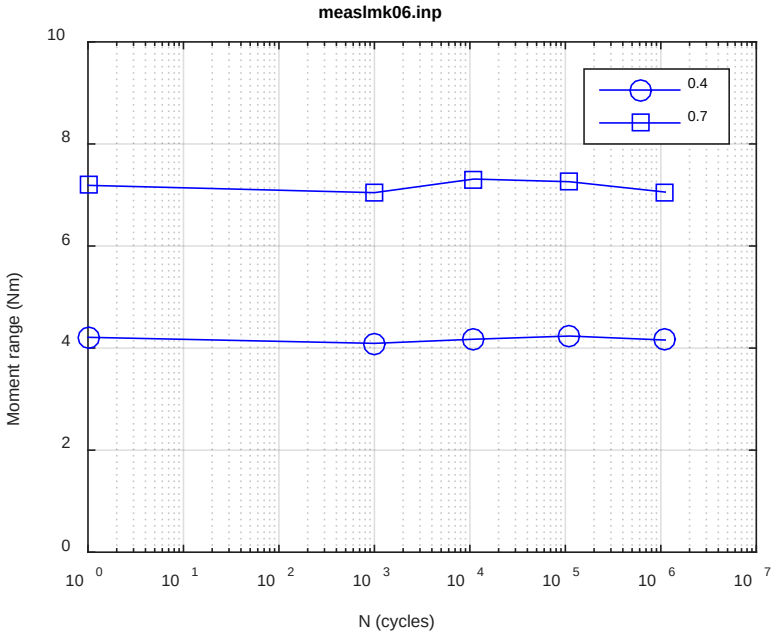
measlmk06.inp
10
8
6
4
2
0
Moment range (Nm)
0.4
0.7
10 0
10 1
10 2
10 3
10 4
10 5
10 6
10 7
N (cycles)

(b)

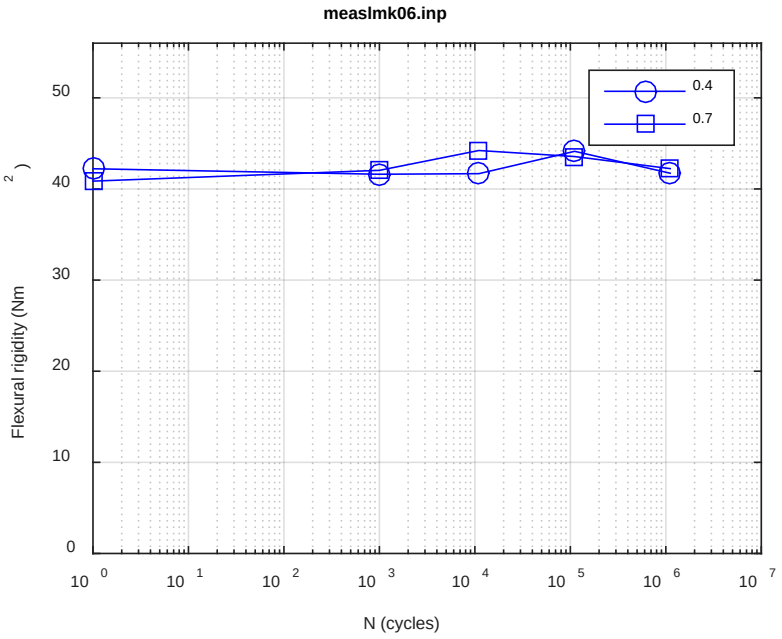
measlmk06.inp
0.4
0.7
Flexural rigidity (Nm 2)
N (cycles)

(c)

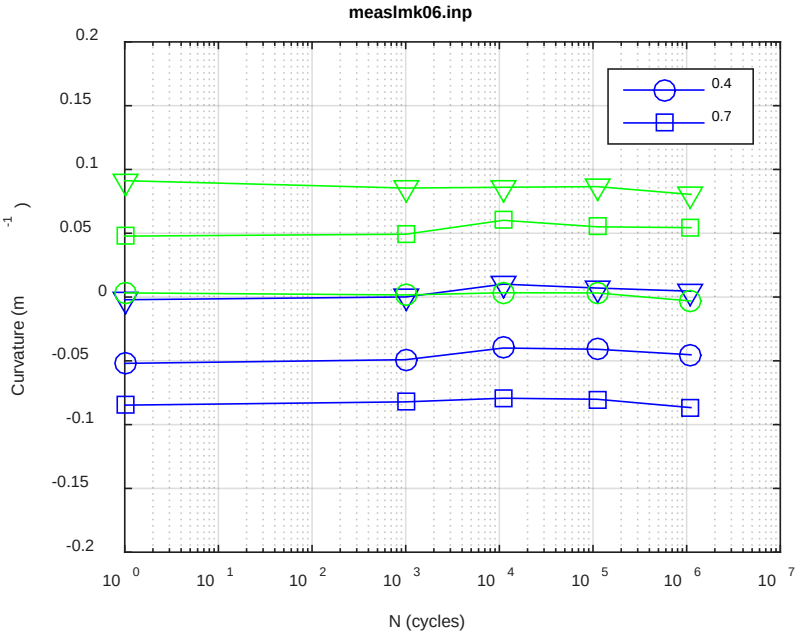
measlmk06.inp
0.4
0.7
Curvature (m -1)
N (cycles)

(d)

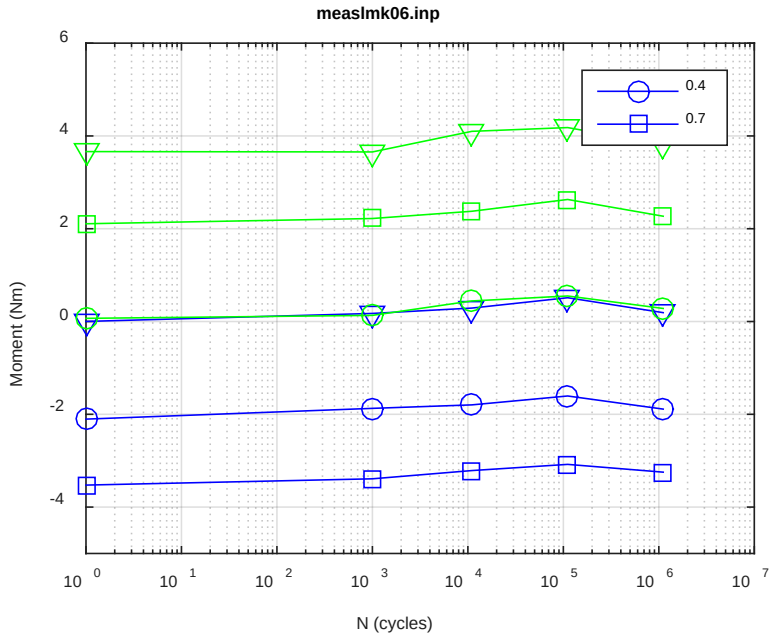

(e)

Fig. A.15. Measurement-based responses: (a) curvature range, (b) moment range, (c) rigidity, (d) curvature peak/valley, (e) moment peak/valley, LMK06, 7.62 Nm.

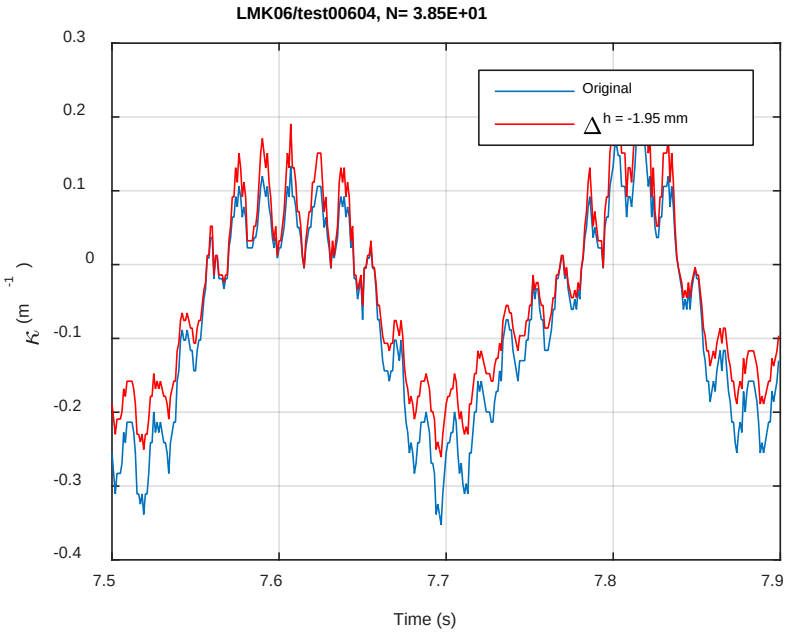
LMK06/test00604, N= 3.85E+01
Original
Δh = -1.95 mm
κ (m-1)
Time (s)

(a)

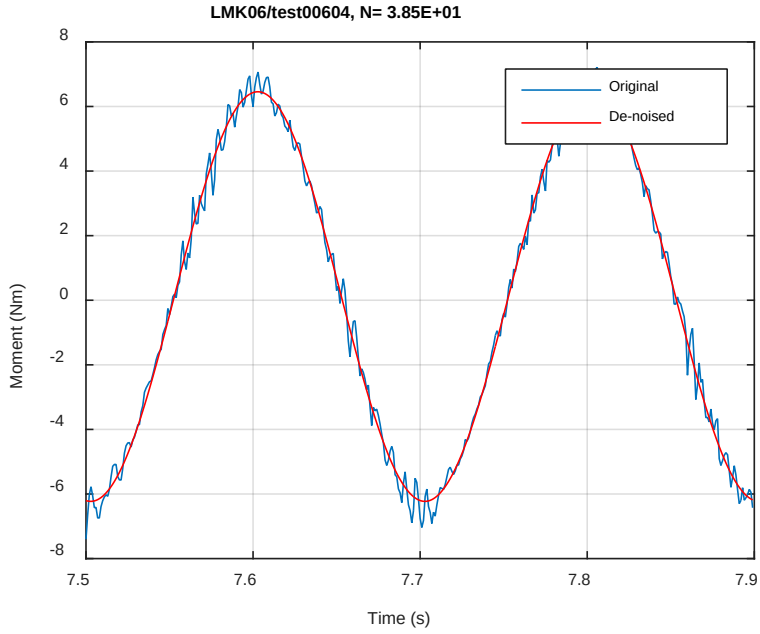
LMK06/test00604, N= 3.85E+01
Original
De-noised
Moment (Nm)
Time (s)

(b)

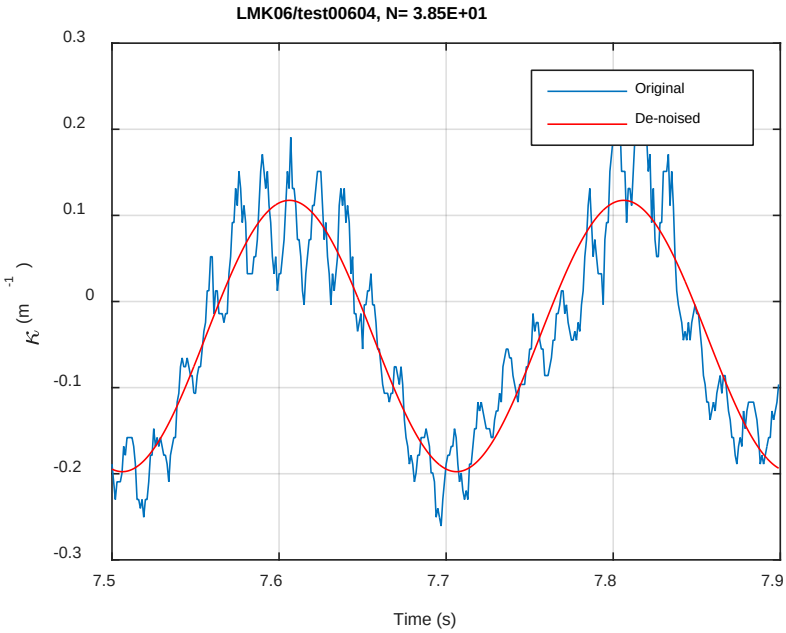

(c)

Fig. A.16. Monitoring-based responses: (a) curvature, (b) moment, (c) curvature, LMK06, 7.62 Nm, Ns = 3.85E+01 cycles.

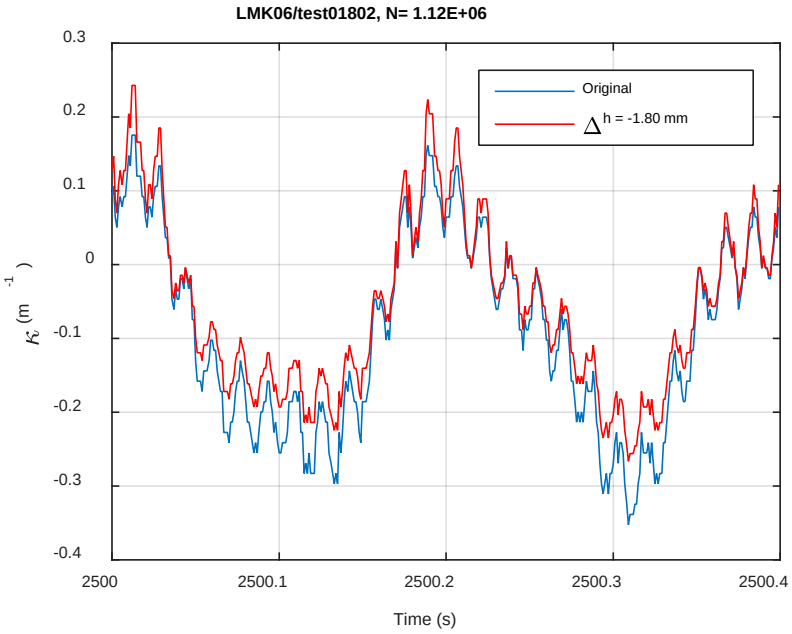
LMK06/test01802, N= 1.12E+06
Original
Δh = -1.80 mm
κ (m-1)
Time (s)
0.3
0.2
0.1
0
-0.1
-0.2
-0.3
-0.4
2500
2500.1
2500.2
2500.3
2500.4

(a)

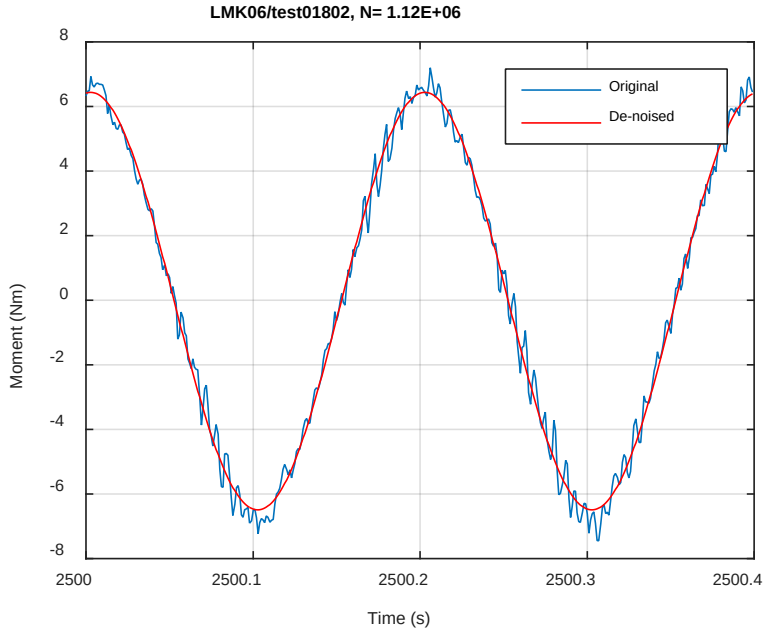
LMK06/test01802, N= 1.12E+06
Original
De-noised
Moment (Nm)
Time (s)
8
6
4
2
0
-2
-4
-6
-8
2500
2500.1
2500.2
2500.3
2500.4

(b)

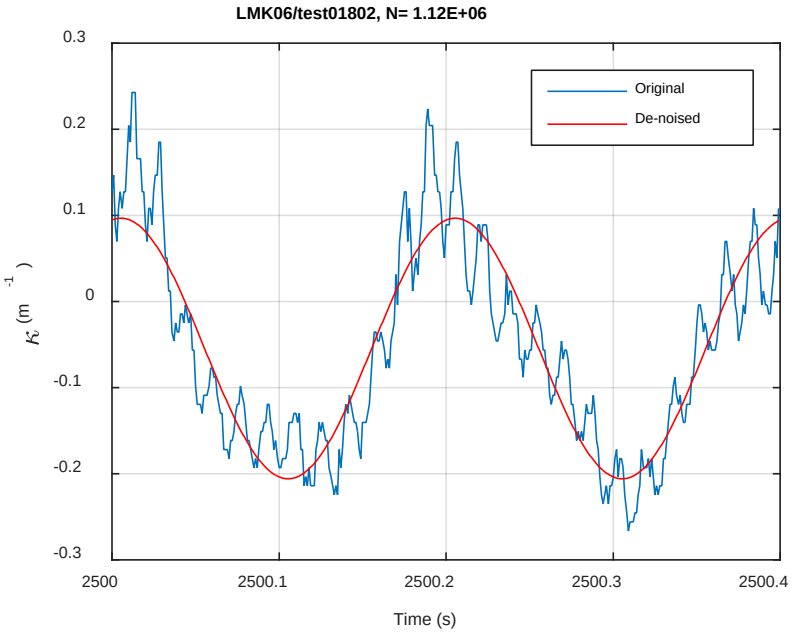

(c)

Fig. A.17. Monitoring-based responses: (a) curvature, (b) moment, (c) curvature, LMK06, 7.62 Nm, Ns = 1.12E+06 cycles.

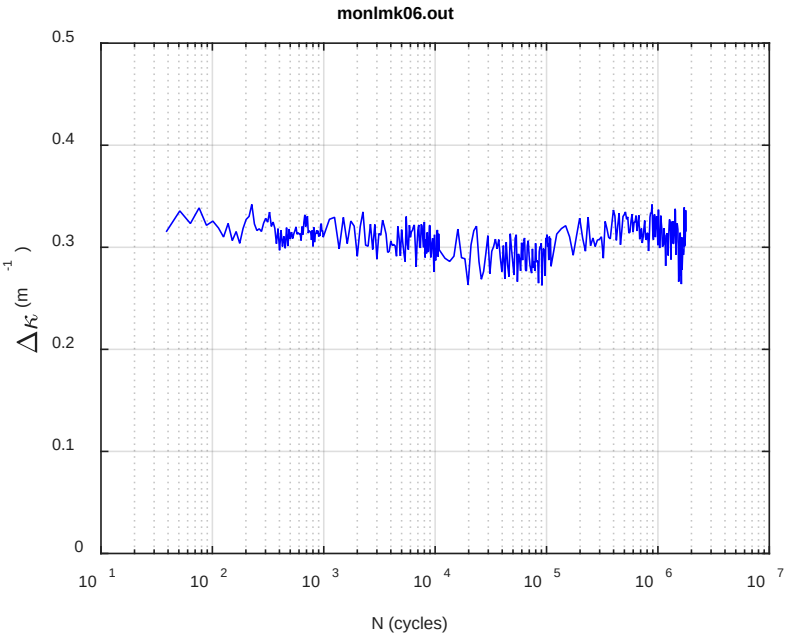
monlmk06.out
0.5
0.4
0.3
0.2
0.1
0
Δκ (m -1)
10 1
10 2
10 3
10 4
10 5
10 6
10 7
N (cycles)

(a)

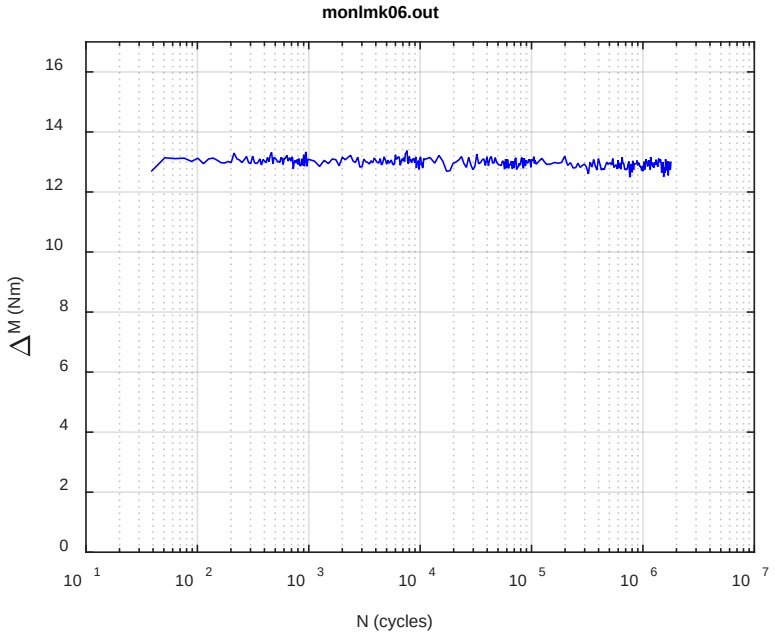
monlmk06.out
16
14
12
10
8
6
4
2
0
Δ M (Nm)
10 1
10 2
10 3
10 4
10 5
10 6
10 7
N (cycles)

(b)

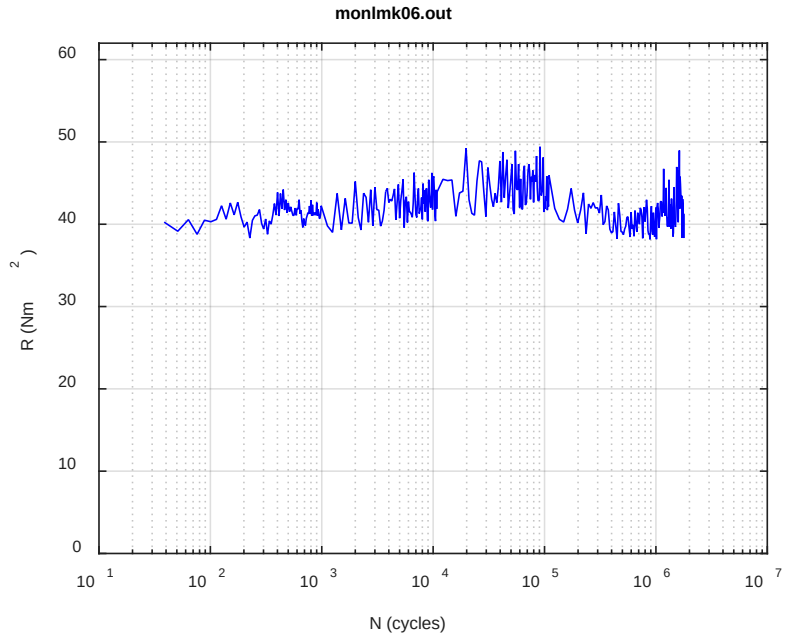
monlmk06.out
R (Nm 2)
N (cycles)

(c)

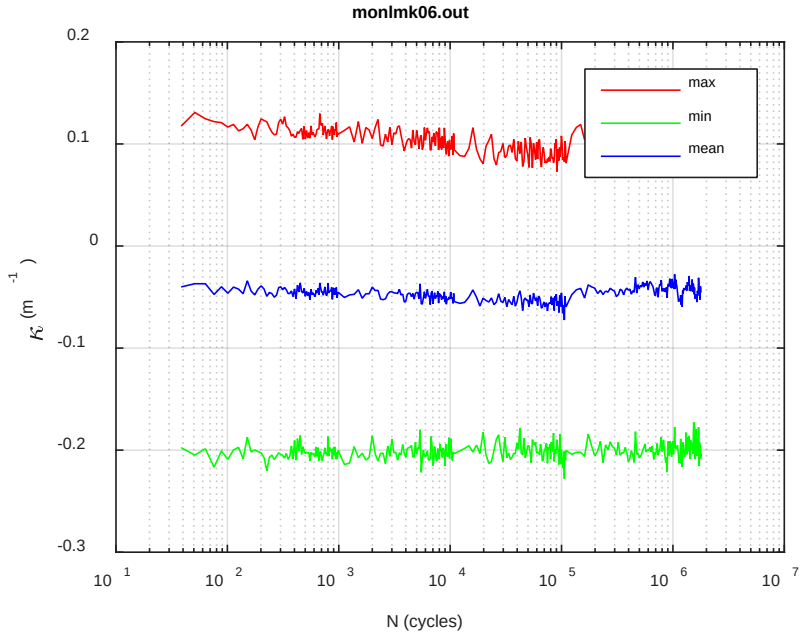
monlmk06.out
max
min
mean
κ (m -1)
N (cycles)

(d)

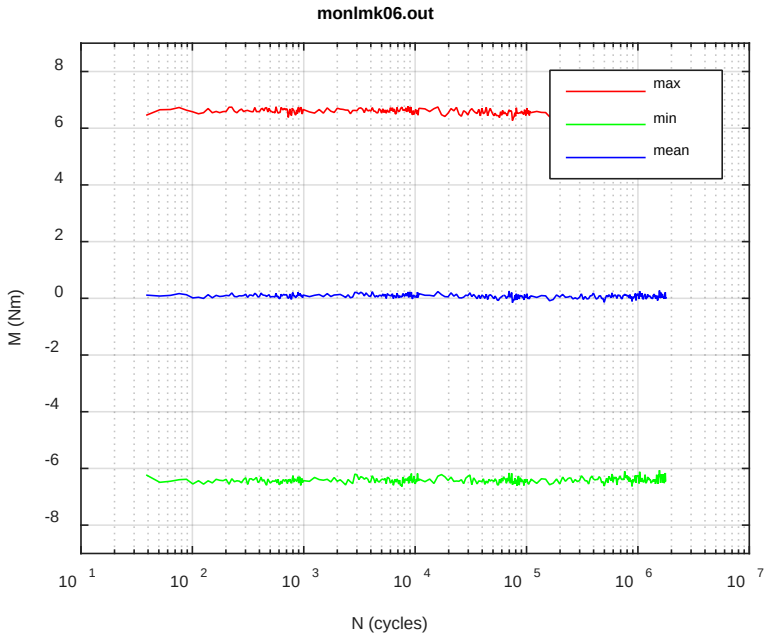

(e)

Fig. A.18. Monitoring-based responses: (a) curvature range, (b) moment range, (c) rigidity, (d) curvature peak/valley, (e) moment peak/valley, LMK06, 7.62 Nm, Nf = 1.79E+06 cycles.

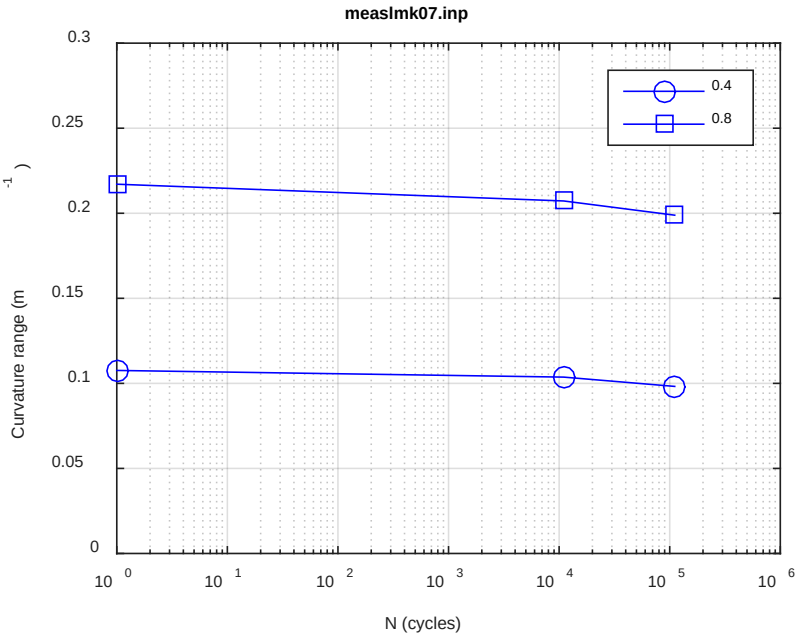
measlmk07.inp
0.3
0.25
0.2
0.15
0.1
0.05
0
Curvature range (m -1)
0.4
0.8
10 0
10 1
10 2
10 3
10 4
10 5
10 6
N (cycles)

(a)

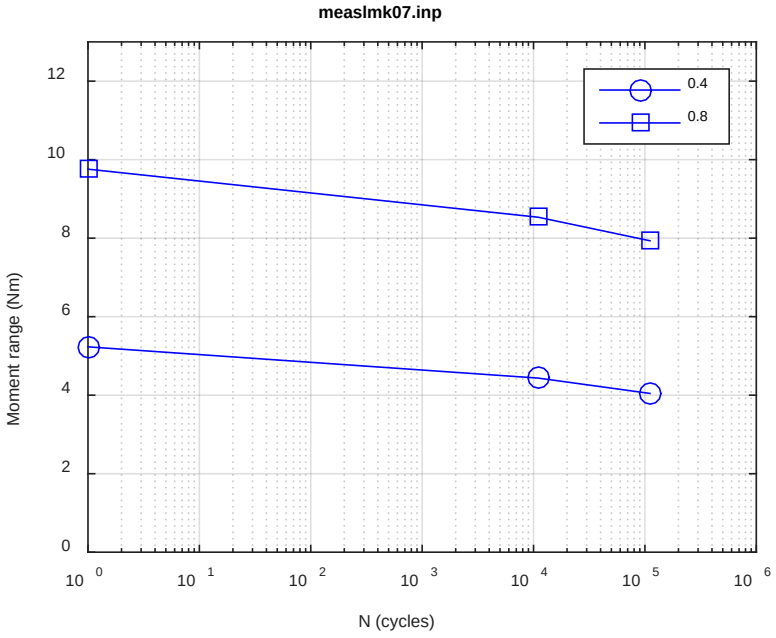
measlmk07.inp
12
10
8
6
4
2
0
Moment range (Nm)
0.4
0.8
10 0
10 1
10 2
10 3
10 4
10 5
10 6
N (cycles)

(b)

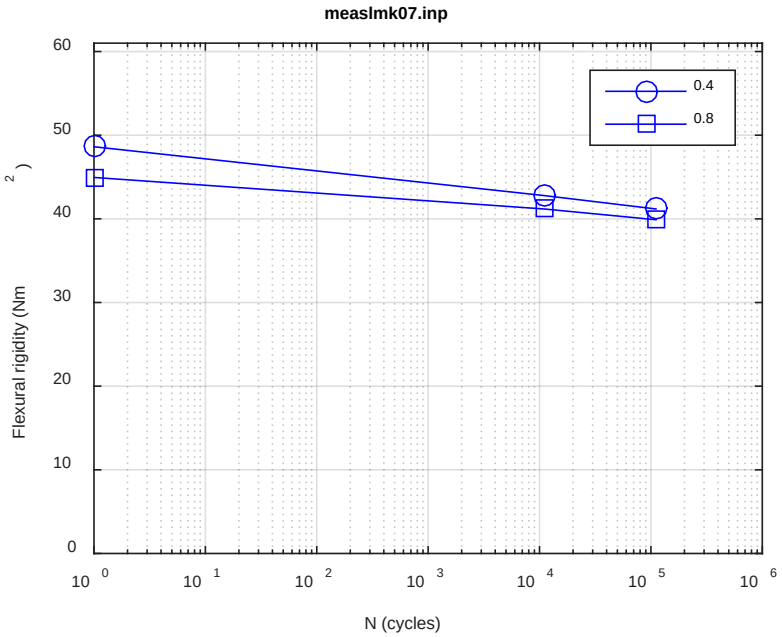
measlmk07.inp
Flexural rigidity (Nm 2)
N (cycles)
0.4
0.8

(c)

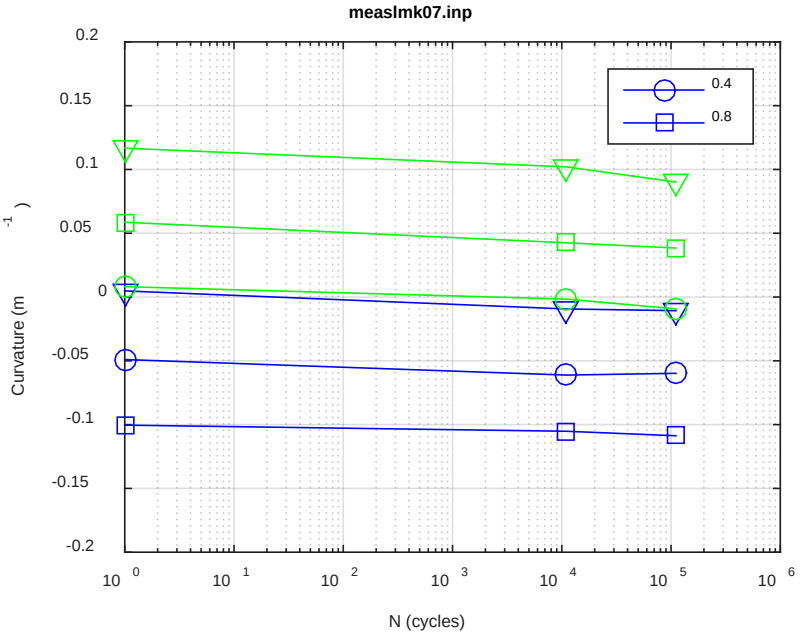
measlmk07.inp
Curvature (m -1)
N (cycles)
0.4
0.8

(d)

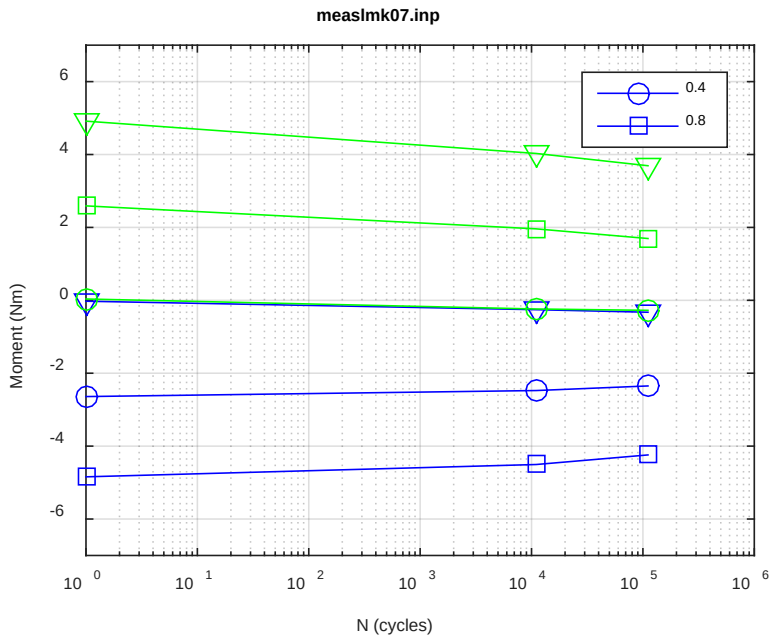

(e)

Fig. A.19. Measurement-based responses: (a) curvature range, (b) moment range, (c) rigidity, (d) curvature peak/valley, (e) moment peak/valley, LMK07, 15.24 Nm.

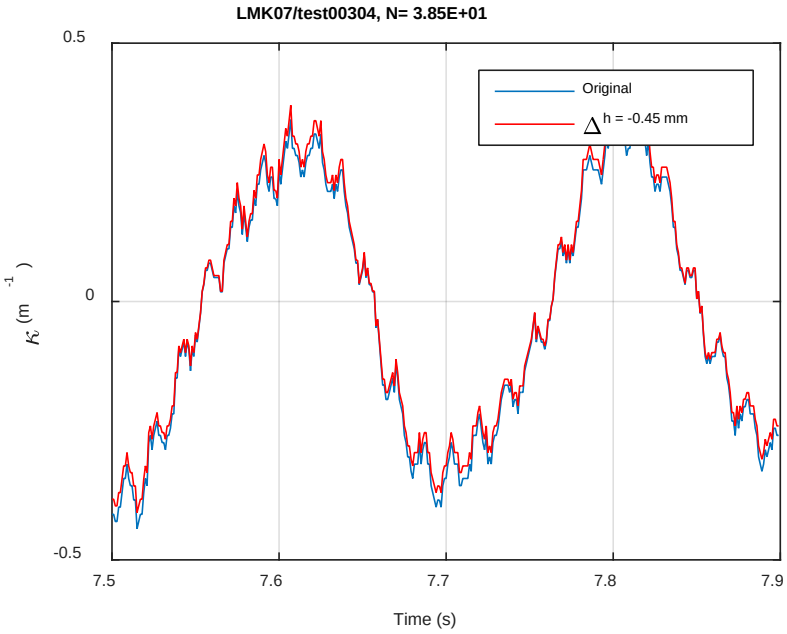
LMK07/test00304, N= 3.85E+01
Original
Δh = -0.45 mm
κ (m-1)
0.5
0
-0.5
7.5
7.6
7.7
7.8
7.9
Time (s)

(a)

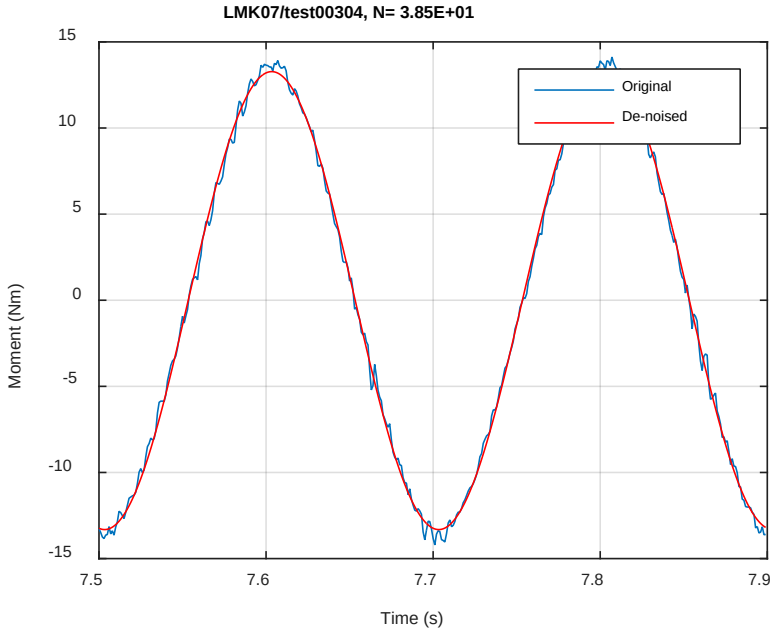
LMK07/test00304, N= 3.85E+01
Original
De-noised
Moment (Nm)
15
10
5
0
-5
-10
-15
7.5
7.6
7.7
7.8
7.9
Time (s)

(b)

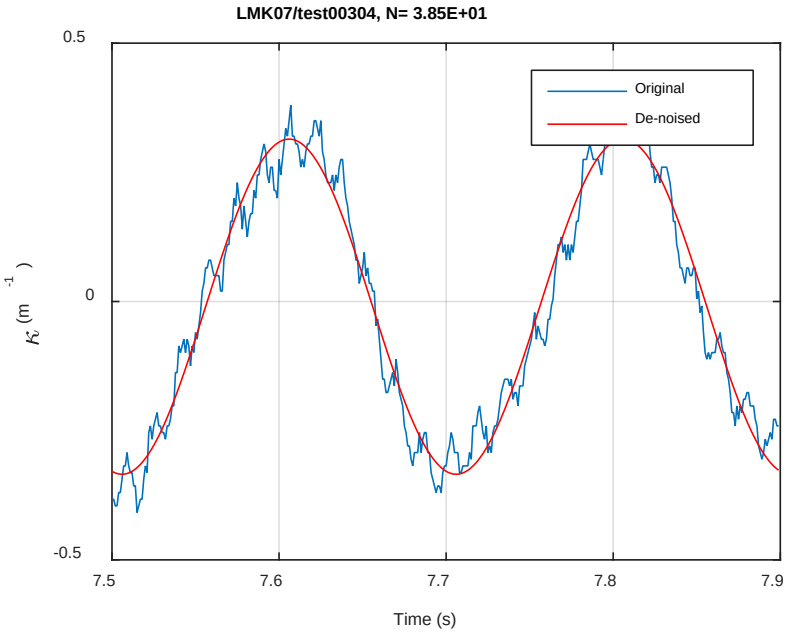

(c)

Fig. A.20. Monitoring-based responses: (a) curvature, (b) moment, (c) curvature, LMK07, 15.24 Nm, Ns = 3.85E+01 cycles.

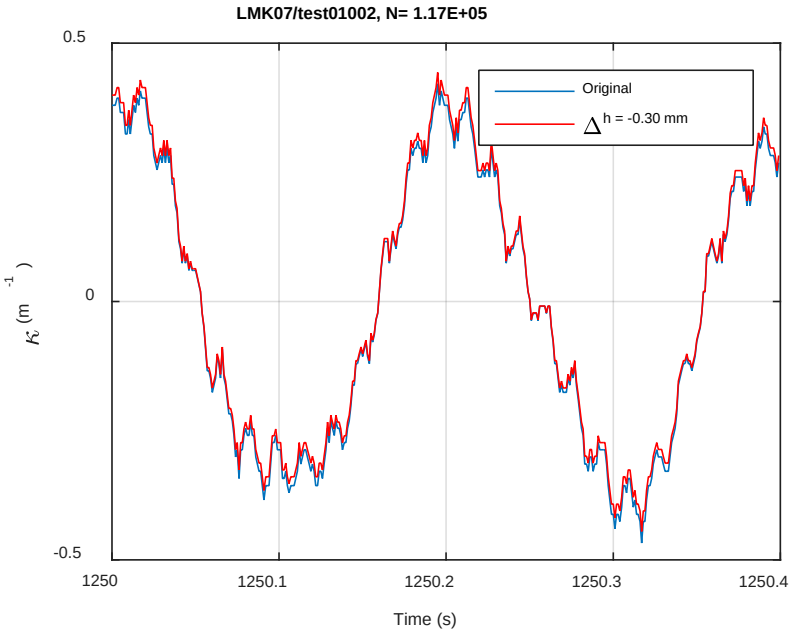
LMK07/test01002, N= 1.17E+05
Original
Δh = -0.30 mm
κ (m-1)
Time (s)
0.5
0
-0.5
1250
1250.1
1250.2
1250.3
1250.4

(a)

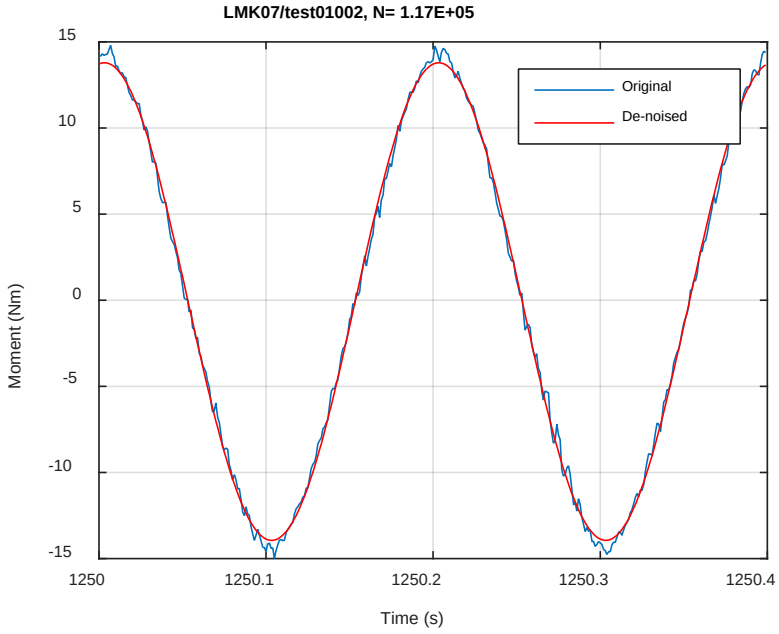
LMK07/test01002, N= 1.17E+05
Original
De-noised
Moment (Nm)
Time (s)
15
10
5
0
-5
-10
-15
1250
1250.1
1250.2
1250.3
1250.4

(b)

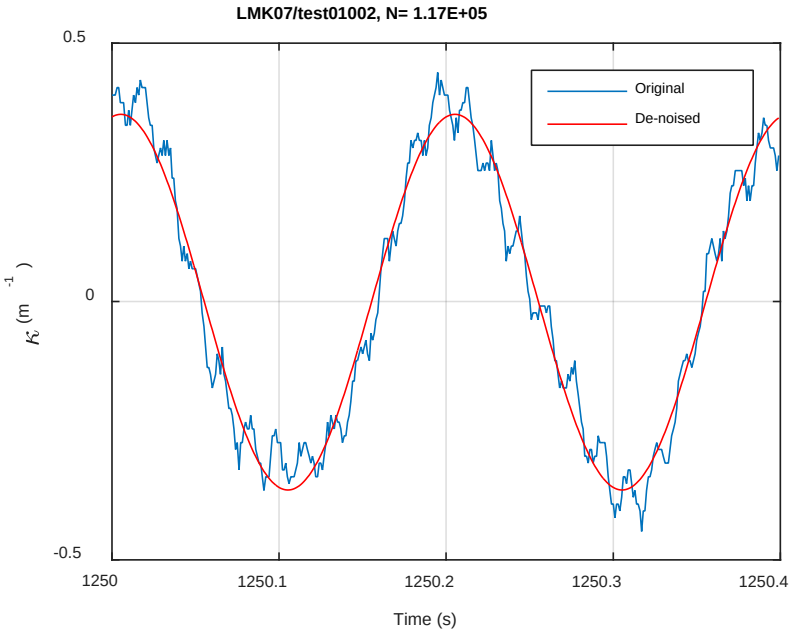

(c)

Fig. A.21. Monitoring-based responses: (a) curvature, (b) moment, (c) curvature, LMK07, 15.24 Nm, Ns = 1.17E+05 cycles.

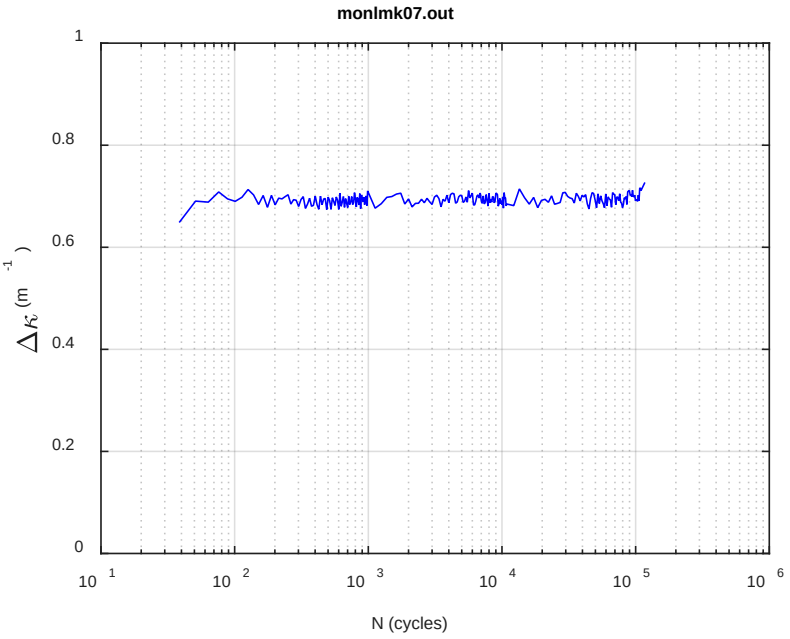
monlmk07.out
1
0.8
0.6
0.4
0.2
0
Δκ (m-1)
10 1
10 2
10 3
10 4
10 5
10 6
N (cycles)

(a)

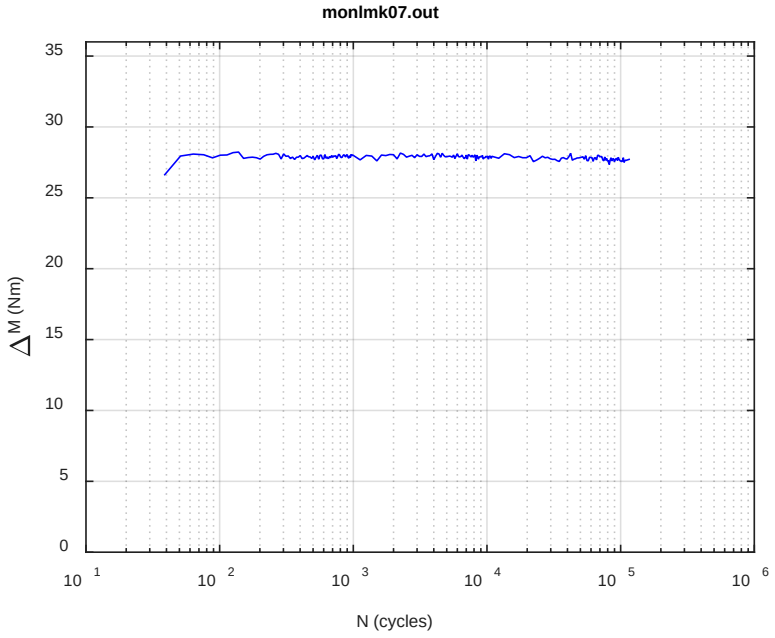
monlmk07.out
35
30
25
20
15
10
5
0
Δ M (Nm)
10 1
10 2
10 3
10 4
10 5
10 6
N (cycles)

(b)

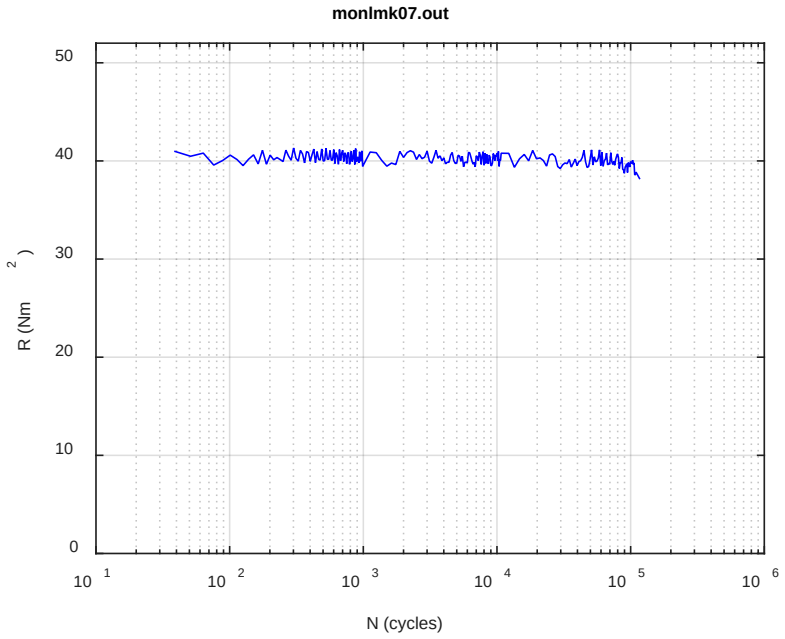
monlmk07.out
50
40
30
20
10
0
R (Nm 2)
10 1
10 2
10 3
10 4
10 5
10 6
N (cycles)

(c)

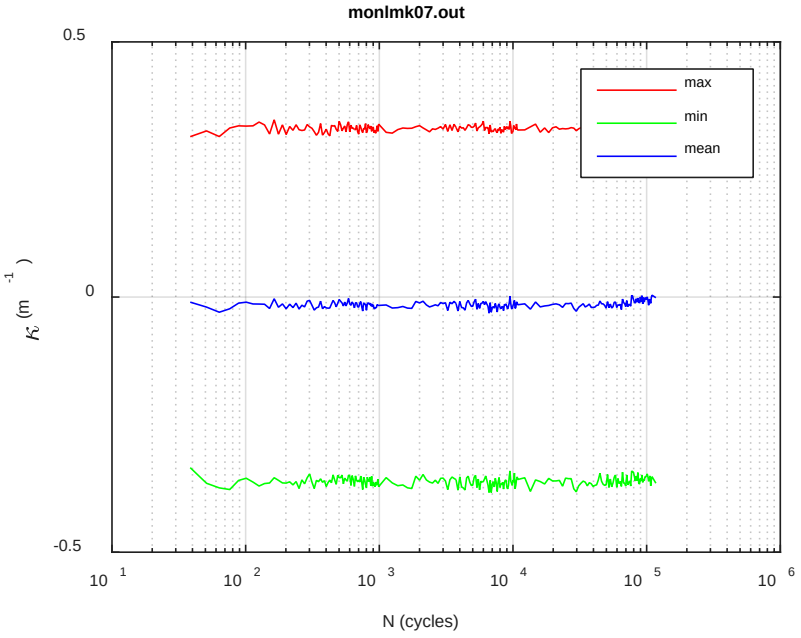
monlmk07.out
0.5
0
-0.5
κ (m -1)
max
min
mean
10 1
10 2
10 3
10 4
10 5
10 6
N (cycles)

(d)

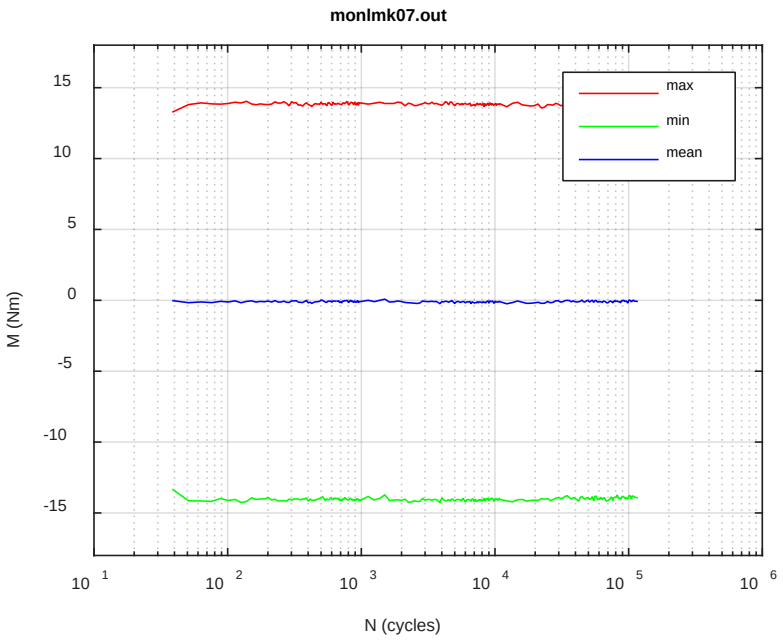

(e)

Fig. A.22. Monitoring-based responses: (a) curvature range, (b) moment range, (c) rigidity, (d) curvature peak/valley, (e) moment peak/valley, LMK07, 15.24 Nm, Nf = 1.22E+05 cycles.

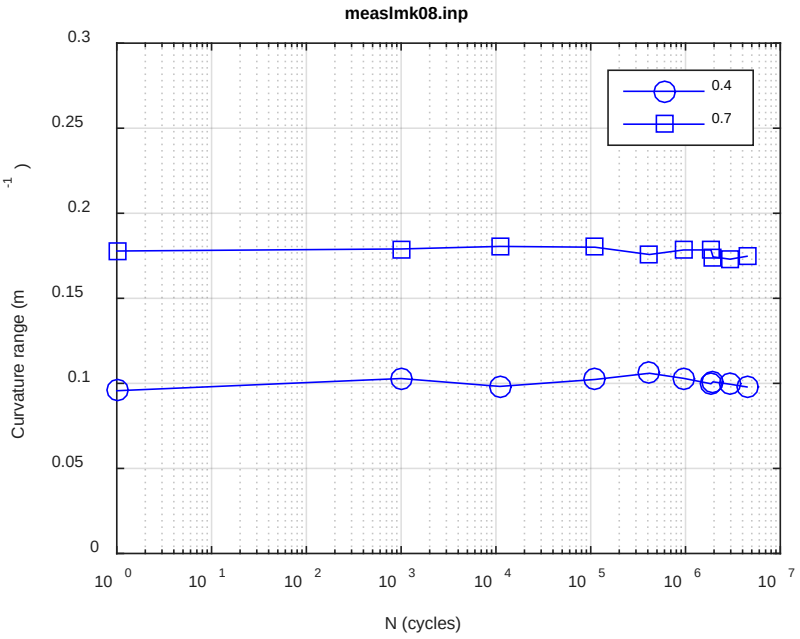
measlmk08.inp
0.3
0.25
0.2
0.15
0.1
0.05
0
Curvature range (m-1)
0.4
0.7
10 0
10 1
10 2
10 3
10 4
10 5
10 6
10 7
N (cycles)

(a)

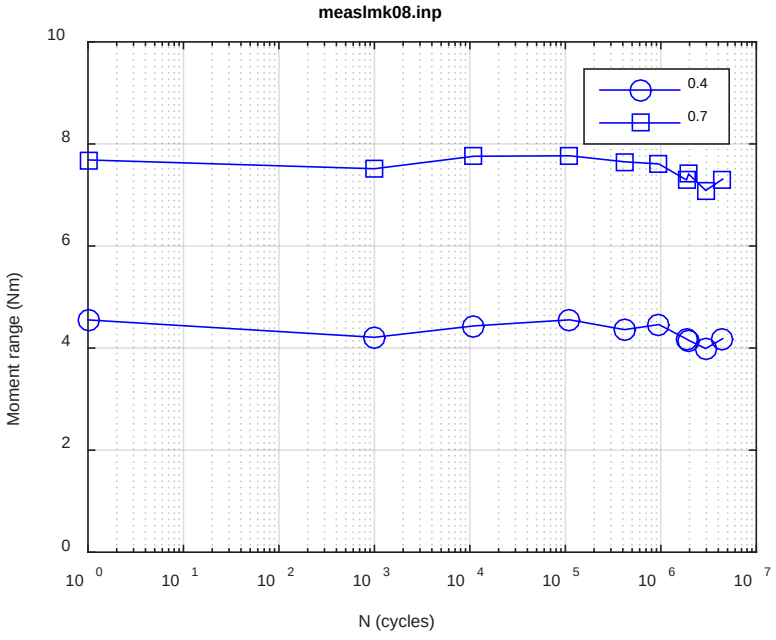
measlmk08.inp
10
8
6
4
2
0
Moment range (Nm)
0.4
0.7
10 0
10 1
10 2
10 3
10 4
10 5
10 6
10 7
N (cycles)

(b)

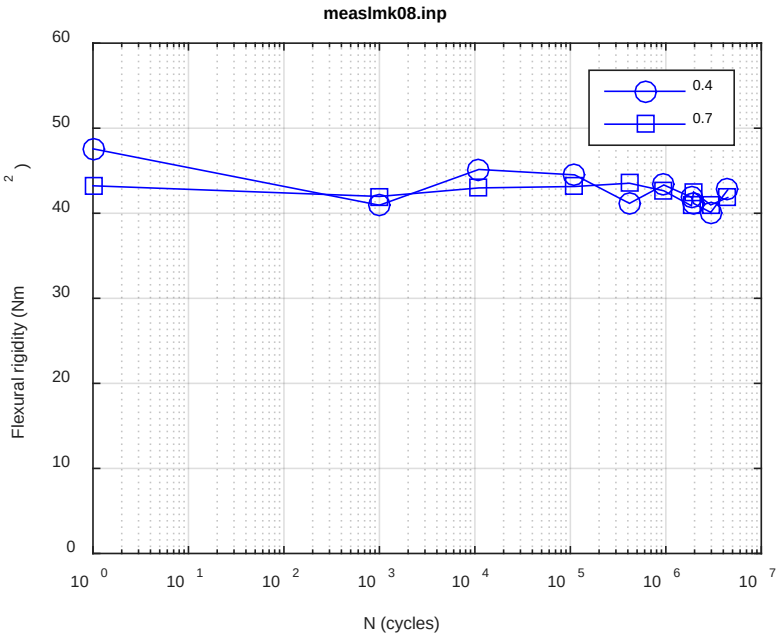
measlmk08.inp
0.4
0.7
Flexural rigidity (Nm 2)
N (cycles)

(c)

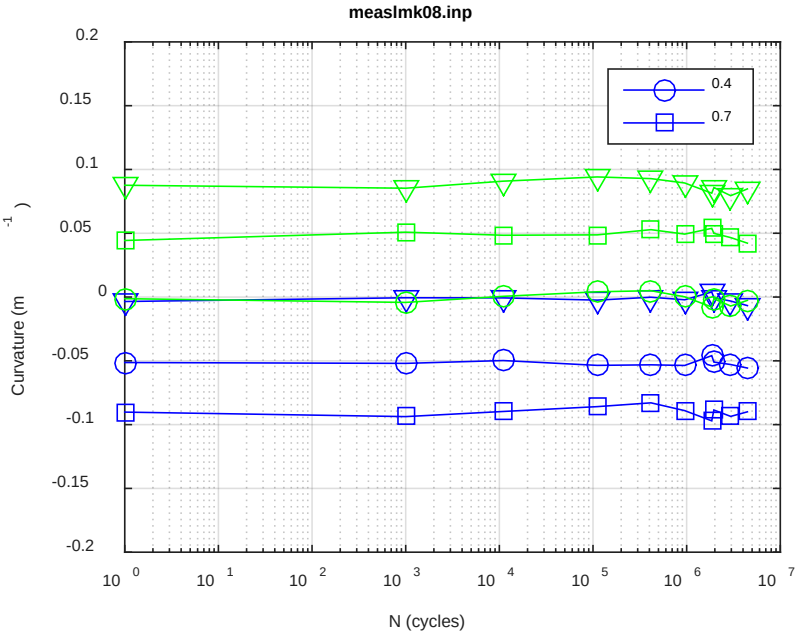
measlmk08.inp
0.4
0.7
Curvature (m -1)
N (cycles)

(d)

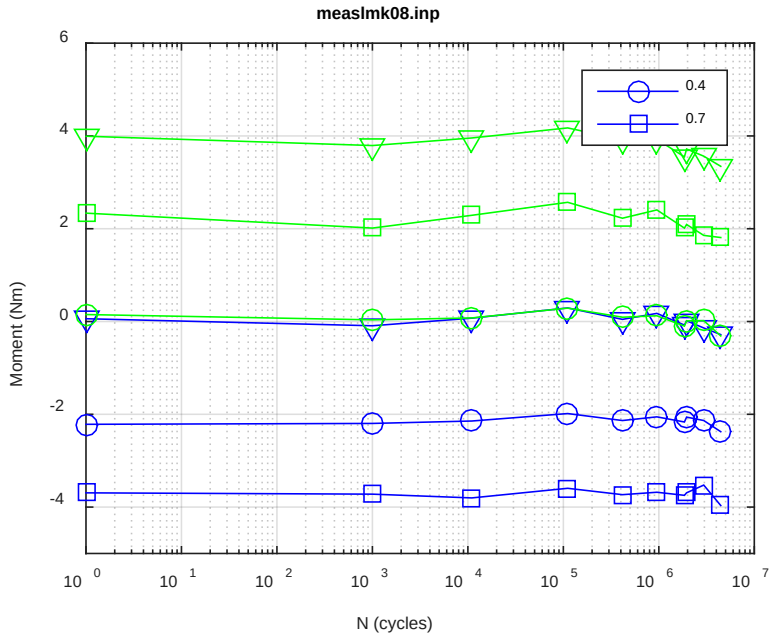

(e)

Fig. A.23. Measurement-based responses: (a) curvature range, (b) moment range, (c) rigidity, (d) curvature peak/valley, (e) moment peak/valley, LMK08, 7.62 Nm.

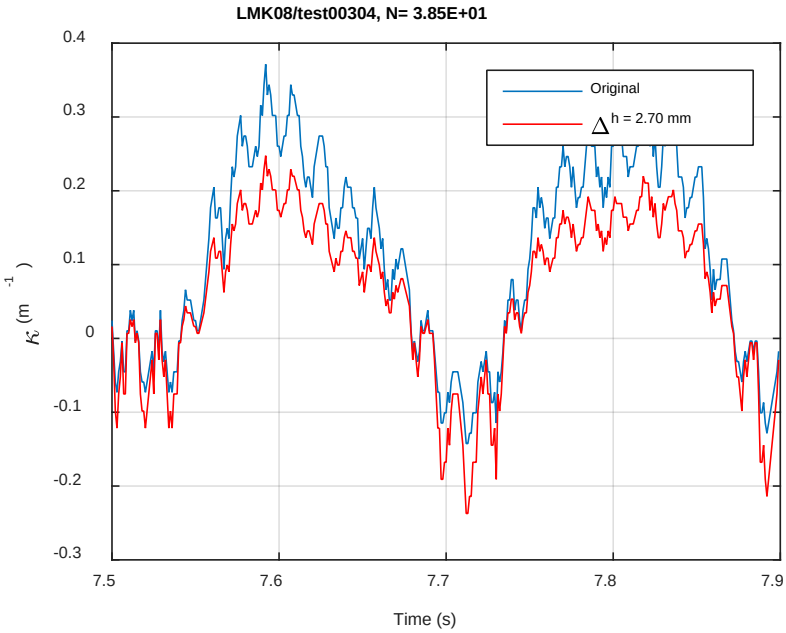
LMK08/test00304, N= 3.85E+01
Original
Δh = 2.70 mm
κ (m-1)
Time (s)

(a)

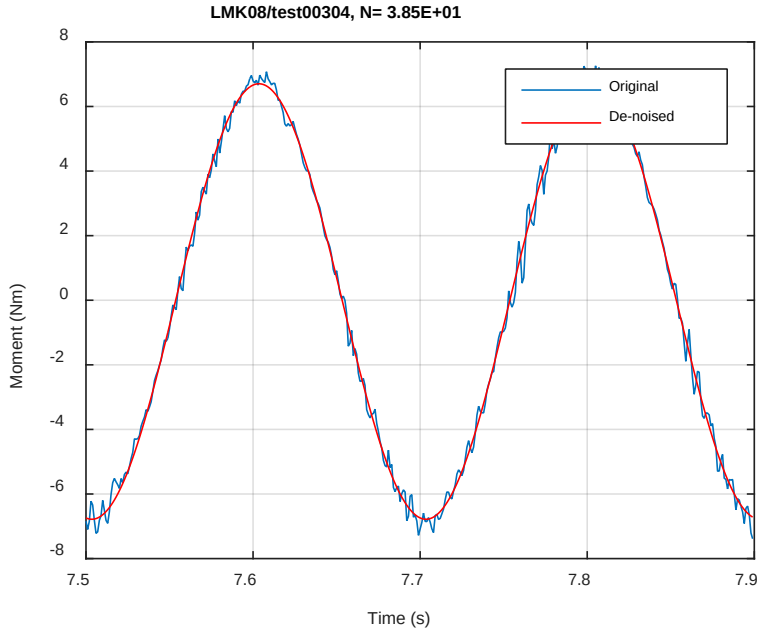
LMK08/test00304, N= 3.85E+01
Original
De-noised
Moment (Nm)
Time (s)

(b)

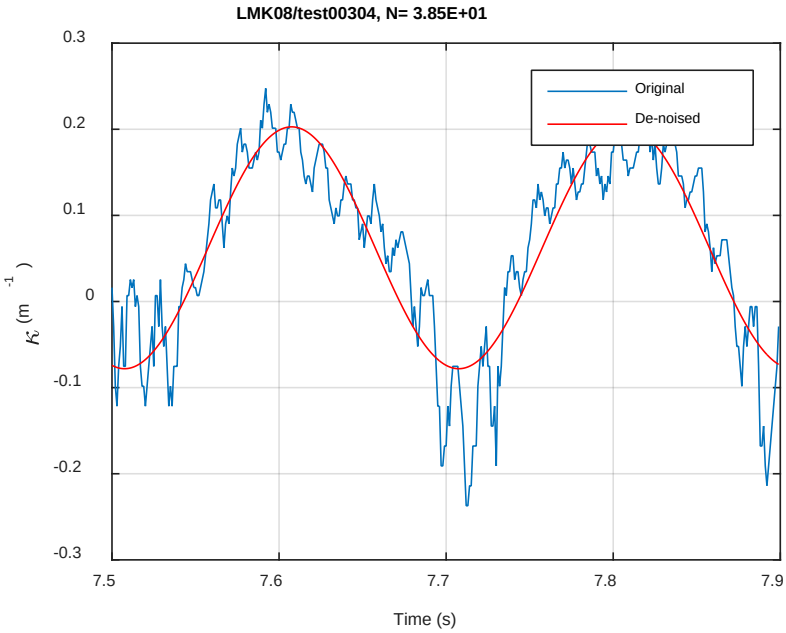

(c)

Fig. A.24. Monitoring-based responses: (a) curvature, (b) moment, (c) curvature, LMK08, 7.62 Nm, Ns = 3.85E+01 cycles.

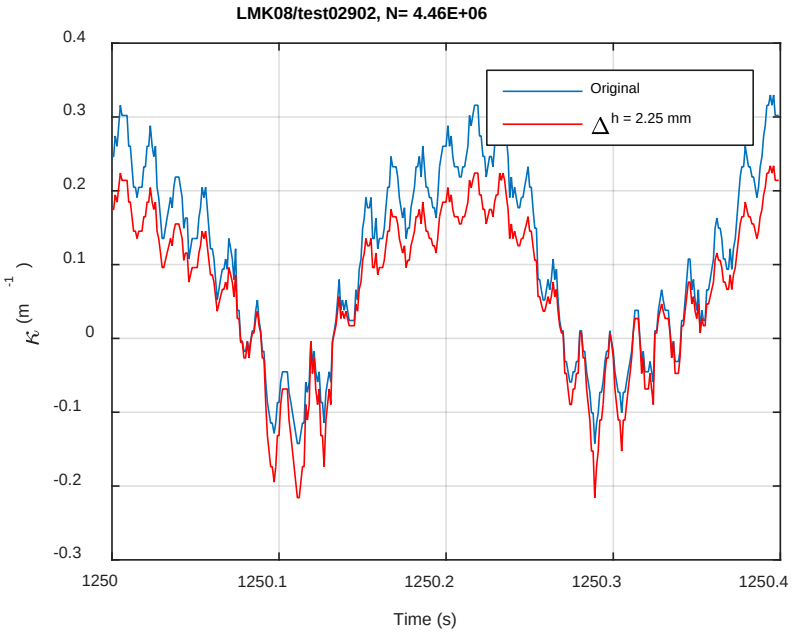
LMK08/test02902, N= 4.46E+06
Original
Δh = 2.25 mm
κ (m-1)
Time (s)
0.4
0.3
0.2
0.1
0
-0.1
-0.2
-0.3
1250
1250.1
1250.2
1250.3
1250.4

(a)

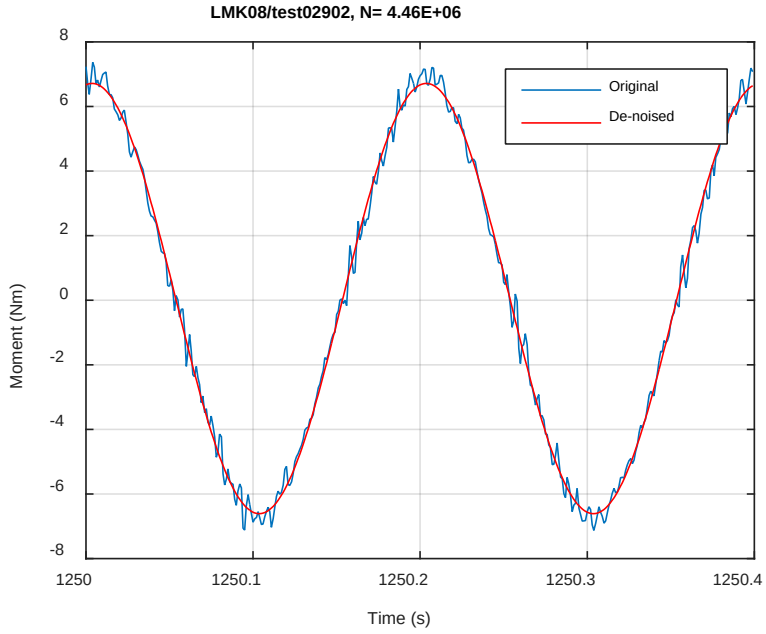
LMK08/test02902, N= 4.46E+06
Original
De-noised
Moment (Nm)
Time (s)
8
6
4
2
0
-2
-4
-6
-8
1250
1250.1
1250.2
1250.3
1250.4

(b)

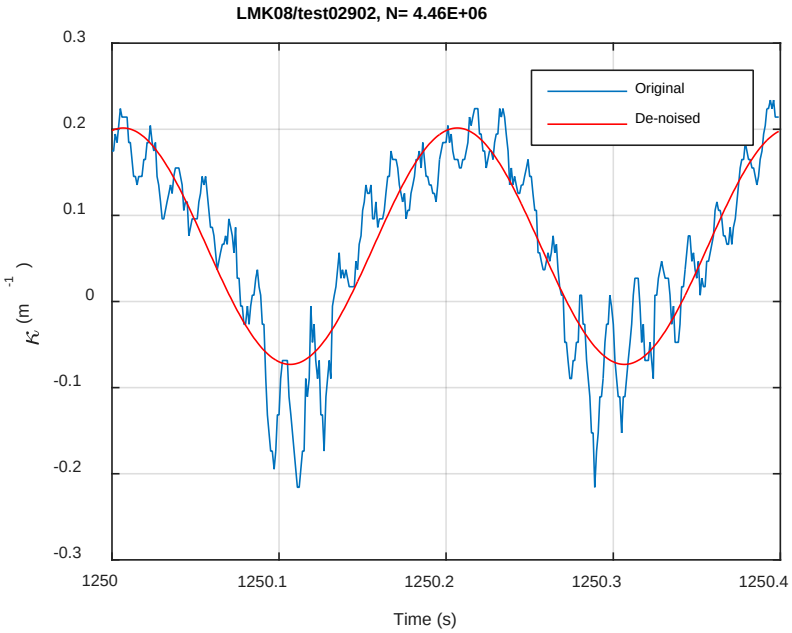

(c)

Fig. A.25. Monitoring-based responses: (a) curvature, (b) moment, (c) curvature, LMK08, 7.62 Nm, Ns = 4.46E+06 cycles.

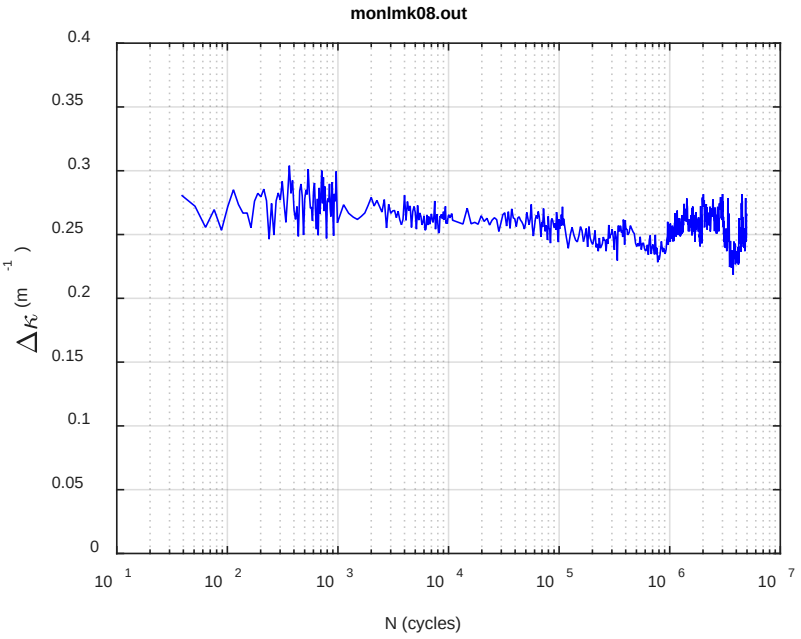
monlmk08.out
0.4
0.35
0.3
0.25
0.2
0.15
0.1
0.05
0
Δκ (m -1)
10 1
10 2
10 3
10 4
10 5
10 6
10 7
N (cycles)

(a)

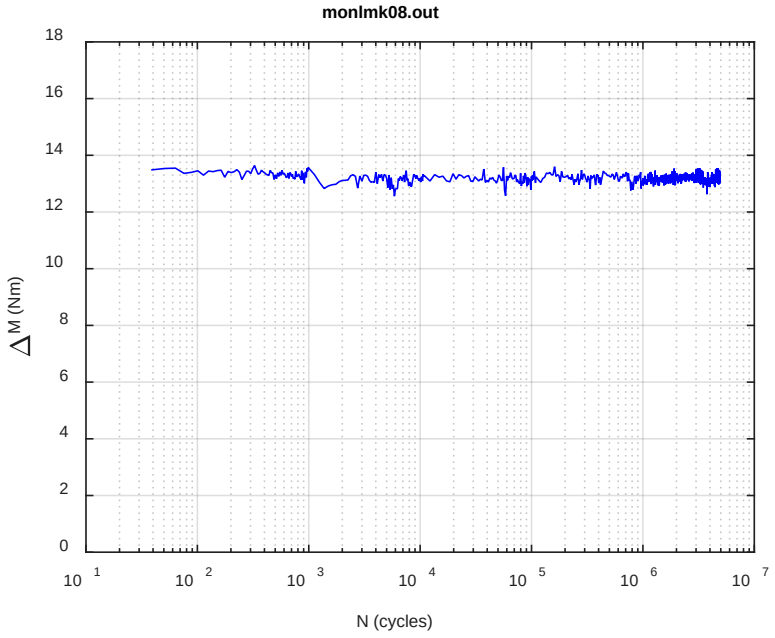
monlmk08.out
18
16
14
12
10
8
6
4
2
0
Δ M (Nm)
10 1
10 2
10 3
10 4
10 5
10 6
10 7
N (cycles)

(b)

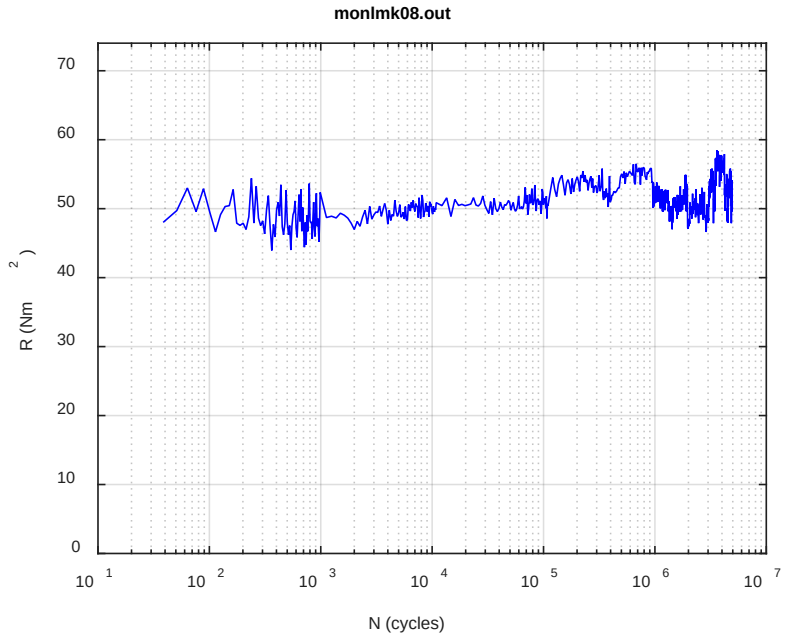
monlmk08.out
R (Nm 2)
N (cycles)

(c)

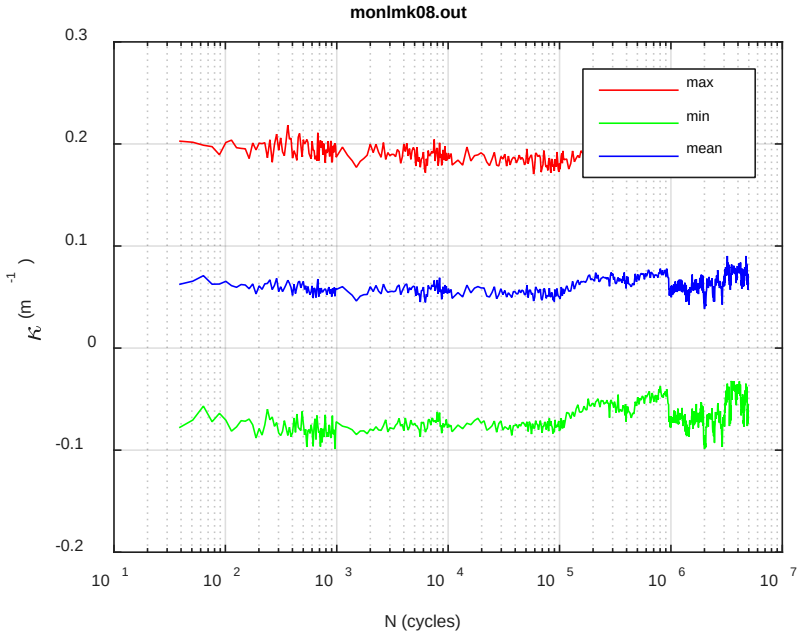
monlmk08.out
max
min
mean
κ (m -1)
N (cycles)

(d)

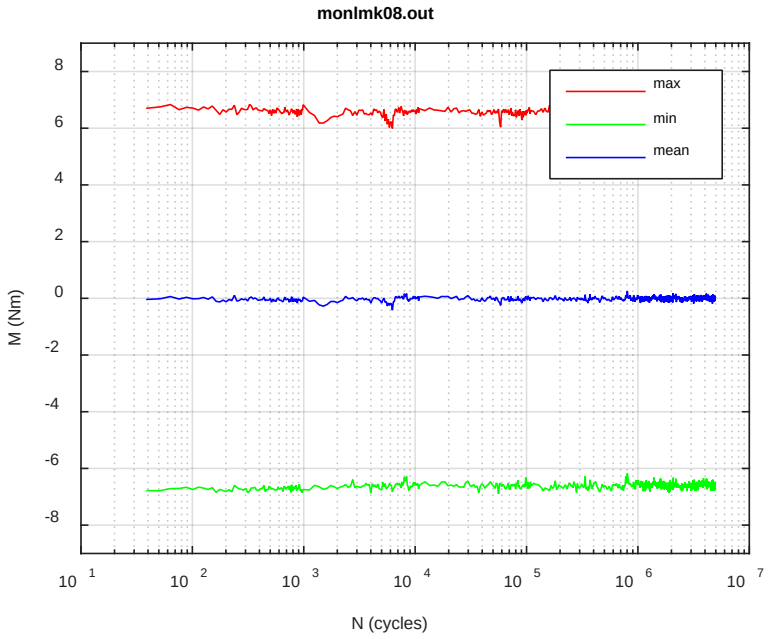

(e)

Fig. A.26. Monitoring-based responses: (a) curvature range, (b) moment range, (c) rigidity, (d) curvature peak/valley, (e) moment peak/valley, LMK08, 7.62 Nm, Nf = 4.70E+06 cycles.

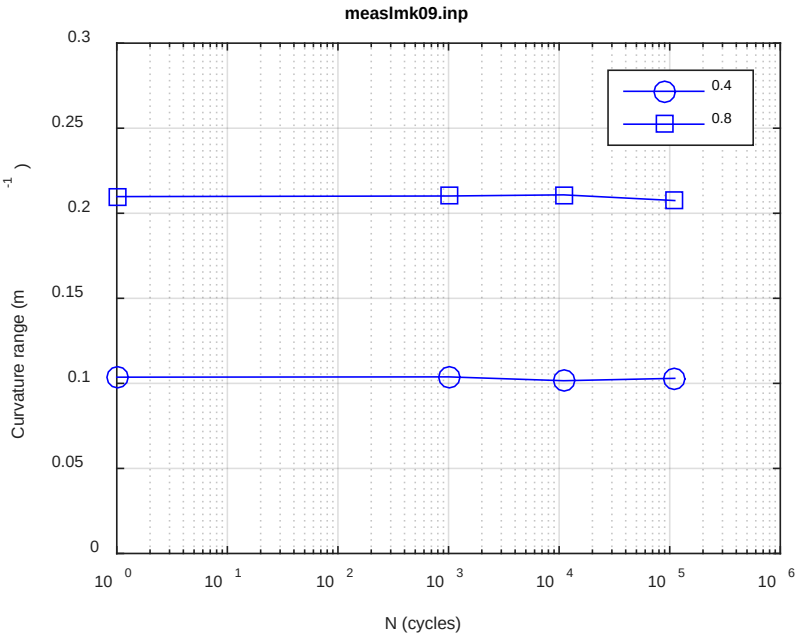
measlmk09.inp
0.3
0.25
0.2
0.15
0.1
0.05
0
Curvature range (m -1)
0.4
0.8
10 0
10 1
10 2
10 3
10 4
10 5
10 6
N (cycles)

(a)

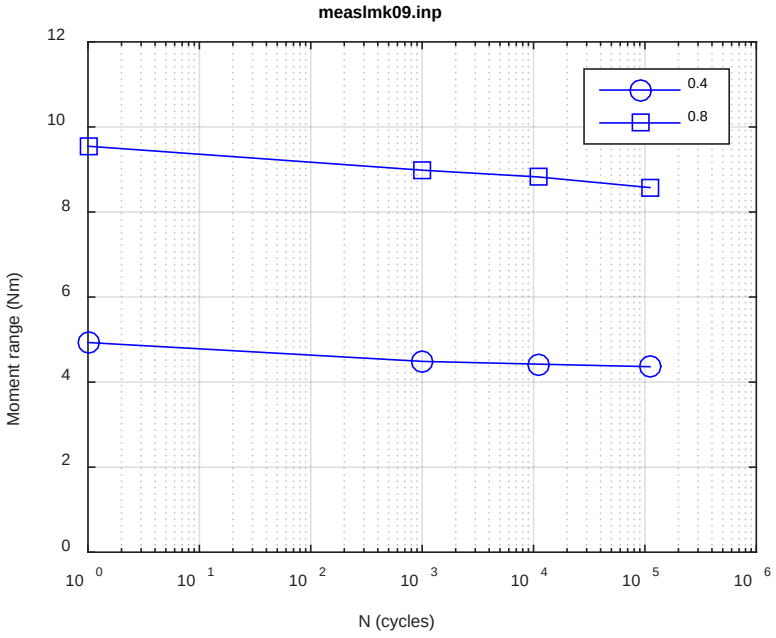
measlmk09.inp
12
10
8
6
4
2
0
Moment range (Nm)
0.4
0.8
10 0
10 1
10 2
10 3
10 4
10 5
10 6
N (cycles)

(b)

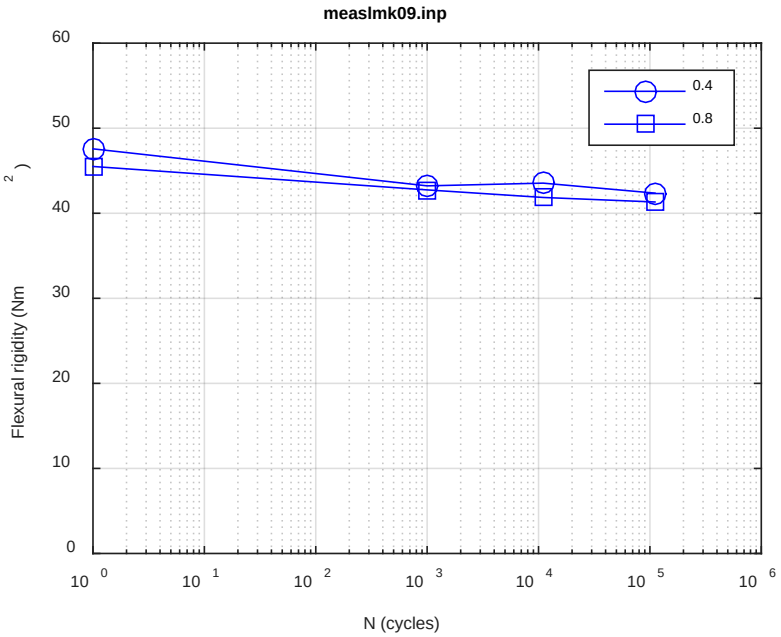
measlmk09.inp
Flexural rigidity (Nm 2)
N (cycles)
0.4
0.8

(c)

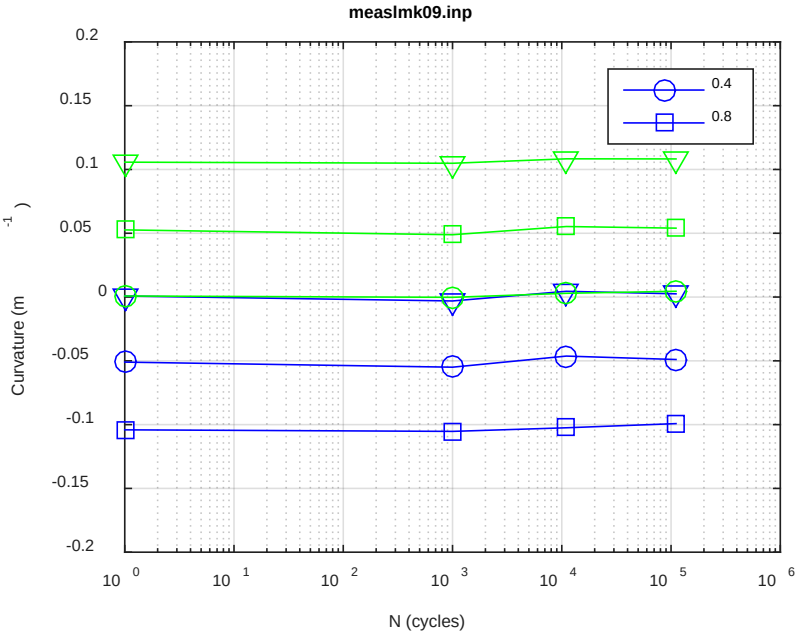
measlmk09.inp
Curvature (m -1)
N (cycles)
0.4
0.8

(d)

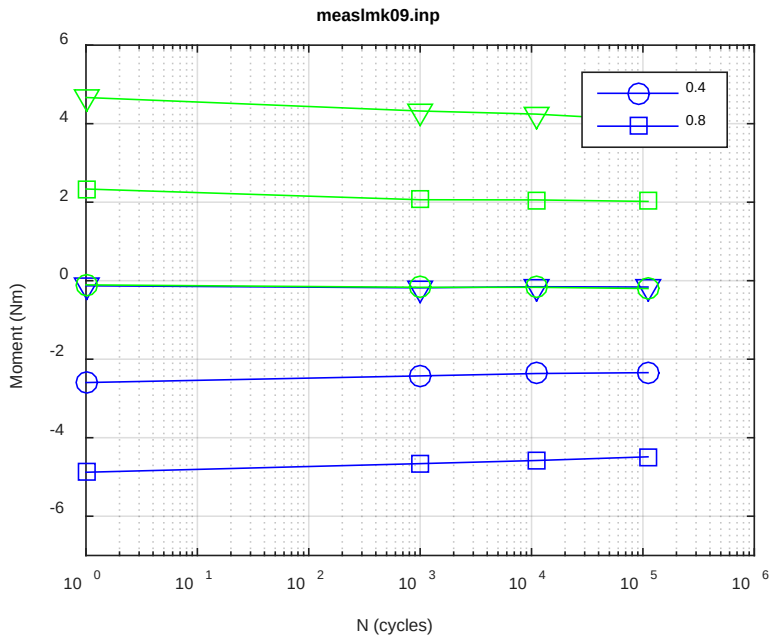

(e)

Fig. A.27. Measurement-based responses: (a) curvature range, (b) moment range, (c) rigidity, (d) curvature peak/valley, (e) moment peak/valley, LMK09, 10.16 Nm.

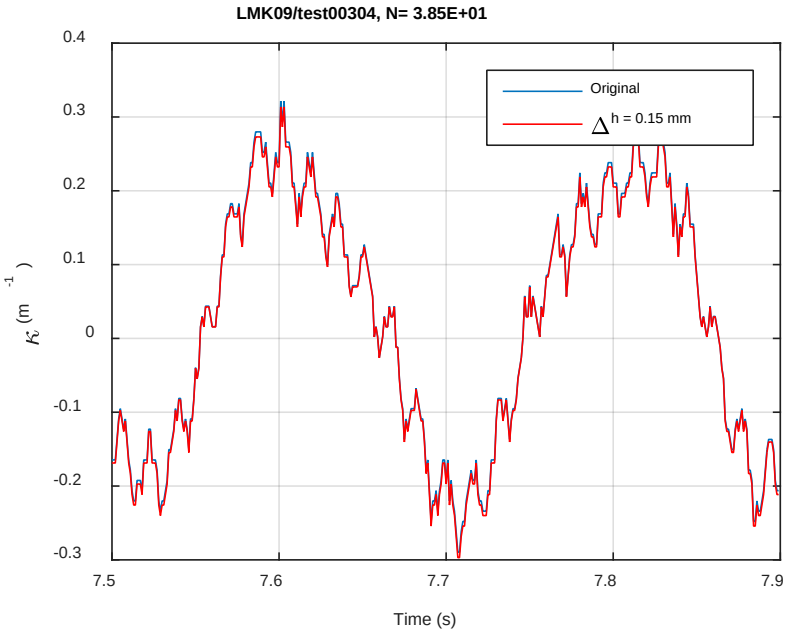
LMK09/test00304, N= 3.85E+01
Original
Δh = 0.15 mm
κ (m-1)
Time (s)

(a)

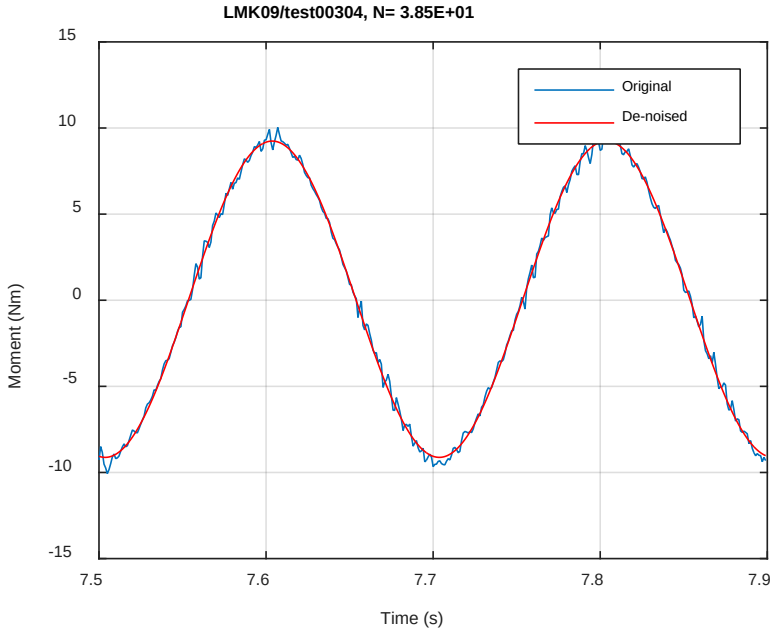
LMK09/test00304, N= 3.85E+01
Original
De-noised
Moment (Nm)
Time (s)

(b)

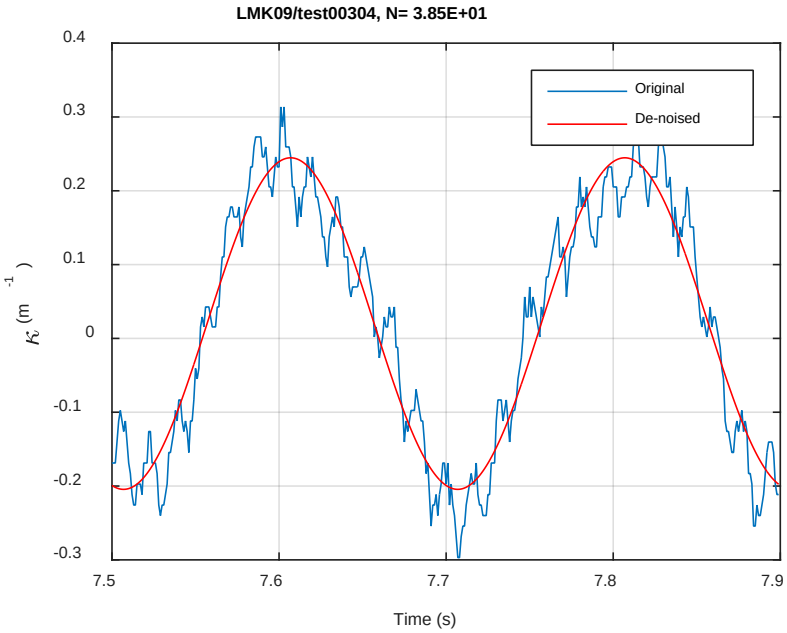

(c)

Fig. A.28. Monitoring-based responses: (a) curvature, (b) moment, (c) curvature, LMK09, 10.16 Nm, Ns = 3.85E+01 cycles.

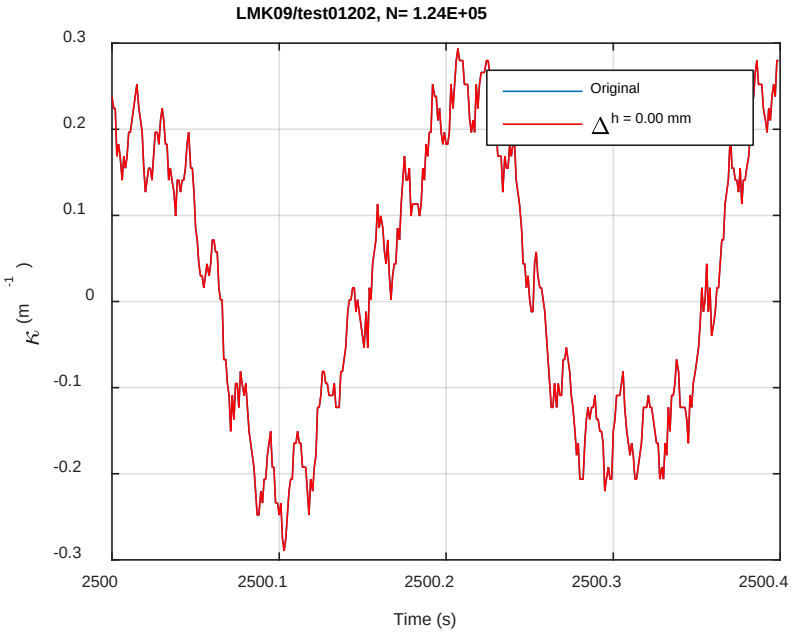
LMK09/test01202, N= 1.24E+05
Original
Δh = 0.00 mm
κ (m-1)
Time (s)
0.3
0.2
0.1
0
-0.1
-0.2
-0.3
2500
2500.1
2500.2
2500.3
2500.4

(a)

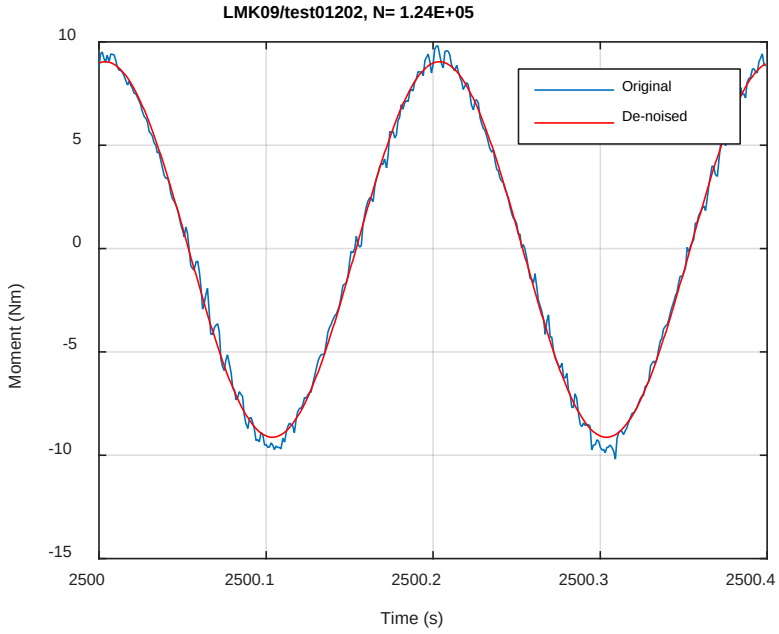
LMK09/test01202, N= 1.24E+05
Original
De-noised
Moment (Nm)
Time (s)
10
5
0
-5
-10
-15
2500
2500.1
2500.2
2500.3
2500.4

(b)

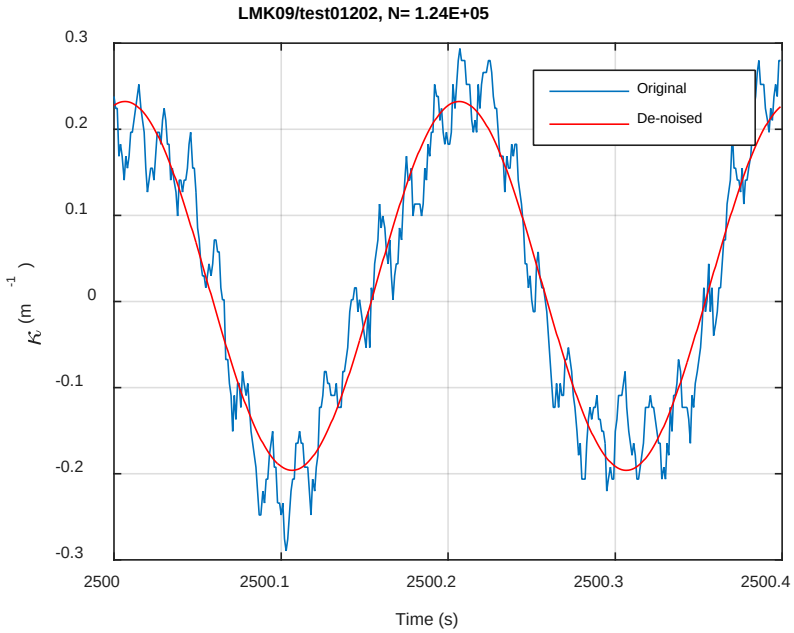

(c)

Fig. A.29. Monitoring-based responses: (a) curvature, (b) moment, (c) curvature, LMK09, 10.16 Nm, Ns = 1.24E+05 cycles.

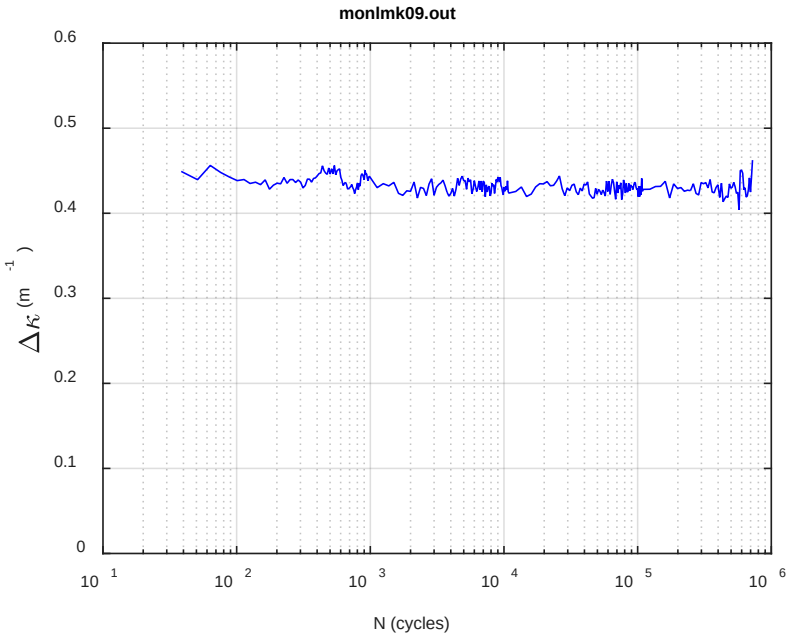
monlmk09.out
0.6
0.5
0.4
0.3
0.2
0.1
0
Δκ (m -1)
10 1
10 2
10 3
10 4
10 5
10 6
N (cycles)

(a)

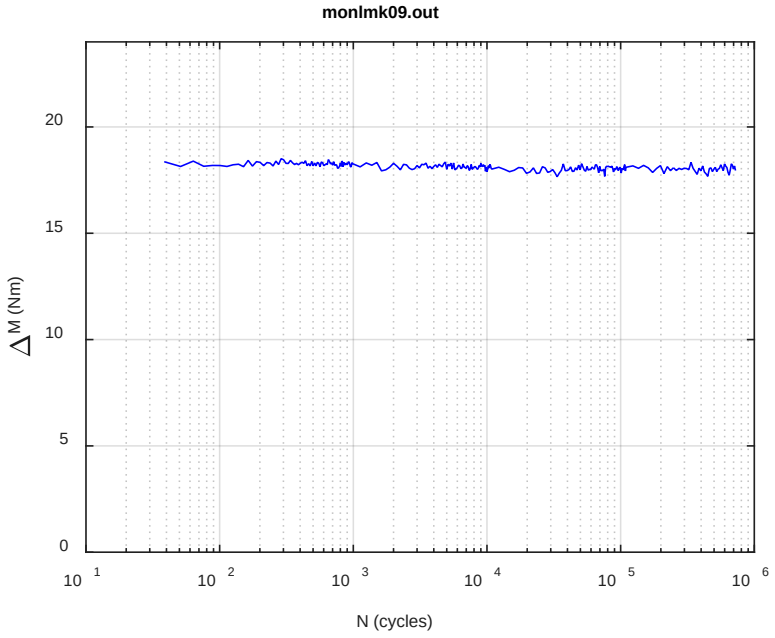
monlmk09.out
20
15
10
5
0
Δ M (Nm)
10 1
10 2
10 3
10 4
10 5
10 6
N (cycles)

(b)

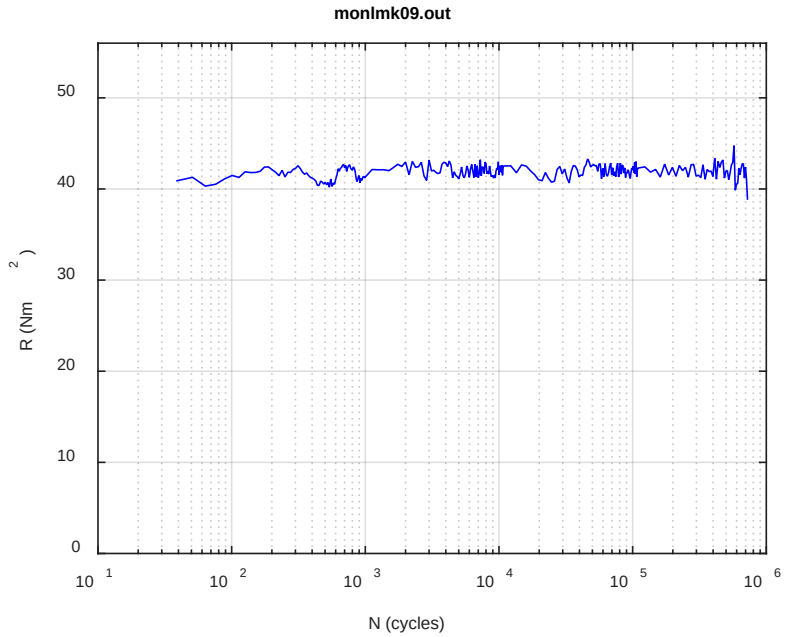
monlmk09.out
R (Nm 2)
N (cycles)

(c)

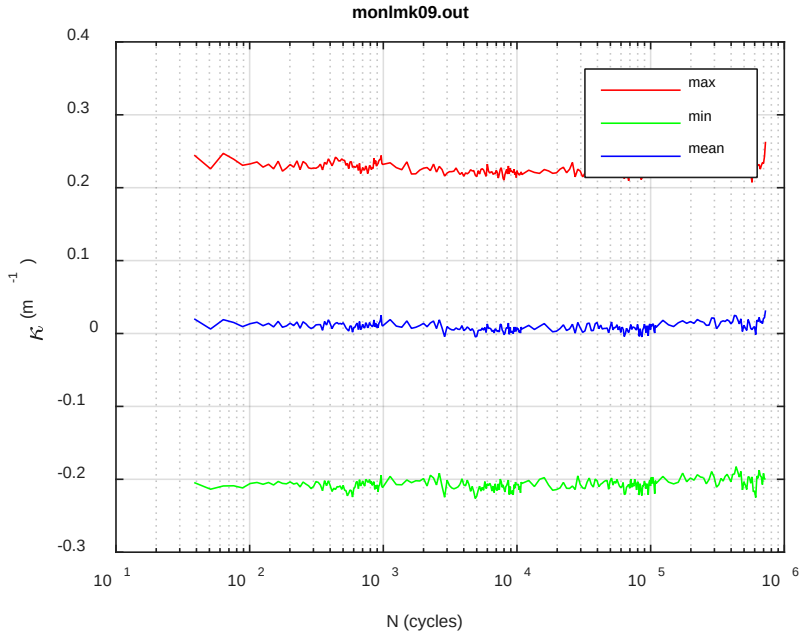
monlmk09.out
max
min
mean
κ (m -1)
N (cycles)

(d)

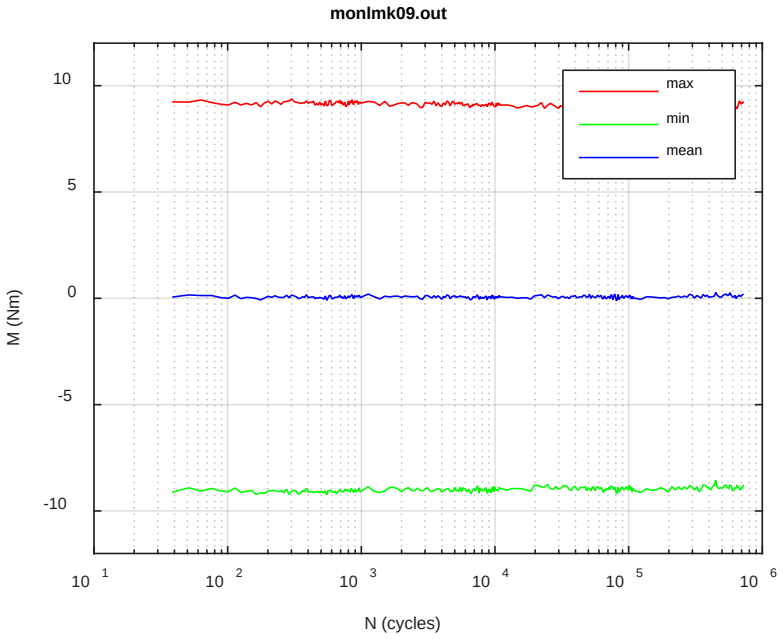

(e)

Fig. A.30. Monitoring-based responses: (a) curvature range, (b) moment range, (c) rigidity, (d) curvature peak/valley, (e) moment peak/valley, LMK09, 10.16 Nm, Nf = 7.31E+05 cycles.

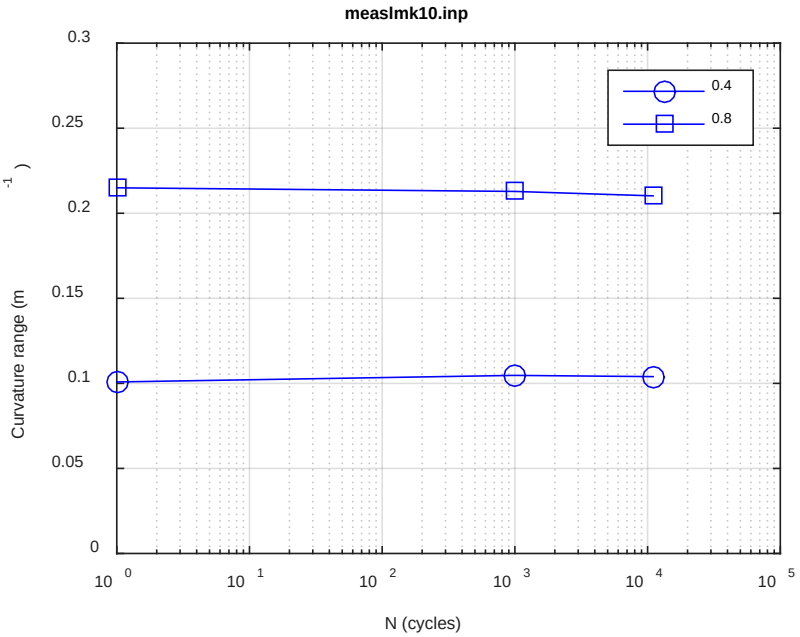
measlmk10.inp
0.3
0.25
0.2
0.15
0.1
0.05
0
Curvature range (m-1)
0.4
0.8
10 0
10 1
10 2
10 3
10 4
10 5
N (cycles)

(a)

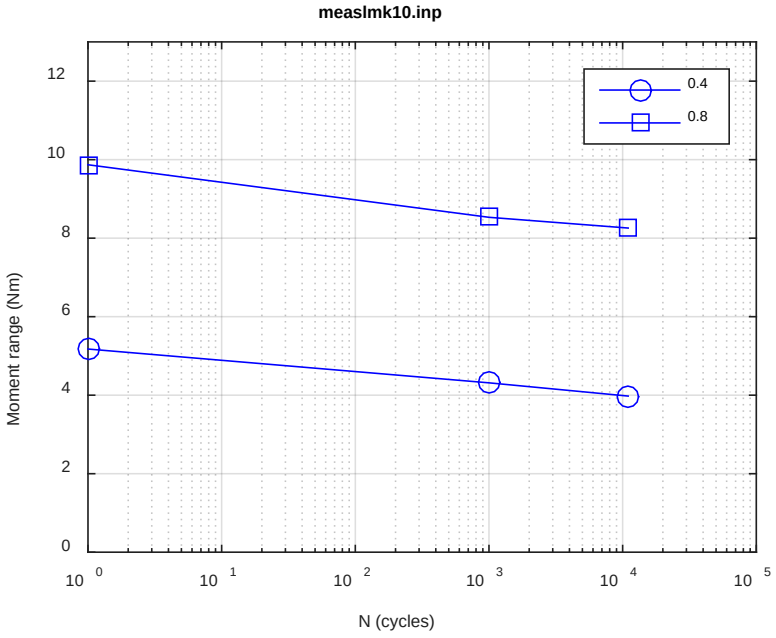
measlmk10.inp
12
10
8
6
4
2
0
Moment range (Nm)
0.4
0.8
10 0
10 1
10 2
10 3
10 4
10 5
N (cycles)

(b)

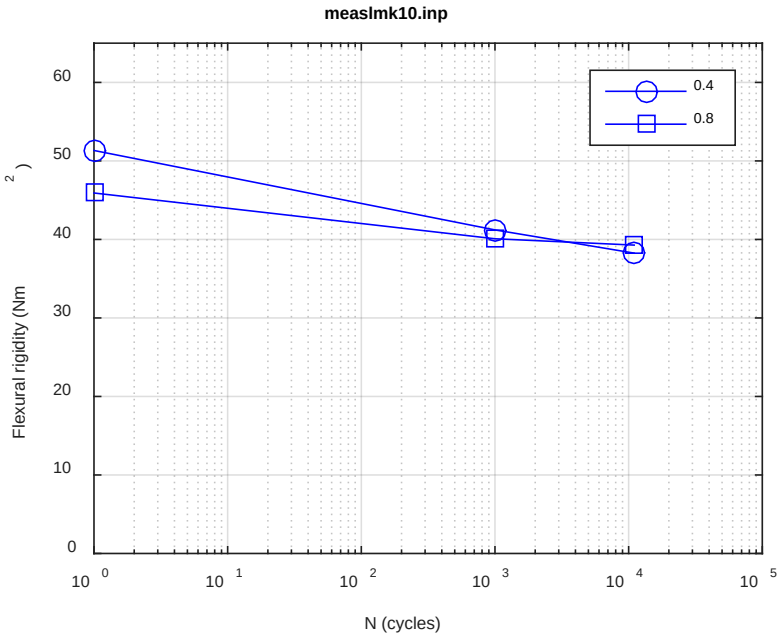
measlmk10.inp
Flexural rigidity (Nm 2)
N (cycles)
0.4
0.8
60
50
40
30
20
10
0
10 0
10 1
10 2
10 3
10 4
10 5

(c)

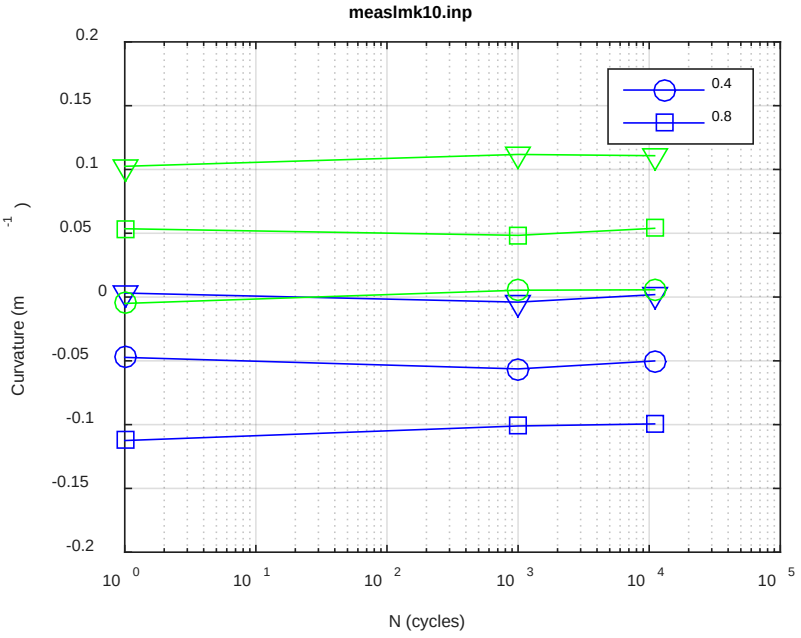
measlmk10.inp
Curvature (m -1)
N (cycles)
0.4
0.8
0.2
0.15
0.1
0.05
0
-0.05
-0.1
-0.15
-0.2
10 0
10 1
10 2
10 3
10 4
10 5

(d)

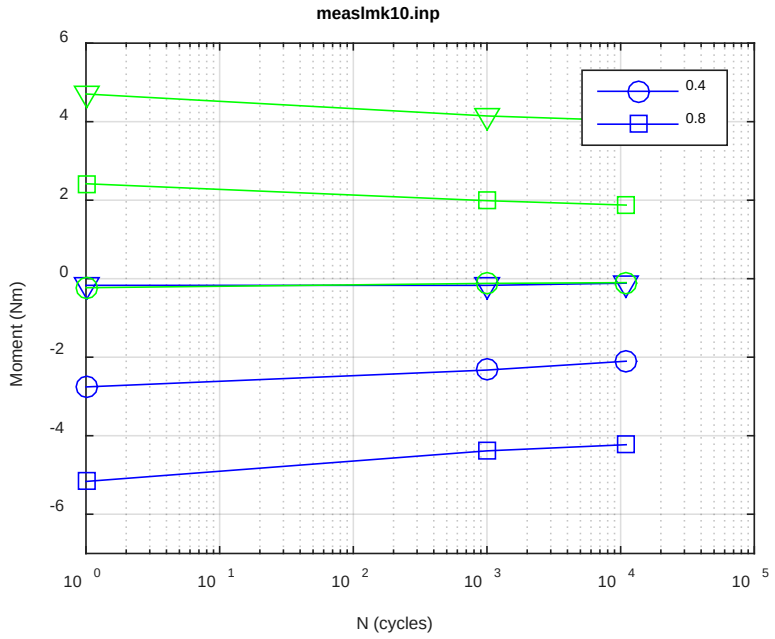

(e)

Fig. A.31. Measurement-based responses: (a) curvature range, (b) moment range, (c) rigidity, (d) curvature peak/valley, (e) moment peak/valley, LMK10, 20.32 Nm.

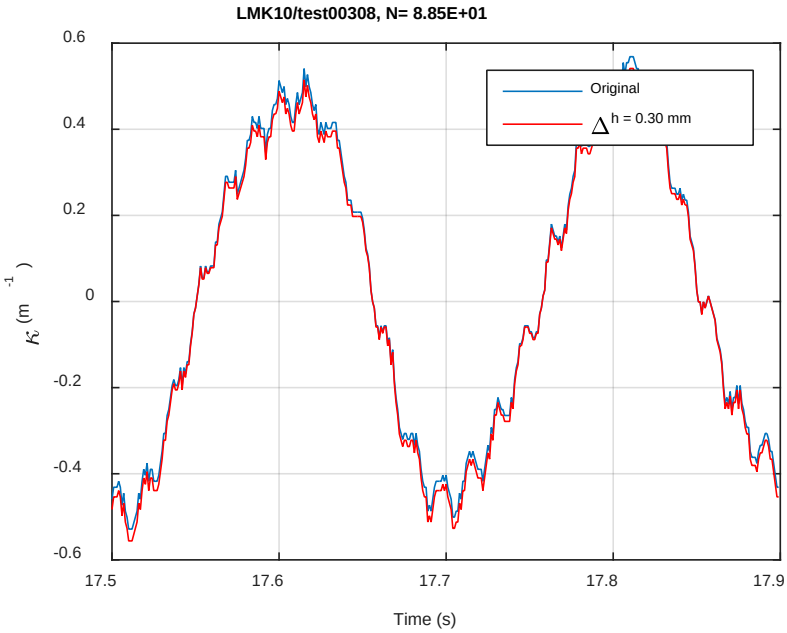
LMK10/test00308, N= 8.85E+01
Original
Δh = 0.30 mm
κ (m-1)
Time (s)
0.6
0.4
0.2
0
-0.2
-0.4
-0.6
17.5
17.6
17.7
17.8
17.9

(a)

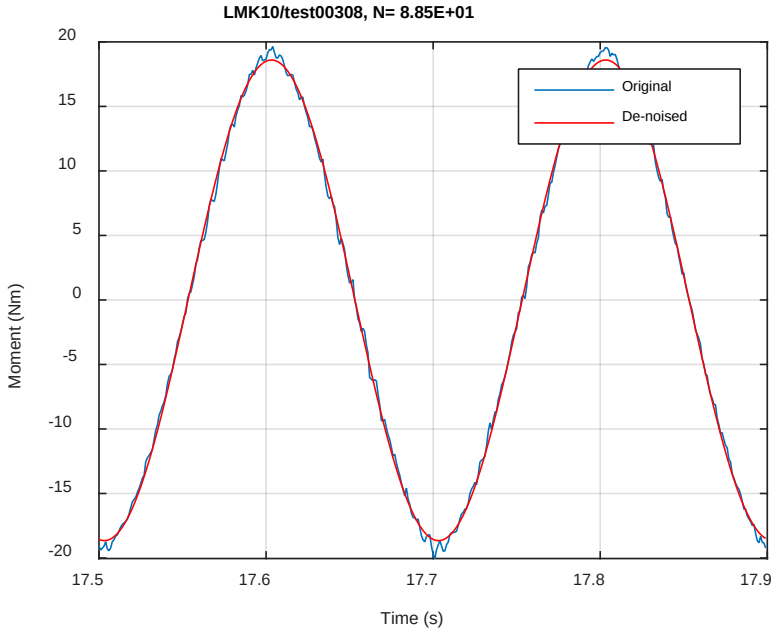
LMK10/test00308, N= 8.85E+01
Original
De-noised
Moment (Nm)
Time (s)
20
15
10
5
0
-5
-10
-15
-20
17.5
17.6
17.7
17.8
17.9

(b)

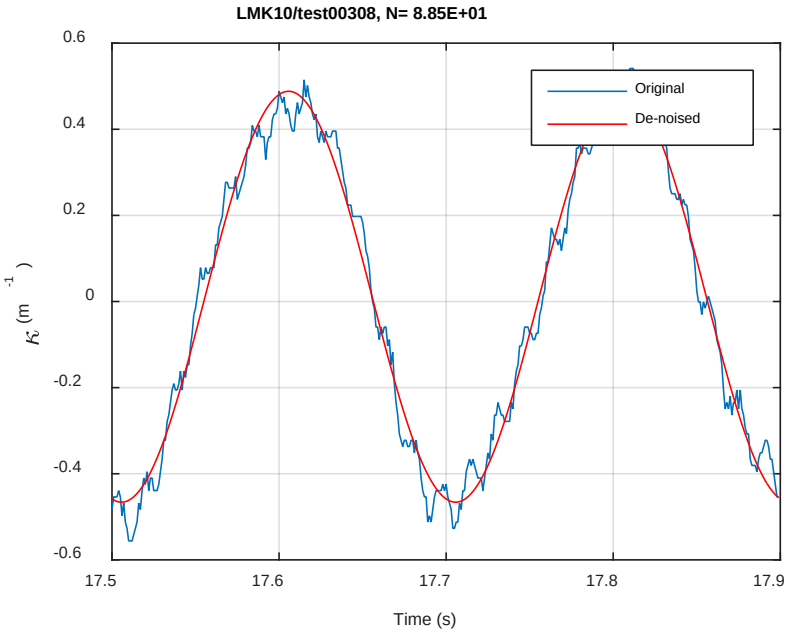

(c)

Fig. A.32. Monitoring-based responses: (a) curvature, (b) moment, (c) curvature, LMK10, 20.32 Nm, Ns = 8.85E+01 cycles.

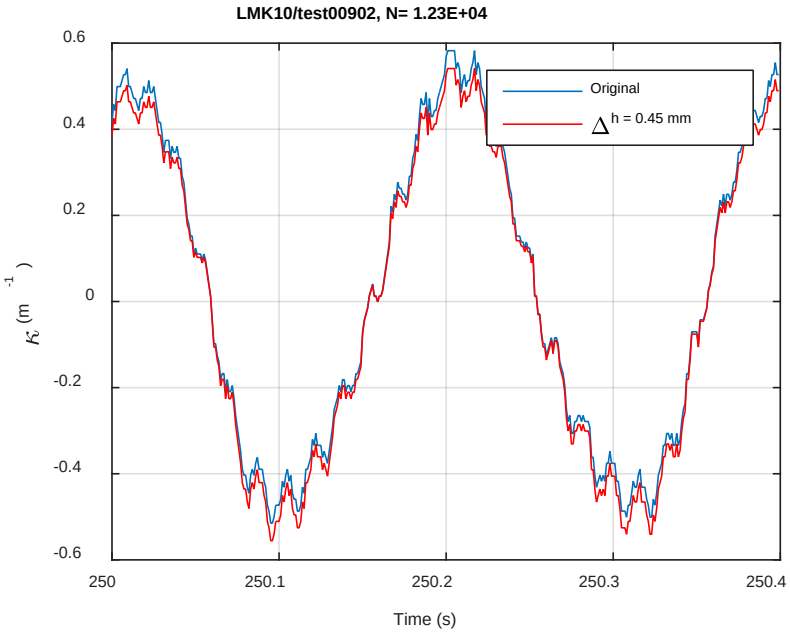
LMK10/test00902, N= 1.23E+04
Original
Δh = 0.45 mm
κ (m-1)
Time (s)
0.6
0.4
0.2
0
-0.2
-0.4
-0.6
250
250.1
250.2
250.3
250.4

(a)

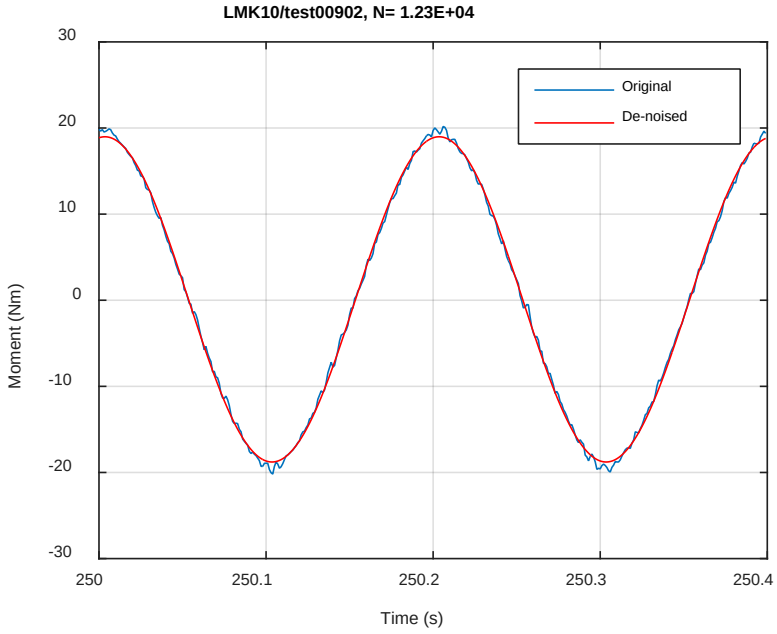
LMK10/test00902, N= 1.23E+04
Original
De-noised
Moment (Nm)
Time (s)
30
20
10
0
-10
-20
-30
250
250.1
250.2
250.3
250.4

(b)

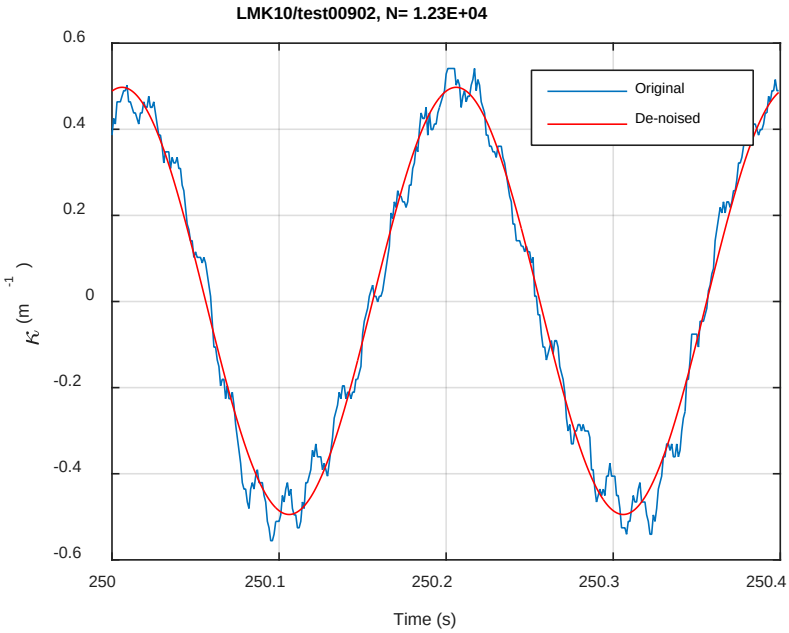

(c)

Fig. A.33. Monitoring-based responses: (a) curvature, (b) moment, (c) curvature, LMK10, 20.32 Nm, Ns = 1.23E+04 cycles.

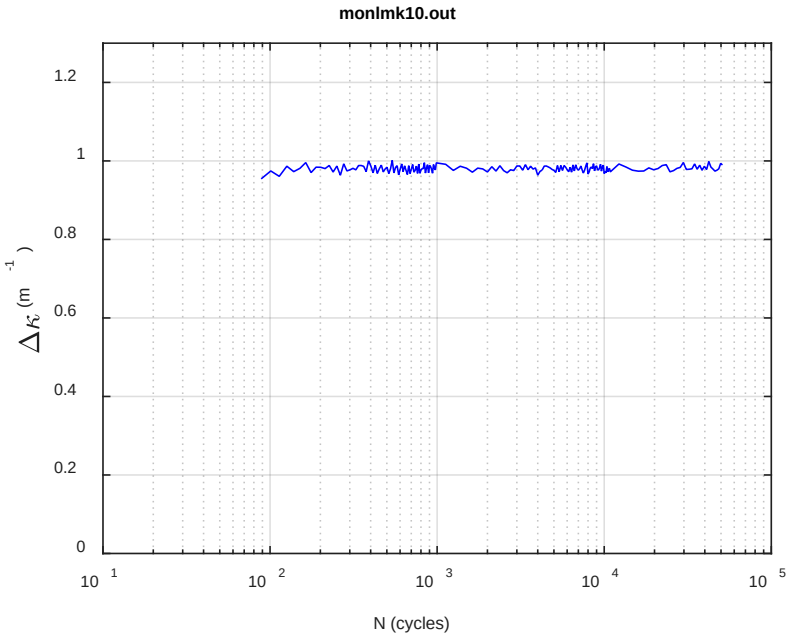
monlmk10.out
1.2
1
0.8
0.6
0.4
0.2
0
$\Delta\kappa$ (m^{-1})
10^1
10^2
10^3
10^4
10^5
N (cycles)

(a)

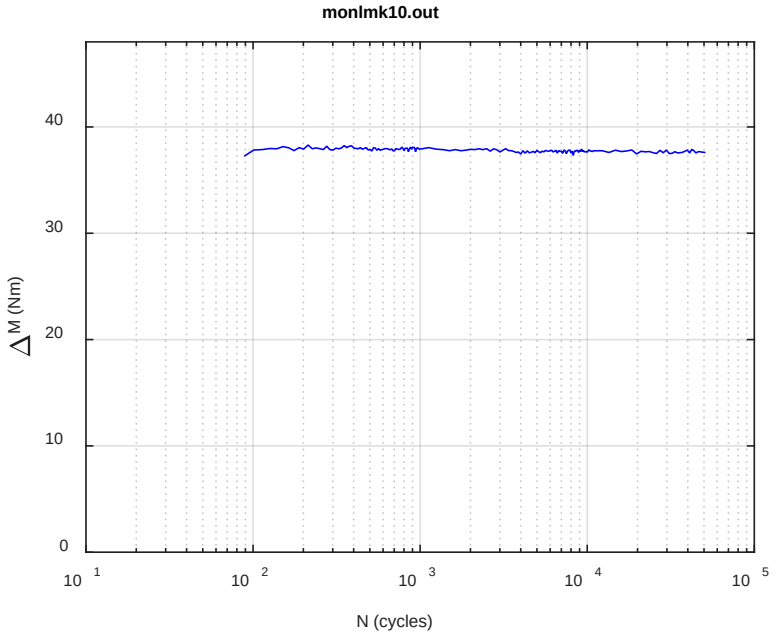
monlmk10.out
40
30
20
10
0
Δ M (Nm)
10^1
10^2
10^3
10^4
10^5
N (cycles)

(b)

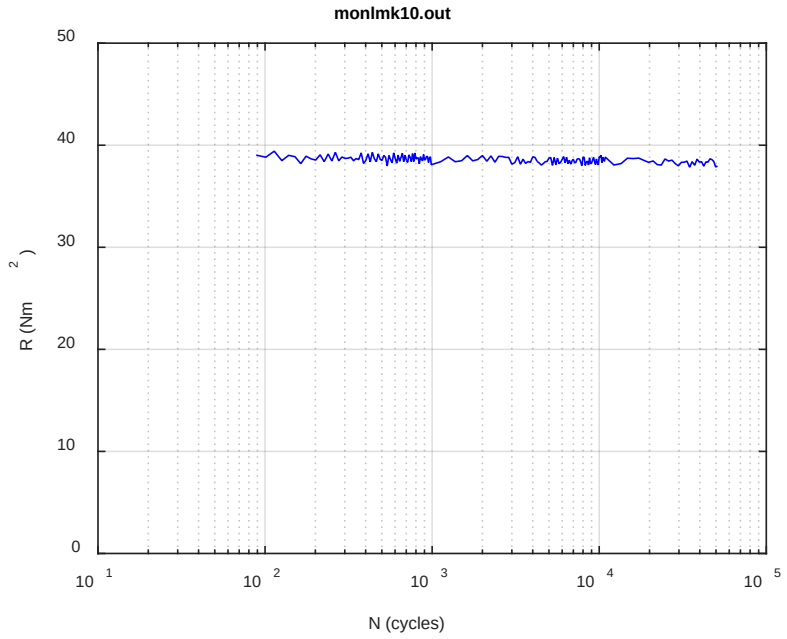
monlmk10.out
R (Nm 2)
N (cycles)

(c)

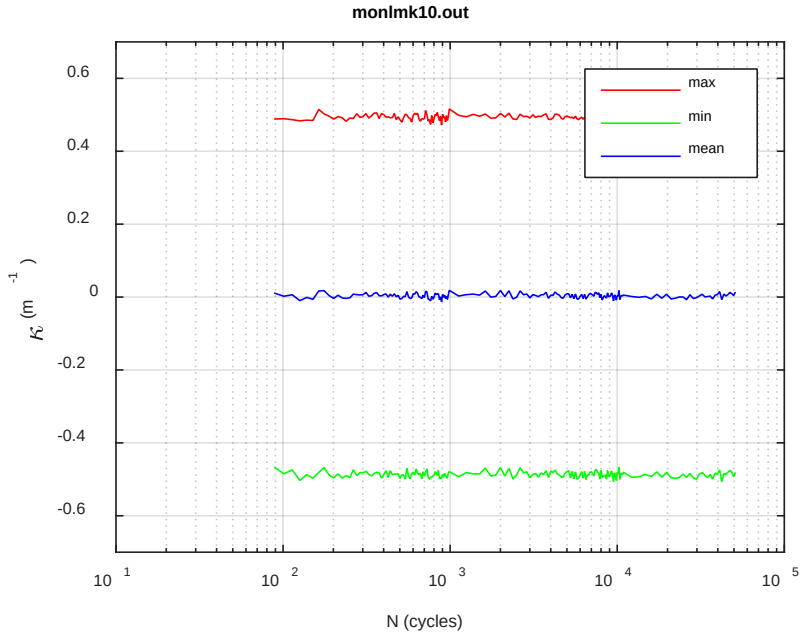
monlmk10.out
max
min
mean
κ (m -1)
N (cycles)

(d)

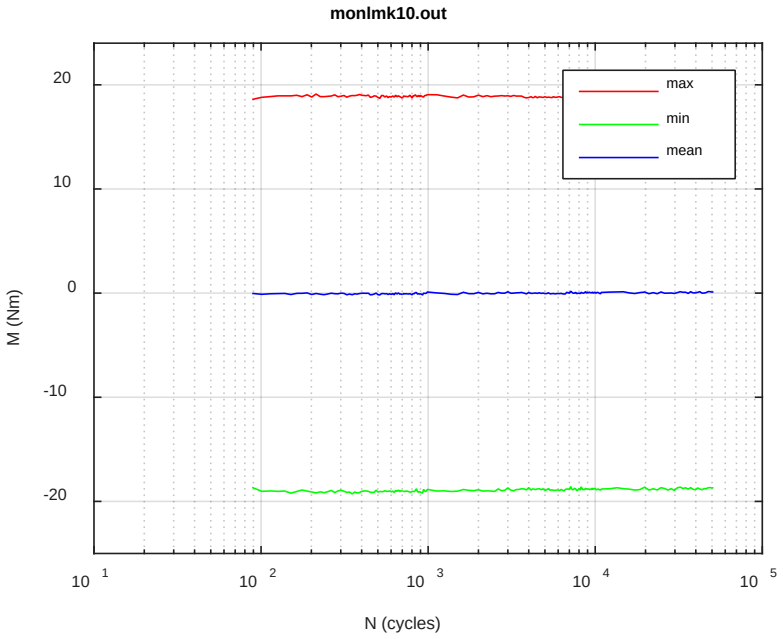

(e)

Fig. A.34. Monitoring-based responses: (a) curvature range, (b) moment range, (c) rigidity, (d) curvature peak/valley, (e) moment peak/valley, LMK10, 20.32 Nm, Nf = 5.20E+04 cycles.

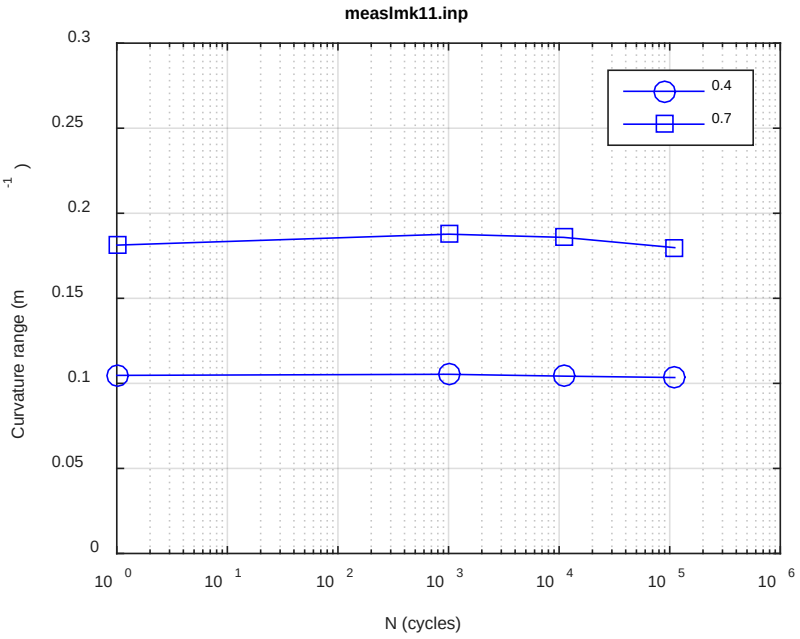
measlmk11.inp
0.3
0.25
0.2
0.15
0.1
0.05
0
Curvature range (m -1)
0.4
0.7
10 0
10 1
10 2
10 3
10 4
10 5
10 6
N (cycles)

(a)

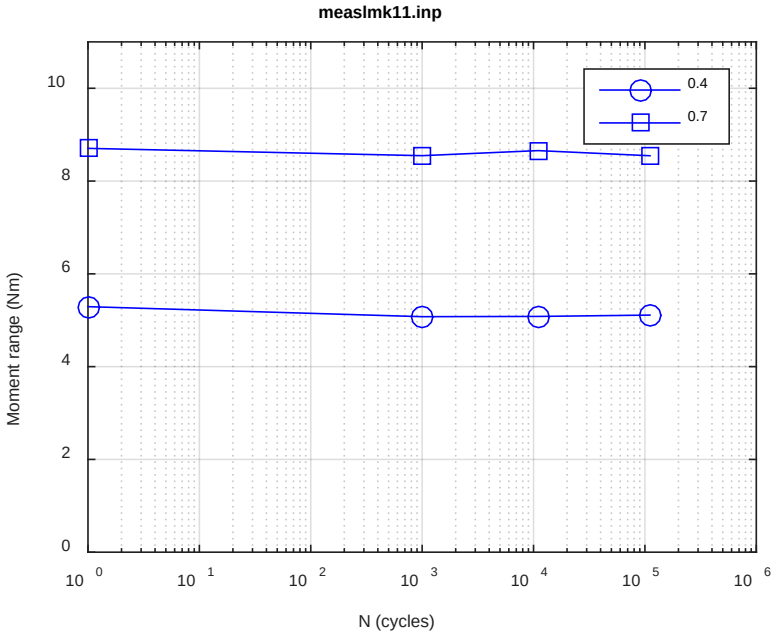
measlmk11.inp
10
8
6
4
2
0
Moment range (Nm)
0.4
0.7
10 0
10 1
10 2
10 3
10 4
10 5
10 6
N (cycles)

(b)

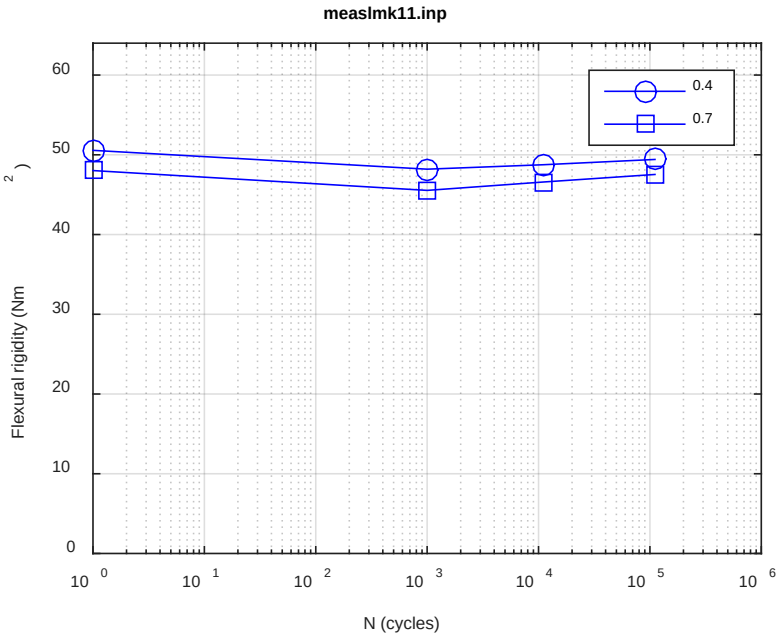
measlmk11.inp
0.4
0.7
Flexural rigidity (Nm 2)
N (cycles)

(c)

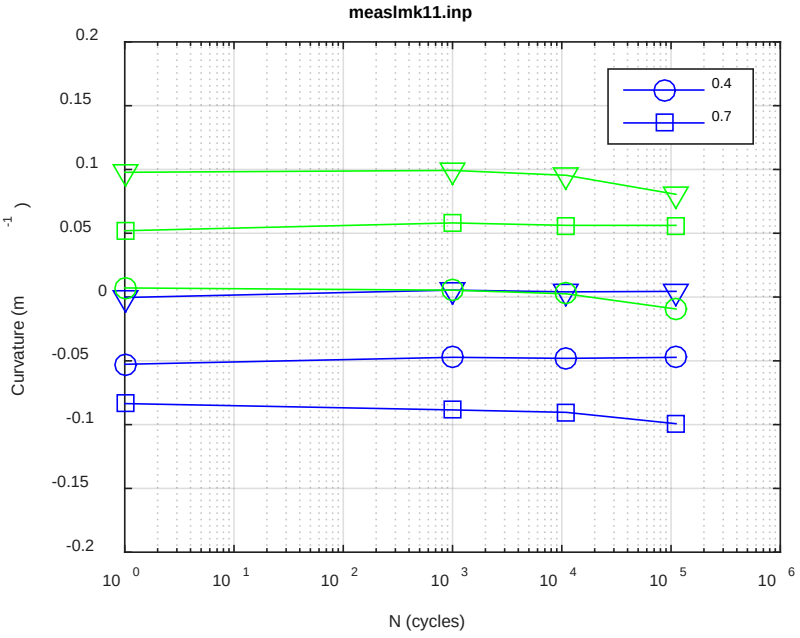
measlmk11.inp
0.4
0.7
Curvature (m -1)
N (cycles)

(d)

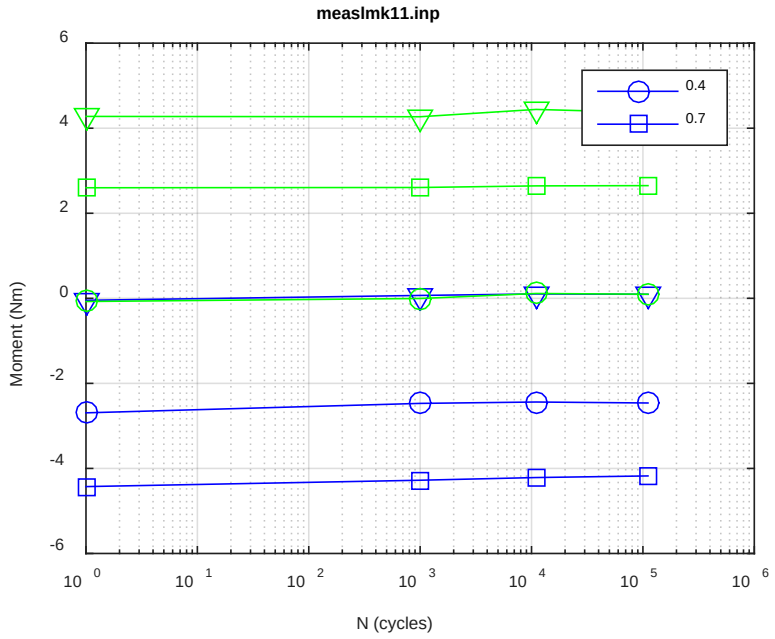

(e)

Fig. A.35. Measurement-based responses: (a) curvature range, (b) moment range, (c) rigidity, (d) curvature peak/valley, (e) moment peak/valley, LMK11, 8.64 Nm.

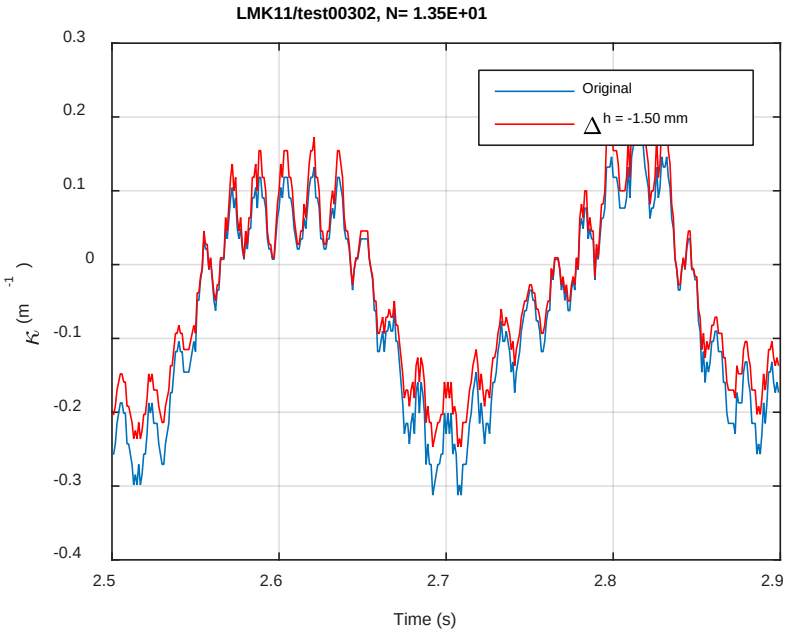
LMK11/test00302, N= 1.35E+01
Original
Δh = -1.50 mm
κ (m-1)
Time (s)

(a)

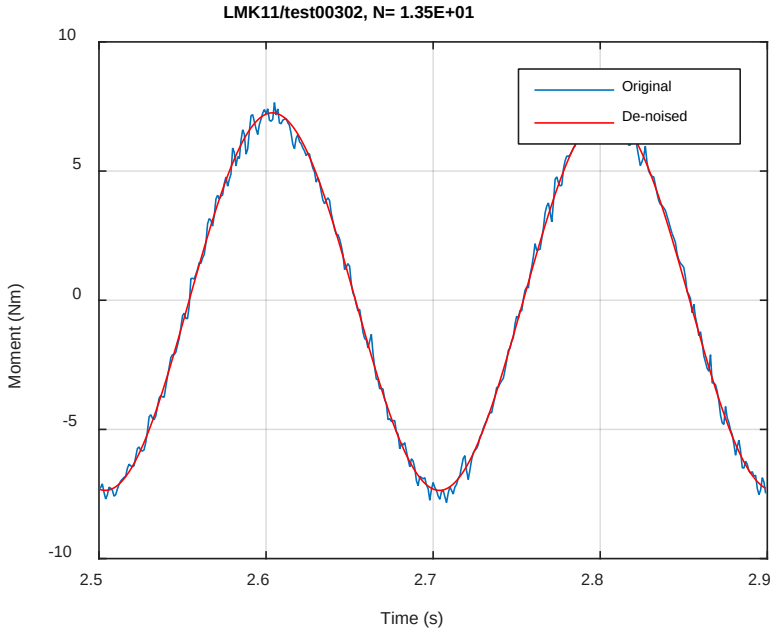
LMK11/test00302, N= 1.35E+01
Original
De-noised
Moment (Nm)
Time (s)

(b)

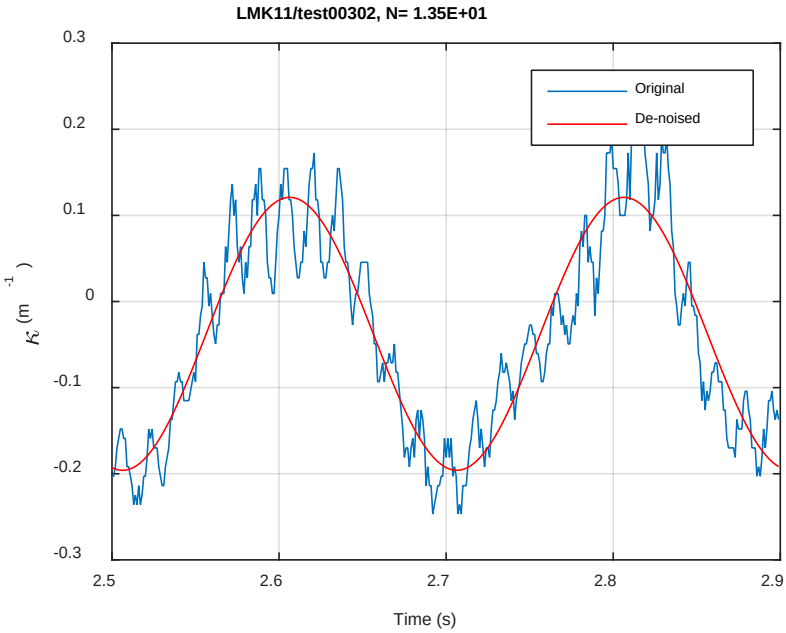

(c)

Fig. A.36. Monitoring-based responses: (a) curvature, (b) moment, (c) curvature, LMK11, 8.64 Nm, Ns = 1.35E+01 cycles.

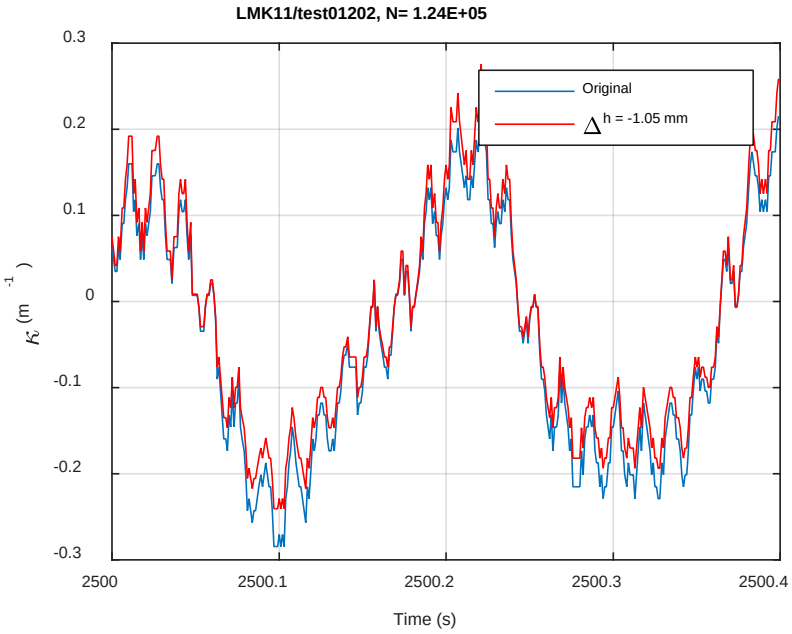
LMK11/test01202, N= 1.24E+05
Original
Δh = -1.05 mm
κ (m-1)
Time (s)
0.3
0.2
0.1
0
-0.1
-0.2
-0.3
2500
2500.1
2500.2
2500.3
2500.4

(a)

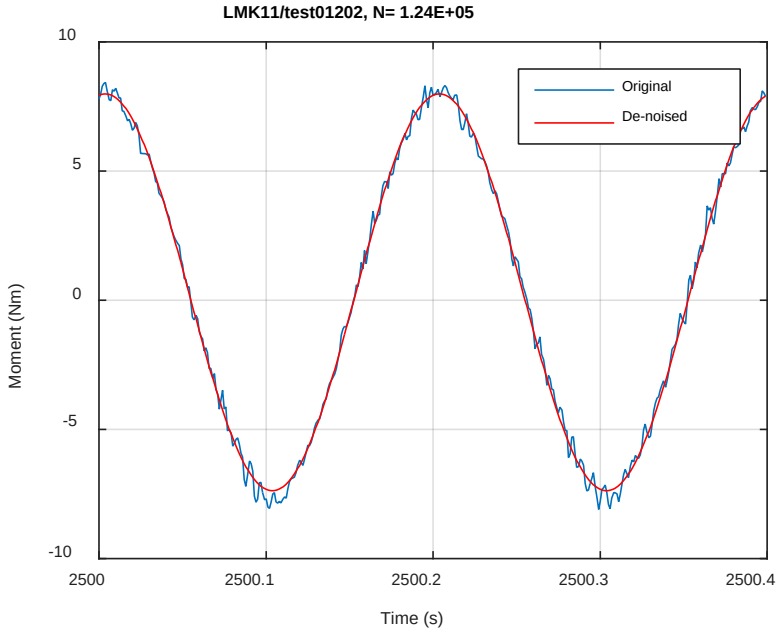
LMK11/test01202, N= 1.24E+05
Original
De-noised
Moment (Nm)
Time (s)
10
5
0
-5
-10
2500
2500.1
2500.2
2500.3
2500.4

(b)

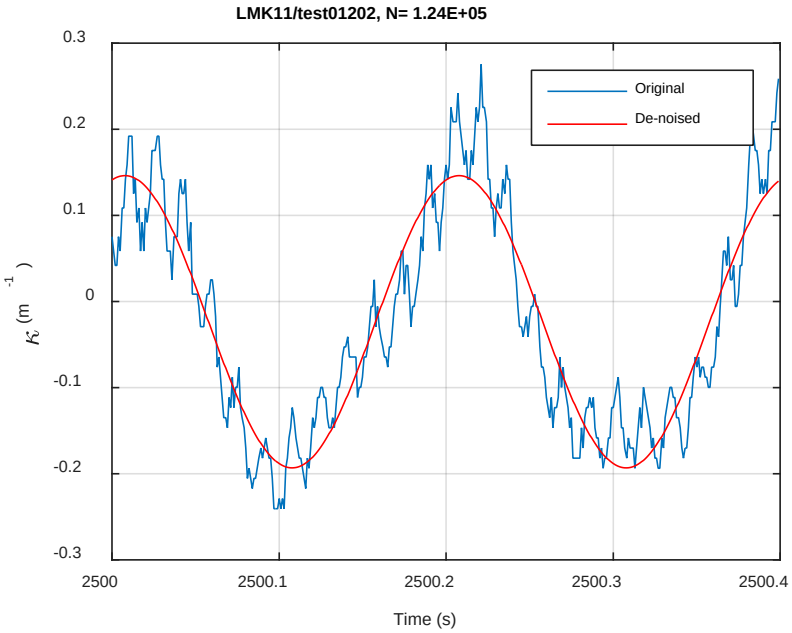

(c)

Fig. A.37. Monitoring-based responses: (a) curvature, (b) moment, (c) curvature, LMK11, 8.64 Nm, Ns = 1.24E+05 cycles.

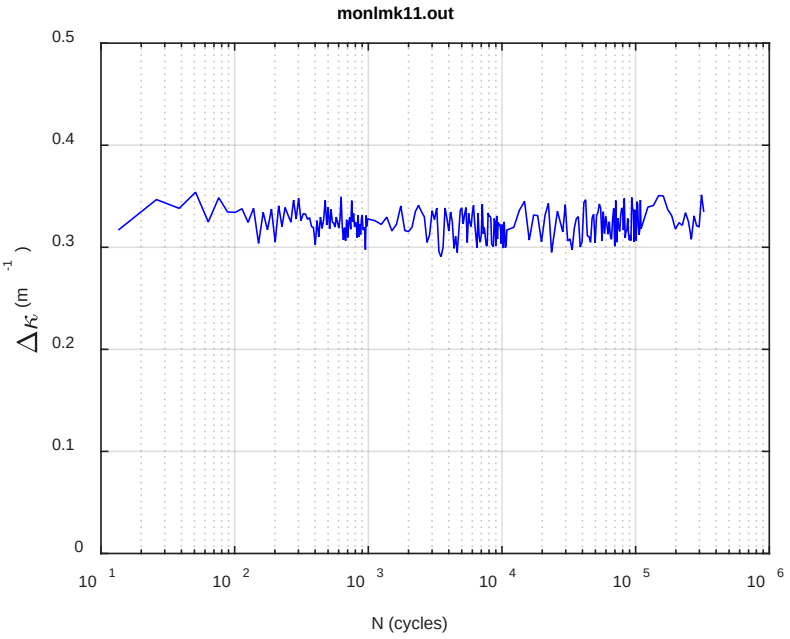
monlmk11.out
0.5
0.4
0.3
0.2
0.1
0
Δκ (m^-1)
10^1
10^2
10^3
10^4
10^5
10^6
N (cycles)

(a)

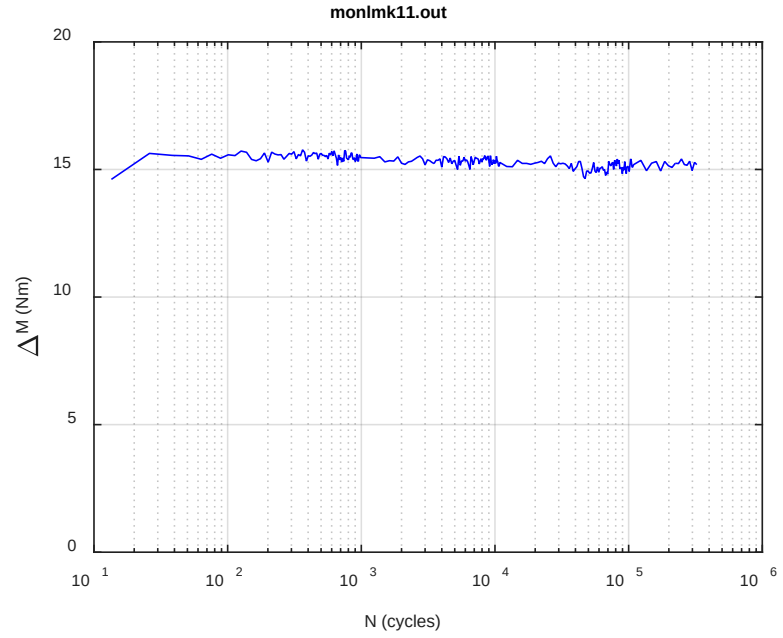
monlmk11.out
20
15
10
5
0
Δ M (Nm)
10^1
10^2
10^3
10^4
10^5
10^6
N (cycles)

(b)

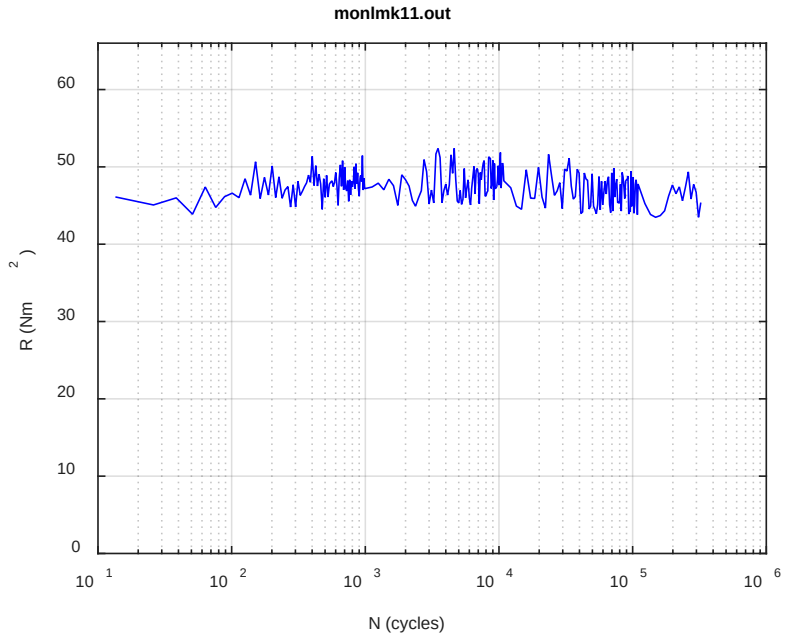
monlmk11.out
R (Nm 2)
N (cycles)

(c)

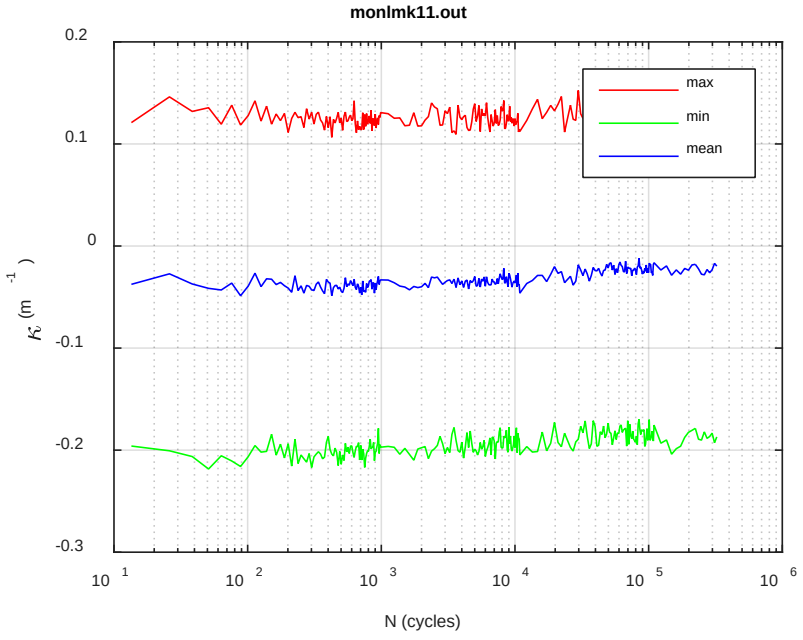
monlmk11.out
max
min
mean
κ (m -1)
N (cycles)

(d)

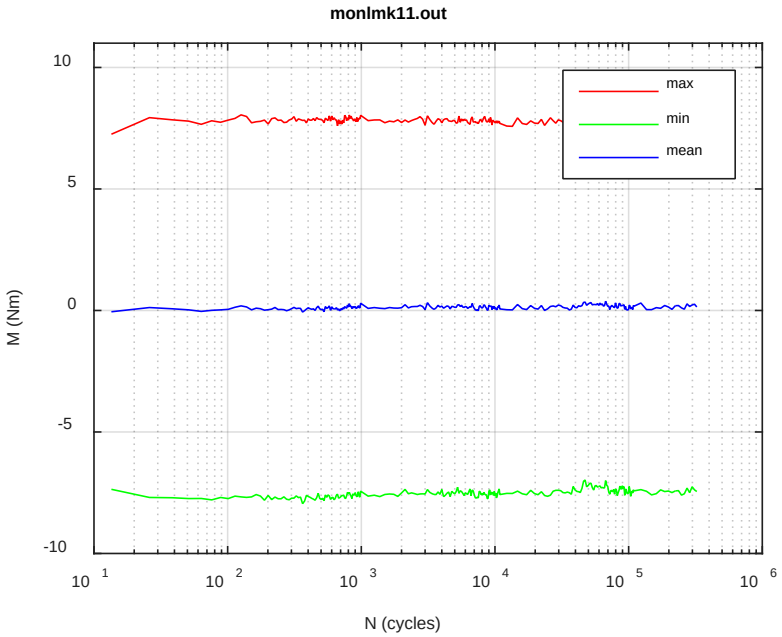

(e)

Fig. A.38. Monitoring-based responses: (a) curvature range, (b) moment range, (c) rigidity, (d) curvature peak/valley, (e) moment peak/valley, LMK11, 8.64 Nm, Nf = 3.55E+05 cycles.

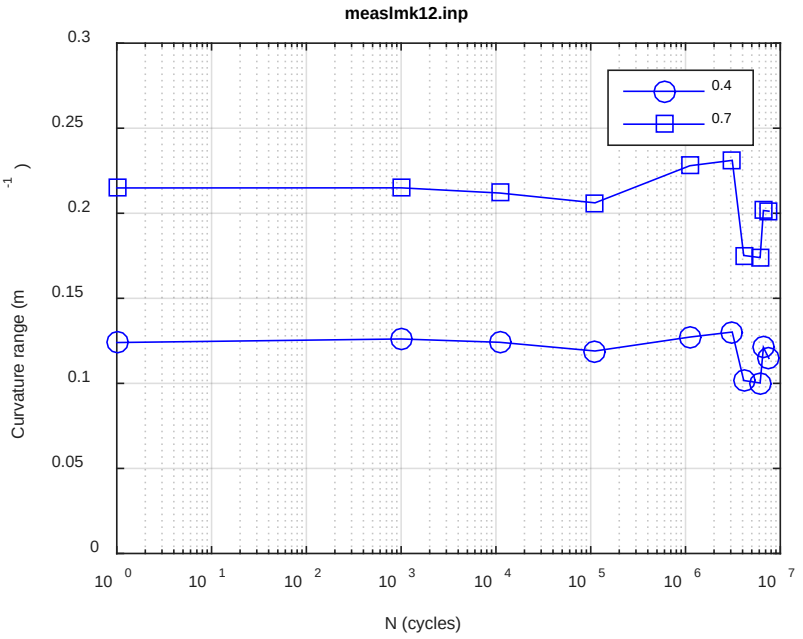
measlmk12.inp
0.4
0.7
Curvature range (m-1)
N (cycles)

(a)

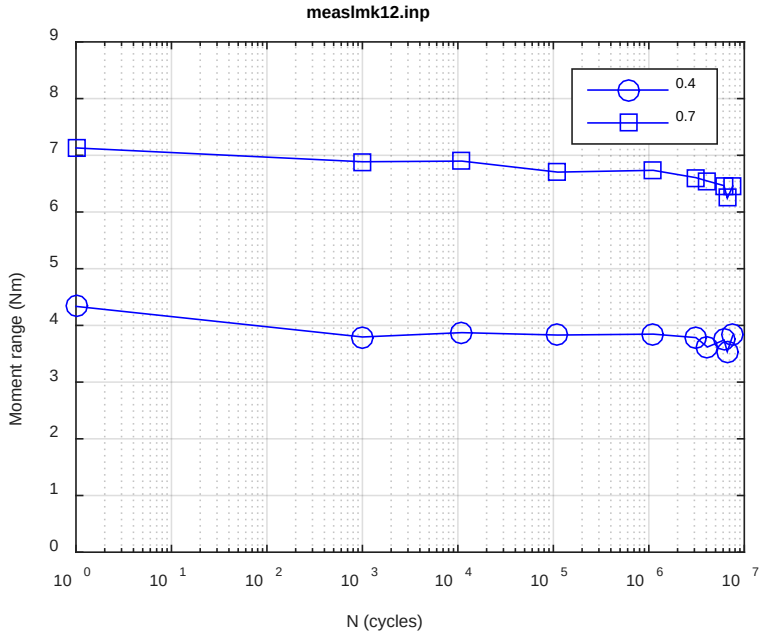
measlmk12.inp
0.4
0.7
Moment range (Nm)
N (cycles)

(b)

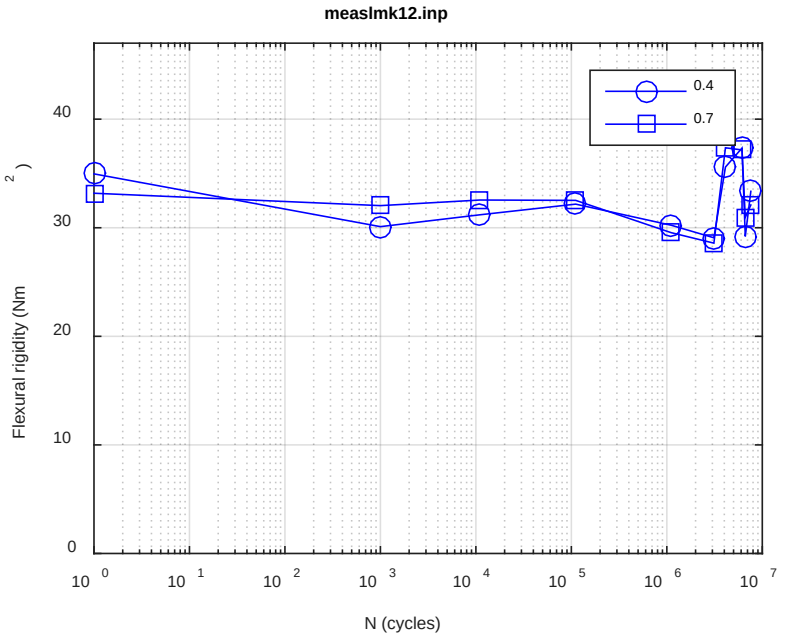
measlmk12.inp
0.4
0.7
Flexural rigidity (Nm 2)
N (cycles)

(c)

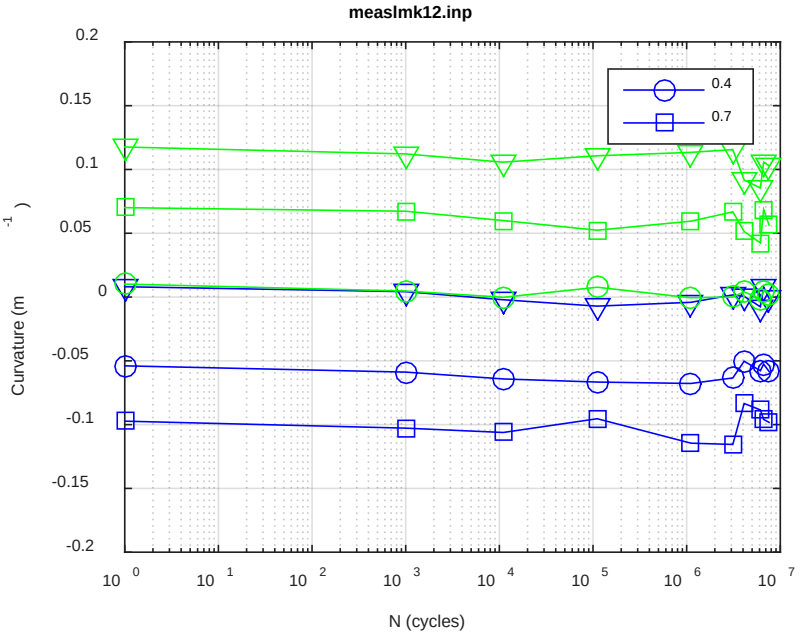
measlmk12.inp
0.4
0.7
Curvature (m -1)
N (cycles)

(d)

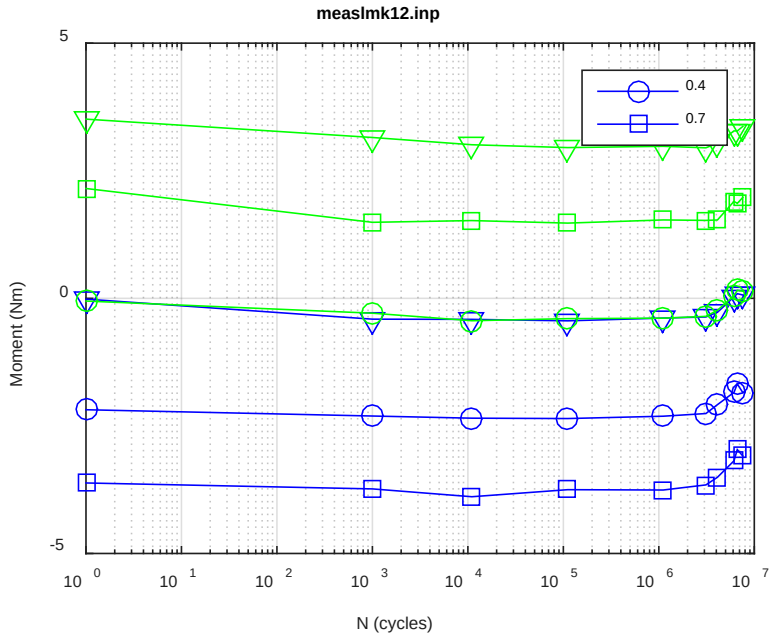

(e)

Fig. A.39. Measurement-based responses: (a) curvature range, (b) moment range, (c) rigidity, (d) curvature peak/valley, (e) moment peak/valley, LMK12, 7.11 Nm.

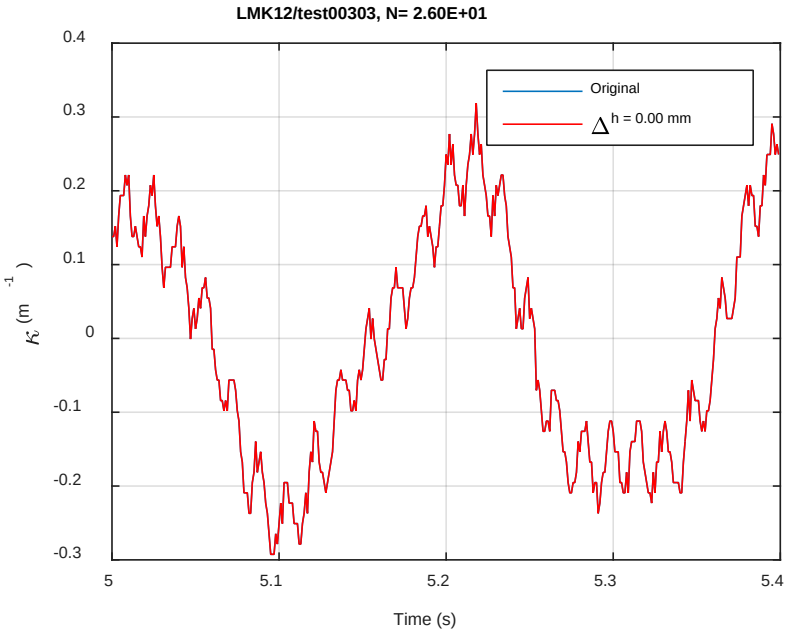
LMK12/test00303, N= 2.60E+01
Original
Δh = 0.00 mm
κ (m-1)
Time (s)

(a)

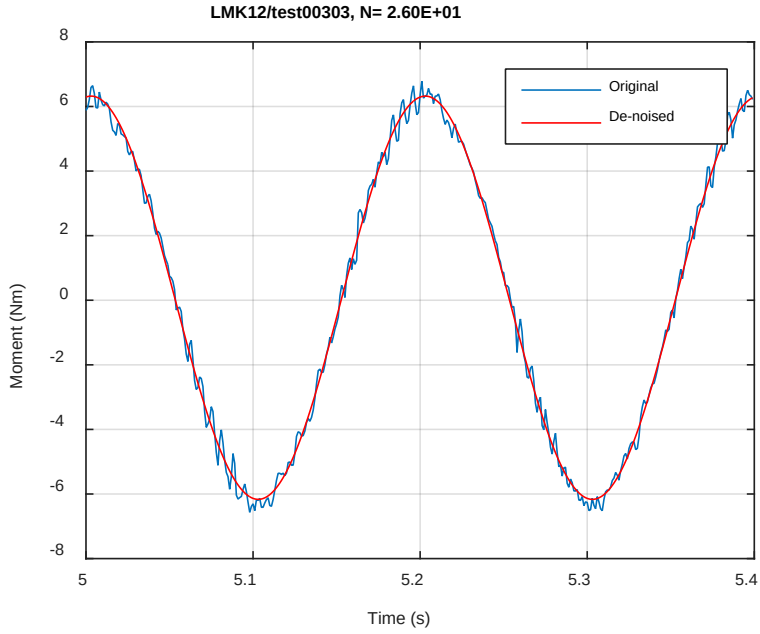
LMK12/test00303, N= 2.60E+01
Original
De-noised
Moment (Nm)
Time (s)

(b)

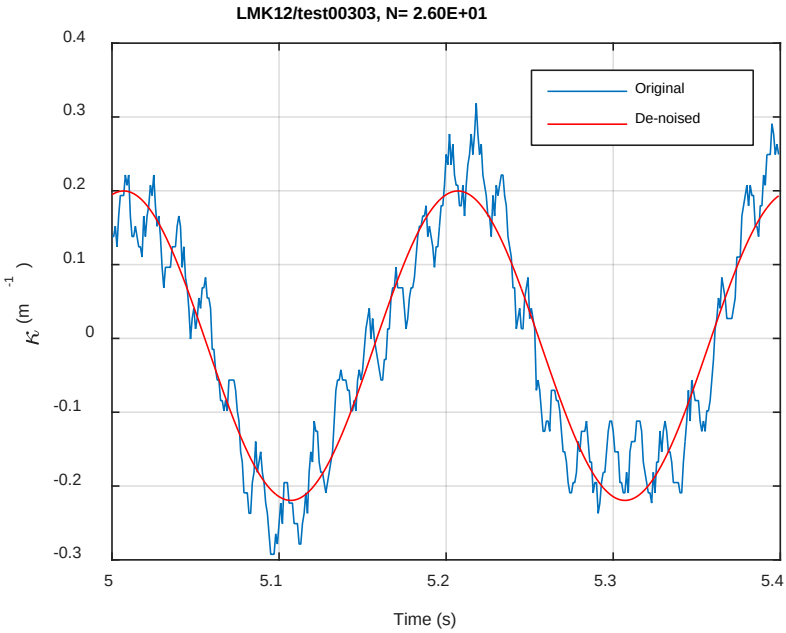

(c)

Fig. A.40. Monitoring-based responses: (a) curvature, (b) moment, (c) curvature, LMK12, 7.11 Nm, Ns = 2.60E+01 cycles.

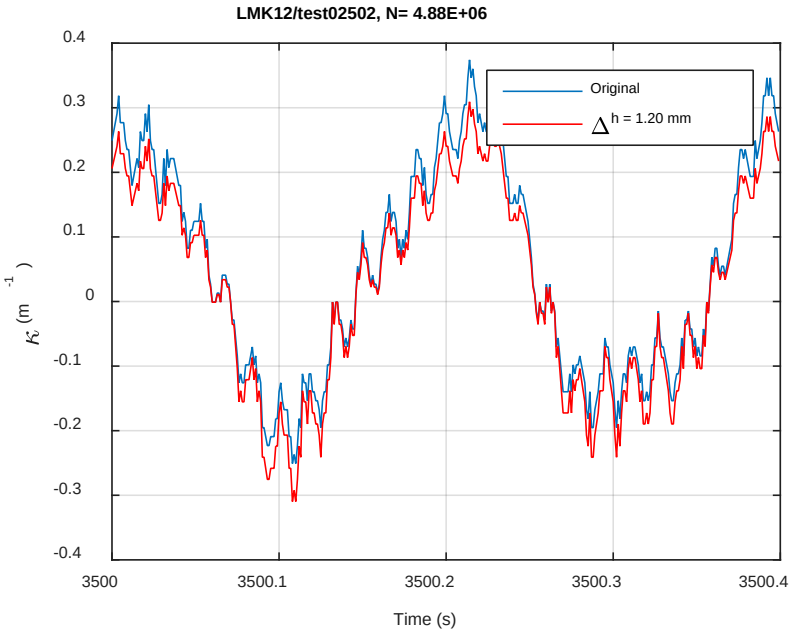
LMK12/test02502, N= 4.88E+06
Original
Δh = 1.20 mm
κ (m-1)
Time (s)
0.4
0.3
0.2
0.1
0
-0.1
-0.2
-0.3
-0.4
3500
3500.1
3500.2
3500.3
3500.4

(a)

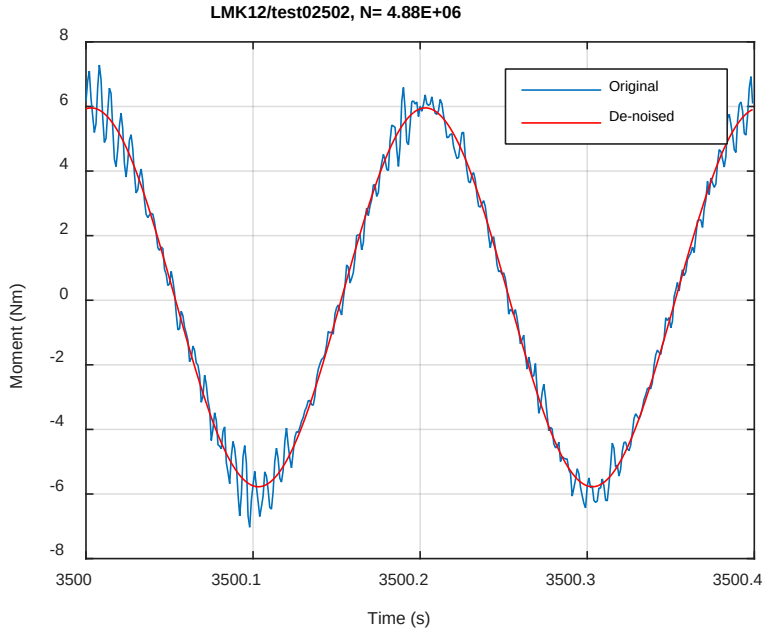
LMK12/test02502, N= 4.88E+06
Original
De-noised
Moment (Nm)
Time (s)
8
6
4
2
0
-2
-4
-6
-8
3500
3500.1
3500.2
3500.3
3500.4

(b)

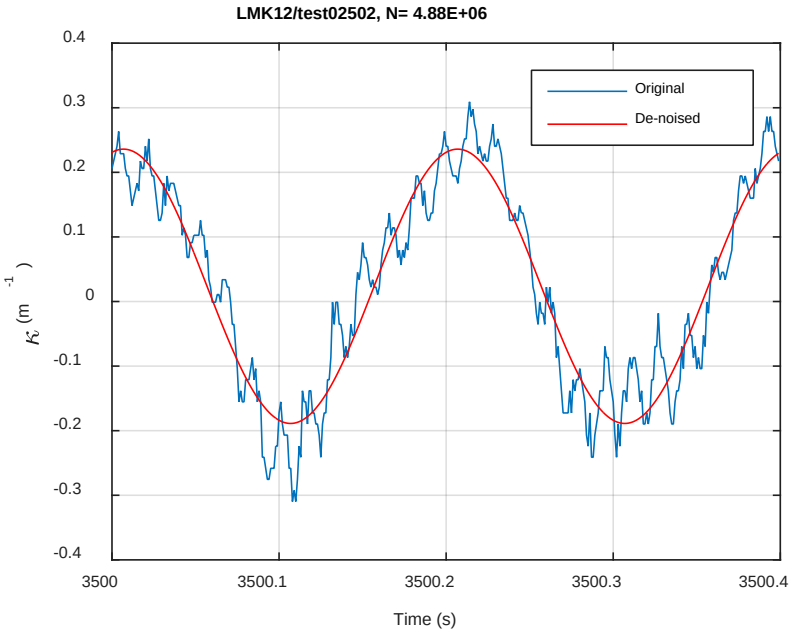

(c)

Fig. A.41. Monitoring-based responses: (a) curvature, (b) moment, (c) curvature, LMK12, 7.11 Nm, Ns = 4.88E+06 cycles.

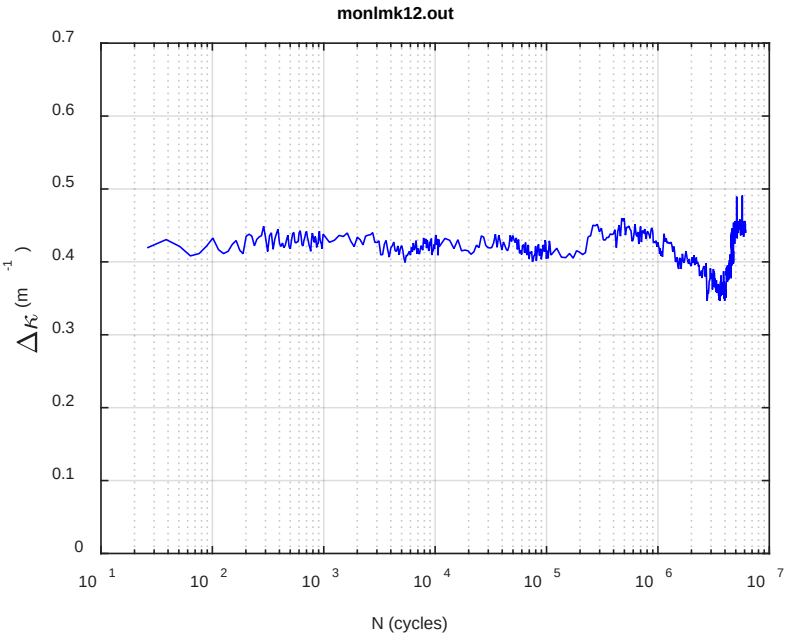
monlmk12.out
0.7
0.6
0.5
0.4
0.3
0.2
0.1
0
Δκ (m -1)
10 1
10 2
10 3
10 4
10 5
10 6
10 7
N (cycles)

(a)

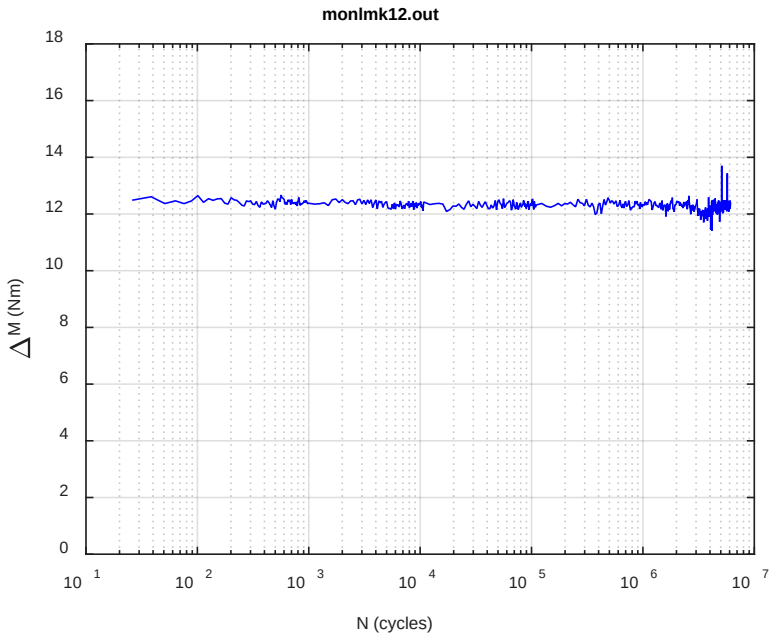
monlmk12.out
18
16
14
12
10
8
6
4
2
0
Δ M (Nm)
10 1
10 2
10 3
10 4
10 5
10 6
10 7
N (cycles)

(b)

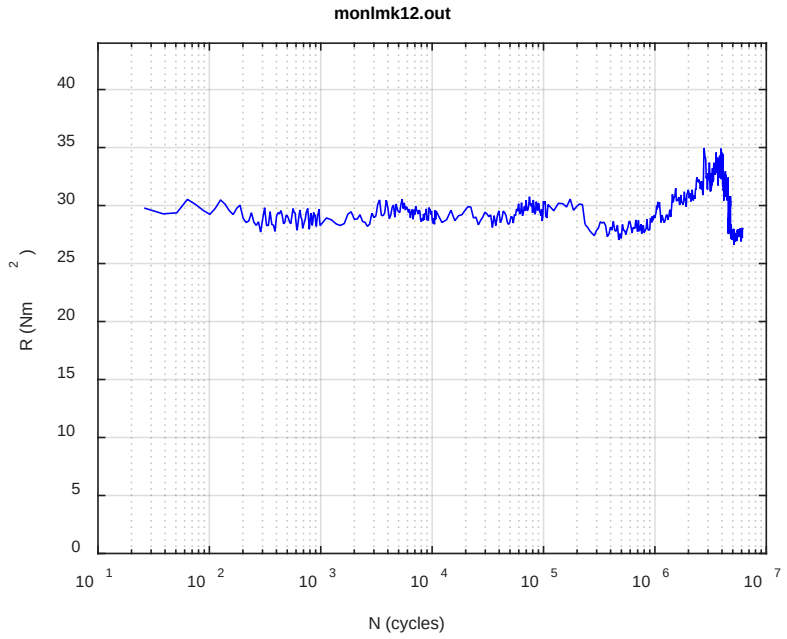
monlmk12.out
R (Nm 2)
N (cycles)

(c)

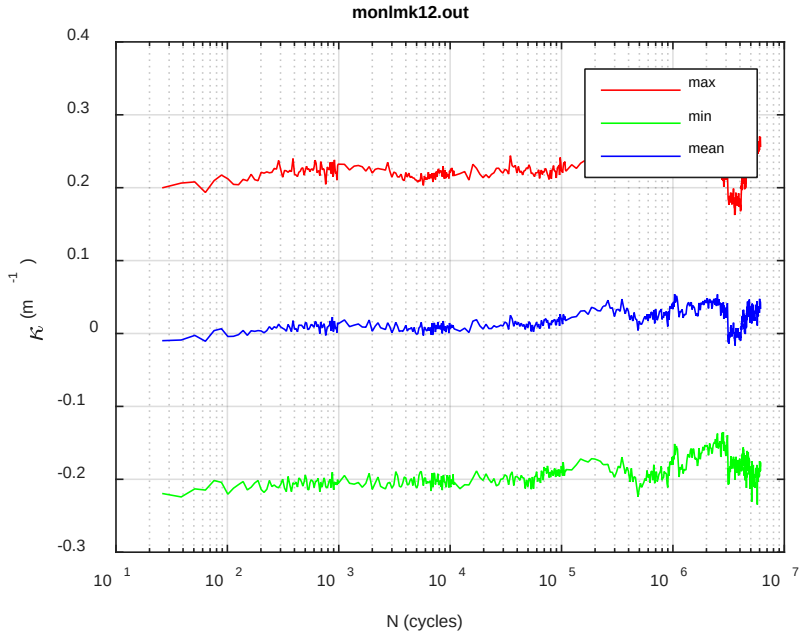
monlmk12.out
max
min
mean
κ (m -1)
N (cycles)

(d)

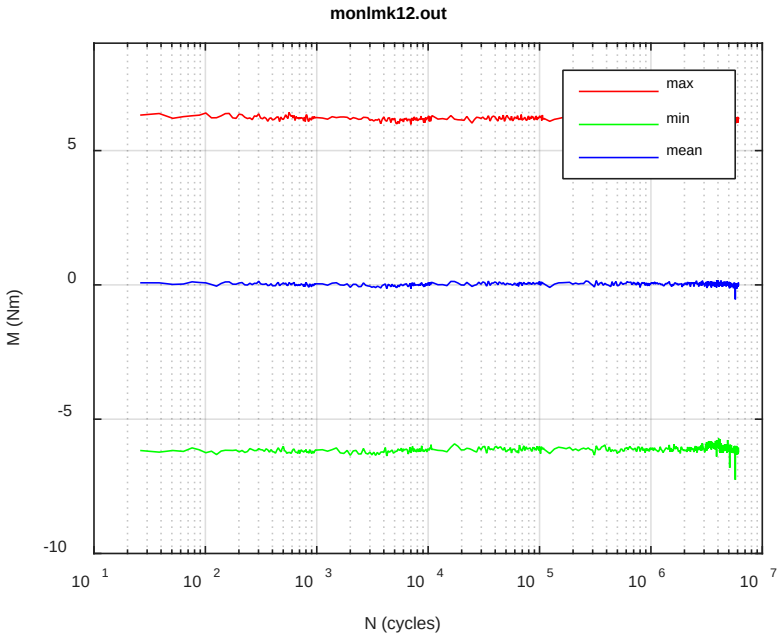

(e)

Fig. A.42. Monitoring-based responses: (a) curvature range, (b) moment range, (c) rigidity, (d) curvature peak/valley, (e) moment peak/valley, LMK12, 7.11 Nm, Nf = 7.58E+06 cycles.

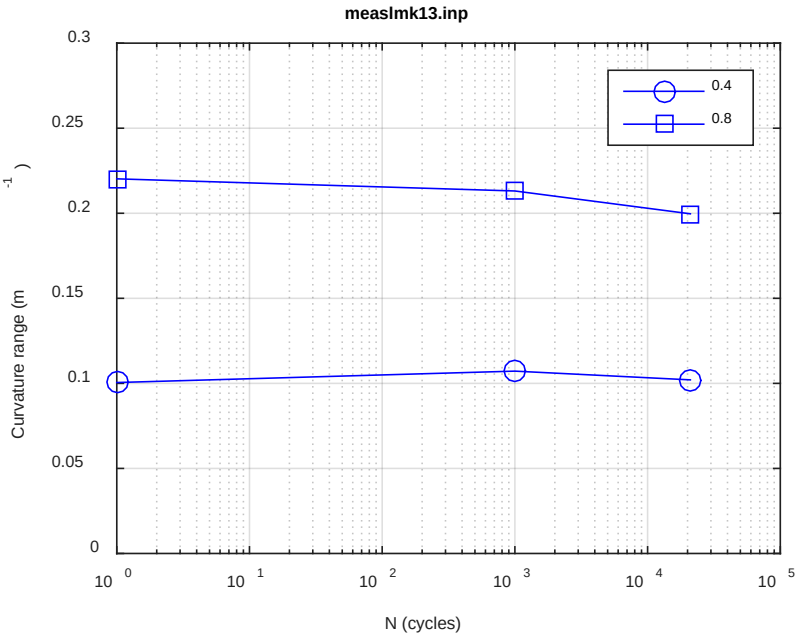
measlmk13.inp
0.3
0.25
0.2
0.15
0.1
0.05
0
Curvature range (m -1)
0.4
0.8
10 0
10 1
10 2
10 3
10 4
10 5
N (cycles)

(a)

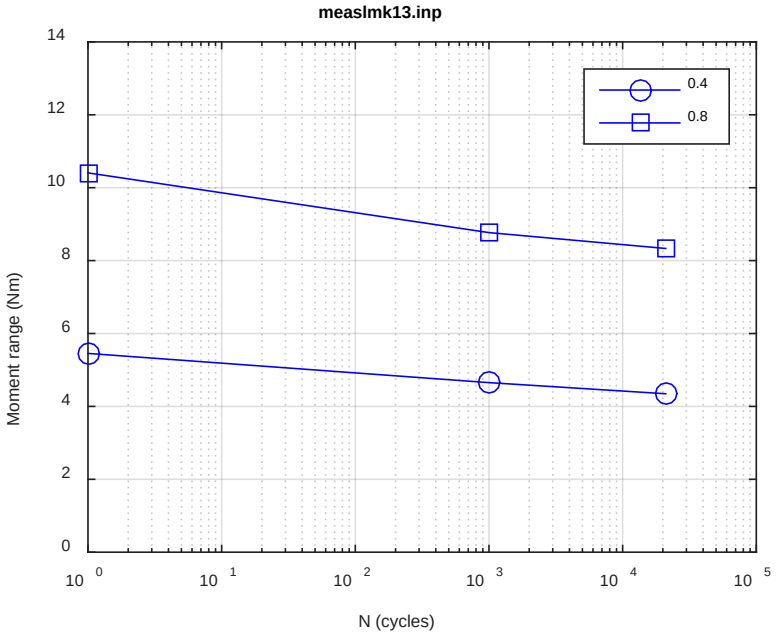
measlmk13.inp
14
12
10
8
6
4
2
0
Moment range (Nm)
0.4
0.8
10 0
10 1
10 2
10 3
10 4
10 5
N (cycles)

(b)

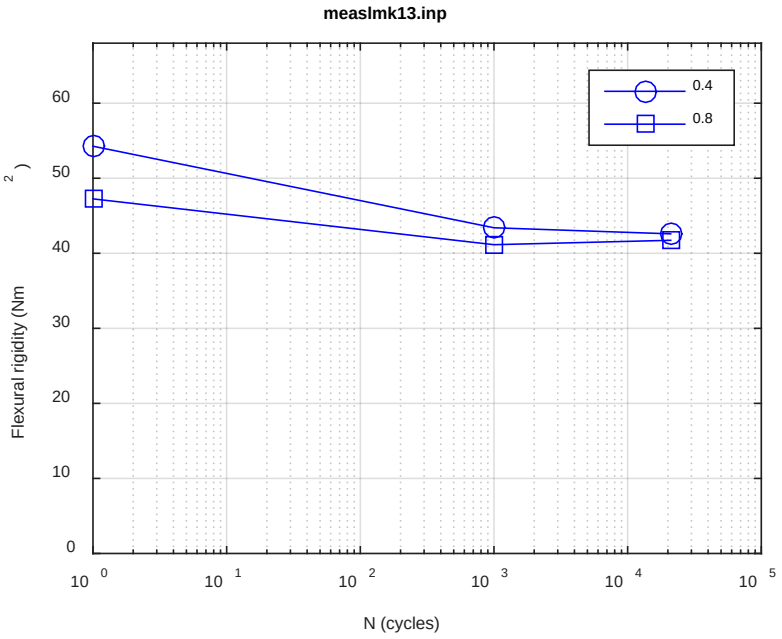
measlmk13.inp
0.4
0.8
Flexural rigidity (Nm 2)
N (cycles)

(c)

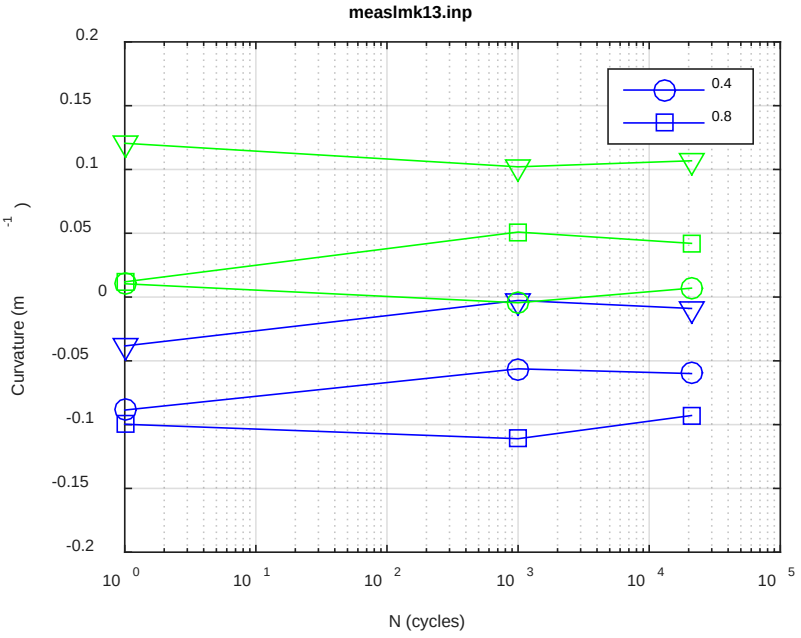
measlmk13.inp
0.4
0.8
Curvature (m -1)
N (cycles)

(d)

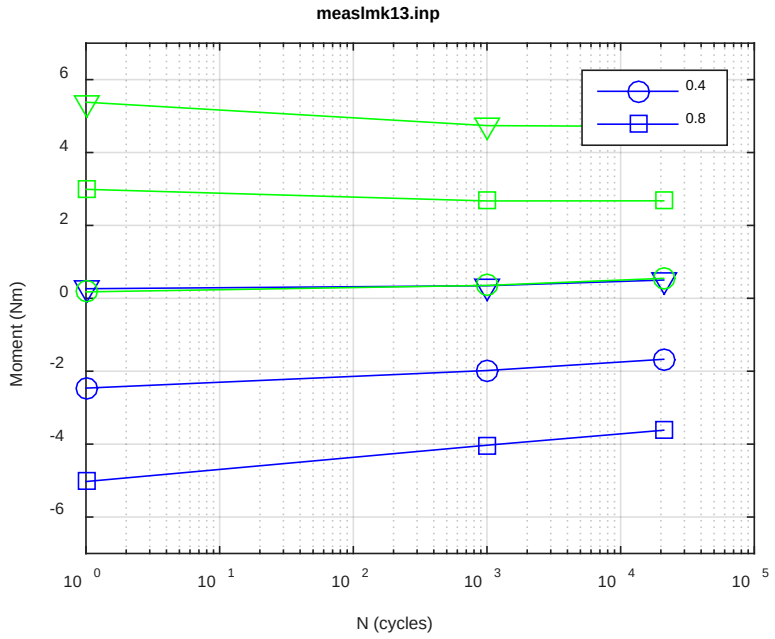

(e)

Fig. A.43. Measurement-based responses: (a) curvature range, (b) moment range, (c) rigidity, (d) curvature peak/valley, (e) moment peak/valley, LMK13, 25.40 Nm.

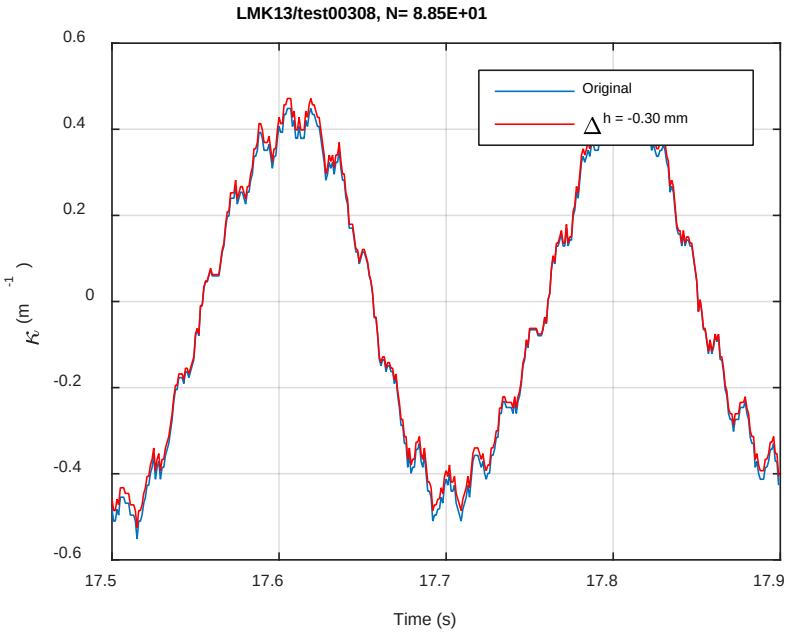
LMK13/test00308, N= 8.85E+01
Original
Δh = -0.30 mm
κ (m-1)
Time (s)
0.6
0.4
0.2
0
-0.2
-0.4
-0.6
17.5
17.6
17.7
17.8
17.9

(a)

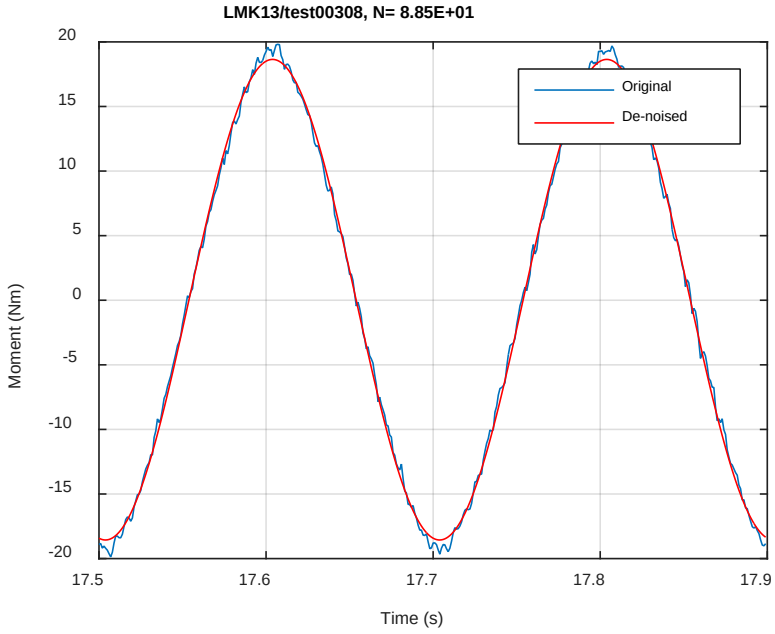
LMK13/test00308, N= 8.85E+01
Original
De-noised
Moment (Nm)
Time (s)
20
15
10
5
0
-5
-10
-15
-20
17.5
17.6
17.7
17.8
17.9

(b)

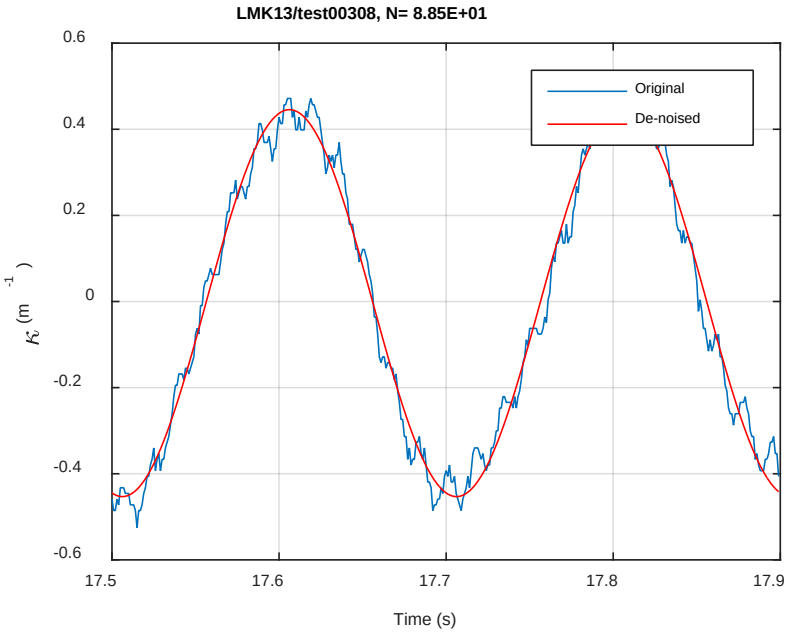

(c)

Fig. A.44. Monitoring-based responses: (a) curvature, (b) moment, (c) curvature, LMK13, 25.40 Nm, Ns = 8.85E+01 cycles.

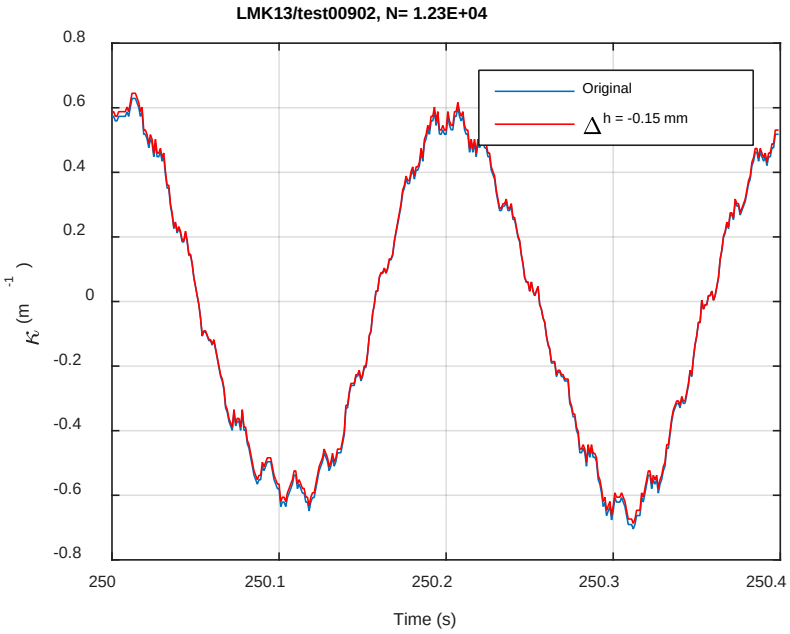
LMK13/test00902, N= 1.23E+04
Original
Δh = -0.15 mm
κ (m-1)
Time (s)
0.8
0.6
0.4
0.2
0
-0.2
-0.4
-0.6
-0.8
250
250.1
250.2
250.3
250.4

(a)

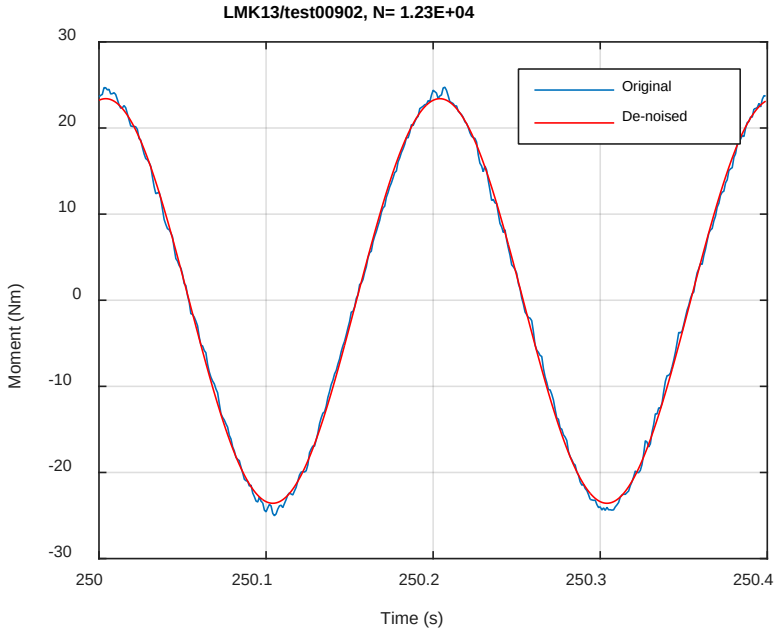
LMK13/test00902, N= 1.23E+04
Original
De-noised
Moment (Nm)
Time (s)
30
20
10
0
-10
-20
-30
250
250.1
250.2
250.3
250.4

(b)

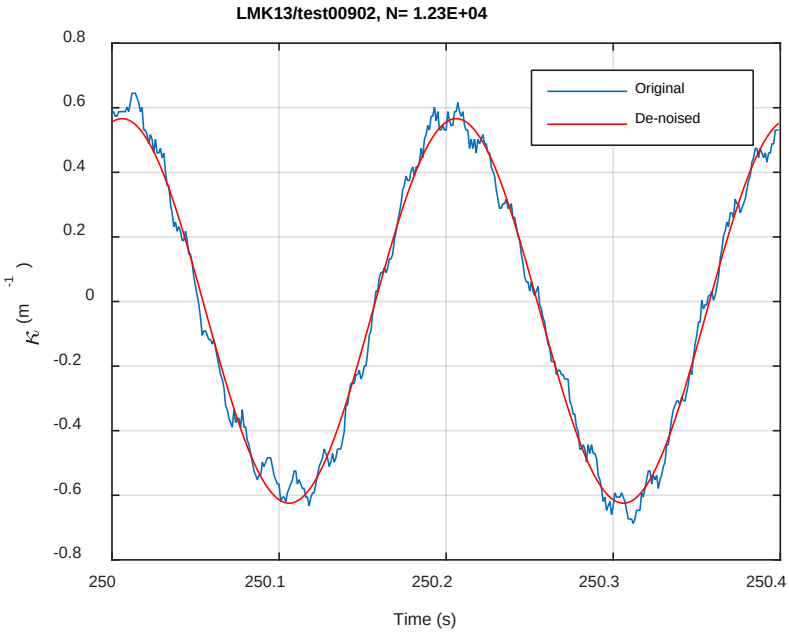

(c)

Fig. A.45. Monitoring-based responses: (a) curvature, (b) moment, (c) curvature, LMK13, 25.40 Nm, Ns = 1.23E+04 cycles.

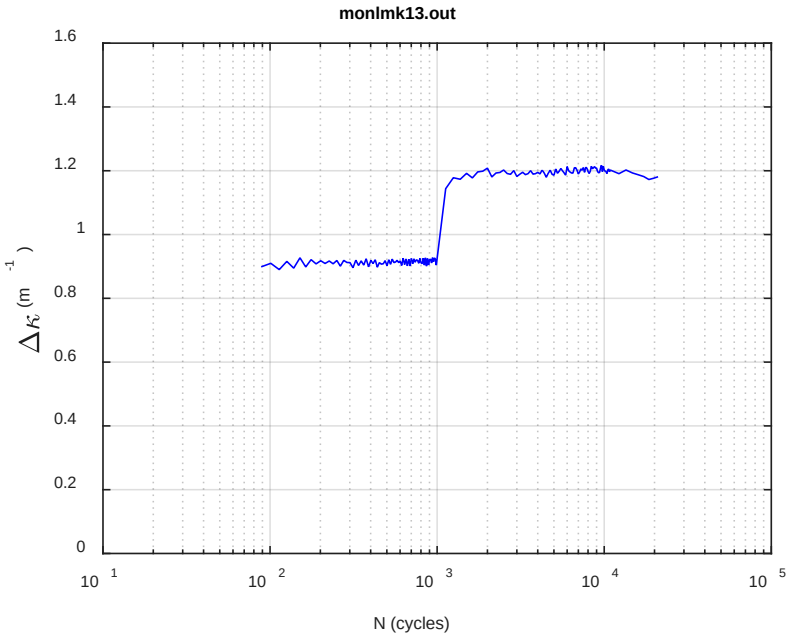
monlmk13.out
1.6
1.4
1.2
1
0.8
0.6
0.4
0.2
0
Δκ (m -1)
10 1
10 2
10 3
10 4
10 5
N (cycles)

(a)

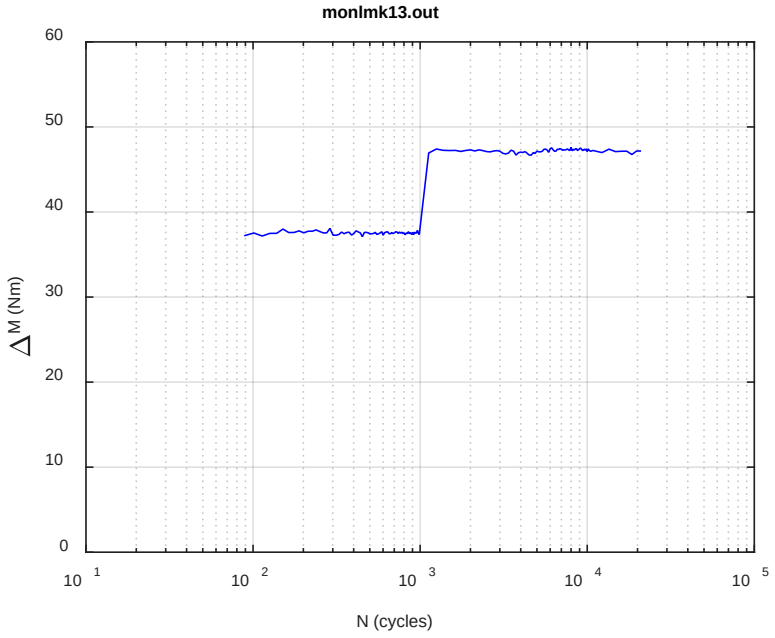
monlmk13.out
60
50
40
30
20
10
0
Δ M (Nm)
10 1
10 2
10 3
10 4
10 5
N (cycles)

(b)

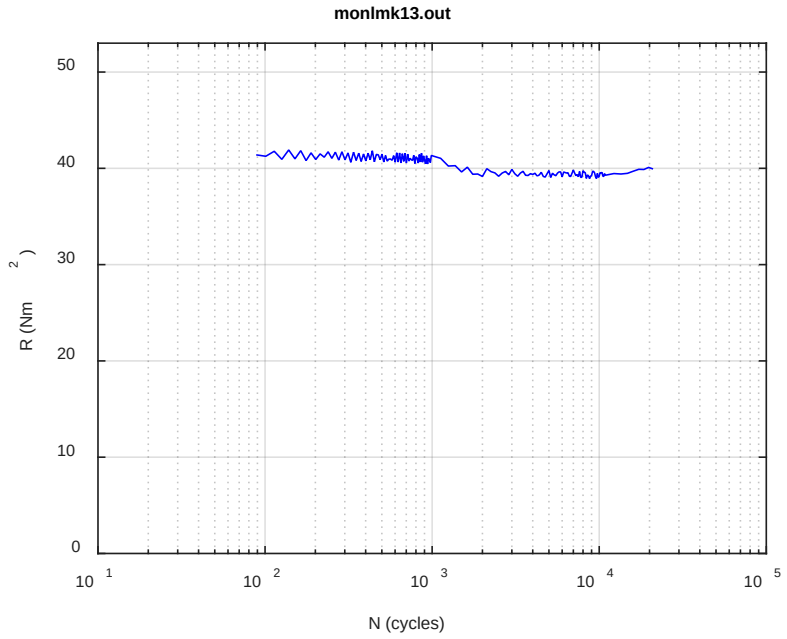
monlmk13.out
R (Nm 2)
N (cycles)

(c)

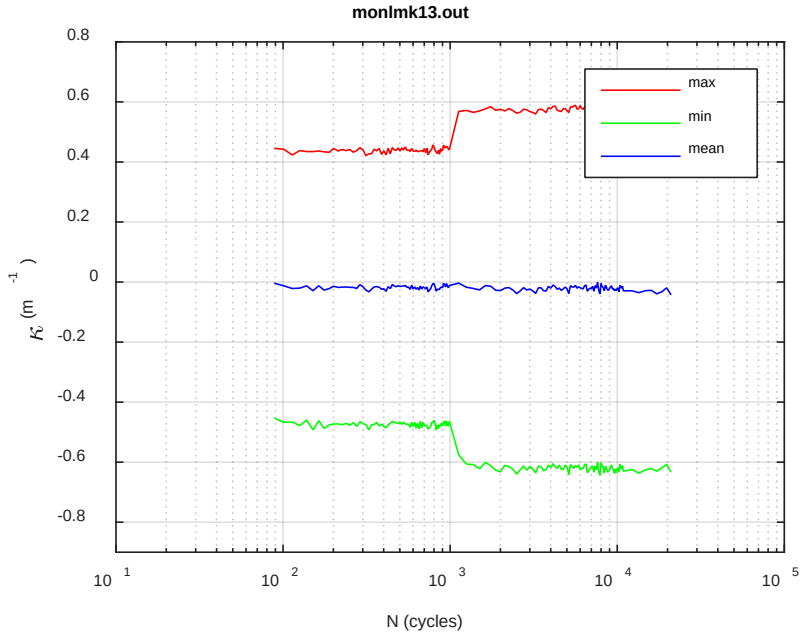
monlmk13.out
max
min
mean
κ (m -1)
N (cycles)

(d)

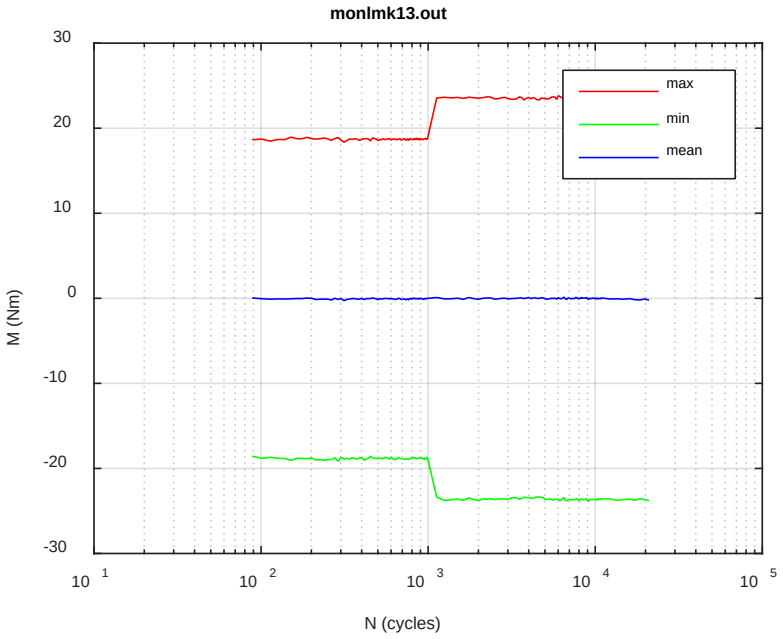

(e)

Fig. A.46. Monitoring-based responses: (a) curvature range, (b) moment range, (c) rigidity, (d) curvature peak/valley, (e) moment peak/valley, LMK13, 25.40 Nm, Nf = 2.10E+04 cycles.

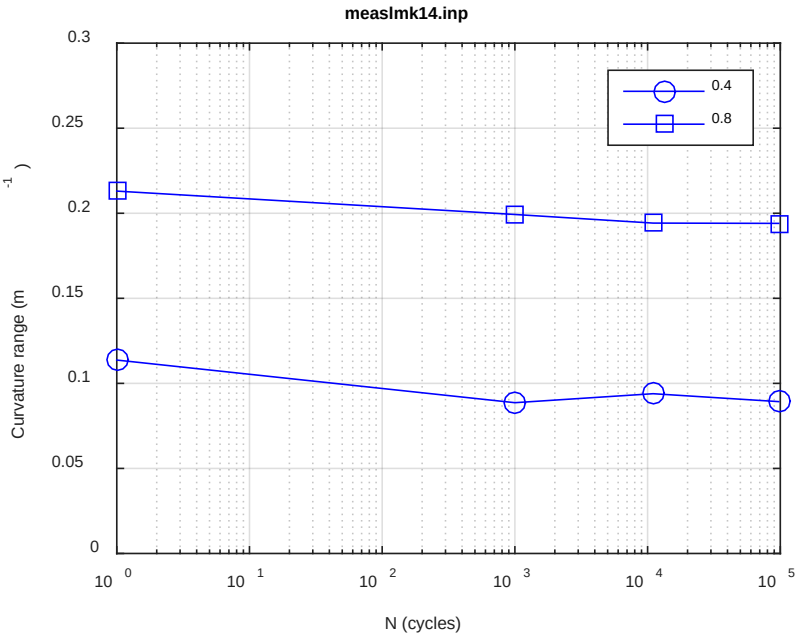
measlmk14.inp
0.3
0.25
0.2
0.15
0.1
0.05
0
Curvature range (m-1)
0.4
0.8
10 0
10 1
10 2
10 3
10 4
10 5
N (cycles)

(a)

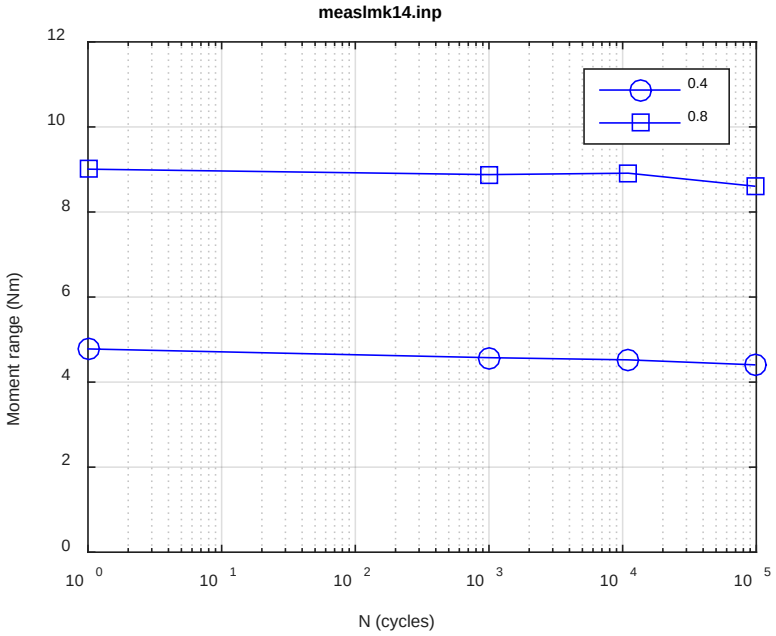
measlmk14.inp
12
10
8
6
4
2
0
Moment range (Nm)
0.4
0.8
10 0
10 1
10 2
10 3
10 4
10 5
N (cycles)

(b)

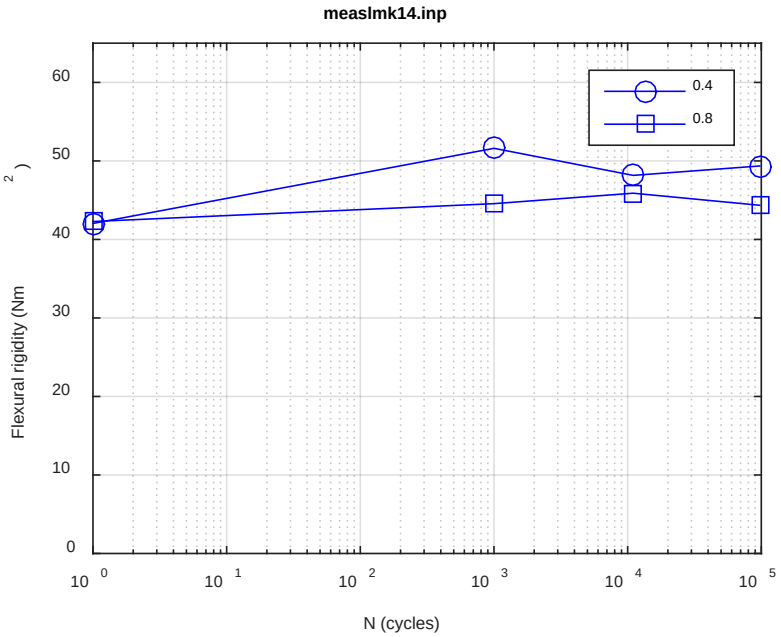
measlmk14.inp
0.4
0.8
Flexural rigidity (Nm 2)
N (cycles)
0
10
20
30
40
50
60
10 0
10 1
10 2
10 3
10 4
10 5

(c)

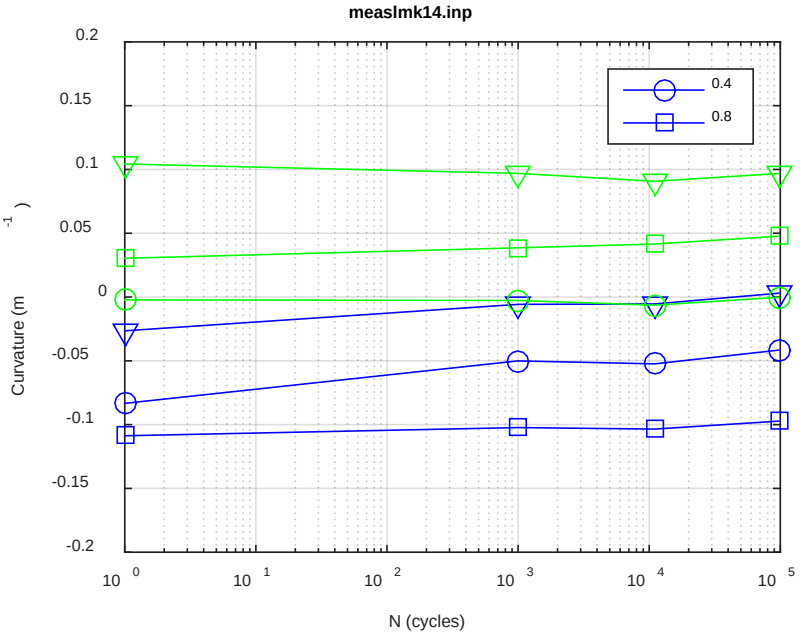
measlmk14.inp
0.4
0.8
Curvature (m -1)
N (cycles)
0.2
0.15
0.1
0.05
0
-0.05
-0.1
-0.15
-0.2
10 0
10 1
10 2
10 3
10 4
10 5

(d)

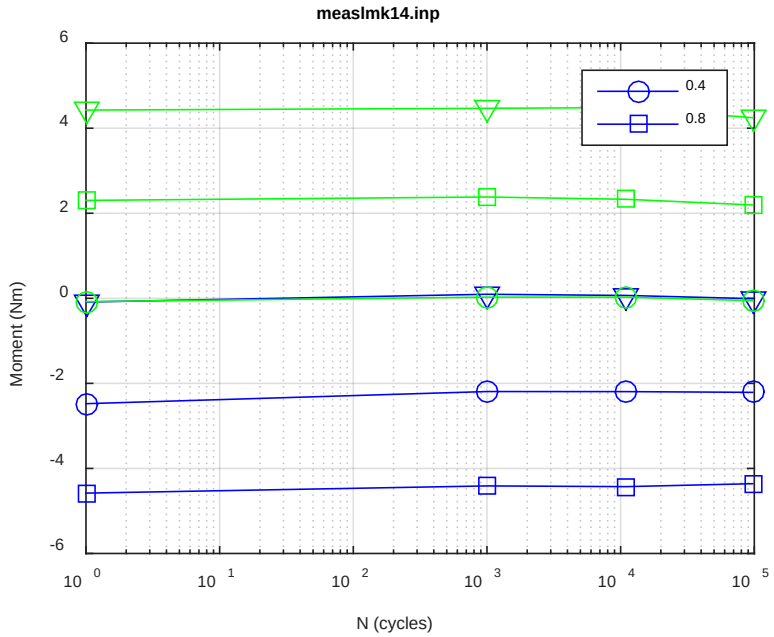

(e)

Fig. A.47. Measurement-based responses: (a) curvature range, (b) moment range, (c) rigidity, (d) curvature peak/valley, (e) moment peak/valley, LMK14, 10.16 Nm.

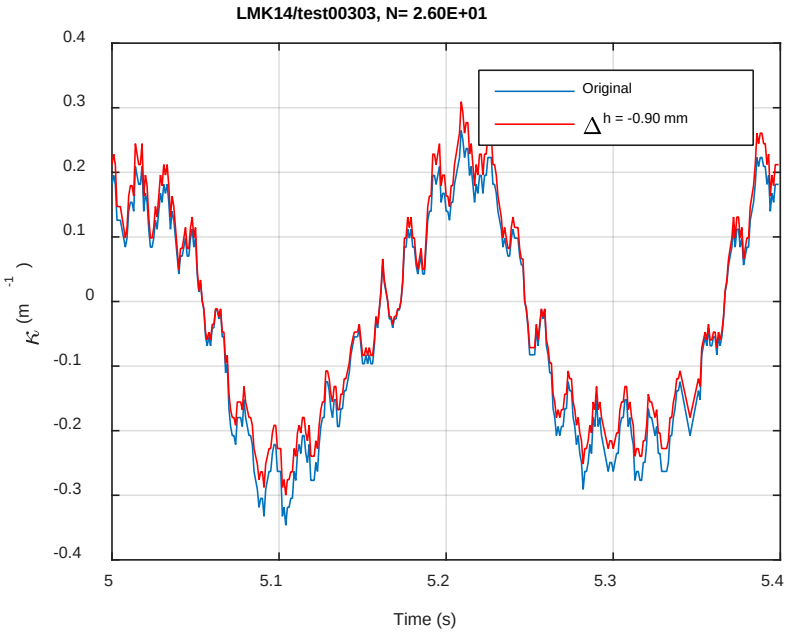
LMK14/test00303, N= 2.60E+01
Original
Δh = -0.90 mm
κ (m-1)
Time (s)

(a)

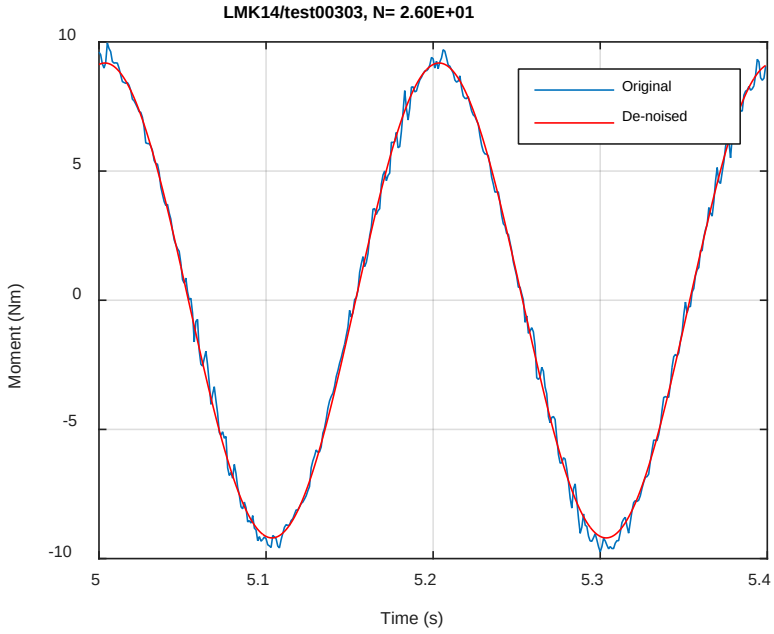
LMK14/test00303, N= 2.60E+01
Original
De-noised
Moment (Nm)
Time (s)

(b)

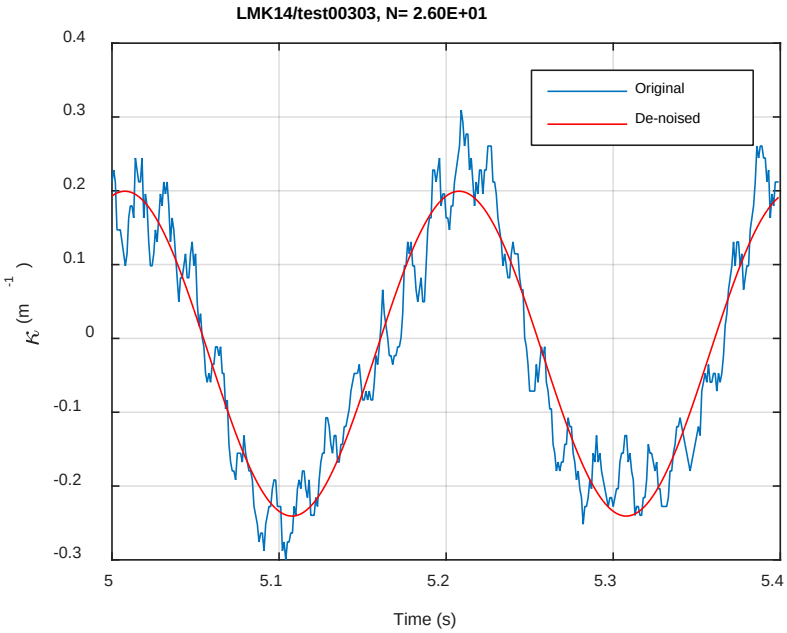

(c)

Fig. A.48. Monitoring-based responses: (a) curvature, (b) moment, (c) curvature, LMK14, 10.16 Nm, Ns = 2.60E+01 cycles.

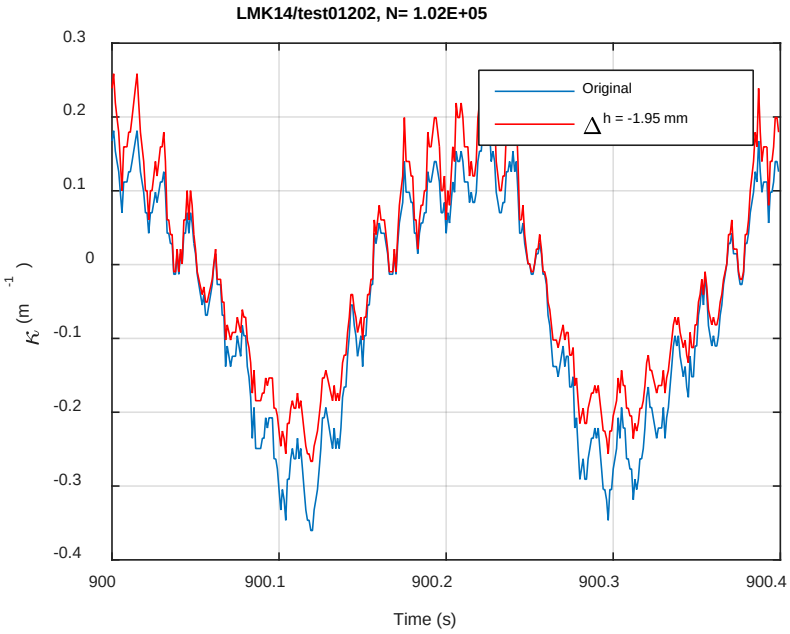
LMK14/test01202, N= 1.02E+05
Original
Δh = -1.95 mm
κ (m-1)
Time (s)
0.3
0.2
0.1
0
-0.1
-0.2
-0.3
-0.4
900
900.1
900.2
900.3
900.4

(a)

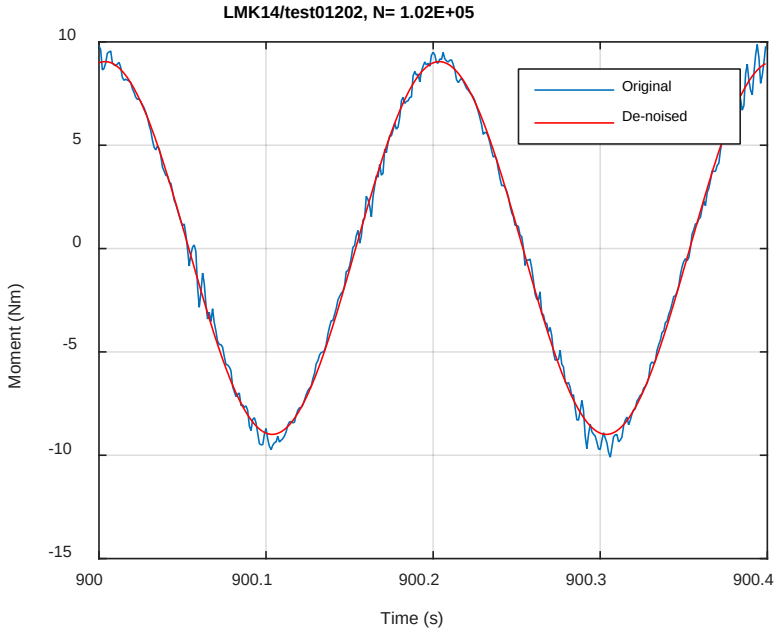
LMK14/test01202, N= 1.02E+05
Original
De-noised
Moment (Nm)
Time (s)
10
5
0
-5
-10
-15
900
900.1
900.2
900.3
900.4

(b)

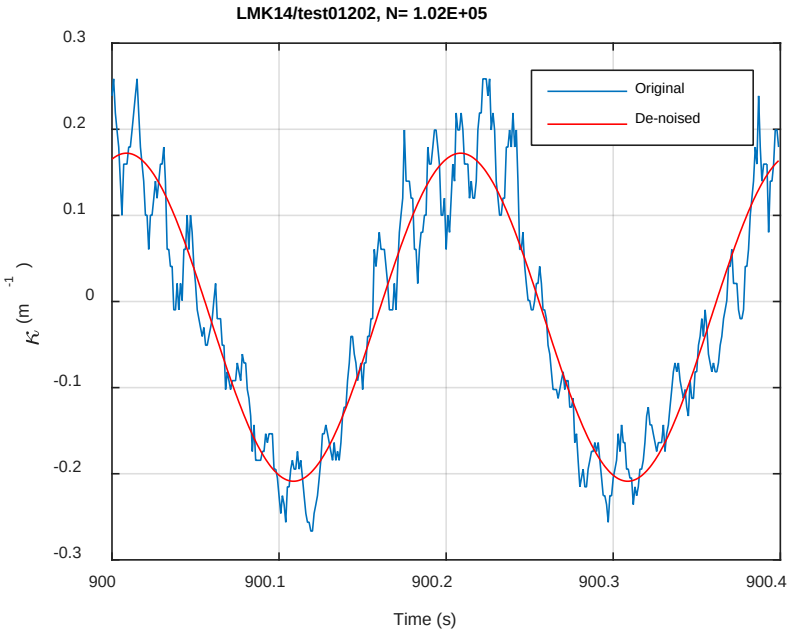

(c)

Fig. A.49. Monitoring-based responses: (a) curvature, (b) moment, (c) curvature, LMK14, 10.16 Nm, Ns = 1.02E+05 cycles.

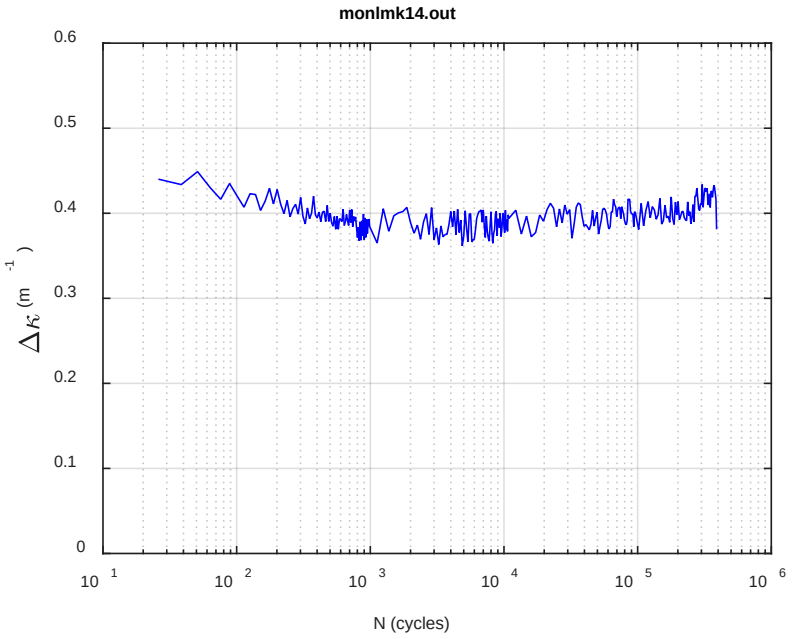
monlmk14.out
0.6
0.5
0.4
0.3
0.2
0.1
0
Δκ (m -1)
10 1
10 2
10 3
10 4
10 5
10 6
N (cycles)

(a)

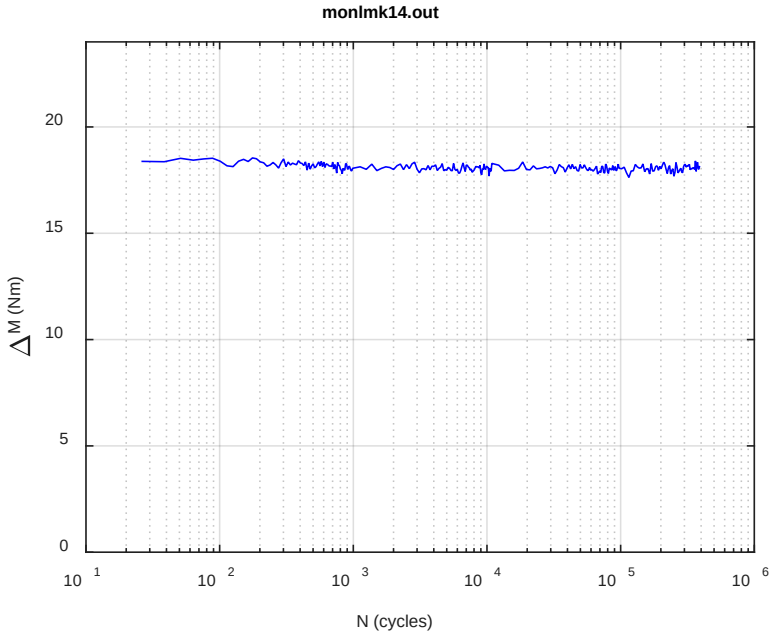
monlmk14.out
20
15
10
5
0
Δ M (Nm)
10 1
10 2
10 3
10 4
10 5
10 6
N (cycles)

(b)

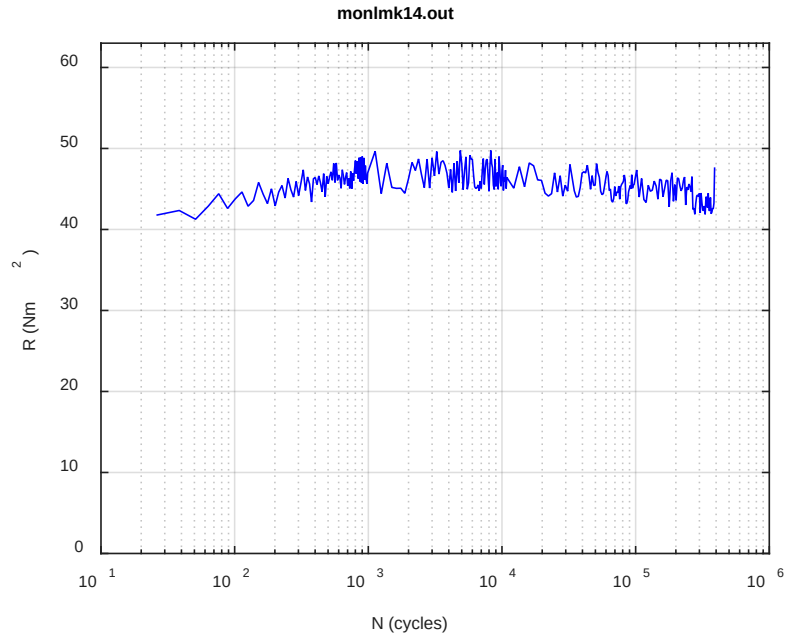
monlmk14.out
R (Nm 2)
N (cycles)

(c)

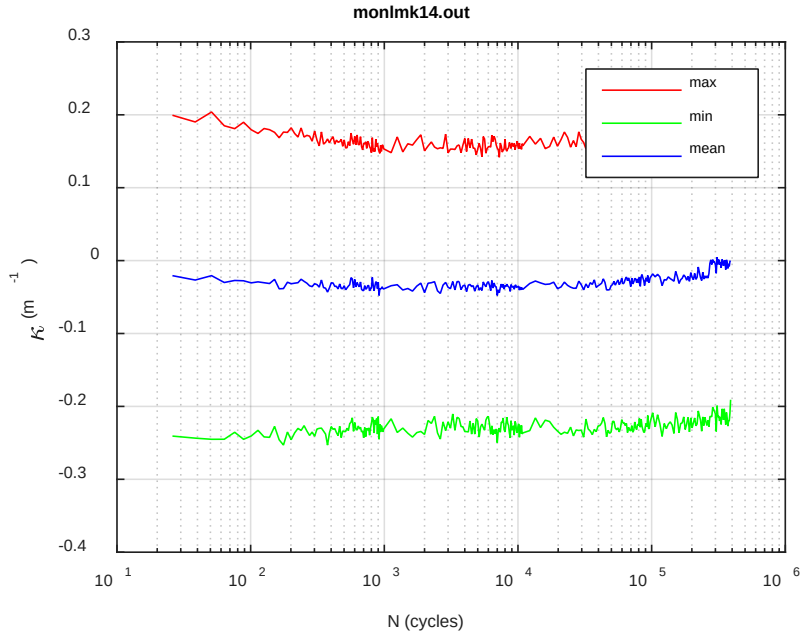
monlmk14.out
max
min
mean
κ (m -1)
N (cycles)

(d)

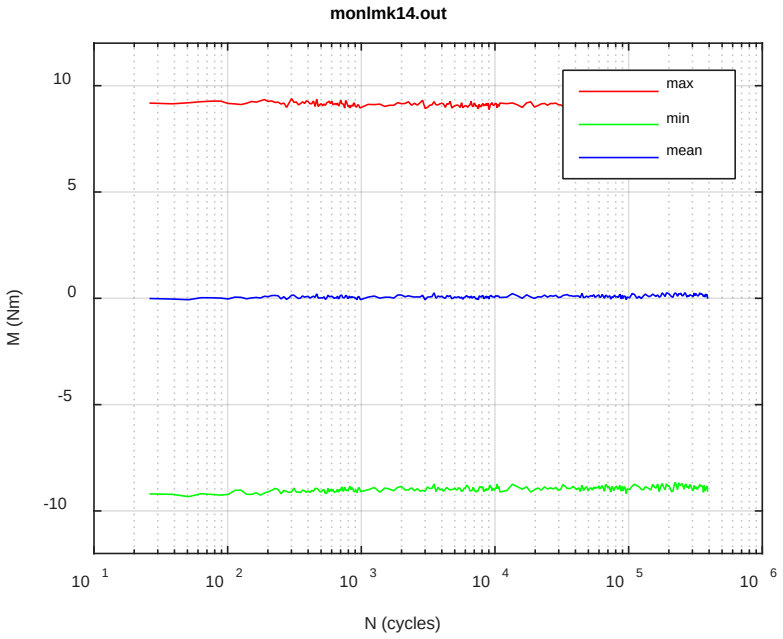

(e)

Fig. A.50. Monitoring-based responses: (a) curvature range, (b) moment range, (c) rigidity, (d) curvature peak/valley, (e) moment peak/valley, LMK14, 10.16 Nm, Nf = 3.90E+05 cycles.

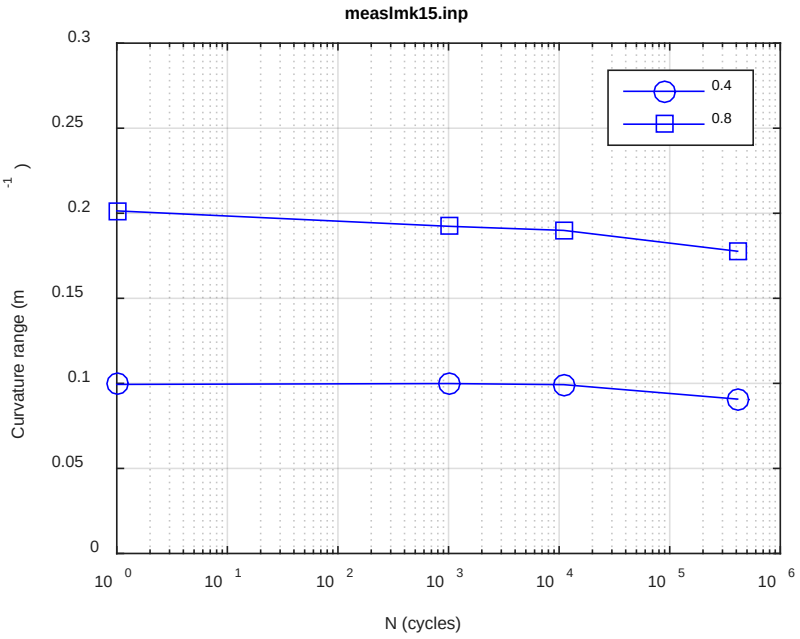
measlmk15.inp
0.3
0.25
0.2
0.15
0.1
0.05
0
Curvature range (m-1)
0.4
0.8
10 0
10 1
10 2
10 3
10 4
10 5
10 6
N (cycles)

(a)

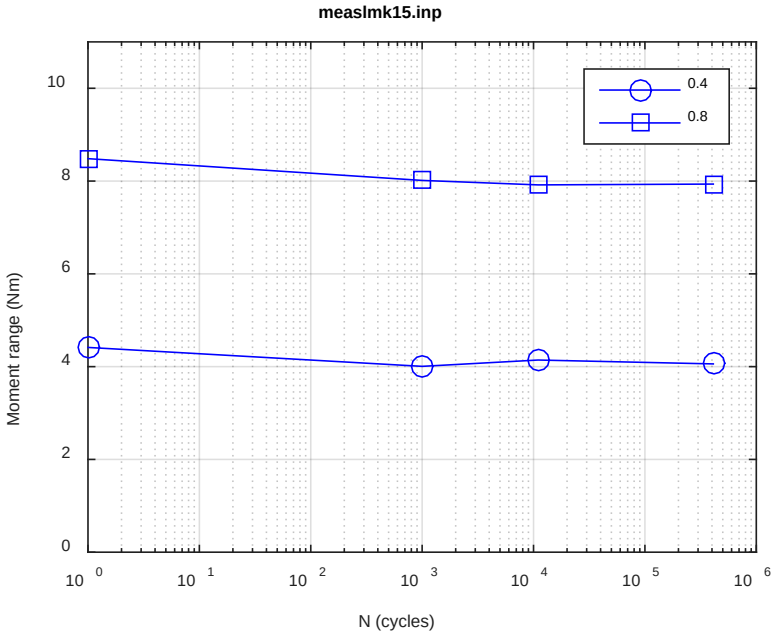
measlmk15.inp
10
8
6
4
2
0
Moment range (Nm)
0.4
0.8
10 0
10 1
10 2
10 3
10 4
10 5
10 6
N (cycles)

(b)

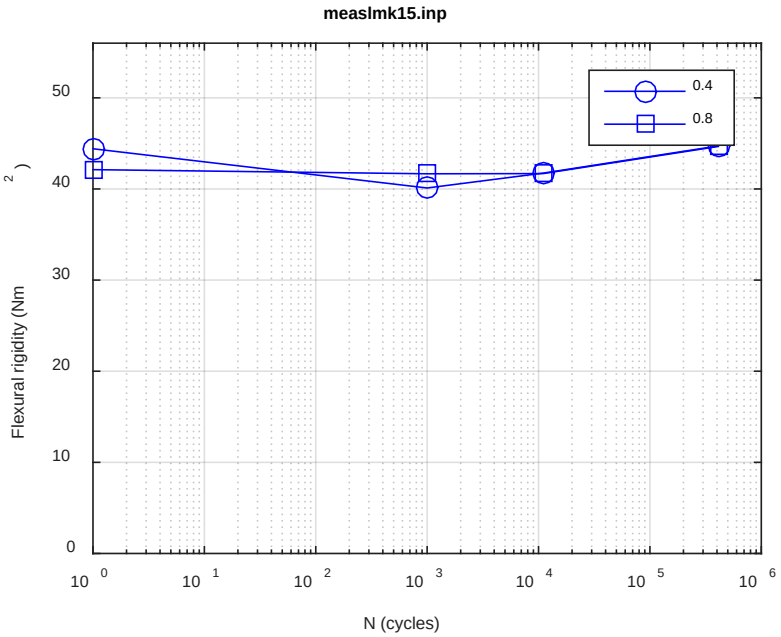
measlmk15.inp
0.4
0.8
Flexural rigidity (Nm 2)
N (cycles)
0
10
20
30
40
50
10 0
10 1
10 2
10 3
10 4
10 5
10 6

(c)

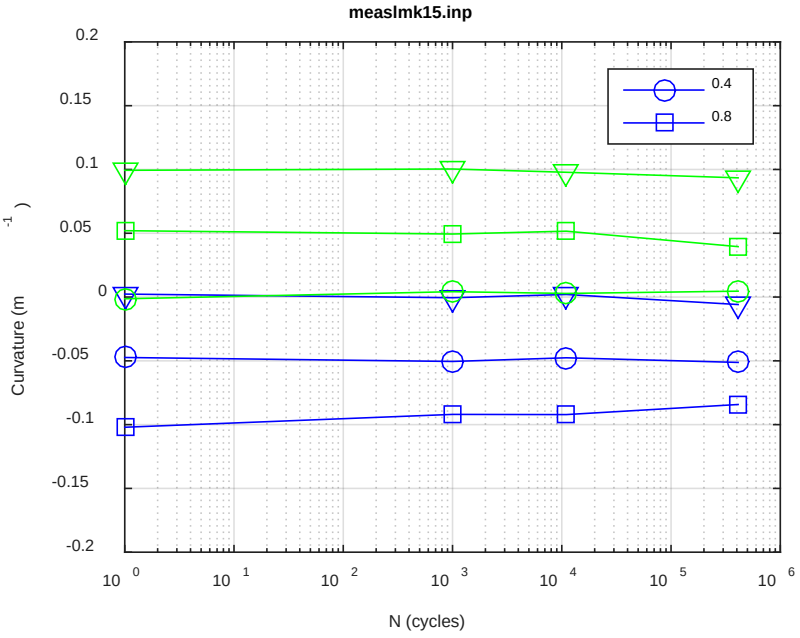
measlmk15.inp
0.4
0.8
Curvature (m -1)
N (cycles)
0.2
0.15
0.1
0.05
0
-0.05
-0.1
-0.15
-0.2
10 0
10 1
10 2
10 3
10 4
10 5
10 6

(d)

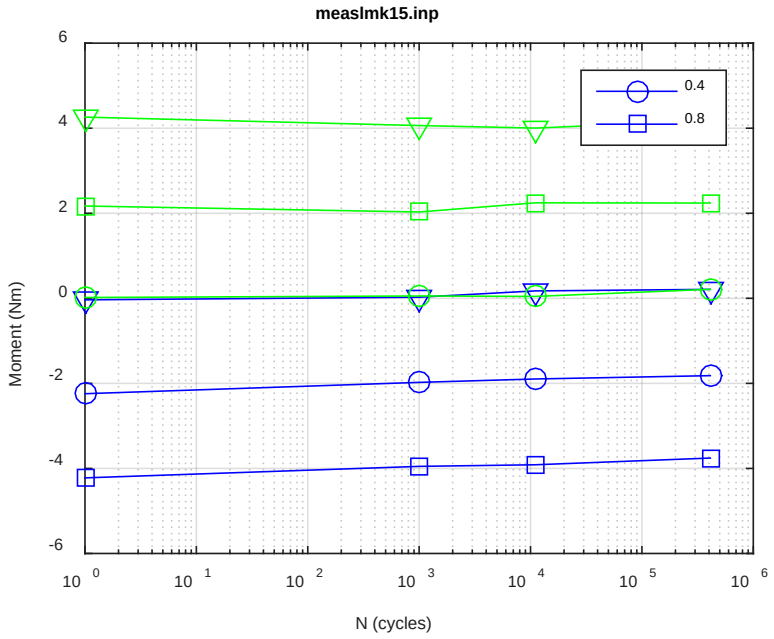

(e)

Fig. A.51. Measurement-based responses: (a) curvature range, (b) moment range, (c) rigidity, (d) curvature peak/valley, (e) moment peak/valley, LMK15, 10.16 Nm.

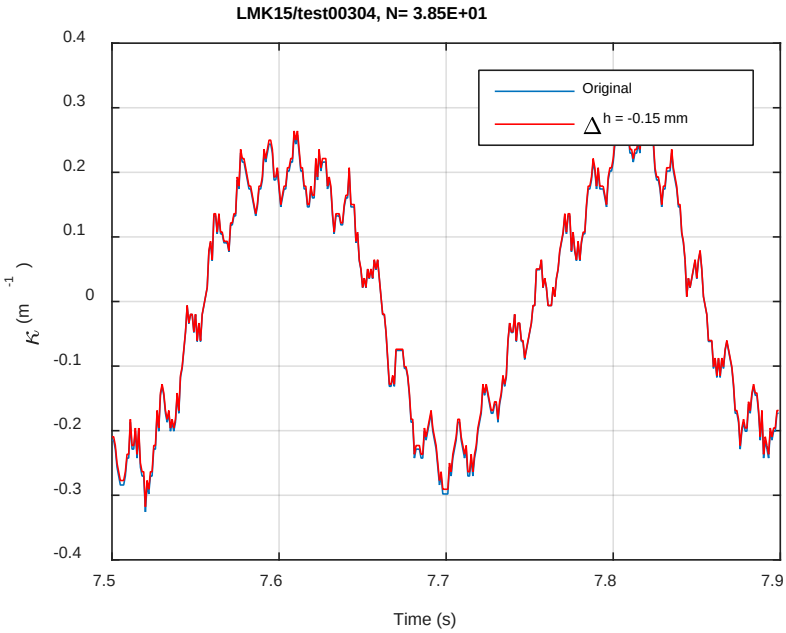
LMK15/test00304, N= 3.85E+01
Original
Δh = -0.15 mm
κ (m-1)
Time (s)

(a)

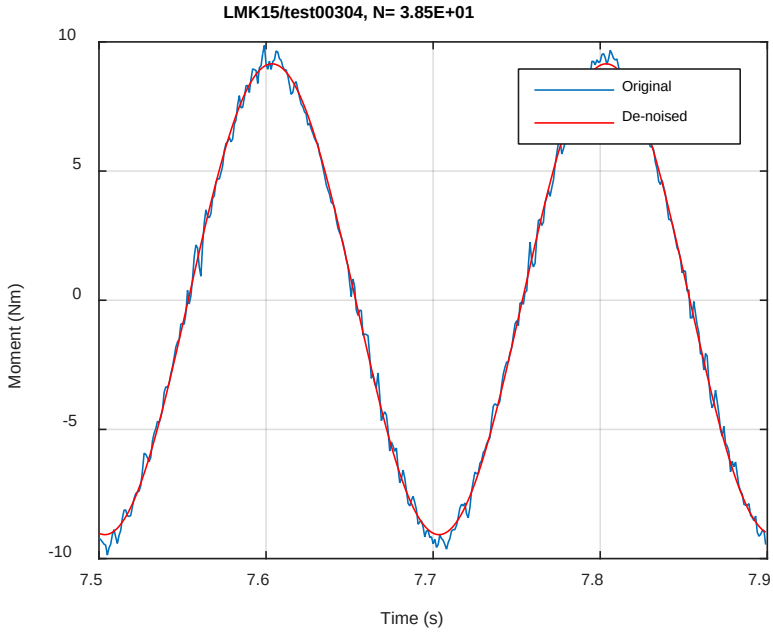
LMK15/test00304, N= 3.85E+01
Original
De-noised
Moment (Nm)
Time (s)

(b)

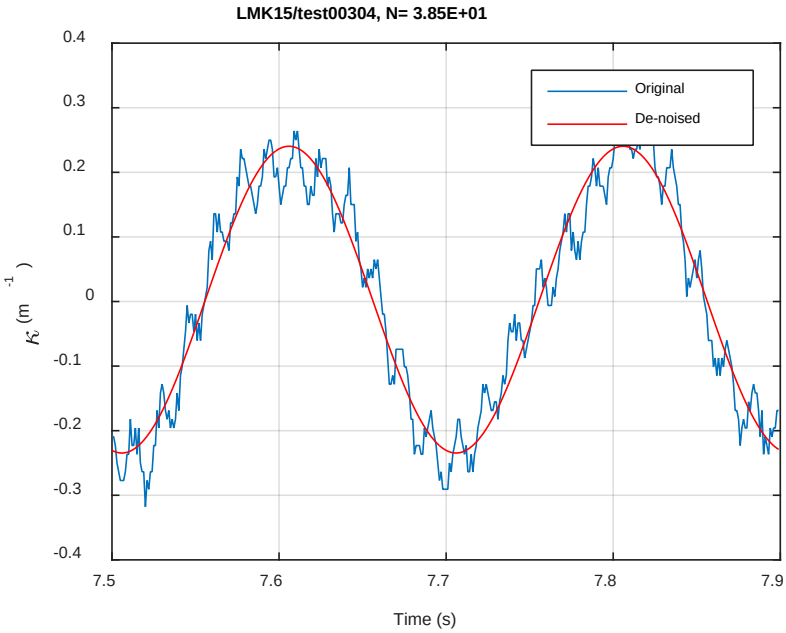

(c)

Fig. A.52. Monitoring-based responses: (a) curvature, (b) moment, (c) curvature, LMK15, 10.16 Nm, Ns = 3.85E+01 cycles.

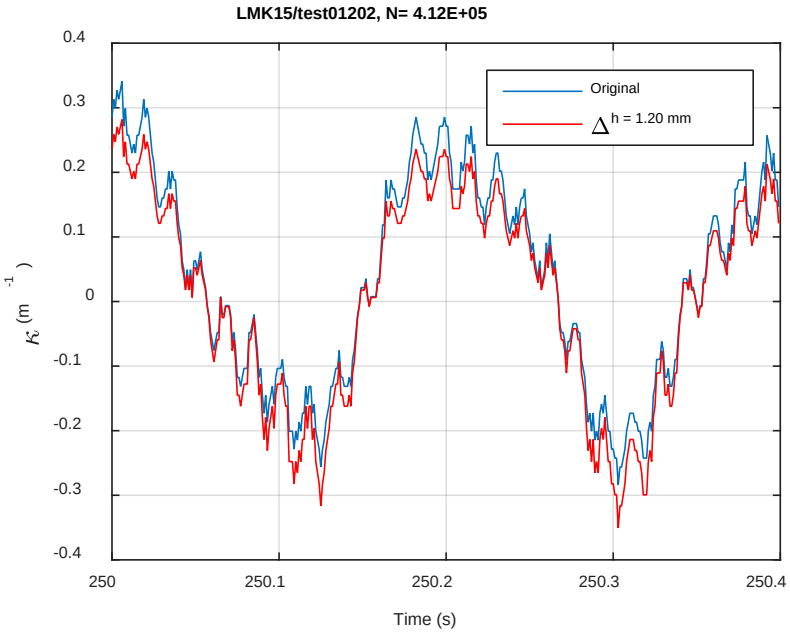
LMK15/test01202, N= 4.12E+05
Original
Δh = 1.20 mm
κ (m-1)
Time (s)

(a)

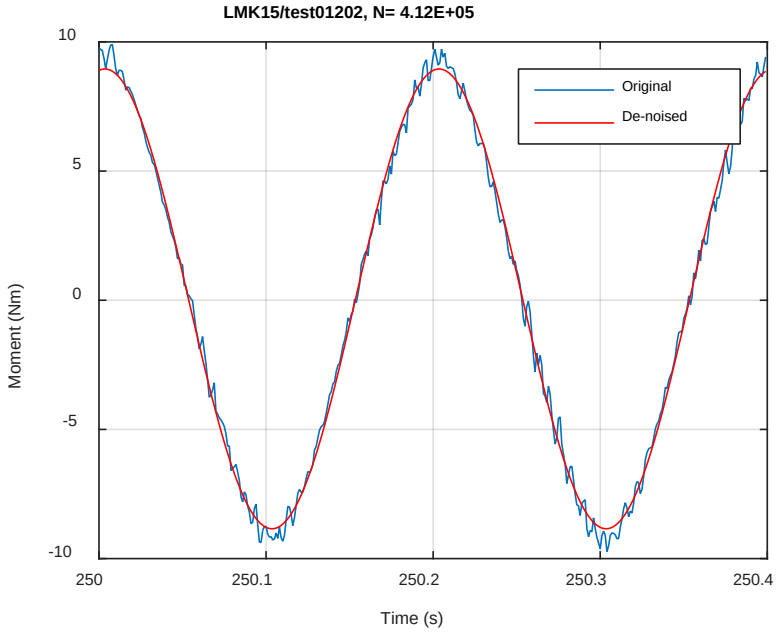
LMK15/test01202, N= 4.12E+05
Original
De-noised
Moment (Nm)
Time (s)

(b)

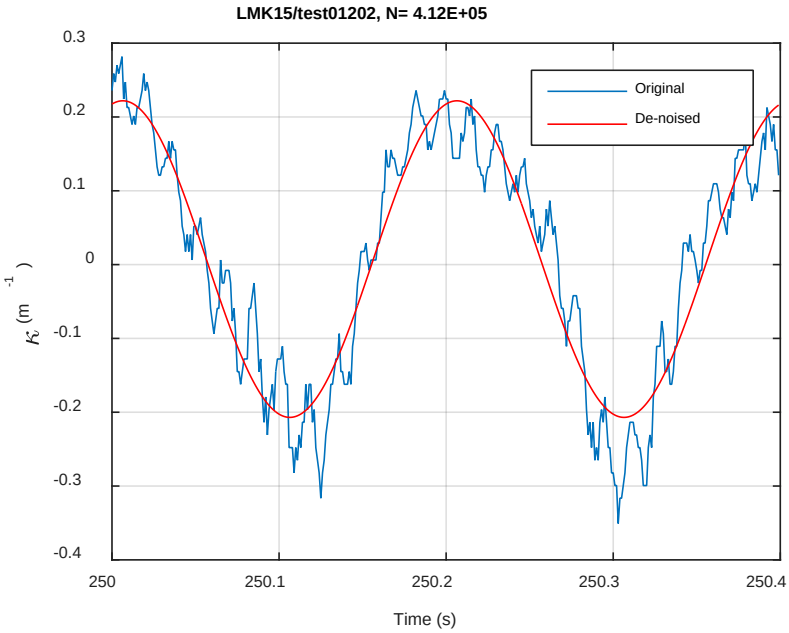

(c)

Fig. A.53. Monitoring-based responses: (a) curvature, (b) moment, (c) curvature, LMK15, 10.16 Nm, Ns = 4.12E+05 cycles.

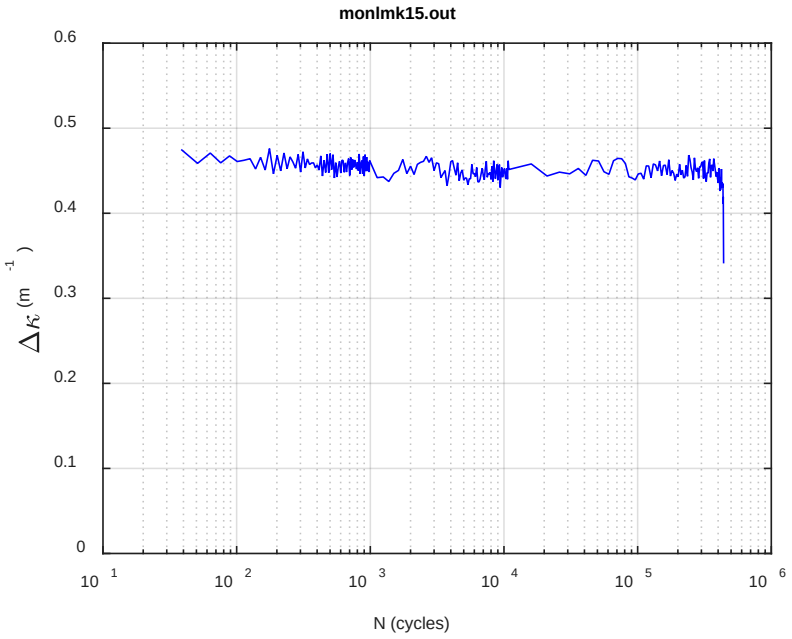
monlmk15.out
0.6
0.5
0.4
0.3
0.2
0.1
0
Δκ (m -1)
10 1
10 2
10 3
10 4
10 5
10 6
N (cycles)

(a)

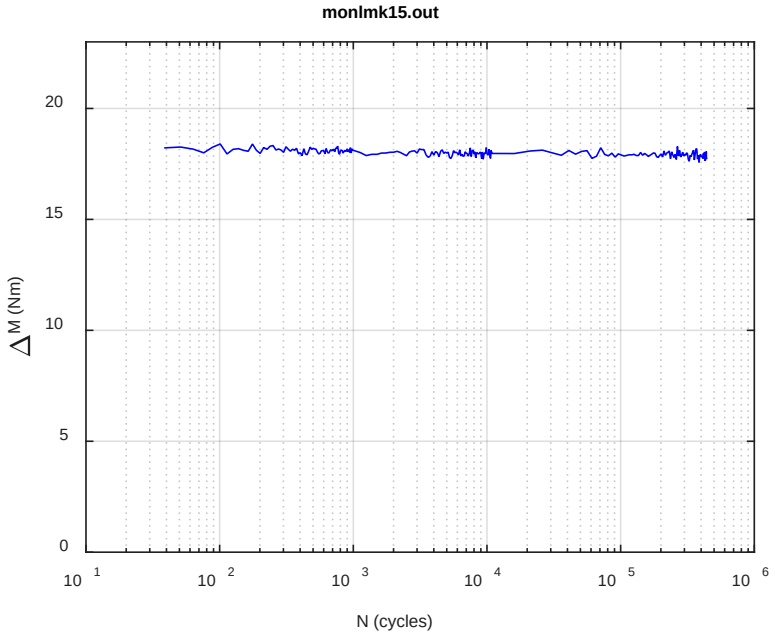
monlmk15.out
20
15
10
5
0
Δ M (Nm)
10 1
10 2
10 3
10 4
10 5
10 6
N (cycles)

(b)

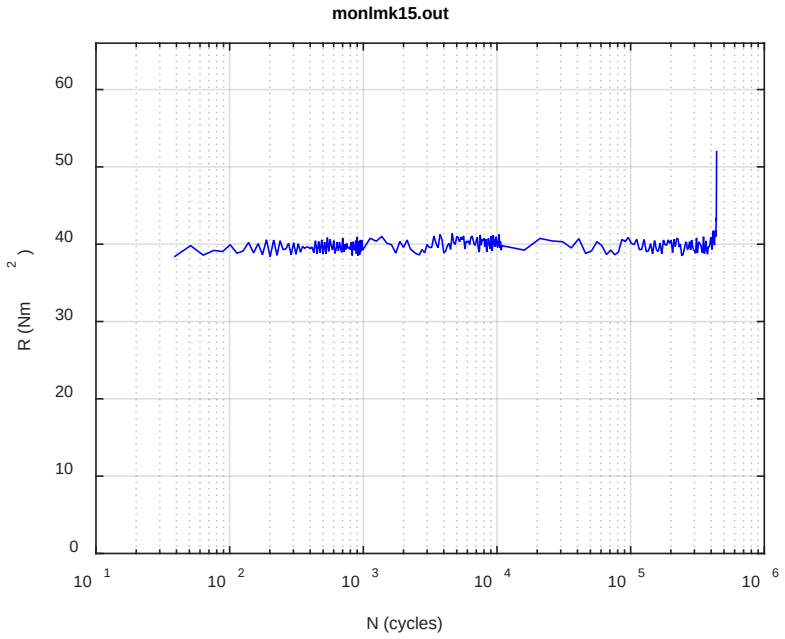
monlmk15.out
R (Nm 2)
N (cycles)

(c)

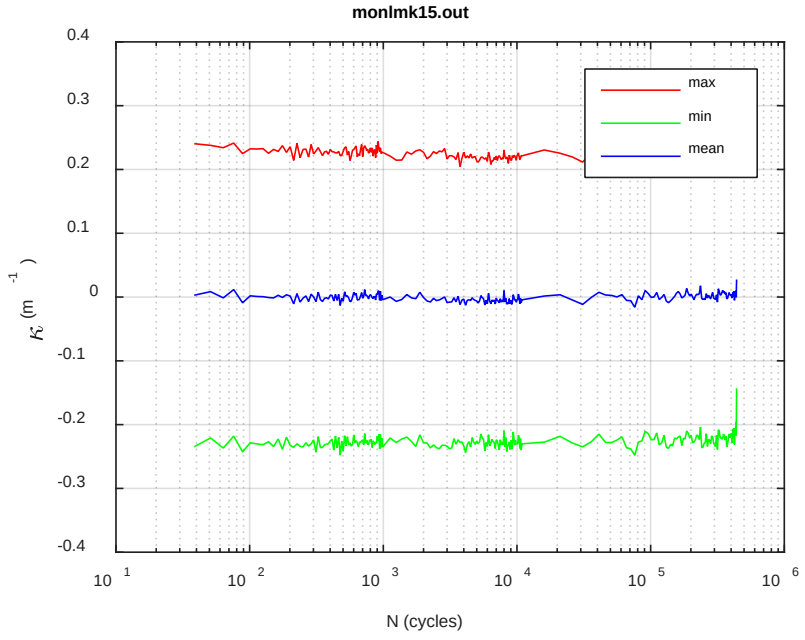
monlmk15.out
max
min
mean
κ (m -1)
N (cycles)

(d)

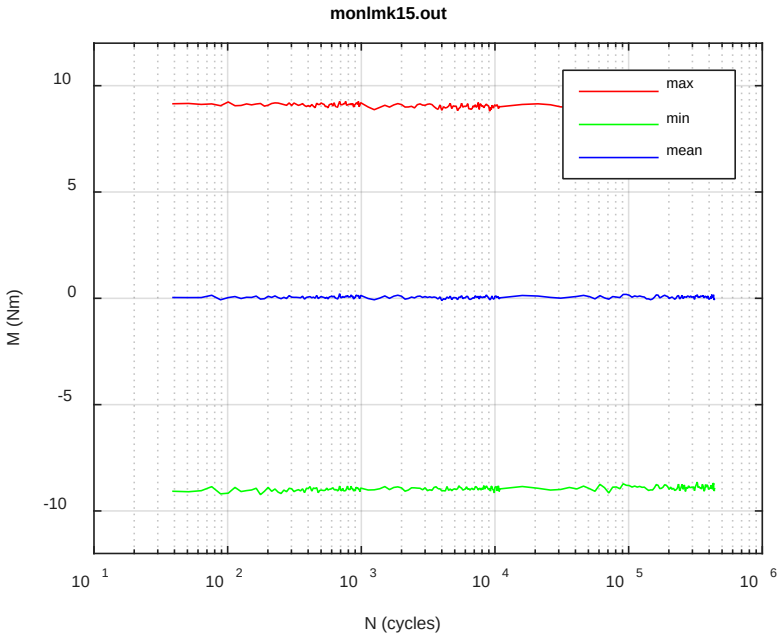

(e)

Fig. A.54. Monitoring-based responses: (a) curvature range, (b) moment range, (c) rigidity, (d) curvature peak/valley, (e) moment peak/valley, LMK15, 10.16 Nm, Nf = 4.41E+05 cycles.

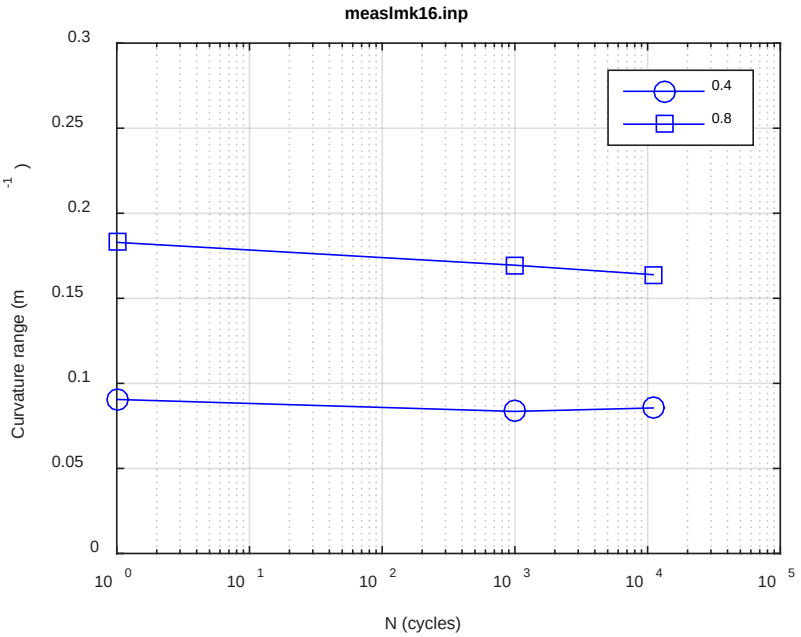
measlmk16.inp
0.3
0.25
0.2
0.15
0.1
0.05
0
Curvature range (m -1)
0.4
0.8
10 0
10 1
10 2
10 3
10 4
10 5
N (cycles)

(a)

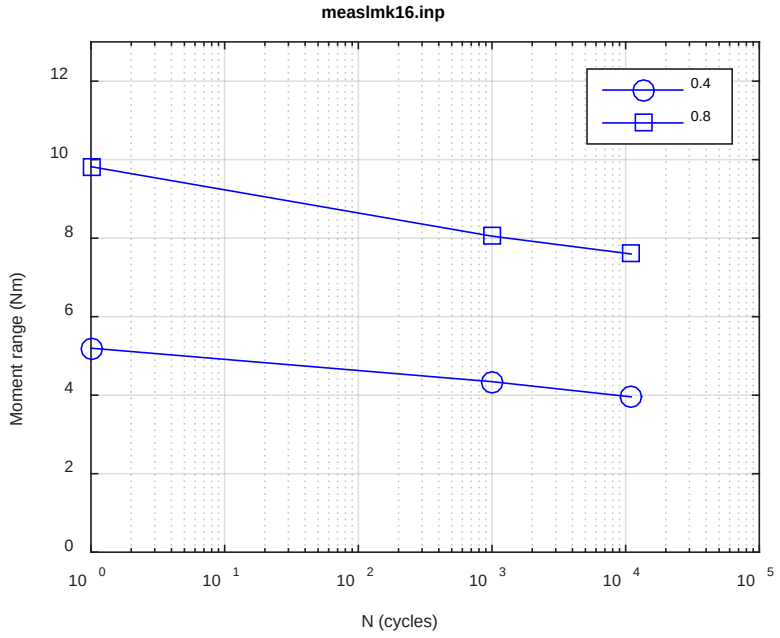
measlmk16.inp
12
10
8
6
4
2
0
Moment range (Nm)
0.4
0.8
10 0
10 1
10 2
10 3
10 4
10 5
N (cycles)

(b)

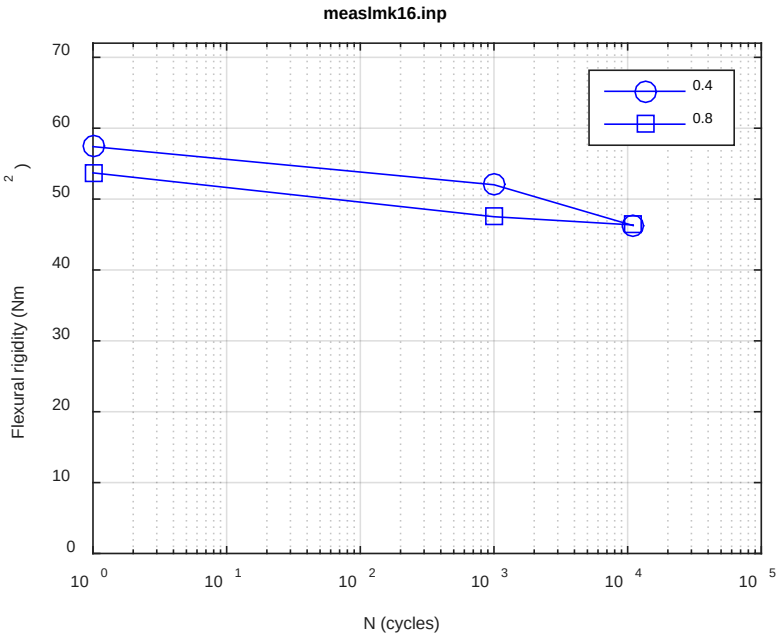
measlmk16.inp
Flexural rigidity (Nm 2)
N (cycles)
0.4
0.8
70
60
50
40
30
20
10
0
10 0
10 1
10 2
10 3
10 4
10 5

(c)

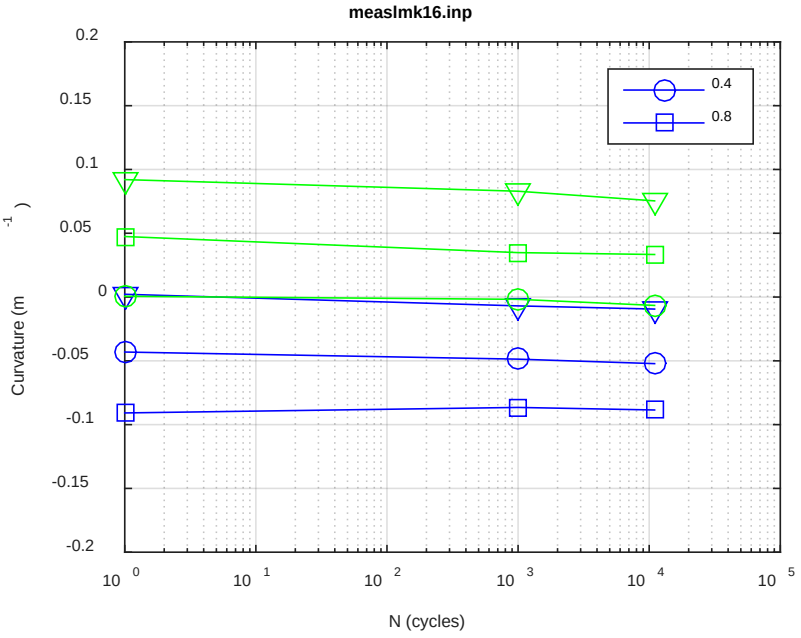
measlmk16.inp
Curvature (m -1)
N (cycles)
0.4
0.8
0.2
0.15
0.1
0.05
0
-0.05
-0.1
-0.15
-0.2
10 0
10 1
10 2
10 3
10 4
10 5

(d)

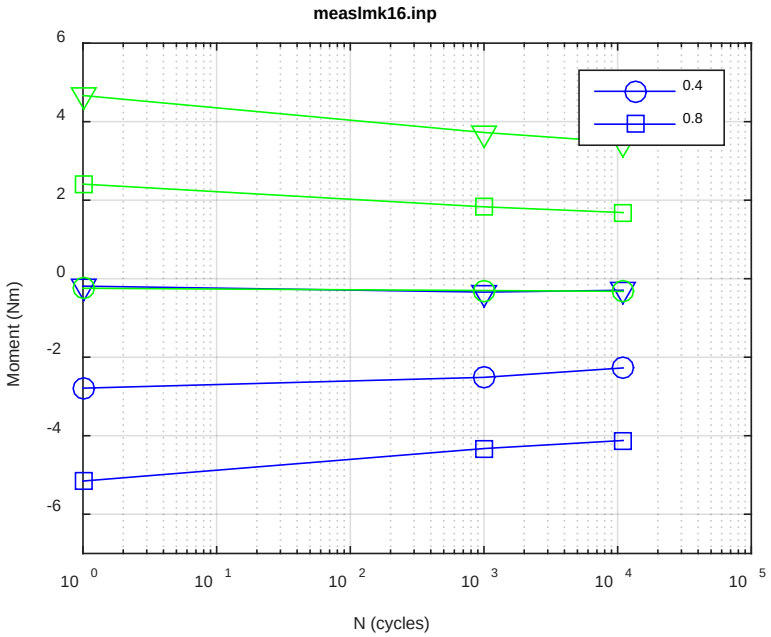

(e)

Fig. A.55. Measurement-based responses: (a) curvature range, (b) moment range, (c) rigidity, (d) curvature peak/valley, (e) moment peak/valley, LMK16, 30.48 Nm.

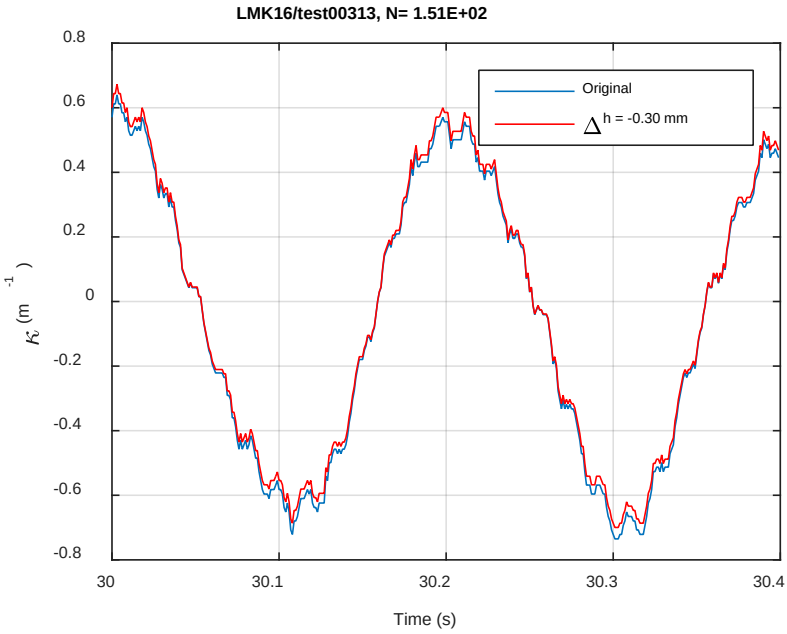
LMK16/test00313, N= 1.51E+02
Original
Δh = -0.30 mm
κ (m-1)
Time (s)
0.8
0.6
0.4
0.2
0
-0.2
-0.4
-0.6
-0.8
30
30.1
30.2
30.3
30.4

(a)

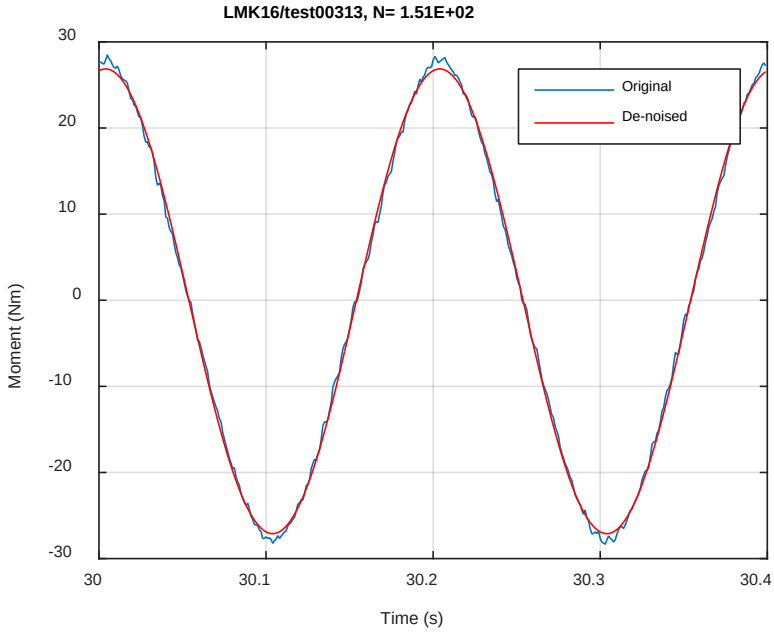
LMK16/test00313, N= 1.51E+02
Original
De-noised
Moment (Nm)
Time (s)
30
20
10
0
-10
-20
-30
30
30.1
30.2
30.3
30.4

(b)

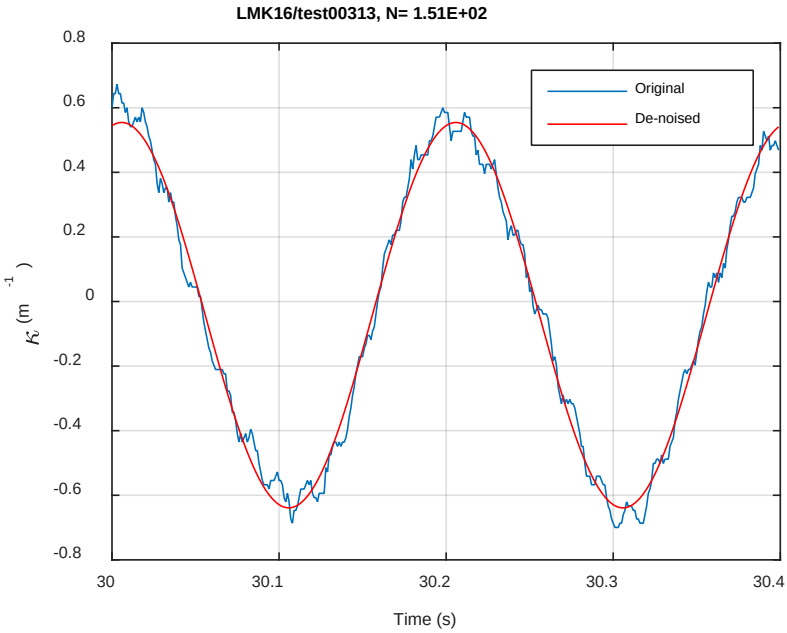

(c)

Fig. A.56. Monitoring-based responses: (a) curvature, (b) moment, (c) curvature, LMK16, 30.48 Nm, Ns = 1.51E+02 cycles.

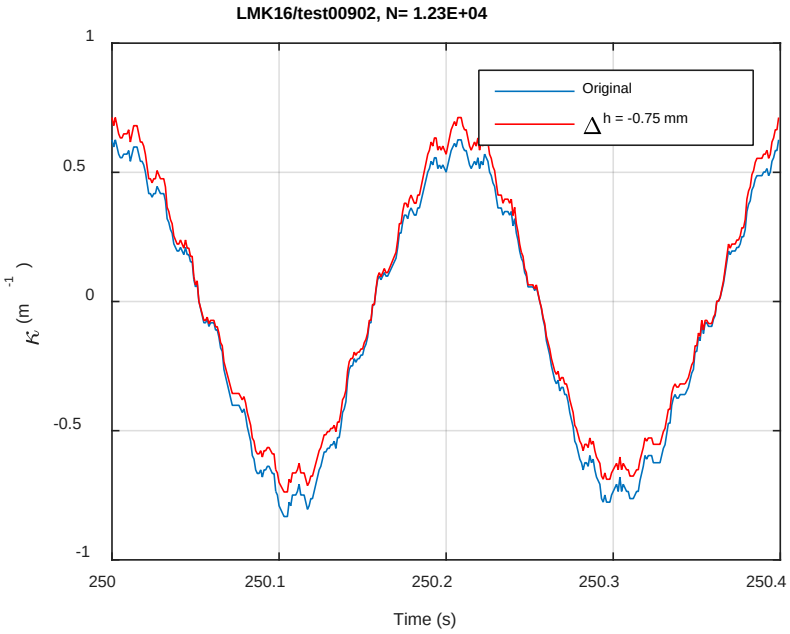
LMK16/test00902, N= 1.23E+04
Original
Δh = -0.75 mm
κ (m-1)
Time (s)
1
0.5
0
-0.5
-1
250
250.1
250.2
250.3
250.4

(a)

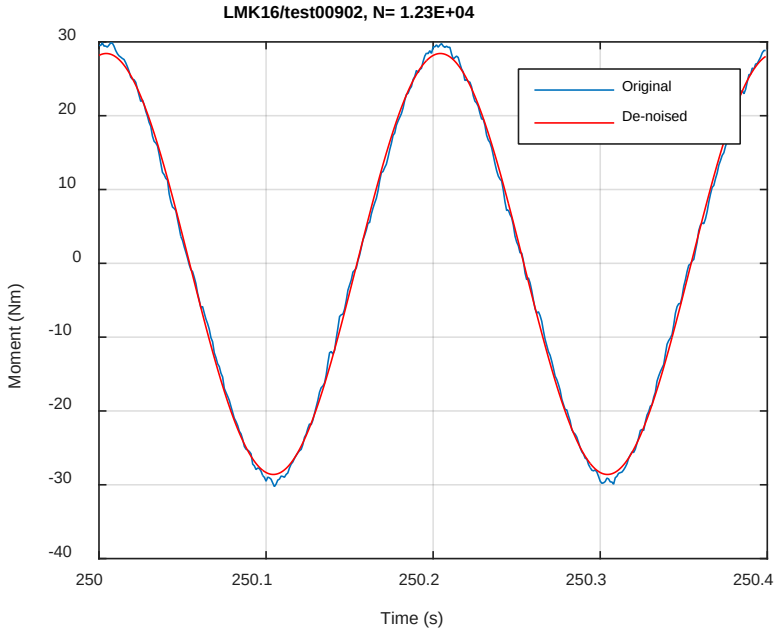
LMK16/test00902, N= 1.23E+04
Original
De-noised
Moment (Nm)
Time (s)
30
20
10
0
-10
-20
-30
-40
250
250.1
250.2
250.3
250.4

(b)

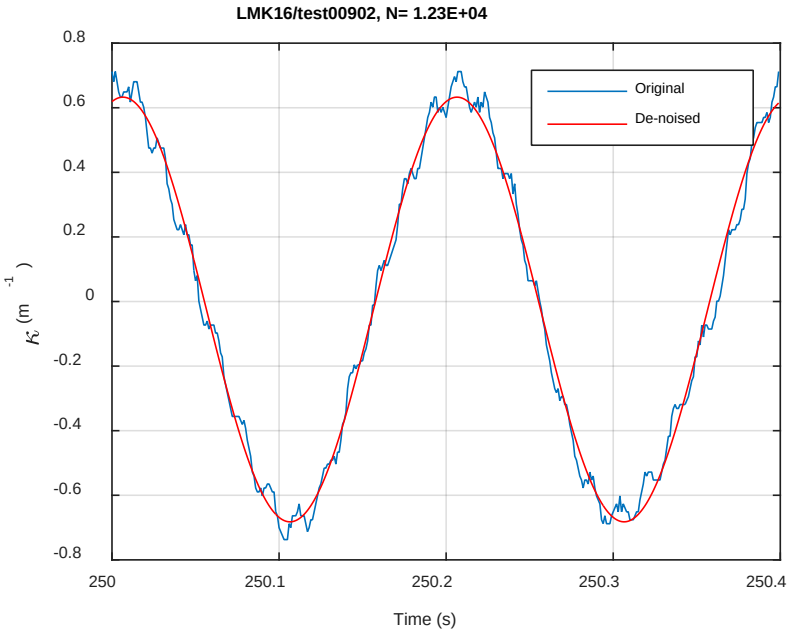

(c)

Fig. A.57. Monitoring-based responses: (a) curvature, (b) moment, (c) curvature, LMK16, 30.48 Nm, Ns = 1.23E+04 cycles.

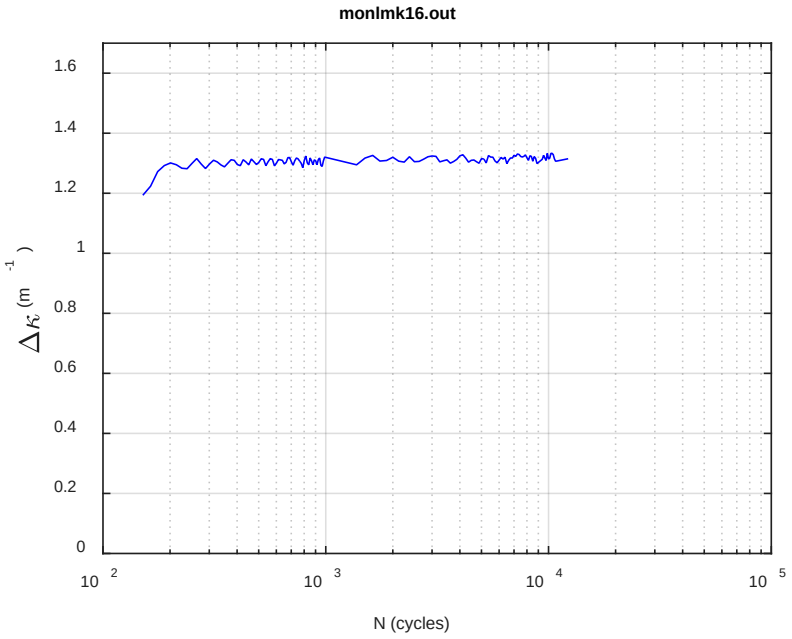
monlmk16.out
1.6
1.4
1.2
1
0.8
0.6
0.4
0.2
0
Δκ (m-1)
10 2
10 3
10 4
10 5
N (cycles)

(a)

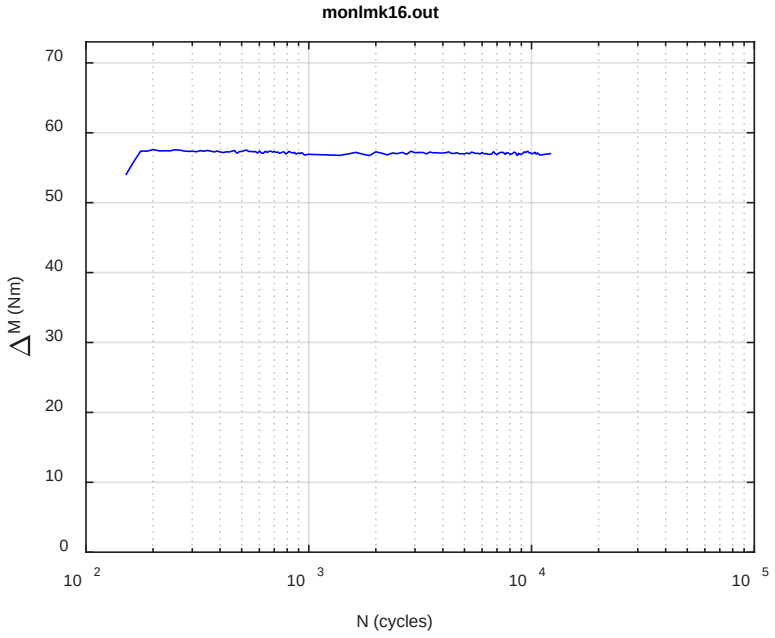
monlmk16.out
70
60
50
40
30
20
10
0
Δ M (Nm)
10 2
10 3
10 4
10 5
N (cycles)

(b)

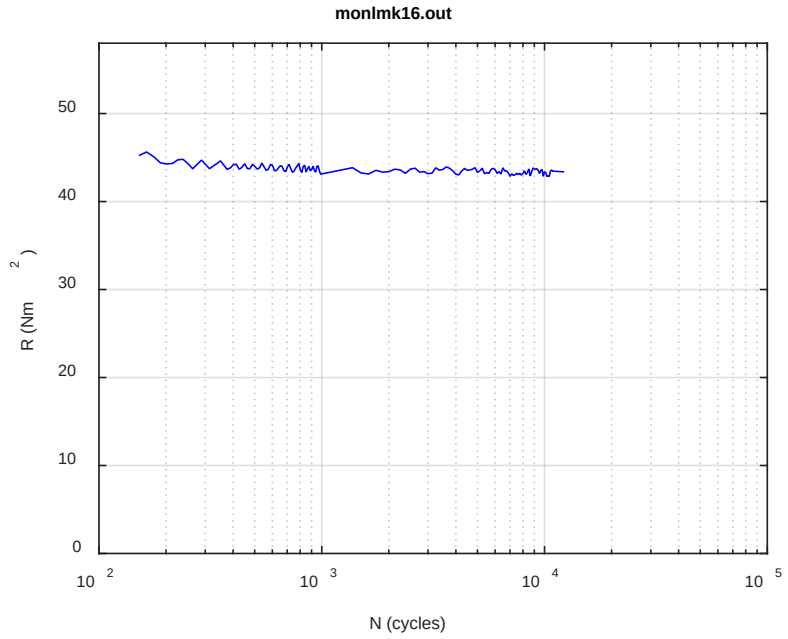
monlmk16.out
R (Nm 2)
50
40
30
20
10
0
10 2
10 3
10 4
10 5
N (cycles)

(c)

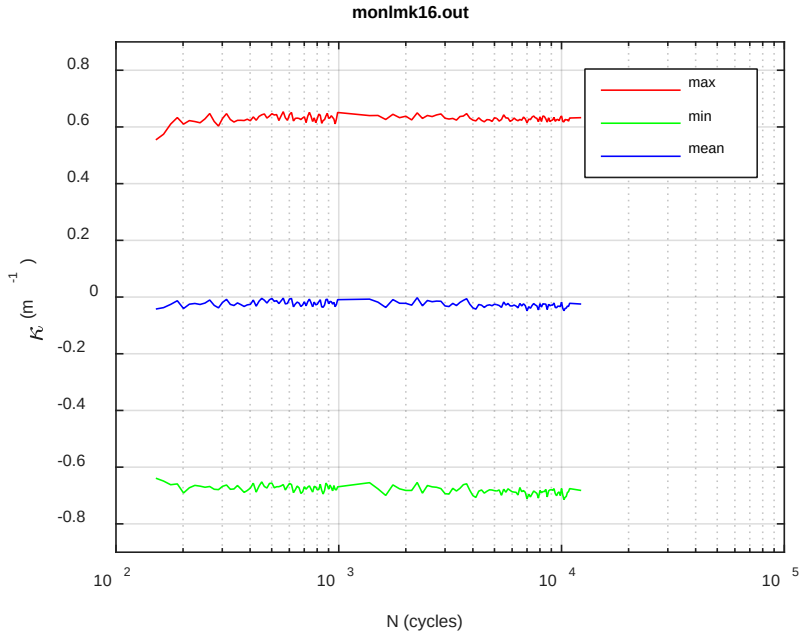
monlmk16.out
max
min
mean
κ (m -1)
0.8
0.6
0.4
0.2
0
-0.2
-0.4
-0.6
-0.8
10 2
10 3
10 4
10 5
N (cycles)

(d)

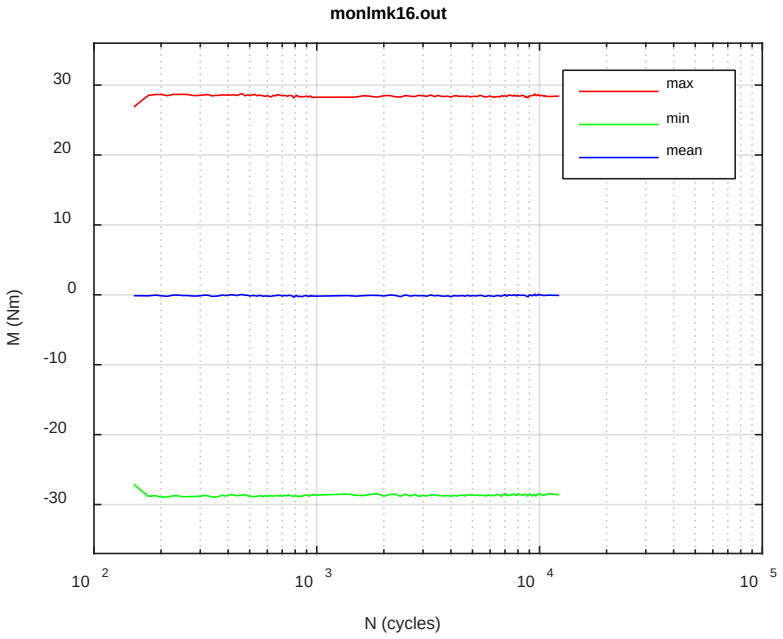

(e)

Fig. A.58. Monitoring-based responses: (a) curvature range, (b) moment range, (c) rigidity, (d) curvature peak/valley, (e) moment peak/valley, LMK16, 30.48 Nm, Nf = 1.36E+04 cycles.

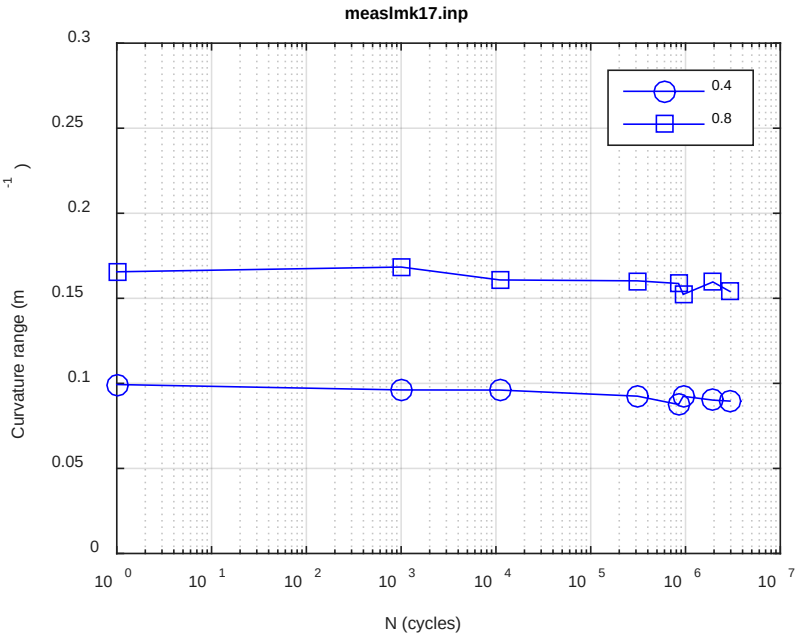
measlmk17.inp
0.4
0.8
Curvature range (m-1)
N (cycles)

(a)

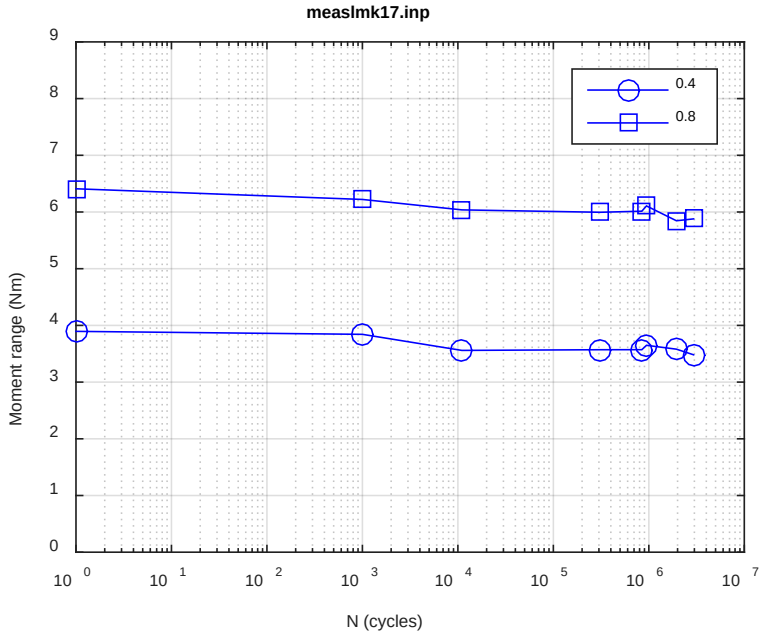
measlmk17.inp
0.4
0.8
Moment range (Nm)
N (cycles)

(b)

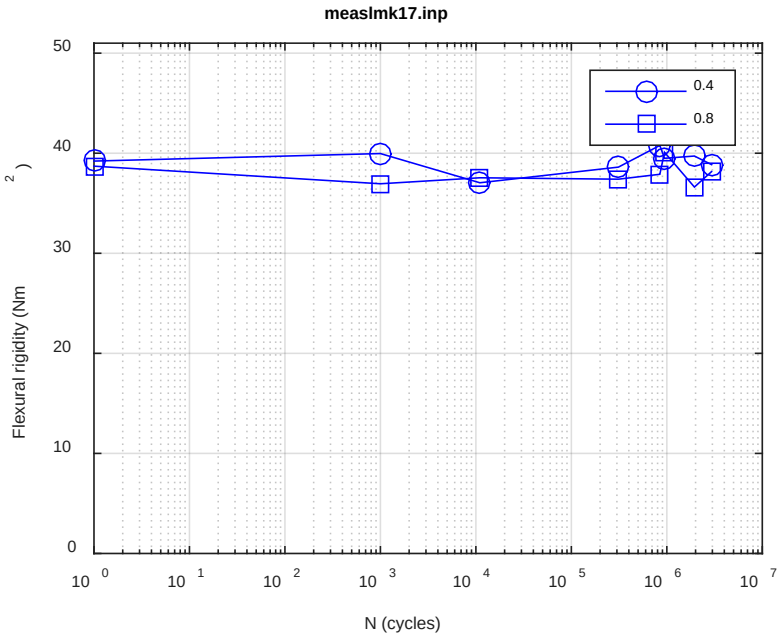
measlmk17.inp
0.4
0.8
Flexural rigidity (Nm 2)
N (cycles)

(c)

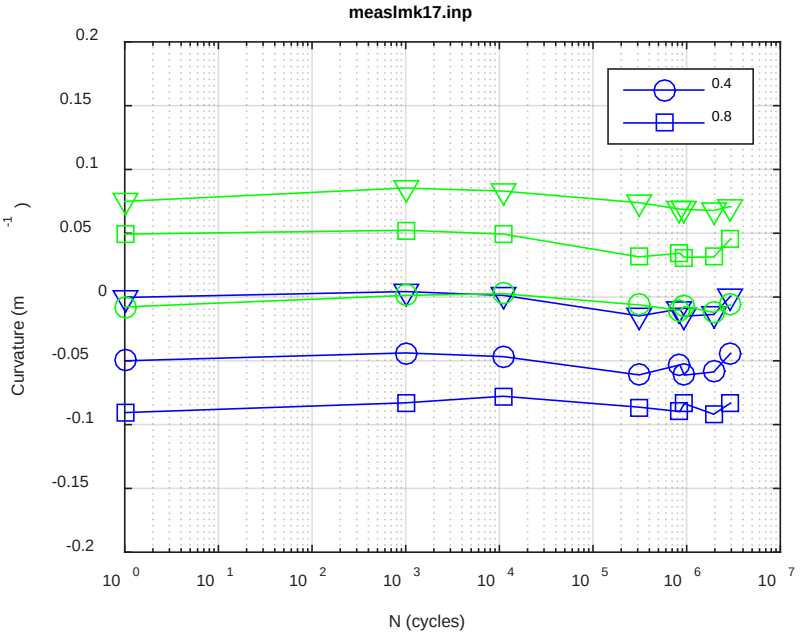
measlmk17.inp
0.4
0.8
Curvature (m -1)
N (cycles)

(d)

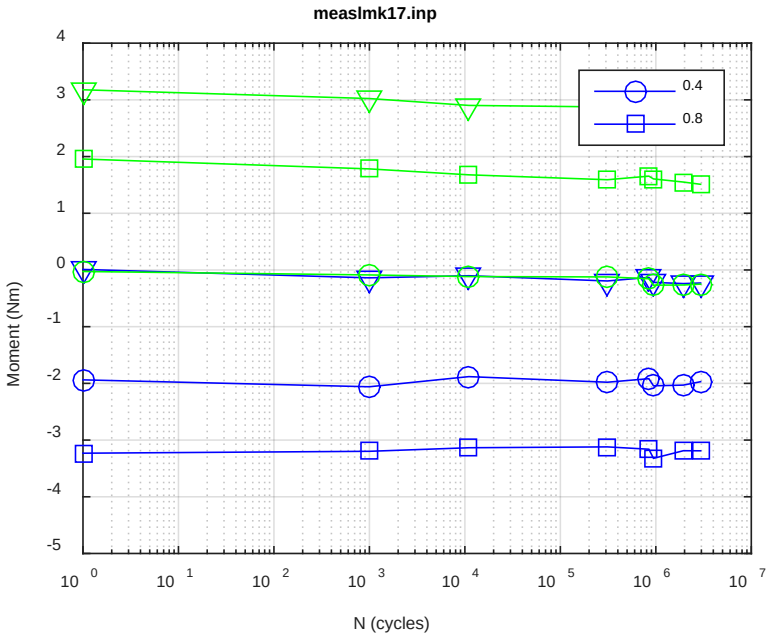

(e)

Fig. A.59. Measurement-based responses: (a) curvature range, (b) moment range, (c) rigidity, (d) curvature peak/valley, (e) moment peak/valley, LMK17, 8.64 Nm.

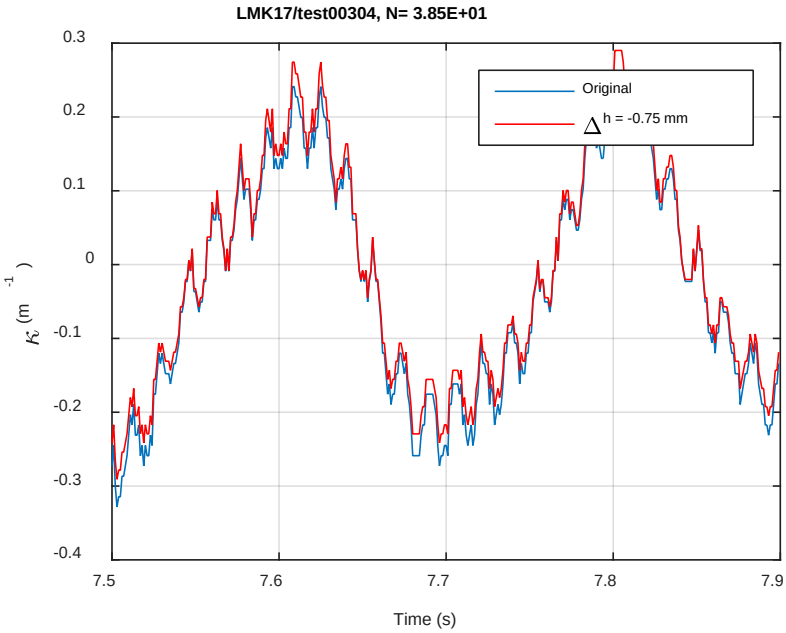
LMK17/test00304, N= 3.85E+01
Original
Δh = -0.75 mm
κ (m-1)
Time (s)

(a)

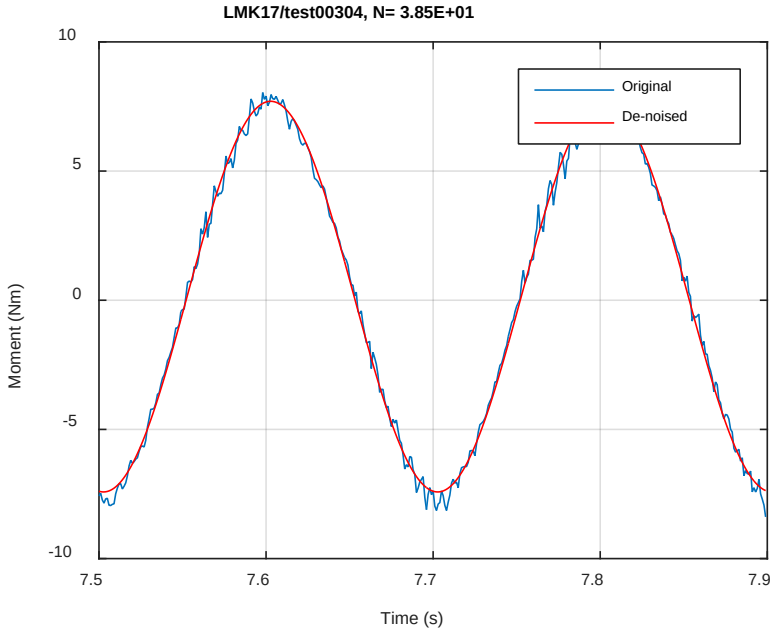
LMK17/test00304, N= 3.85E+01
Original
De-noised
Moment (Nm)
Time (s)

(b)

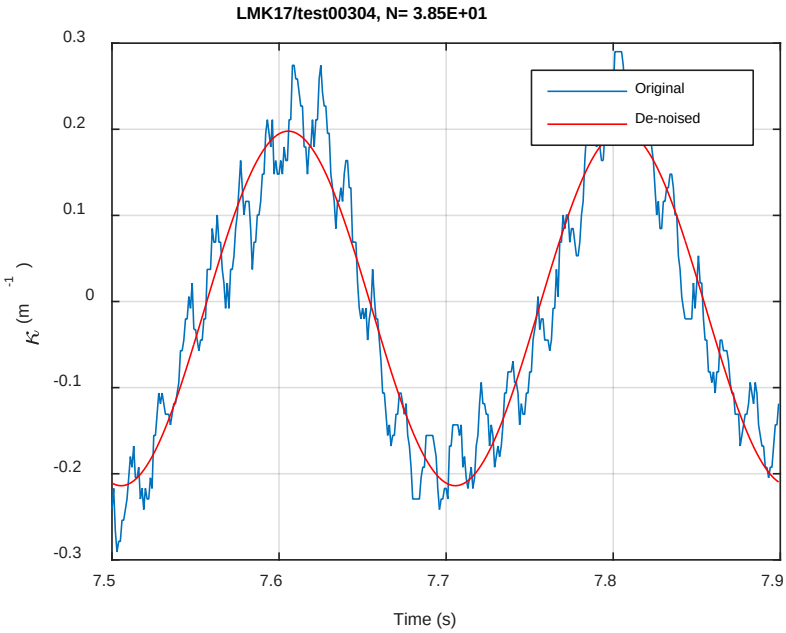

(c)

Fig. A.60. Monitoring-based responses: (a) curvature, (b) moment, (c) curvature, LMK17, 8.64 Nm, Ns = 3.85E+01 cycles.

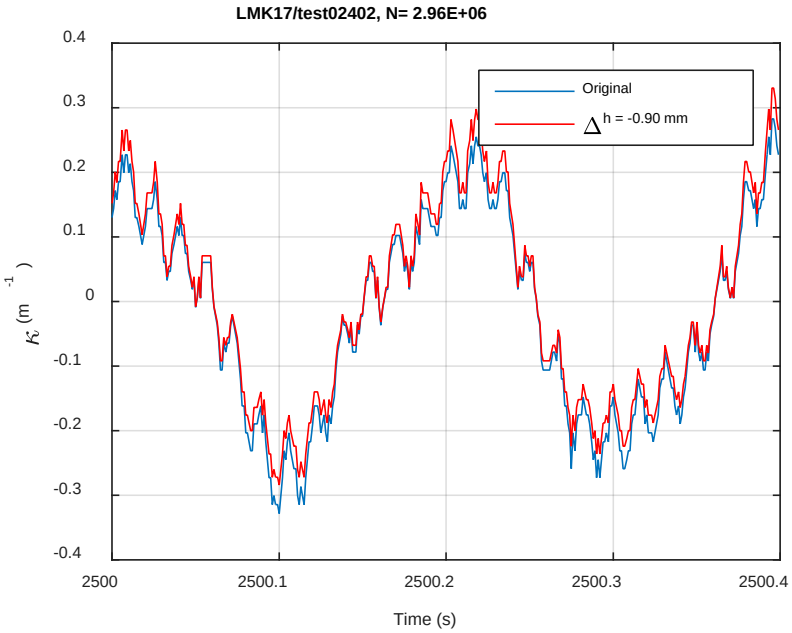
LMK17/test02402, N= 2.96E+06
Original
Δh = -0.90 mm
κ (m-1)
Time (s)
0.4
0.3
0.2
0.1
0
-0.1
-0.2
-0.3
-0.4
2500
2500.1
2500.2
2500.3
2500.4

(a)

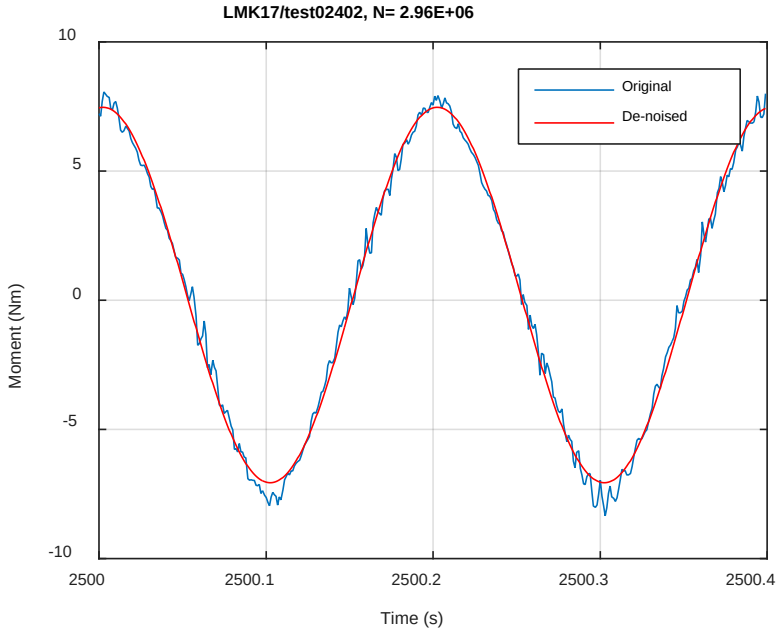
LMK17/test02402, N= 2.96E+06
Original
De-noised
Moment (Nm)
Time (s)
10
5
0
-5
-10
2500
2500.1
2500.2
2500.3
2500.4

(b)

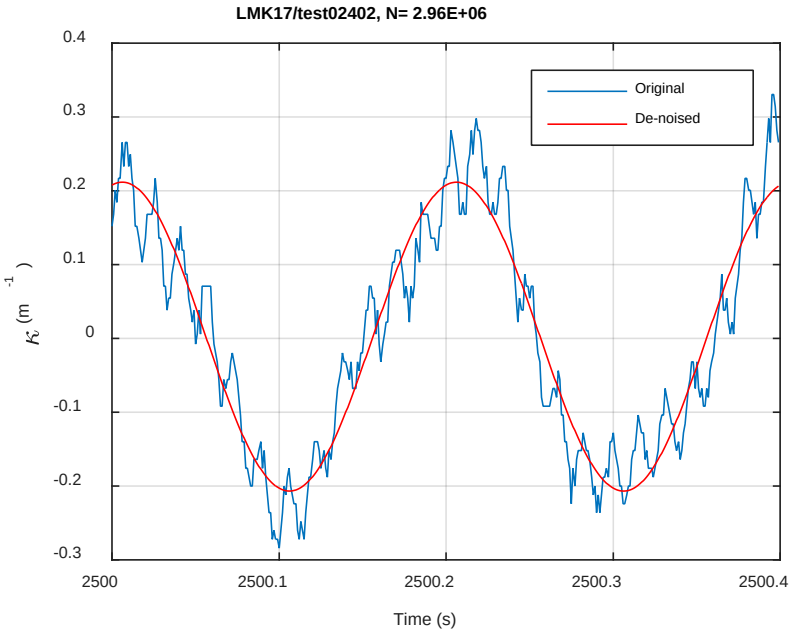

(c)

Fig. A.61. Monitoring-based responses: (a) curvature, (b) moment, (c) curvature, LMK17, 8.64 Nm, Ns = 2.96E+06 cycles.

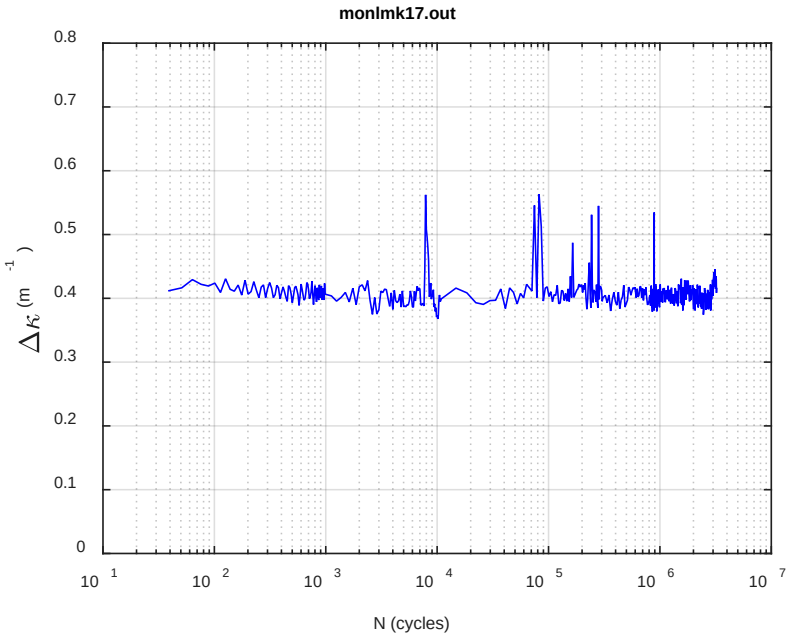
monlmk17.out
0.8
0.7
0.6
0.5
0.4
0.3
0.2
0.1
0
Δκ (m -1)
10 1
10 2
10 3
10 4
10 5
10 6
10 7
N (cycles)

(a)

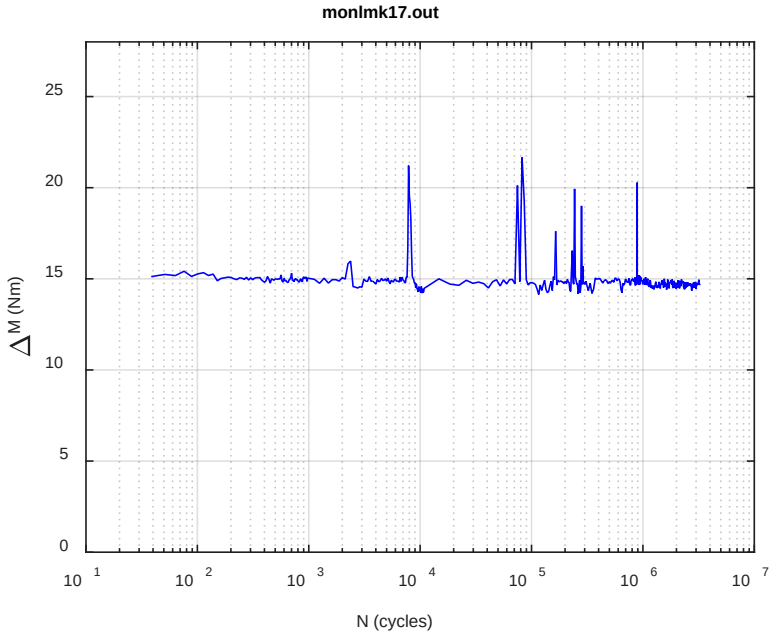
monlmk17.out
25
20
15
10
5
0
Δ M (Nm)
10 1
10 2
10 3
10 4
10 5
10 6
10 7
N (cycles)

(b)

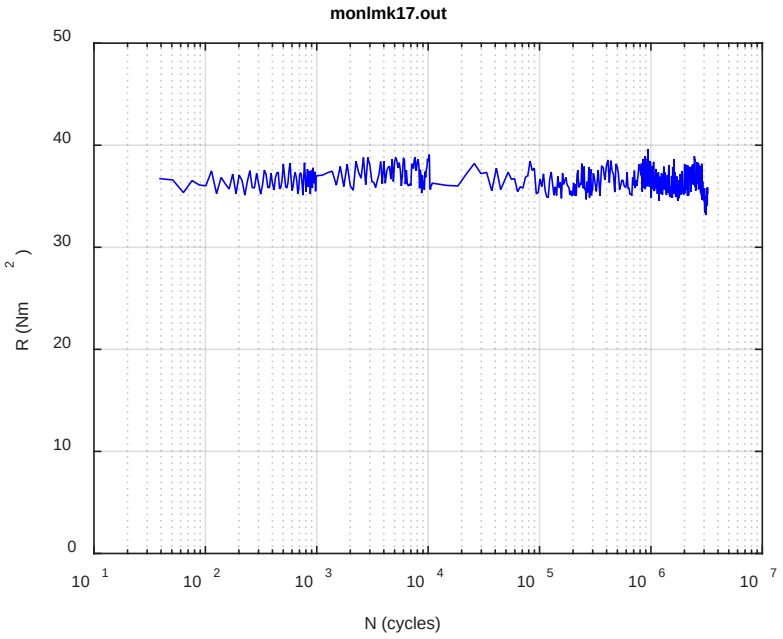
monlmk17.out
R (Nm 2)
N (cycles)

(c)

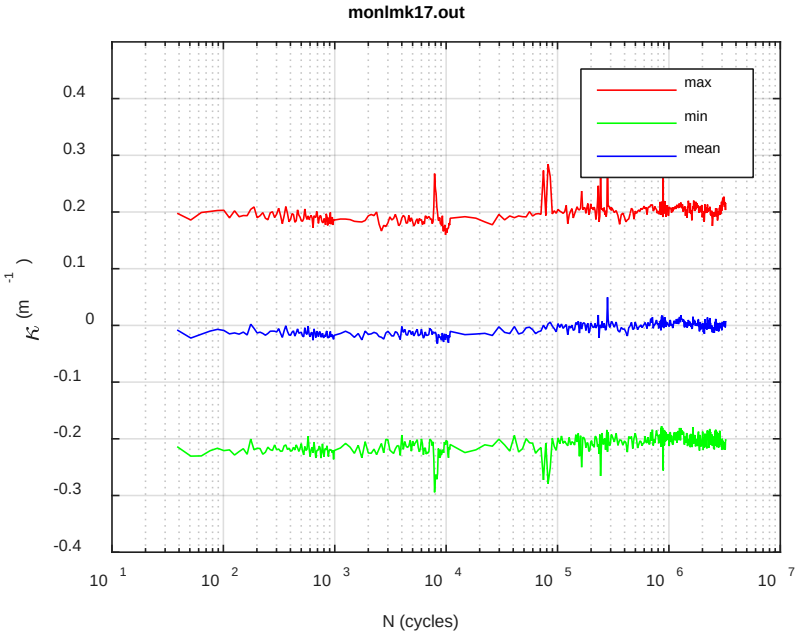
monlmk17.out
max
min
mean
κ (m -1)
N (cycles)

(d)

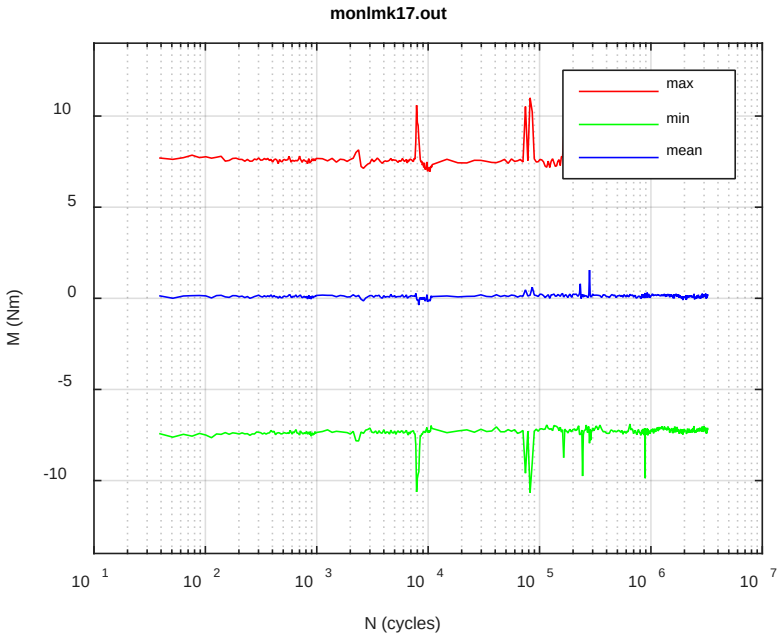

(e)

Fig. A.62. Monitoring-based responses: (a) curvature range, (b) moment range, (c) rigidity, (d) curvature peak/valley, (e) moment peak/valley, LMK17, 8.64 Nm, Nf = 3.37E+06 cycles.

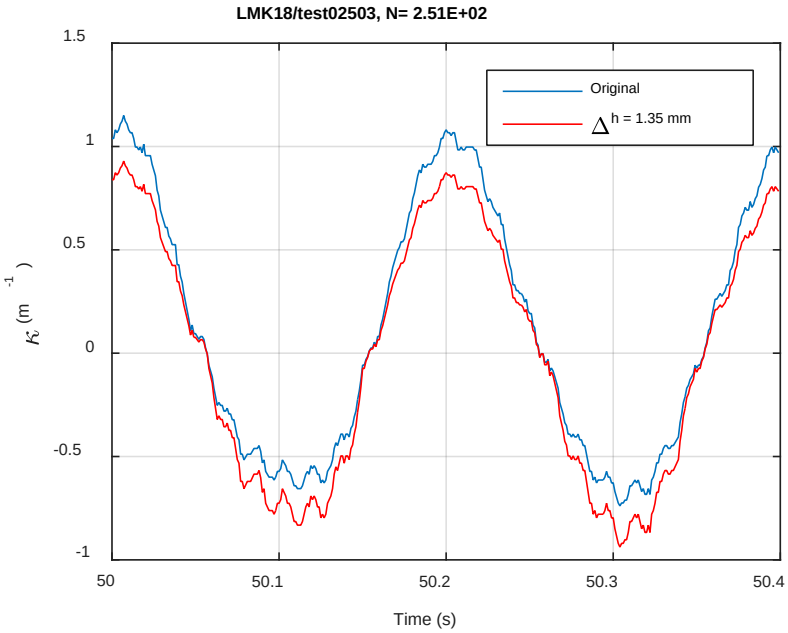
LMK18/test02503, N= 2.51E+02
Original
Δh = 1.35 mm
κ (m-1)
Time (s)
1.5
1
0.5
0
-0.5
-1
50
50.1
50.2
50.3
50.4

(a)

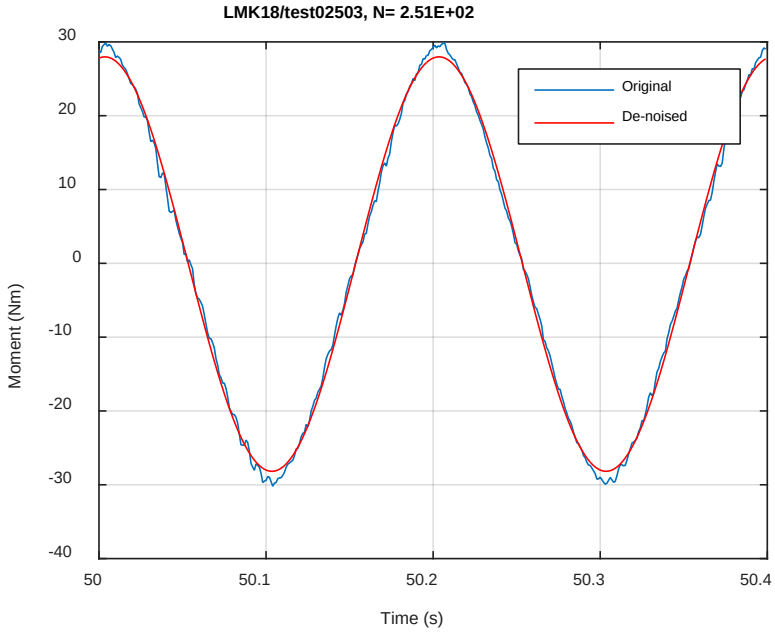
LMK18/test02503, N= 2.51E+02
Original
De-noised
Moment (Nm)
Time (s)
30
20
10
0
-10
-20
-30
-40
50
50.1
50.2
50.3
50.4

(b)

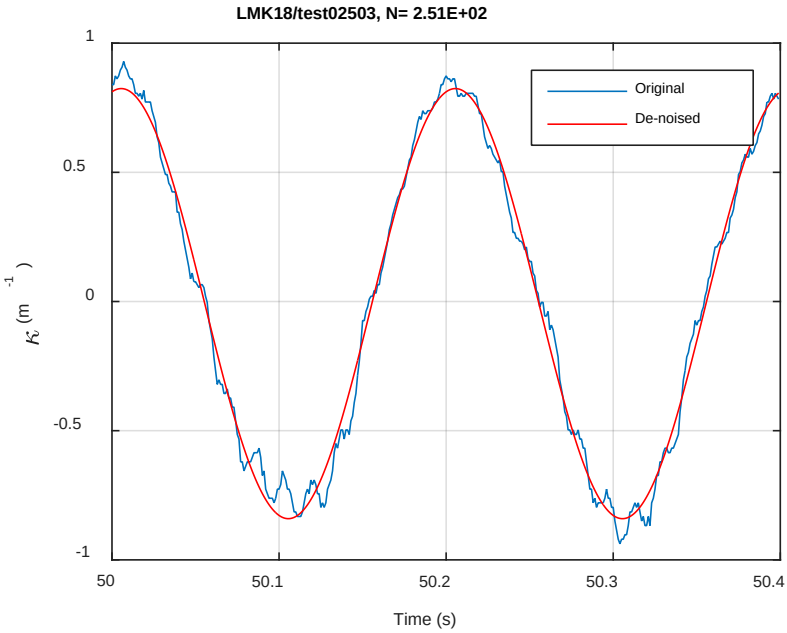

(c)

Fig. A.63. Monitoring-based responses: (a) curvature, (b) moment, (c) curvature, LMK18, 30.48 Nm, Ns = 2.51E+02 cycles.

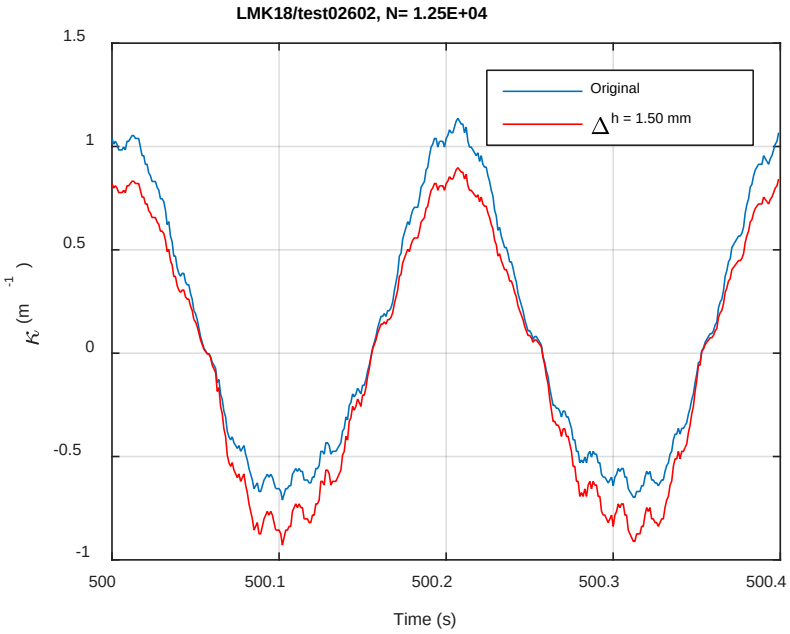
LMK18/test02602, N= 1.25E+04
Original
Δh = 1.50 mm
κ (m-1)
Time (s)
1.5
1
0.5
0
-0.5
-1
500
500.1
500.2
500.3
500.4

(a)

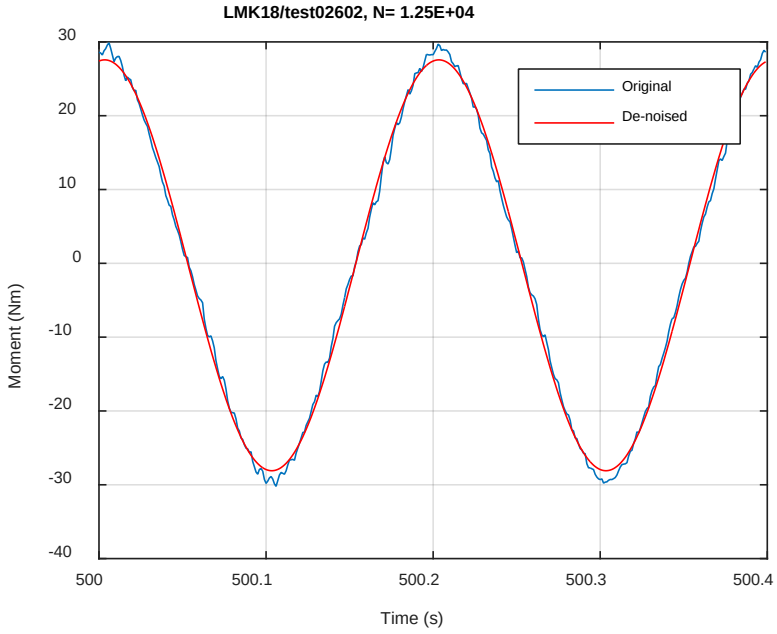
LMK18/test02602, N= 1.25E+04
Original
De-noised
Moment (Nm)
Time (s)
30
20
10
0
-10
-20
-30
-40
500
500.1
500.2
500.3
500.4

(b)

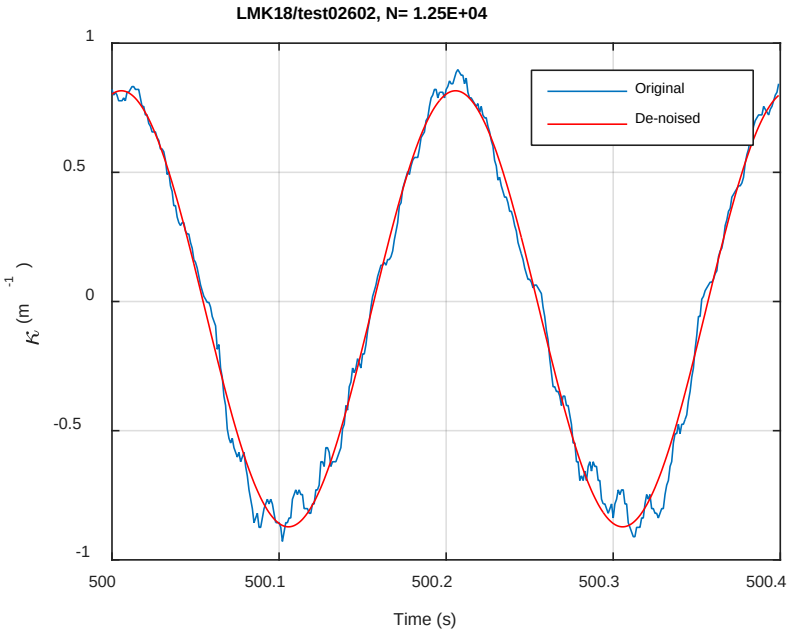

(c)

Fig. A.64. Monitoring-based responses: (a) curvature, (b) moment, (c) curvature, LMK18, 30.48 Nm, Ns = 1.25E+04 cycles.

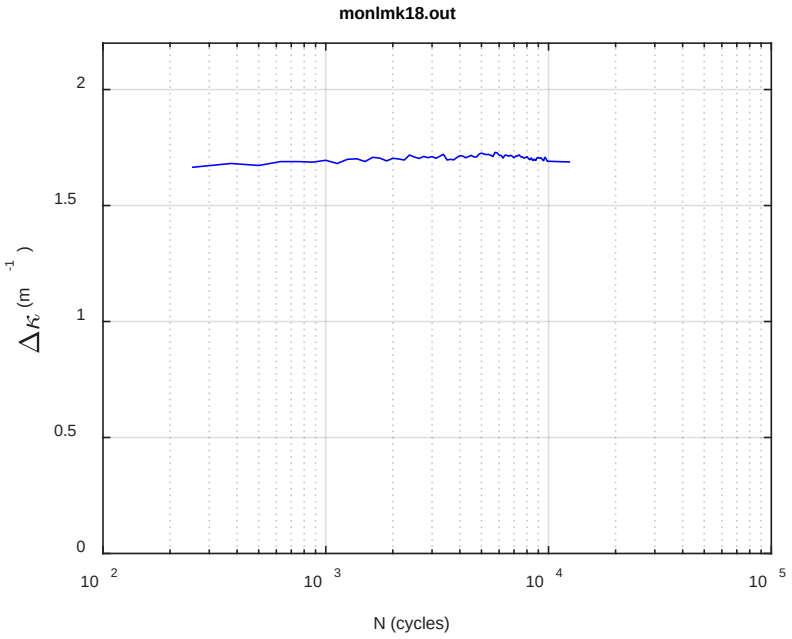
monlmk18.out
2
1.5
1
0.5
0
Δκ (m -1)
10 2
10 3
10 4
10 5
N (cycles)

(a)

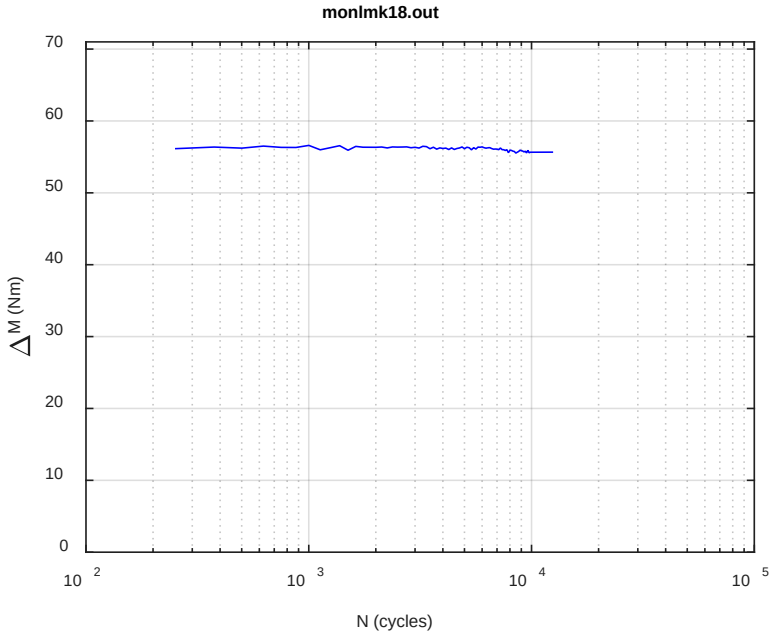
monlmk18.out
70
60
50
40
30
20
10
0
Δ M (Nm)
10 2
10 3
10 4
10 5
N (cycles)

(b)

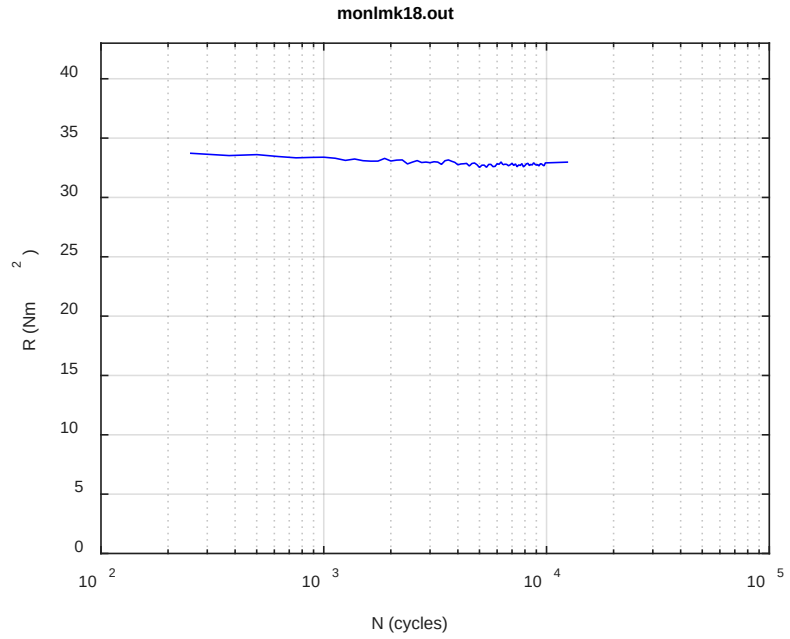
monlmk18.out
R (Nm 2)
N (cycles)

(c)

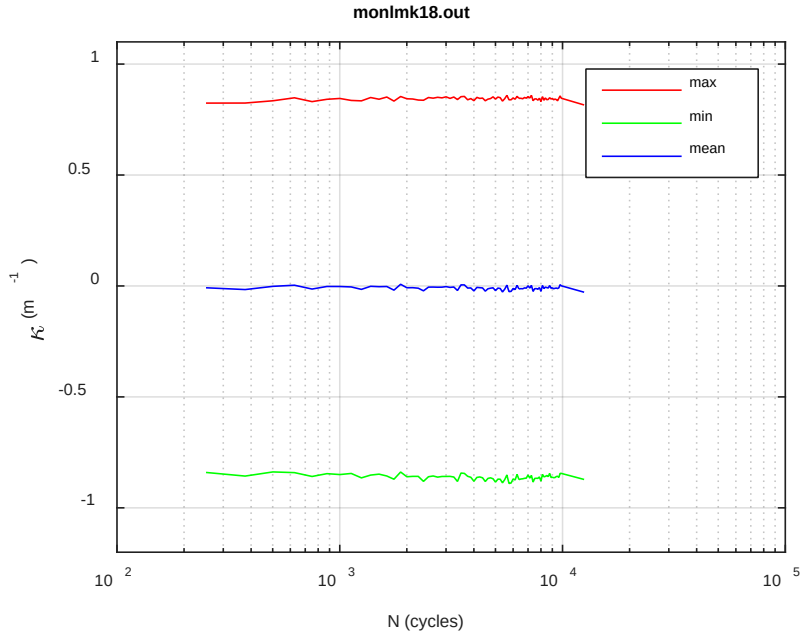
monlmk18.out
max
min
mean
κ (m -1)
N (cycles)

(d)

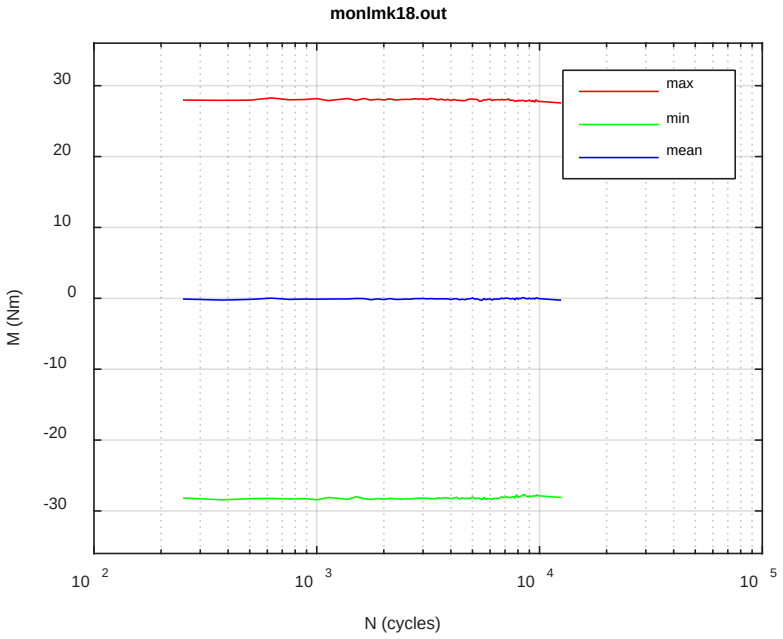

(e)

Fig. A.65. Monitoring-based responses: (a) curvature range, (b) moment range, (c) rigidity, (d) curvature peak/valley, (e) moment peak/valley, LMK18, 30.48 Nm, Nf = 1.31E+04 cycles.

This page intentionally left blank.

APPENDIX B CIRFT TESTING RESULTS OF NA

TABLE OF CONTENTS

Measurement and monitoring rigidity curves of North Anna Spent Nuclear Fuel

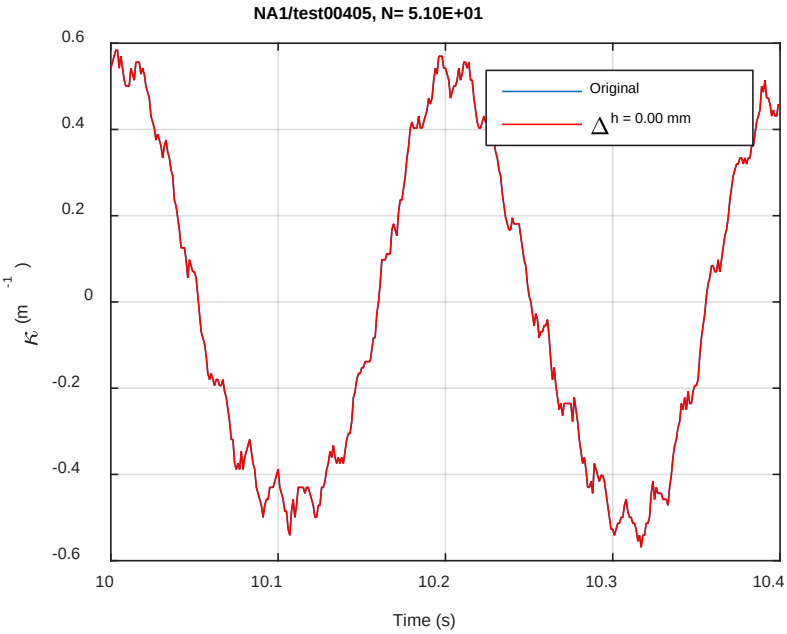
NA1/test00405, N= 5.10E+01
Original
Δh = 0.00 mm
κ (m-1)
Time (s)
0.6
0.4
0.2
0
-0.2
-0.4
-0.6
10
10.1
10.2
10.3
10.4

(a)

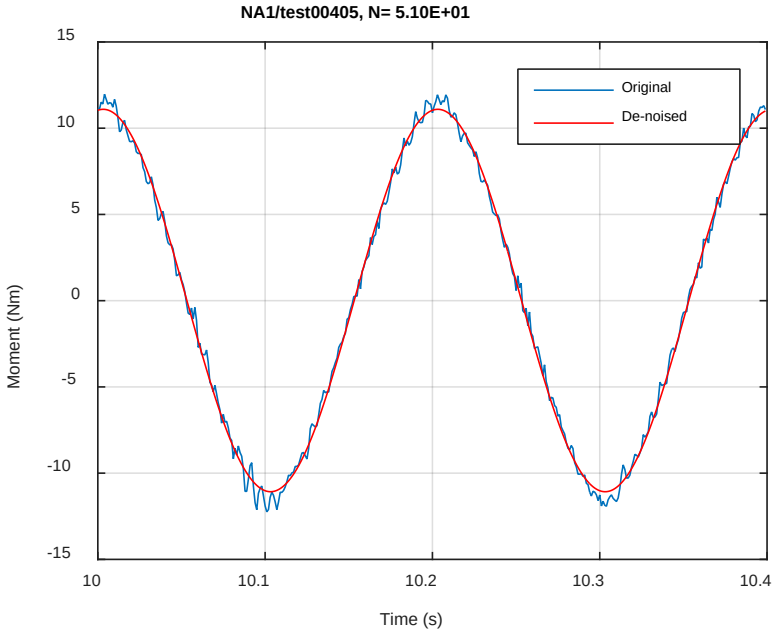
NA1/test00405, N= 5.10E+01
Original
De-noised
Moment (Nm)
Time (s)
15
10
5
0
-5
-10
-15
10
10.1
10.2
10.3
10.4

(b)

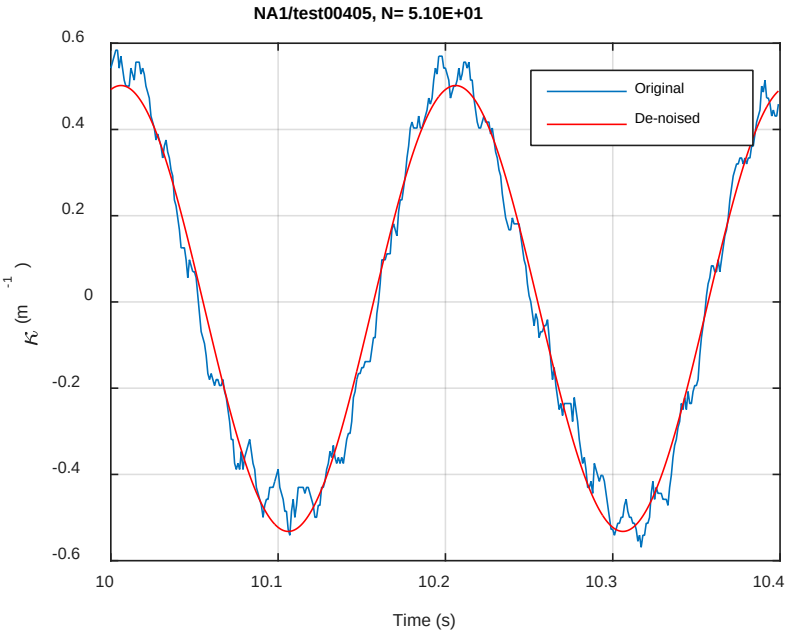

(c)

Fig. B.1. Monitoring-based responses: (a) curvature, (b) moment, (c) curvature, NA1, 12.70 Nm, Ns = 5.10E+01 cycles.

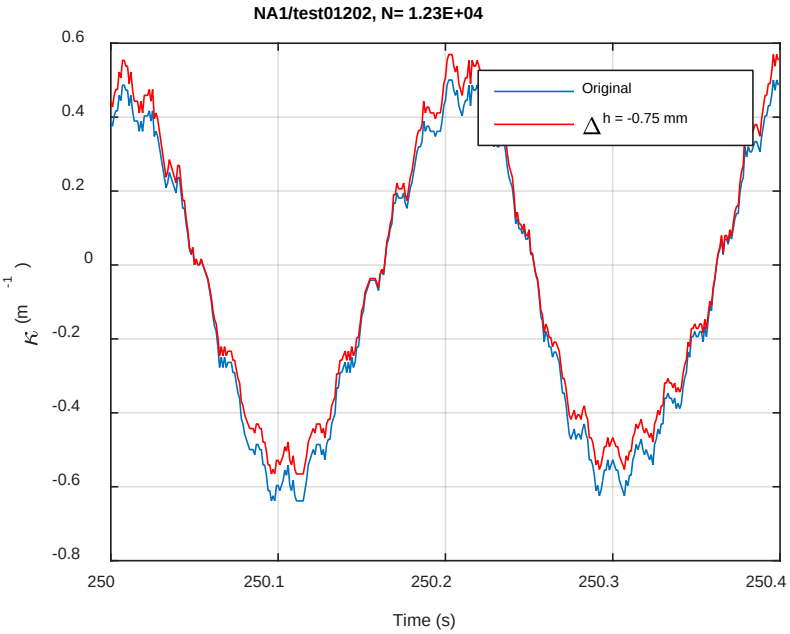
NA1/test01202, N= 1.23E+04
Original
Δh = -0.75 mm
κ (m-1)
Time (s)

(a)

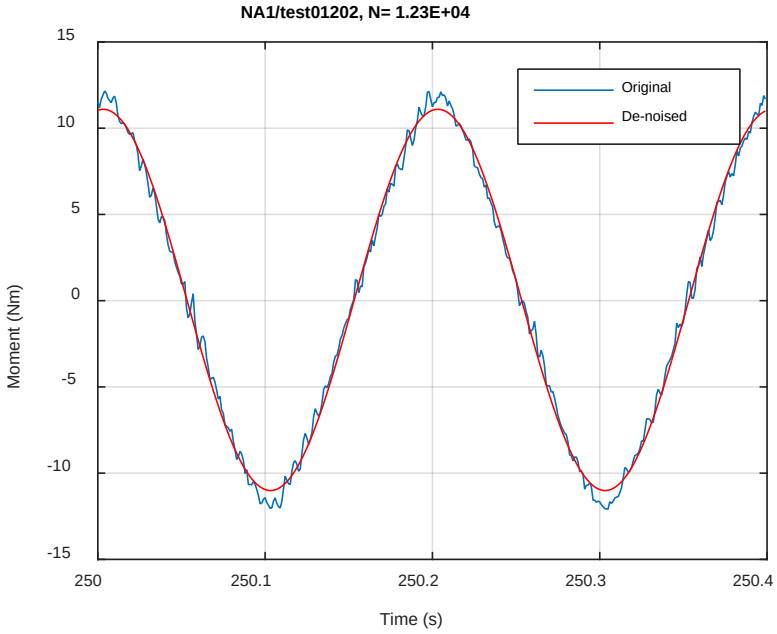
NA1/test01202, N= 1.23E+04
Original
De-noised
Moment (Nm)
Time (s)

(b)

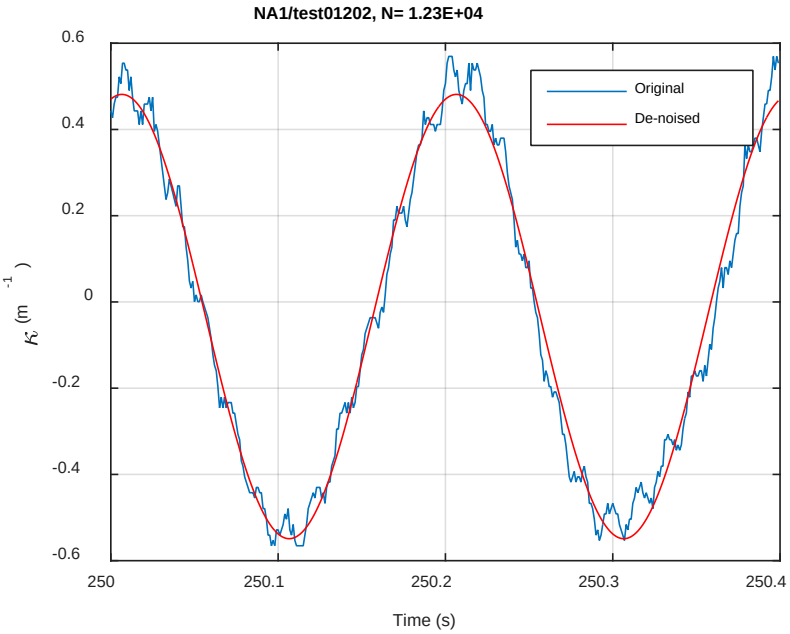

(c)

Fig. B.2. Monitoring-based responses: (a) curvature, (b) moment, (c) curvature, NA1, 12.70 Nm, Ns = 1.23E+04 cycles.

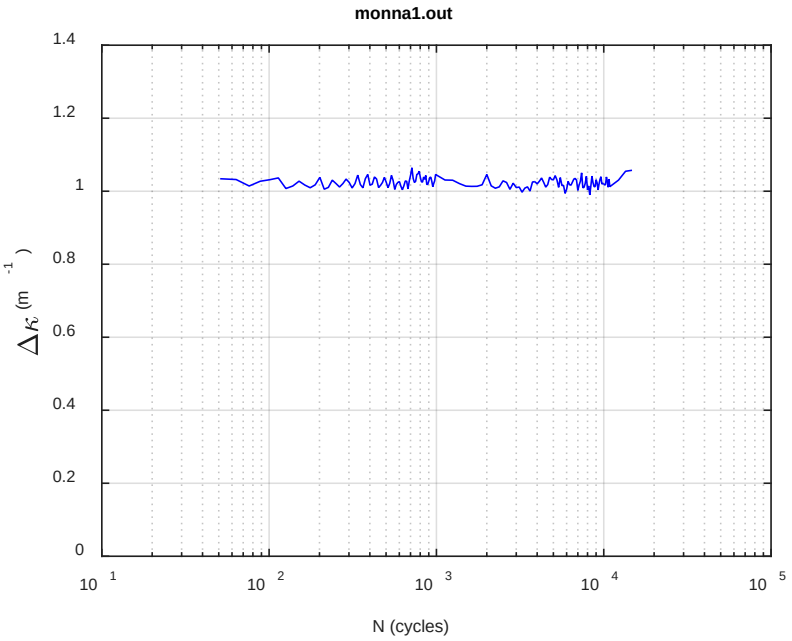
monna1.out
1.4
1.2
1
0.8
0.6
0.4
0.2
0
$\Delta\kappa$ (m^{-1})
10^1
10^2
10^3
10^4
10^5
N (cycles)

(a)

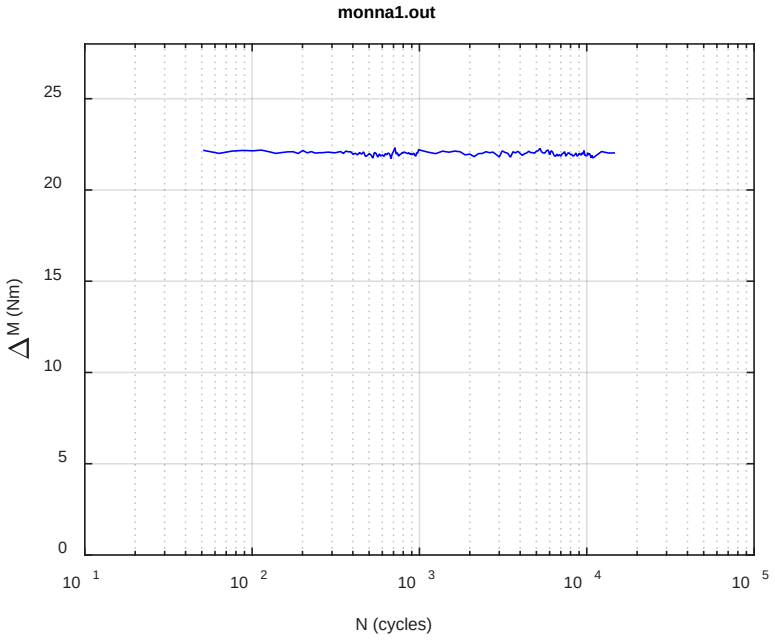
monna1.out
25
20
15
10
5
0
Δ M (Nm)
10^1
10^2
10^3
10^4
10^5
N (cycles)

(b)

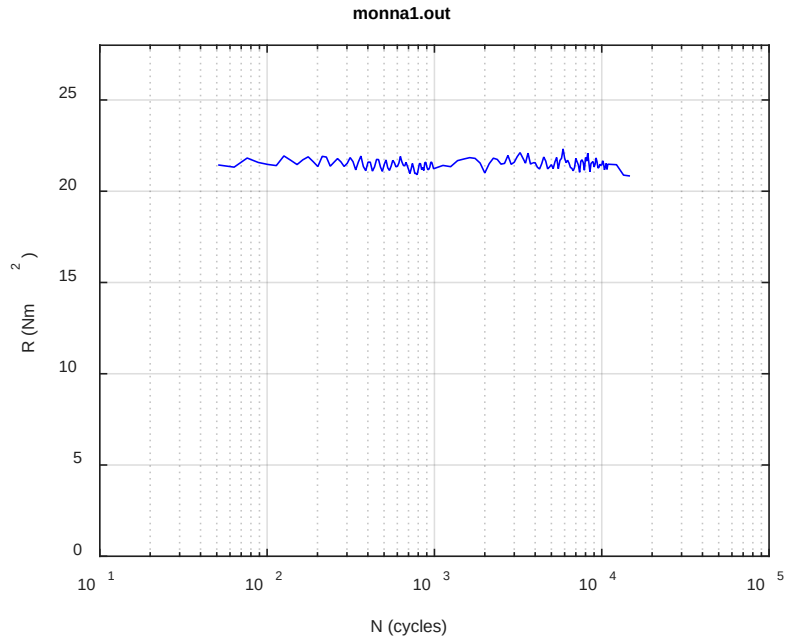

(c)

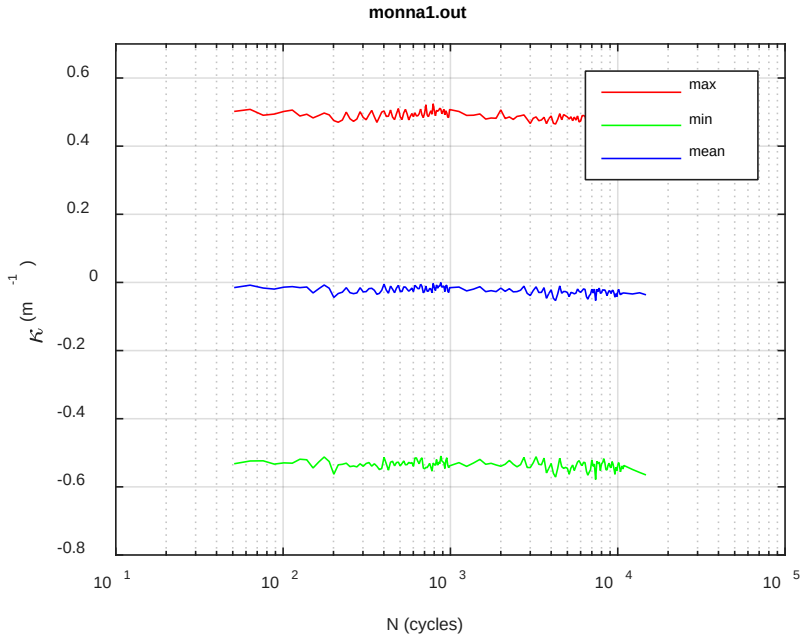

(d)

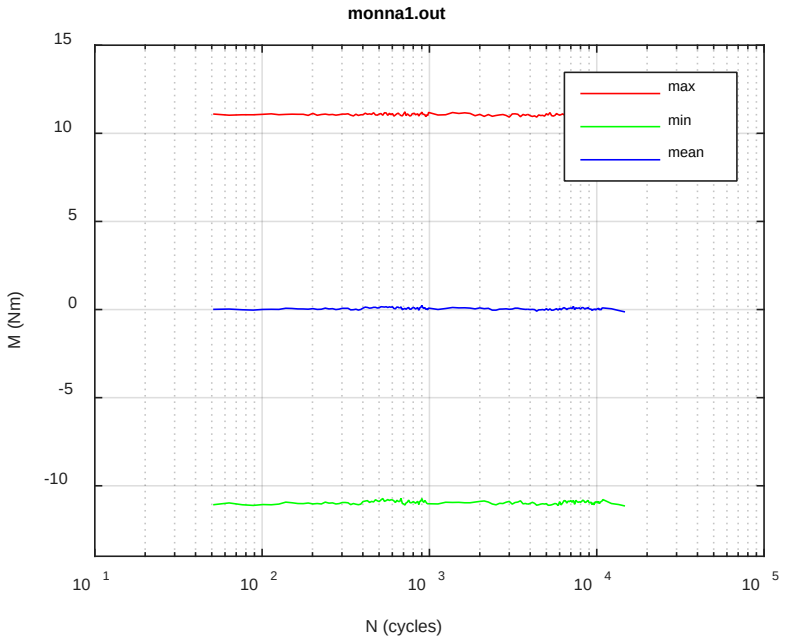

(e)

Fig. B.3. Monitoring-based responses: (a) curvature range, (b) moment range, (c) rigidity, (d) curvature peak/valley, (e) moment peak/valley, NA1, 12.70 Nm, Nf = 1.57E+04 cycles.

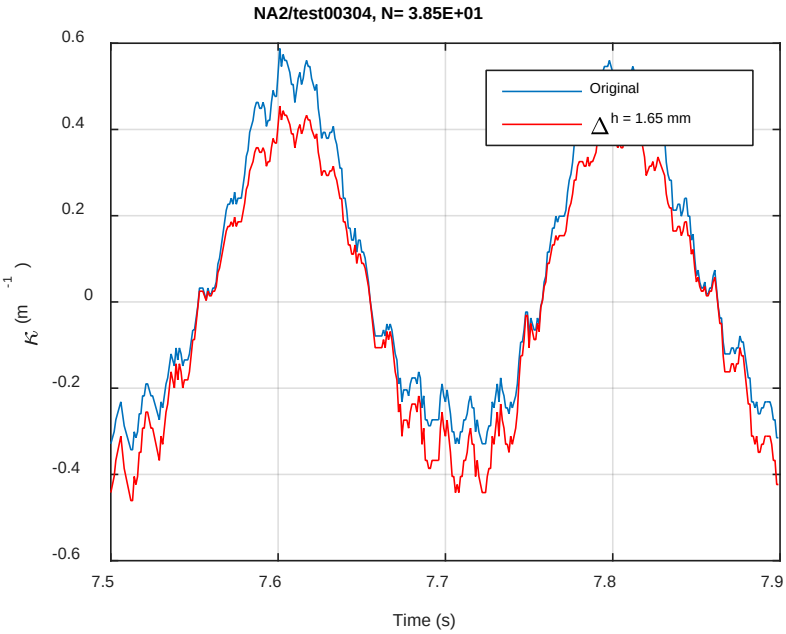
NA2/test00304, N= 3.85E+01
Original
Δh = 1.65 mm
κ (m-1)
Time (s)
0.6
0.4
0.2
0
-0.2
-0.4
-0.6
7.5
7.6
7.7
7.8
7.9

(a)

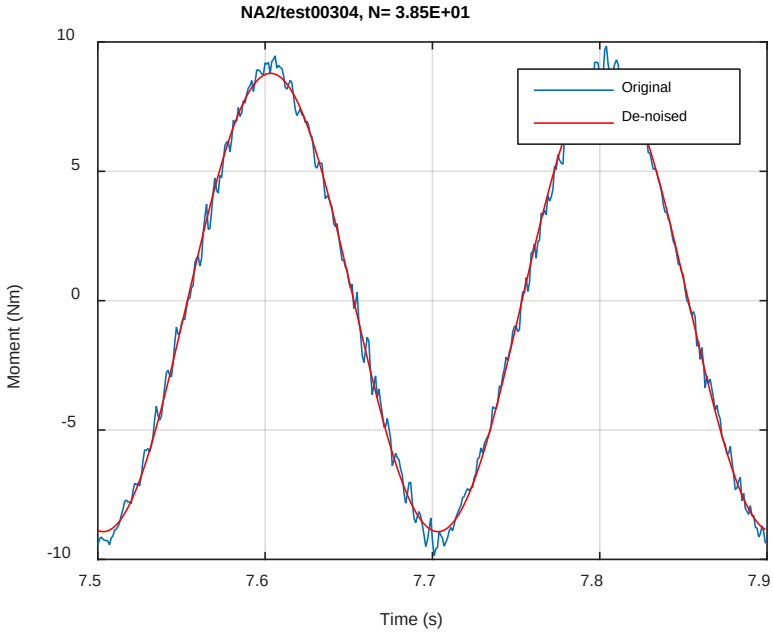
NA2/test00304, N= 3.85E+01
Original
De-noised
Moment (Nm)
Time (s)
10
5
0
-5
-10
7.5
7.6
7.7
7.8
7.9

(b)

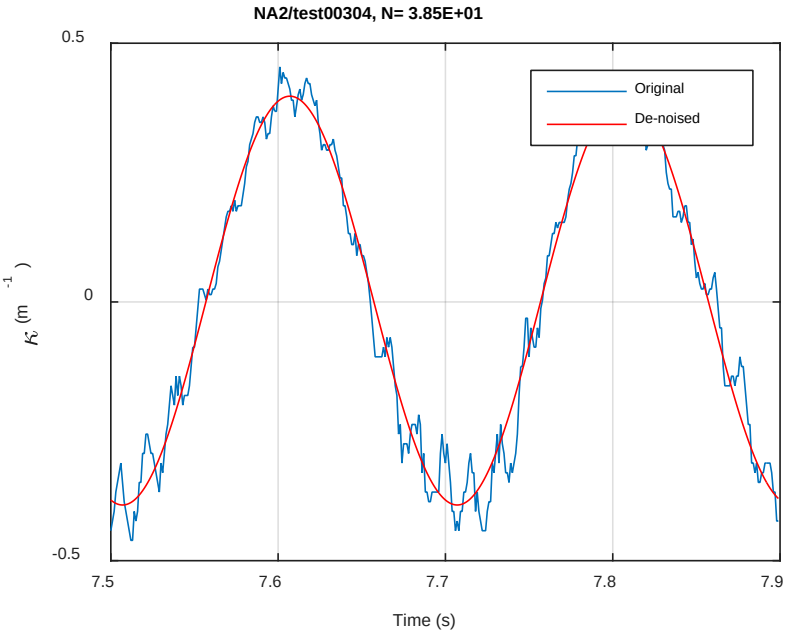

(c)

Fig. B.4. Monitoring-based responses: (a) curvature, (b) moment, (c) curvature, NA2, 10.16 Nm, Ns = 3.85E+01 cycles.

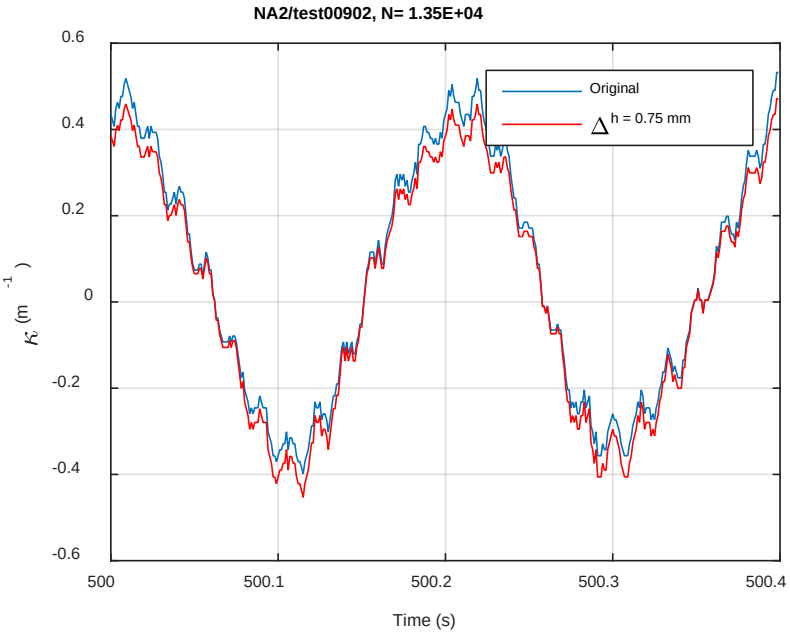
NA2/test00902, N= 1.35E+04
Original
Δh = 0.75 mm
κ (m-1)
Time (s)
0.6
0.4
0.2
0
-0.2
-0.4
-0.6
500
500.1
500.2
500.3
500.4

(a)

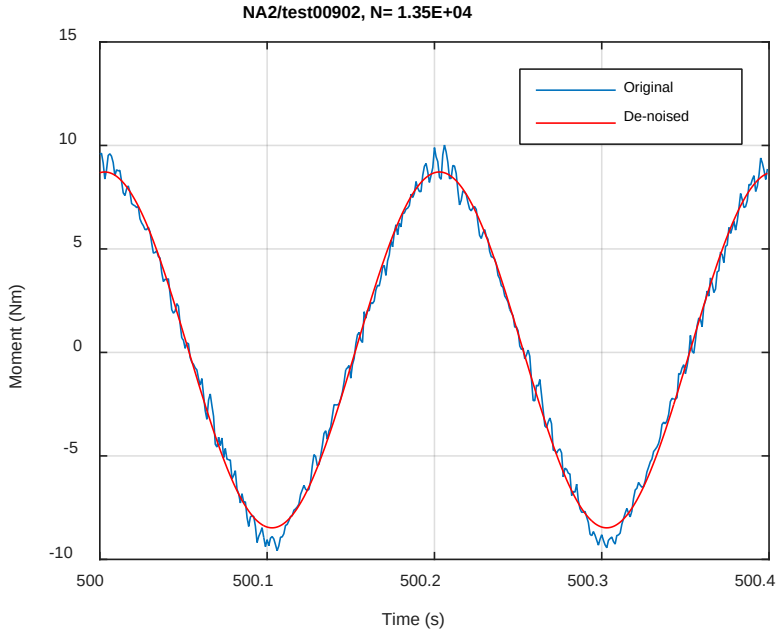
NA2/test00902, N= 1.35E+04
Original
De-noised
Moment (Nm)
Time (s)
15
10
5
0
-5
-10
500
500.1
500.2
500.3
500.4

(b)

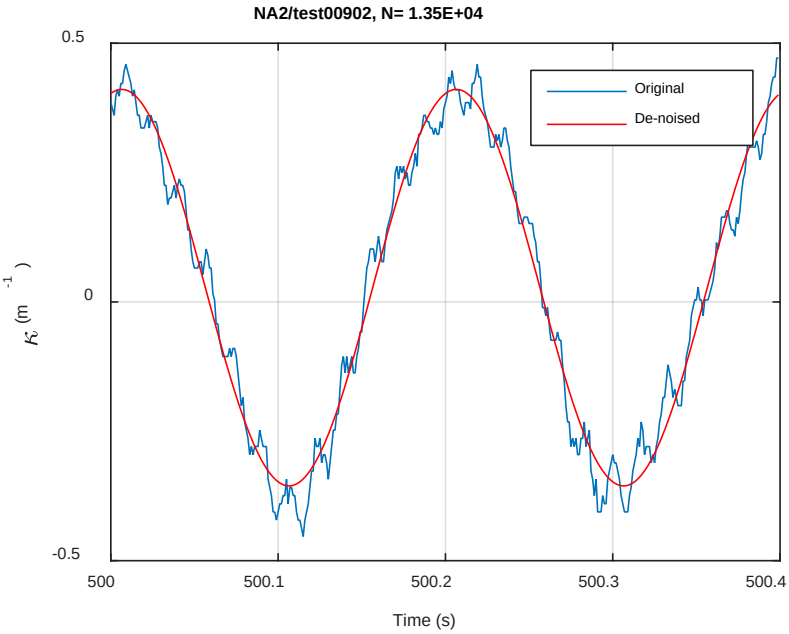

(c)

Fig. B.5. Monitoring-based responses: (a) curvature, (b) moment, (c) curvature, NA2, 10.16 Nm, Ns = 1.35E+04 cycles.

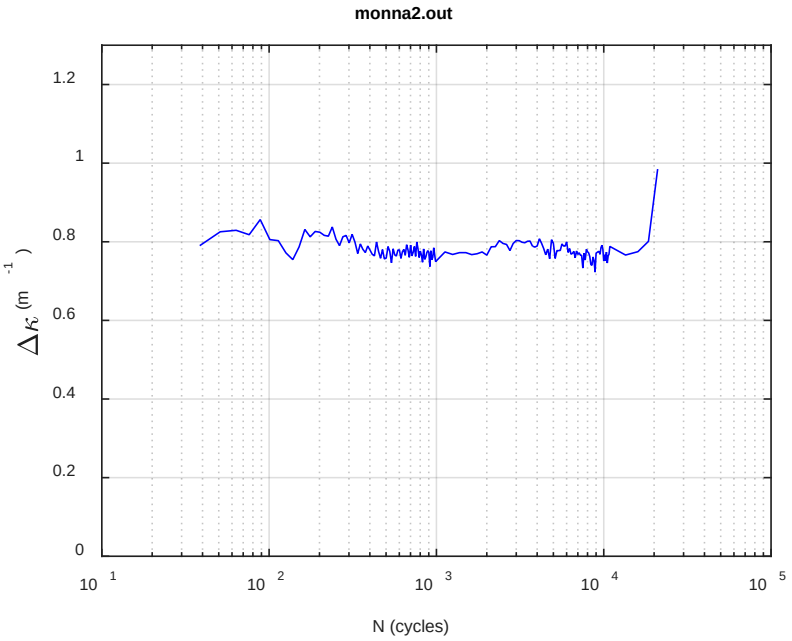
monna2.out
1.2
1
0.8
0.6
0.4
0.2
0
$\Delta\kappa$ (m^{-1})
10^1
10^2
10^3
10^4
10^5
N (cycles)

(a)

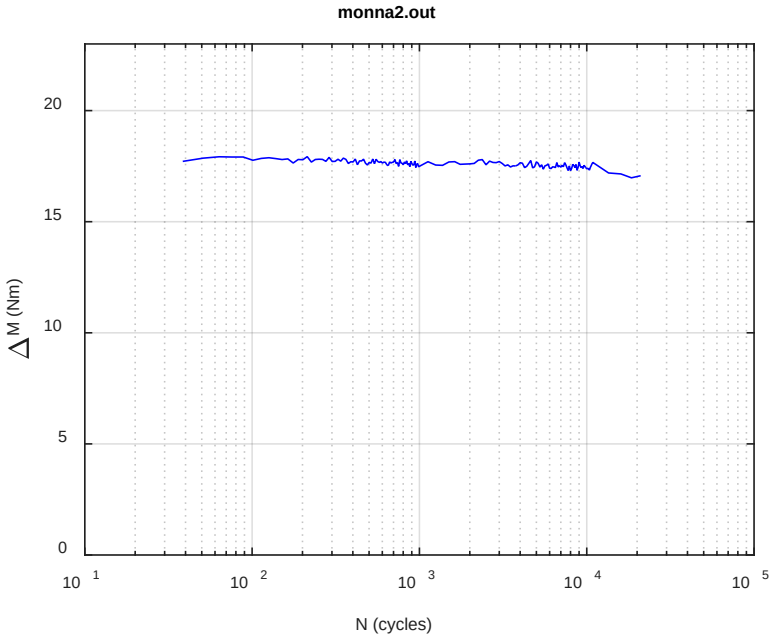
monna2.out
20
15
10
5
0
Δ M (Nm)
10^1
10^2
10^3
10^4
10^5
N (cycles)

(b)

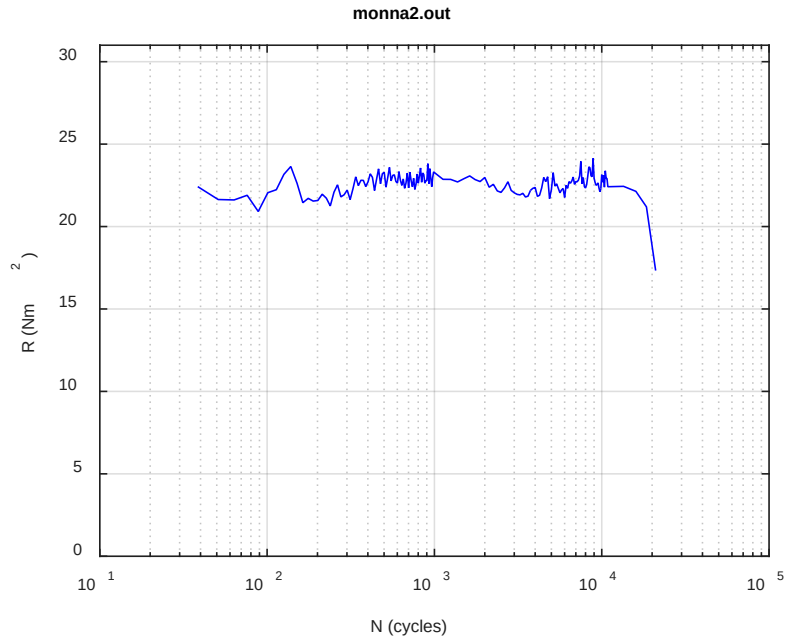

(c)

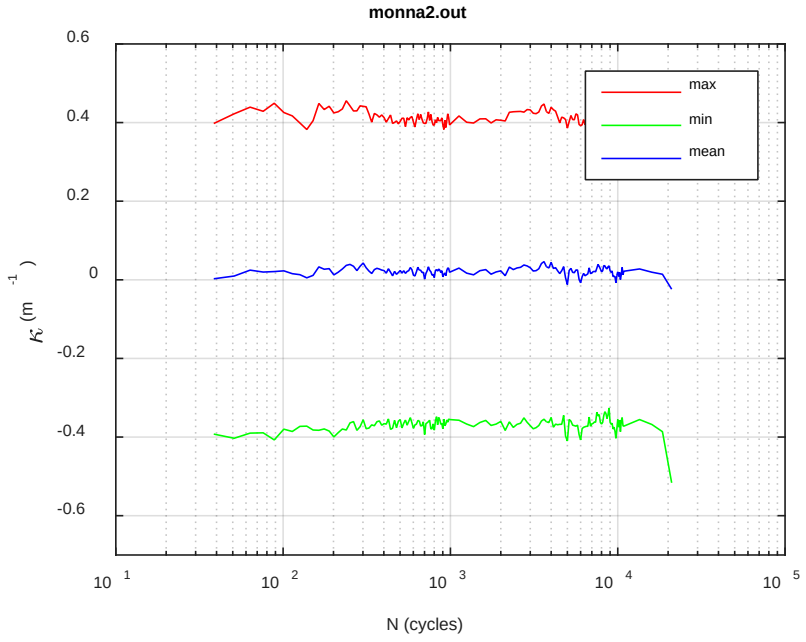

(d)

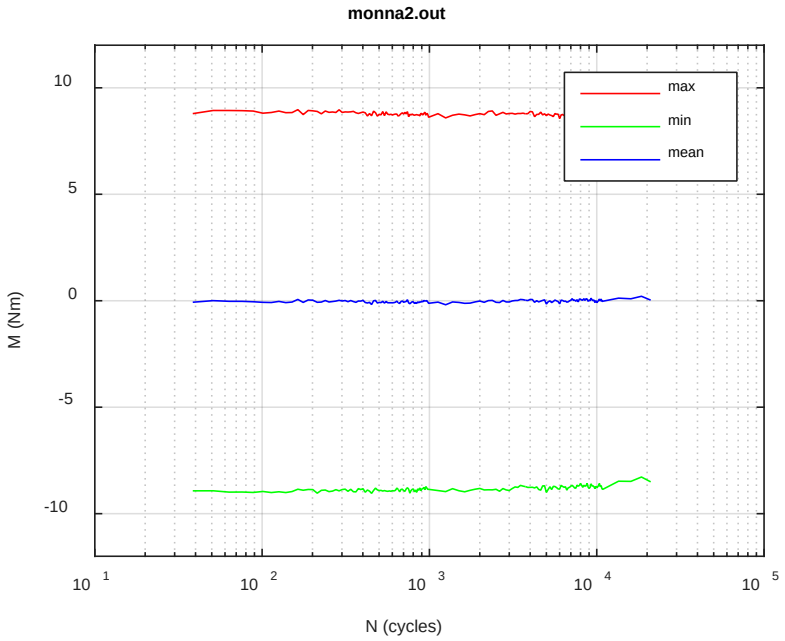

(e)

Fig. B.6. Monitoring-based responses: (a) curvature range, (b) moment range, (c) rigidity, (d) curvature peak/valley, (e) moment peak/valley, NA2, 10.16 Nm, Nf = 2.20E+04 cycles.

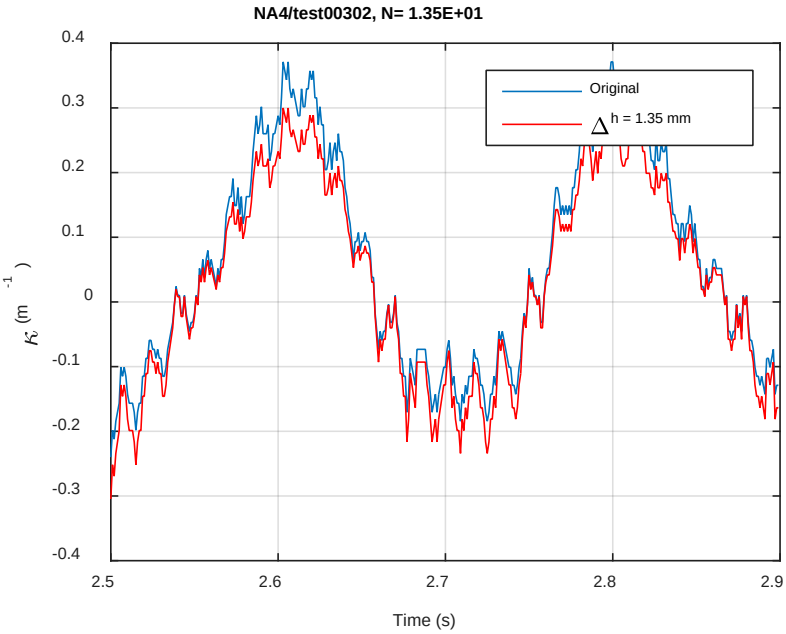
NA4/test00302, N= 1.35E+01
Original
Δh = 1.35 mm
κ (m-1)
Time (s)

(a)

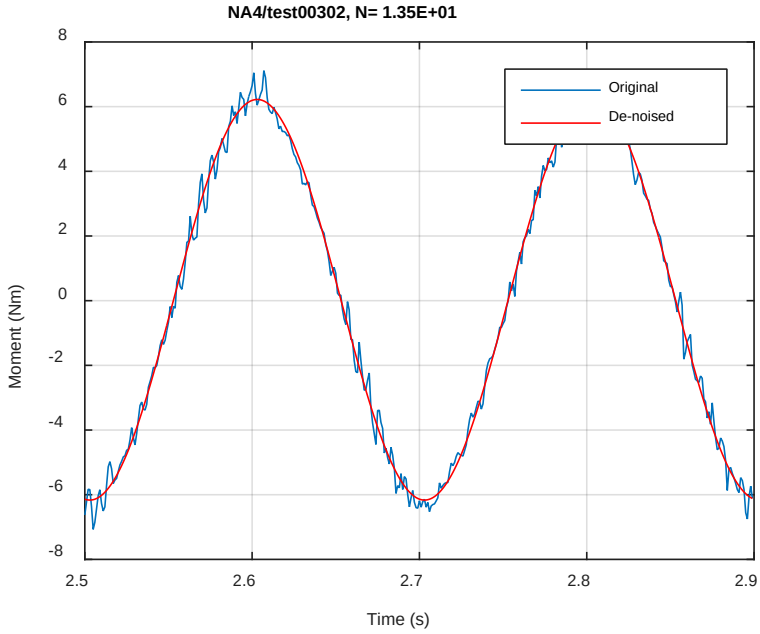
NA4/test00302, N= 1.35E+01
Original
De-noised
Moment (Nm)
Time (s)

(b)

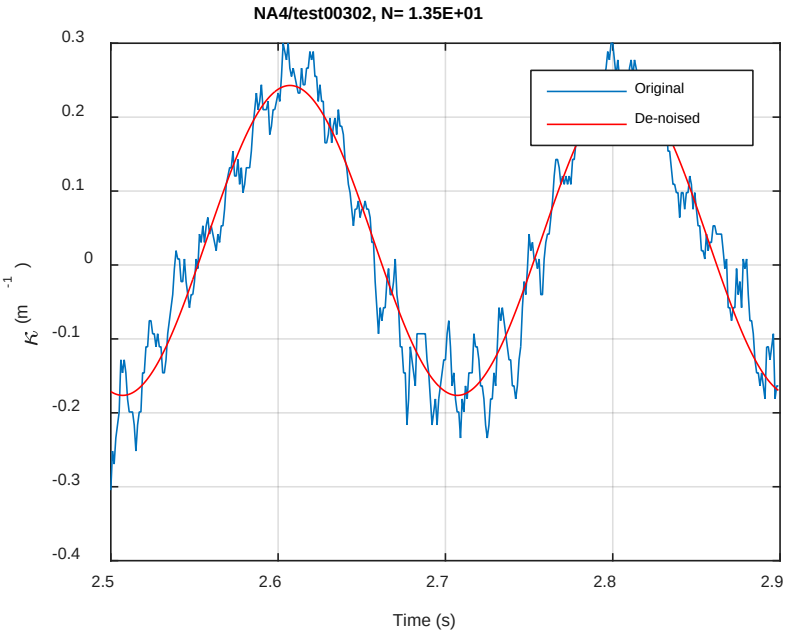

(c)

Fig. B.7. Monitoring-based responses: (a) curvature, (b) moment, (c) curvature, NA4, 7.62 Nm, Ns = 1.35E+01 cycles.

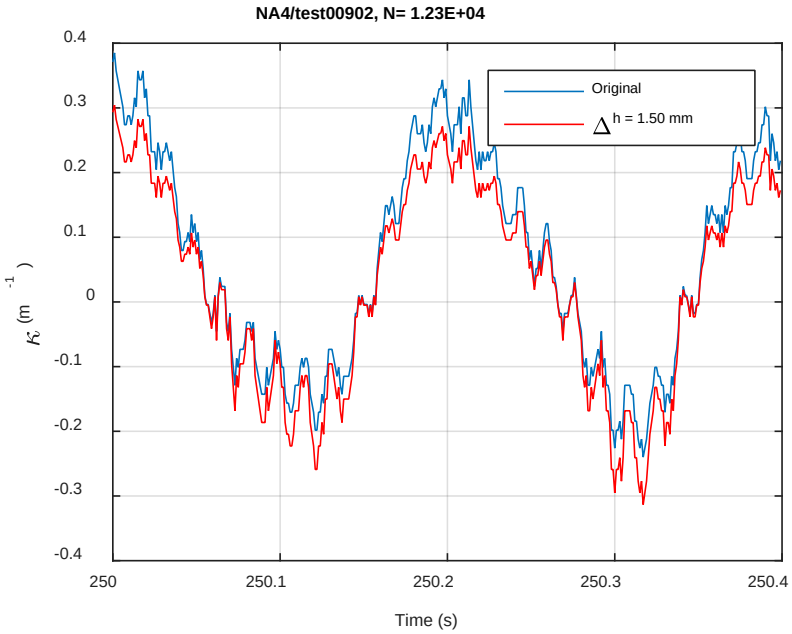
NA4/test00902, N= 1.23E+04
Original
Δh = 1.50 mm
κ (m-1)
Time (s)
0.4
0.3
0.2
0.1
0
-0.1
-0.2
-0.3
-0.4
250
250.1
250.2
250.3
250.4

(a)

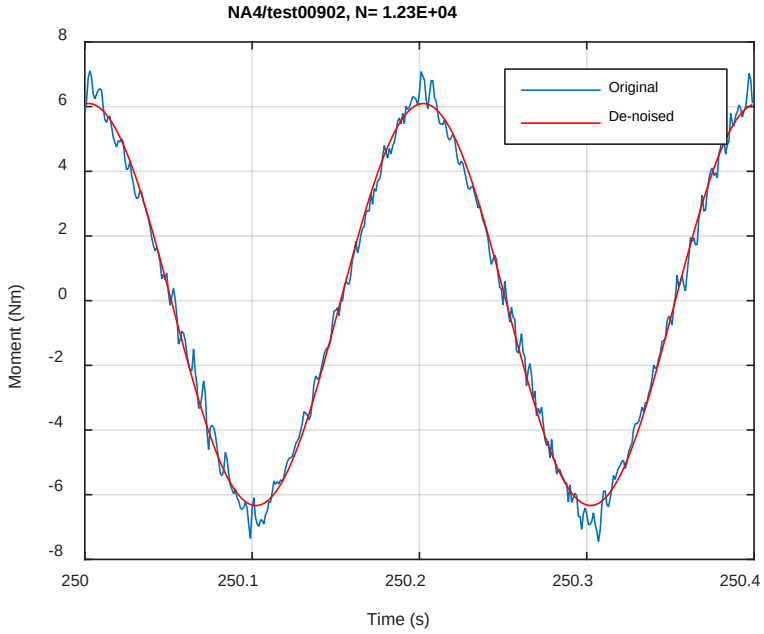
NA4/test00902, N= 1.23E+04
Original
De-noised
Moment (Nm)
Time (s)
8
6
4
2
0
-2
-4
-6
-8
250
250.1
250.2
250.3
250.4

(b)

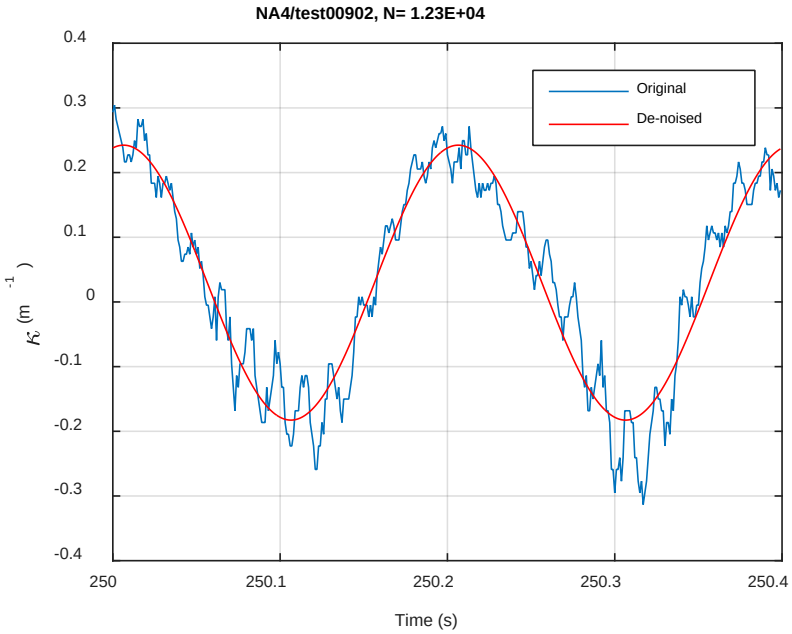

(c)

Fig. B.8. Monitoring-based responses: (a) curvature, (b) moment, (c) curvature, NA4, 7.62 Nm, Ns = 1.23E+04 cycles.

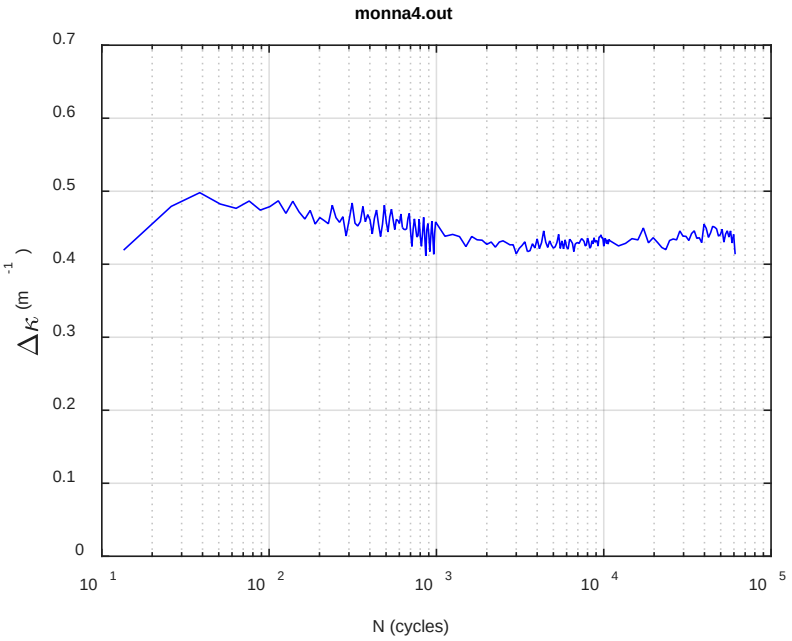
monna4.out
0.7
0.6
0.5
0.4
0.3
0.2
0.1
0
Δκ (m -1)
10 1
10 2
10 3
10 4
10 5
N (cycles)

(a)

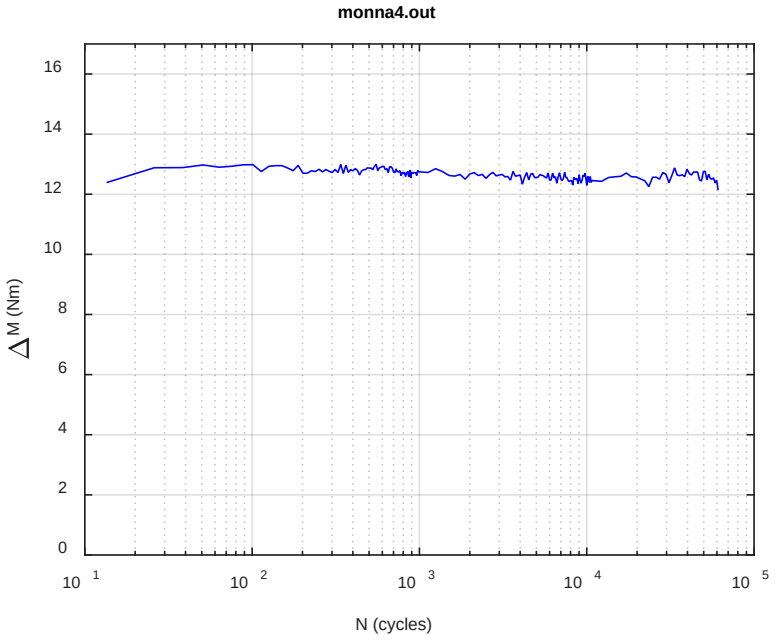
monna4.out
16
14
12
10
8
6
4
2
0
Δ M (Nm)
10 1
10 2
10 3
10 4
10 5
N (cycles)

(b)

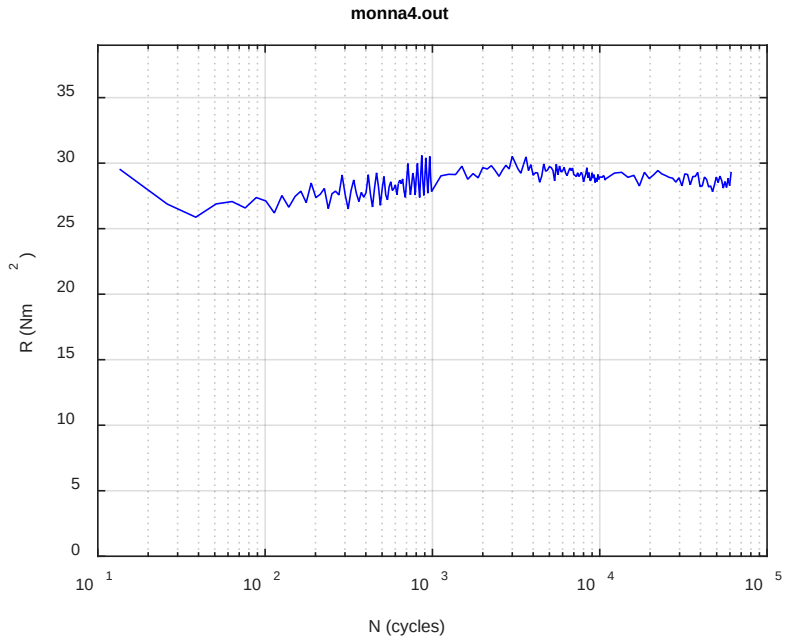

(c)

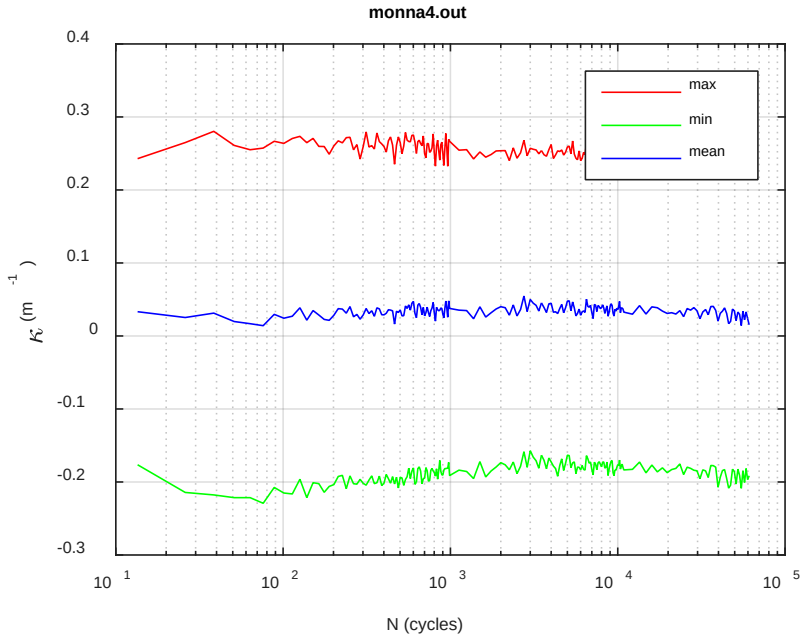

(d)

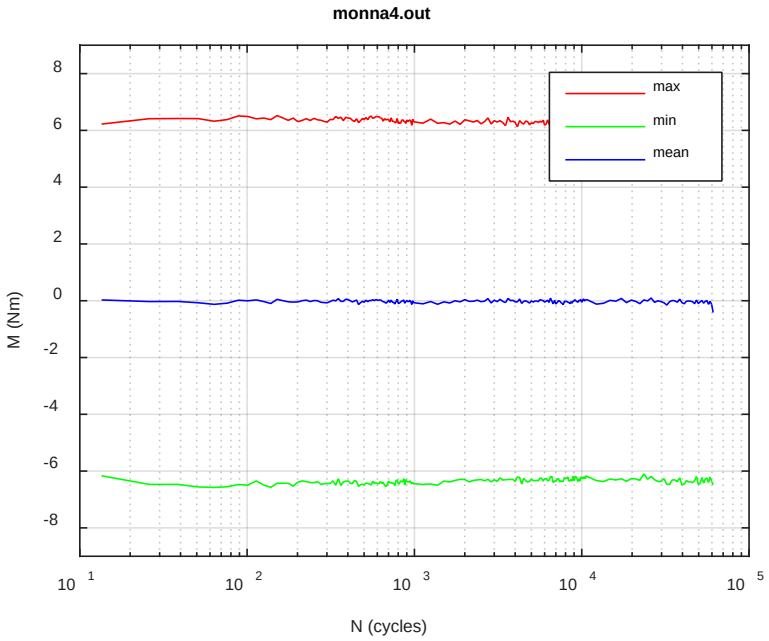

(e)

Fig. B.9. Monitoring-based responses: (a) curvature range, (b) moment range, (c) rigidity, (d) curvature peak/valley, (e) moment peak/valley, NA4, 7.62 Nm, Nf = 6.10E+04 cycles.

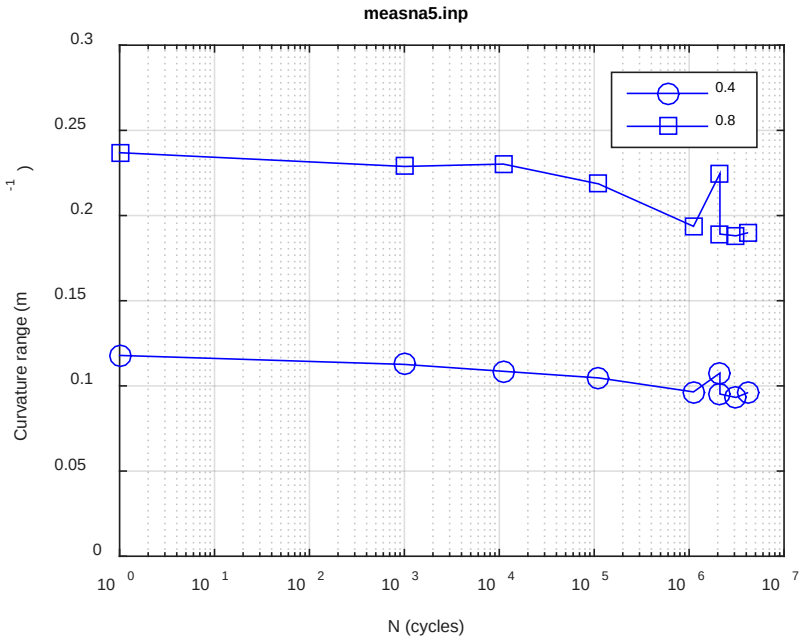
measna5.inp
0.4
0.8
Curvature range (m -1)
N (cycles)

(a)

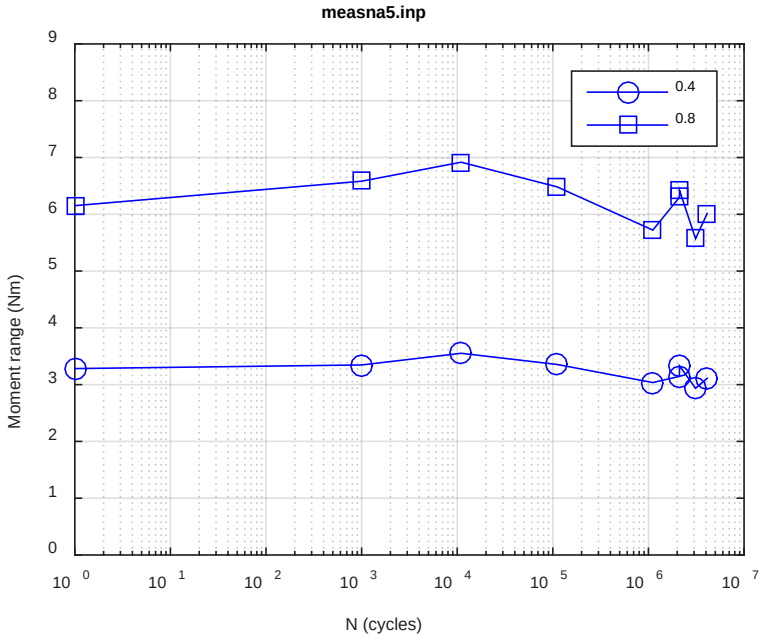
measna5.inp
0.4
0.8
Moment range (Nm)
N (cycles)

(b)

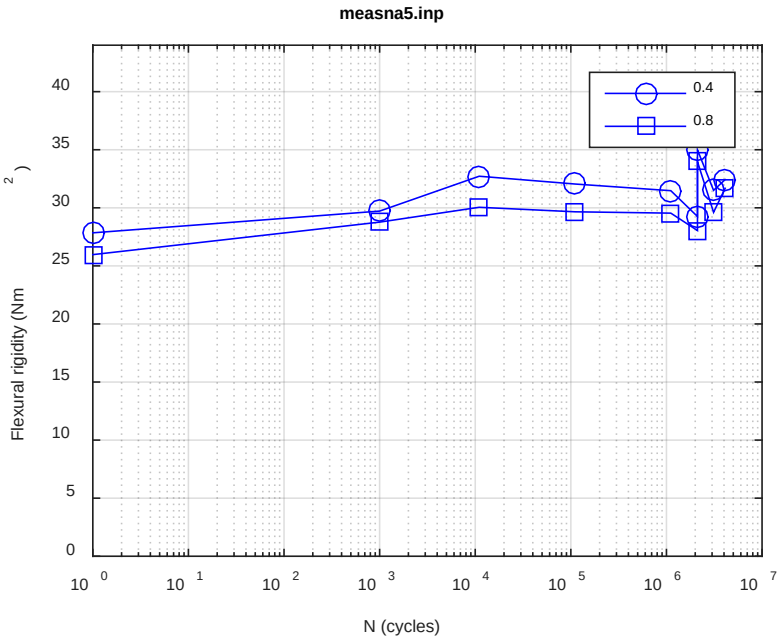
measna5.inp
0.4
0.8
Flexural rigidity (Nm 2)
N (cycles)

(c)

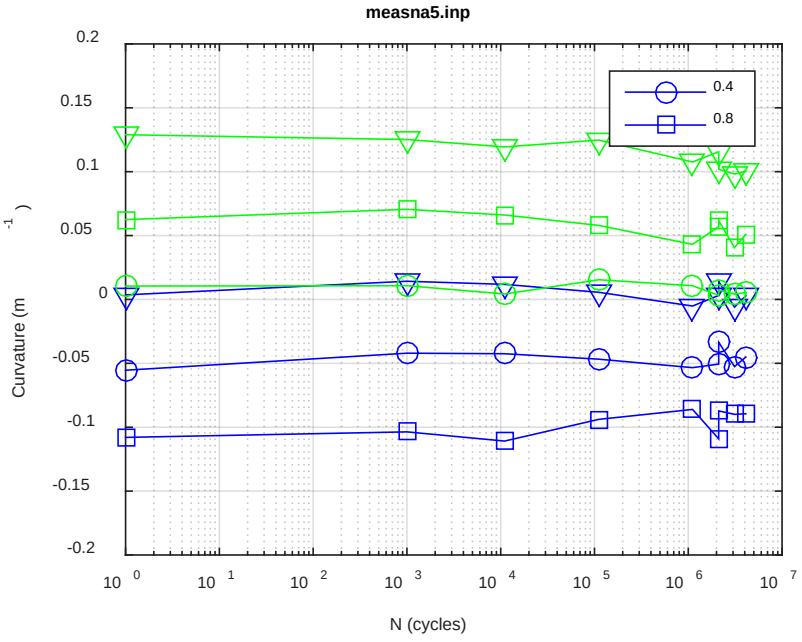
measna5.inp
0.4
0.8
Curvature (m -1)
N (cycles)

(d)

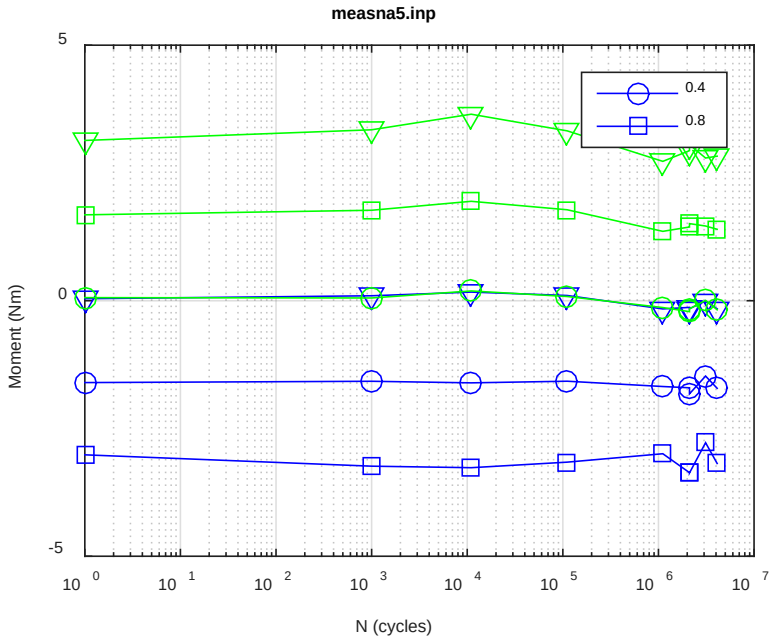

(e)

Fig. B.10. Measurement-based responses: (a) curvature range, (b) moment range, (c) rigidity, (d) curvature peak/valley, (e) moment peak/valley, NA5, 5.08 Nm.

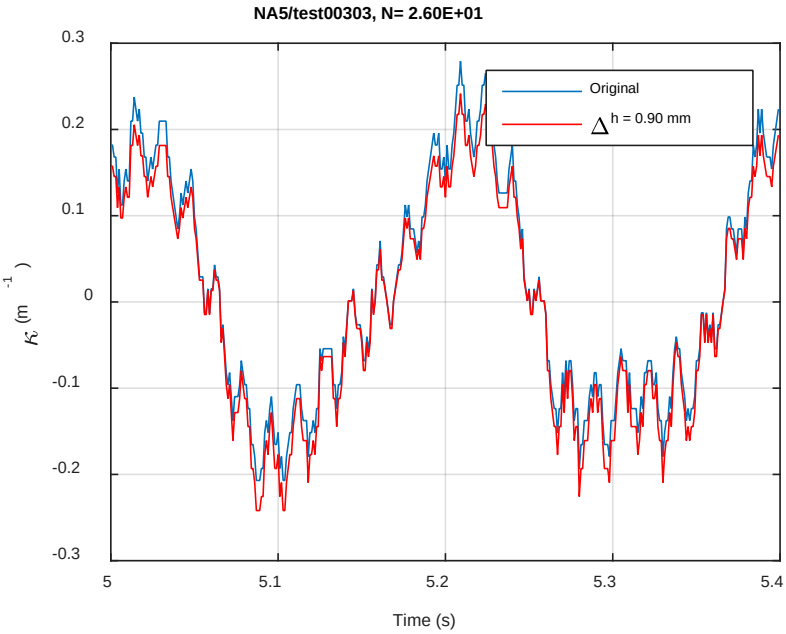
NA5/test00303, N= 2.60E+01
Original
Δh = 0.90 mm
κ (m-1)
Time (s)

(a)

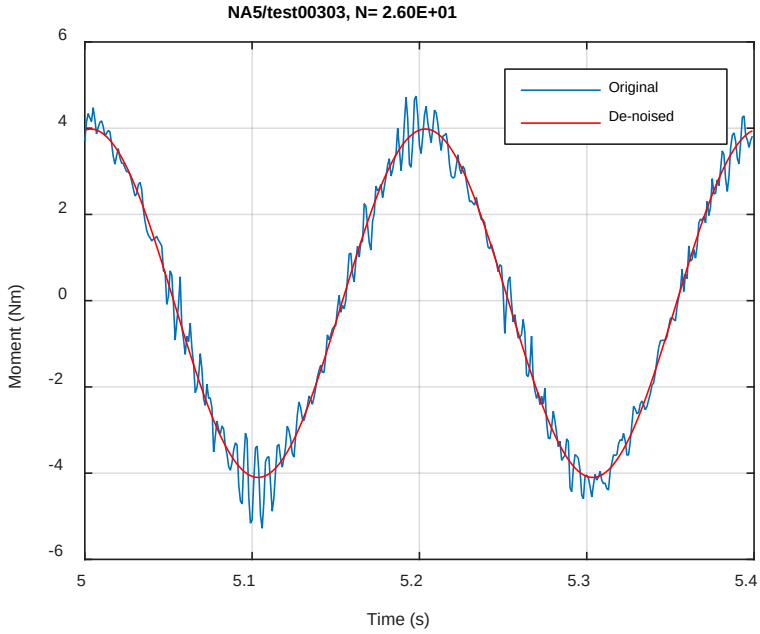
NA5/test00303, N= 2.60E+01
Original
De-noised
Moment (Nm)
Time (s)

(b)

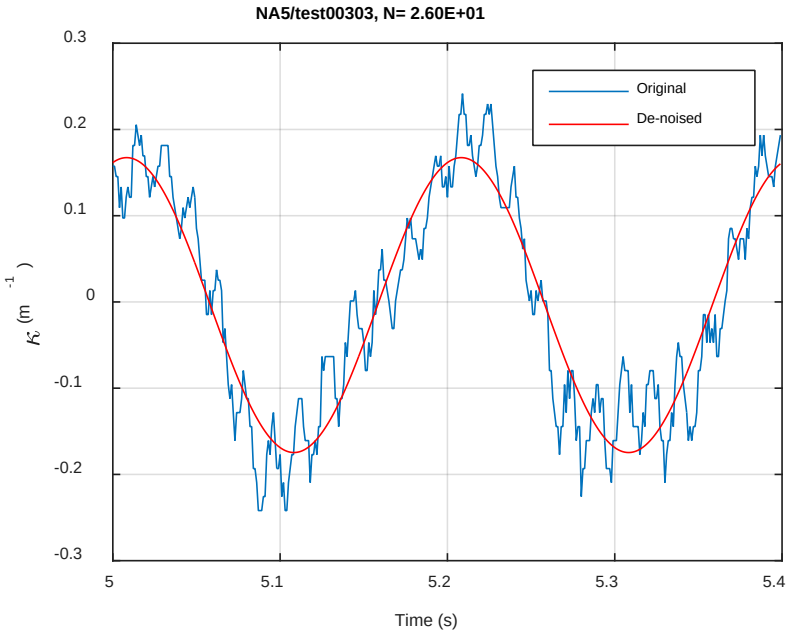

(c)

Fig. B.11. Monitoring-based responses: (a) curvature, (b) moment, (c) curvature, NA5, 5.08 Nm, Ns = 2.60E+01 cycles.

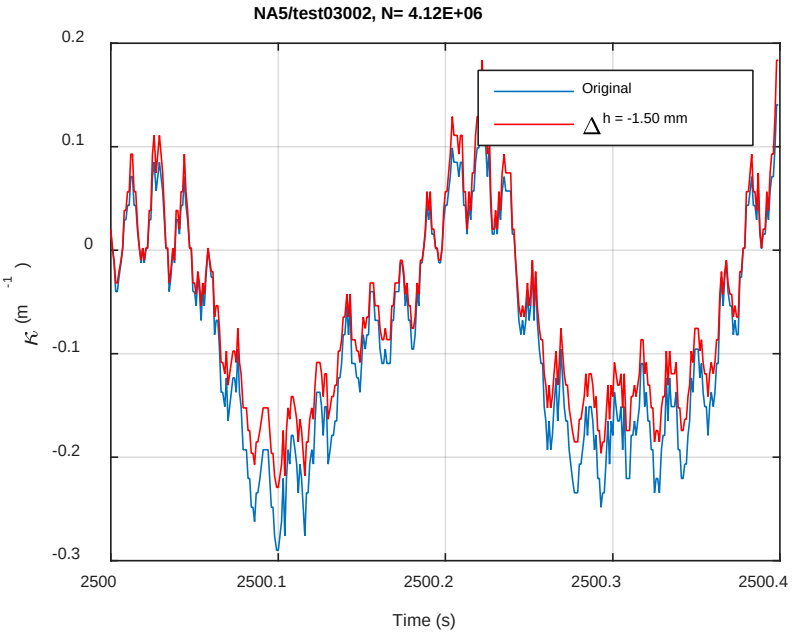
NA5/test03002, N= 4.12E+06
Original
Δh = -1.50 mm
κ (m-1)
0.2
0.1
0
-0.1
-0.2
-0.3
2500
2500.1
2500.2
2500.3
2500.4
Time (s)

(a)

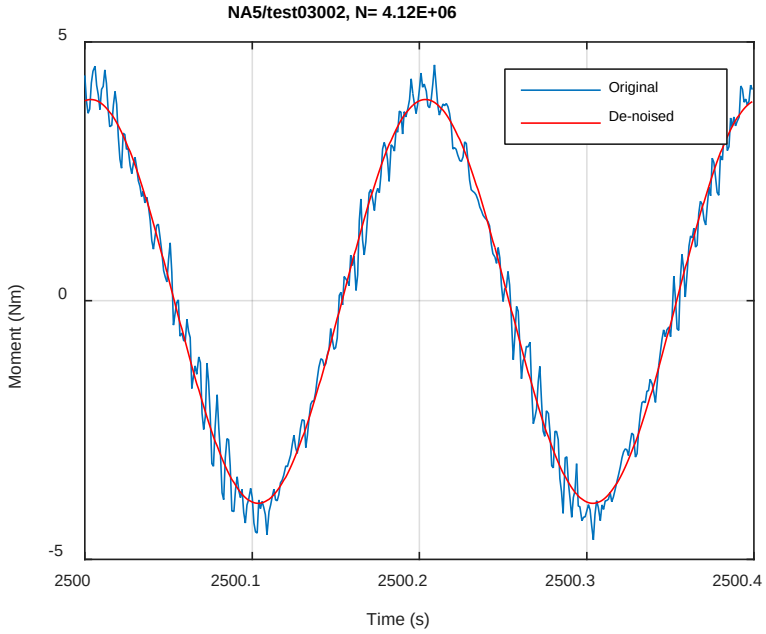
NA5/test03002, N= 4.12E+06
Original
De-noised
Moment (Nm)
5
0
-5
2500
2500.1
2500.2
2500.3
2500.4
Time (s)

(b)

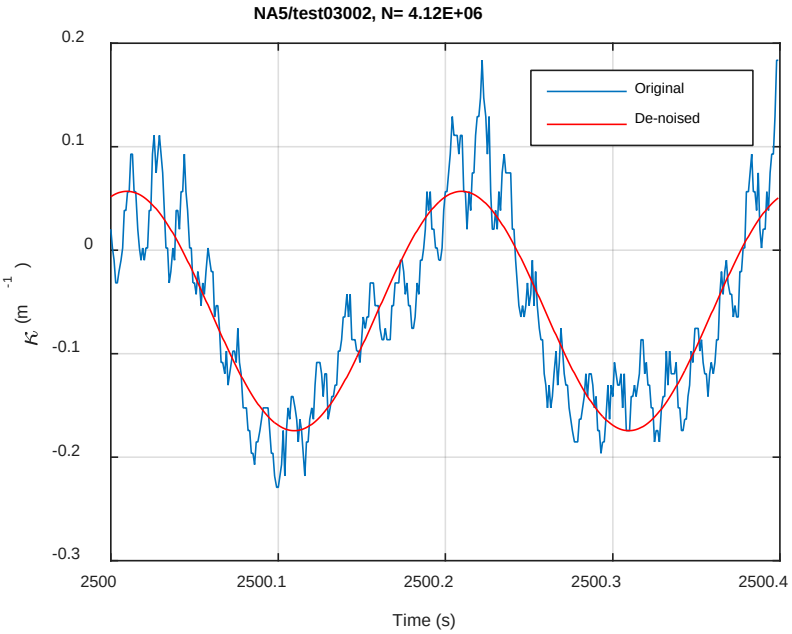

(c)

Fig. B.12. Monitoring-based responses: (a) curvature, (b) moment, (c) curvature, NA5, 5.08 Nm, Ns = 4.12E+06 cycles.

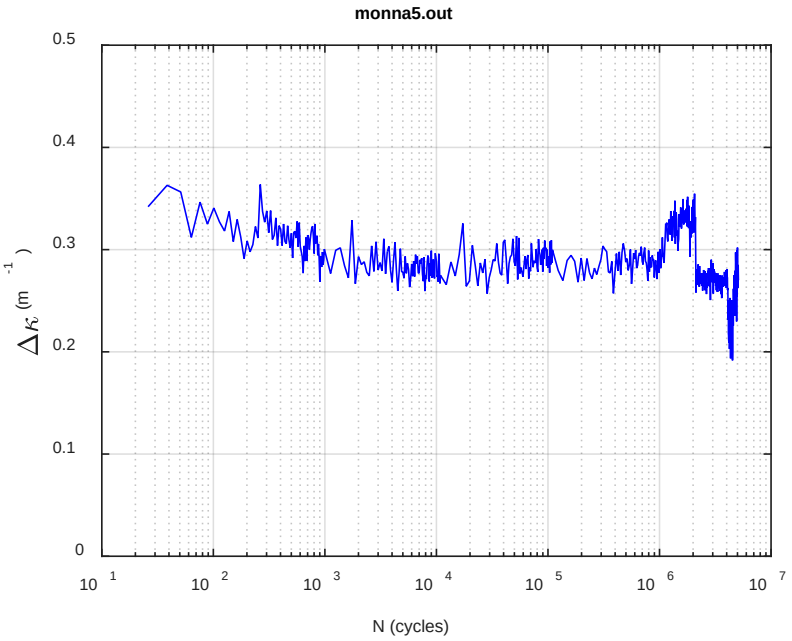
monna5.out
0.5
0.4
0.3
0.2
0.1
0
Δκ (m -1)
10 1
10 2
10 3
10 4
10 5
10 6
10 7
N (cycles)

(a)

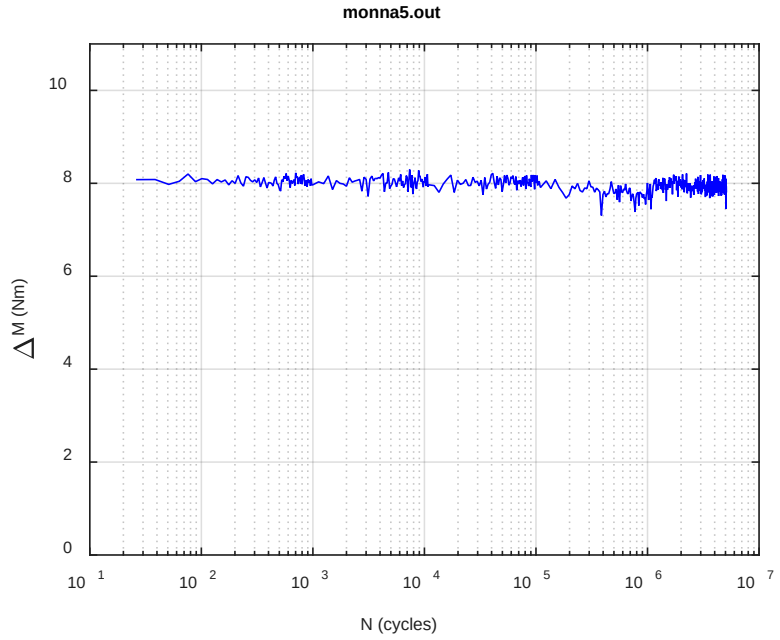
monna5.out
10
8
6
4
2
0
Δ M (Nm)
10 1
10 2
10 3
10 4
10 5
10 6
10 7
N (cycles)

(b)

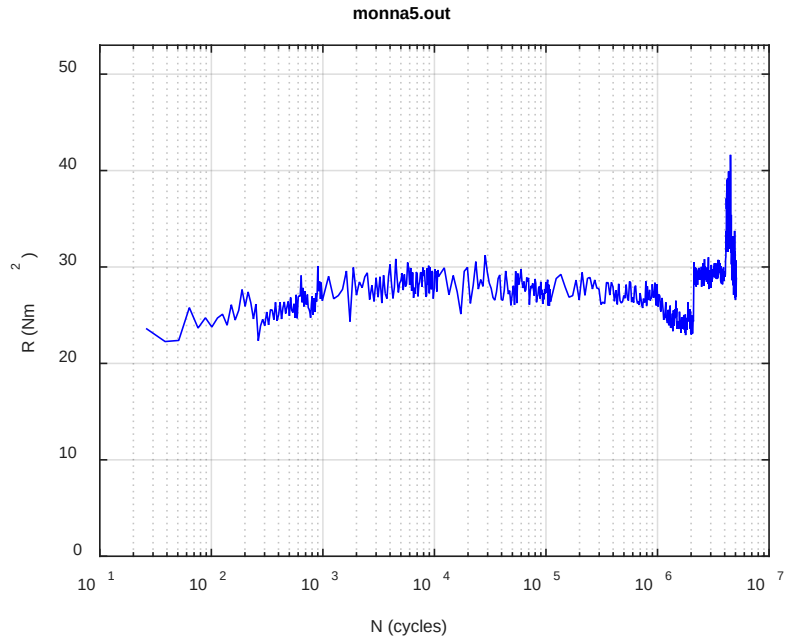

(c)

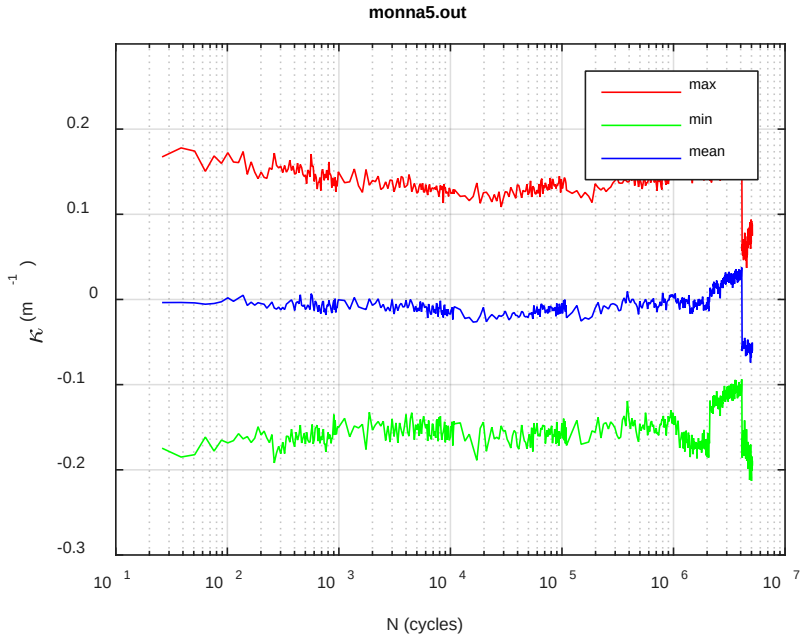

(d)

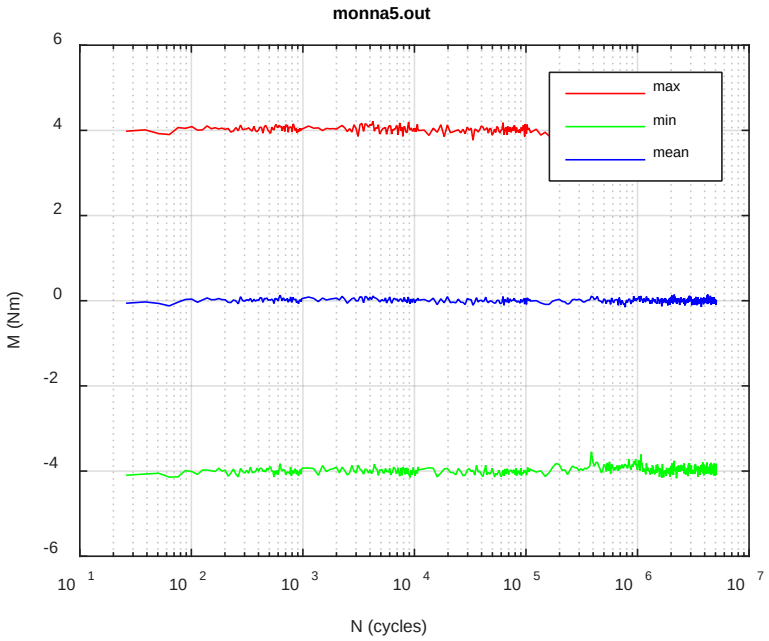

(e)

Fig. B.13. Monitoring-based responses: (a) curvature range, (b) moment range, (c) rigidity, (d) curvature peak/valley, (e) moment peak/valley, NA5, 5.08 Nm, Nf = 5.11E+06 cycles.

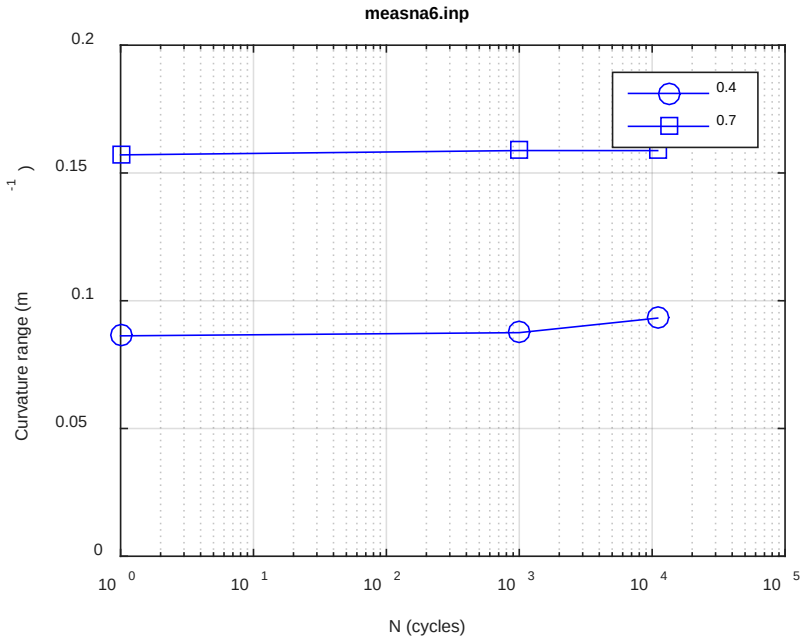
measna6.inp
0.2
0.15
0.1
0.05
0
Curvature range (m-1)
0.4
0.7
10 0
10 1
10 2
10 3
10 4
10 5
N (cycles)

(a)

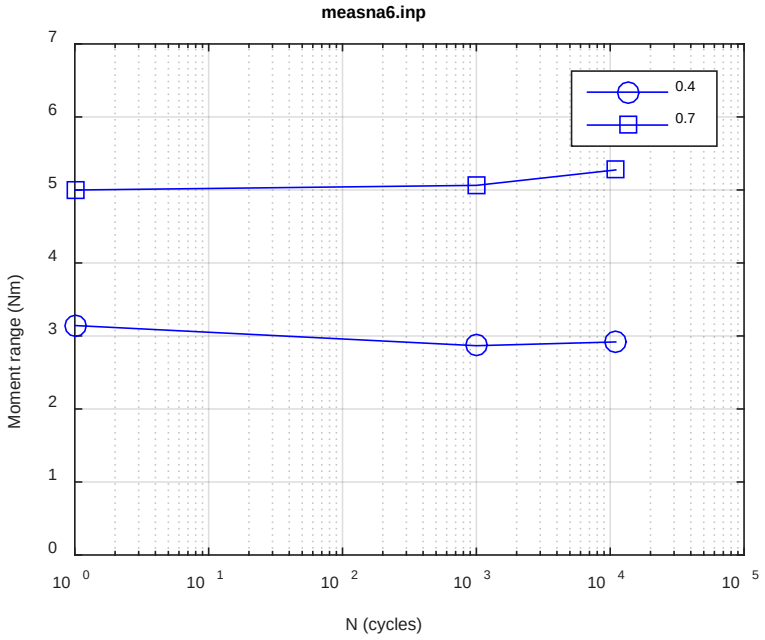
measna6.inp
7
6
5
4
3
2
1
0
Moment range (Nm)
0.4
0.7
10 0
10 1
10 2
10 3
10 4
10 5
N (cycles)

(b)

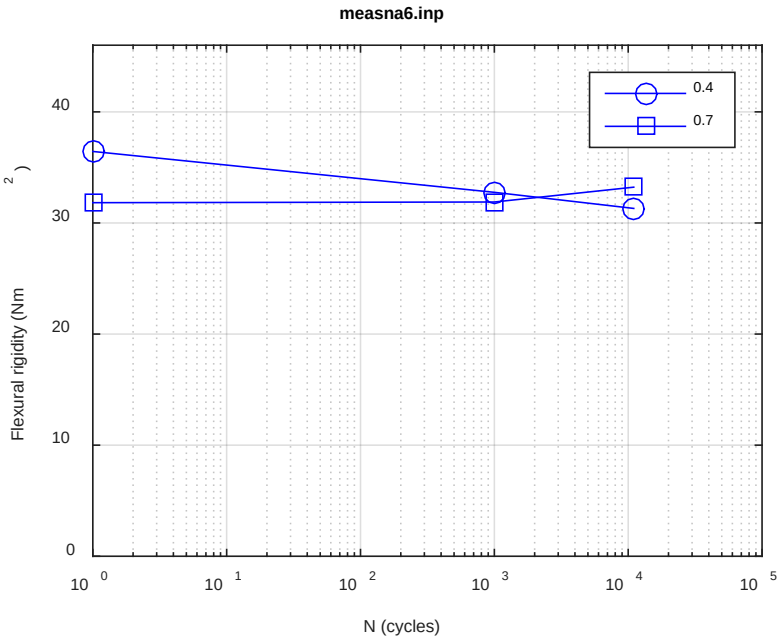
measna6.inp
0.4
0.7
Flexural rigidity (Nm 2)
N (cycles)

(c)

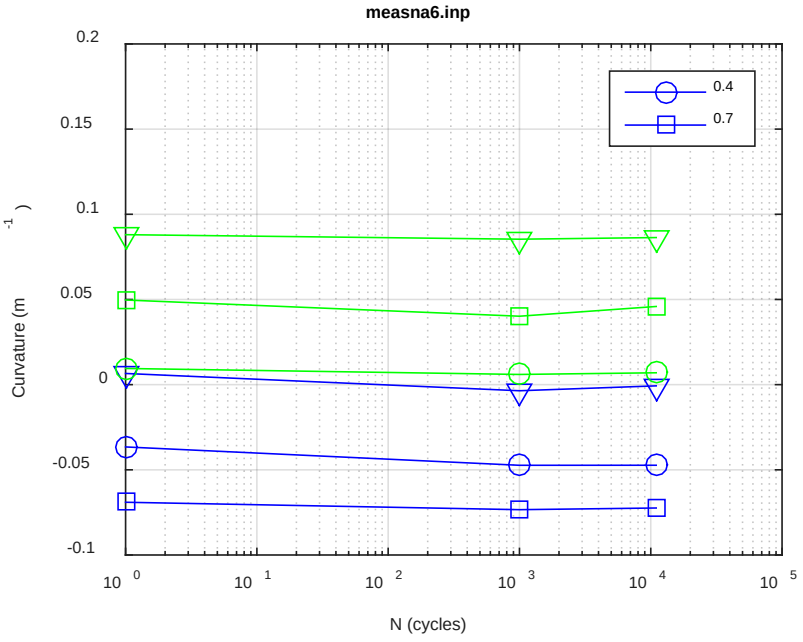
measna6.inp
0.4
0.7
Curvature (m -1)
N (cycles)

(d)

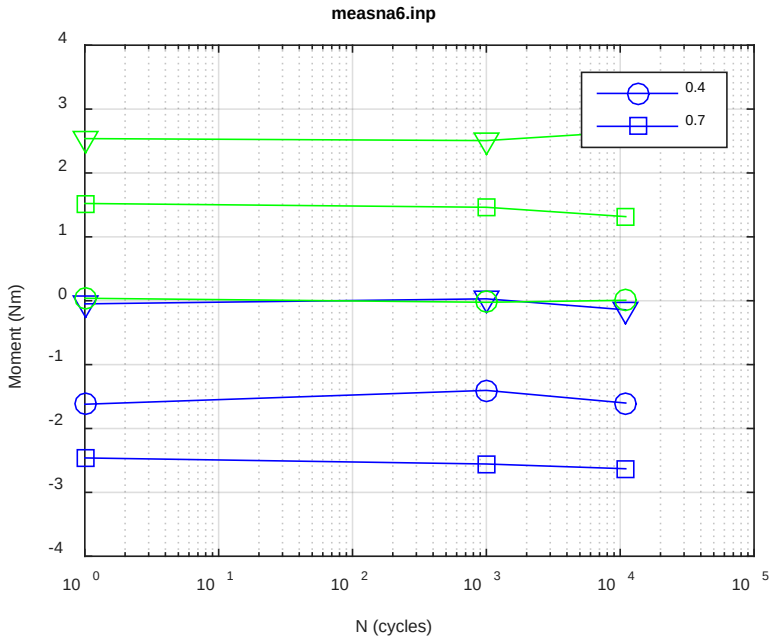

(e)

Fig. B.14. Measurement-based responses: (a) curvature range, (b) moment range, (c) rigidity, (d) curvature peak/valley, (e) moment peak/valley, NA6, 5.08 Nm.

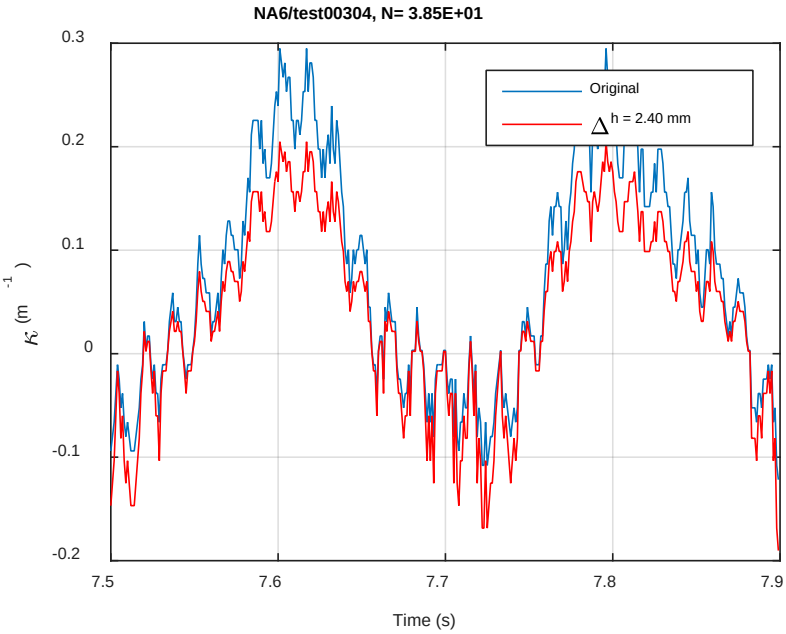
NA6/test00304, N= 3.85E+01
Original
Δh = 2.40 mm
κ (m-1)
Time (s)

(a)

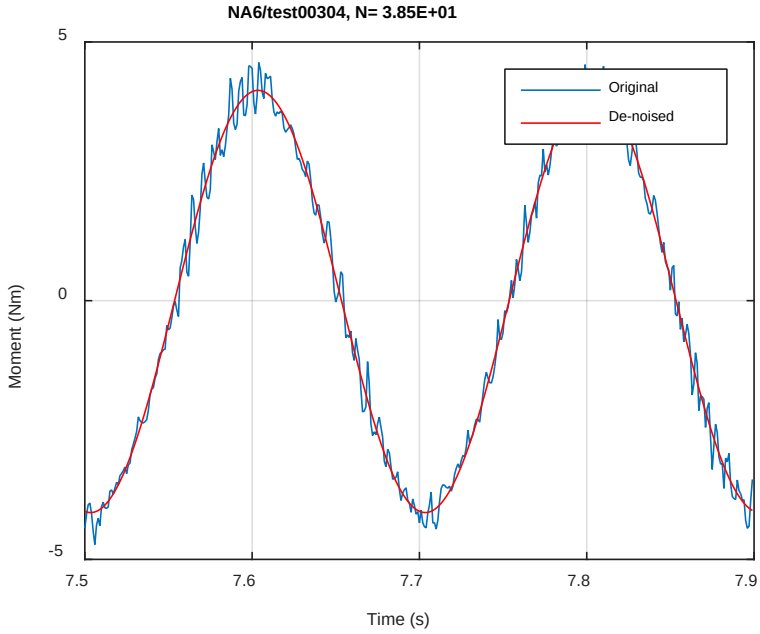
NA6/test00304, N= 3.85E+01
Original
De-noised
Moment (Nm)
Time (s)

(b)

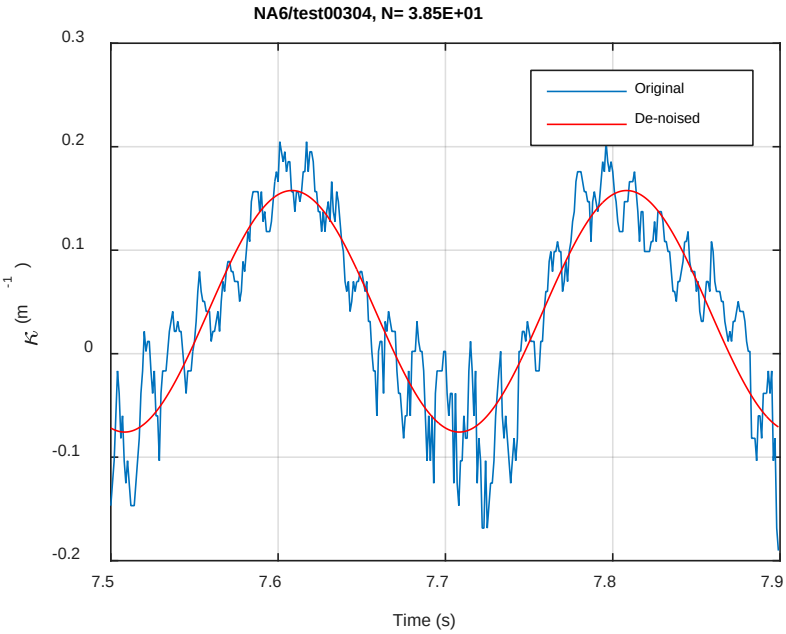

(c)

Fig. B.15. Monitoring-based responses: (a) curvature, (b) moment, (c) curvature, NA6, 5.08 Nm, Ns = 3.85E+01 cycles.

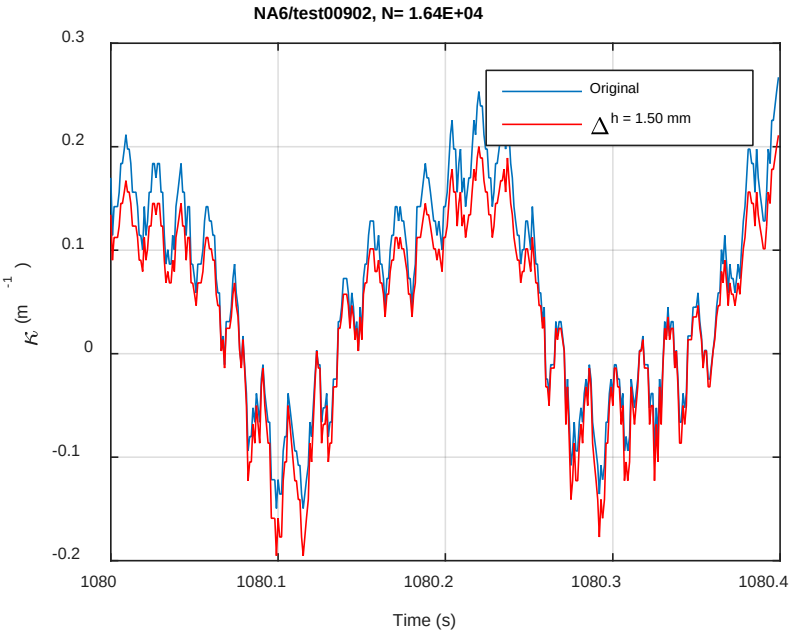
NA6/test00902, N= 1.64E+04
Original
Δh = 1.50 mm
κ (m-1)
Time (s)
0.3
0.2
0.1
0
-0.1
-0.2
1080
1080.1
1080.2
1080.3
1080.4

(a)

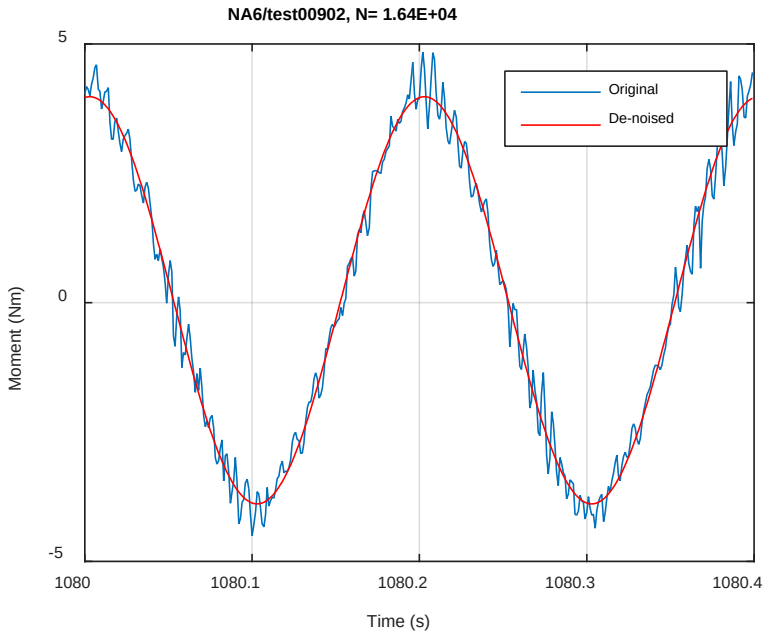
NA6/test00902, N= 1.64E+04
Original
De-noised
Moment (Nm)
Time (s)
5
0
-5
1080
1080.1
1080.2
1080.3
1080.4

(b)

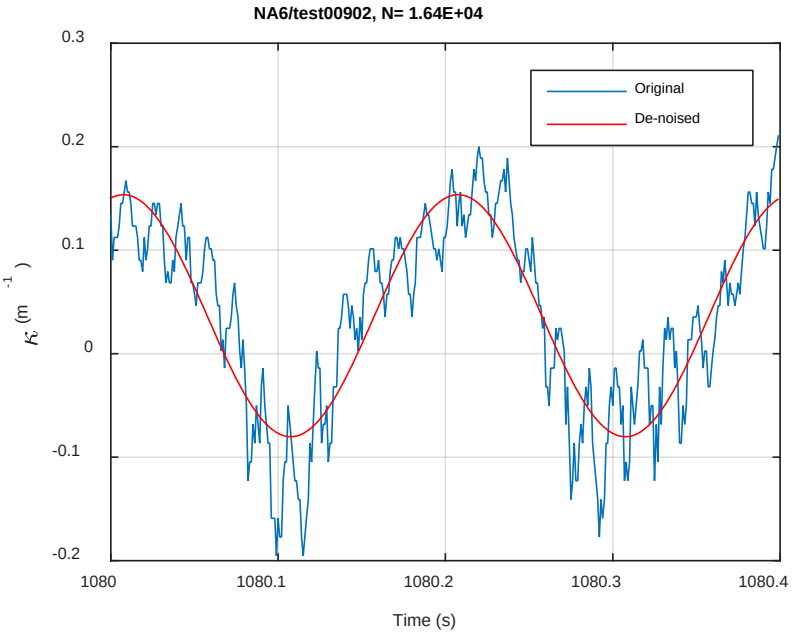

(c)

Fig. B.16. Monitoring-based responses: (a) curvature, (b) moment, (c) curvature, NA6, 5.08 Nm, Ns = 1.64E+04 cycles.

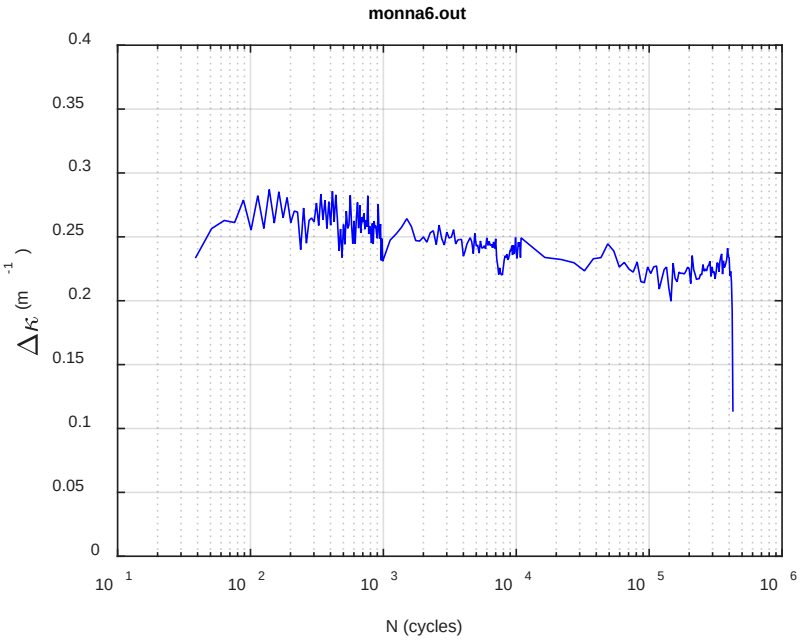
monna6.out
0.4
0.35
0.3
0.25
0.2
0.15
0.1
0.05
0
Δκ (m -1)
10 1
10 2
10 3
10 4
10 5
10 6
N (cycles)

(a)

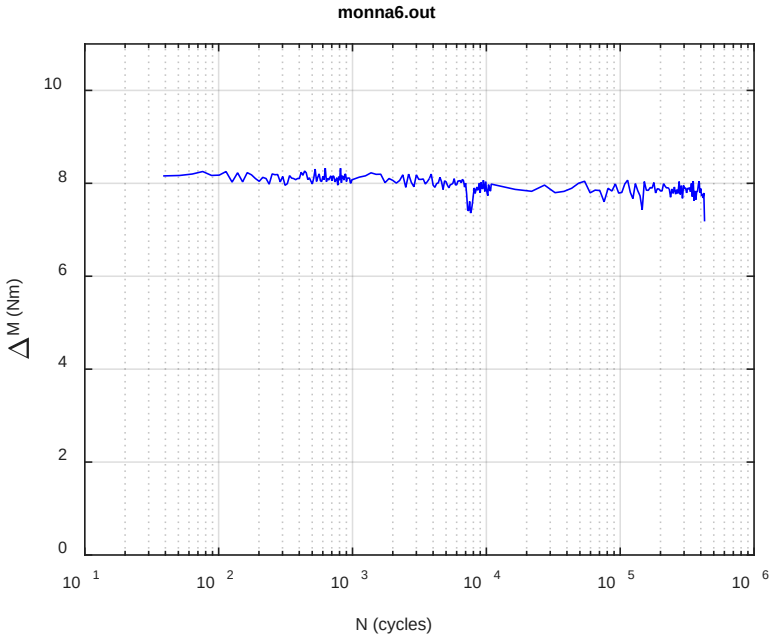
monna6.out
10
8
6
4
2
0
Δ M (Nm)
10 1
10 2
10 3
10 4
10 5
10 6
N (cycles)

(b)

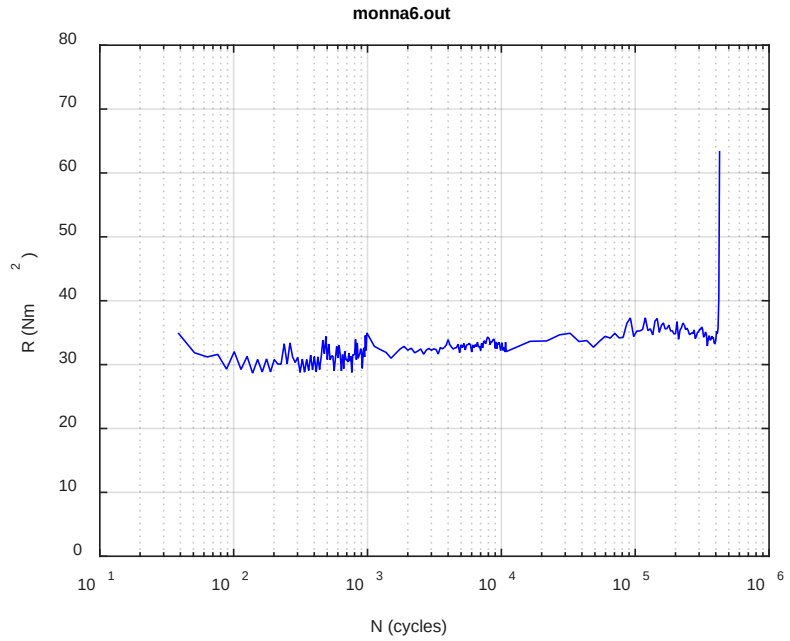

(c)

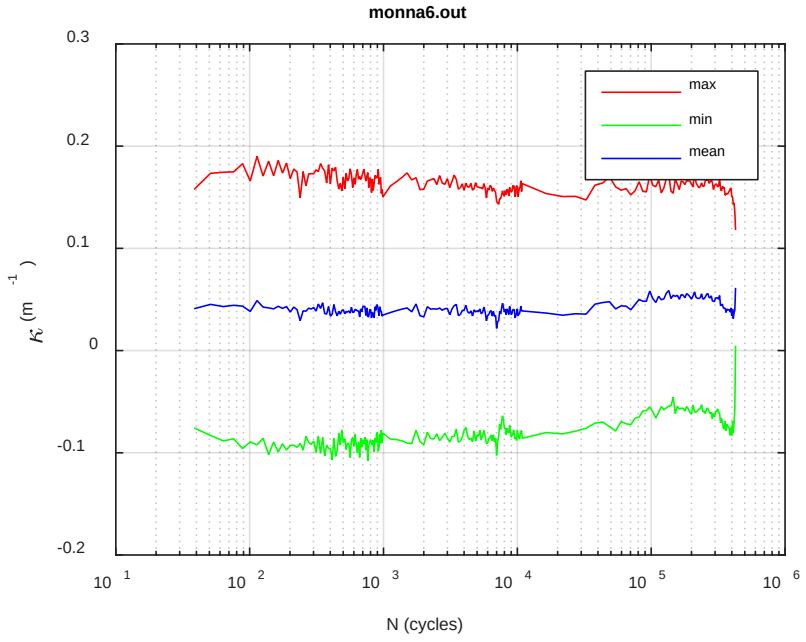

(d)

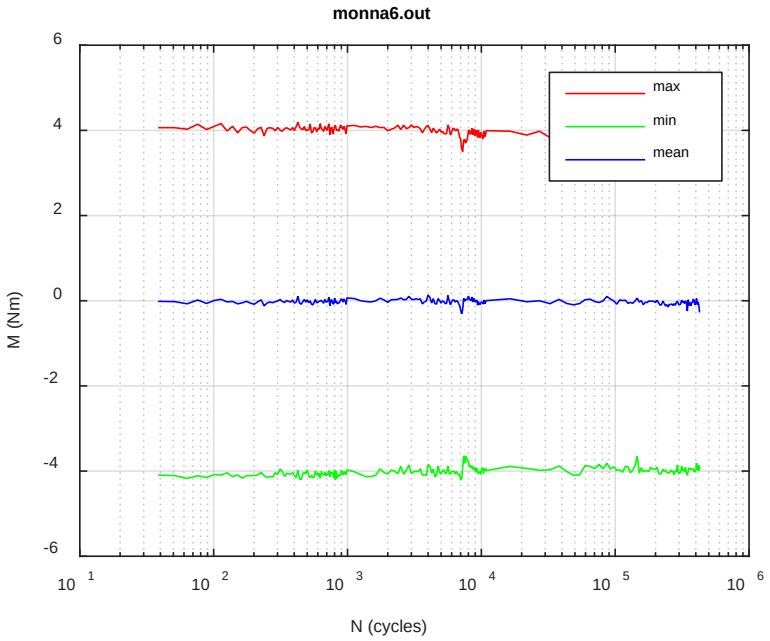

(e)

Fig. B.17. Monitoring-based responses: (a) curvature range, (b) moment range, (c) rigidity, (d) curvature peak/valley, (e) moment peak/valley, NA6, 5.08 Nm, Nf = 4.27E+05 cycles.

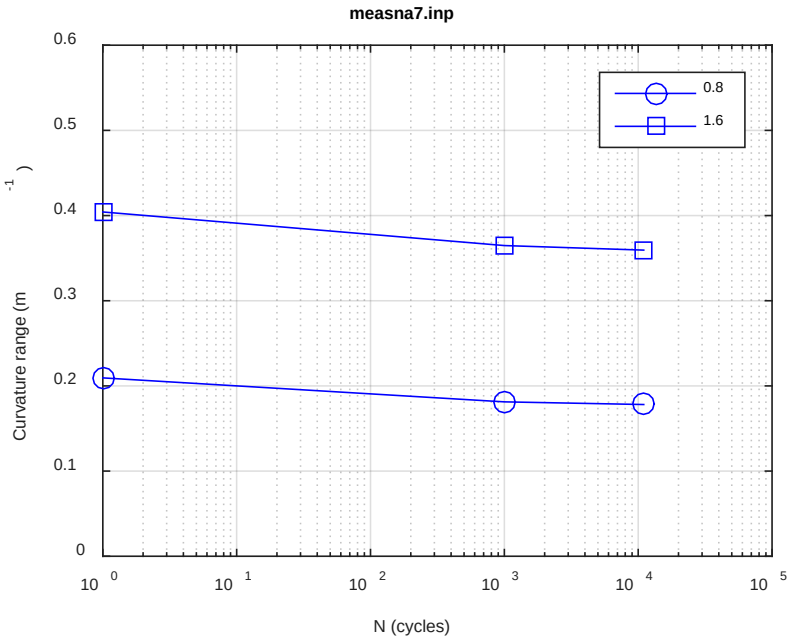
measna7.inp
0.8
1.6
Curvature range (m -1)
N (cycles)
0
0.1
0.2
0.3
0.4
0.5
0.6
10 0
10 1
10 2
10 3
10 4
10 5

(a)

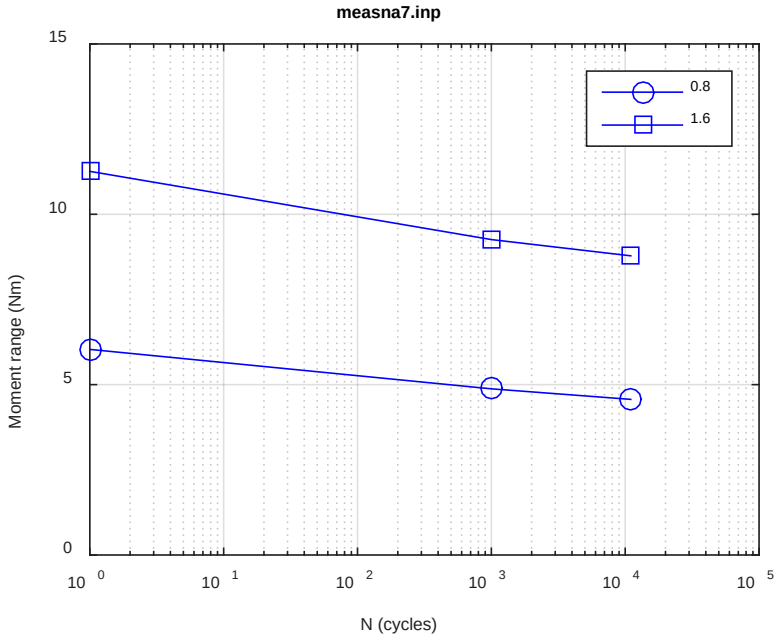
measna7.inp
0.8
1.6
Moment range (Nm)
N (cycles)
0
5
10
15
10 0
10 1
10 2
10 3
10 4
10 5

(b)

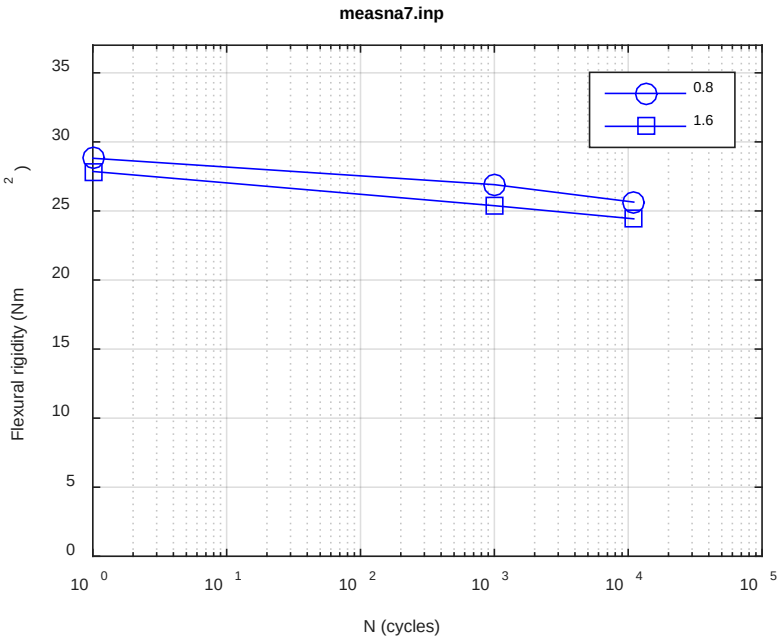
measna7.inp
0.8
1.6
Flexural rigidity (Nm 2)
N (cycles)

(c)

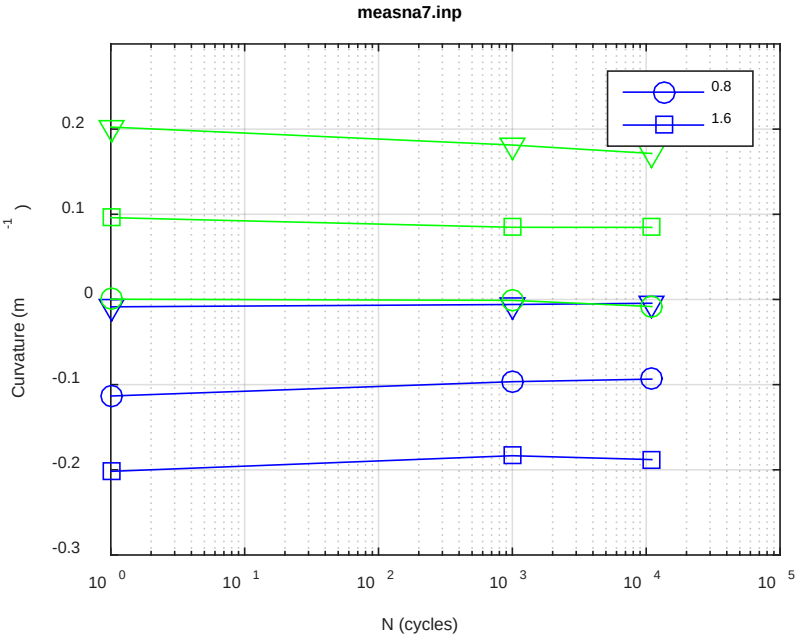
measna7.inp
0.8
1.6
Curvature (m -1)
N (cycles)

(d)

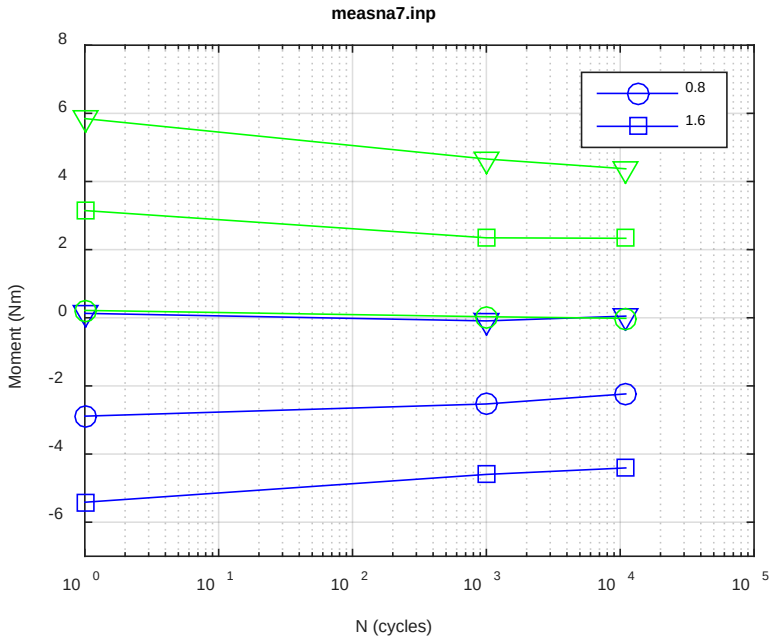

(e)

Fig. B.18. Measurement-based responses: (a) curvature range, (b) moment range, (c) rigidity, (d) curvature peak/valley, (e) moment peak/valley, NA7, 15.24 Nm.

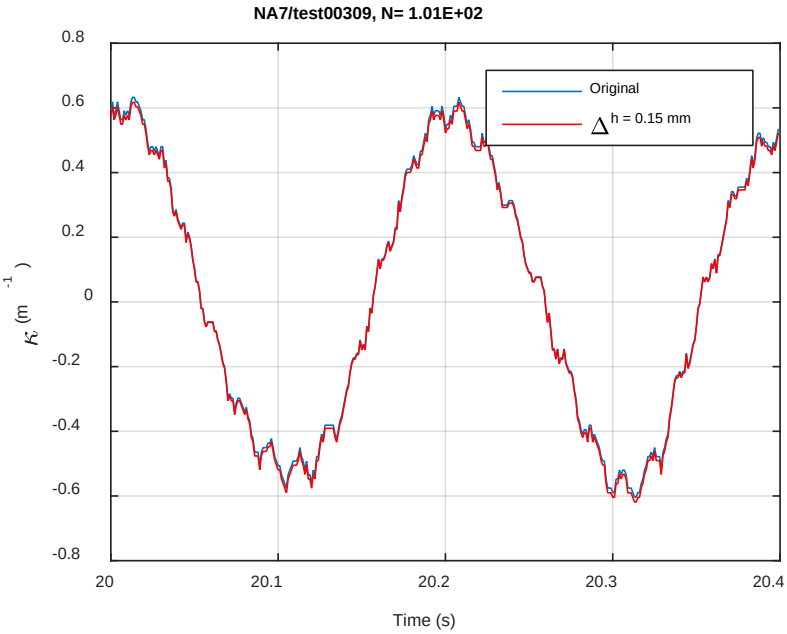
NA7/test00309, N= 1.01E+02
Original
Δh = 0.15 mm
κ (m-1)
Time (s)

(a)

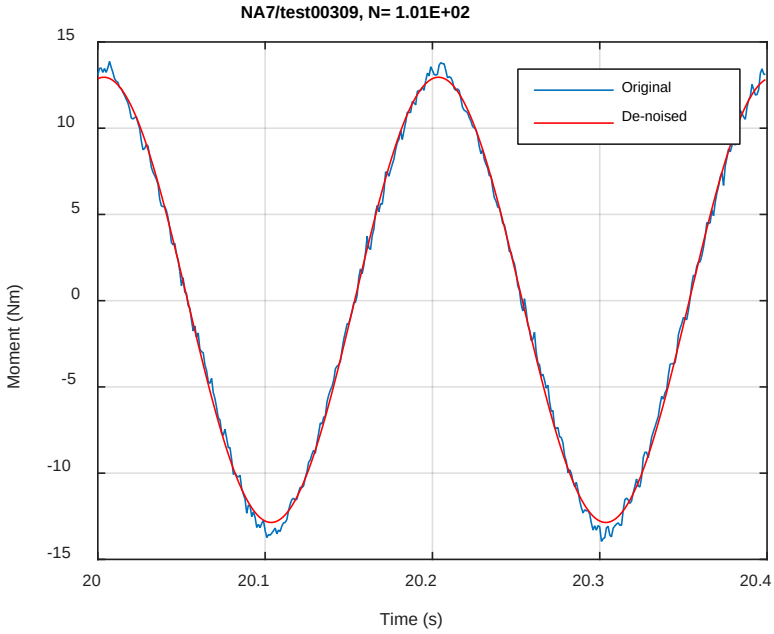
NA7/test00309, N= 1.01E+02
Original
De-noised
Moment (Nm)
Time (s)

(b)

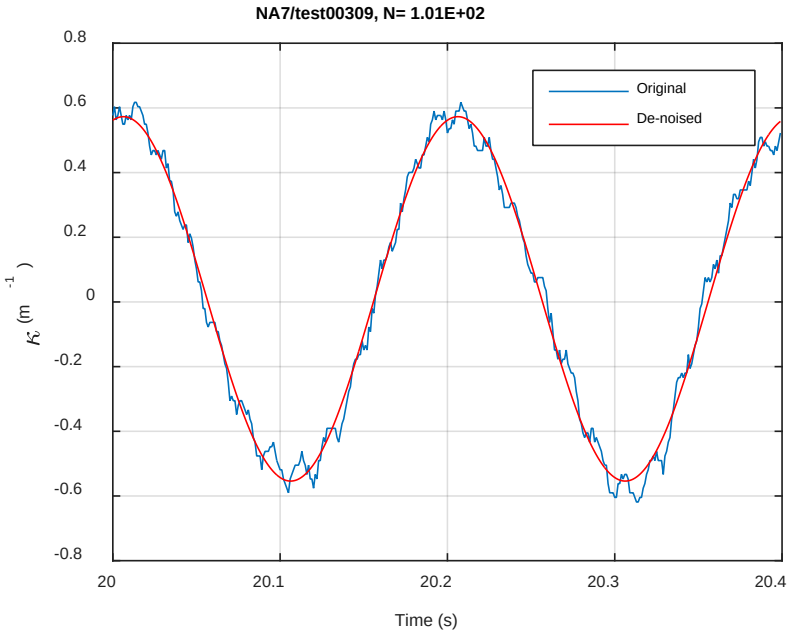

(c)

Fig. B.19. Monitoring-based responses: (a) curvature, (b) moment, (c) curvature, NA7, 15.24 Nm, Ns = 1.01E+02 cycles.

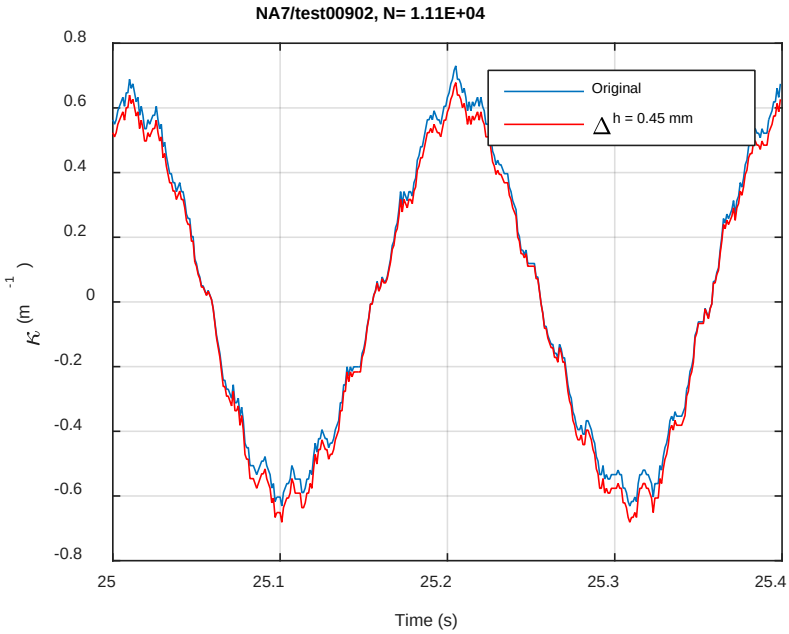
NA7/test00902, N= 1.11E+04
Original
Δh = 0.45 mm
κ (m-1)
Time (s)

(a)

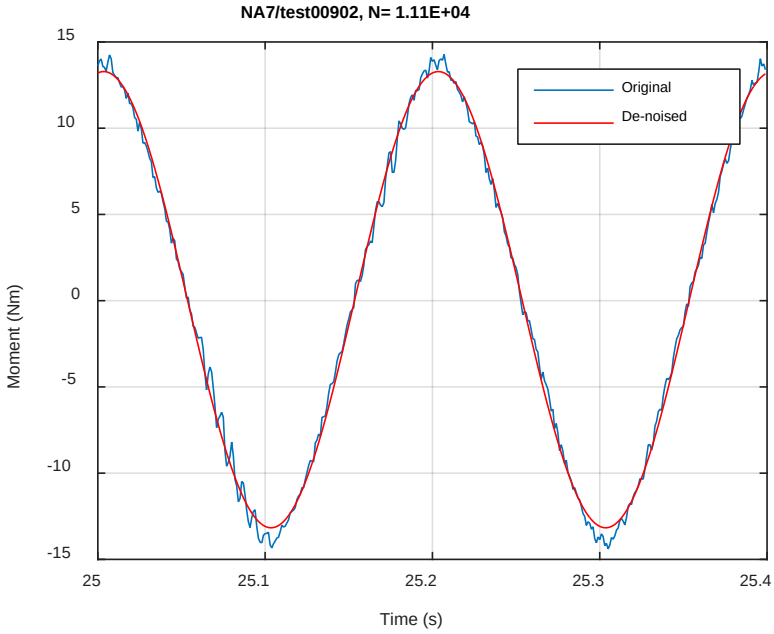
NA7/test00902, N= 1.11E+04
Original
De-noised
Moment (Nm)
Time (s)

(b)

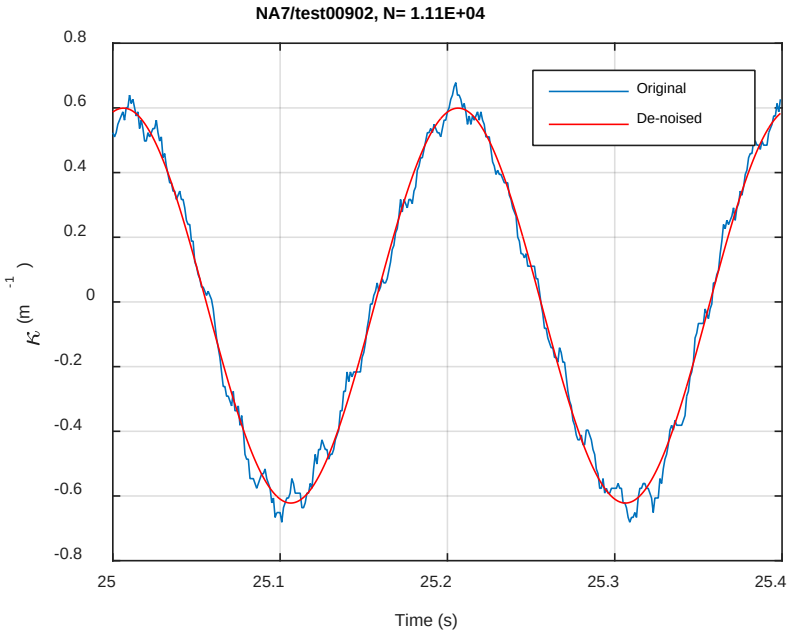

(c)

Fig. B.20. Monitoring-based responses: (a) curvature, (b) moment, (c) curvature, NA7, 15.24 Nm, Ns = 1.11E+04 cycles.

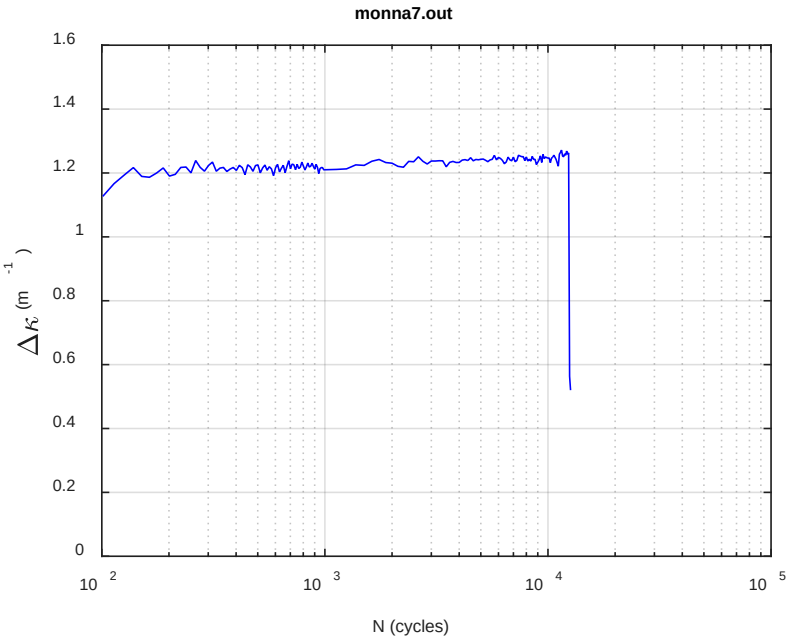
monna7.out
1.6
1.4
1.2
1
0.8
0.6
0.4
0.2
0
Δκ (m -1)
10 2
10 3
10 4
10 5
N (cycles)

(a)

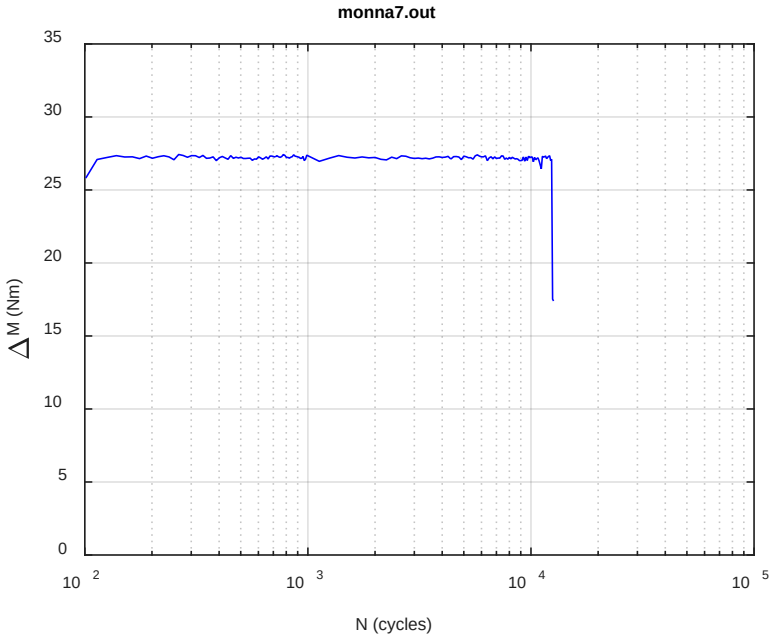
monna7.out
35
30
25
20
15
10
5
0
Δ M (Nm)
10 2
10 3
10 4
10 5
N (cycles)

(b)

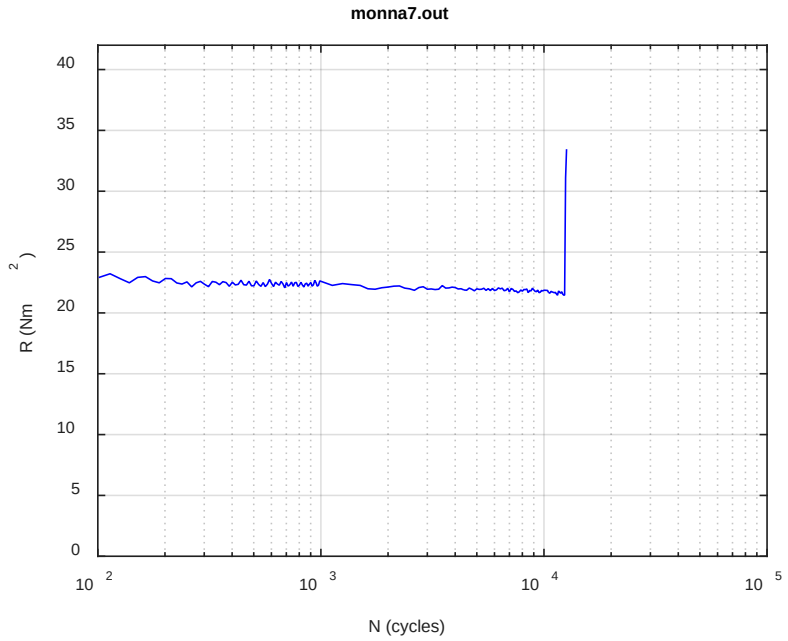

(c)

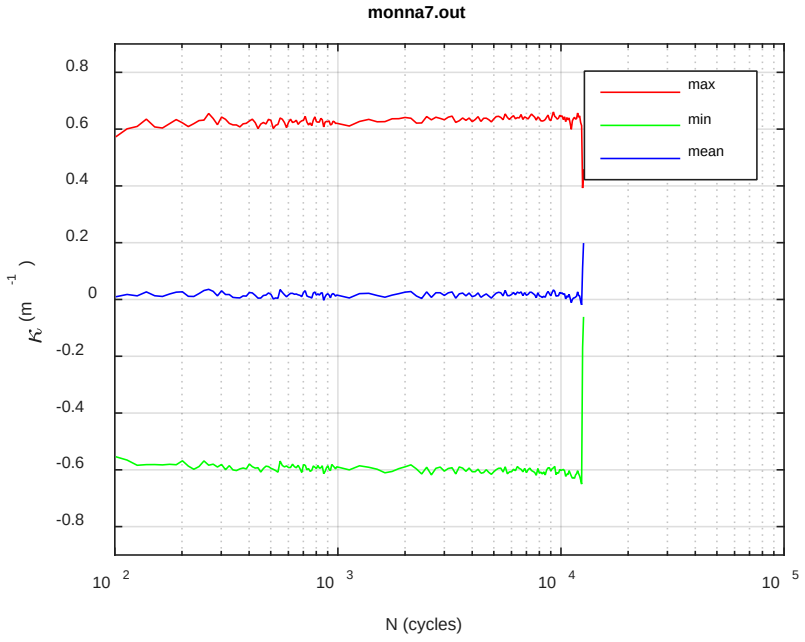

(d)

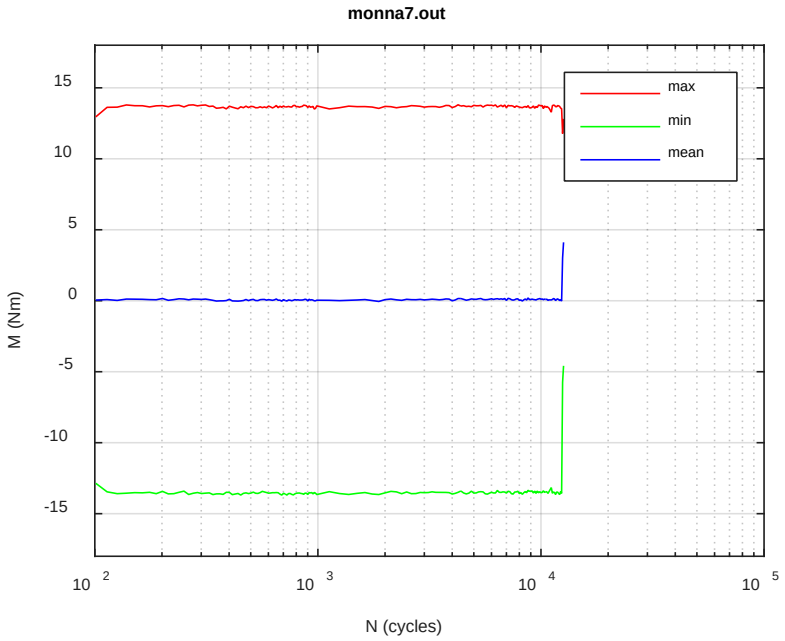

(e)

Fig. B.21. Monitoring-based responses: (a) curvature range, (b) moment range, (c) rigidity, (d) curvature peak/valley, (e) moment peak/valley, NA7, 15.24 Nm, Nf = 1.26E+04 cycles.

APPENDIX C CIRFT TESTING RESULTS OF MOX

TABLE OF CONTENTS

Measurement and monitoring rigidity curves of CATAWBA MOX Spent Nuclear Fuel

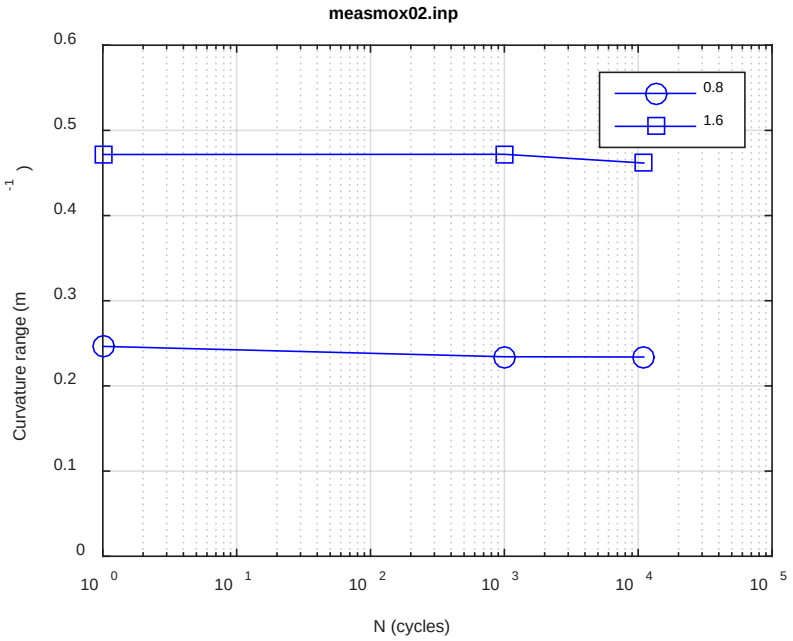
measmox02.inp
0.8
1.6
Curvature range (m -1)
N (cycles)

(a)

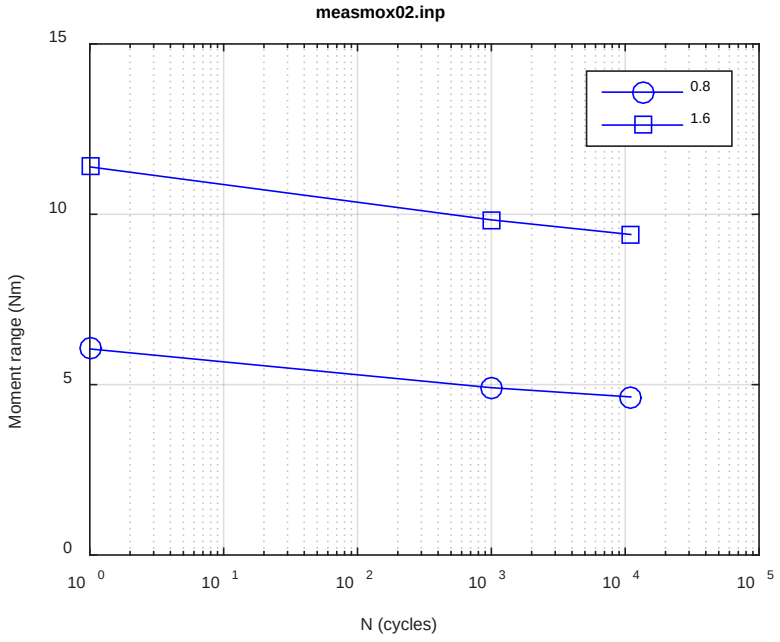
measmox02.inp
0.8
1.6
Moment range (Nm)
N (cycles)

(b)

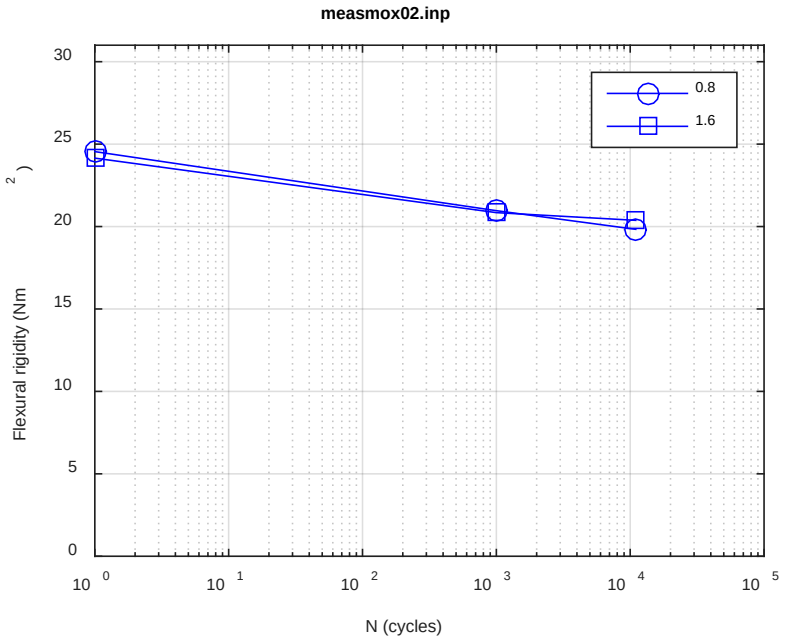
measmox02.inp
Flexural rigidity (Nm^2)
N (cycles)
0.8
1.6
30
25
20
15
10
5
0
10^0
10^1
10^2
10^3
10^4
10^5

(c)

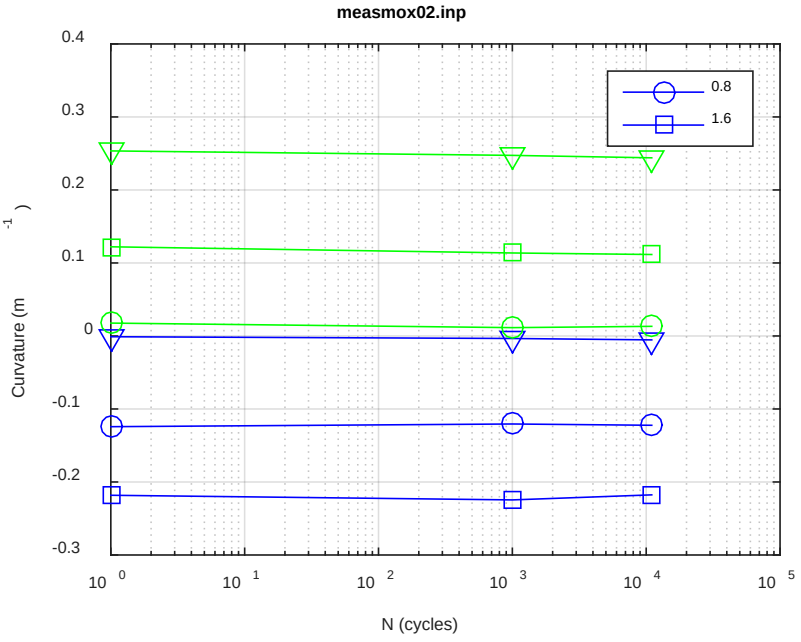
measmox02.inp
Curvature (m^-1)
N (cycles)
0.8
1.6
0.4
0.3
0.2
0.1
0
-0.1
-0.2
-0.3
10^0
10^1
10^2
10^3
10^4
10^5

(d)

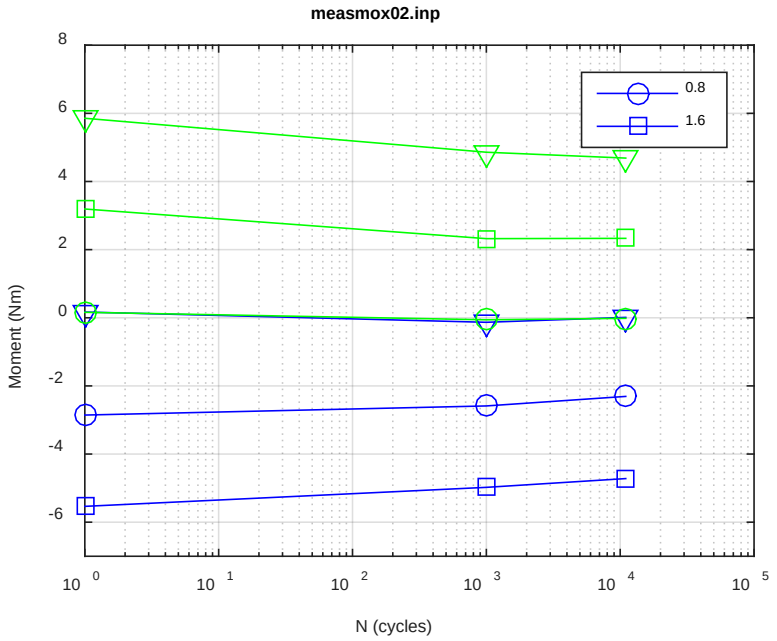

(e)

Fig. C.1. Measurement-based responses: (a) curvature range, (b) moment range, (c) rigidity, (d) curvature peak/valley, (e) moment peak/valley, MOX02, 10.16 Nm.

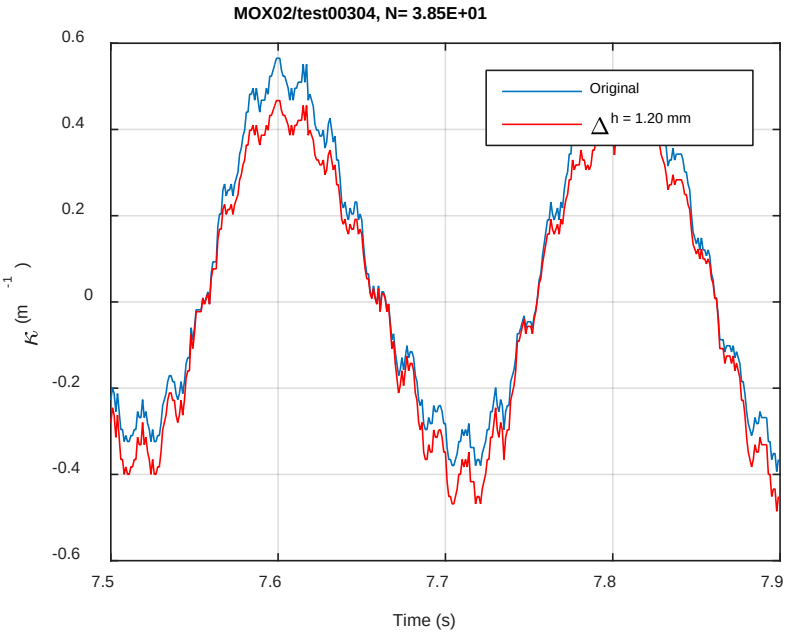
MOX02/test00304, N= 3.85E+01
Original
Δh = 1.20 mm
κ (m-1)
Time (s)
0.6
0.4
0.2
0
-0.2
-0.4
-0.6
7.5
7.6
7.7
7.8
7.9

(a)

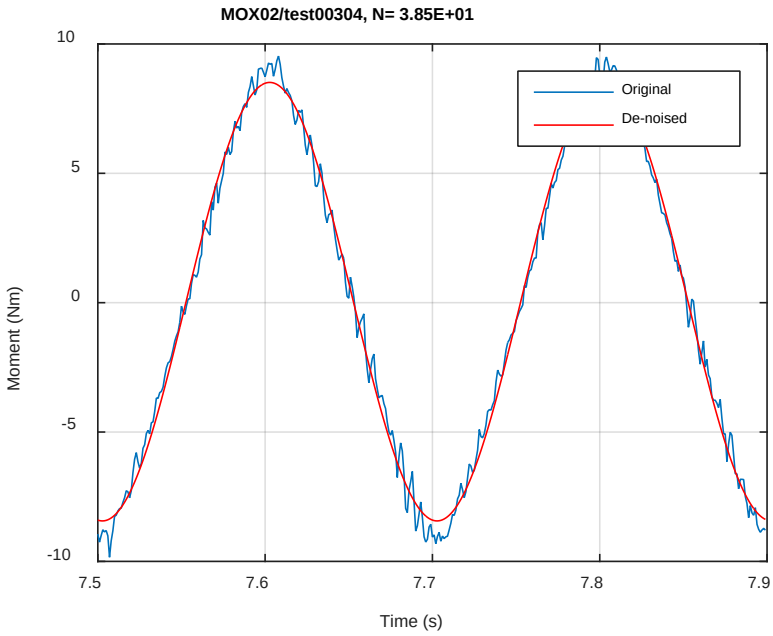
MOX02/test00304, N= 3.85E+01
Original
De-noised
Moment (Nm)
Time (s)
10
5
0
-5
-10
7.5
7.6
7.7
7.8
7.9

(b)

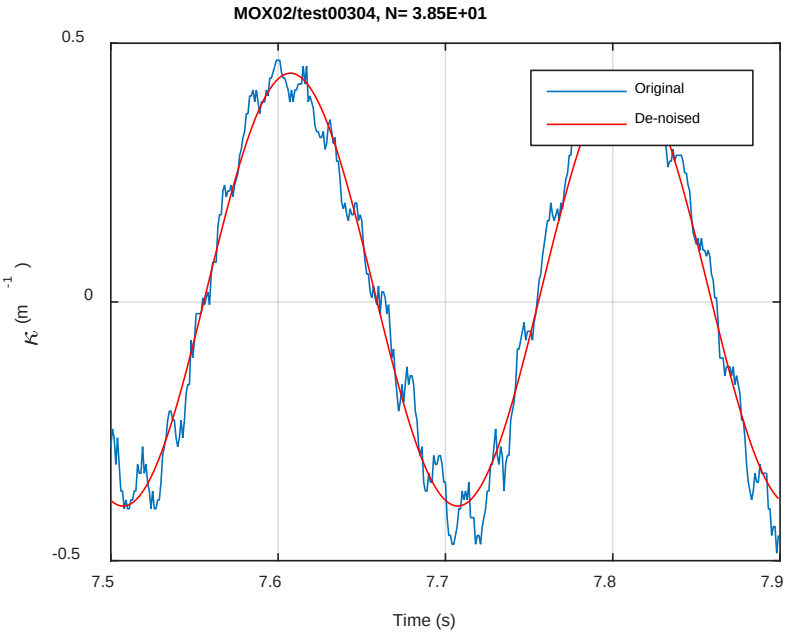

(c)

Fig. C.2. Monitoring-based responses: (a) curvature, (b) moment, (c) curvature, MOX02, 10.16 Nm, Ns = 3.85E+01 cycles.

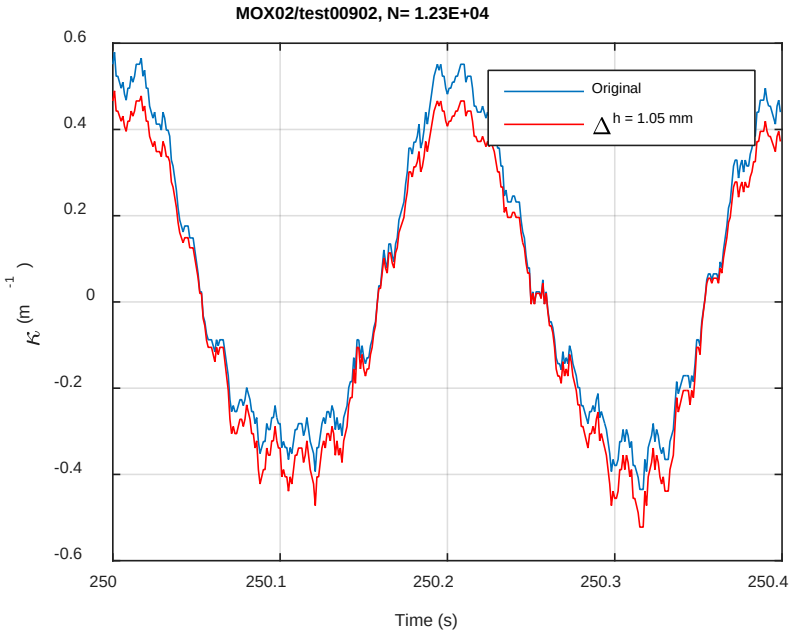
MOX02/test00902, N= 1.23E+04
Original
Δh = 1.05 mm
κ (m-1)
Time (s)
0.6
0.4
0.2
0
-0.2
-0.4
-0.6
250
250.1
250.2
250.3
250.4

(a)

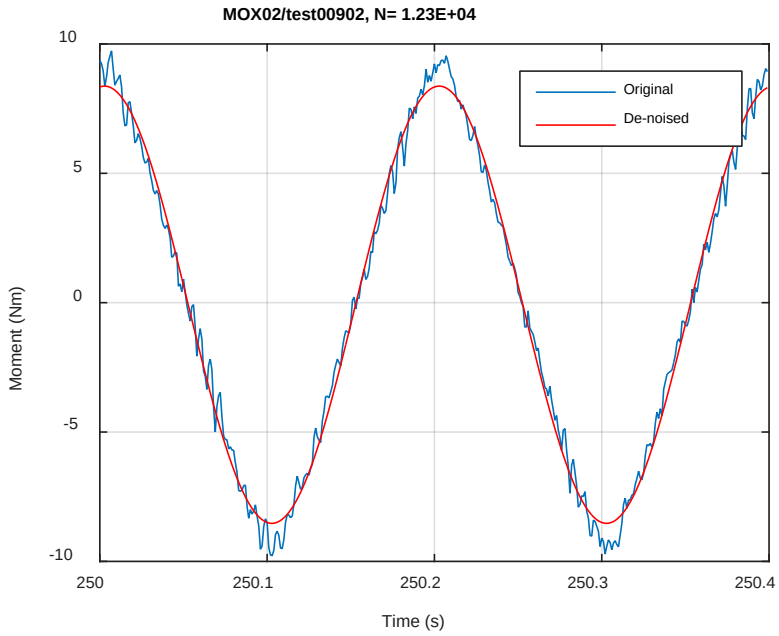
MOX02/test00902, N= 1.23E+04
Original
De-noised
Moment (Nm)
Time (s)
10
5
0
-5
-10
250
250.1
250.2
250.3
250.4

(b)

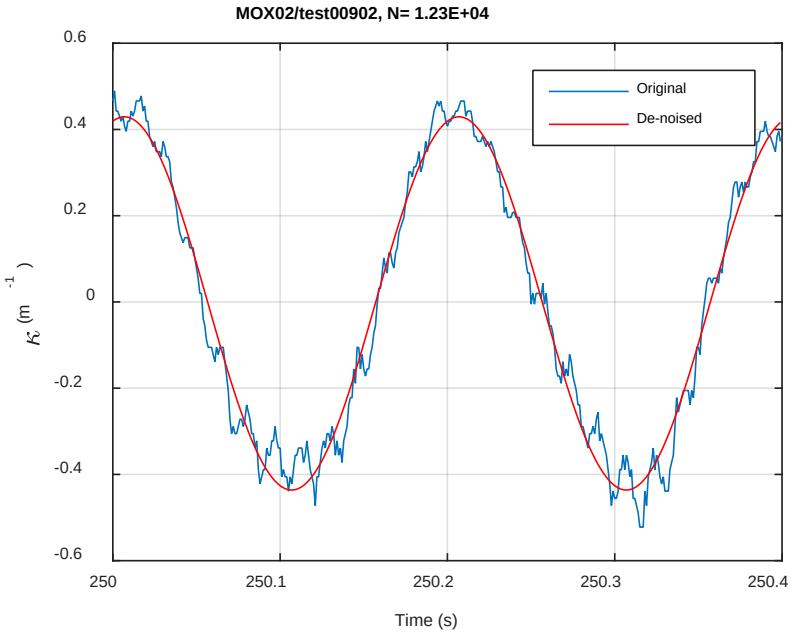

(c)

Fig. C.3. Monitoring-based responses: (a) curvature, (b) moment, (c) curvature, MOX02, 10.16 Nm, Ns = 1.23E+04 cycles.

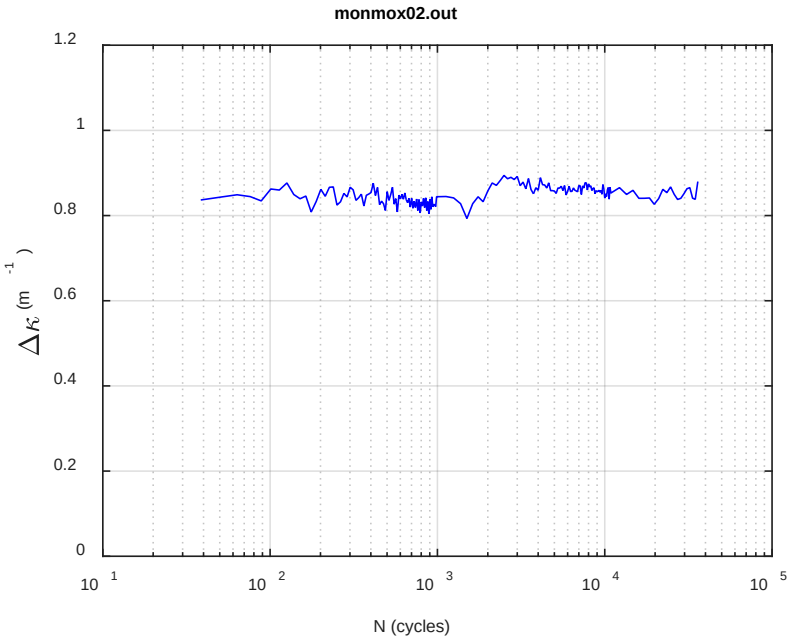
monmox02.out
1.2
1
0.8
0.6
0.4
0.2
0
Δκ (m-1)
10 1
10 2
10 3
10 4
10 5
N (cycles)

(a)

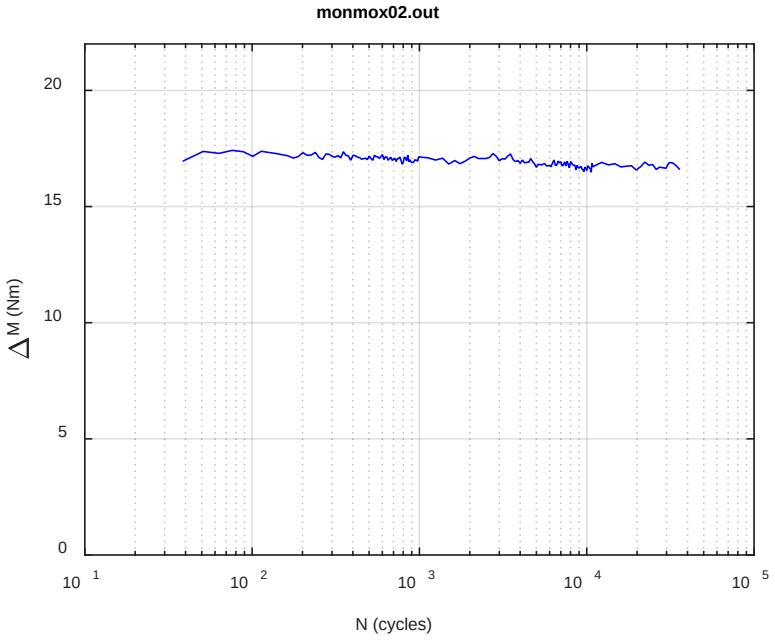
monmox02.out
20
15
10
5
0
Δ M (Nm)
10 1
10 2
10 3
10 4
10 5
N (cycles)

(b)

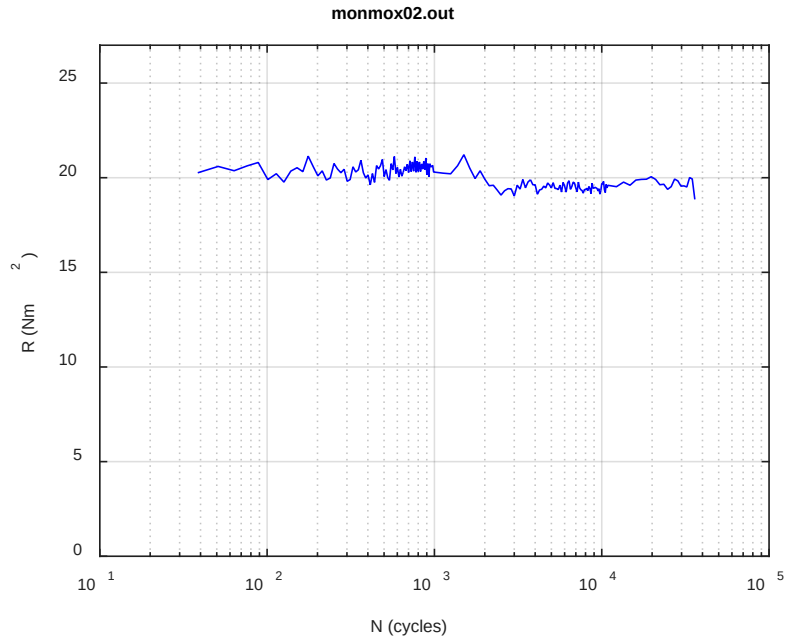
monmox02.out
R (Nm 2)
25
20
15
10
5
0
10 1
10 2
10 3
10 4
10 5
N (cycles)

(c)

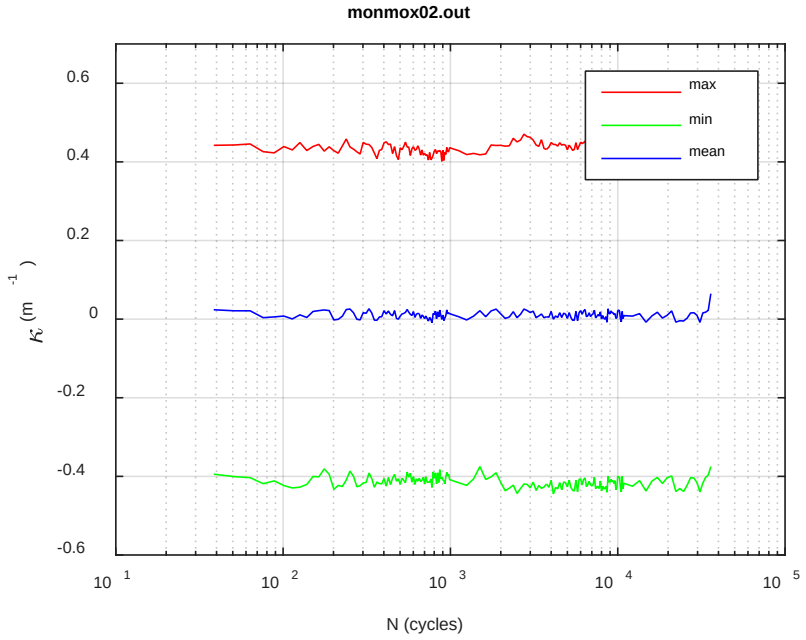
monmox02.out
max
min
mean
κ (m -1)
0.6
0.4
0.2
0
-0.2
-0.4
-0.6
10 1
10 2
10 3
10 4
10 5
N (cycles)

(d)

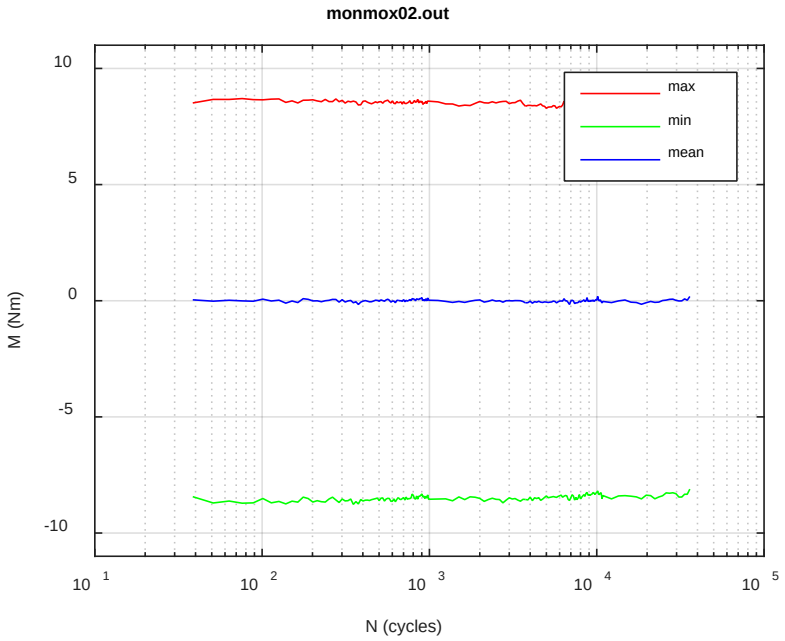

(e)

Fig. C.4. Monitoring-based responses: (a) curvature range, (b) moment range, (c) rigidity, (d) curvature peak/valley, (e) moment peak/valley, MOX02, 10.16 Nm, Nf = 3.70E+04 cycles.

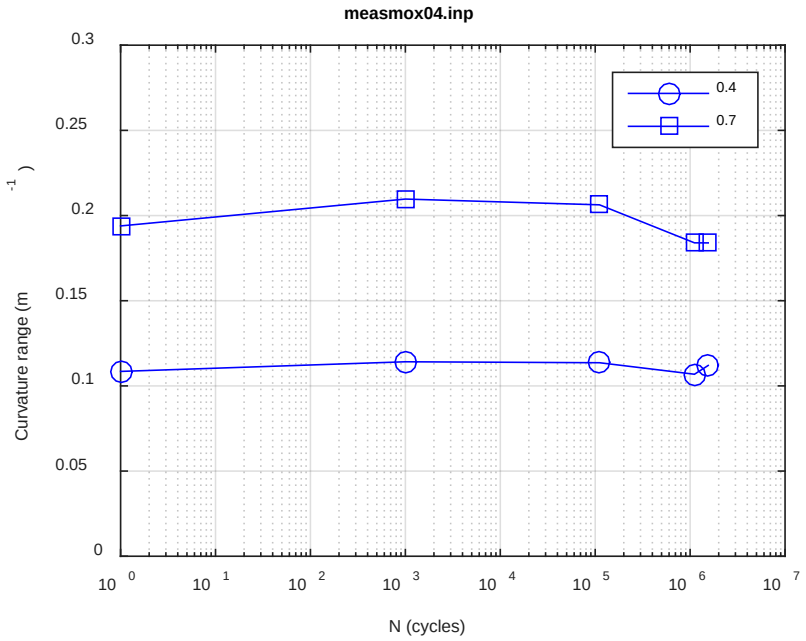
measmox04.inp
0.3
0.25
0.2
0.15
0.1
0.05
0
Curvature range (m -1)
0.4
0.7
10 0
10 1
10 2
10 3
10 4
10 5
10 6
10 7
N (cycles)

(a)

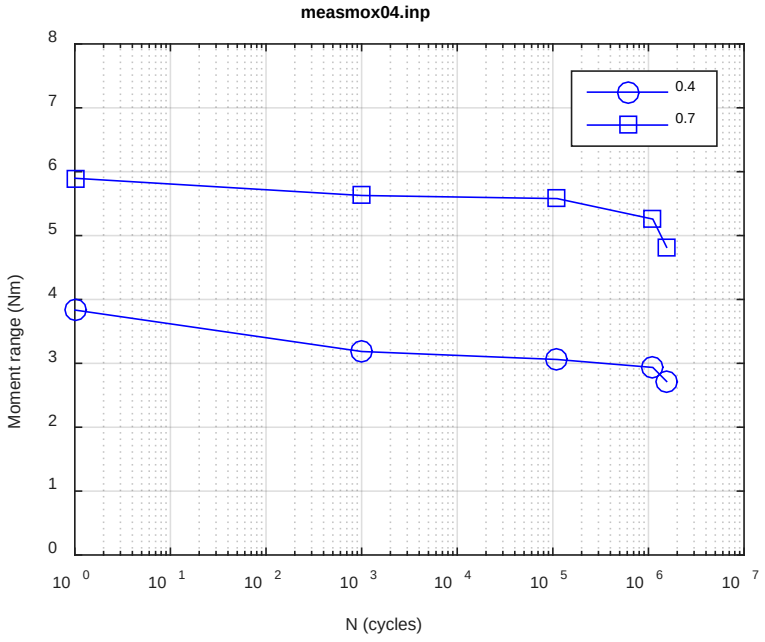
measmox04.inp
8
7
6
5
4
3
2
1
0
Moment range (Nm)
0.4
0.7
10 0
10 1
10 2
10 3
10 4
10 5
10 6
10 7
N (cycles)

(b)

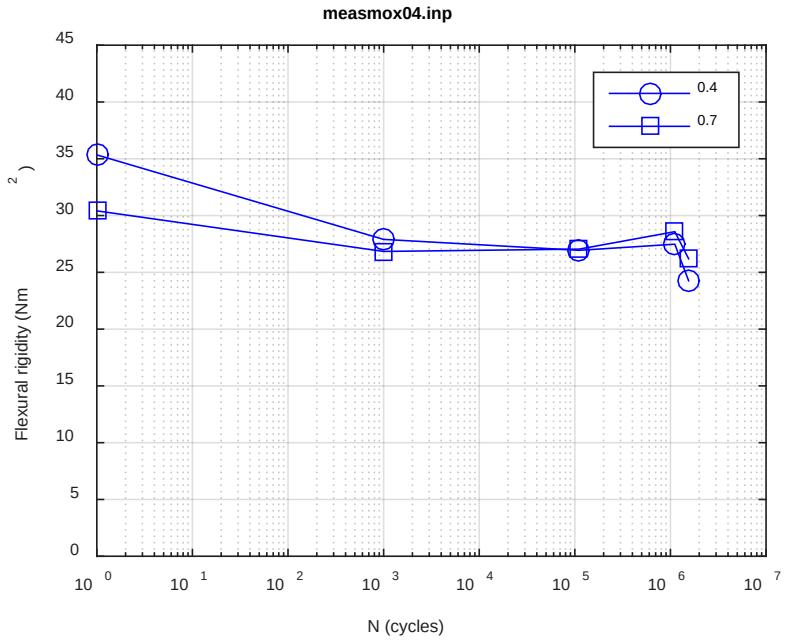
measmox04.inp
0.4
0.7
Flexural rigidity (Nm 2)
N (cycles)

(c)

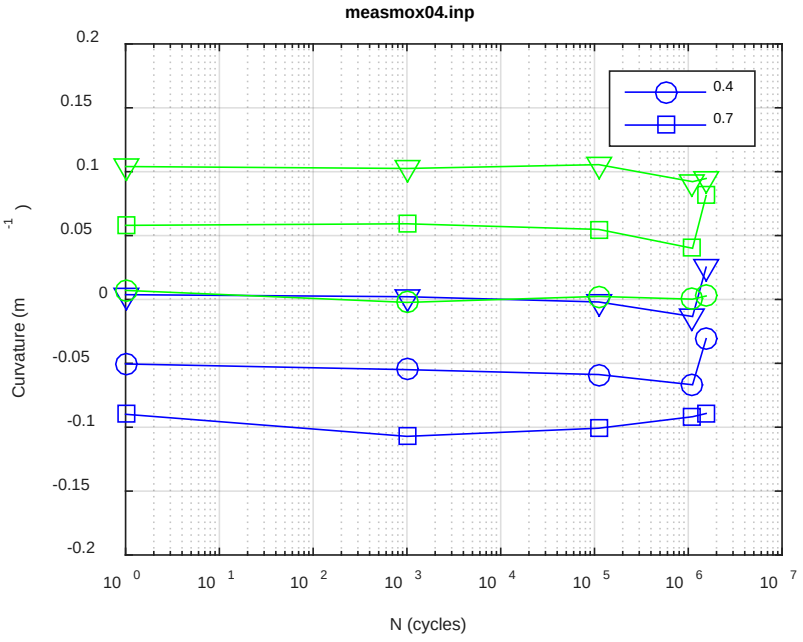
measmox04.inp
0.4
0.7
Curvature (m -1)
N (cycles)

(d)

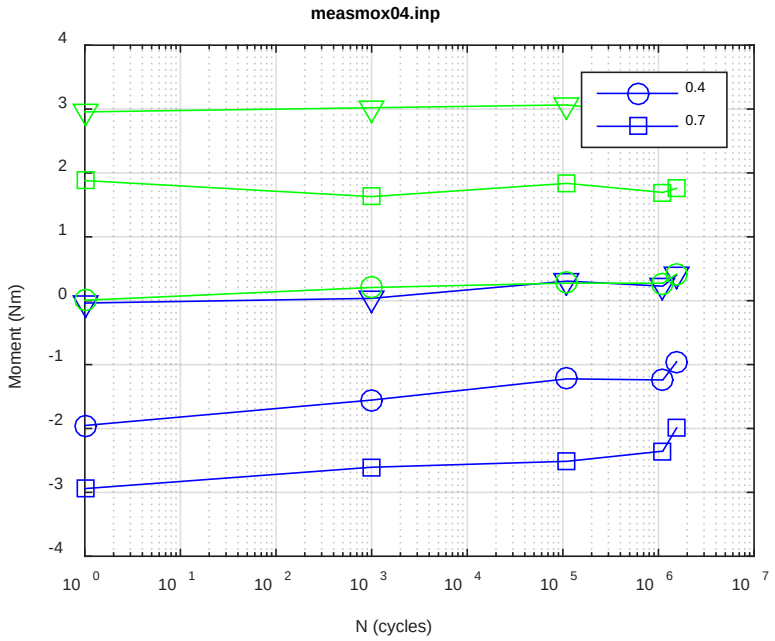

(e)

Fig. C.5. Measurement-based responses: (a) curvature range, (b) moment range, (c) rigidity, (d) curvature peak/valley, (e) moment peak/valley, MOX04, 5.08 Nm.

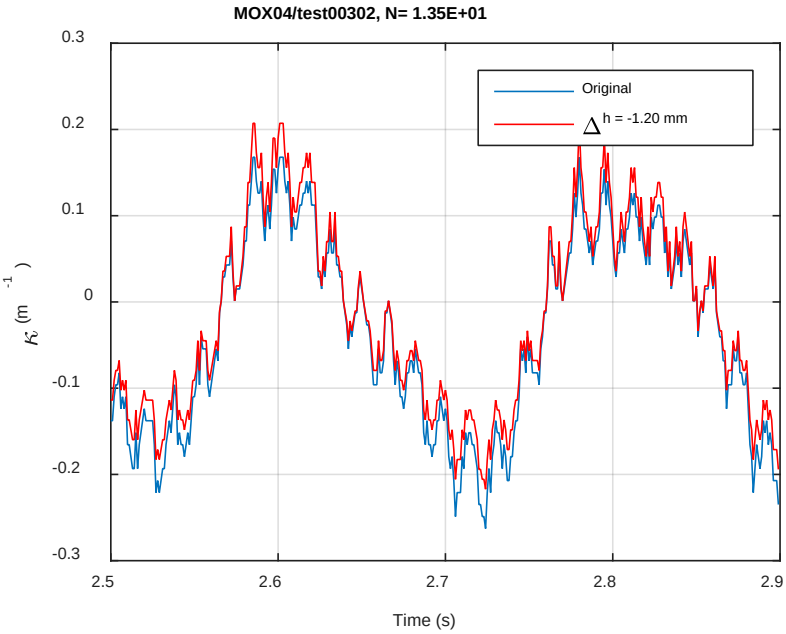
MOX04/test00302, N= 1.35E+01
Original
Δh = -1.20 mm
κ (m-1)
Time (s)

(a)

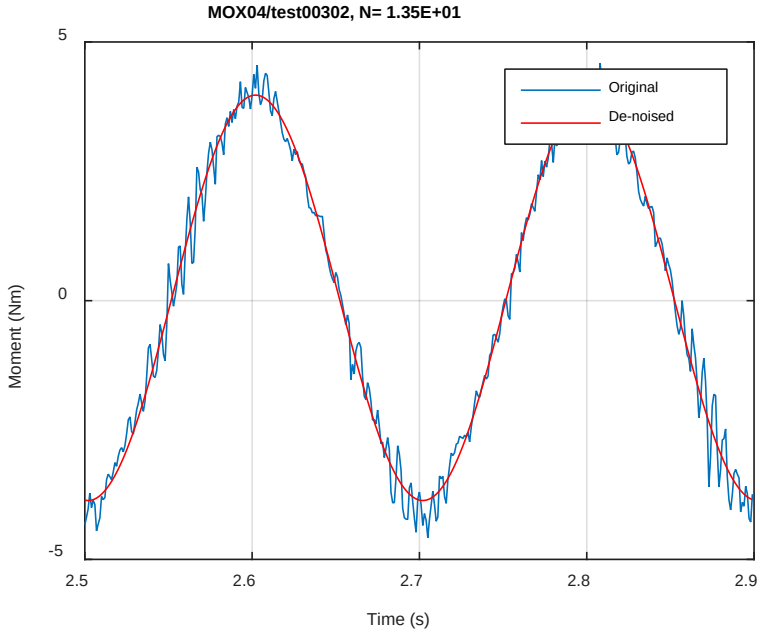
MOX04/test00302, N= 1.35E+01
Original
De-noised
Moment (Nm)
Time (s)

(b)

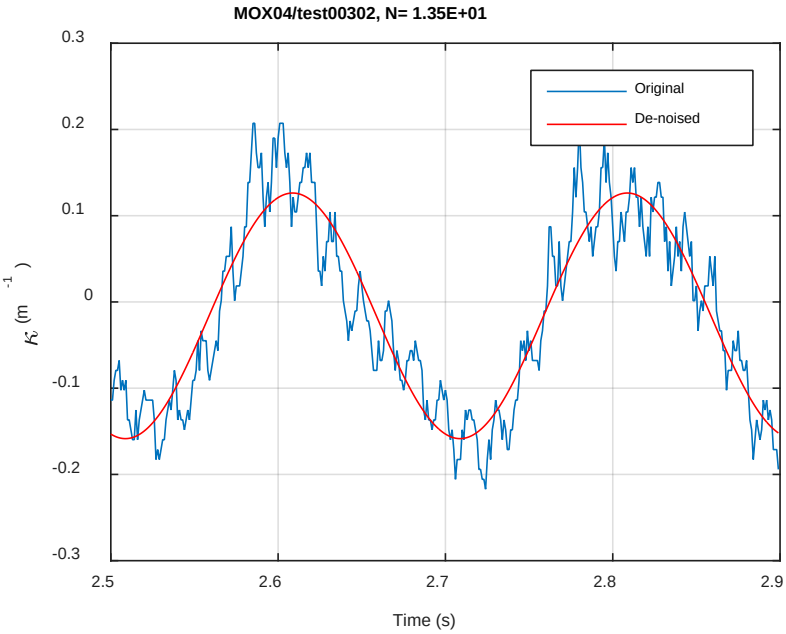

(c)

Fig. C.6. Monitoring-based responses: (a) curvature, (b) moment, (c) curvature, MOX04, 5.08 Nm, Ns = 1.35E+01 cycles.

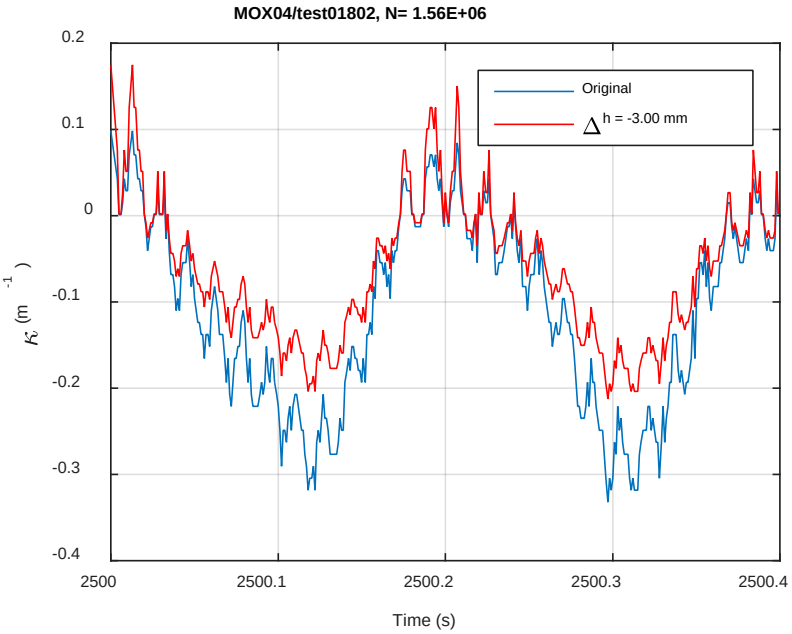
MOX04/test01802, N= 1.56E+06
Original
Δh = -3.00 mm
κ (m-1)
Time (s)

(a)

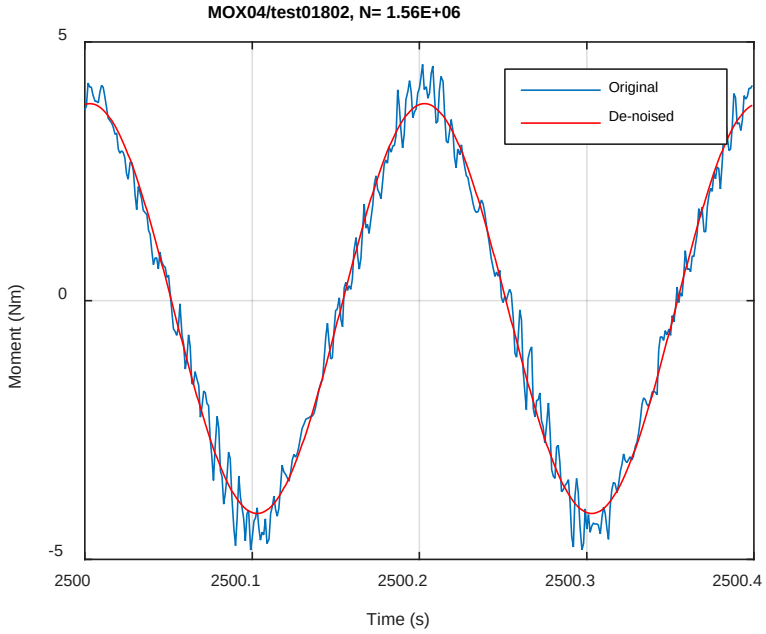
MOX04/test01802, N= 1.56E+06
Original
De-noised
Moment (Nm)
Time (s)

(b)

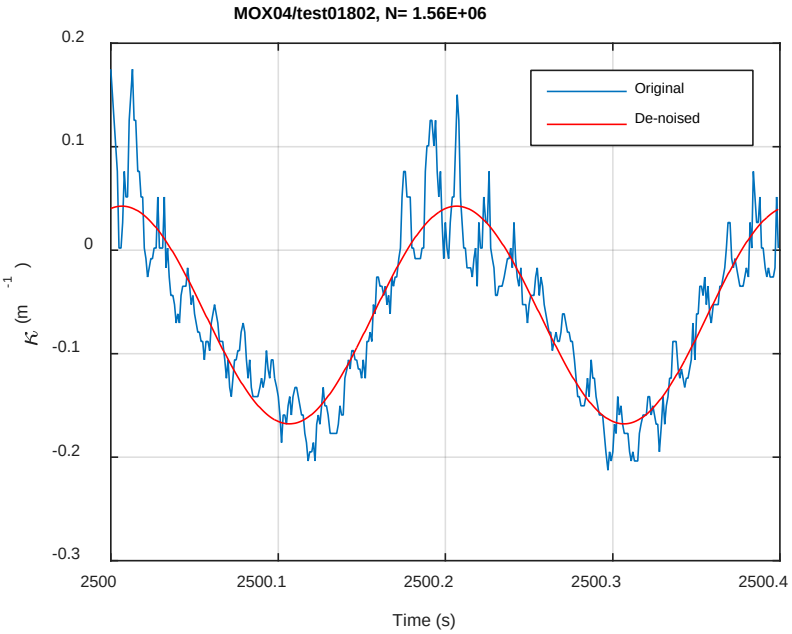

(c)

Fig. C.7. Monitoring-based responses: (a) curvature, (b) moment, (c) curvature, MOX04, 5.08 Nm, Ns = 1.56E+06 cycles.

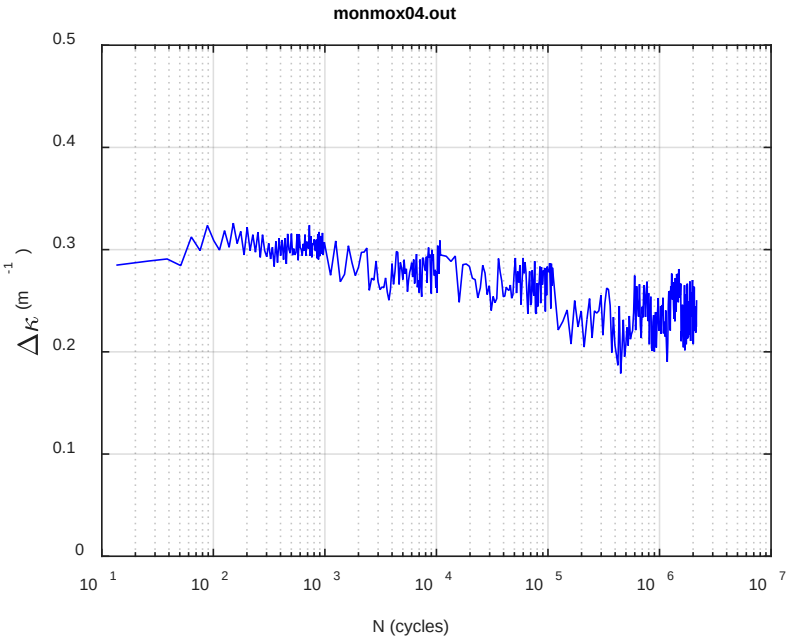
monmox04.out
0.5
0.4
0.3
0.2
0.1
0
Δκ (m -1)
10 1
10 2
10 3
10 4
10 5
10 6
10 7
N (cycles)

(a)

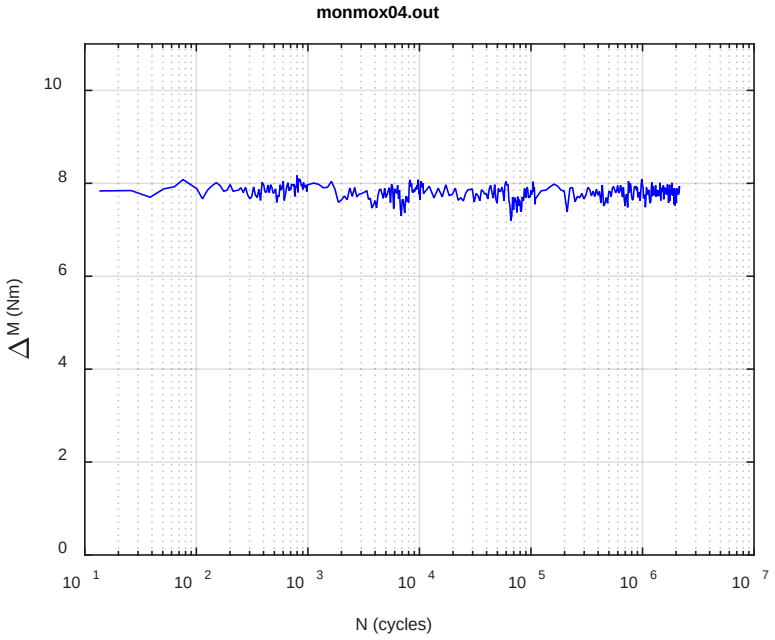
monmox04.out
10
8
6
4
2
0
Δ M (Nm)
10 1
10 2
10 3
10 4
10 5
10 6
10 7
N (cycles)

(b)

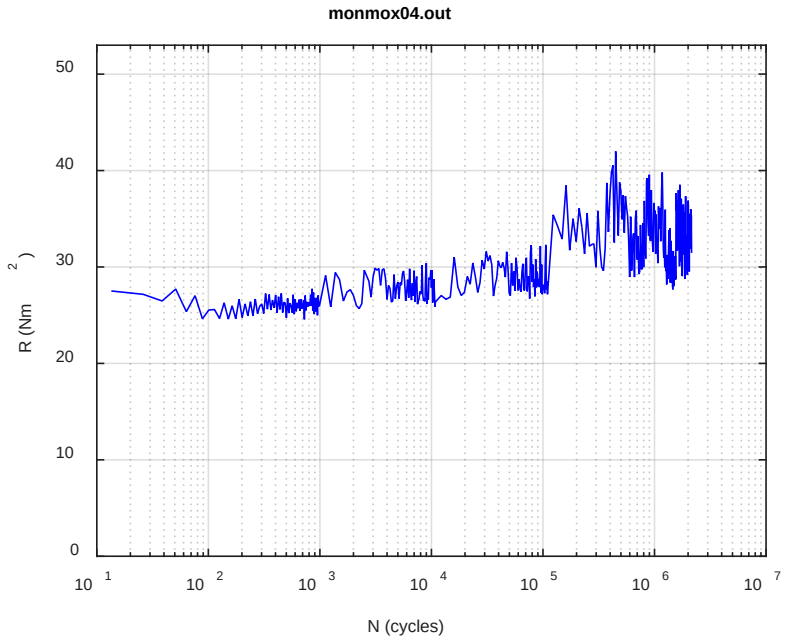
monmox04.out
R (Nm 2)
N (cycles)

(c)

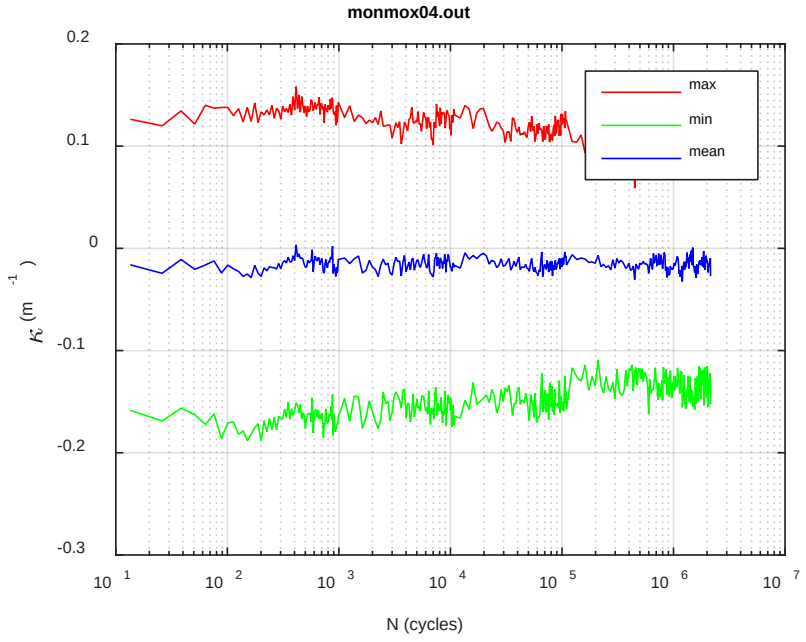
monmox04.out
max
min
mean
κ (m -1)
N (cycles)

(d)

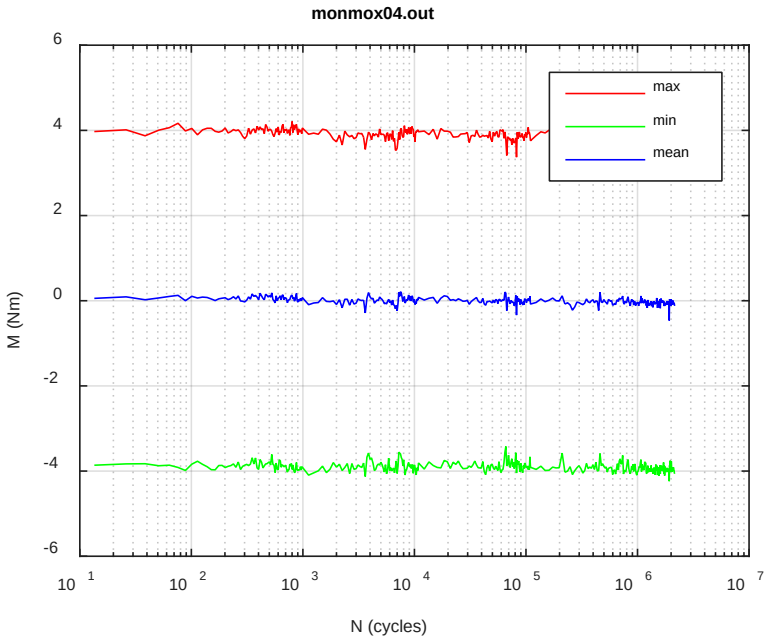

(e)

Fig. C.8. Monitoring-based responses: (a) curvature range, (b) moment range, (c) rigidity, (d) curvature peak/valley, (e) moment peak/valley, MOX04, 5.08 Nm, Nf = 2.15E+06 cycles.

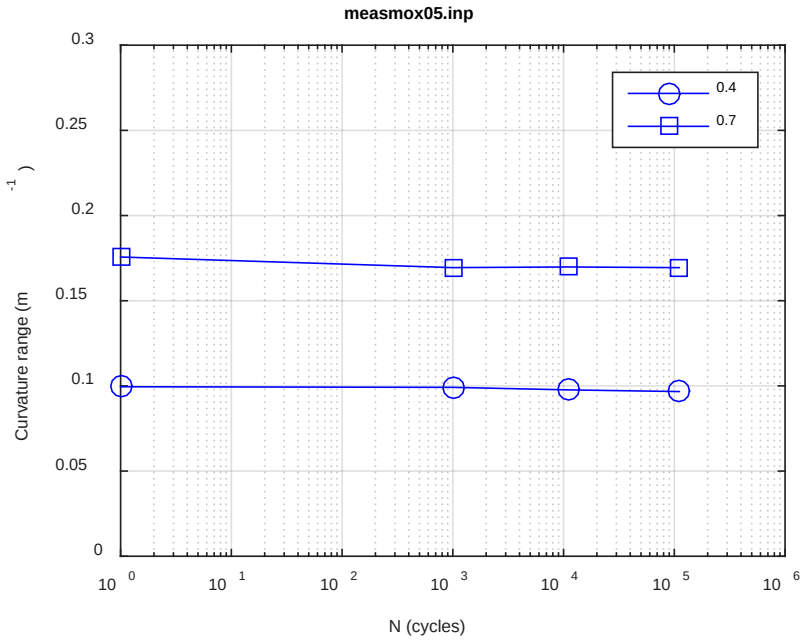
measmox05.inp
0.3
0.25
0.2
0.15
0.1
0.05
0
Curvature range (m -1)
0.4
0.7
10 0
10 1
10 2
10 3
10 4
10 5
10 6
N (cycles)

(a)

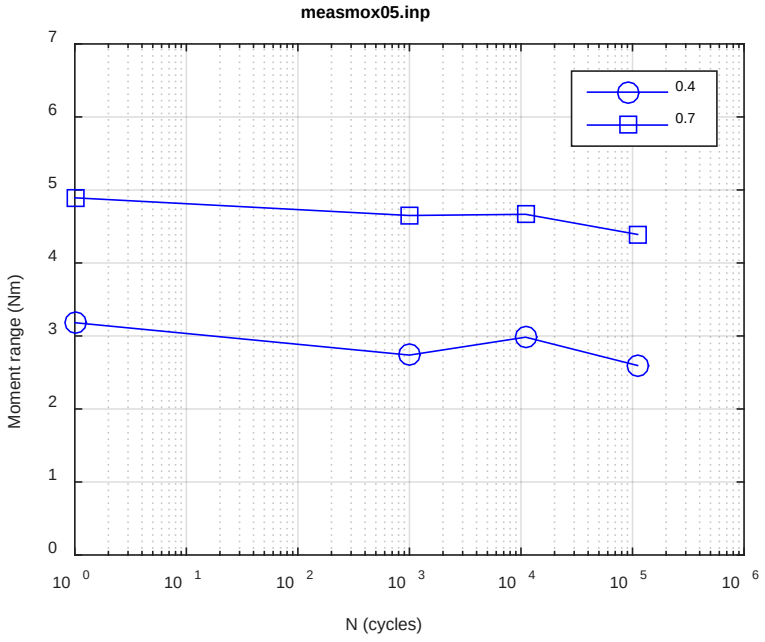
measmox05.inp
7
6
5
4
3
2
1
0
Moment range (Nm)
0.4
0.7
10 0
10 1
10 2
10 3
10 4
10 5
10 6
N (cycles)

(b)

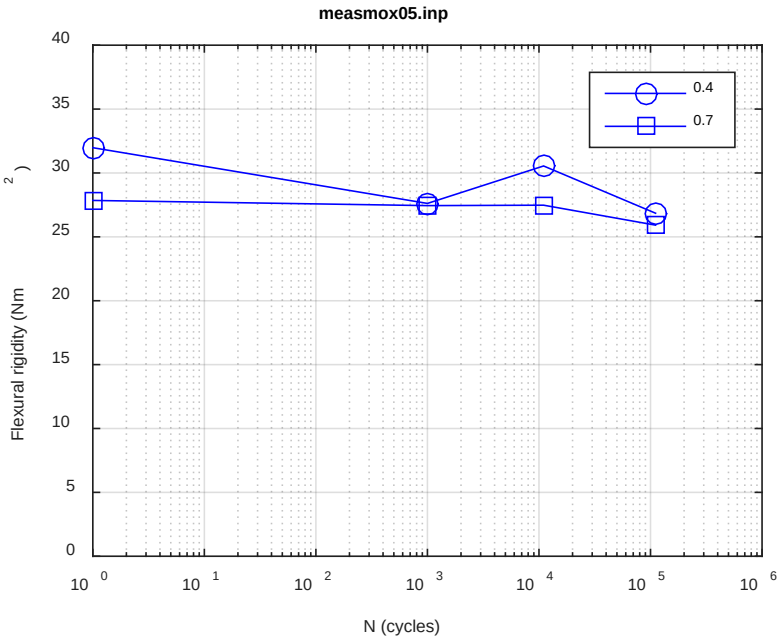
measmox05.inp
Flexural rigidity (Nm^2)
N (cycles)
0.4
0.7
40
35
30
25
20
15
10
5
0
10^0
10^1
10^2
10^3
10^4
10^5
10^6

(c)

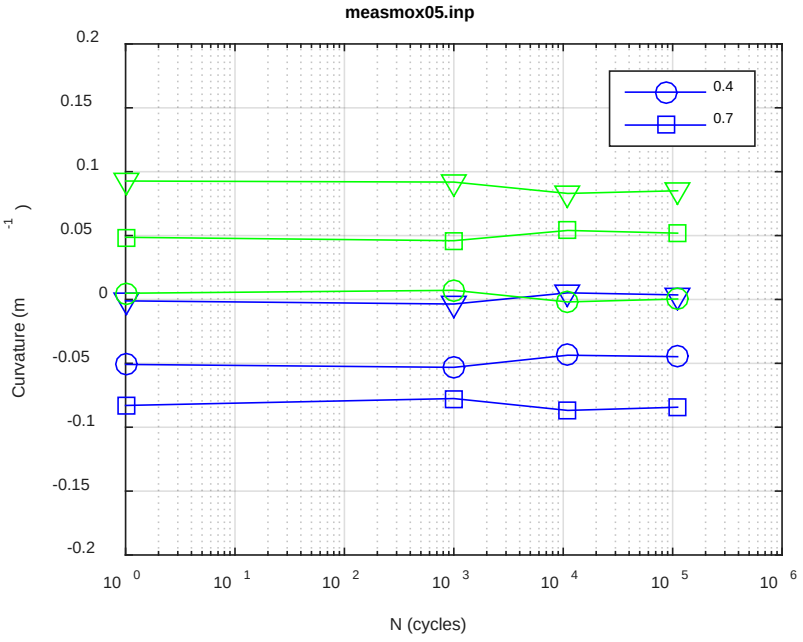
measmox05.inp
Curvature (m^-1)
N (cycles)
0.4
0.7
0.2
0.15
0.1
0.05
0
-0.05
-0.1
-0.15
-0.2
10^0
10^1
10^2
10^3
10^4
10^5
10^6

(d)

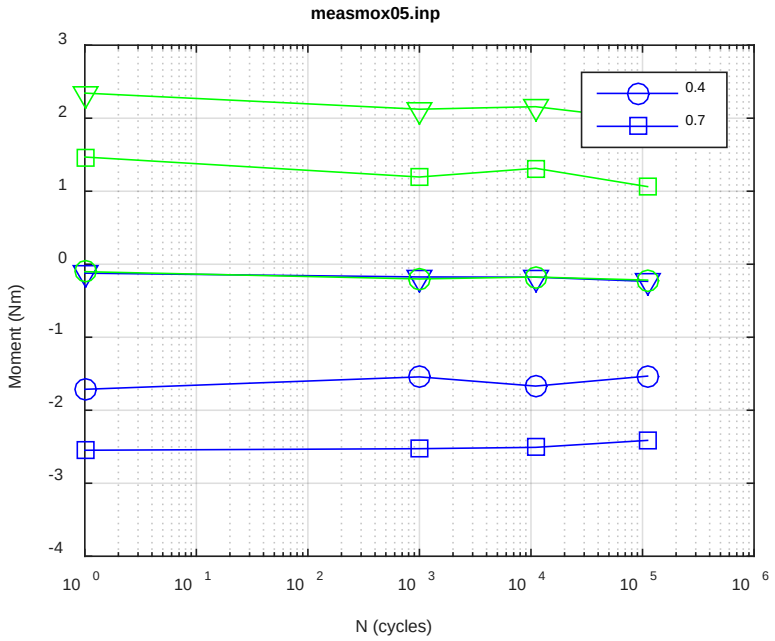

(e)

Fig. C.9. Measurement-based responses: (a) curvature range, (b) moment range, (c) rigidity, (d) curvature peak/valley, (e) moment peak/valley, MOX05, 6.10 Nm.

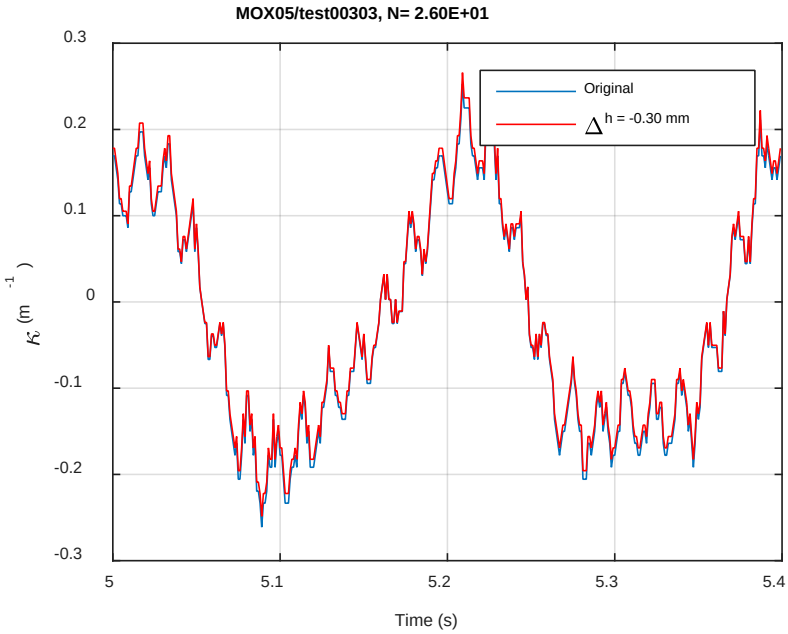
MOX05/test00303, N= 2.60E+01
Original
Δh = -0.30 mm
κ (m-1)
Time (s)

(a)

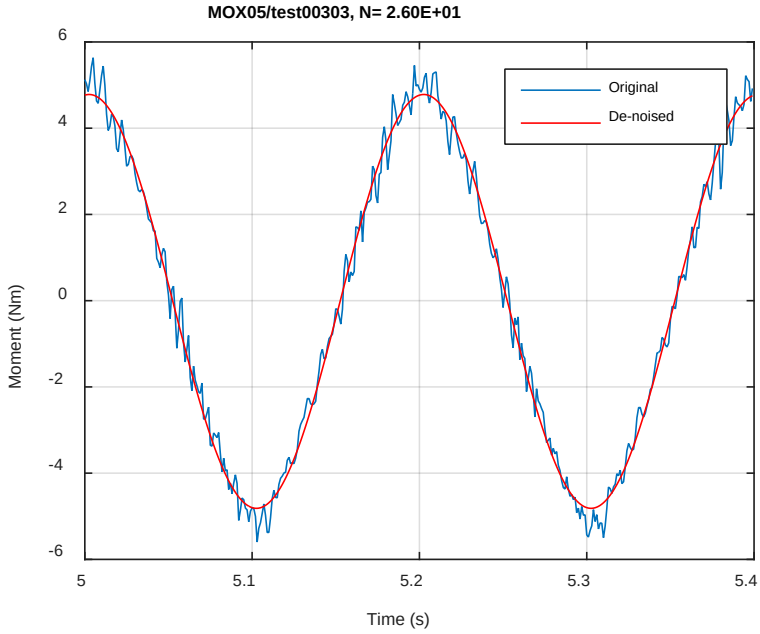
MOX05/test00303, N= 2.60E+01
Original
De-noised
Moment (Nm)
Time (s)

(b)

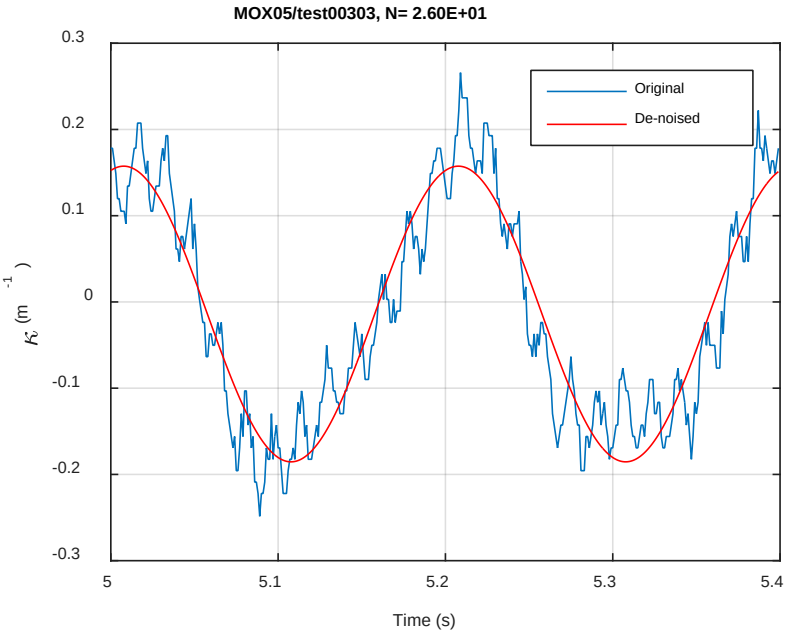

(c)

Fig. C.10. Monitoring-based responses: (a) curvature, (b) moment, (c) curvature, MOX05, 6.10 Nm, Ns = 2.60E+01 cycles.

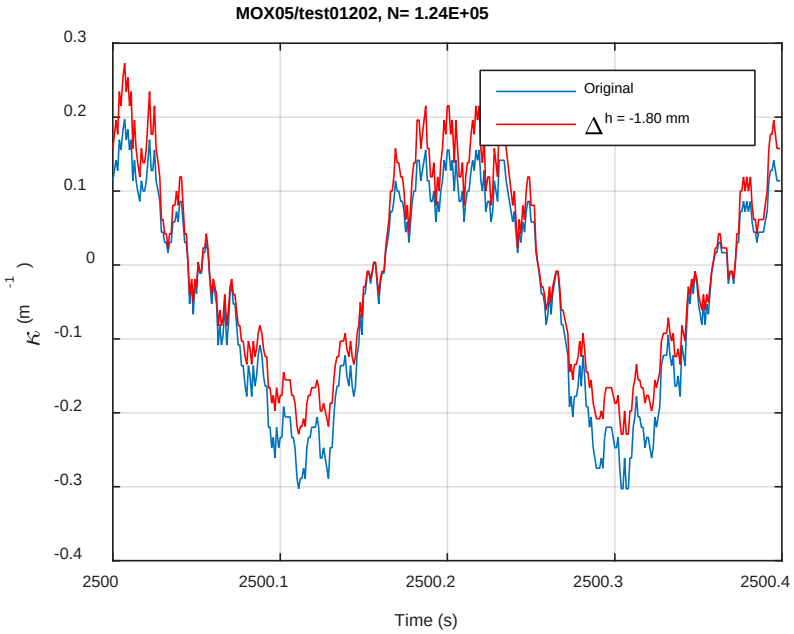
MOX05/test01202, N= 1.24E+05
Original
Δh = -1.80 mm
κ (m-1)
Time (s)
0.3
0.2
0.1
0
-0.1
-0.2
-0.3
-0.4
2500
2500.1
2500.2
2500.3
2500.4

(a)

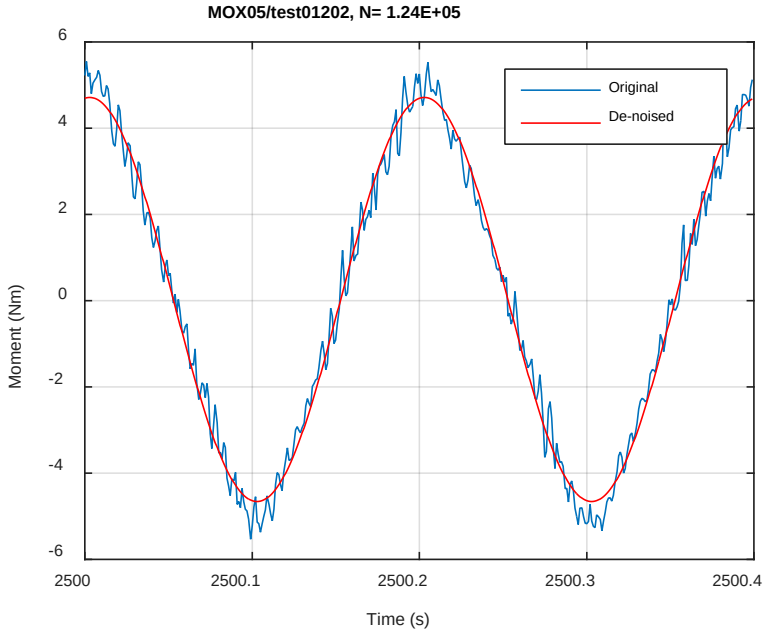
MOX05/test01202, N= 1.24E+05
Original
De-noised
Moment (Nm)
Time (s)
6
4
2
0
-2
-4
-6
2500
2500.1
2500.2
2500.3
2500.4

(b)

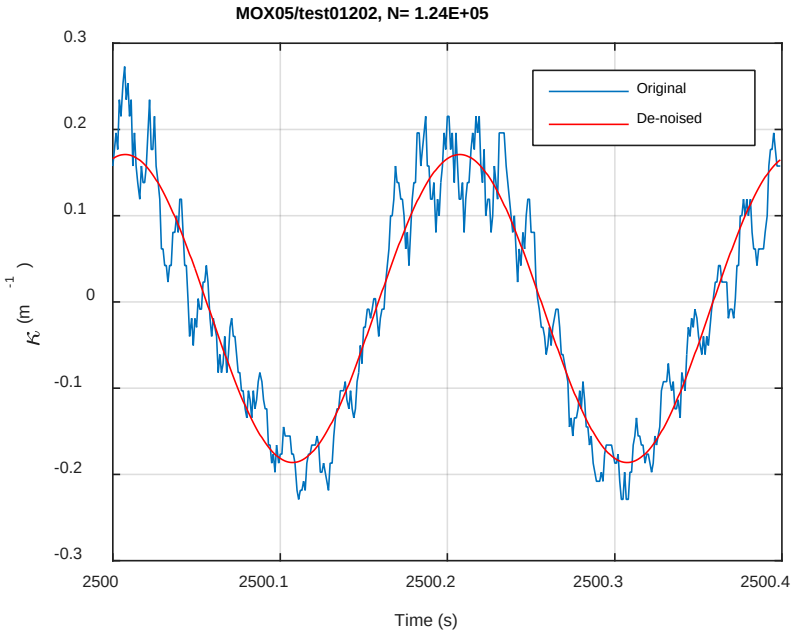

(c)

Fig. C.11. Monitoring-based responses: (a) curvature, (b) moment, (c) curvature, MOX05, 6.10 Nm, Ns = 1.24E+05 cycles.

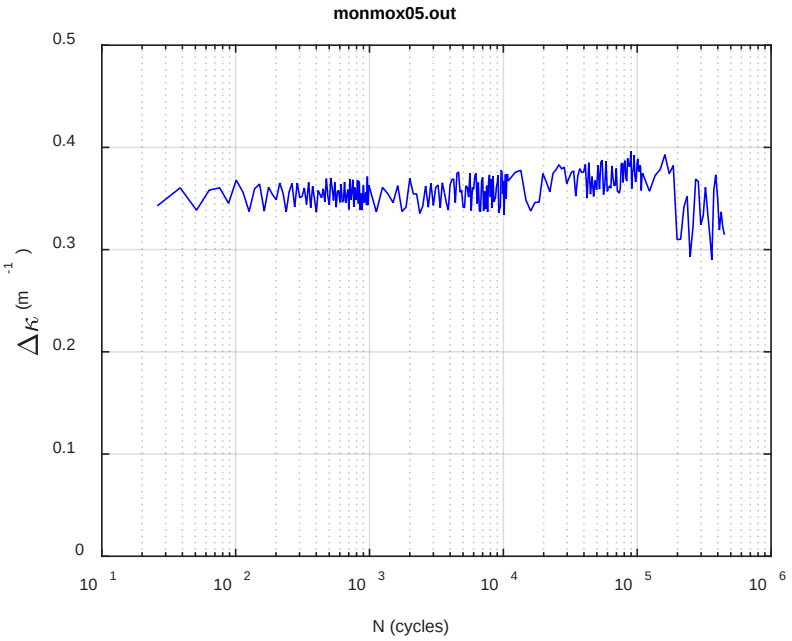
monmox05.out
0.5
0.4
0.3
0.2
0.1
0
Δκ (m -1)
10 1
10 2
10 3
10 4
10 5
10 6
N (cycles)

(a)

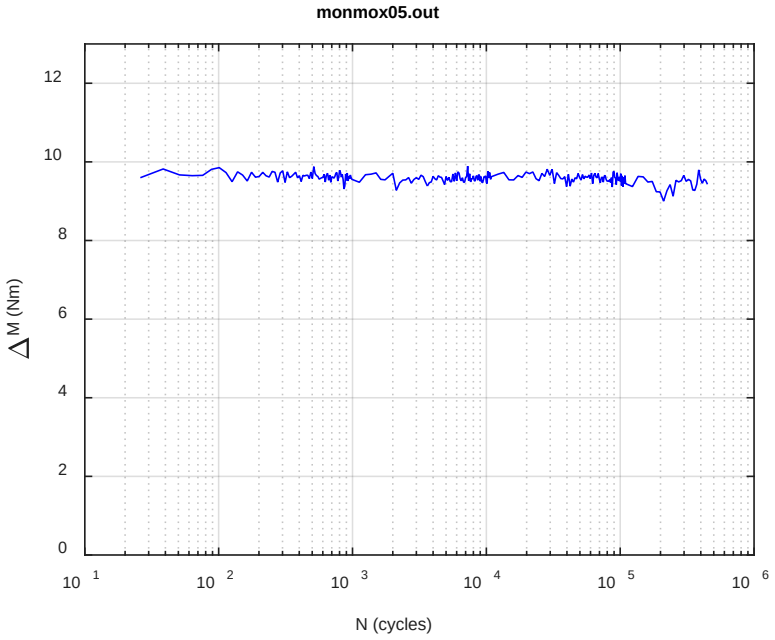
monmox05.out
12
10
8
6
4
2
0
Δ M (Nm)
10 1
10 2
10 3
10 4
10 5
10 6
N (cycles)

(b)

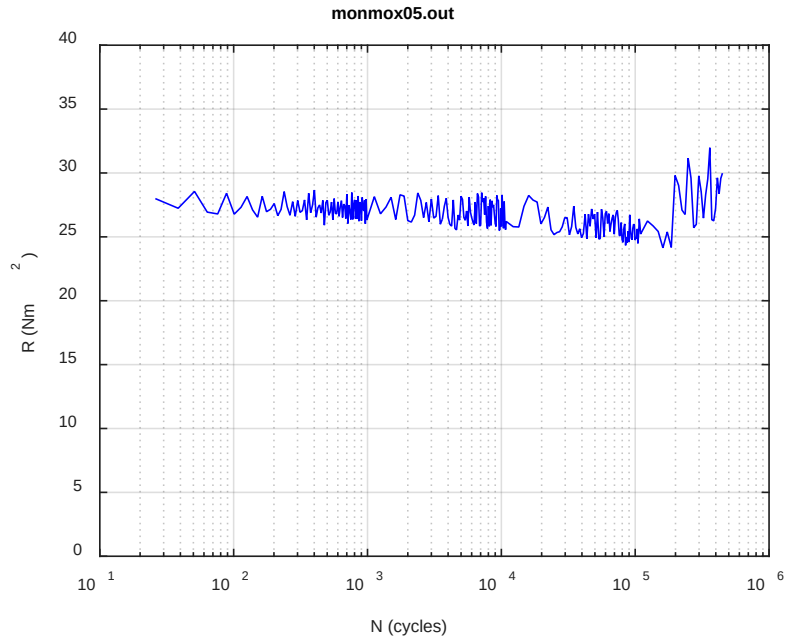
monmox05.out
R (Nm 2)
N (cycles)

(c)

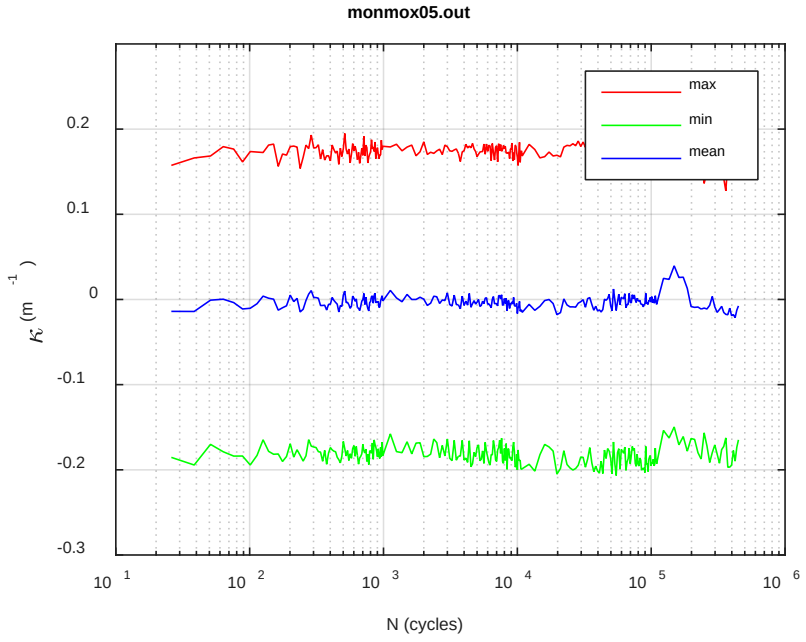
monmox05.out
max
min
mean
κ (m -1)
N (cycles)

(d)

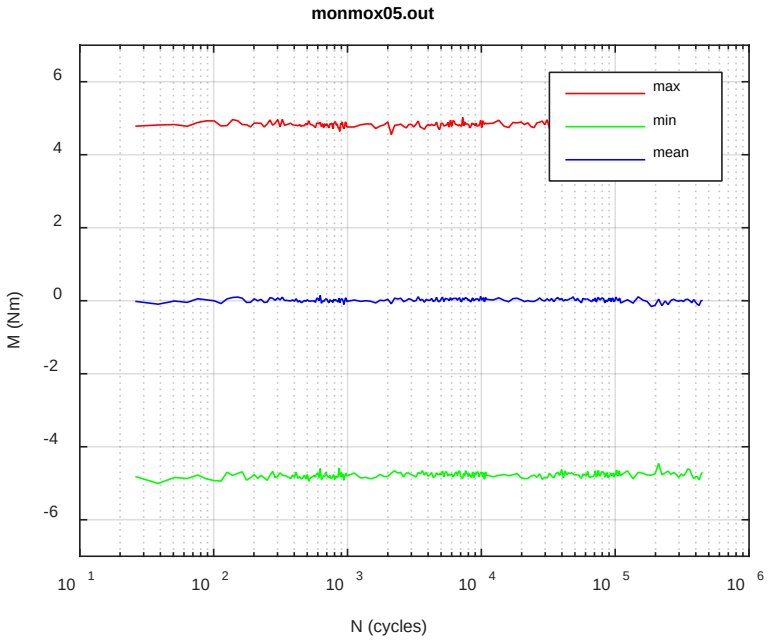

(e)

Fig. C.12. Monitoring-based responses: (a) curvature range, (b) moment range, (c) rigidity, (d) curvature peak/valley, (e) moment peak/valley, MOX05, 6.10 Nm, Nf = 4.49E+05 cycles.

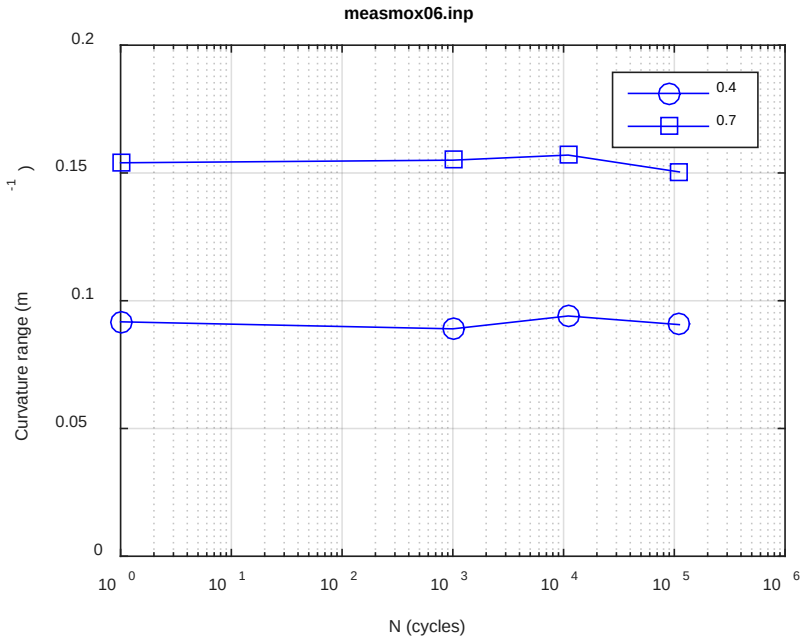
measmox06.inp
0.2
0.15
0.1
0.05
0
Curvature range (m -1)
0.4
0.7
10 0
10 1
10 2
10 3
10 4
10 5
10 6
N (cycles)

(a)

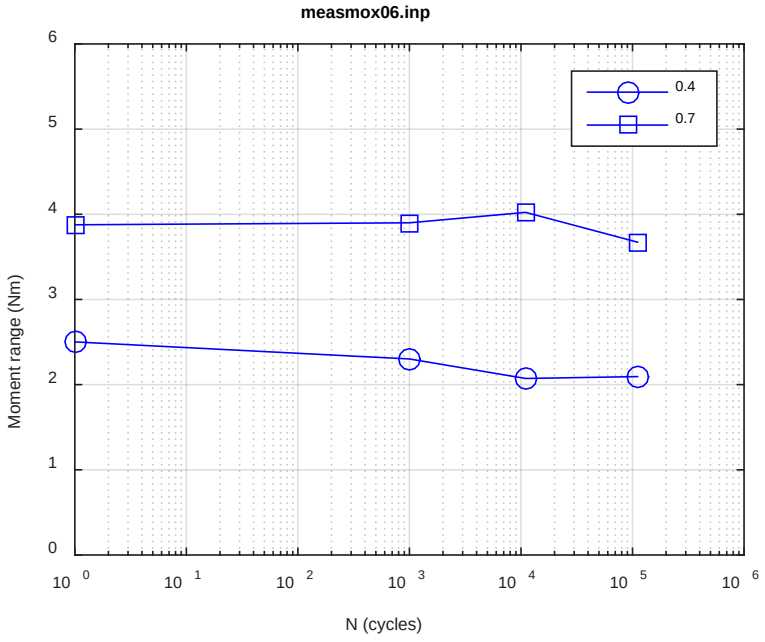
measmox06.inp
6
5
4
3
2
1
0
Moment range (Nm)
0.4
0.7
10 0
10 1
10 2
10 3
10 4
10 5
10 6
N (cycles)

(b)

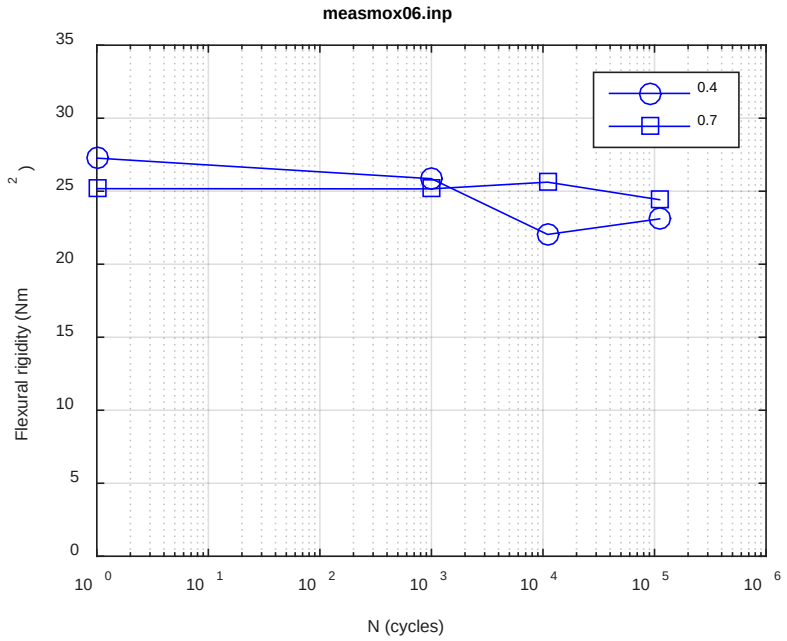
measmox06.inp
0.4
0.7
Flexural rigidity (Nm 2)
N (cycles)
35
30
25
20
15
10
5
0
10 0
10 1
10 2
10 3
10 4
10 5
10 6

(c)

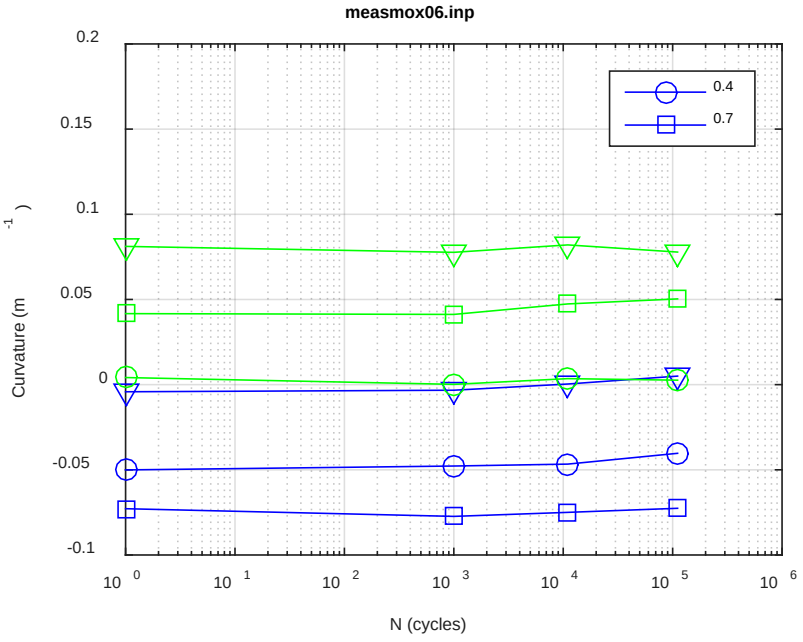
measmox06.inp
0.4
0.7
Curvature (m -1)
N (cycles)
0.2
0.15
0.1
0.05
0
-0.05
-0.1
10 0
10 1
10 2
10 3
10 4
10 5
10 6

(d)

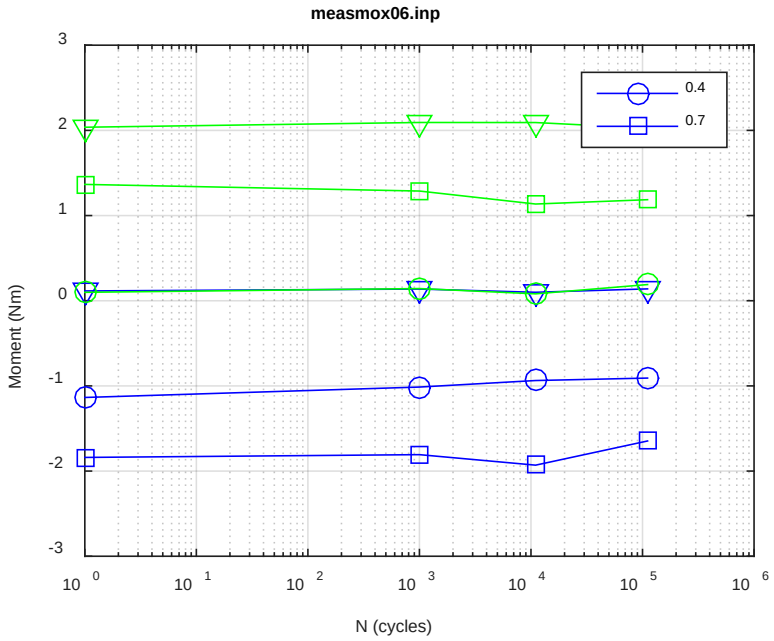

(e)

Fig. C.13. Measurement-based responses: (a) curvature range, (b) moment range, (c) rigidity, (d) curvature peak/valley, (e) moment peak/valley, MOX06, 5.08 Nm.

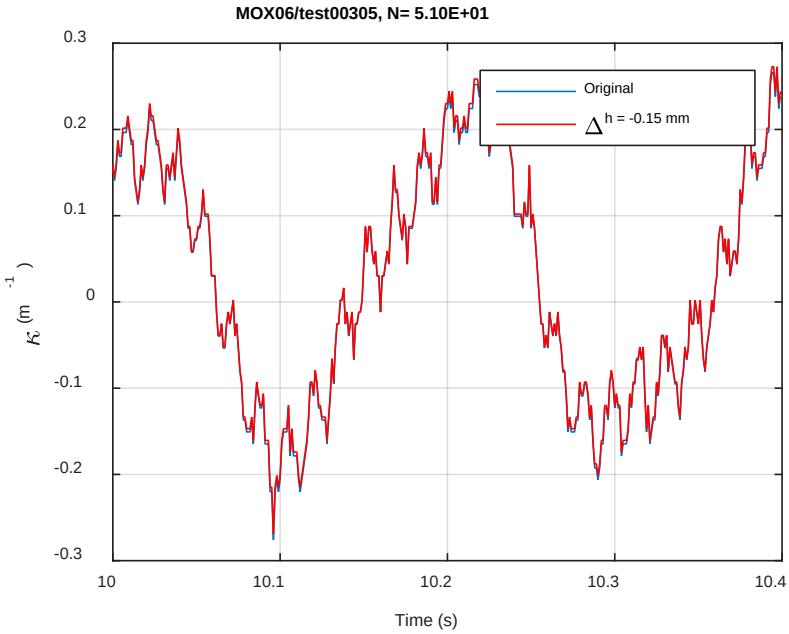
MOX06/test00305, N= 5.10E+01
Original
Δh = -0.15 mm
κ (m-1)
Time (s)
0.3
0.2
0.1
0
-0.1
-0.2
-0.3
10
10.1
10.2
10.3
10.4

(a)

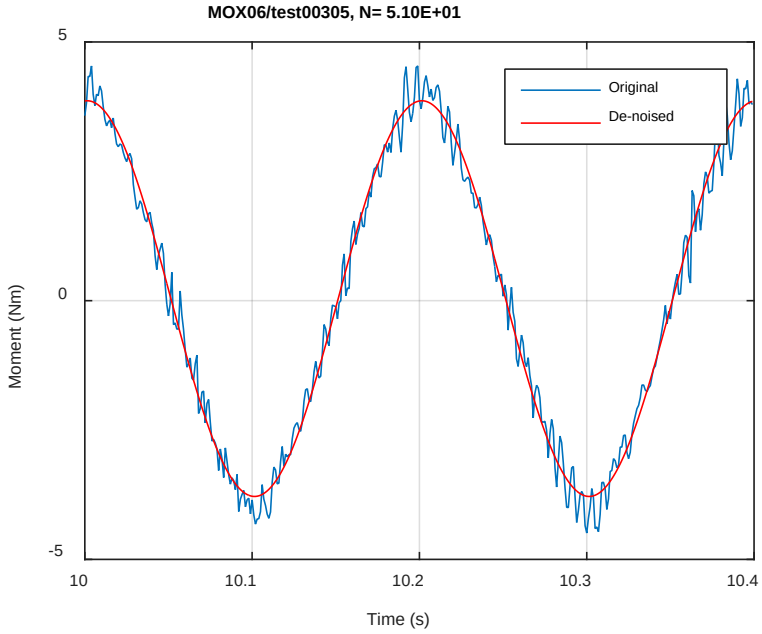
MOX06/test00305, N= 5.10E+01
Original
De-noised
Moment (Nm)
Time (s)
5
0
-5
10
10.1
10.2
10.3
10.4

(b)

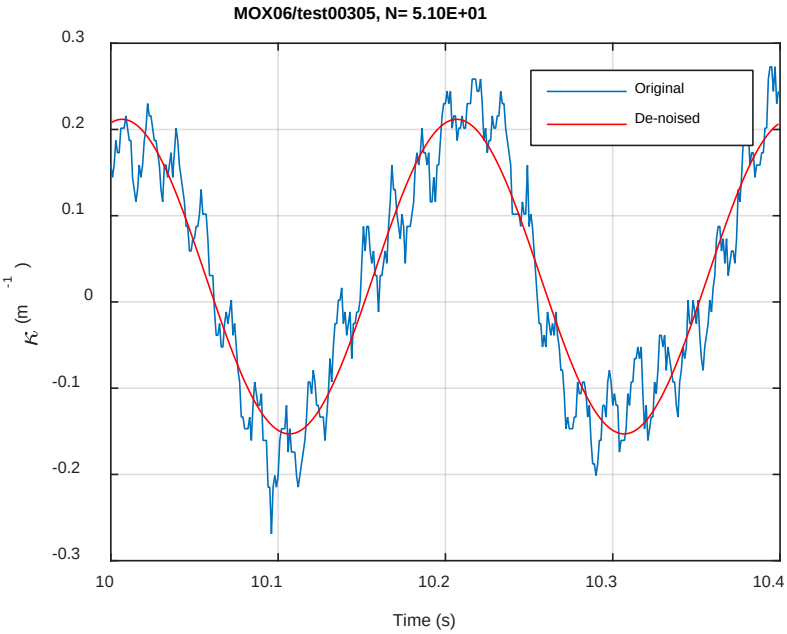

(c)

Fig. C.14. Monitoring-based responses: (a) curvature, (b) moment, (c) curvature, MOX06, 5.08 Nm, Ns = 5.10E+01 cycles.

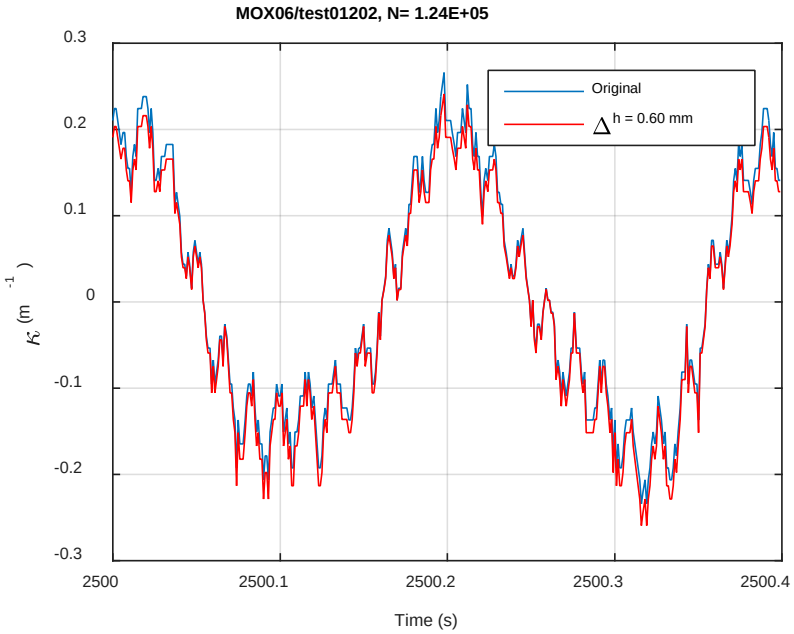
MOX06/test01202, N= 1.24E+05
Original
Δh = 0.60 mm
κ (m-1)
Time (s)
0.3
0.2
0.1
0
-0.1
-0.2
-0.3
2500
2500.1
2500.2
2500.3
2500.4

(a)

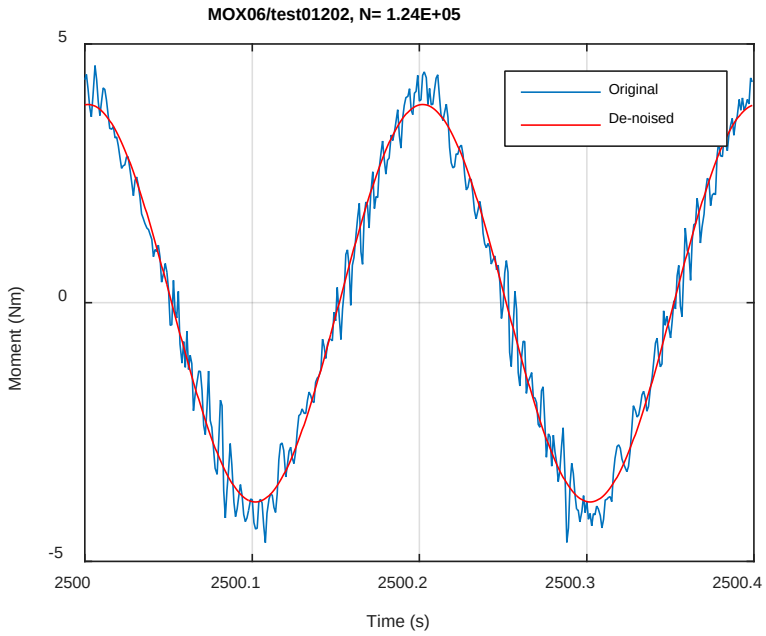
MOX06/test01202, N= 1.24E+05
Original
De-noised
Moment (Nm)
Time (s)
5
0
-5
2500
2500.1
2500.2
2500.3
2500.4

(b)

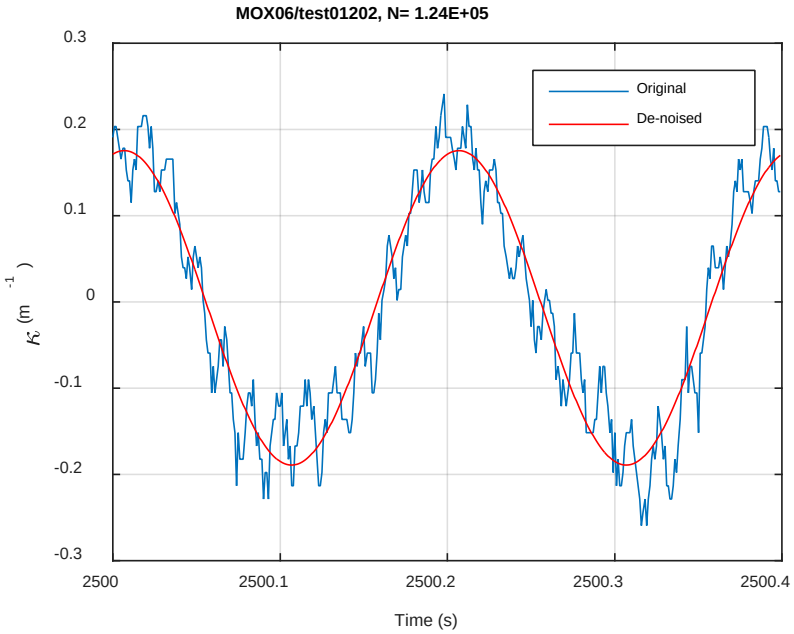

(c)

Fig. C.15. Monitoring-based responses: (a) curvature, (b) moment, (c) curvature, MOX06, 5.08 Nm, Ns = 1.24E+05 cycles.

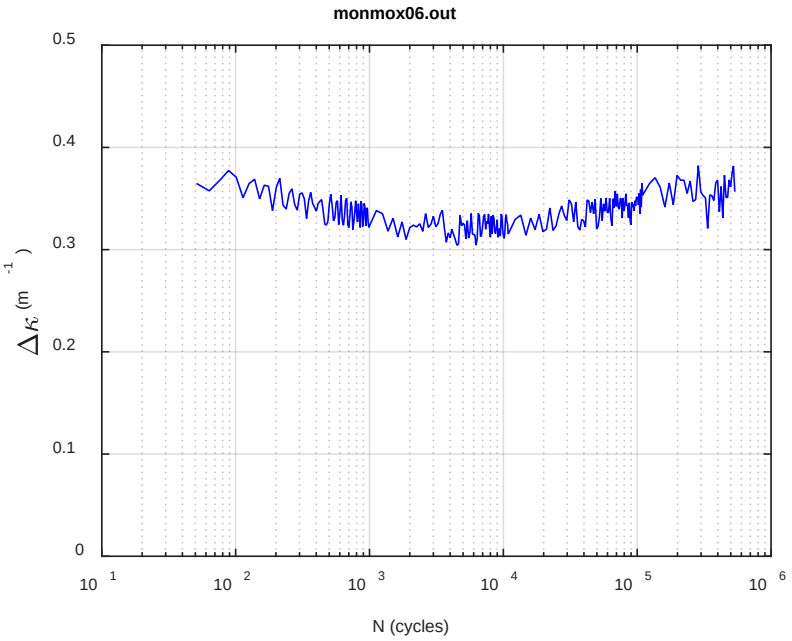
monmox06.out
0.5
0.4
0.3
0.2
0.1
0
Δκ (m -1)
10 1
10 2
10 3
10 4
10 5
10 6
N (cycles)

(a)

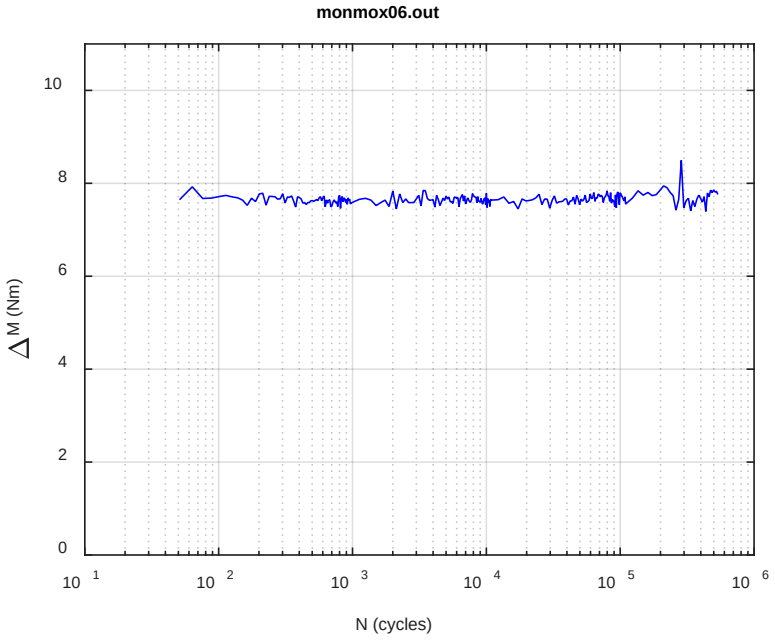
monmox06.out
10
8
6
4
2
0
Δ M (Nm)
10 1
10 2
10 3
10 4
10 5
10 6
N (cycles)

(b)

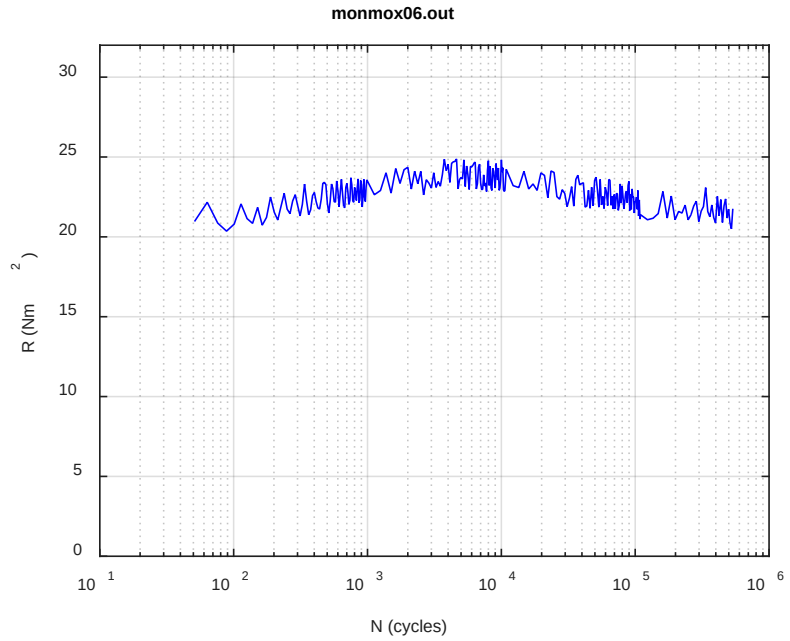
monmox06.out
R (Nm 2)
N (cycles)

(c)

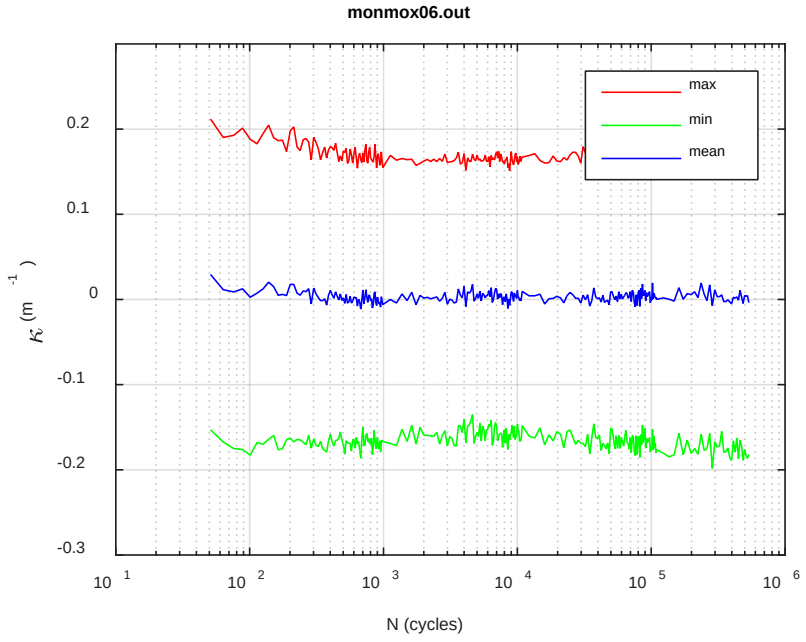
monmox06.out
max
min
mean
κ (m -1)
N (cycles)

(d)

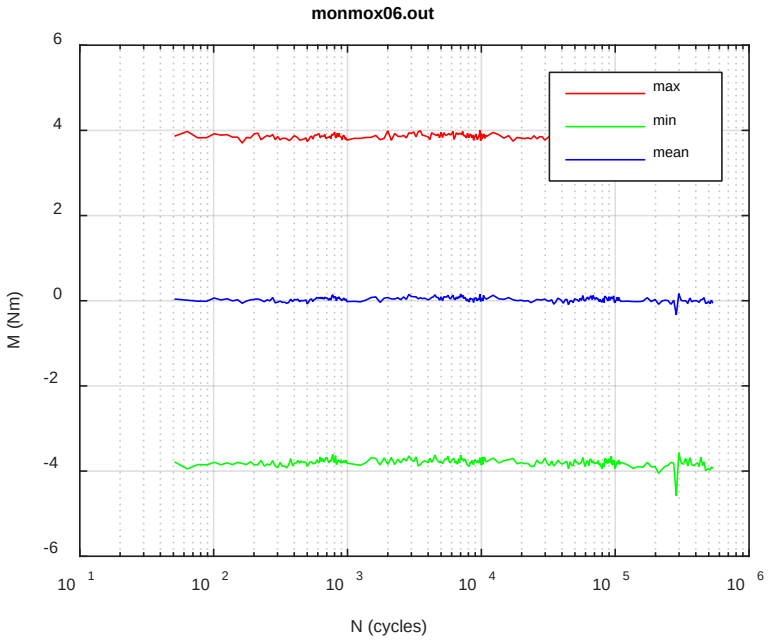

(e)

Fig. C.16. Monitoring-based responses: (a) curvature range, (b) moment range, (c) rigidity, (d) curvature peak/valley, (e) moment peak/valley, MOX06, 5.08 Nm, Nf = 5.42E+05 cycles.

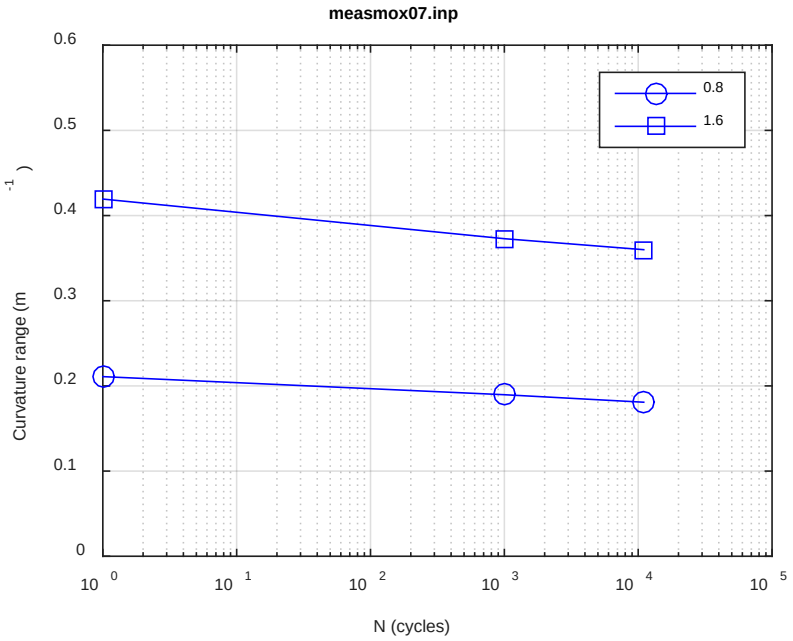
measmox07.inp
0.6
0.5
0.4
0.3
0.2
0.1
0
Curvature range (m -1)
0.8
1.6
10 0
10 1
10 2
10 3
10 4
10 5
N (cycles)

(a)

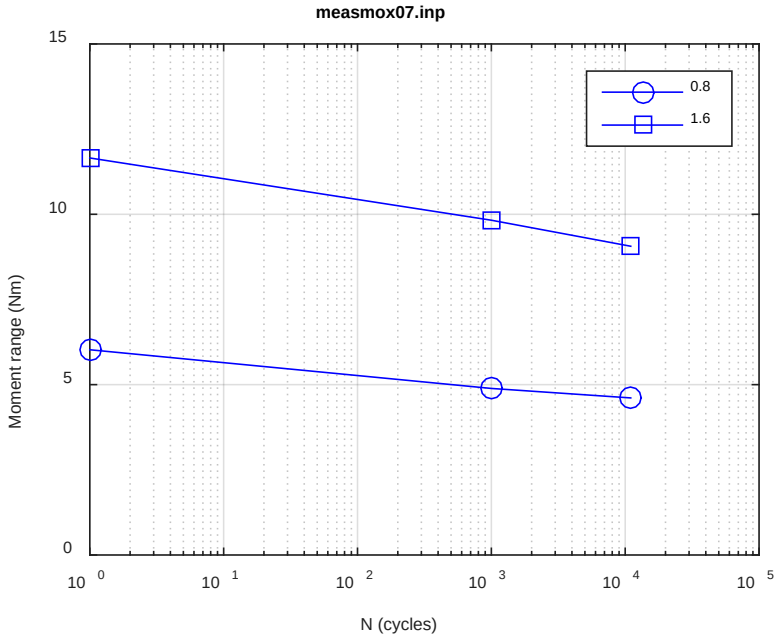
measmox07.inp
15
10
5
0
Moment range (Nm)
0.8
1.6
10 0
10 1
10 2
10 3
10 4
10 5
N (cycles)

(b)

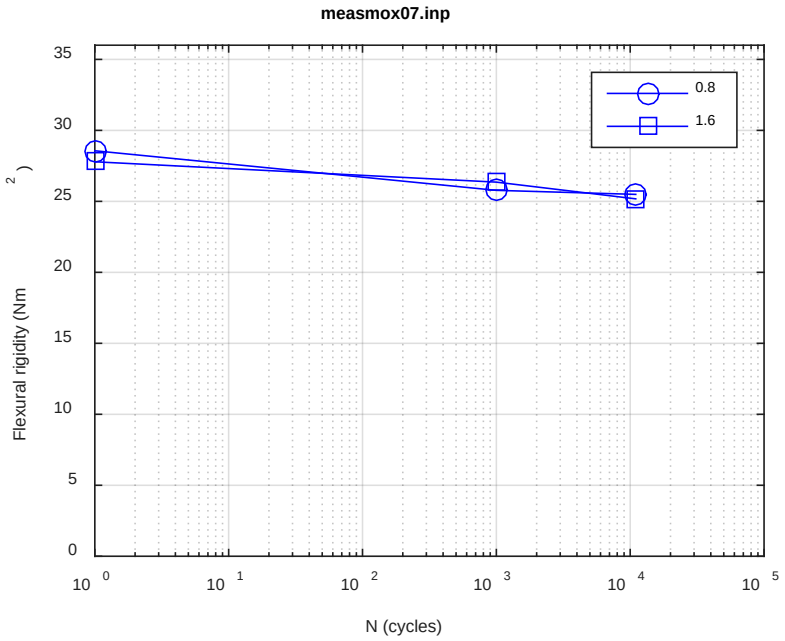
measmox07.inp
0.8
1.6
Flexural rigidity (Nm 2)
N (cycles)
0
5
10
15
20
25
30
35
10 0
10 1
10 2
10 3
10 4
10 5

(c)

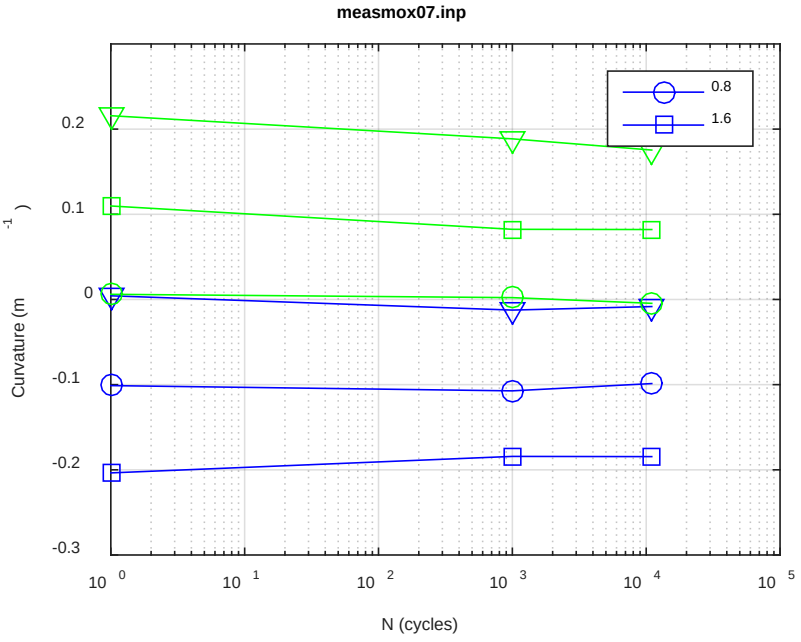
measmox07.inp
0.8
1.6
Curvature (m -1)
N (cycles)
0.2
0.1
0
-0.1
-0.2
-0.3
10 0
10 1
10 2
10 3
10 4
10 5

(d)

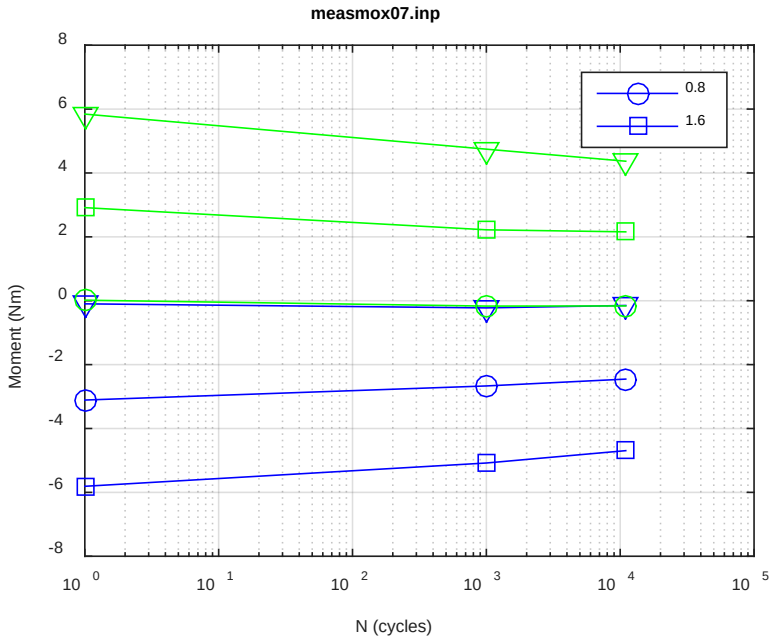

(e)

Fig. C.17. Measurement-based responses: (a) curvature range, (b) moment range, (c) rigidity, (d) curvature peak/valley, (e) moment peak/valley, MOX07, 15.24 Nm.

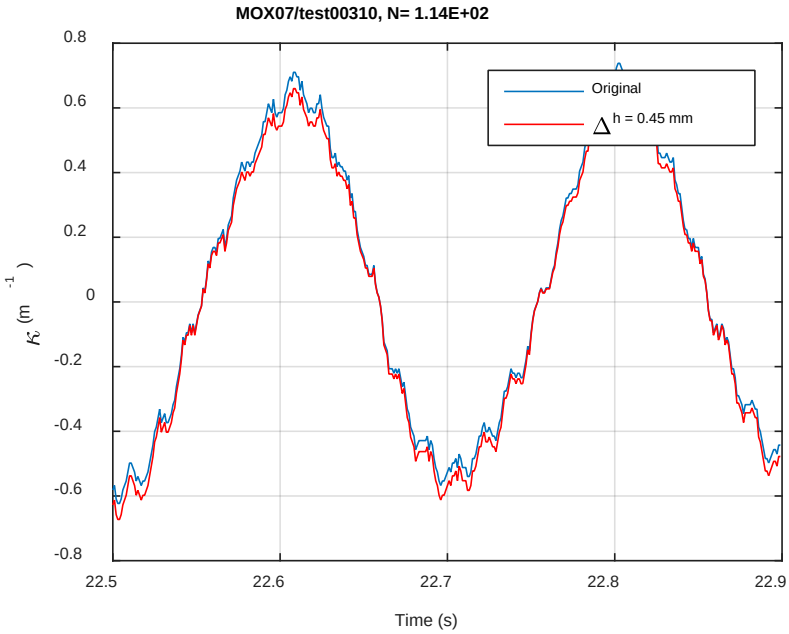
MOX07/test00310, N= 1.14E+02
Original
Δh = 0.45 mm
κ (m-1)
Time (s)

(a)

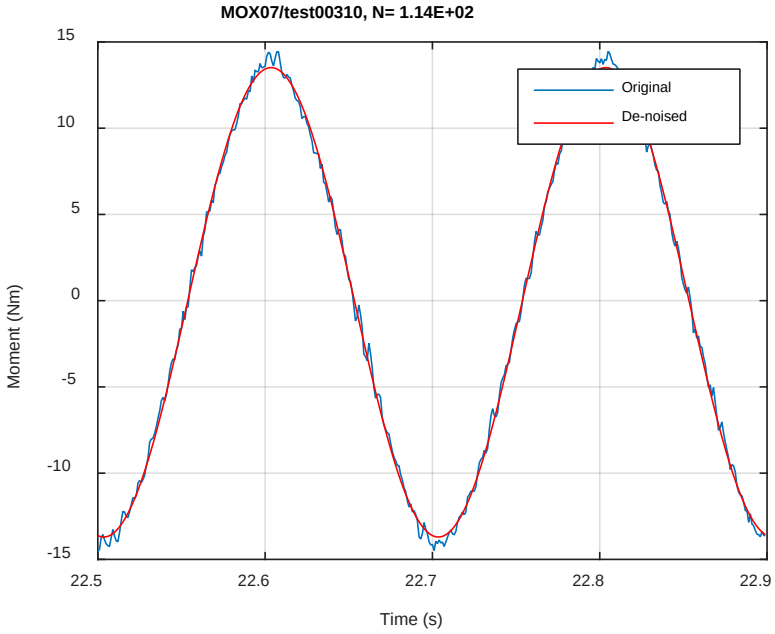
MOX07/test00310, N= 1.14E+02
Original
De-noised
Moment (Nm)
Time (s)

(b)

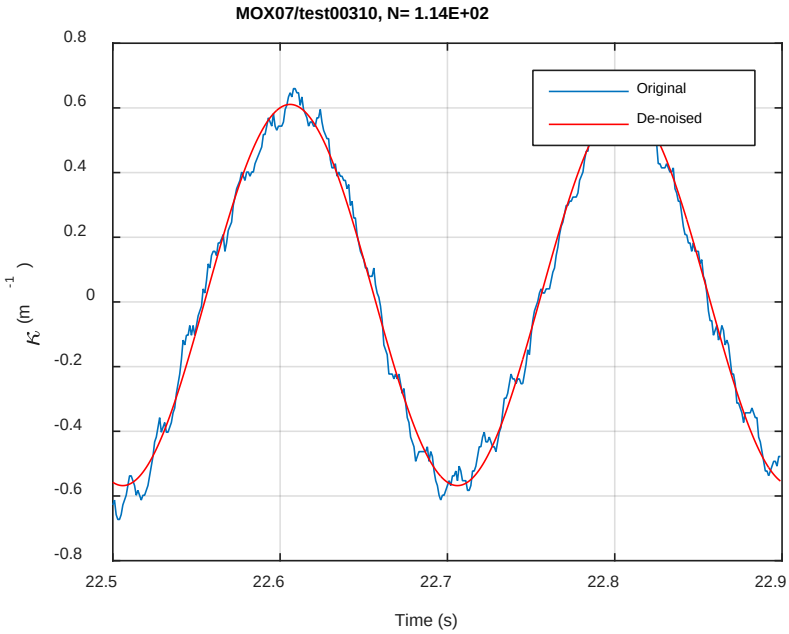

(c)

Fig. C.18. Monitoring-based responses: (a) curvature, (b) moment, (c) curvature, MOX07, 15.24 Nm, Ns = 1.14E+02 cycles.

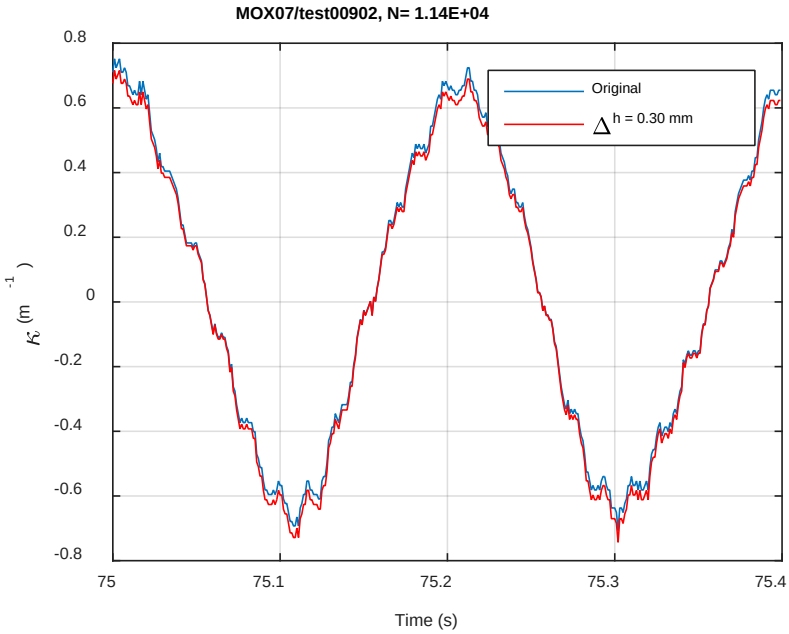
MOX07/test00902, N= 1.14E+04
Original
Δh = 0.30 mm
κ (m-1)
Time (s)
0.8
0.6
0.4
0.2
0
-0.2
-0.4
-0.6
-0.8
75
75.1
75.2
75.3
75.4

(a)

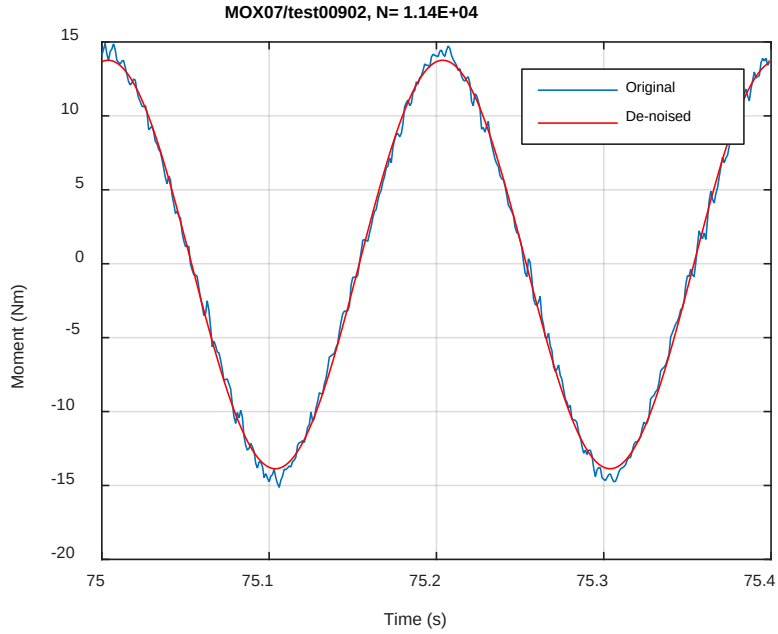
MOX07/test00902, N= 1.14E+04
Original
De-noised
Moment (Nm)
Time (s)
15
10
5
0
-5
-10
-15
-20
75
75.1
75.2
75.3
75.4

(b)

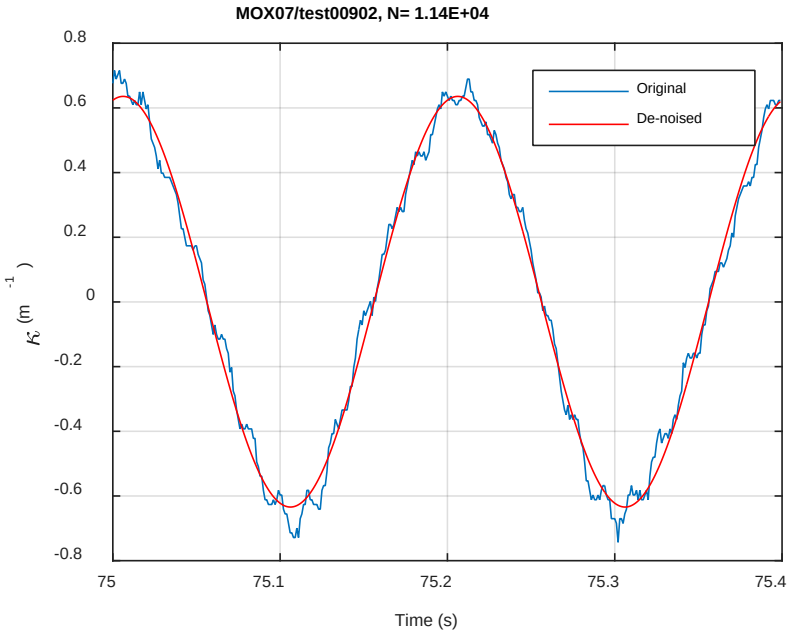

(c)

Fig. C.19. Monitoring-based responses: (a) curvature, (b) moment, (c) curvature, MOX07, 15.24 Nm, Ns = 1.14E+04 cycles.

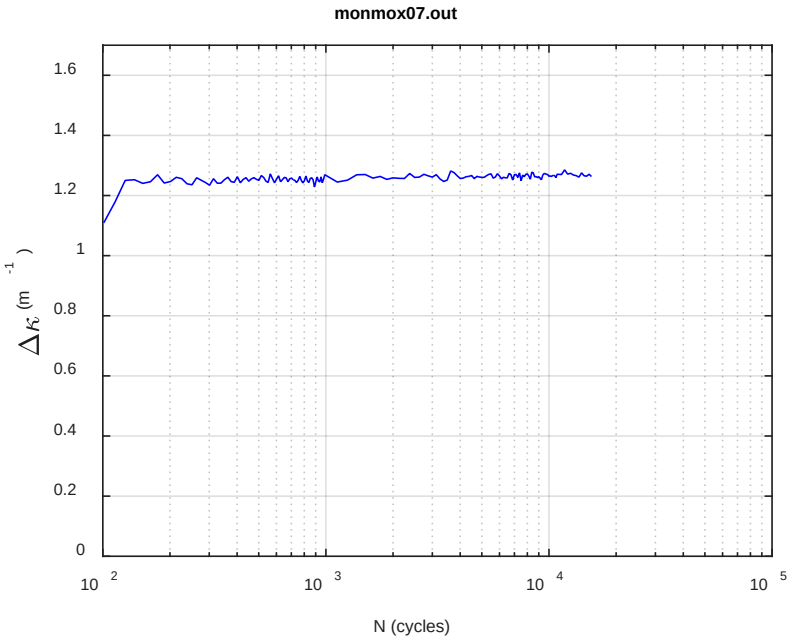
monmox07.out
1.6
1.4
1.2
1
0.8
0.6
0.4
0.2
0
Δκ (m-1)
10 2
10 3
10 4
10 5
N (cycles)

(a)

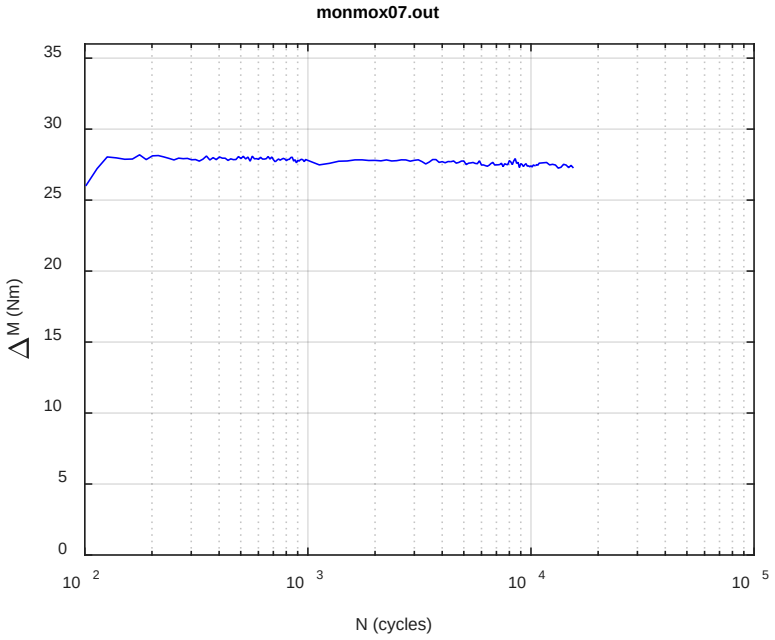
monmox07.out
35
30
25
20
15
10
5
0
ΔM (Nm)
10 2
10 3
10 4
10 5
N (cycles)

(b)

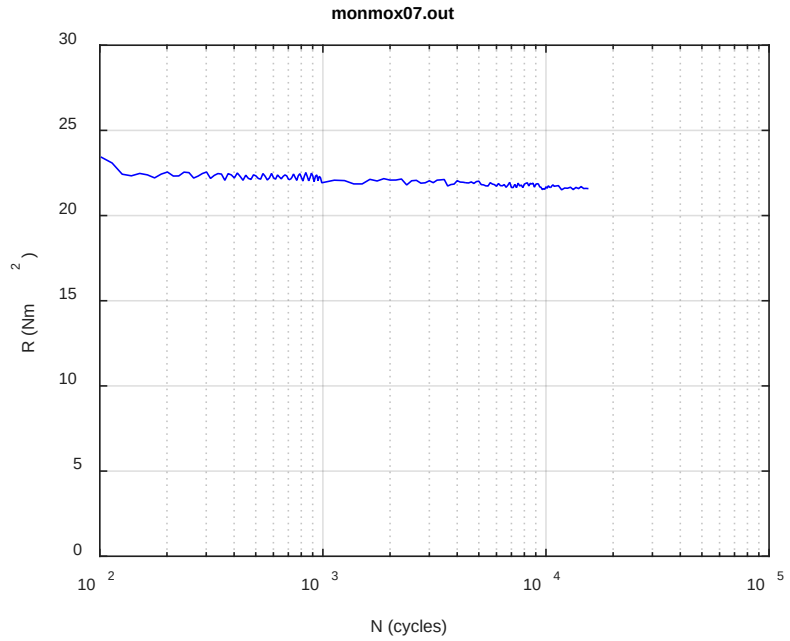
monmox07.out
R (Nm 2)
N (cycles)

(c)

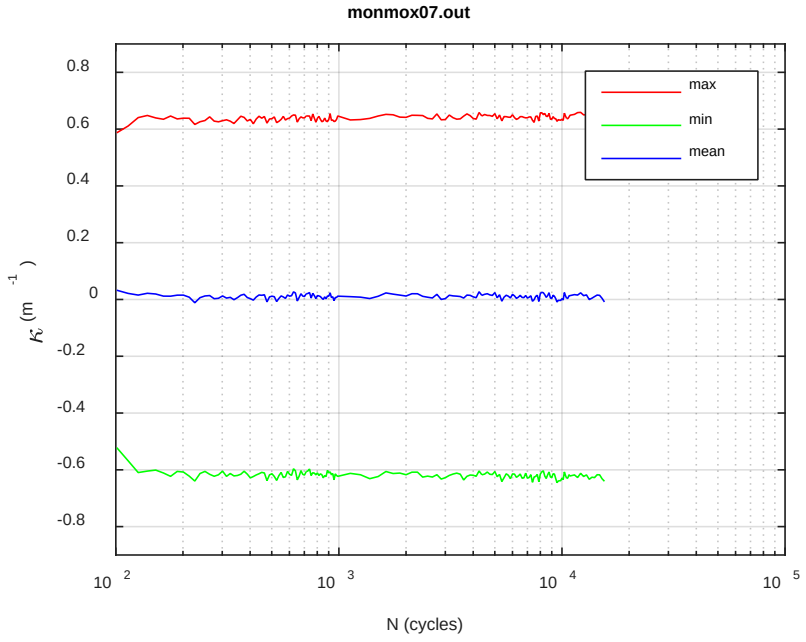
monmox07.out
max
min
mean
κ (m -1)
N (cycles)

(d)

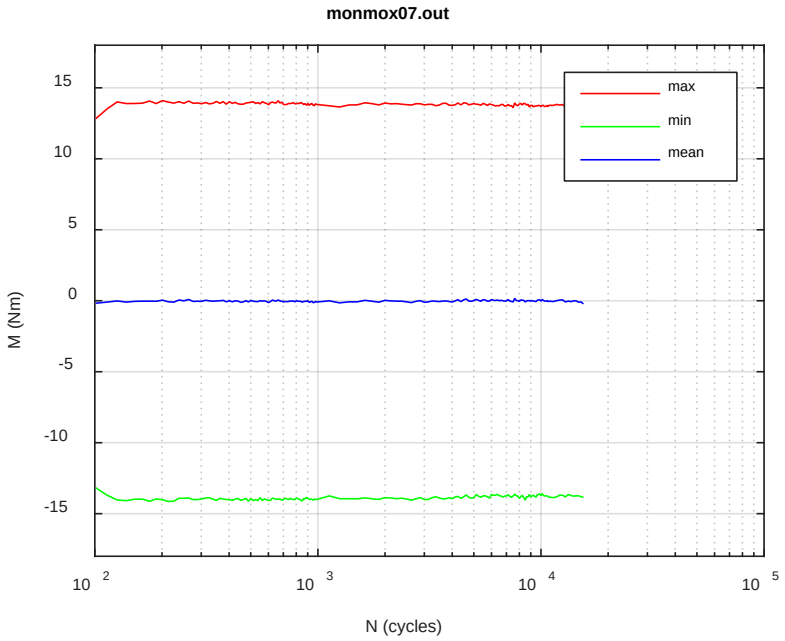

(e)

Fig. C.20. Monitoring-based responses: (a) curvature range, (b) moment range, (c) rigidity, (d) curvature peak/valley, (e) moment peak/valley, MOX07, 15.24 Nm, Nf = 1.55E+04 cycles.

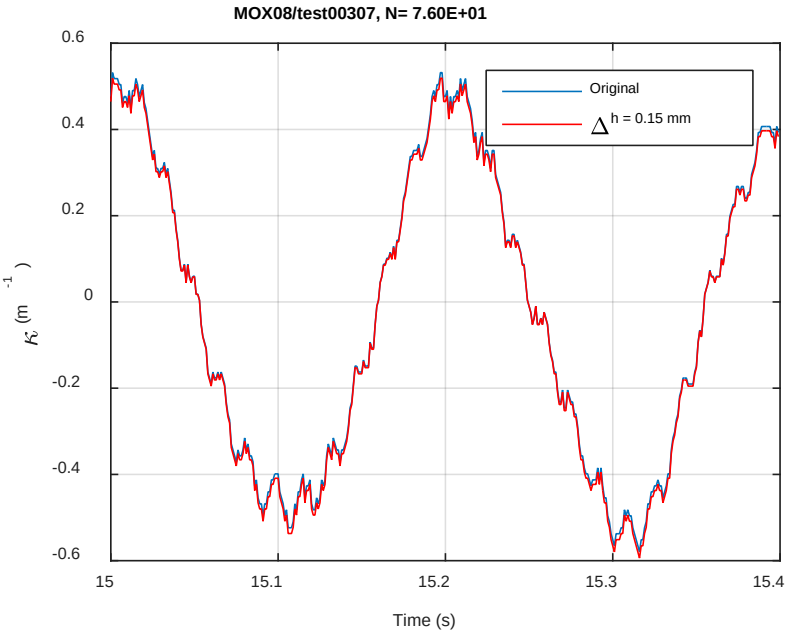
MOX08/test00307, N= 7.60E+01
Original
Δh = 0.15 mm
κ (m-1)
Time (s)

(a)

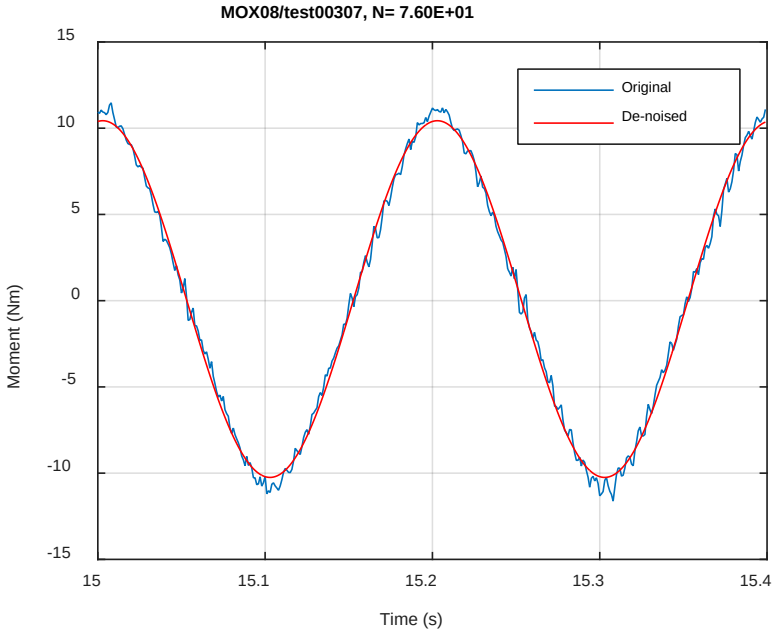
MOX08/test00307, N= 7.60E+01
Original
De-noised
Moment (Nm)
Time (s)

(b)

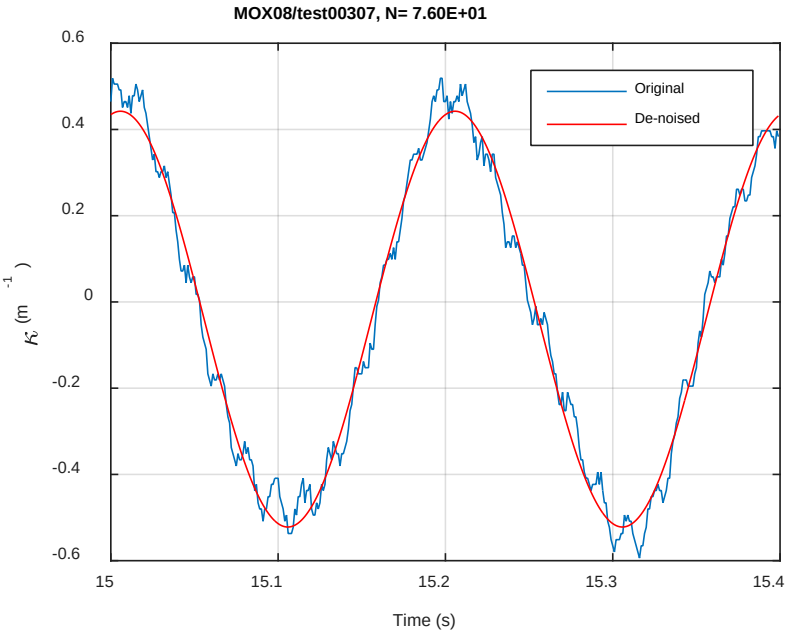

(c)

Fig. C.21. Monitoring-based responses: (a) curvature, (b) moment, (c) curvature, MOX08, 12.70 Nm, Ns = 7.60E+01 cycles.

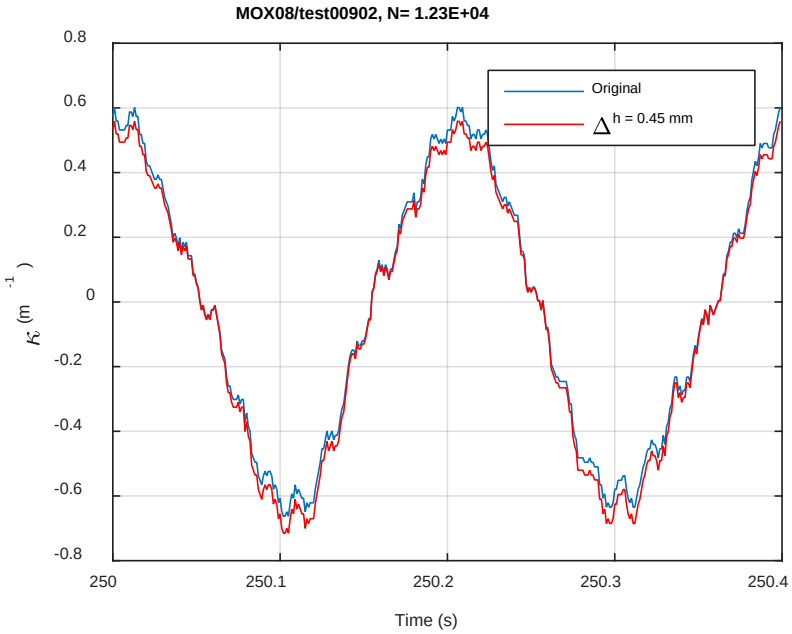
MOX08/test00902, N= 1.23E+04
Original
Δh = 0.45 mm
κ (m-1)
Time (s)
0.8
0.6
0.4
0.2
0
-0.2
-0.4
-0.6
-0.8
250
250.1
250.2
250.3
250.4

(a)

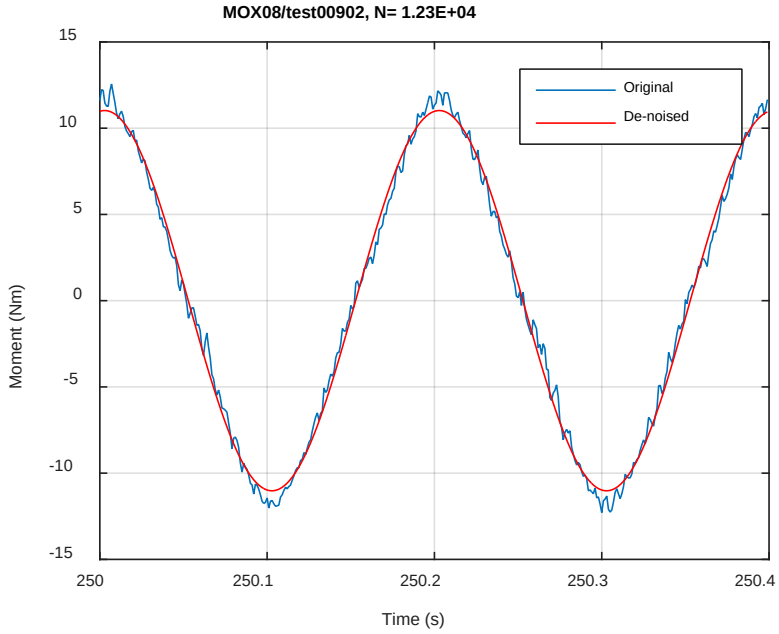
MOX08/test00902, N= 1.23E+04
Original
De-noised
Moment (Nm)
Time (s)
15
10
5
0
-5
-10
-15
250
250.1
250.2
250.3
250.4

(b)

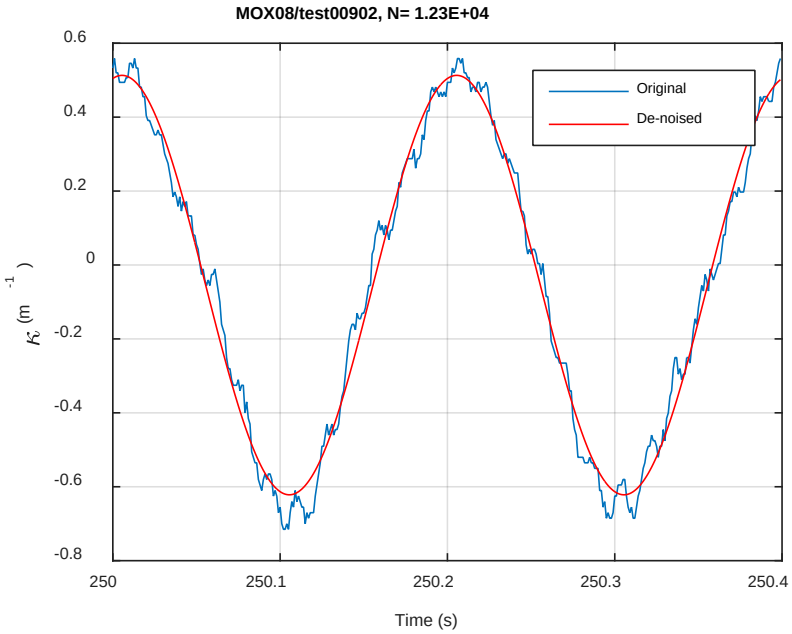

(c)

Fig. C.22. Monitoring-based responses: (a) curvature, (b) moment, (c) curvature, MOX08, 12.70 Nm, Ns = 1.23E+04 cycles.

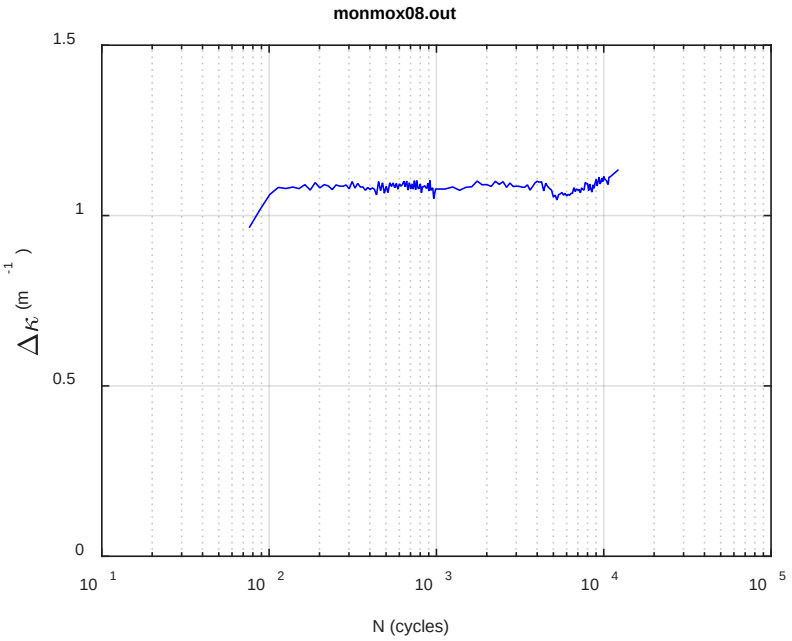
monmox08.out
1.5
1
0.5
0
$\Delta\kappa$ (m^{-1})
10^1
10^2
10^3
10^4
10^5
N (cycles)

(a)

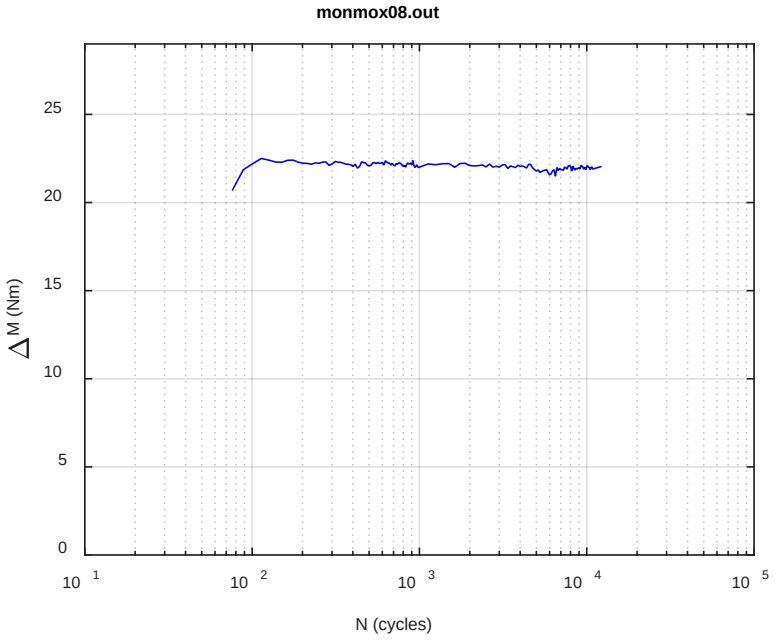
monmox08.out
25
20
15
10
5
0
Δ M (Nm)
10^1
10^2
10^3
10^4
10^5
N (cycles)

(b)

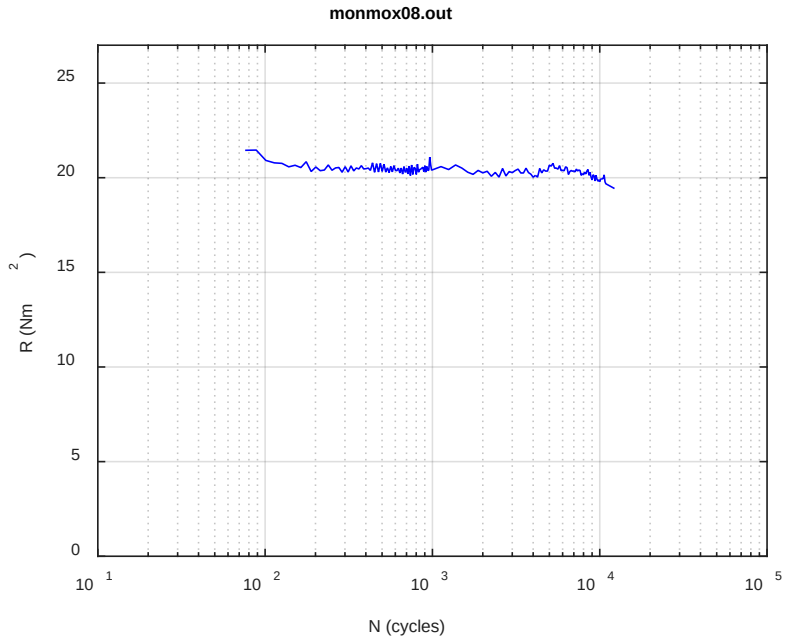
monmox08.out
25
20
15
10
5
0
R (Nm 2)
10 1
10 2
10 3
10 4
10 5
N (cycles)

(c)

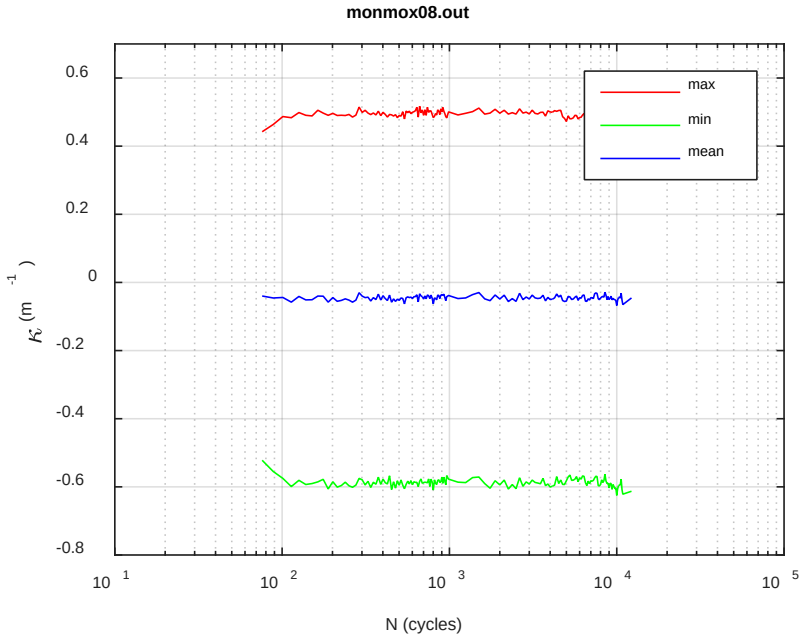
monmox08.out
max
min
mean
0.6
0.4
0.2
0
-0.2
-0.4
-0.6
-0.8
κ (m -1)
10 1
10 2
10 3
10 4
10 5
N (cycles)

(d)

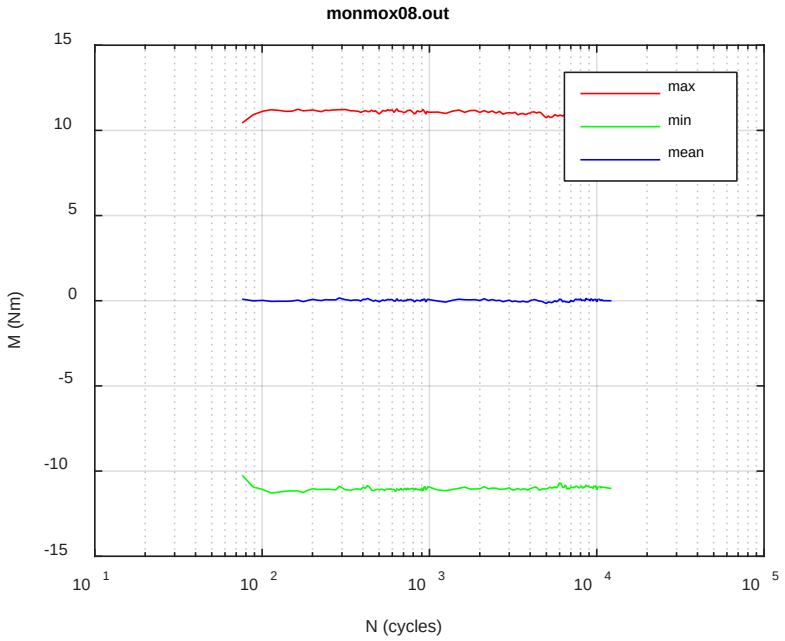

(e)

Fig. C.23. Monitoring-based responses: (a) curvature range, (b) moment range, (c) rigidity, (d) curvature peak/valley, (e) moment peak/valley, MOX08, 12.70 Nm, Nf = 1.29E+04 cycles.

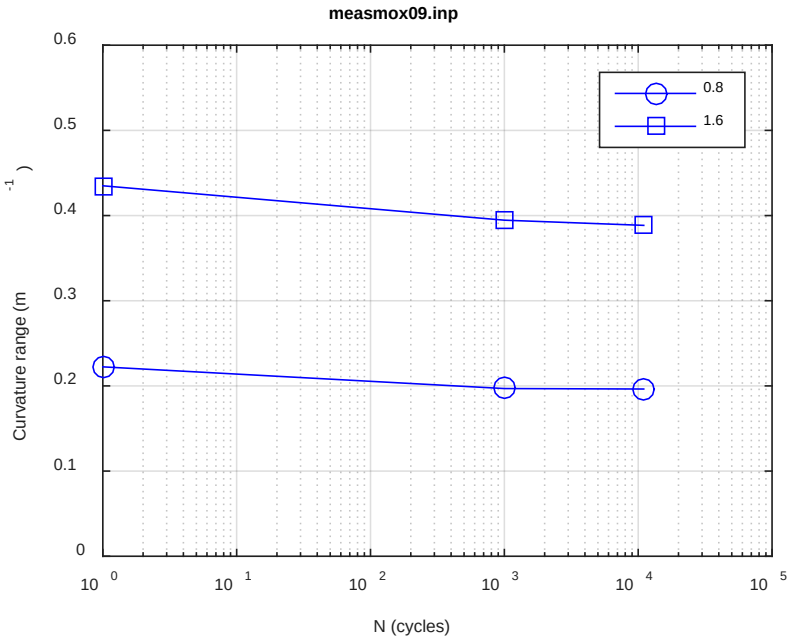
measmox09.inp
0.8
1.6
Curvature range (m -1)
N (cycles)
0
0.1
0.2
0.3
0.4
0.5
0.6
10 0
10 1
10 2
10 3
10 4
10 5

(a)

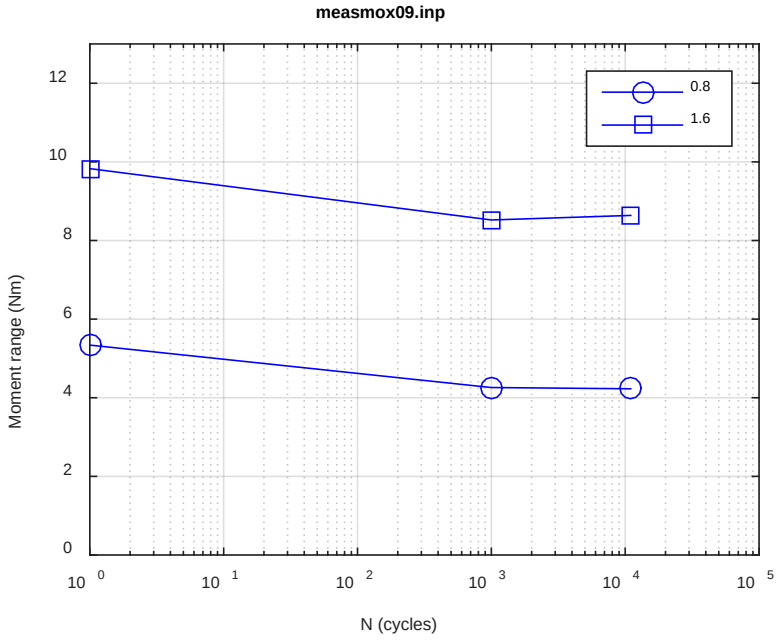
measmox09.inp
0.8
1.6
Moment range (Nm)
N (cycles)
0
2
4
6
8
10
12
10 0
10 1
10 2
10 3
10 4
10 5

(b)

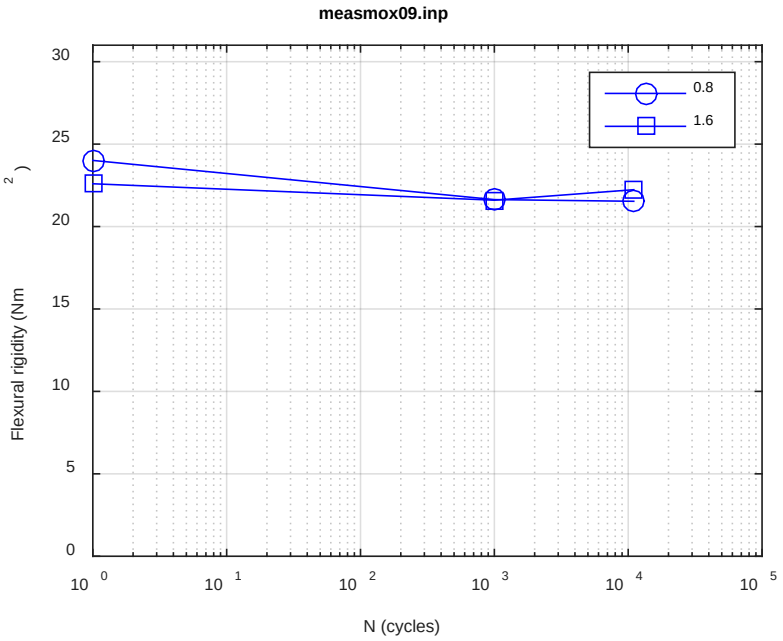
measmox09.inp
0.8
1.6
Flexural rigidity (Nm 2)
N (cycles)

(c)

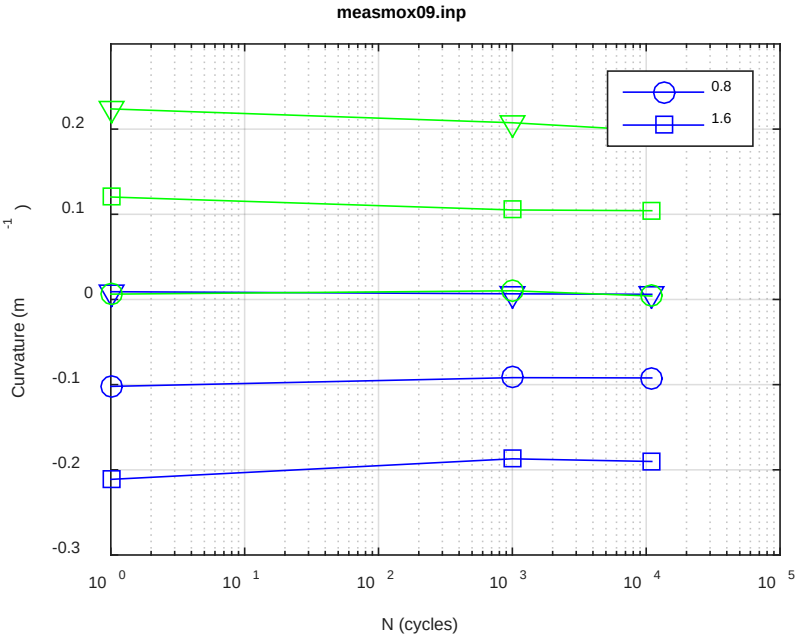
measmox09.inp
0.8
1.6
Curvature (m -1)
N (cycles)

(d)

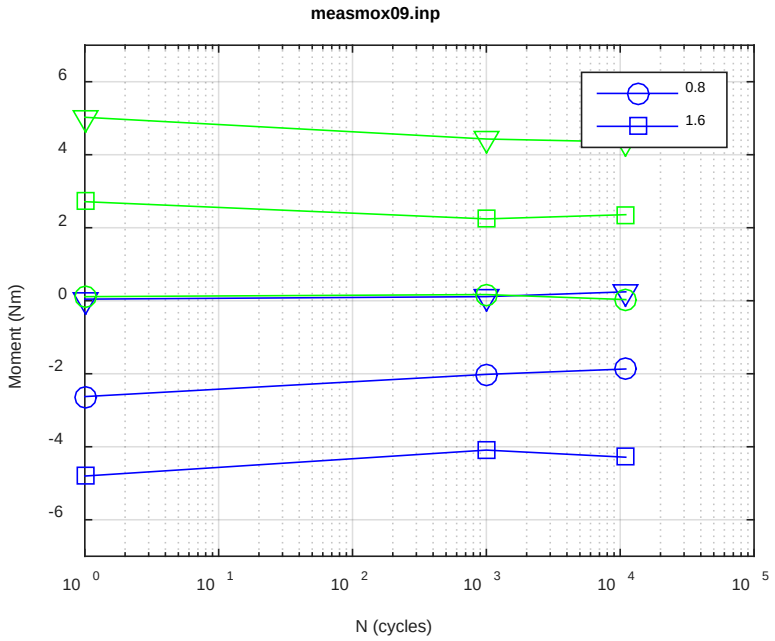

(e)

Fig. C.24. Measurement-based responses: (a) curvature range, (b) moment range, (c) rigidity, (d) curvature peak/valley, (e) moment peak/valley, MOX09, 7.62 Nm.

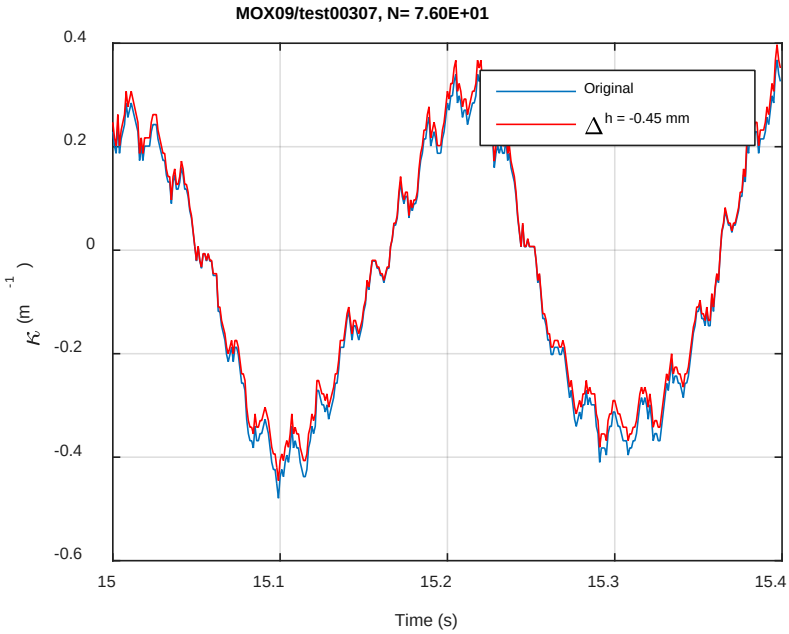
MOX09/test00307, N= 7.60E+01
Original
Δh = -0.45 mm
κ (m-1)
Time (s)
0.4
0.2
0
-0.2
-0.4
-0.6
15
15.1
15.2
15.3
15.4

(a)

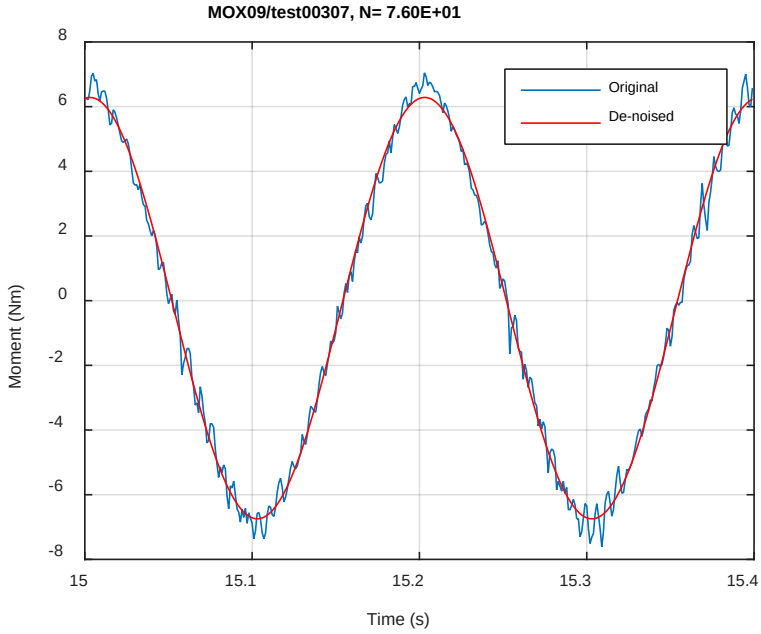
MOX09/test00307, N= 7.60E+01
Original
De-noised
Moment (Nm)
Time (s)
8
6
4
2
0
-2
-4
-6
-8
15
15.1
15.2
15.3
15.4

(b)

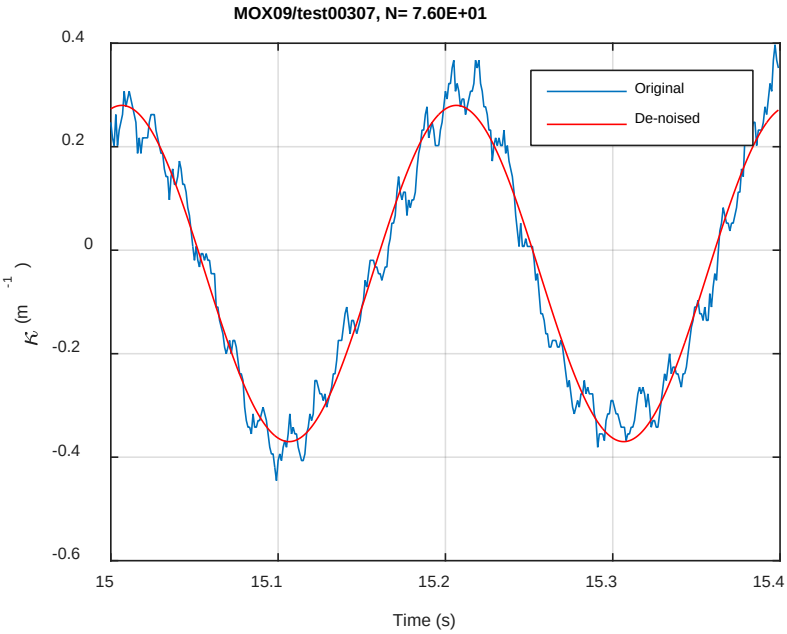

(c)

Fig. C.25. Monitoring-based responses: (a) curvature, (b) moment, (c) curvature, MOX09, 7.62 Nm, Ns = 7.60E+01 cycles.

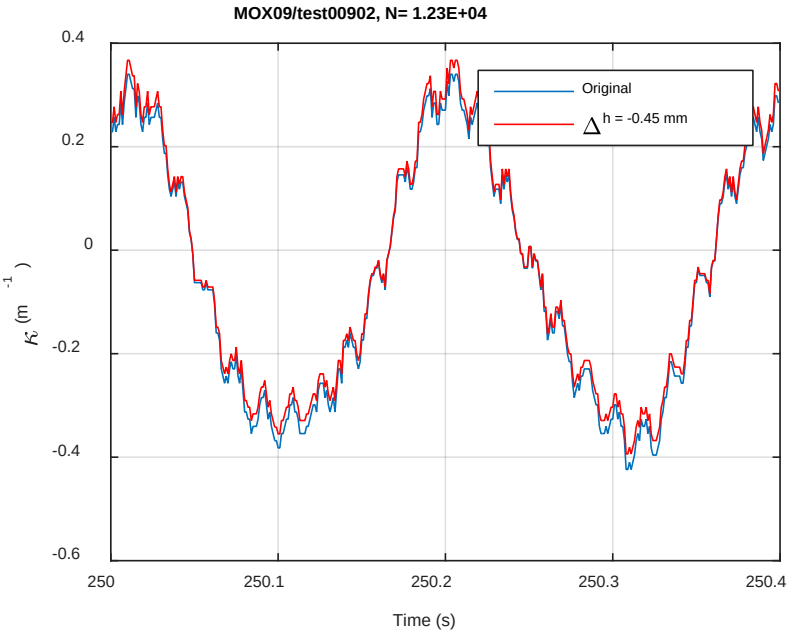
MOX09/test00902, N= 1.23E+04
Original
Δh = -0.45 mm
κ (m-1)
Time (s)
0.4
0.2
0
-0.2
-0.4
-0.6
250
250.1
250.2
250.3
250.4

(a)

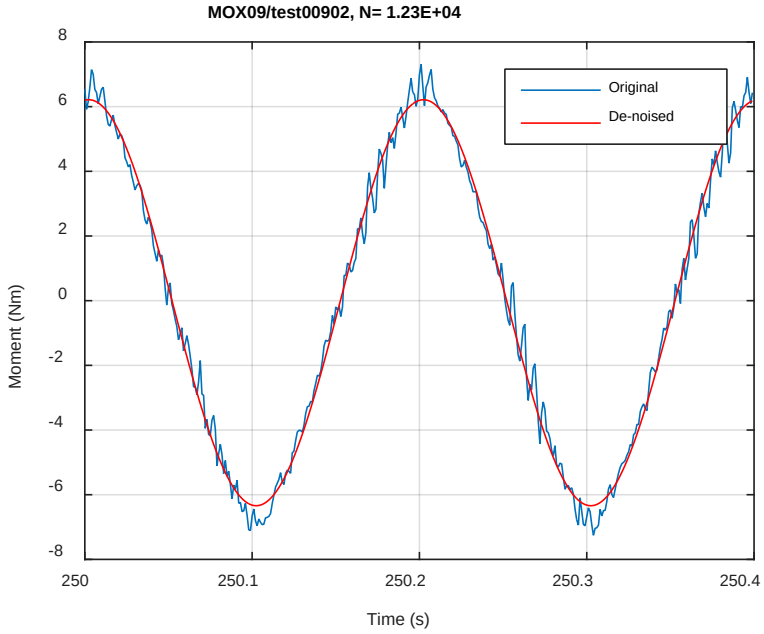
MOX09/test00902, N= 1.23E+04
Original
De-noised
Moment (Nm)
Time (s)
8
6
4
2
0
-2
-4
-6
-8
250
250.1
250.2
250.3
250.4

(b)

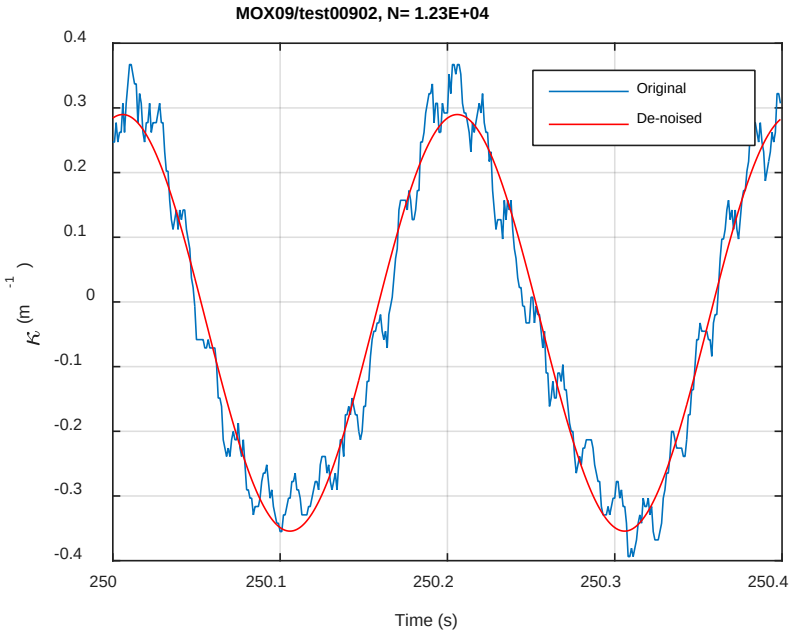

(c)

Fig. C.26. Monitoring-based responses: (a) curvature, (b) moment, (c) curvature, MOX09, 7.62 Nm, Ns = 1.23E+04 cycles.

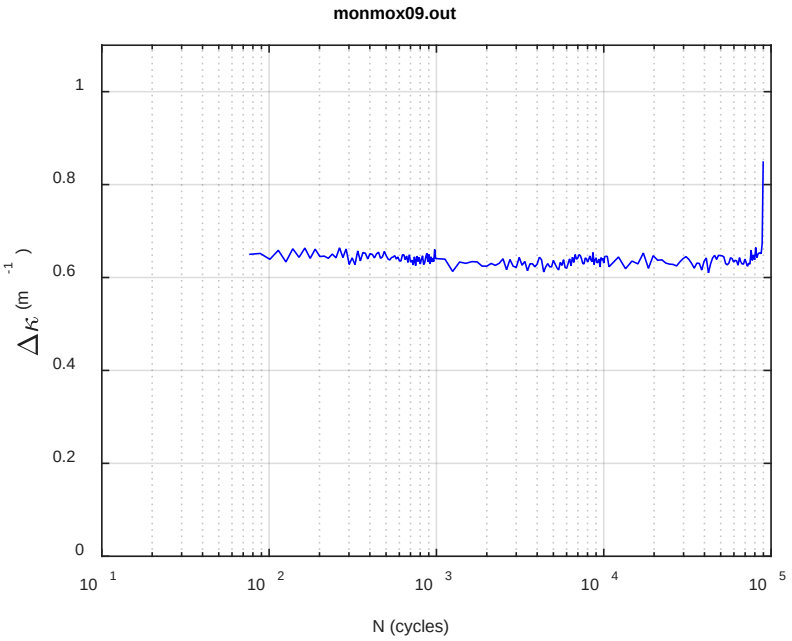
monmox09.out
1
0.8
0.6
0.4
0.2
0
Δκ (m -1)
10 1
10 2
10 3
10 4
10 5
N (cycles)

(a)

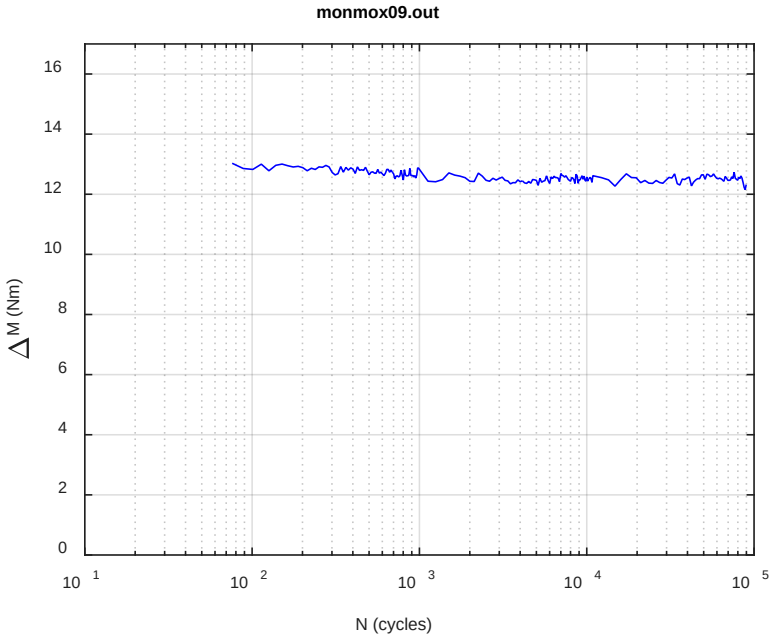
monmox09.out
16
14
12
10
8
6
4
2
0
Δ M (Nm)
10 1
10 2
10 3
10 4
10 5
N (cycles)

(b)

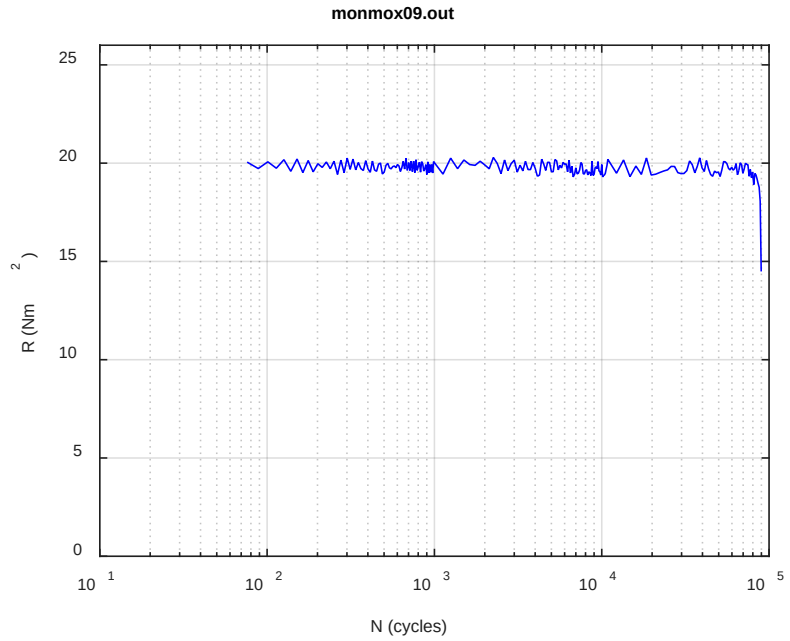
monmox09.out
25
20
15
10
5
0
R (Nm 2)
10 1
10 2
10 3
10 4
10 5
N (cycles)

(c)

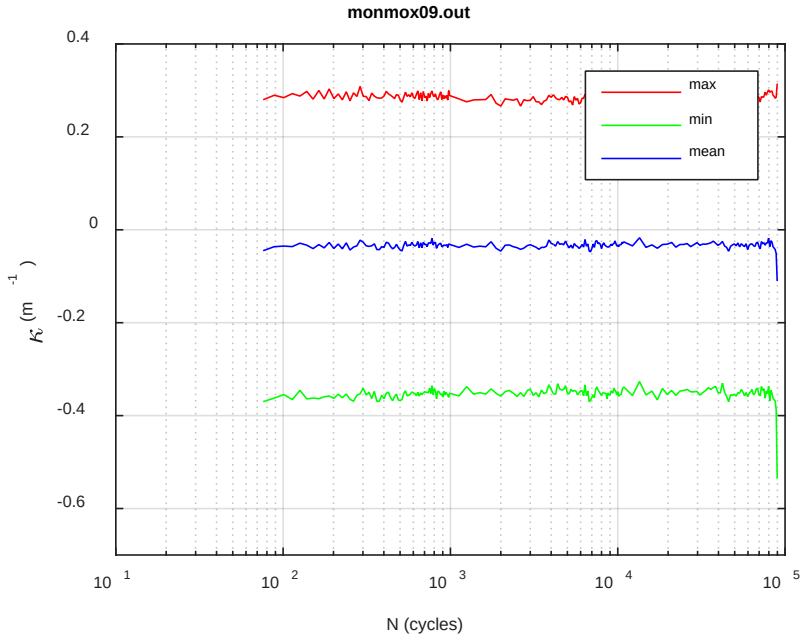
monmox09.out
max
min
mean
0.4
0.2
0
-0.2
-0.4
-0.6
κ (m -1)
10 1
10 2
10 3
10 4
10 5
N (cycles)

(d)

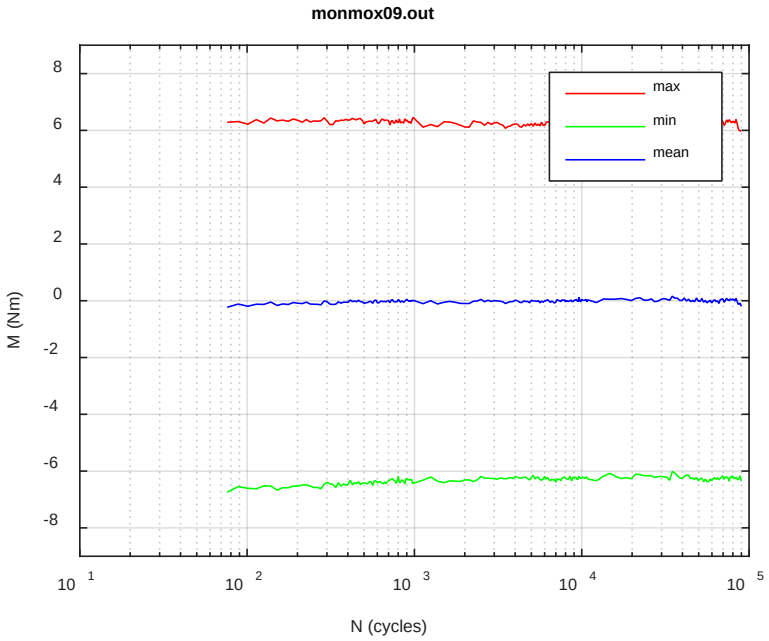

(e)

Fig. C.27. Monitoring-based responses: (a) curvature range, (b) moment range, (c) rigidity, (d) curvature peak/valley, (e) moment peak/valley, MOX09, 7.62 Nm, Nf = 8.98E+04 cycles.

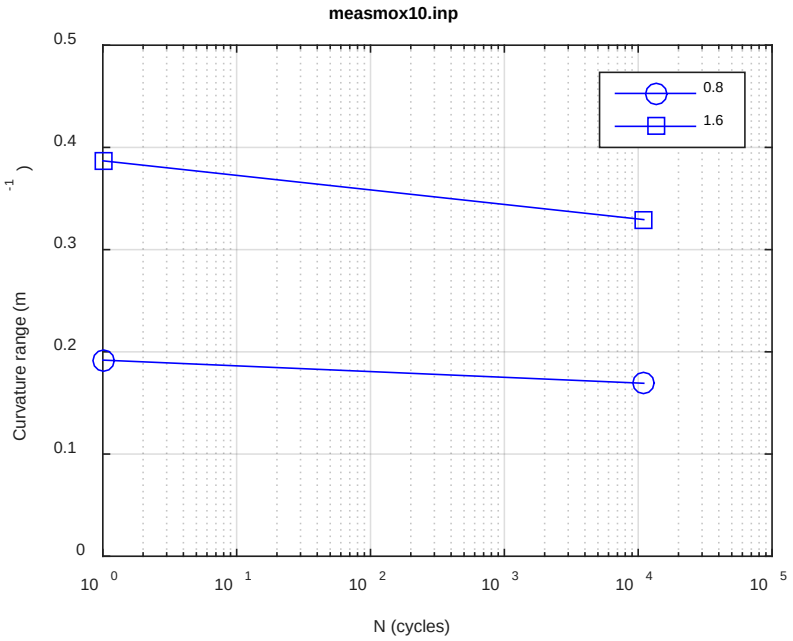
measmox10.inp
0.8
1.6
Curvature range (m-1)
N (cycles)
0
0.1
0.2
0.3
0.4
0.5
10 0
10 1
10 2
10 3
10 4
10 5

(a)

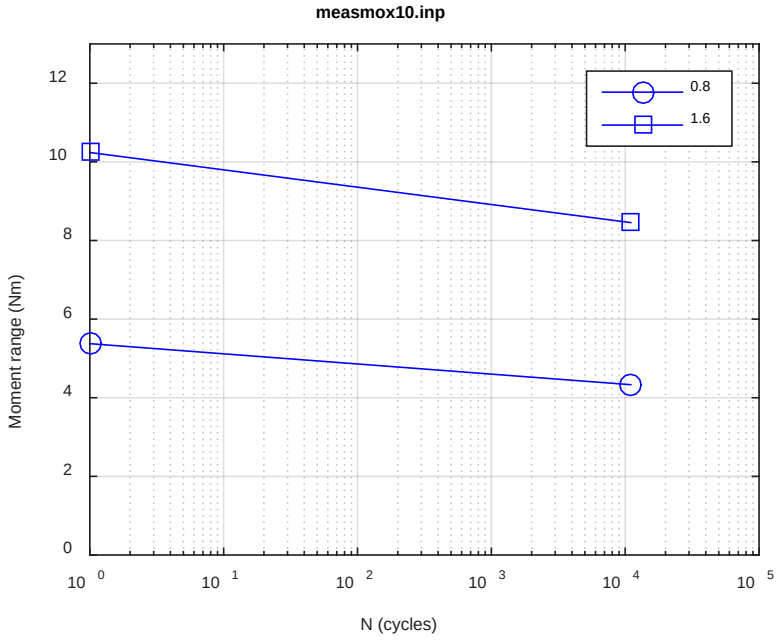
measmox10.inp
0.8
1.6
Moment range (Nm)
N (cycles)
0
2
4
6
8
10
12
10 0
10 1
10 2
10 3
10 4
10 5

(b)

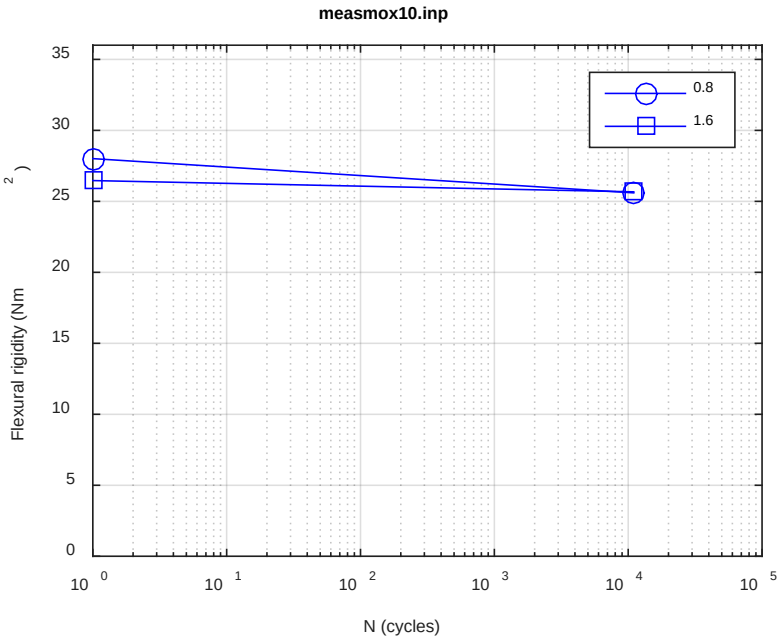
measmox10.inp
0.8
1.6
Flexural rigidity (Nm 2)
N (cycles)

(c)

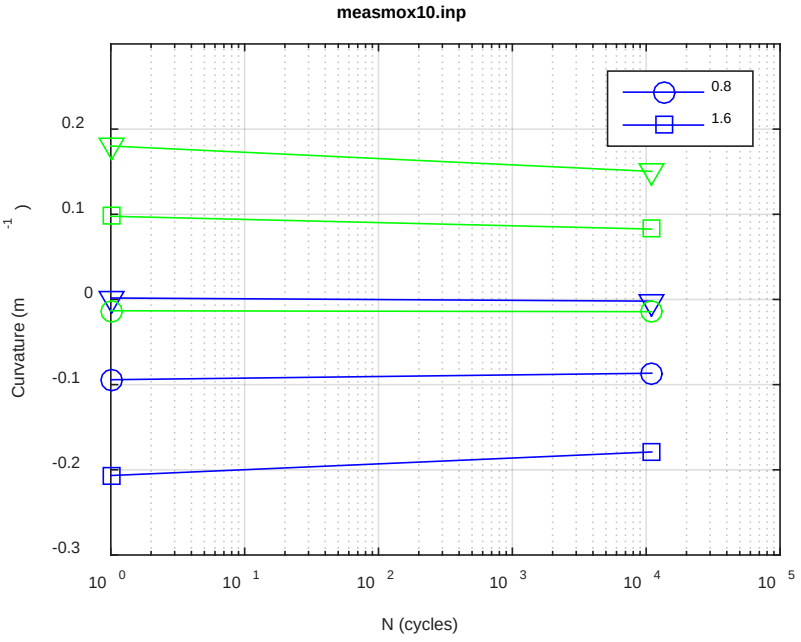
measmox10.inp
0.8
1.6
Curvature (m -1)
N (cycles)

(d)

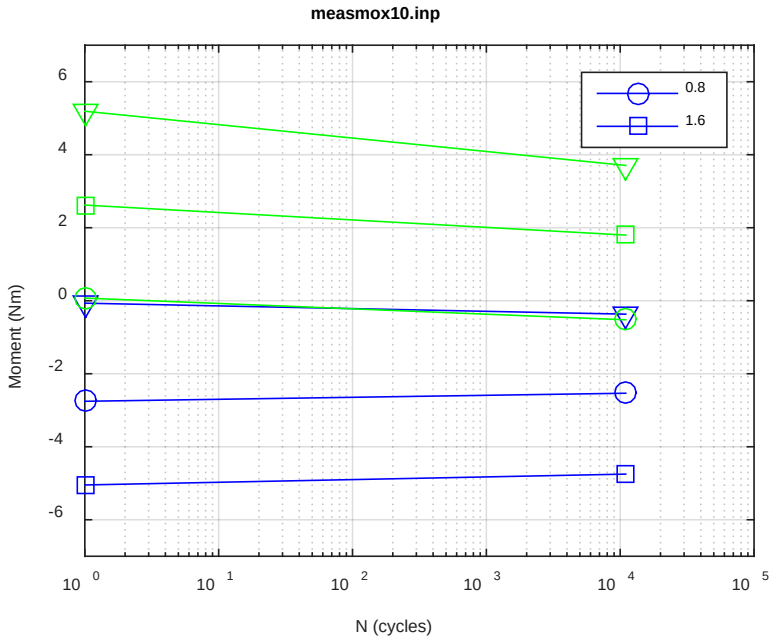

(e)

Fig. C.28. Measurement-based responses: (a) curvature range, (b) moment range, (c) rigidity, (d) curvature peak/valley, (e) moment peak/valley, MOX10, 10.16 Nm.

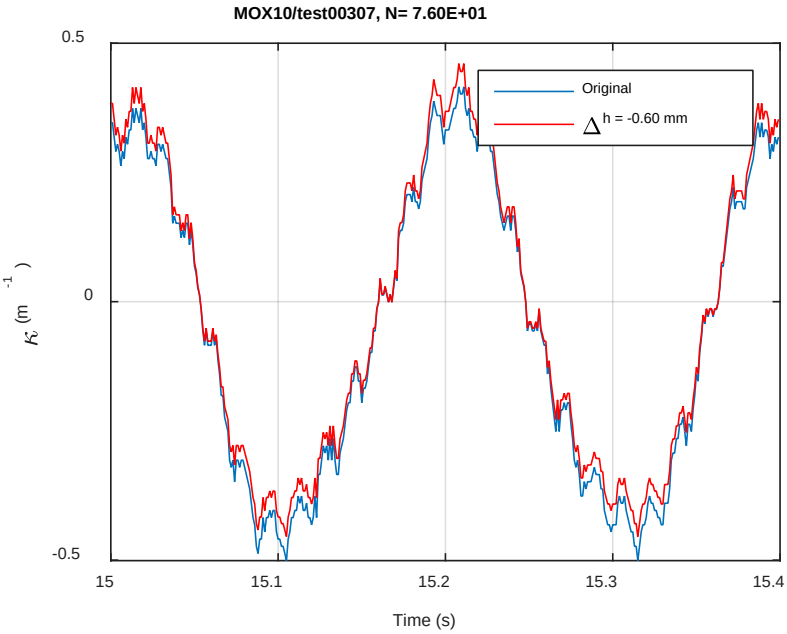
MOX10/test00307, N= 7.60E+01
Original
Δh = -0.60 mm
κ (m-1)
Time (s)
0.5
0
-0.5
15
15.1
15.2
15.3
15.4

(a)

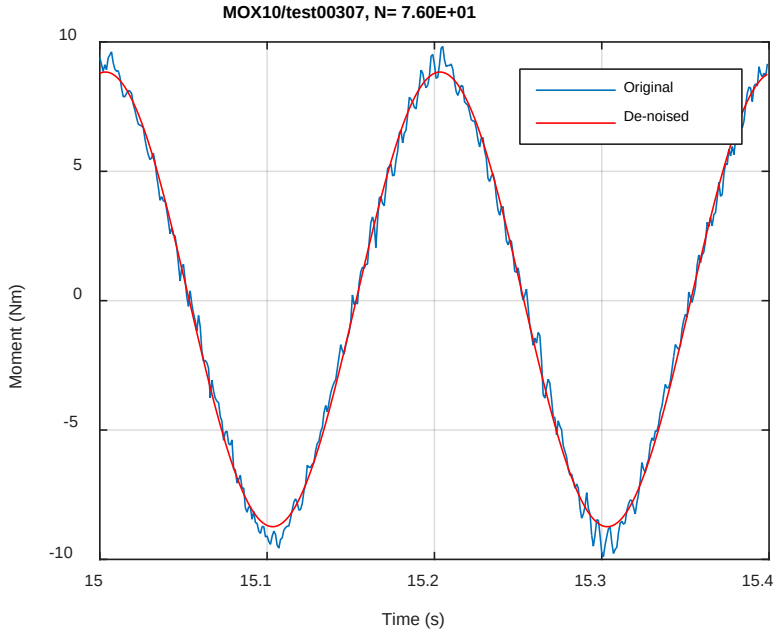
MOX10/test00307, N= 7.60E+01
Original
De-noised
Moment (Nm)
Time (s)
10
5
0
-5
-10
15
15.1
15.2
15.3
15.4

(b)

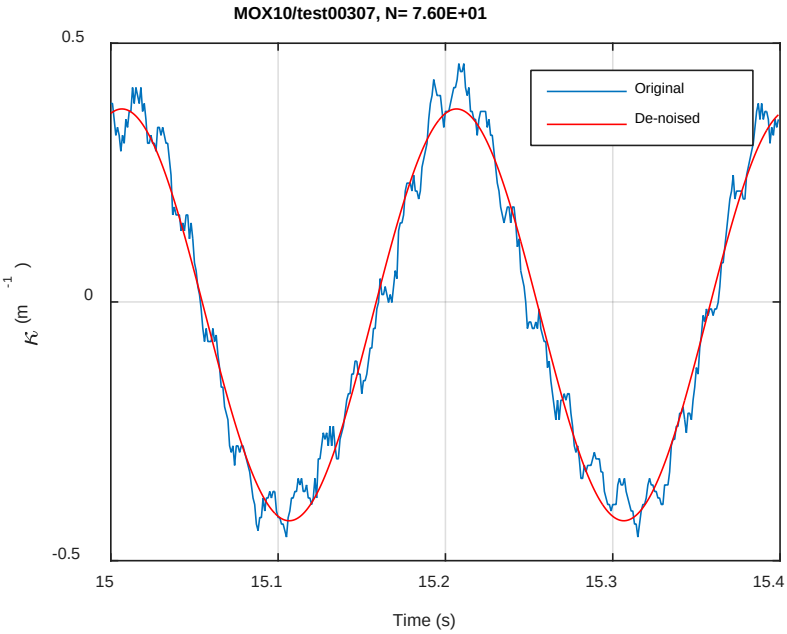

(c)

Fig. C.29. Monitoring-based responses: (a) curvature, (b) moment, (c) curvature, MOX10, 10.16 Nm, Ns = 7.60E+01 cycles.

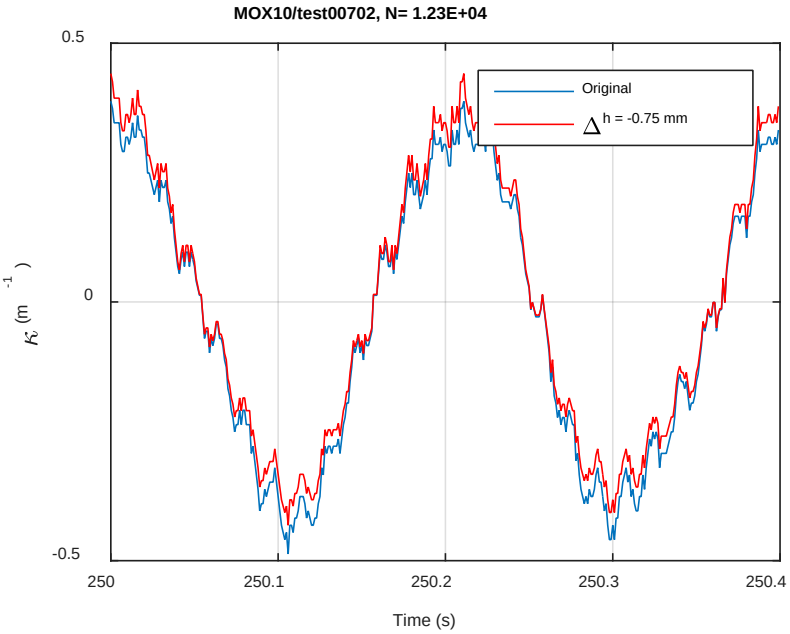
MOX10/test00702, N= 1.23E+04
Original
Δh = -0.75 mm
κ (m-1)
0.5
0
-0.5
250
250.1
250.2
250.3
250.4
Time (s)

(a)

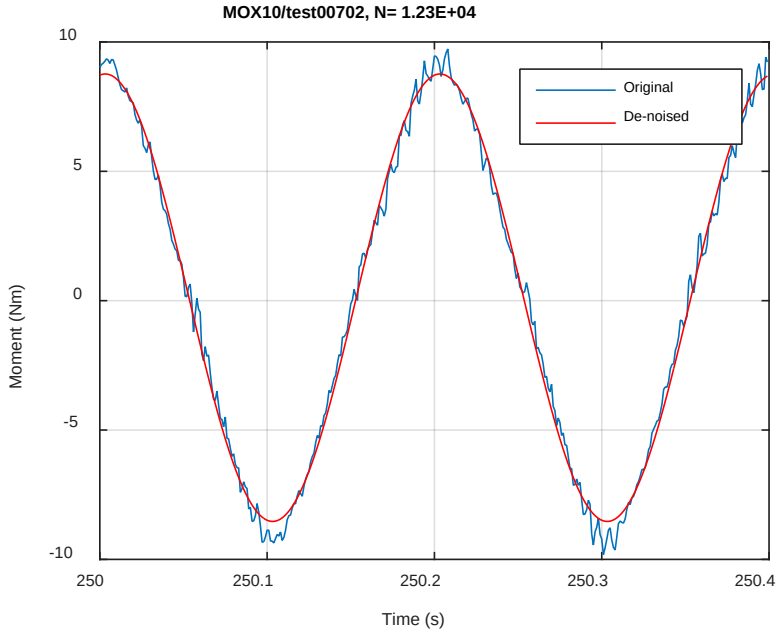
MOX10/test00702, N= 1.23E+04
Original
De-noised
Moment (Nm)
10
5
0
-5
-10
250
250.1
250.2
250.3
250.4
Time (s)

(b)

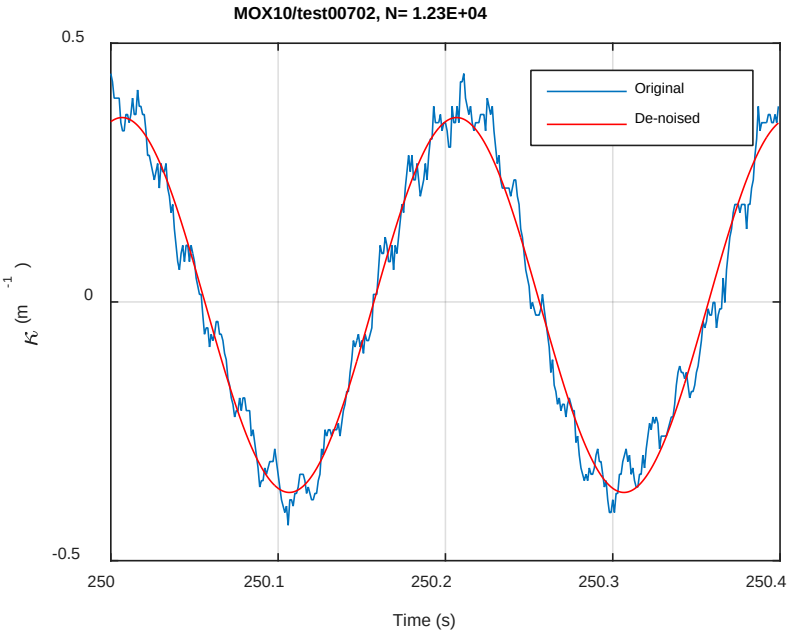

(c)

Fig. C.30. Monitoring-based responses: (a) curvature, (b) moment, (c) curvature, MOX10, 10.16 Nm, Ns = 1.23E+04 cycles.

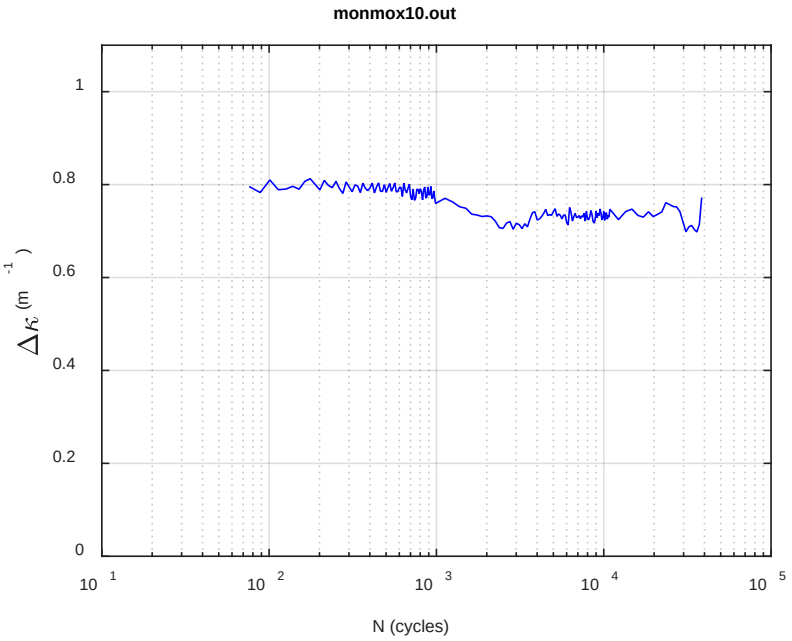
monmox10.out
1
0.8
0.6
0.4
0.2
0
Δκ (m -1)
10 1
10 2
10 3
10 4
10 5
N (cycles)

(a)

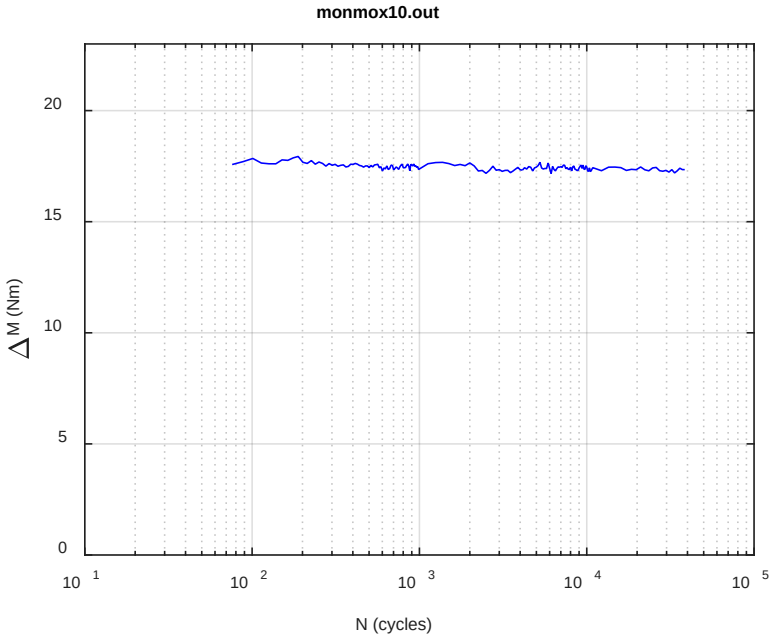
monmox10.out
20
15
10
5
0
ΔM (Nm)
10 1
10 2
10 3
10 4
10 5
N (cycles)

(b)

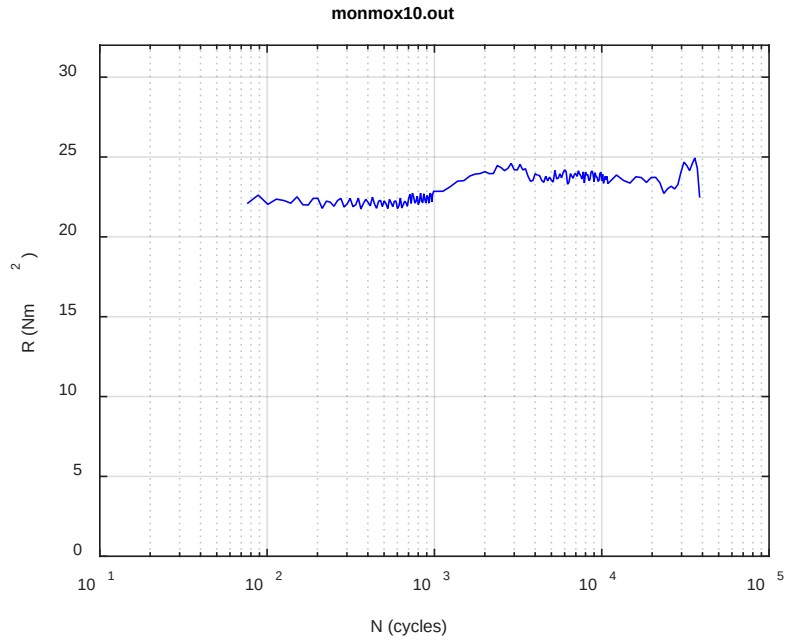
monmox10.out
30
25
20
15
10
5
0
R (Nm 2)
10 1
10 2
10 3
10 4
10 5
N (cycles)

(c)

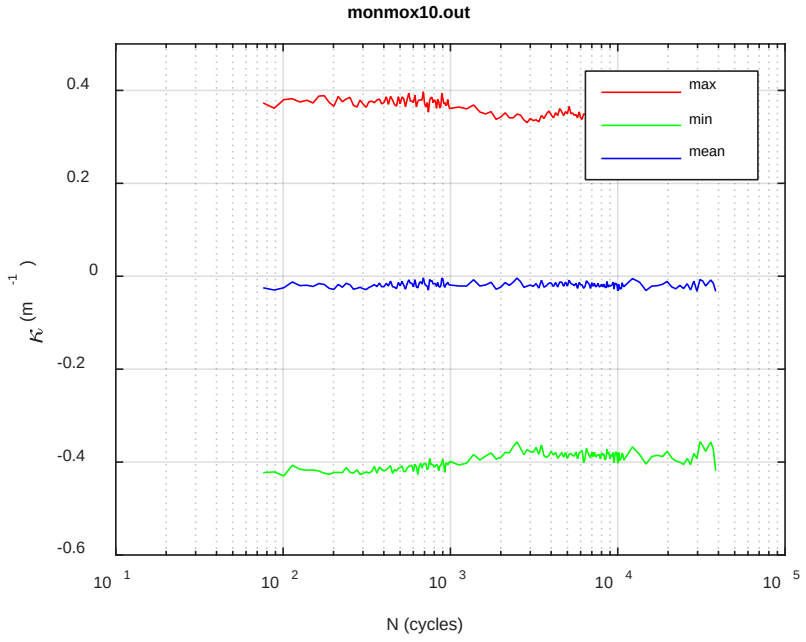
monmox10.out
max
min
mean
0.4
0.2
0
-0.2
-0.4
-0.6
κ (m -1)
10 1
10 2
10 3
10 4
10 5
N (cycles)

(d)

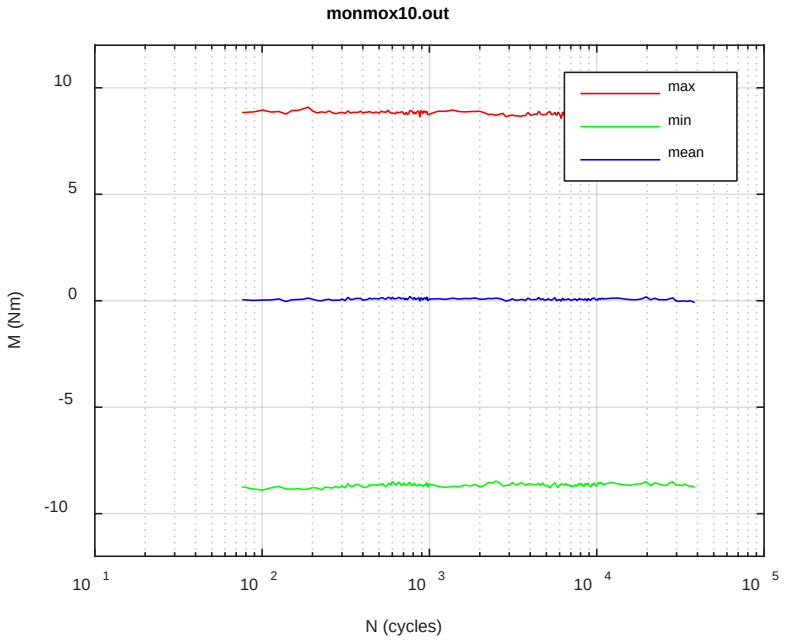

(e)

Fig. C.31. Monitoring-based responses: (a) curvature range, (b) moment range, (c) rigidity, (d) curvature peak/valley, (e) moment peak/valley, MOX10, 10.16 Nm, Nf = 3.85E+04 cycles.

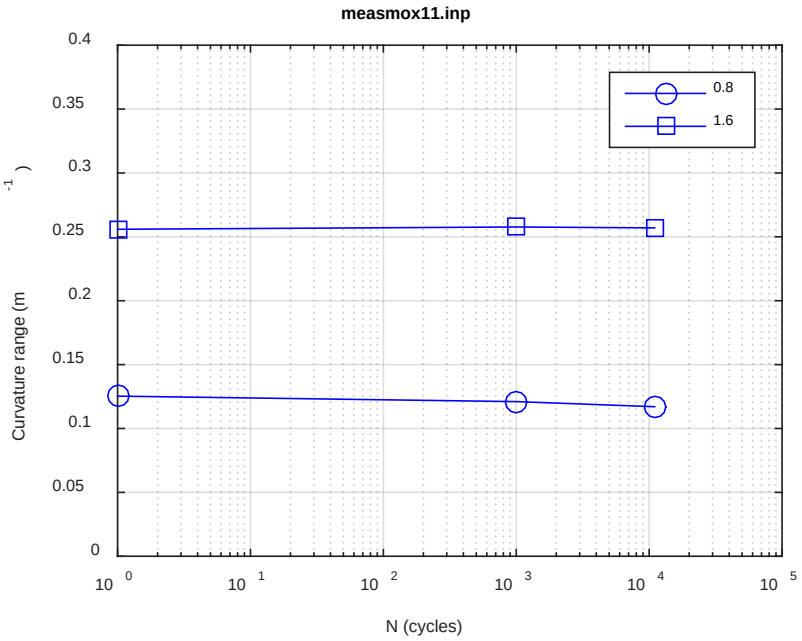
measmox11.inp
0.8
1.6
Curvature range (m-1)
N (cycles)
0
0.05
0.1
0.15
0.2
0.25
0.3
0.35
0.4
10 0
10 1
10 2
10 3
10 4
10 5

(a)

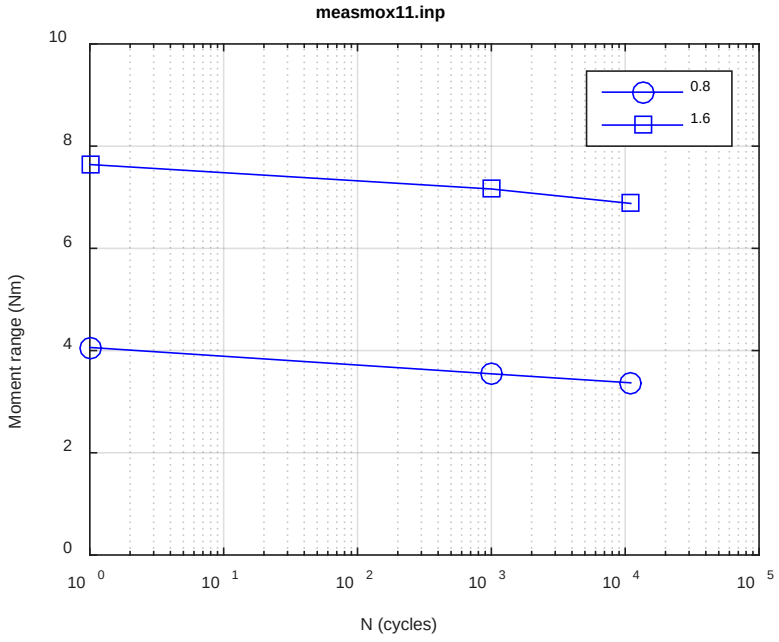
measmox11.inp
0.8
1.6
Moment range (Nm)
N (cycles)
0
2
4
6
8
10
10 0
10 1
10 2
10 3
10 4
10 5

(b)

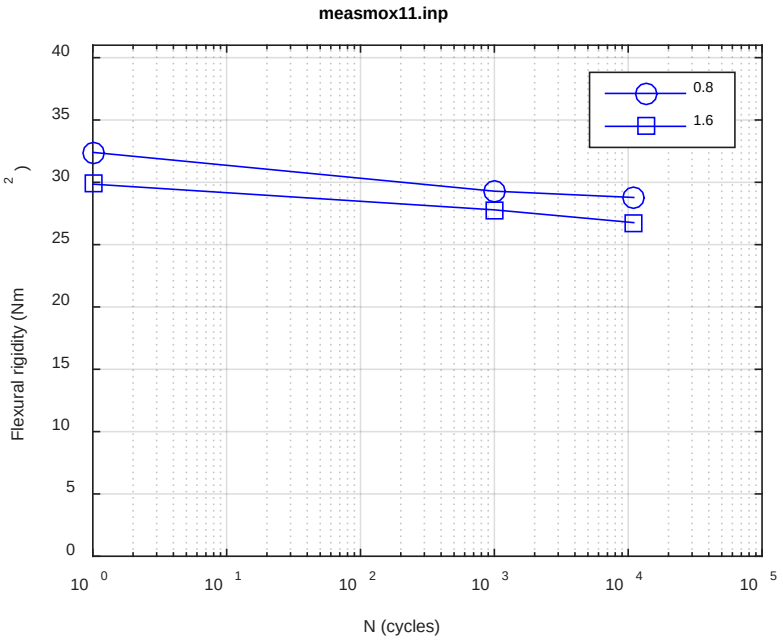
measmox11.inp
0.8
1.6
Flexural rigidity (Nm 2)
N (cycles)
40
35
30
25
20
15
10
5
0
10 0
10 1
10 2
10 3
10 4
10 5

(c)

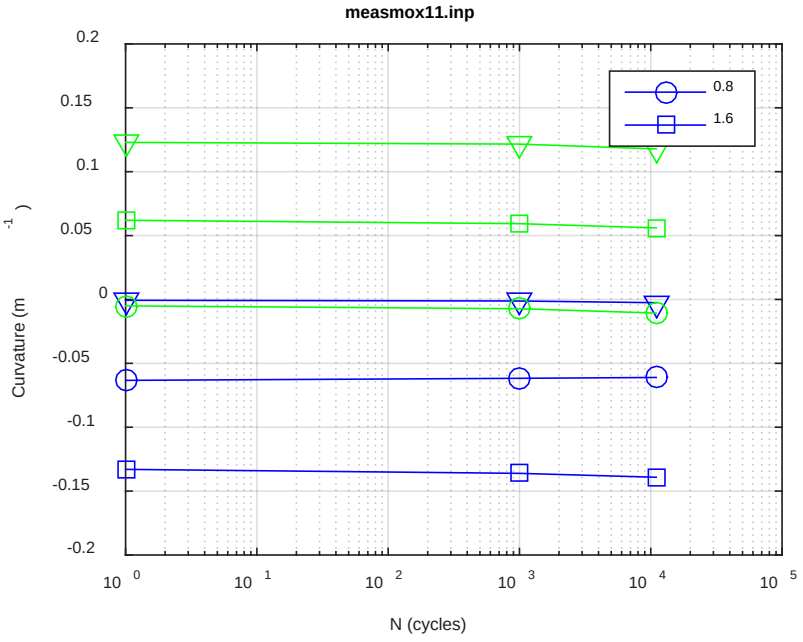
measmox11.inp
0.8
1.6
Curvature (m -1)
N (cycles)
0.2
0.15
0.1
0.05
0
-0.05
-0.1
-0.15
-0.2
10 0
10 1
10 2
10 3
10 4
10 5

(d)

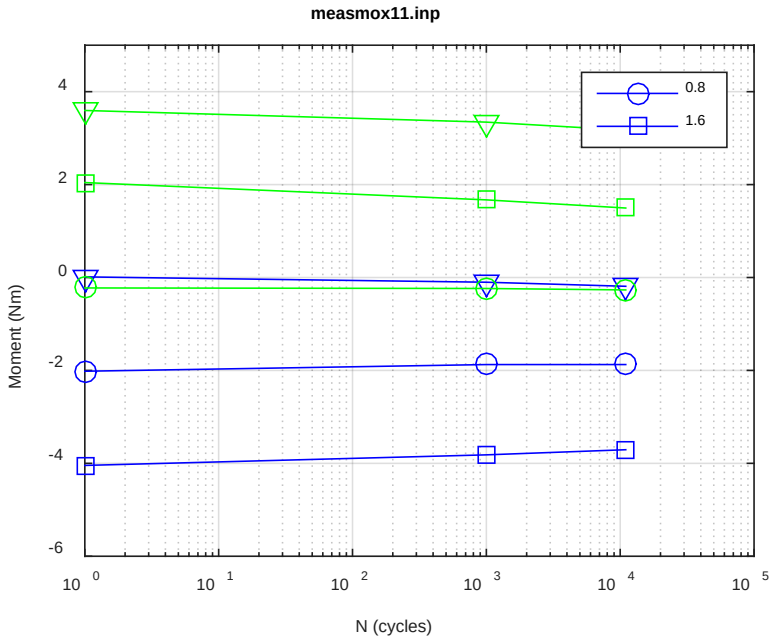

(e)

Fig. C.32. Measurement-based responses: (a) curvature range, (b) moment range, (c) rigidity, (d) curvature peak/valley, (e) moment peak/valley, MOX11, 10.16 Nm.

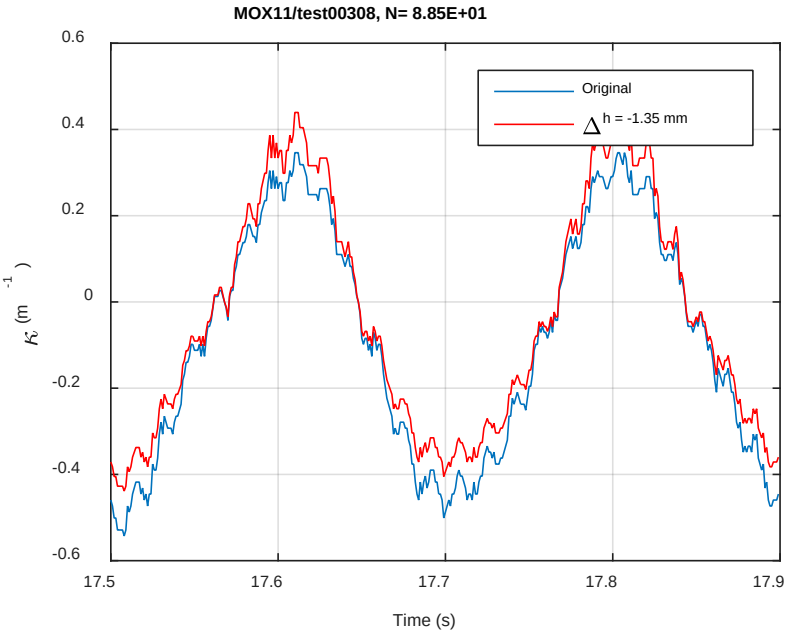
MOX11/test00308, N= 8.85E+01
Original
Δh = -1.35 mm
κ (m-1)
Time (s)

(a)

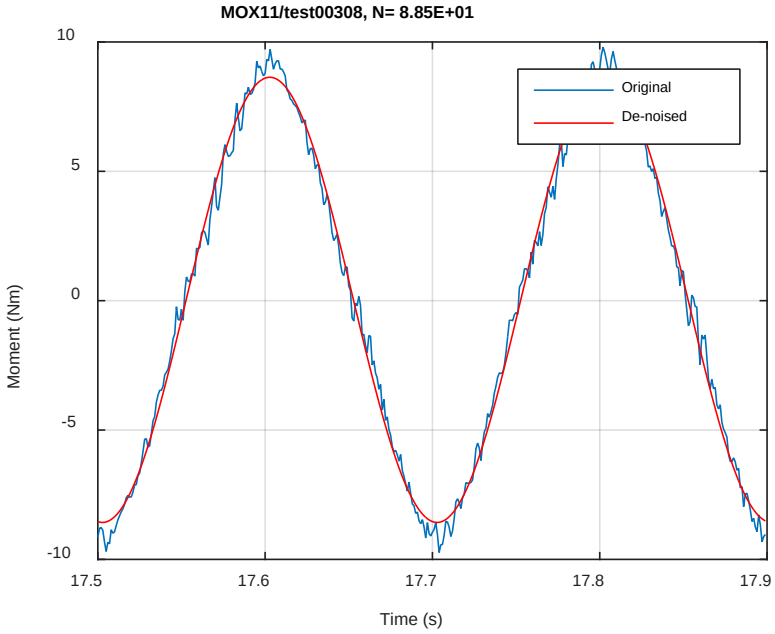
MOX11/test00308, N= 8.85E+01
Original
De-noised
Moment (Nm)
Time (s)

(b)

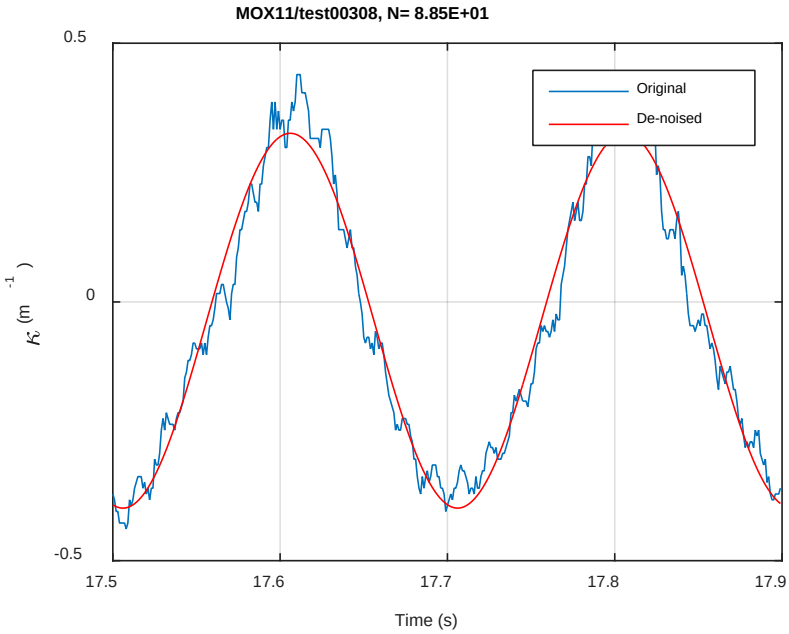

(c)

Fig. C.33. Monitoring-based responses: (a) curvature, (b) moment, (c) curvature, MOX11, 10.16 Nm, Ns = 8.85E+01 cycles.

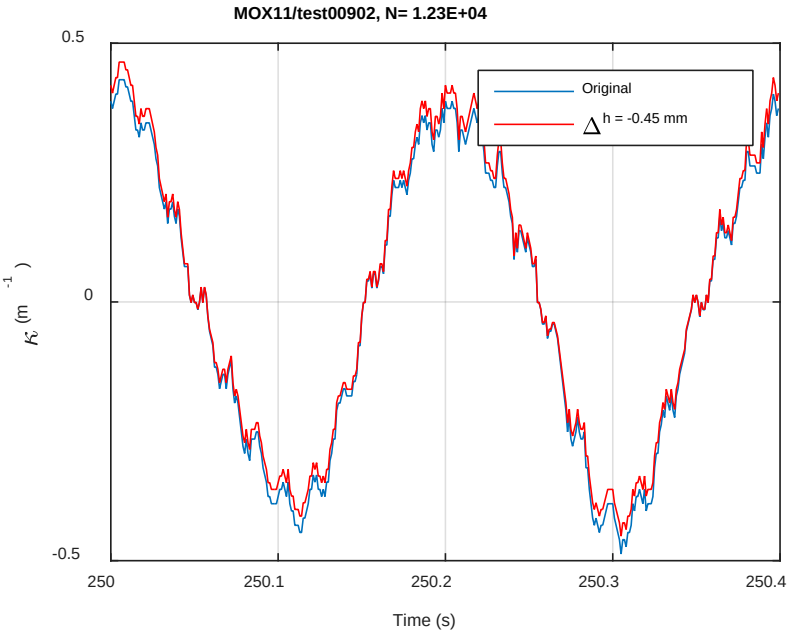
MOX11/test00902, N= 1.23E+04
Original
Δh = -0.45 mm
κ (m-1)
Time (s)
0.5
0
-0.5
250
250.1
250.2
250.3
250.4

(a)

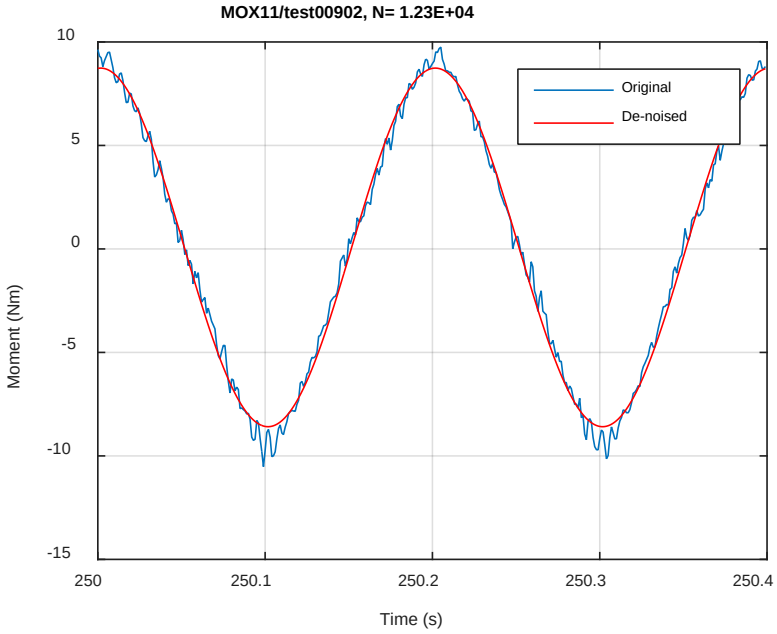
MOX11/test00902, N= 1.23E+04
Original
De-noised
Moment (Nm)
Time (s)
10
5
0
-5
-10
-15
250
250.1
250.2
250.3
250.4

(b)

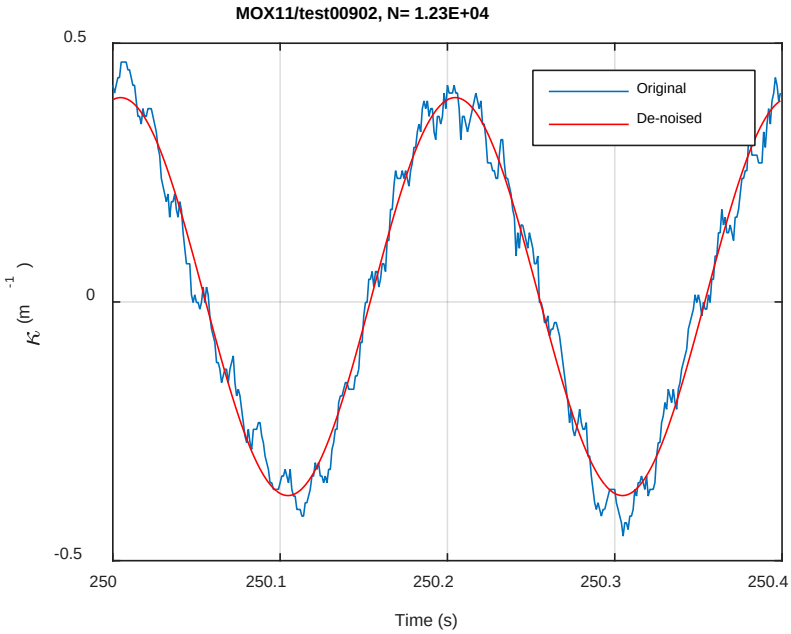

(c)

Fig. C.34. Monitoring-based responses: (a) curvature, (b) moment, (c) curvature, MOX11, 10.16 Nm, Ns = 1.23E+04 cycles.

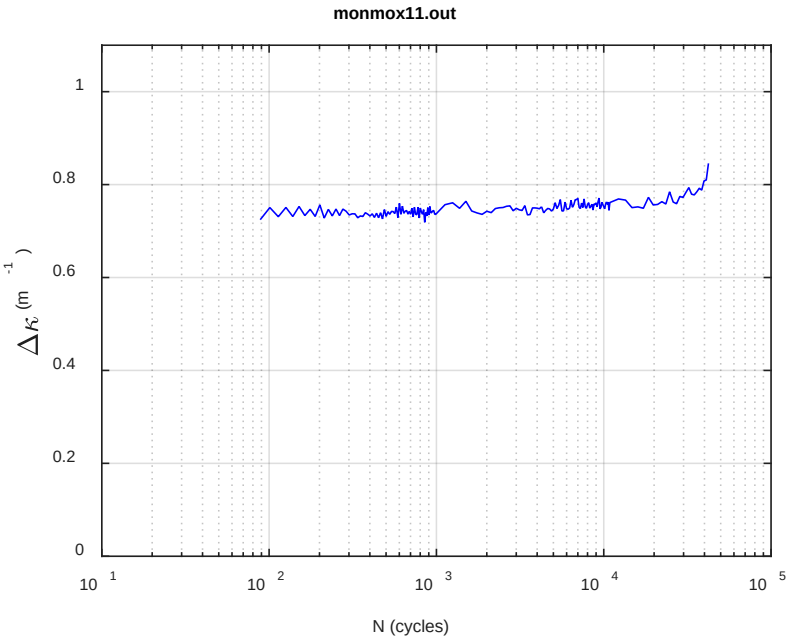
monmox11.out
1
0.8
0.6
0.4
0.2
0
Δκ (m-1)
10 1
10 2
10 3
10 4
10 5
N (cycles)

(a)

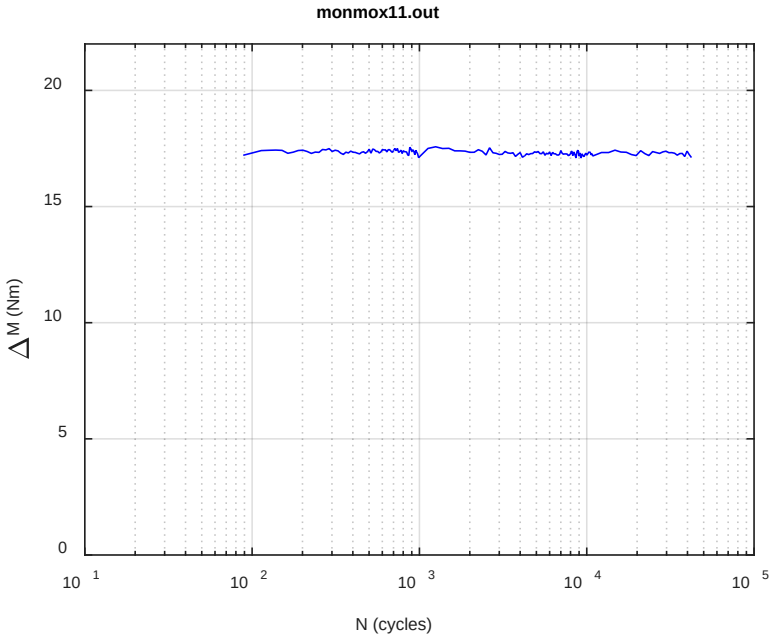
monmox11.out
20
15
10
5
0
Δ M (Nm)
10 1
10 2
10 3
10 4
10 5
N (cycles)

(b)

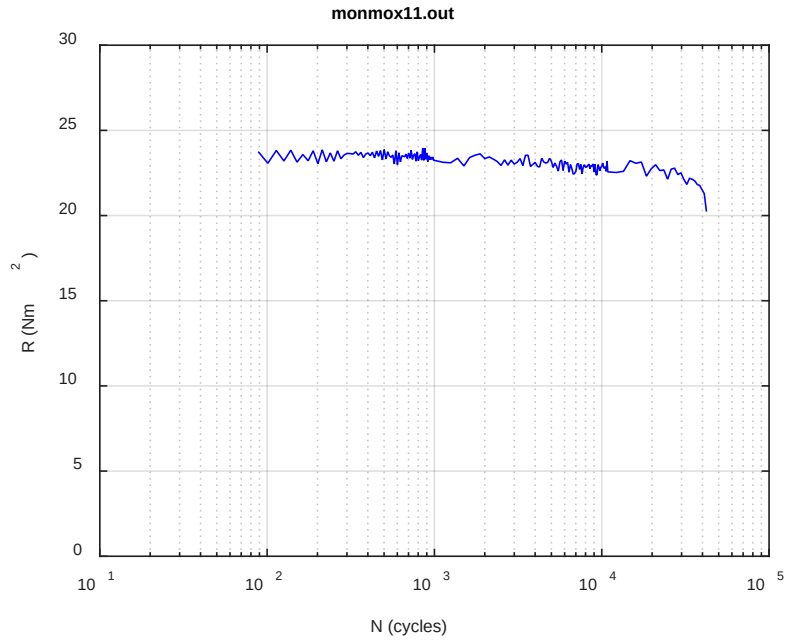
monmox11.out
R (Nm 2)
N (cycles)

(c)

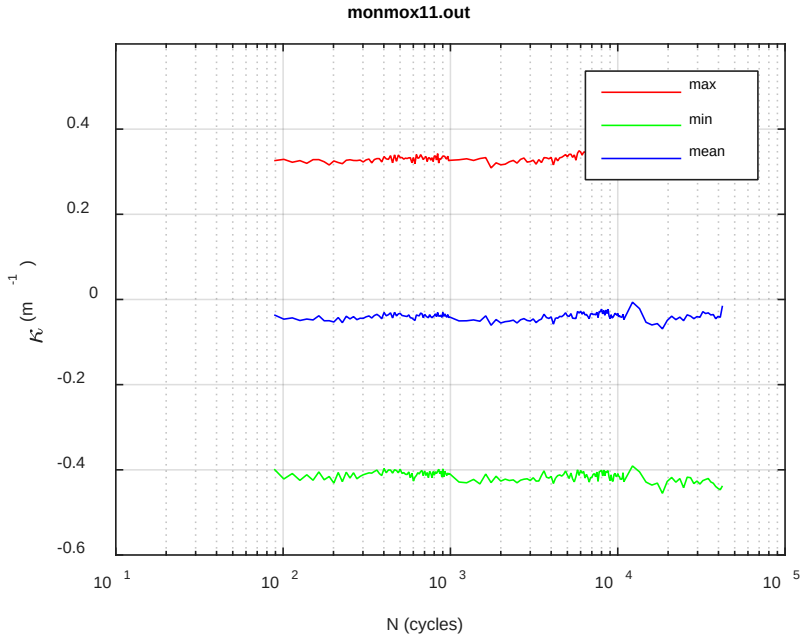
monmox11.out
max
min
mean
κ (m -1)
N (cycles)

(d)

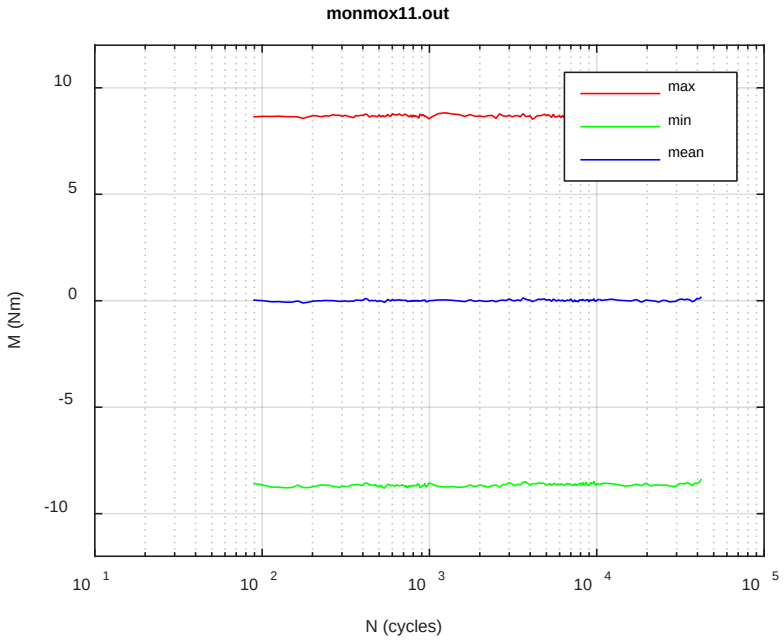

(e)

Fig. C.35. Monitoring-based responses: (a) curvature range, (b) moment range, (c) rigidity, (d) curvature peak/valley, (e) moment peak/valley, MOX11, 10.16 Nm, Nf = 4.23E+04 cycles.

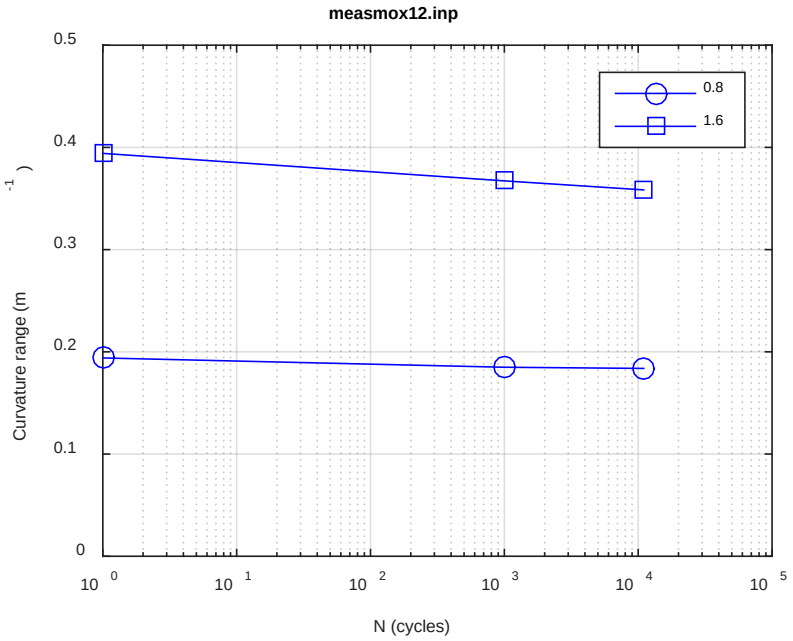
measmox12.inp
0.5
0.4
0.3
0.2
0.1
0
Curvature range (m -1)
0.8
1.6
10 0
10 1
10 2
10 3
10 4
10 5
N (cycles)

(a)

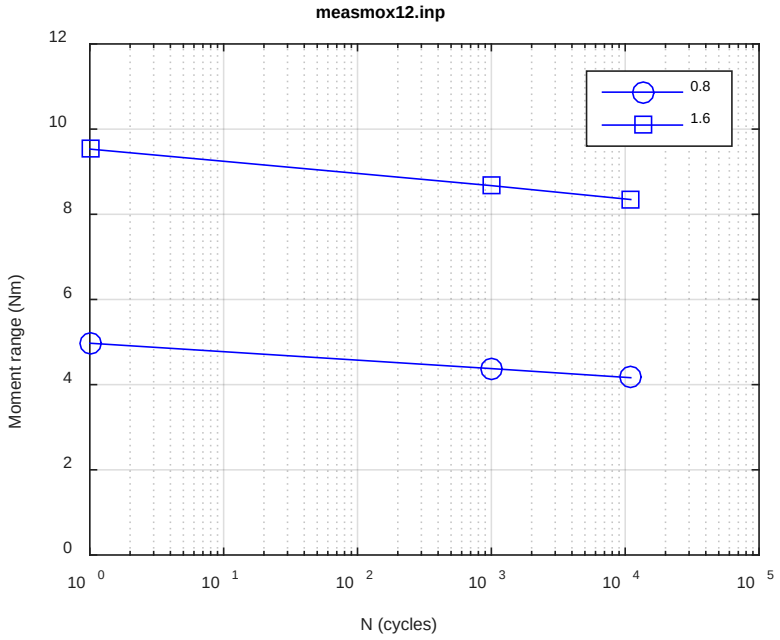
measmox12.inp
12
10
8
6
4
2
0
Moment range (Nm)
0.8
1.6
10 0
10 1
10 2
10 3
10 4
10 5
N (cycles)

(b)

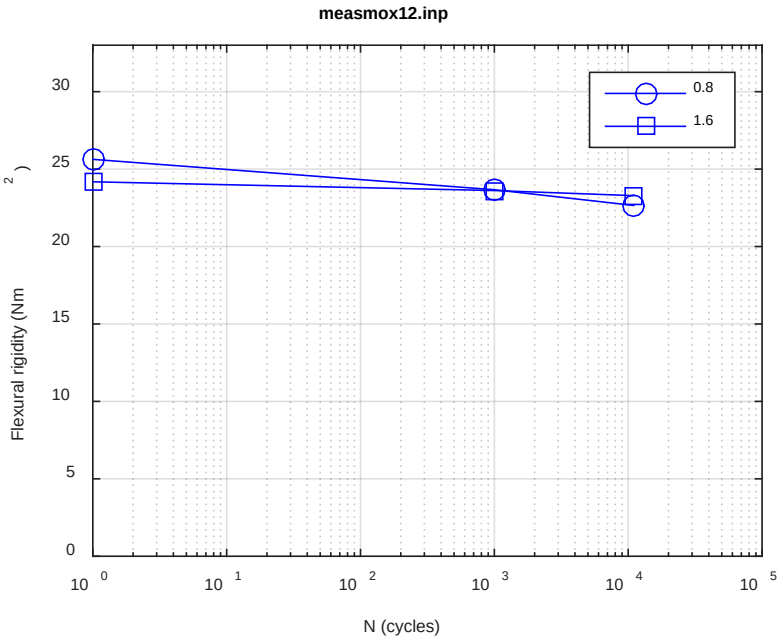
measmox12.inp
0.8
1.6
Flexural rigidity (Nm 2)
N (cycles)

(c)

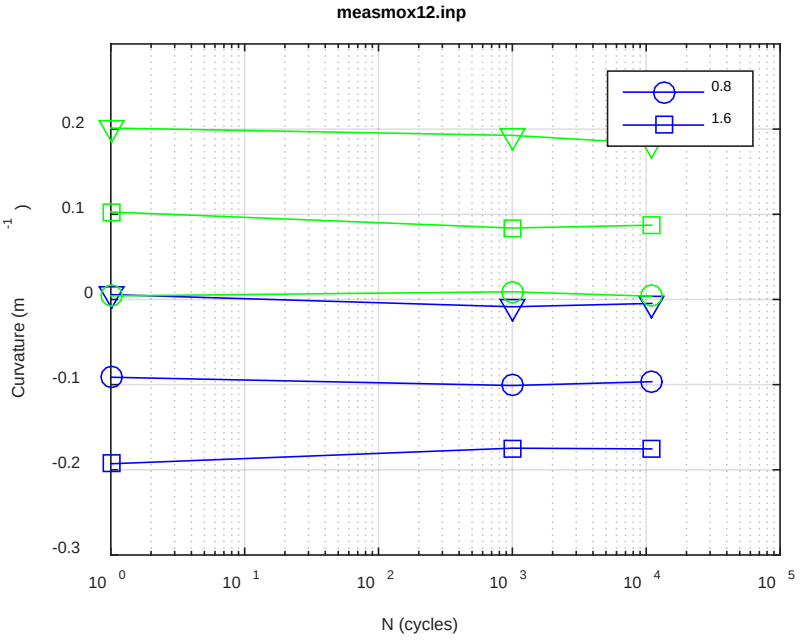
measmox12.inp
0.8
1.6
Curvature (m -1)
N (cycles)

(d)

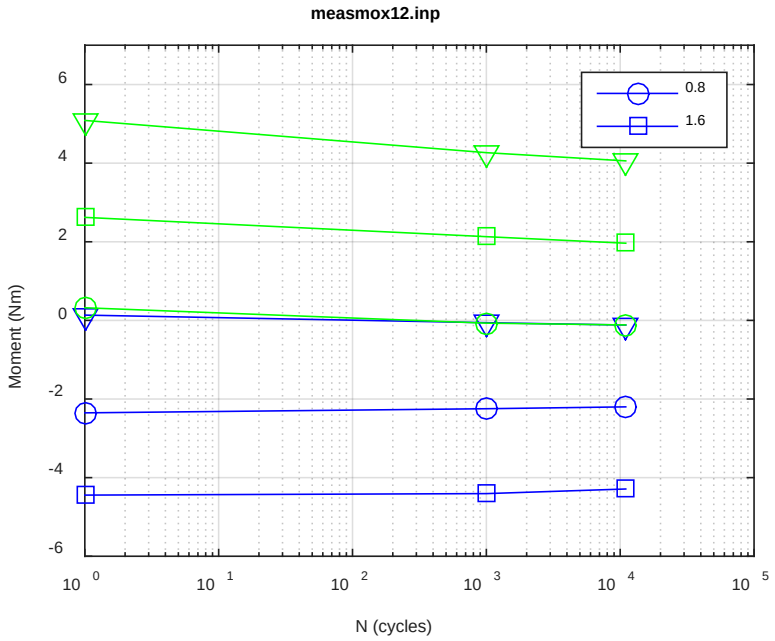

(e)

Fig. C.36. Measurement-based responses: (a) curvature range, (b) moment range, (c) rigidity, (d) curvature peak/valley, (e) moment peak/valley, MOX12, 10.16 Nm.

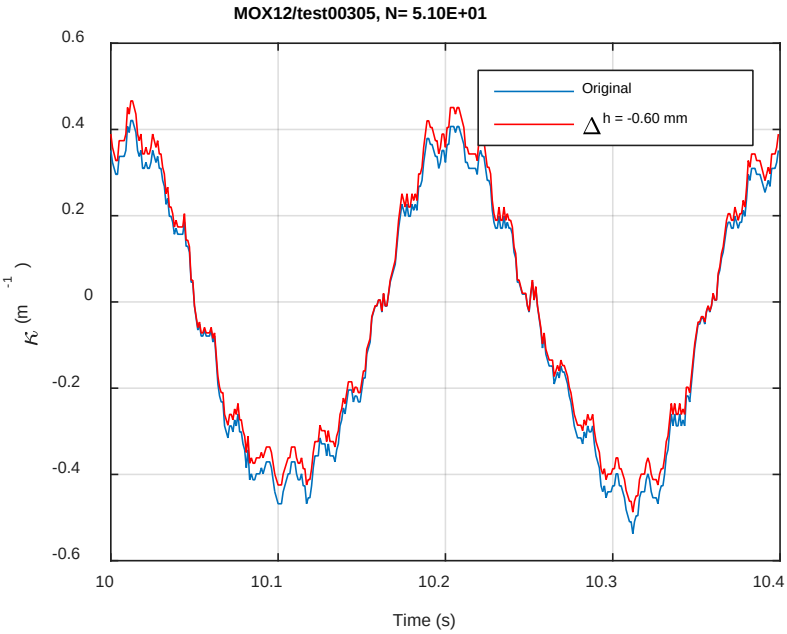
MOX12/test00305, N= 5.10E+01
Original
Δh = -0.60 mm
κ (m-1)
Time (s)
0.6
0.4
0.2
0
-0.2
-0.4
-0.6
10
10.1
10.2
10.3
10.4

(a)

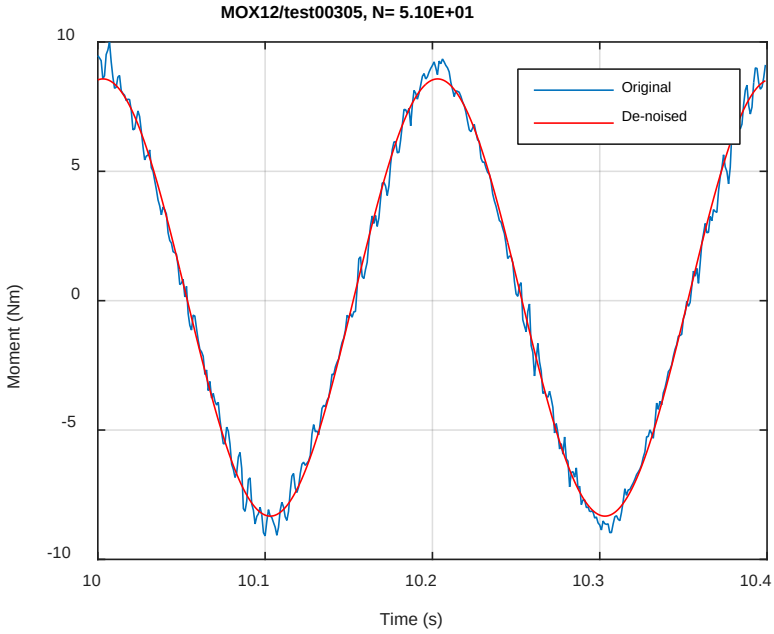
MOX12/test00305, N= 5.10E+01
Original
De-noised
Moment (Nm)
Time (s)
10
5
0
-5
-10
10
10.1
10.2
10.3
10.4

(b)

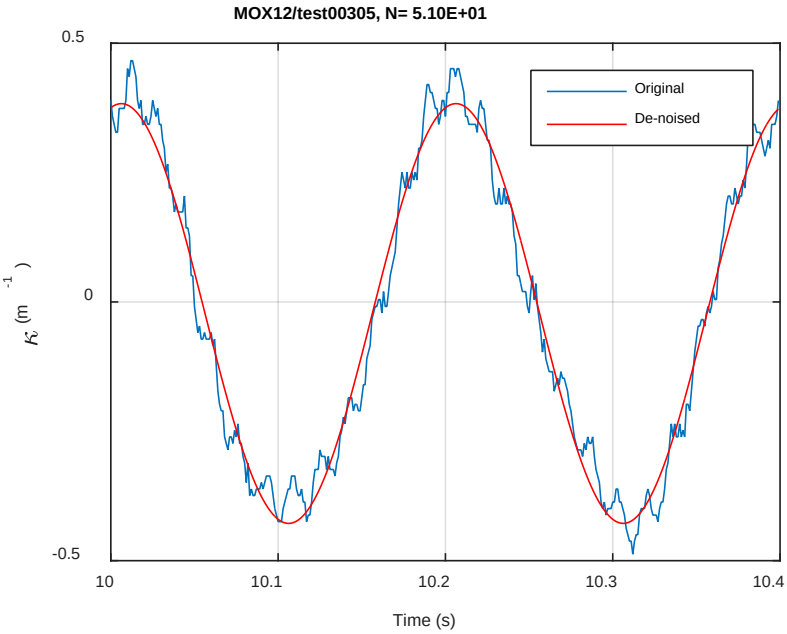

(c)

Fig. C.37. Monitoring-based responses: (a) curvature, (b) moment, (c) curvature, MOX12, 10.16 Nm, Ns = 5.10E+01 cycles.

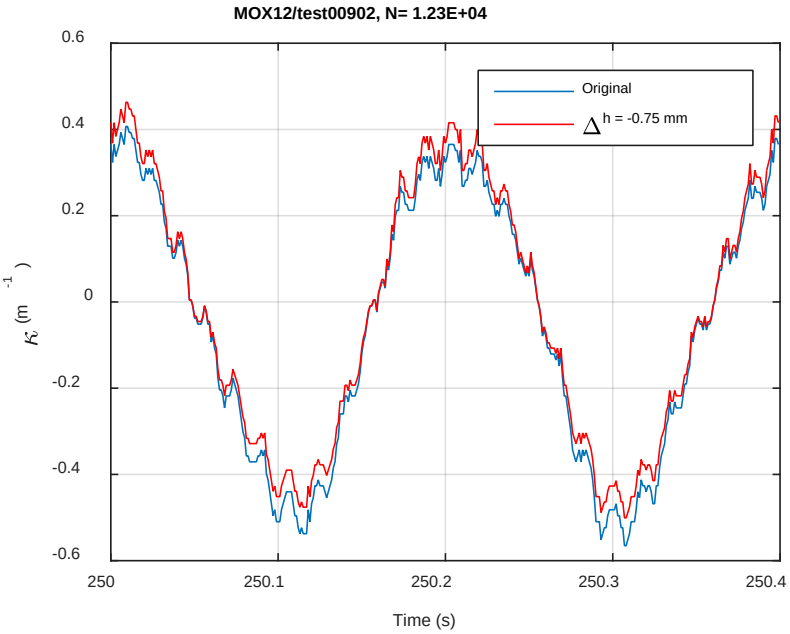
MOX12/test00902, N= 1.23E+04
Original
Δh = -0.75 mm
κ (m-1)
Time (s)
0.6
0.4
0.2
0
-0.2
-0.4
-0.6
250
250.1
250.2
250.3
250.4

(a)

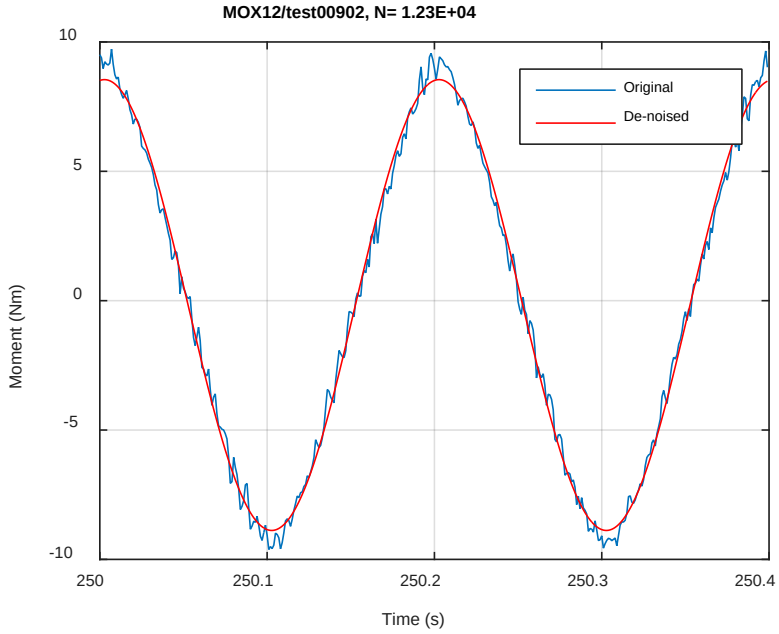
MOX12/test00902, N= 1.23E+04
Original
De-noised
Moment (Nm)
Time (s)
10
5
0
-5
-10
250
250.1
250.2
250.3
250.4

(b)

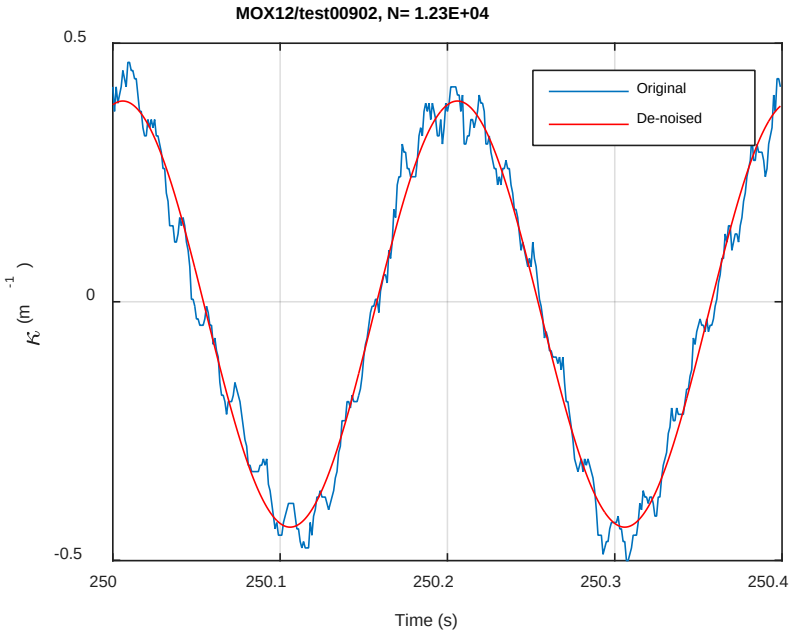

(c)

Fig. C.38. Monitoring-based responses: (a) curvature, (b) moment, (c) curvature, MOX12, 10.16 Nm, Ns = 1.23E+04 cycles.

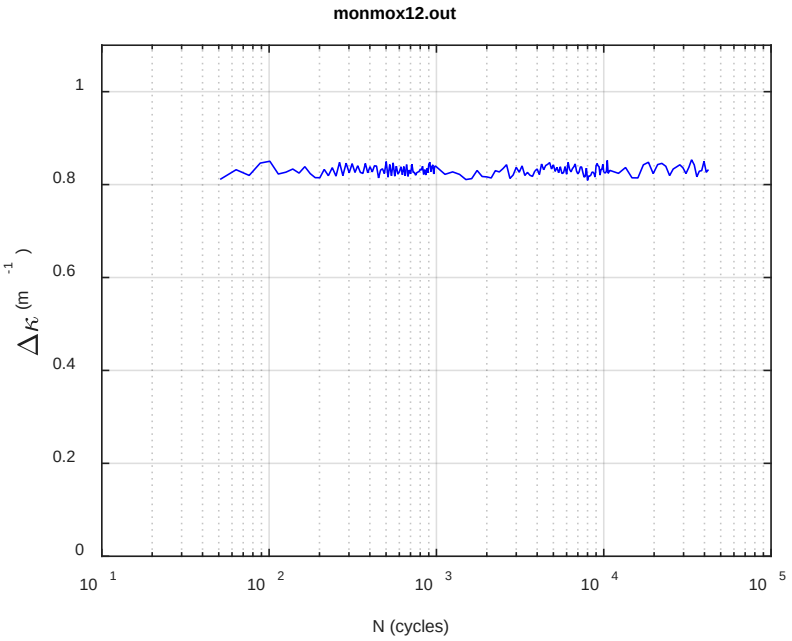
monmox12.out
1
0.8
0.6
0.4
0.2
0
Δκ (m -1)
10 1
10 2
10 3
10 4
10 5
N (cycles)

(a)

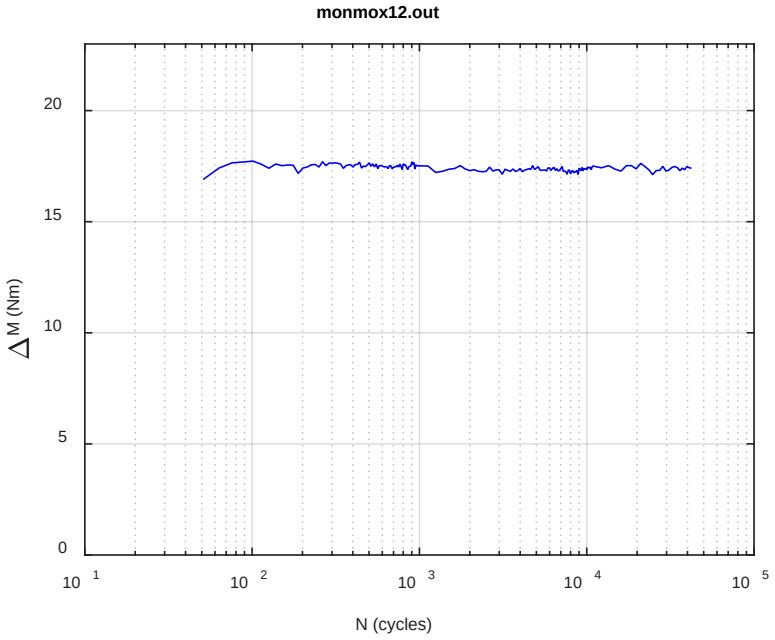
monmox12.out
20
15
10
5
0
Δ M (Nm)
10 1
10 2
10 3
10 4
10 5
N (cycles)

(b)

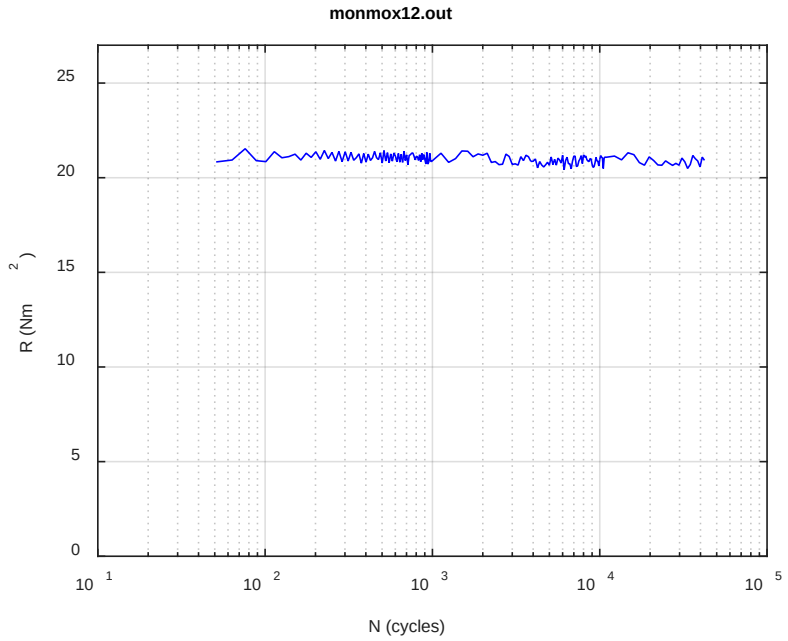
monmox12.out
25
20
15
10
5
0
R (Nm 2)
10 1
10 2
10 3
10 4
10 5
N (cycles)

(c)

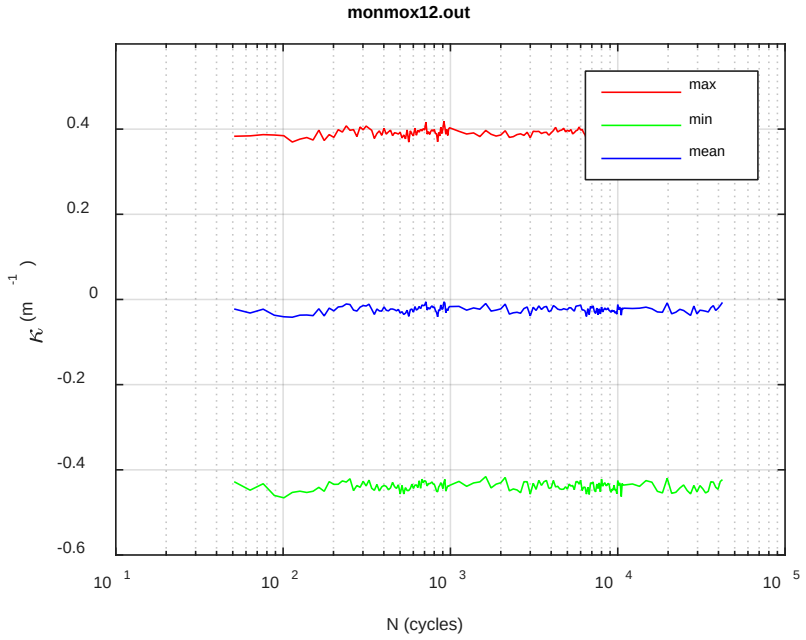
monmox12.out
max
min
mean
0.4
0.2
0
-0.2
-0.4
-0.6
κ (m -1)
10 1
10 2
10 3
10 4
10 5
N (cycles)

(d)

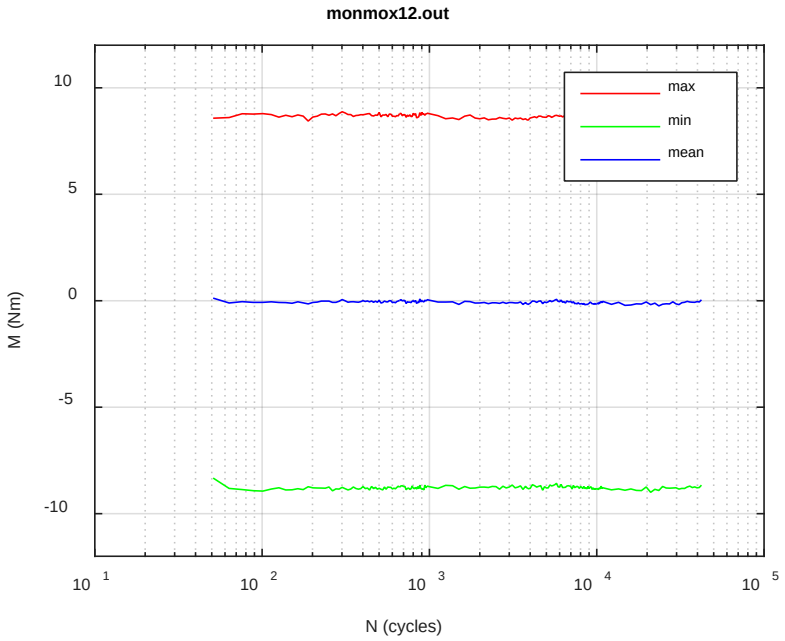

(e)

Fig. C.39. Monitoring-based responses: (a) curvature range, (b) moment range, (c) rigidity, (d) curvature peak/valley, (e) moment peak/valley, MOX12, 10.16 Nm, Nf = 4.23E+04 cycles.